



ACTINOBACTERIA, A SOURCE OF BIOCATALYTIC TOOLS

EDITED BY: Dirk Tischler, Willem J. H. van Berkel and Marco W. Fraaije
PUBLISHED IN: *Frontiers in Microbiology*



frontiers

Frontiers Copyright Statement

© Copyright 2007-2019 Frontiers Media SA. All rights reserved.

All content included on this site, such as text, graphics, logos, button icons, images, video/audio clips, downloads, data compilations and software, is the property of or is licensed to Frontiers Media SA ("Frontiers") or its licensees and/or subcontractors. The copyright in the text of individual articles is the property of their respective authors, subject to a license granted to Frontiers.

The compilation of articles constituting this e-book, wherever published, as well as the compilation of all other content on this site, is the exclusive property of Frontiers. For the conditions for downloading and copying of e-books from Frontiers' website, please see the Terms for Website Use. If purchasing Frontiers e-books from other websites or sources, the conditions of the website concerned apply.

Images and graphics not forming part of user-contributed materials may not be downloaded or copied without permission.

Individual articles may be downloaded and reproduced in accordance with the principles of the CC-BY licence subject to any copyright or other notices. They may not be re-sold as an e-book.

As author or other contributor you grant a CC-BY licence to others to reproduce your articles, including any graphics and third-party materials supplied by you, in accordance with the Conditions for Website Use and subject to any copyright notices which you include in connection with your articles and materials.

All copyright, and all rights therein, are protected by national and international copyright laws.

The above represents a summary only. For the full conditions see the Conditions for Authors and the Conditions for Website Use.

ISSN 1664-8714
ISBN 978-2-88945-922-3
DOI 10.3389/978-2-88945-922-3

About Frontiers

Frontiers is more than just an open-access publisher of scholarly articles: it is a pioneering approach to the world of academia, radically improving the way scholarly research is managed. The grand vision of Frontiers is a world where all people have an equal opportunity to seek, share and generate knowledge. Frontiers provides immediate and permanent online open access to all its publications, but this alone is not enough to realize our grand goals.

Frontiers Journal Series

The Frontiers Journal Series is a multi-tier and interdisciplinary set of open-access, online journals, promising a paradigm shift from the current review, selection and dissemination processes in academic publishing. All Frontiers journals are driven by researchers for researchers; therefore, they constitute a service to the scholarly community. At the same time, the Frontiers Journal Series operates on a revolutionary invention, the tiered publishing system, initially addressing specific communities of scholars, and gradually climbing up to broader public understanding, thus serving the interests of the lay society, too.

Dedication to Quality

Each Frontiers article is a landmark of the highest quality, thanks to genuinely collaborative interactions between authors and review editors, who include some of the world's best academicians. Research must be certified by peers before entering a stream of knowledge that may eventually reach the public - and shape society; therefore, Frontiers only applies the most rigorous and unbiased reviews.

Frontiers revolutionizes research publishing by freely delivering the most outstanding research, evaluated with no bias from both the academic and social point of view. By applying the most advanced information technologies, Frontiers is catapulting scholarly publishing into a new generation.

What are Frontiers Research Topics?

Frontiers Research Topics are very popular trademarks of the Frontiers Journals Series: they are collections of at least ten articles, all centered on a particular subject. With their unique mix of varied contributions from Original Research to Review Articles, Frontiers Research Topics unify the most influential researchers, the latest key findings and historical advances in a hot research area! Find out more on how to host your own Frontiers Research Topic or contribute to one as an author by contacting the Frontiers Editorial Office: researchtopics@frontiersin.org

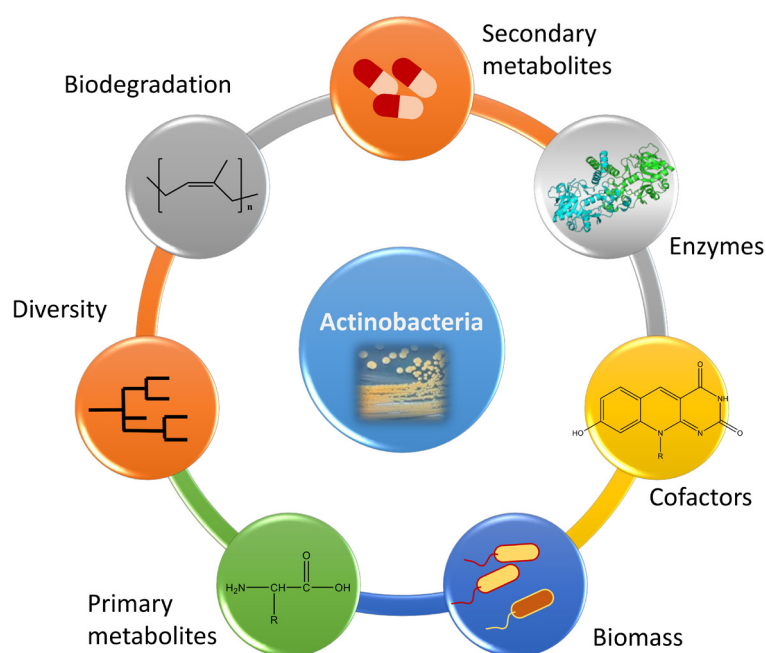
ACTINOBACTERIA, A SOURCE OF BIOCATALYTIC TOOLS

Topic Editors:

Dirk Tischler, Ruhr-Universität Bochum, Germany

Willem J. H. van Berkel, Wageningen University & Research, Netherlands

Marco W. Fraaije, University of Groningen, Netherlands



Landscape of *Actinobacteria* in biotechnology related topics. Image: Dirk Tischler.

Actinobacteria (Actinomycetes) represent one of the largest and most diverse phyla among Bacteria. The remarkable diversity is displayed by various lifestyles, distinct morphologies, a wide spectrum of physiological and metabolic activities, as well as genetics. Interestingly, most *Actinobacteria* have a high GC-content (ranging from 51% to >70%) and belong to Gram-positive or Gram-variable type microbes. Many species are well known for large genomes which may be of linear style as in case of rhodococci or circular. Many of those harbor linear megaplastids as a kind of genetic storage device. Frequently gene redundancy is reported and in most cases the evolutionary history or a functional role remains enigmatic.

Nevertheless these large genomes and megaplastids provide access to a number of potential (homologous) biocatalysts which await elucidation. *Actinobacteria* are well known for their biotechnological potential which is exemplarily described for amino

acid producing *Corynebacteria*, secondary metabolite producing *Streptomyces*, pathogenic targets as *Nocardia* and *Mycobacteria*, carotenoid building *Micrococcus* strains, acid fermenting *Propionibacteria*, health and food related *Bifidobacterium* strains, rubber degrading *Gordonia* species, and organic pollutant degrading rhodococci among others.

In many cases individual pathways or enzymes can be modified or recombinantly employed for biocatalysis. Even some genetic tools to work directly in those microbes have been successfully used as for example in *Corynebacterium* or in *Rhodococcus* species. During the last decade more and more genomes have been sequenced and made available for data mining and become accessible by state of the art genomic manipulation methods as minimal genomes, knock-out or artificial evolution.

With respect to this large and ancient phylum many questions can be asked either from a scientific or industrial point of view. In order to provide some crystallization points we like to raise some examples as follows. How small can be an actinobacterial genome? What is the driving force to comprise large and repetitive genomes/megaplasms? What is needed to generate an actinobacterial power house for industry? Can we annotate novel biocatalysts from scratch and improve functional annotation? What are common and different features with respect to other bacteria and/or fungi? How many novel antibiotics are hidden among *Actinobacteria*? Is there more potential among extremophile members or are they only specialized?

Here especially the production of natural compounds is of high interest.

Citation: Tischler, D., van Berkel, W. J. H., Fraaije, M. W., eds. (2019). *Actinobacteria*, a Source of Biocatalytic Tools. Lausanne: Frontiers Media.
doi: 10.3389/978-2-88945-922-3

Table of Contents

- 06 Editorial: Actinobacteria, a Source of Biocatalytic Tools**
Dirk Tischler, Willem J. H. van Berkel and Marco W. Fraaije
- 10 *Mycobacterial $F_{420}H_2$ -Dependent Reductases Promiscuously Reduce Diverse Compounds Through a Common Mechanism***
Chris Greening, Thanavit Jirapanjawat, Shahana Afroze, Blair Ney, Colin Scott, Gunjan Pandey, Brendon M. Lee, Robyn J. Russell, Colin J. Jackson, John G. Oakeshott, Matthew C. Taylor and Andrew C. Warden
- 20 *Cofactor Tail Length Modulates Catalysis of Bacterial F_{420} -Dependent Oxidoreductases***
Blair Ney, Carlo R. Carere, Richard Sparling, Thanavit Jirapanjawat, Matthew B. Stott, Colin J. Jackson, John G. Oakeshott, Andrew C. Warden and Chris Greening
- 31 *3-Hydroxybenzoate 6-Hydroxylase From *Rhodococcus jostii* RHA1 Contains a Phosphatidylinositol Cofactor***
Stefania Montersino, Evelien te Poele, Roberto Orru, Adrie H. Westphal, Arjan Barendregt, Albert J. R. Heck, Robert van der Geize, Lubbert Dijkhuizen, Andrea Mattevi and Willem J. H. van Berkel
- 42 *Pyridine Nucleotide Coenzyme Specificity of p-Hydroxybenzoate Hydroxylase and Related Flavoprotein Monooxygenases***
Adrie H. Westphal, Dirk Tischler, Florian Heinke, Sarah Hofmann, Janosch A. D. Gröning, Dirk Labudde and Willem J. H. van Berkel
- 59 *Mining the Genome of *Streptomyces leeuwenhoekii*: Two New Type I Baeyer–Villiger Monooxygenases From Atacama Desert***
Alejandro Gran-Scheuch, Milos Trajkovic, Loreto Parra and Marco W. Fraaije
- 69 *Catalytic Performance of a Class III Old Yellow Enzyme and its Cysteine Variants***
Anika Scholtissek, Eric Gädke, Caroline E. Paul, Adrie H. Westphal, Willem J. H. van Berkel and Dirk Tischler
- 79 *Development of a Novel *Escherichia coli*–*Kocuria* Shuttle Vector Using the Cryptic *pKPAL3* Plasmid From *K. palustris* IPUFS-1 and its Utilization in Producing Enantiopure (S)-Styrene Oxide***
Hiroshi Toda and Nobuya Itoh
- 90 *Real Time Monitoring of NADPH Concentrations in *Corynebacterium glutamicum* and *Escherichia coli* via the Genetically Encoded Sensor mBFP***
Oliver Goldbeck, Alexander W. Eck and Gerd M. Seibold
- 100 *Efficient Production of the Dicarboxylic Acid Glutarate by *Corynebacterium glutamicum* via a Novel Synthetic Pathway***
Fernando Pérez-García, João M. P. Jorge, Annika Dreyszas, Joe Max Risse and Volker F. Wendisch
- 113 *Expression and Characteristics of Two Glucose-Tolerant GH1 β -glucosidases From *Actinomadura amylolytica* YIM 77502^T for Promoting Cellulose Degradation***
Yi-Rui Yin, Peng Sang, Wen-Dong Xian, Xin Li, Jian-Yu Jiao, Lan Liu, Wael N. Hozzein, Min Xiao and Wen-Jun Li

- 126 **Whole Cell Actinobacteria as Biocatalysts**
Yitayal Shiferaw Anteneh and Christopher Milton Mathew Franco
- 141 **A Waking Review: Old and Novel Insights Into the Spore Germination in Streptomyces**
Jan Bobek, Klára Šmídová and Matouš Čihák
- 153 **Germination and Growth Analysis of Streptomyces lividans at the Single-Cell Level Under Varying Medium Compositions**
Joachim Koepff, Christian Carsten Sachs, Wolfgang Wiechert, Dietrich Kohlheyer, Katharina Nöh, Marco Oldiges and Alexander Grünberger
- 163 **Secondary Metabolites Produced During the Germination of Streptomyces coelicolor**
Matouš Čihák, Zdeněk Kameník, Klára Šmídová, Natalie Bergman, Oldřich Benada, Olga Kofroňová, Kateřina Petříčková and Jan Bobek
- 176 **RNase III-Binding-mRNAs Revealed Novel Complementary Transcripts in Streptomyces**
Dita Šetinová, Klára Šmídová, Pavel Pohl, Inesa Musić and Jan Bobek
- 188 **The SCO4117 ECF Sigma Factor Pleiotropically Controls Secondary Metabolism and Morphogenesis in Streptomyces coelicolor**
María T. López-García, Paula Yagüe, Nathaly González-Quiñónez, Beatriz Rioseras and Angel Manteca
- 200 **ArgR of Streptomyces coelicolor is a Pleiotropic Transcriptional Regulator: Effect on the Transcriptome, Antibiotic Production, and Differentiation in Liquid Cultures**
Alma Botas, Rosario Pérez-Redondo, Antonio Rodríguez-García, Rubén Álvarez-Álvarez, Paula Yagüe, Angel Manteca and Paloma Liras
- 218 **Plant-Growth Promotion and Biocontrol Properties of Three Streptomyces spp. Isolates to Control Bacterial Rice Pathogens**
Zulma Rocío Suárez-Moreno, Diana Marcela Vinchira-Villarraga, Diana Isabel Vergara-Morales, Leonardo Castellanos, Freddy A. Ramos, Corrado Guarnaccia, Giuliano Degrassi, Vittorio Venturi and Nubia Moreno-Sarmiento



Editorial: *Actinobacteria*, a Source of Biocatalytic Tools

Dirk Tischler^{1*}, Willem J. H. van Berkel² and Marco W. Fraaije³

¹ Microbial Biotechnology, Biology and Biotechnology, Ruhr University Bochum, Bochum, Germany, ² Laboratory of Biochemistry, Wageningen University & Research, Wageningen, Netherlands, ³ Molecular Enzymology, University of Groningen, Groningen, Netherlands

Keywords: actinomycetes, secondary metabolites, high GC genetics, novel biocatalysts, extremophile actinobacteria, biotechnology, biocatalysis, germination

Editorial on the Research Topic

Actinobacteria, a Source of Biocatalytic Tools

ACTINOBACTERIA: ANCIENT PHYLUM WITH LARGE BIOTECHNOLOGICAL POTENTIAL STILL TO BE UNCOVERED

OPEN ACCESS

Edited by:

Marc Strous,
University of Calgary, Canada

Reviewed by:

Dmitry A. Rodionov,
Sanford Burnham Prebys Medical
Discovery Institute, United States

*Correspondence:

Dirk Tischler
dirk.tischler@rub.de;
dirk-tischler@email.de

Specialty section:

This article was submitted to
Microbial Physiology and Metabolism,
a section of the journal
Frontiers in Microbiology

Received: 25 January 2019

Accepted: 28 March 2019

Published: 16 April 2019

Citation:

Tischler D, van Berkel WJH and
Fraaije MW (2019) Editorial:
Actinobacteria, a Source of
Biocatalytic Tools.
Front. Microbiol. 10:800.
doi: 10.3389/fmicb.2019.00800

Actinobacteria (Actinomycetes) represent one of the largest and most diverse phyla among the Bacteria. The characteristics and phylogeny of actinobacteria have been well-described throughout the years (Anteneh and Franco; Embley et al., 1994; Stackebrandt et al., 1997a,b; Stach and Bull, 2005; Stackebrandt and Schumann, 2006; Ventura et al., 2007; Gao and Gupta, 2012; Goodfellow, 2012a,b; Schrempf, 2013; Lawson, 2018; Lewin et al., 2016). Still actinobacteria are hotspots for discovery of new biomolecules and enzyme activities, fueling an active field of research. The remarkable diversity is displayed by various lifestyles, distinct morphologies, a wide spectrum of physiological and metabolic activities, as well as genetics.

Most actinobacteria have a high GC-content (ranging from 51% to over 70%) and belong to Gram-positive or Gram-variable type microbes (Stackebrandt and Schumann, 2006; Ventura et al., 2007; Lawson, 2018). Many species are well-known for their large genomes, which may be of linear style, as in case of rhodococci, or circular (Ventura et al., 2007; Sen et al., 2014; Lewin et al., 2016). Many also harbor linear megaplasmids as a kind of genetic storage device (König et al., 2004; Medema et al., 2010; Wagenknecht et al., 2010; Bottacini et al., 2015). These plasmids often encode special metabolic features such as secondary metabolite synthetic machineries or alternative degradation pathways. However, a number of representatives comprise smaller genomes such as some *Bifidobacteria*, *Corynebacteria*, *Mycobacteria*, and *Propionibacteria* species (Ventura et al., 2007; Lewin et al., 2016). Interestingly, smaller genomes are often encountered in pathogens or in those, which live in ecological niches. The smallest actinobacterial genomes can be found among *Tropheryma*, which is known as the Whipple's disease microbe (Bentley et al., 2003; Raoult et al., 2003). Gene redundancy or genes encoding for closely related enzymes are frequently reported and in most cases the evolutionary history or a functional role remains enigmatic (McLeod et al., 2006; Tischler et al., 2009, 2010, 2013; Roberts et al., 2011; Riebel et al., 2012; Gröning et al., 2014; Riedel et al., 2015a,b; Nguyen et al., 2017; Chen et al., 2018; Gran-Scheuch et al.). In this context horizontal gene transfer was found to play a major role in the genome fluidity of actinobacteria (Ventura et al., 2007). However, this seems not to be true for all actinobacteria or limited to some features such as secondary metabolism as discussed for *Streptomyces* and *Rhodococcus*, respectively (McLeod et al., 2006; Lewin et al., 2016).

The large actinobacterial genomes and megaplastids provide access to an impressive number of potential biocatalysts and pathways (Lewin et al., 2016). A few examples of novel biocatalysts linked to gene redundancy are cited above, but still more truly novel enzymes or pathways await elucidation. Actinobacteria are well-known for their biotechnological potential which is exemplarily described for amino acid producing *Corynebacteria* (Poetsch et al., 2011; Goldbeck et al.; Pérez-García et al.), secondary metabolite producing *Streptomyces* (Niu et al., 2016; Senges et al., 2018), pathogenic targets as *Nocardia* and *Mycobacteria* (Cosma et al., 2003; Wilson, 2012), carotenoid building *Micrococcus* strains (Rostami et al., 2016), acid fermenting *Propionibacteria* (Rabah et al., 2017), health and food related *Bifidobacterium* strains (Lawson, 2018), rubber degrading *Gordonia* species (Linos et al., 1999; Heine et al., 2018), and organic pollutant degrading rhodococci (McLeod et al., 2006; Kim et al., 2018) among others.

In many cases individual pathways can be exploited for the production of valuable products, or enzymes can be recombinantly produced and exploited for biocatalysis. Even some genetic tools to work directly in actinobacteria have been successfully used as for example in *Corynebacterium* (Nešvera and Pátek, 2011). Recently some additional systems have been established to create e.g., *Kocuria* and *Rhodococcus* hosts (MonTERSINO et al.; Toda and Itoh). The first system allowed actually to express genes of various origins in *Kocuria*, whereas the *Rhodococcus* system was used for identification of the natural phospholipid ligand of a monooxygenase. During the last decade more and more genomes have been sequenced and made available for data mining and become accessible by state-of-the-art genomic manipulation methods. Novel pathways and enzymes are frequently described from actinobacteria as a result of the progress in various omics approaches and high-throughput methods. Except for novel pathways or enzymes, genome analyses have revealed that actinobacteria also employ rather unique cofactors, such as the F₄₂₀ cofactor (Selengut and Haft, 2010; Greening et al., 2016; Nguyen et al., 2017; Ney et al.). With respect to biocatalysis and derived applications a number of recent studies can be mentioned. These comprise whole-cell systems (Oelschlägel et al., 2015; Okamoto et al., 2017; de Carvalho, 2017; Goldbeck et al.; Yin et al.) enzymatic cascades (Kara et al., 2015; Ni et al., 2016; Zimmerling et al., 2017), structure-function relationships (Riebel et al., 2012; MonTERSINO et al., 2013; Riedel et al., 2015a,b; Sucharitakul et al., 2016; Scholtissek et al., 2017; Scholtissek et al.) as well as mechanistic insights (Greening et al.; Ney et al.; Westphal et al.).

Secondary metabolite production is of industrial interest and here especially *Streptomyces* has to be mentioned which provides access to antibiotics as well as siderophores (Medema et al., 2010; Čihák et al.; Botas et al.; López-García et al.; Senges et al., 2018; Suárez Moreno et al.). Secondary metabolite production is

frequently investigated either on a regulatory level (Botas et al.) or *via* metabolomics (Senges et al., 2018) and of course within biotechnological studies. It was found that the lifestyle and the development stage seem to be crucial for secondary metabolism. Spore formation among *Streptomyces* is such a specialized development stage and of importance for cell regulatory processes, but also with respect to applications (Bobek et al.). Further, some regulatory elements are solely present among actinobacteria and need to be functionally tested (Koepff et al.; López-García et al.; Šetinová et al.). Growth limiting conditions (Fe-, N-, S-limitations or presence of toxic compounds/elements) are often used to overproduce target compounds and among those the secondary metabolites siderophores (Retamal-Morales et al., 2017, 2018b; Senges et al., 2018) and biosurfactants (Kügler et al., 2015; Retamal-Morales et al., 2018a) can be mentioned.

Actinobacteria also harbor extremophile branches, which become more and more attractive for biotechnological investigations (Shivlata and Satyanarayana, 2015). Examples include antimicrobial compound producers as many *Streptomyces* spp. (Radhakrishnan et al., 2007; Xue et al., 2013), siderophore producing strains as *Thermobifida fusca* (Dimise et al., 2008) and *Thermocristum agreste* (Heine et al., 2017), and many rhizosphere specialists with various interactions toward plants, fungi and/or other bacteria (Palaniyandi et al., 2013). Besides the above described actinobacteria mainly derived from soil, also other habitats and ecological niches are explored and successfully conquered by various actinobacteria. Among those interesting resources for biotechnology are present (Shivlata and Satyanarayana, 2015).

In conclusion, it becomes obvious that the large and diverse group of actinobacteria is of interest from different perspectives such as general microbiology, ecology, phylogeny, biochemistry, and regulation, environmental concerns, pathogenicity as well as biotechnology. Still there are new members being discovered that belong to this phylum or reclassifications occur according to new findings with respect to morphology and phylogeny. The increasing amount of data from various omics fields allows us to uncover more and more properties which can be of use for various (biotechnological) purposes. We believe that the potential of actinobacteria for biotechnology was only touched lightly thus far: there is more to be uncovered!

AUTHOR CONTRIBUTIONS

DT, WB, and MF drafted this editorial together and approved it prior submission.

ACKNOWLEDGMENTS

The authors thank the Frontiers Team for support during handling of the Research Topic and all Contributors for providing insides into their research.

REFERENCES

- Bentley, S. D., Maiwald, M., Murphy, L. D., Pallen, M. J., Yeats, C. A., Dover, L. G., et al. (2003). Sequencing and analysis of the genome of the Whipple's disease bacterium *Tropheryma whippelii*. *Lancet* 361, 637–644. doi: 10.1016/S0140-6736(03)12597-4
- Bottacini, F., O'Connell Motherway, M., Casey, E., McDonnell, B., Mahony, J., Ventura, M., et al. (2015). Discovery of a conjugative megaplasmid in *Bifidobacterium breve*. *Appl. Environ. Microbiol.* 81, 166–176. doi: 10.1128/AEM.02871-14
- Chen, B. S., Médiçi, R., van der Helm, M. P., van Zwet, Y., Gjonaj, L., van der Geest, R., et al. (2018). *Rhodococcus* strains as source for ene-reductase activity. *Appl. Microbiol. Biotechnol.* 102, 5545–5556. doi: 10.1007/s00253-018-8984-7
- Cosma, C. L., Sherman, D. R., and Ramakrishnan, L. (2003). The secret lives of the pathogenic mycobacteria. *Annu. Rev. Microbiol.* 57, 641–676. doi: 10.1146/annurev.micro.57.030502.091033
- de Carvalho, C. C. (2017). Whole cell biocatalysts: Essential workers from Nature to the industry. *Microb. Biotechnol.* 10, 250–263. doi: 10.1111/1751-7915.12363
- Dimise, E. J., Widdboom, P. F., and Bruner, S. D. (2008). Structure elucidation and biosynthesis of fuscachelins, peptide siderophores from the moderate thermophile *Thermobifida fusca*. *Proc. Natl. Acad. Sci. U.S.A.* 105, 15311–15316. doi: 10.1073/pnas.0805451105
- Embley, T. M., Hirt, R. P., and Williams, D. M. (1994). Biodiversity at the molecular level: the domains, kingdoms and phyla of life. *Phil. Trans. R. Soc. B* 345, 21–33. doi: 10.1098/rstb.1994.0083
- Gao, B., and Gupta, R. S. (2012). Phylogenetic framework and molecular signatures for the main clades of the phylum actinobacteria. *Microbiol. Mol. Biol. Rev.* 76, 66–112. doi: 10.1128/MMBR.05011-11
- Goodfellow, M. (2012a). "Class I. Actinobacteria," in *Bergey's Manual of Systematic Bacteriology*, eds M. Goodfellow, P. Kämpfer, H.-J. Busse, M. E. Trujillo, K.-I. Suzuki, W. Ludwig, and B. Whitman (New York, NY: Springer), 34–45.
- Goodfellow, M. (2012b). "Phylum XXVI. Actinobacteria phyl. nov," in *Bergey's Manual of Systematic Bacteriology*, eds M. Goodfellow, P. Kämpfer, H.-J. Busse, M. E. Trujillo, K.-I. Suzuki, W. Ludwig, and B. Whitman (New York, NY: Springer), 33–2028.
- Greening, C., Ahmed, F. H., Mohamed, A. E., Lee, B. M., Pandey, G., Warden, A. C., et al. (2016). Physiology, biochemistry, and applications of F420- and Fo-dependent redox reactions. *Microbiol. Mol. Biol. Rev.* 80, 451–493. doi: 10.1128/MMBR.00070-15
- Gröning, J. A., Eulberg, D., Tischler, D., Kaschabek, S. R., and Schlömann, M. (2014). Gene redundancy of two-component (chloro)phenol hydroxylases in *Rhodococcus opacus* 1CP. *FEMS Microbiol. Lett.* 361: 68–75. doi: 10.1111/1574-6968.12616
- Heine, T., Mehnert, M., Schwabe, R., and Tischler, D. (2017). Thermochelin, a hydroxamate siderophore from *Thermocristum agreste* DSM 44070. *Solid State Phenomena* 262, 505–508. doi: 10.4028/www.scientific.net/SSP.262.501
- Heine, T., Zimmerling, J., Ballmann, A., Kleeberg, S. B., Rückert, C., Busche, T., et al. (2018). On the enigma of glutathione-dependent styrene degradation in *Gordonia rubripertincta* CWB2. *Appl. Environ. Microbiol.* 84:e00154–e00118. doi: 10.1128/AEM.00154-18
- Kara, S., Schrittwieser, J. H., Gargiulo, S., Ni, Y., Yanase, H., Opperman, D. J., et al. (2015). Complete enzymatic oxidation of methanol to carbon dioxide: Towards more eco-efficient NAD(P)H regeneration systems. *Adv. Synth. Catal.* 357, 1687–1691. doi: 10.1002/adsc.201500173
- Kim, D., Choi, K. Y., Yoo, M., Zylstra, G. J., and Kim, E. (2018). Biotechnological potential of *Rhodococcus* biodegradative pathways. *J. Microbiol. Biotechnol.* 28, 1037–1051. doi: 10.4014/jmb.1712.12017
- König, C., Eulberg, D., Gröning, J. A., Lakner, S., Seibert, V., Kaschabek, S. R., et al. (2004). A linear megaplasmid, p1CP, carrying the genes for chlorocatechol catabolism of *Rhodococcus opacus* 1CP. *Microbiology* 150, 3075–3087. doi: 10.1099/mic.0.27217-0
- Kügler, J. H., Le Roes-Hill, M., Syldatk, C., and Hausmann, R. (2015). Surfactants tailored by the class actinobacteria. *Front. Microbiol.* 6:212. doi: 10.3389/fmicb.2015.00212
- Lawson, P. A. (2018). "The phylum actinobacteria," in *The Bifidobacteria and Related Organisms. Biology, Taxonomy, Applications*, eds P. Mattarelli, B. Biavati, W. H. Holzapel, and B. J. B Wood (London: Elsevier; Academic Press), 1–8. doi: 10.1016/B978-0-12-805060-6.00001-6
- Lewin, G. R., Carlos, C., Chevrette, M. G., Horn, H. A., McDonald, B. R., Stankey, R. J., et al. (2016). Evolution and ecology of actinobacteria and their bioenergy applications. *Annu. Rev. Microbiol.* 70, 235–254. doi: 10.1146/annurev-micro-102215-095748
- Linós, A., Steinbüchel, A., Spröer, C., and Kroppenstedt, R. M. (1999). *Gordonia polyisoprenivorans* sp. nov., a rubber-degrading actinomycete isolated from an automobile tyre. *Int. J. Syst. Bacteriol.* 49, 1785–1791. doi: 10.1099/00207713-49-4-1785
- McLeod, M. P., Warren, R. L., Hsiao, W. W., Araki, N., Myhre, M., Fernandes, C., et al. (2006). The complete genome of *Rhodococcus* sp. RHA1 provides insights into a catabolic powerhouse. *Proc. Natl. Acad. Sci. U.S.A.* 103, 15582–15587. doi: 10.1073/pnas.0607048103
- Medema, M. H., Trefzer, A., Kovalchuk, A., van den Berg, M., Müller, U., Heijne, W., et al. (2010). The sequence of a 1.8-mb bacterial linear plasmid reveals a rich evolutionary reservoir of secondary metabolic pathways. *Genome Biol. Evol.* 12, 212–224. doi: 10.1093/gbe/evq013
- Monterisino, S., Orru, R., Barendregt, A., Westphal, A. H., van Duijn, E., Mattevi, A., et al. (2013). Crystal structure of 3-hydroxybenzoate 6-hydroxylase uncovers lipid-assisted flavoprotein strategy for regioselective aromatic hydroxylation. *J. Biol. Chem.* 288, 26235–26245. doi: 10.1074/jbc.M113.479303
- Nešvera, J., and Pátek, M. (2011). Tools for genetic manipulations in *Corynebacterium glutamicum* and their applications. *Appl. Microbiol. Biotechnol.* 90, 1641–1654. doi: 10.1007/s00253-011-3272-9
- Nguyen, Q. T., Trinco, G., Binda, C., Mattevi, A., and Fraaije, M. W. (2017). Discovery and characterization of an F420-dependent glucose-6-phosphate dehydrogenase (Rh-FGD1) from *Rhodococcus jostii* RHA1. *Appl. Microbiol. Biotechnol.* 101, 2831–2842. doi: 10.1007/s00253-016-8038-y
- Ni, Y., Fernández-Fueyo, E., Gomez Baraibar, A., Ullrich, R., Hofrichter, M., Yanase, H., et al. (2016). Peroxygenase-catalyzed oxyfunctionalization reactions promoted by the complete oxidation of methanol. *Angew. Chem. Int. Ed. Engl.* 55, 798–801. doi: 10.1002/anie.201507881
- Niu, G., Chater, K. F., Tian, Y., Zhang, J., and Tan, H. (2016). Specialised metabolites regulating antibiotic biosynthesis in *Streptomyces* spp. *FEMS Microbiol. Rev.* 40, 554–573. doi: 10.1093/femsre/fuw012
- Oelschlägel, M., Kaschabek, S. R., Zimmerling, J., Schlömann, M., and Tischler, D. (2015). Co-metabolic formation of substituted phenylacetic acids by styrene-degrading bacteria. *Biotechnol. Rep.* 6, 20–26. doi: 10.1016/j.btre.2015.01.003
- Okamoto, D. N., Ferrari, V. B., Lago, J. H. G., de Melo, I. S., and Vasconcellos, S. P. (2017). Actinomycetes as tools for biotransformations of lignans. *Biomed. J. Sci. Tech. Res.* 1, 1–3. doi: 10.26717/BJSTR.2017.01.000448
- Palaniyandi, S. A., Yang, S. H., Zhang, L., and Suh, J. W. (2013). Effects of actinobacteria on plant disease suppression and growth promotion. *Appl. Microbiol. Biotechnol.* 97, 9621–9636. doi: 10.1007/s00253-013-5206-1
- Poetsch, A., Haussmann, U., and Burkovski, A. (2011). Proteomics of corynebacteria: from biotechnology workhorses to pathogens. *Proteomics* 11, 3244–3255. doi: 10.1002/pmic.201000786
- Rabah, H., Rosa do Carmo, F. L., and Jan, G. (2017). Dairy propionibacteria: versatile probiotics. *Microorganisms* 5:E24. doi: 10.3390/microorganisms5020024
- Radhakrishnan, M., Balaji, S., and Balagurunathan, R. (2007). Thermotolerant actinomycetes from Himalayan Mountain - antagonistic potential, characterization and identification of selected strains. *Malaysian Appl. Biol.* 36, 59–65.
- Raoult, D., Ogata, H., Audic, S., Robert, C., Suhre, K., Drancourt, M., et al. (2003). *Tropheryma whippelii* Twist: a human pathogenic *Actinobacteria* with a reduced genome. *Genome Res.* 13, 1800–1809. doi: 10.1101/gr.1474603
- Retamal-Morales, G., Heine, T., Tischler, J. S., Erler, B., Gröning, J. A. D., Kaschabek, S. R., et al. (2018a). Draft genome sequence of *Rhodococcus erythropolis* B7g, a biosurfactant producing actinobacterium. *J. Biotechnol.* 280, 38–41. doi: 10.1016/j.jbiotec.2018.06.001
- Retamal-Morales, G., Mehnert, M., Schwabe, R., Tischler, D., Schlömann, M., and Levićan, G. J. (2017). Genomic characterization of the arsenic-tolerant actinobacterium, *Rhodococcus erythropolis* S43. *Solid State Phenomena* 262, 660–663. doi: 10.4028/www.scientific.net/SSP.262.660
- Retamal-Morales, G., Mehnert, M., Schwabe, R., Tischler, D., Zapata, C., Chávez, R., et al. (2018b). Detection of arsenic-binding siderophores in arsenic-tolerating actinobacteria by a modified CAS assay. *Ecotoxicol. Environ. Saf.* 157, 176–181. doi: 10.1016/j.ecoenv.2018.03.087

- Riebel, A., Dudek, H. M., de Gonzalo, G., Stepniak, P., Rychlewski, L., and Fraaije, M. W. (2012). Expanding the set of rhodococcal Baeyer-Villiger monooxygenases by high-throughput cloning, expression and substrate screening. *Appl. Microbiol. Biotechnol.* 95, 1479–1489. doi: 10.1007/s00253-011-3823-0
- Riedel, A., Heine, T., Westphal, A. H., Conrad, C., Rathack, P., van Berkel, W. J., et al. (2015a). Catalytic and hydrodynamic properties of styrene monooxygenases from *Rhodococcus opacus* 1CP are modulated by cofactor binding. *AMB Express* 5, 30. doi: 10.1186/s13568-015-0112-9
- Riedel, A., Mehnert, M., Paul, C. E., Westphal, A. H., van Berkel, W. J., and Tischler, D. (2015b). Functional characterization and stability improvement of a 'thermophilic-like' ene-reductase from *Rhodococcus opacus* 1CP. *Front. Microbiol.* 6:1073. doi: 10.3389/fmicb.2015.01073
- Roberts, J. N., Singh, R., Grigg, J. C., Murphy, M. E., Bugg, T. D., and Eltis, L. D. (2011). Characterization of dye-decolorizing peroxidases from *Rhodococcus jostii* RHA1. *Biochemistry* 50, 5108–5119. doi: 10.1021/bi200427h
- Rostami, H., Hamed, H., and Yolmeh, M. (2016). Some biological activities of pigments extracted from *Micrococcus roseus* (PTCC 1411) and *Rhodotorula glutinis* (PTCC 5257). *Int. J. Immunopathol. Pharmacol.* 29, 684–695. doi: 10.1177/0394632016673846
- Scholtissek, A., Tischler, D., Westphal, A. H., van Berkel, W. J. H., and Paul, C. E. (2017). Old Yellow Enzyme-catalysed asymmetric hydrogenation: linking family roots with improved catalysis. *Catalysts* 7:130. doi: 10.3390/catal7050130
- Schrempf, H. (2013). Actinobacteria within soils: capacities for mutualism, symbiosis and pathogenesis. *FEMS Microbiol. Lett.* 342, 77–78. doi: 10.1111/1574-6968.12147
- Selengut, J. D., and Haft, D. H. (2010). Unexpected abundance of coenzyme F(420)-dependent enzymes in *Mycobacterium tuberculosis* and other actinobacteria. *J. Bacteriol.* 192, 5788–5798. doi: 10.1128/JB.00425-10
- Sen, A., Daubin, V., Abrouk, D., Gifford, I., Berry, A. M., and Normand, P. (2014). Phylogeny of the class actinobacteria revisited in the light of complete genomes. The orders 'Frankiales' and Micrococcales should be split into coherent entities: proposal of Frankiales ord. nov., *Geodermatophilales* ord. nov., *Acidothermales* ord. nov. and *Nakamurellales* ord. nov. *Int. J. Syst. Evol. Microbiol.* 64, 3821–3832. doi: 10.1099/ijs.0.063966-0
- Senges, C. H. R., Al-Dilaimi, A., Marchbank, D. H., Wibberg, D., Winkler, A., Haltli, B., et al. (2018). The secreted metabolome of *Streptomyces chartreusis* and implications for bacterial chemistry. *Proc. Natl. Acad. Sci. U.S.A.* 115, 2490–2495. doi: 10.1073/pnas.1715713115
- Shivlata, L., and Satyanarayana, T. (2015). Thermophilic and alkaliphilic actinobacteria: biology and potential applications. *Front. Microbiol.* 6:1014. doi: 10.3389/fmicb.2015.01014
- Stach, J. E., and Bull, A. T. (2005). Estimating and comparing the diversity of marine actinobacteria. *Antonie Van Leeuwenhoek* 87, 3–9. doi: 10.1007/s10482-004-6524-1
- Stackebrandt, E., Rainey, F. A., and Ward-Rainey, N. L. (1997a). Proposal for a new hierarchic classification system, *Actinobacteria* classis nov.. *Int. J. Syst. Evol. Microbiol.* 47, 479–491.
- Stackebrandt, E., and Schumann, P. (2006). "Introduction to the taxonomy of actinobacteria," in *The Prokaryotes*, eds M. Dworkin, S. Falkow, E. Rosenberg, K.-H. Schleifer, and F. Stackebrandt (New York, NY: Springer), 297–321.
- Stackebrandt, E., Sproer, C., Rainey, F. A., Burghardt, J., Päuker, O., and Hippe, H. (1997b). Phylogenetic analysis of the genus *Desulfotomaculum*: evidence for the misclassification of *Desulfotomaculum guttoideum* and description of *Desulfotomaculum orientis* as *Desulfosporosinus orientis* gen. nov., comb. nov.. *Int. J. Syst. Evol. Microbiol.* 47, 1134–1139.
- Sucharitakul, J., Medhanavyn, D., Pakotiprapha, D., van Berkel, W. J., and Chaiyen, P. (2016). Tyr217 and His213 are important for substrate binding and hydroxylation of 3-hydroxybenzoate 6-hydroxylase from *Rhodococcus jostii* RHA1. *FEBS J.* 283, 860–881. doi: 10.1111/febs.13636
- Tischler, D., Eulberg, D., Lakner, S., Kaschabek, S. R., van Berkel, W. J., and Schlömann, M. (2009). Identification of a novel self-sufficient styrene monooxygenase from *Rhodococcus opacus* 1CP. *J. Bacteriol.* 191, 4996–5009. doi: 10.1128/JB.00723-10
- Tischler, D., Kermer, R., Gröning, J. A., Kaschabek, S. R., van Berkel, W. J., and Schlömann, M. (2010). StyA1 and StyA2B from *Rhodococcus opacus* 1CP: a multifunctional styrene monooxygenase system. *J. Bacteriol.* 192, 5220–5227. doi: 10.1128/JB.00723-10
- Tischler, D., Niescher, S., Kaschabek, S. R., and Schlömann, M. (2013). Trehalose phosphate synthases otsa1 and otsa2 of *Rhodococcus opacus* 1CP. *FEMS Microbiol. Lett.* 342, 113–122. doi: 10.1111/1574-6968.12096
- Ventura, M., Canchaya, C., Tauch, A., Chandra, G., Fitzgerald, G. F., Chater, K. F., et al. (2007). Genomics of actinobacteria: tracing the evolutionary history of an ancient phylum. *Microbiol. Mol. Biol. Rev.* 71, 495–548. doi: 10.1128/MMBR.00005-07
- Wagenknecht, M., Dib, J. R., Thürmer, A., Daniel, R., Fariás, M. E., and Meinhardt, F. (2010). Structural peculiarities of linear megaplasmid, pLMA1, from *Micrococcus luteus* interfere with pyrosequencing reads assembly. *Biotechnol. Lett.* 32, 1853–1862. doi: 10.1007/s10529-010-0357-y
- Wilson, J. W. (2012). Nocardiosis: updates and clinical overview. *Mayo Clin. Proc.* 87, 403–407. doi: 10.1016/j.mayocp.2011.11.016
- Xue, L., Xue, Q., Chen, Q., Lin, C., Shen, G., and Zhao, J. (2013). Isolation and evaluation of rhizosphere actinomycetes with potential application for biocontrol of *Verticillium* wilt of cotton. *Crop Prot.* 43, 231–240. doi: 10.1016/j.cropro.2012.10.002
- Zimmerling, J., Tischler, D., Großmann, C., Schlömann, M., and Oelschlägel, M. (2017). Characterization of aldehyde dehydrogenases applying an enzyme assay with *in situ* formation of phenylacetaldehydes. *Appl. Biochem. Biotechnol.* 182, 1095–1107. doi: 10.1007/s12010-016-2384-1

Conflict of Interest Statement: The authors declare that the research was conducted in the absence of any commercial or financial relationships that could be construed as a potential conflict of interest.

Copyright © 2019 Tischler, van Berkel and Fraaije. This is an open-access article distributed under the terms of the Creative Commons Attribution License (CC BY). The use, distribution or reproduction in other forums is permitted, provided the original author(s) and the copyright owner(s) are credited and that the original publication in this journal is cited, in accordance with accepted academic practice. No use, distribution or reproduction is permitted which does not comply with these terms.



Mycobacterial F₄₂₀H₂-Dependent Reductases Promiscuously Reduce Diverse Compounds through a Common Mechanism

Chris Greening^{1,2*}†, Thanavit Jirapanjawat^{1,2,3†}, Shahana Afroze^{1,3†}, Blair Ney^{1,2,3}, Colin Scott¹, Gunjan Pandey¹, Brendon M. Lee^{1,3}, Robyn J. Russell¹, Colin J. Jackson³, John G. Oakeshott¹, Matthew C. Taylor¹ and Andrew C. Warden^{1*}

OPEN ACCESS

Edited by:

Dirk Tischler,
Freiburg University of Mining
and Technology, Germany

Reviewed by:

David E. Graham,
Oak Ridge National Laboratory (DOE),
United States
Alberto A. Iglesias,
National University of the Littoral,
Argentina

*Correspondence:

Chris Greening
chris.greening@monash.edu
Andrew C. Warden
andrew.warden@csiro.au

†These authors have contributed
equally to this work.

Specialty section:

This article was submitted to
Microbial Physiology and Metabolism,
a section of the journal
Frontiers in Microbiology

Received: 31 March 2017

Accepted: 18 May 2017

Published: 31 May 2017

Citation:

Greening C, Jirapanjawat T,
Afroze S, Ney B, Scott C, Pandey G,
Lee BM, Russell RJ, Jackson CJ,
Oakeshott JG, Taylor MC and
Warden AC (2017) Mycobacterial
F₄₂₀H₂-Dependent Reductases
Promiscuously Reduce Diverse
Compounds through a Common
Mechanism. *Front. Microbiol.* 8:1000.
doi: 10.3389/fmicb.2017.01000

¹ Land and Water Flagship, The Commonwealth Scientific and Industrial Research Organisation, Acton, ACT, Australia,
² School of Biological Sciences, Monash University, Clayton, VIC, Australia, ³ Research School of Chemistry, Australian
National University, Acton, ACT, Australia

An unusual aspect of actinobacterial metabolism is the use of the redox cofactor F₄₂₀. Studies have shown that actinobacterial F₄₂₀H₂-dependent reductases promiscuously hydrogenate diverse organic compounds in biodegradative and biosynthetic processes. These enzymes therefore represent promising candidates for next-generation industrial biocatalysts. In this work, we undertook the first broad survey of these enzymes as potential industrial biocatalysts by exploring the extent, as well as mechanistic and structural bases, of their substrate promiscuity. We expressed and purified 11 enzymes from seven subgroups of the flavin/deazaflavin oxidoreductase (FDOR) superfamily (A1, A2, A3, B1, B2, B3, B4) from the model soil actinobacterium *Mycobacterium smegmatis*. These enzymes reduced compounds from six chemical classes, including fundamental monocycles such as a cyclohexenone, a dihydropyran, and pyrones, as well as more complex quinone, coumarin, and arylmethane compounds. Substrate range and reduction rates varied between the enzymes, with the A1, A3, and B1 groups exhibiting greatest promiscuity. Molecular docking studies suggested that structurally diverse compounds are accommodated in the large substrate-binding pocket of the most promiscuous FDOR through hydrophobic interactions with conserved aromatic residues and the isoalloxazine headgroup of F₄₂₀H₂. Liquid chromatography-mass spectrometry (LC/MS) and gas chromatography-mass spectrometry (GC/MS) analysis of derivatized reaction products showed reduction occurred through a common mechanism involving hydride transfer from F₄₂₀H[−] to the electron-deficient alkene groups of substrates. Reduction occurs when the hydride donor (C5 of F₄₂₀H[−]) is proximal to the acceptor (electrophilic alkene of the substrate). These findings suggest that engineered actinobacterial F₄₂₀H₂-dependent reductases are promising novel biocatalysts for the facile transformation of a wide range of α,β-unsaturated compounds.

Keywords: F₄₂₀, redox, biocatalysis, promiscuity, biodegradation, *Mycobacterium*, Actinobacteria

INTRODUCTION

Industrial biocatalysts are making a substantial impact in the selective synthesis of pharmaceuticals and other specialist chemicals (Nestl et al., 2011; Clouthier and Pelletier, 2012). Enzymes that mediate selective alkene reduction are in particular demand (Stuermer et al., 2007). The most widely investigated of these enzymes are the “old yellow enzyme” family of NAD(P)H-dependent flavoproteins. These often-promiscuous enzymes have been shown to catalyze hydride addition to activated alkene groups of diverse substrates of both natural (e.g., quinones) and synthetic (e.g., cyclohexenones) origin (Williams and Bruce, 2002; Stuermer et al., 2007; Amato and Stewart, 2015). Their catalytic cycle proceeds by hydride transfer from bound FMN H_2 to the substrate, protonation of the reduced substrate by a conserved tyrosine, and reduction of the cofactor by the external hydride donor NAD(P)H (Fox and Karplus, 1994). Such enzymes are in development as *in vitro* biocatalysts and are critical in several industrial fermentation processes (e.g., levodione synthesis; Stuermer et al., 2007; Amato and Stewart, 2015). Despite these successes, there is still demand for the discovery of novel reductive biocatalysts to provide more flexible platforms for development of specific *in vitro* and *in vivo* syntheses.

Actinobacteria represent a particularly promising source of novel biocatalysts. This phylum includes genera reputed for their biodegradative capacity, notably *Mycobacterium* and *Rhodococcus*, as well as *Streptomyces* strains that are vital sources of natural products (Barka et al., 2016). One reason these organisms are so metabolically versatile is that they synthesize the unusual redox cofactor F_{420} (Greening et al., 2016; Ney et al., 2017). The low standard redox potential ($E^{\circ'} = -340$ mV) and obligate two-electron chemistry of $F_{420}H_2$ means that it can reduce compounds otherwise recalcitrant to activation (Walsh, 1986; Greening et al., 2016). Actinobacteria reduce F_{420} using either the F_{420} -dependent glucose-6-phosphate dehydrogenase (Fgd) (Bashiri et al., 2008; Nguyen et al., 2017) or the F_{420} -NADP oxidoreductase (Fno) (Eker et al., 1989; Ebert et al., 1999). They subsequently couple the reoxidation of $F_{420}H_2$ to the hydrogenation of diverse organic compounds. This depends on a suite of $F_{420}H_2$ -dependent reductases from two different superfamilies, the luciferase-like hydride transferases (LLHT superfamily; Ebert et al., 1999; Heiss et al., 2003; Ikeno et al., 2006) and the flavin/deazaflavin oxidoreductases (FDOR superfamily; Taylor et al., 2010; Gurumurthy et al., 2013; Ahmed et al., 2015; Greening et al., 2016). The enzymatic activities and industrial potential of these enzymes have remained largely unexplored.

$F_{420}H_2$ -dependent reductases of the FDOR superfamily have been advocated as particularly promising reductive biocatalysts (Ahmed et al., 2015; Greening et al., 2016). These reductases are abundant in mycobacteria and other Actinobacteria, where they have diverged into at least 14 distinct subgroups (A1–A3, B1–B6, AA1–AA5; Ahmed et al., 2015). While several native functions have been proposed, e.g., menaquinone and biliverdin reduction (Gurumurthy et al., 2013; Ahmed et al., 2015, 2016), the enzymes also mediate promiscuous activities, such as

nitroimidazole prodrug activation (Cellitti et al., 2012; Mohamed et al., 2016a,b), biodegradation of furanocoumarins (Taylor et al., 2010; Lapalikar et al., 2012b; Jirapanjawat et al., 2016), and decolorization of triarylmethane dyes (Guerra-Lopez et al., 2007; Jirapanjawat et al., 2016). The findings that these enzymes can reduce such structurally and chemically diverse compounds suggests that they may also have the latent capacity to act upon industrially relevant non-natural chemicals. Mechanistic studies focused on mycobacteria indicate that these enzymes adopt a distinct mechanism from old yellow enzymes that may be relevant for selective synthesis (Greening et al., 2016; Mohamed et al., 2016b). For example, the reduced cofactor is thought to bind the enzyme from the solvent phase and directly mediate hydride addition to the substrate (Mohamed et al., 2016a,b); The cofactor can then be re-reduced *in vitro* and *in vivo* by Fgd (Purwantini and Daniels, 1996; Bashiri et al., 2008). In addition, the proton donor for reduced substrates is a solvent-accessible hydroxonium ion rather than a tyrosine residue (Mohamed et al., 2016b).

In this study, we explored the substrate promiscuity across multiple subgroups of the $F_{420}H_2$ -dependent FDORs to determine their potential value as next-generation biocatalysts. To do this, we tested 11 of these enzymes from the model laboratory organism *Mycobacterium smegmatis* against 47 different substrates, ranging from synthetic building blocks to more complex polycyclic compounds. This revealed that, in common with old yellow enzymes, several of these enzymes can promiscuously reduce diverse cyclic and polycyclic compounds harboring activated alkene groups. Subsequent structural modeling and mechanistic studies suggested that these enzymes reduced these diverse substrates through a common mechanism: regioselective hydride transfer from $F_{420}H^-$ to the proximal electrophilic alkene group. The considerable promiscuity of these enzymes suggests they are promising candidate biocatalysts, but engineering will be required to optimize their rates in industrial processes.

MATERIALS AND METHODS

Recombinant Protein Expression and Purification

Eleven $F_{420}H_2$ -dependent reductases of the FDOR superfamily (MSMEG loci 5998, 2850, 2027, 5030, 6325, 3380, 0048, 6848, 6526, 5170, 3880; Supplementary Table S1) and the F_{420} -reducing glucose-6-phosphate dehydrogenase (Fgd) were recombinantly overexpressed in *E. coli* BL21(DE3). MSMEG_6325, MSMEG_6526, MSMEG_3880 and *fgd* were expressed overnight in modified auto-induction TB2.0 media at 28°C (200 rpm) as previously described (Taylor et al., 2010; Lapalikar et al., 2012b). For the remaining proteins, cells were grown in lysogeny broth (LB) at 37°C (200 rpm) and induced at OD₆₀₀ 0.6 with 0.2% L-arabinose for 2 h. Cells were harvested by centrifugation (10,000 × g, 20 min, 4°C), resuspended in lysis buffer (50 mM NaH₂PO₄, 300 mM NaCl, 10 mM imidazole, pH 8.0), and lysed in a EmulsiFlex-C3 homogenizer (ATA Scientific, Australia). The enzymes

were purified from soluble extracts by Ni-nitrilotriacetic acid (NTA) affinity chromatography using gravity columns as previously described (Taylor et al., 2010; Ahmed et al., 2015) and stored in elution buffer (50 mM NaH_2PO_4 300 mM NaCl, 250 mM imidazole, pH 8.0) until use in enzymatic assays. The high purity of the proteins was confirmed by running the fractions on NuPAGE Novex 10% Bis-Tris gels (Invitrogen, Australia) at 200 V and staining with Coomassie Brilliant Blue. Protein concentration was determined by measuring absorbance at 280 nm using a NanoDrop ND1000 (NanoDrop Technologies) and calculating concentration with the Beer-Lambert equation. Molar absorption coefficients were calculated for each protein based on amino acid sequences (Supplementary Table S1). F_{420} was extracted, purified, and concentrated from a recombinant F_{420} overexpression strain of *M. smegmatis* mc²4517 (Bashiri et al., 2010) as previously described (Isabelle et al., 2002).

Enzyme Activity Assays

Forty-seven different compounds were sourced from Sigma-Aldrich and dissolved into 1 M working stocks in dimethyl sulfoxide, except hypoxanthine and guanine that were dissolved in 1 M NaOH solution. The structures of the compounds tested are shown in Supplementary Tables S2, S3. Enzymatic assays were performed by spectroscopically monitoring the reoxidation of pre-reduced $F_{420}H_2$ in the presence of FDOR and substrate. F_{420} was enzymatically reduced to $F_{420}H_2$ by overnight incubation with 1 μ M Fgd and 12 mM glucose 6-phosphate as described (Ahmed et al., 2015). The enzyme was subsequently repurified as described (Ahmed et al., 2015). All reaction mixtures contained degassed Tris buffer [200 mM Tris, 0.1% (w/v) Triton X-100, pH 8.0] sequentially supplemented with 50 μ M substrate, 25 μ M $F_{420}H_2$, and 1 μ M of the FDOR. Enzyme concentration was decreased to 10 nM for substrates observed to be rapidly reduced, i.e., quinone compounds. Reaction rates were monitored by recording the initial linear increase in 420 nm absorbance using an Epoch 2 Microplate Spectrophotometer (BioTek). All assays were performed at room temperature (approximately 25°C). We only detected significant levels of enzyme-independent, substrate-dependent $F_{420}H_2$ reoxidation for quinone and arylmethane substrates, at rates that we previously reported (Jirapanjawat et al., 2016). We observed no enzyme-dependent, substrate-independent or spontaneous $F_{420}H_2$ reoxidation in the timeframe of our assays. Specific activities were calculated after subtracting rates of enzyme-independent $F_{420}H_2$ reoxidation and were expressed in $nmol\ s^{-1}\ \mu mol^{-1}$ enzyme as previously described (Taylor et al., 2010). The rate of reduction of three of these compounds, namely 1,4-naphthoquinone, 3-cyanocoumarin, and 5,6-dihydro-2H-pyran-2-one, was also measured in cofactor-recycling assays. Assays used 100 μ M substrate, 0.1 μ M enzyme, 10 μ M F_{420} , 2.5 mM glucose-6-phosphate, and 0.45 μ M Fgd. Time course high performance liquid chromatography (HPLC) assays, performed according to published methodologies (Lapalikar et al., 2012b), measured loss of absorbance (at λ_{max}) of the substrates at regular time intervals.

Molecular Docking

Substrates were docked into the previously solved X-ray crystal structures of MSMEG_2027 (1.5 Å resolution; PDB: 4Y9I; Ahmed et al., 2015) and MSMEG_6526 (1.7 Å resolution; PDB: 4KZY; Ahmed et al., 2015). F_{420} was docked into the cofactor-binding pockets based on the cofactor-bound structures of Rv3547 (PDB: 3R5R; Cellitti et al., 2012) and Rv2074 (PDB: 5JAB; Ahmed et al., 2016) respectively. AutoDock Vina was used to computationally dock the substrates into their corresponding enzymes, with enzymes and ligands prepared using AutoDockTools operating with default settings (Morris et al., 2009). The docking results were visualized and analyzed in UCSF Chimera (Pettersen et al., 2004).

Substrate Reduction and Derivatization

The chemical standards and reaction products of menadione, 3-cyanocoumarin, and 2-cyclohexen-1-one were detected by mass spectrometry. These compounds were reduced by incubating them with the promiscuous $F_{420}H_2$ -dependent reductase MSMEG_2027 for 2 h at 37°C. The assay mixture comprised 100 μ M substrate, 10 μ M F_{420} , 1 μ M Fgd, 1 μ M MSMEG_2027, and excess G-6-P in either 20 mM Tris buffer, pH 8.0 (for menadione and 2-cyclohexen-1-one) or 50 mM ammonium acetate buffer, pH 7.5 (for 3-cyanocoumarin). For menadione, the standard and reaction products were derivatized with methoxyamine. Specifically, the standard and products were dried by rotary evaporation, resuspended in 20 μ l pyridine containing 20 mg mL^{-1} methoxyamine hydrochloride, and incubated at 37°C for 1.5 h. To this solution, 20 μ l of *N*-methyl-*N*-(trimethylsilyl)trifluoroacetamide (MSTFA) was added and the solution was incubated at 37°C for 1 h. For cyclohexenone, the standard and reaction products were derivatized by spiking the solution with 1 mM 2,4-dinitrophenylhydrazine and incubating the solution at 30°C for 2 h.

LC/MS and GC/MS

The standard and reaction products of 3-cyanocoumarin were measured on an Agilent 6100 Series Single Quadrupole liquid chromatography-mass spectrometry (LC/MS) with diode array detector. Samples were separated on an Agilent Poroshell 120 EC-C18 column (2.7 μ m, 2.1 \times 100 mm). A gradient of two buffers, buffer A (0.1% formic acid in H_2O) and buffer B (0.1% formic acid in acetonitrile), was applied as follows: 0–0.5 min, held at 10% B; 0.5–6.5 min, 10–60% B; 6.5–7 min, held at 90% B. A positive mode electron ionisation (EI) scan was undertaken, and in these conditions the molecular ion could not be detected as the loss of the cyano (CN) group was universal. The derivatized cyclohexenone standard and reactions products were determined on an Agilent 1290 Infinity/6550 quadrupole time-of-flight (Q-TOF) LC/MS system equipped with an Agilent Poroshell 120 EC-C18 2.1 \times 50 mm 2.7 μ m column. A gradient comprising two buffers, buffer A (20 mM ammonium acetate, pH 7.0) and buffer B (100% acetonitrile), was applied as follows: 0–1 min, held at 10% B; 1–10 min, 10–90% B. Positive mode electrospray ionisation (ESI) was utilized, and a scan from 50 to 300 *m/z* was conducted. The menadione standard, its reaction

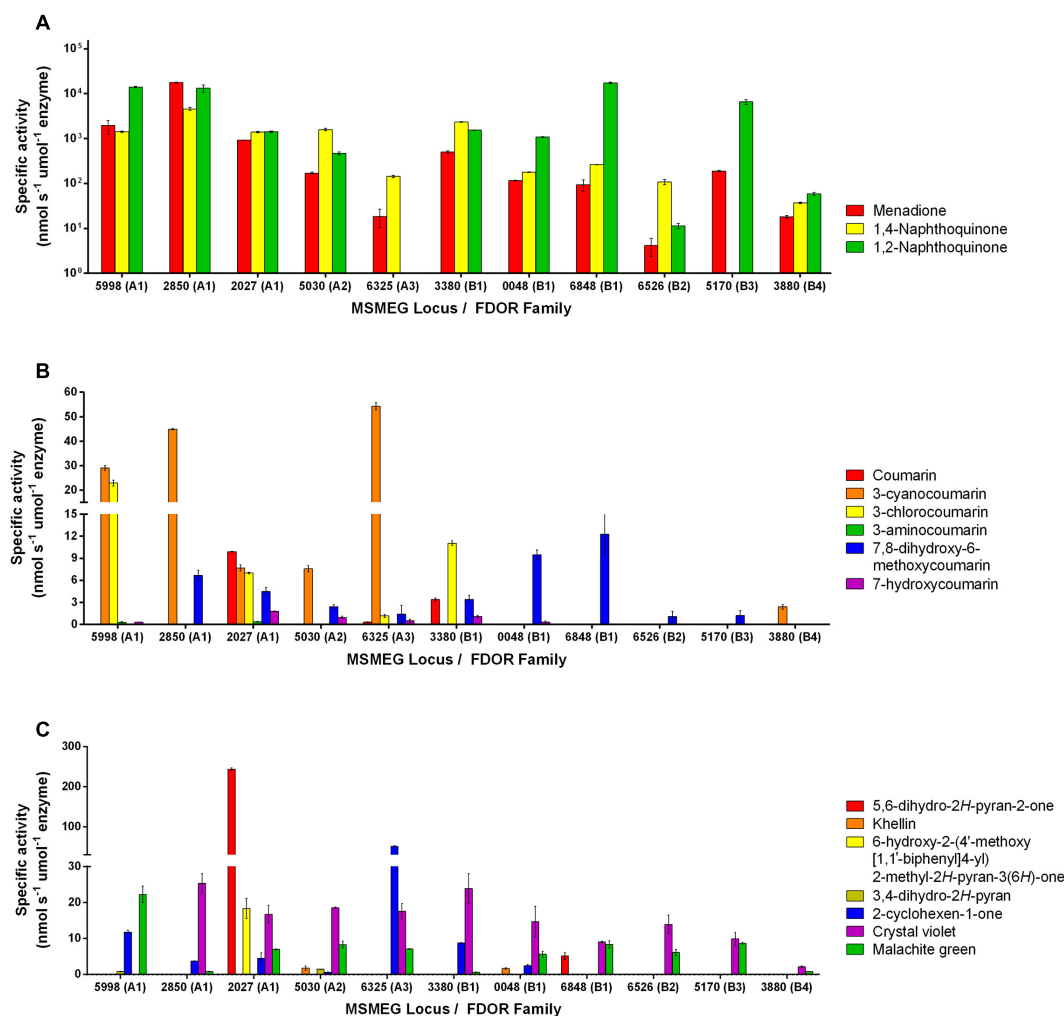


FIGURE 1 | Substrate range of the $F_{420}H_2$ -dependent reductases. The results show the specific activities of five FDOR-A and six FDOR-B enzymes with 16 organic compounds. Specific activities are shown with **(A)** quinones, **(B)** coumarins, and **(C)** pyrones, pyrans, cyclohexenones, and triarylmethanes. Error bars show standard deviations from three independent replicates. The reactivity of six of the enzymes with quinone and triarylmethane compounds was previously reported (Jirapanjawat et al., 2016). The structures of the substrates are shown in Supplementary Table S2. The 32 compounds tested that were not compatible with the FDORs are listed in Supplementary Table S3.

product, and their methoxime derivatives were detected on an Agilent 7010 gas chromatography-mass spectrometry (GC/MS) triple quadrupole system. Samples were separated on an Agilent 19091S 30 m × 250 μm × 0.25 μm HP-5 ms column over a gradient of 60–320°C at a rate of 7°C min⁻¹, and a positive EI scan at 70 eV was conducted.

RESULTS

$F_{420}H_2$ -Dependent Reductases Reduce Structurally Diverse Cyclic and Polycyclic Compounds

Eleven $F_{420}H_2$ -dependent FDORs from *M. smegmatis* were expressed recombinantly and purified (Supplementary Table S1). We purified enzymes spanning multiple phylogenetically

distinct subgroups, namely three enzymes each from the well-described FDOR-A1 and FDOR-B1 subgroups (Taylor et al., 2010; Lapalikar et al., 2012b; Ahmed et al., 2015), as well as representatives from five other subgroups (A2, A3, B1, B2, B3, B4; Ahmed et al., 2015). On the basis of previously reported data (Lapalikar et al., 2012b; Gurumurthy et al., 2013; Jirapanjawat et al., 2016), we determined the specific activities of the purified enzymes with 47 organic compounds following addition of the pre-reduced cofactor $F_{420}H_2$ (Supplementary Tables S2, S3). Of these, 16 compounds were enzymatically transformed. These compounds included fundamental monocyclic compounds, such as 3,4-dihydro-2H-pyran, 2-cyclohexen-1-one, and 5,6-dihydro-2H-pyran-2-one, as well as aromatic bicyclic and tricyclic compounds from the quinone, coumarin, and arylmethane chemical classes (Supplementary Table S2). Specific activities for the 16 substrates ranged from very low if reproducible

for some compounds (e.g., $<1 \text{ nmol s}^{-1} \mu\text{mol enzyme}^{-1}$ for the pyran compound) to high for the quinones (e.g., $>10^4 \text{ nmol s}^{-1} \mu\text{mol enzyme}^{-1}$ for 1,2-naphthoquinone) (**Figure 1**). Enzymes purified from the A1, A3, and B1 classes had the broadest and highest activities, with MSMEG_2027 (A1) proving catalytically compatible with all but two of the 16 substrates, whereas enzymes from the A2, B2, B3, and B4 classes had low activities with all non-quinone substrates.

Comparisons across the compounds tested for activity suggest that the presence of an electrophilic alkene is necessary for reduction to occur and implicates this group as the hydride acceptor. For example, activity was observed with pyrones that were α -substituted (e.g., 5,6-dihydro-2*H*-pyran-2-one; **Figure 1C**) but not γ -substituted (e.g., chelidonic acid; Supplementary Table S3). This is also supported by the finding that, whereas malachite green and crystal violet can be reduced, azure B cannot; while all three compounds contain triphenyl and *N,N*-dimethyliminium moieties, azure B lacks the central delocalized alkene group (Supplementary Tables S2, S3). Consistent with the proposal that the activated alkene is the hydride acceptor of $F_{420}H_2$ -dependent reductases, enzymatic activity with coumarin derivatives was modulated by the nature of aromatic directing groups at the C3 position (**Figure 1**); moderate activities were observed with electron-withdrawing cyano and chloro groups, very low activities with an electron-donating amino group, and no activity with 3-hydroxycoumarin (**Figure 1B**). This suggests that electron-withdrawing groups render these compounds susceptible to nucleophilic attack by removing electron density from the π system. It is possible that differential interactions of these substrates with the substrate-binding pockets also contribute to the differences in the rates of reduction both between substrates and between enzymes.

For three of the compounds, we also measured specific activities with another independent assay that measured substrate reduction by HPLC in a cofactor-recycling system containing the Fgd (Supplementary Figure S1). While the relative activities between enzymes were comparable, initial reduction rates were generally higher in the cofactor-recycling systems and resulted in substrate conversions exceeding 90%.

$F_{420}H_2$ -Dependent Reductases Selectively Reduce Electrophilic Alkene Groups

We subsequently sought to understand the structural basis of how FDORs could reduce such diverse substrates. To do this, we used automated substrate docking to compare the binding of representative substrates to the high-resolution crystal structures of the highly promiscuous MSMEG_2720 (Ahmed et al., 2015) (A1) and the more specific MSMEG_6526 (Ahmed et al., 2015) (B2) enzyme. Compounds representing four major substrate classes were tested, namely menadione (quinone class), 3-cyanocoumarin (coumarin class), 2-cyclohexen-1-one (monocyclic compounds), and malachite green (arylmethane class). Consistent with the results of the activity assays (**Figure 1**), all substrates were predicted to be structurally compatible with MSMEG_2027, whereas only menadione

and malachite green were predicted to specifically bind MSMEG_6526 (Supplementary Figure S2 and Table S4).

In the MSMEG_2027 models, substrates are accommodated in the large substrate-binding pocket adjacent to the cofactor-binding site (**Figure 2**). All four substrates are predicted to make extensive hydrophobic interactions with aromatic residues in the active site, including a triad of tyrosine residues (Tyr120, Tyr123, Tyr126) that have previously been shown to facilitate hydrophobic shielding during nitroimidazole activation (Mohamed et al., 2016b). There was also evidence of hydrophobic interactions between substrate and cofactor, including different degrees of π -stacking interactions with the isoalloxazine ring (**Figure 2**). Few polar interactions were predicted, except hydrogen bonds between the cyano group of 3-cyanocoumarin and the carbonyl oxygen of 2-cyclohexen-1-one with the hydroxyl group of Tyr123. The orientation of the substrates is likely to be realistic. For example, the binding poise of menadione suggests that menaquinone (the proposed physiological substrate of FDOR-A1 enzymes (Gurumurthy et al., 2013; Ahmed et al., 2015), which comprises a menadiene headgroup and a polyisoprene tail) can be accommodated in the active site, given the polyisoprene tail at the C2 position is predicted to be oriented away from the active site.

The docking results indicate that hydride transfer can occur directly between cofactor and substrate within the hydrophobic environment of the MSMEG_2027 active site. Menadione, 3-cyanocoumarin, and 2-cyclohexen-1-one are predicted to be oriented such that their activated alkene groups are within 5 Å of the nucleophilic C5 center of $F_{420}H^-$ (**Figures 2A–C**). This suggests that, in line with the activity assays (**Figure 1**) and previously proposed mechanisms (Taylor et al., 2010; Lapalikar et al., 2012b; Ahmed et al., 2015; Mohamed et al., 2016b), catalysis will occur through nucleophilic attack of the C5 hydride to the electrophilic alkene. In the case of malachite green, the alkene moiety (C1 position) of the substrate is 4.2 Å away from C5 of the cofactor, whereas the *N,N*-dimethylamine and *N,N*-dimethyliminium moieties point toward the solvent phase (**Figure 2D**). Binding modes in which the *N,N*-dimethyliminium moiety was proximal to the cofactor caused steric occlusion. This again suggests that the alkene rather than imine moiety serves as the initial site of hydride transfer from $F_{420}H^-$. In comparison, docking with the less promiscuous MSMEG_6526 enzyme suggested that menadione and malachite green are only accommodated at orientations where the distance between the hydride donor and acceptor exceeds 7 Å, which will be suboptimal for catalysis (Supplementary Table S4). This reflects that MSMEG_6526 has a smaller binding pocket than MSMEG_2027 due to its larger flanking loops (Ahmed et al., 2015).

$F_{420}H_2$ -Dependent Reductases Mediate Substrate Reduction by Direct Hydride Transfer

We determined the mechanistic basis of substrate promiscuity among the $F_{420}H_2$ -dependent reductases. To do so, we used

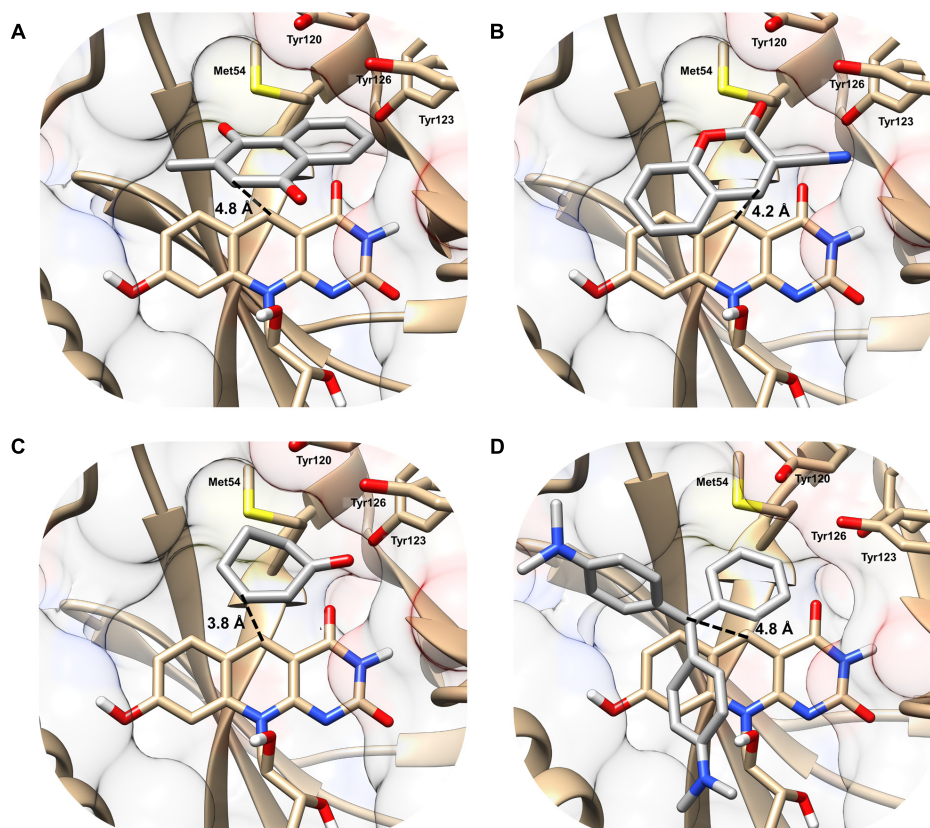


FIGURE 2 | Structural basis of substrate activation by $F_{420}H_2$ -dependent reductases. The secondary structure and surface rendering of the cofactor- and substrate-binding site of MSMEG_2027 are shown based on the 1.5 Å resolution crystal structure (PDB: 4Y9I) (Ahmed et al., 2015) of the enzyme. The structures are computationally docked with (A) menadione, (B) 3-cyanocoumarin, (C) 2-cyclohexen-1-one, and (D) malachite green. The distance between the proposed hydride donor (C5 of $F_{420}H_2^-$) and hydride acceptor (electrophilic carbon of the substrate) are shown. Residues within 5 Å of the substrate are shown. Docking results with the more specific $F_{420}H_2$ -dependent reductase MSMEG_6526 are shown in Supplementary Figure S2 and are compared with MSMEG_2027 in Supplementary Table S4.

mass spectrometry to determine the products formed by the reduction of three representative substrates. LC/MS and GC/MS studies demonstrated that, following incubation of menadione, 3-cyanocoumarin, and 2-cyclohexen-1-one with MSMEG_2027, each substrate peak increased by 2 m/z (Figure 3). This suggests that this enzyme catalyses the reduction of menadione (172 Da) to either menadiol or 2,3-dihydromenadione (both 174 Da) (Supplementary Figure S3), 3-cyanocoumarin (171 Da) to 3-cyanochroman-2-one (173 Da) (Figures 3C,D), and 2-cyclohexen-1-one (96 Da) to either 2-cyclohexen-1-ol or cyclohexanone (both 98 Da) (Figures 3E,F). This is consistent with previous observations that $F_{420}H_2$ -dependent reductases mediate hydride transfer and subsequent protonation of their substrates (Taylor et al., 2010; Lapalikar et al., 2012b; Ahmed et al., 2015; Jirapanjawat et al., 2016; Mohamed et al., 2016b). In previous LC/MS studies, we demonstrated that malachite green (329 Da) was transformed by MSMEG_2027 to produce a decolorized product likely to be the protonated form of leucomalachite green (331 Da) (Jirapanjawat et al., 2016).

While these findings suggest $F_{420}H_2$ -dependent reductases mediate hydride transfer from $F_{420}H_2$ to substrate, they do not

resolve whether the site of attack is the alkene or carbonyl groups of the compounds. To resolve this, we derivatized the standard and reaction products of menadione with methoxyamine hydrochloride (carbonyl-specific) and MSTFA (alcohol-specific). GC/MS analysis of the reaction products revealed that reduction of menadione occurred exclusively *via* the alkene group (Figures 3A,B). Single and double methoxime derivatives of reduced menadione could be detected, indicating 2,3-dihydromenadione was formed as the major reaction product. No trimethylsilyl ester derivatives were formed under these conditions, underlining the absence of menadiol and other quinol products. Menadiol is nevertheless likely to form under physiological conditions through keto–enol tautomerism. In the case of cyclohexenone, the standard and reaction products were derivatized with 2,4-dinitrophenylhydrazine (carbonyl-specific), and analyzed by LC/MS. Analysis of product formation revealed the emergence of the hydrazone derivative of cyclohexanone, again indicating that reduction was mediated through the alkene (Figures 3E,F). Previous studies have inferred that coumarin reduction also occurs through the activated alkene group (Taylor et al., 2010; Lapalikar et al., 2012a,b).

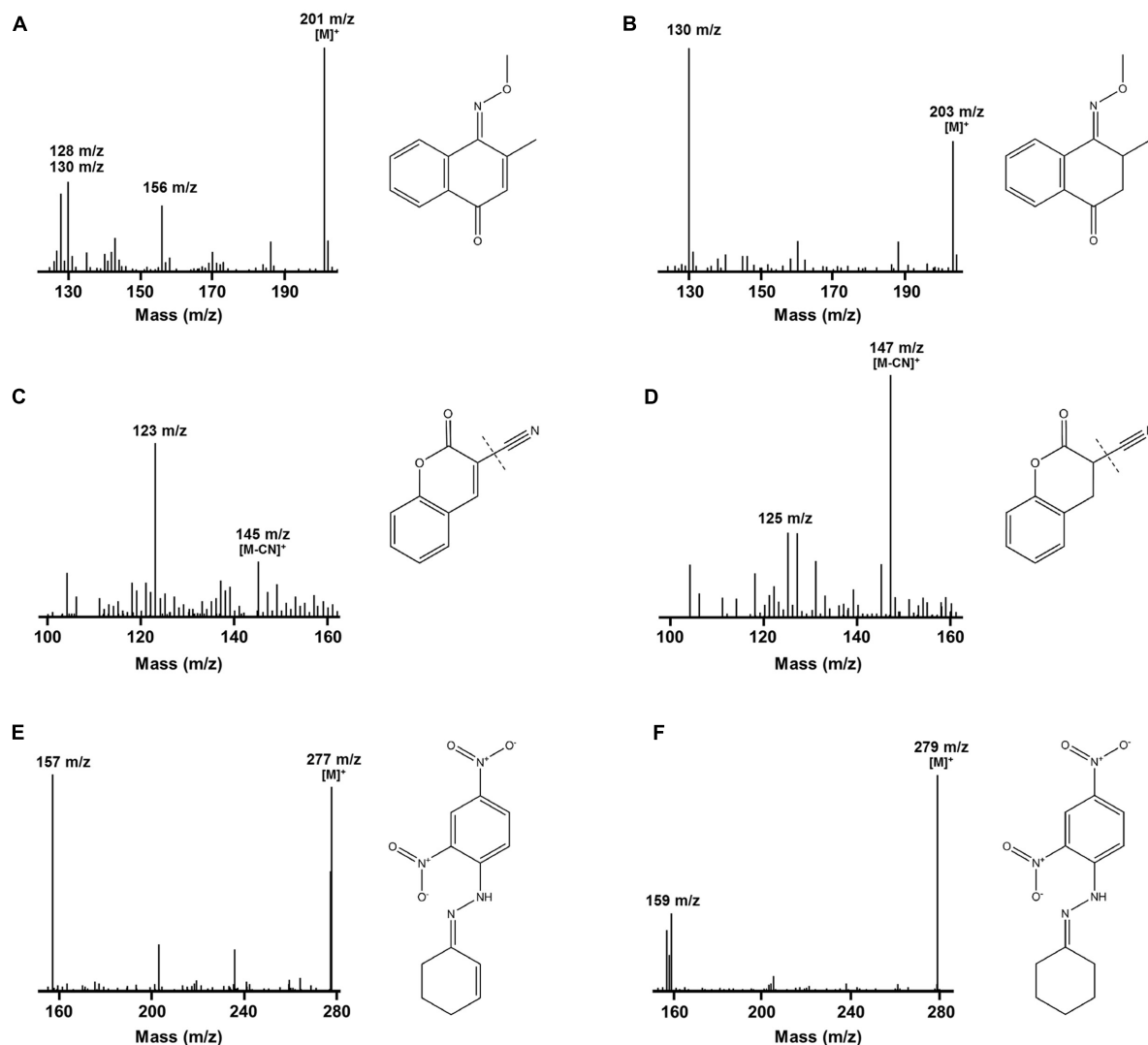
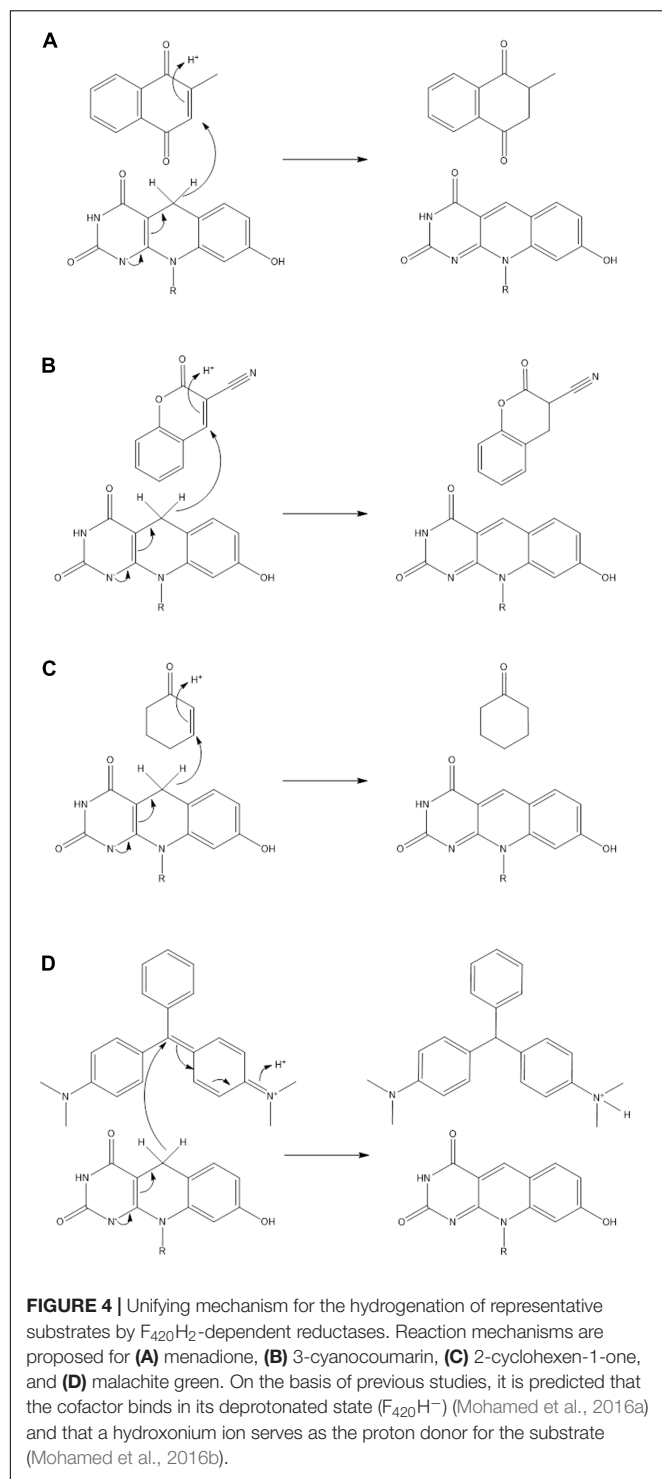


FIGURE 3 | Mass spectra infer that $F_{420}H_2$ -dependent reductases mediate hydrogenation of substrates. The spectra show the detection of substrate standards and reaction products following reduction with MSMEG_2027. GC/MS spectra of the single methoxime derivatives of the (A) menadione standard and (B) 2,3-dihydromenadione product. Mass spectra of the underivatized compounds are shown in Supplementary Figure S3. Keto-enol tautomerization is likely to result in menadiol formation under physiological conditions. LC/MS spectra of the (C) 3-cyanocoumarin standard and (D) 3-cyanochroman-2-one product. The cyano groups were ionized by in-source fragmentation. LC/MS spectra of the dinitrophenylhydrazone derivatives of the (E) 2-cyclohexen-1-one standard and (F) cyclohexanone product. A mass spectrum of the underivatized product could not be obtained. In all cases, corresponding compounds are shown to the right of the spectra. A mass spectrum showing the reduction of malachite green to leucomalachite green was previously published (Jirapanjawan et al., 2016).

DISCUSSION

In this study, we explored the potential of actinobacterial $F_{420}H_2$ -dependent reductases as industrial biocatalysts. We show that mycobacterial FDORs use the electron donor $F_{420}H_2$ to hydrogenate diverse organic compounds at a wide range of rates. On the basis of these findings, we propose in **Figure 4** that all FDOR substrates studied can be reduced through a common hydrogenation mechanism: The cofactor binds the FDOR in its deprotonated state ($F_{420}H^-$; Mohamed et al., 2016a) and the substrate thereafter binds the adjacent pocket through hydrophobic interactions with aromatic residues and

the cofactor. Alignment of the nucleophilic C5 center of $F_{420}H^-$ with the electrophilic alkene group of the substrate will promote direct hydride transfer. Subsequent steps will result in delocalization of electron charge and protonation of the substrate by a solvent-accessible hydroxonium ion (Mohamed et al., 2016b). The FDORs promote this mechanism in multiple ways: binding the substrate and cofactor in proximal sites; generating a hydrophobic environment that promotes hydride transfer; and facilitating protonation by binding hydroxonium ions through conserved tyrosine residues (Mohamed et al., 2016b). The overall mechanism of these enzymes is therefore equivalent to the old yellow enzymes



(Stuermer et al., 2007), though the hydride and proton donors are distinct.

The hydrogenation mechanism proposed here is supported by our studies exploring the observed substrate range of the FDORs (Figure 1). We showed that, in line with findings about the substrate range of old yellow enzymes (Stuermer et al., 2007), the presence of an electrophilic alkene group was a prerequisite

for reduction to occur and that rates were enhanced in electron-withdrawing conjugated systems. The outlined mechanism is also consistent with the results of the structural modeling (Figure 2) and mechanistic studies (Figure 3 and Supplementary Figure S3) that identified the probable sites of hydride attack and inferred hydrogenated reaction products using four model substrates, menadione, 3-cyanocoumarin, 2-cyclohexen-1-one, and malachite green. Similar mechanisms have been proposed for other important reactions known to be mediated by $F_{420}H_2$ -dependent reductases of the FDOR superfamily, namely activation of nitroimidazole prodrugs (Mohamed et al., 2016a,b), reduction of biliverdin to bilirubin (Ahmed et al., 2015, 2016), and the terminal step in the biosynthesis of tetracyclines (Wang et al., 2013). Our mass spectral analysis suggests that these mechanisms are regioselective, with hydride transfer only favorable to electrophilic alkene groups proximal to the nucleophilic C5 center. It will be necessary to extend studies to substrates that will produce prochiral products to determine whether this process also occurs stereoselectively, i.e., through *cis* or *trans* hydrogenation. The observation that substrate reduction is faster in the cofactor-recycling assays is also of interest, and suggests that there is a mechanism that enhances cofactor exchange between FDORs and Fgd (e.g., complex formation).

Our findings warrant the further exploration of $F_{420}H_2$ -dependent FDORs in *in vitro* and *in vivo* biocatalytic processes. Their inherent substrate range, combined with their ease of heterologous overexpression and the presence of a viable cofactor-recycling system, suggests that these enzymes have promise in *in vitro* systems. There may be particular value in exploring the use of these enzymes for hydrogenating substrates incompatible with inorganic catalysts or old yellow enzymes (Stuermer et al., 2007; Clouthier and Pelletier, 2012). Particularly promising are the findings that enzymes in the FDOR superfamily mediate critical steps in the biosynthesis of tetracycline antibiotics (Wang et al., 2013) and the preliminary results that the membrane-bound FDOR-AA family can saturate linear fatty acid chains (Ahmed et al., 2015). However, at least two major innovations are needed if $F_{420}H_2$ -dependent reductases are to be more widely developed: Firstly, given the observation that most substrates were reduced at low rates, the directed evolution of promising FDORs (e.g., MSMEG_2027) will be required to enhance their activities with desirable substrates. Secondly, new processes must be developed if F_{420} is to be cheaply and conveniently produced (Greening et al., 2016). It may be possible to engineer the production of this cofactor in recombinant systems, but this depends on the resolution of the complete F_{420} biosynthesis pathway. Alternatively, it is plausible to synthesize deazaflavin analogs that are catalytically compatible with $F_{420}H_2$ -dependent reductases, which have previously been shown to exhibit cofactor promiscuity (Lapalika et al., 2012a). There is more immediate promise in using these enzymes within actinobacterial hosts and recombinant systems to produce natural products or bioremediate contaminants. With the vast majority of F_{420} -dependent oxidoreductases remaining functionally unannotated, it is expected that further study of these enzymes will reveal novel reactions of potential industrial and pharmaceutical relevance.

AUTHOR CONTRIBUTIONS

CG, AW, JO, MT, BN, CJ, TJ, CS, GP, RR, and BL designed experiments. TJ, CG, SA, BN, AW, MT, and BL performed experiments. CG, JO, CJ, AW, MT, RR, CS, GP, and BL supervised students. CG, AW, JO, BN, TJ, MT, CJ, and SA analyzed data. CG, TJ, AW, BN, and JO wrote the paper. Specific authors were responsible for the specific activity assays (TJ, CG, SA, BL, AW, MT, JO, CJ), substrate-docking experiments (CG, TJ, CJ), and analytical chemistry assays (BN, CG, TJ, AW).

FUNDING

This work was supported by a CSIRO Office of the Chief Executive Postdoctoral Fellowship and an ARC DECRA

Fellowship (DE170100310) awarded to CG, a CSIRO Office of the Chief Executive PhD Scholarship awarded to SA, and Australian Research Council grants (DE120102673, DP130102144) awarded to CJ.

ACKNOWLEDGMENTS

We thank the two reviewers for their helpful feedback.

SUPPLEMENTARY MATERIAL

The Supplementary Material for this article can be found online at: <http://journal.frontiersin.org/article/10.3389/fmicb.2017.01000/full#supplementary-material>

REFERENCES

- Ahmed, F. H., Carr, P. D., Lee, B. M., Afriat-Jurnou, L., Mohamed, A. E., Hong, N.-S., et al. (2015). Sequence-structure-function classification of a catalytically diverse oxidoreductase superfamily in mycobacteria. *J. Mol. Biol.* 427, 3554–3571. doi: 10.1016/j.jmb.2015.09.021
- Ahmed, F. H., Mohamed, A. E., Carr, P. D., Lee, B. M., Condic-Jurkic, K., O'Mara, M. L., et al. (2016). Rv2074 is a novel F420H2-dependent biliverdin reductase in *Mycobacterium tuberculosis*. *Protein Sci.* 25, 1692–1709. doi: 10.1002/pro.2975
- Amato, E. D., and Stewart, J. D. (2015). Applications of protein engineering to members of the old yellow enzyme family. *Biotechnol. Adv.* 33, 624–631. doi: 10.1016/j.biotechadv.2015.04.011
- Barka, E. A., Vatsa, P., Sanchez, L., Gaveau-Vaillant, N., Jacquard, C., Klenk, H.-P., et al. (2016). Taxonomy, physiology, and natural products of Actinobacteria. *Microbiol. Mol. Biol. Rev.* 80, 1–43. doi: 10.1128/MMBR.00019-15
- Bashiri, G., Rehan, A. M., Greenwood, D. R., Dickson, J. M. J., and Baker, E. N. (2010). Metabolic engineering of cofactor F420 production in *Mycobacterium smegmatis*. *PLoS ONE* 5:e15803. doi: 10.1371/journal.pone.0015803
- Bashiri, G., Squire, C. J., Moreland, N. J., and Baker, E. N. (2008). Crystal structures of F420-dependent glucose-6-phosphate dehydrogenase FGD1 involved in the activation of the anti-tuberculosis drug candidate PA-824 reveal the basis of coenzyme and substrate binding. *J. Biol. Chem.* 283, 17531–17541. doi: 10.1074/jbc.M801854200
- Cellitti, S. E., Shaffer, J., Jones, D. H., Mukherjee, T., Gurumurthy, M., Bursulaya, B., et al. (2012). Structure of Ddn, the deazaflavin-dependent nitroreductase from *Mycobacterium tuberculosis* involved in bioreductive activation of PA-824. *Structure* 20, 101–112. doi: 10.1016/j.str.2011.11.001
- Clouthier, C. M., and Pelletier, J. N. (2012). Expanding the organic toolbox: a guide to integrating biocatalysis in synthesis. *Chem. Soc. Rev.* 41, 1585–1605. doi: 10.1039/c2cs15286j
- Ebert, S., Rieger, P.-G., and Knackmuss, H.-J. (1999). Function of coenzyme F420 in aerobic catabolism of 2,4,6-trinitrophenol and 2,4-dinitrophenol by *Nocardioideis simplex* FJ2-1A. *J. Bacteriol.* 181, 2669–2674.
- Eker, A. P., Hessels, J. K., and Meerwaldt, R. (1989). Characterization of an 8-hydroxy-5-deazaflavin:NADPH oxidoreductase from *Streptomyces griseus*. *Biochim. Biophys. Acta* 990, 80–86. doi: 10.1016/S0304-4165(89)80015-7
- Fox, K. M., and Karplus, P. A. (1994). Old yellow enzyme at 2 Å resolution: overall structure, ligand binding, and comparison with related flavoproteins. *Structure* 2, 1089–1105. doi: 10.1016/S0969-2126(94)00111-1
- Greening, C., Ahmed, F. H., Mohamed, A. E., Lee, B. M., Pandey, G., Warden, A. C., et al. (2016). Physiology, biochemistry, and applications of F420- and Fo-dependent redox reactions. *Microbiol. Mol. Biol. Rev.* 80, 451–493. doi: 10.1128/MMBR.00070-15
- Guerra-Lopez, D., Daniels, L., and Rawat, M. (2007). *Mycobacterium smegmatis* mc2155 fbiC and MSMEG_2392 are involved in triphenylmethane dye decolorization and coenzyme F420 biosynthesis. *Microbiology* 153, 2724–2732. doi: 10.1099/mic.0.2006/009241-0
- Gurumurthy, M., Rao, M., Mukherjee, T., Rao, S. P. S., Boshoff, H. I., Dick, T., et al. (2013). A novel F420-dependent anti-oxidant mechanism protects *Mycobacterium tuberculosis* against oxidative stress and bactericidal agents. *Mol. Microbiol.* 87, 744–755. doi: 10.1111/mmi.12127
- Heiss, G., Trachtmann, N., Abe, Y., Takeo, M., and Knackmuss, H.-J. (2003). Homologous npdGI genes in 2,4-dinitrophenol- and 4-nitrophenol-degrading *Rhodococcus* spp. *Appl. Environ. Microbiol.* 69, 2748–2754. doi: 10.1128/AEM.69.5.2748-2754.2003
- Ikeno, S., Aoki, D., Hamada, M., Hori, M., and Tsuchiya, K. S. (2006). DNA sequencing and transcriptional analysis of the kasugamycin biosynthetic gene cluster from *Streptomyces kasugaensis* M338-M1. *J. Antibiot. (Tokyo)* 59, 18–28. doi: 10.1038/ja.2006.4
- Isabelle, D., Simpson, D. R., and Daniels, L. (2002). Large-scale production of coenzyme F420-5,6 by using *Mycobacterium smegmatis*. *Appl. Environ. Microbiol.* 68, 5750–5755. doi: 10.1128/AEM.68.11.5750-5755.2002
- Jirapanjawat, T., Ney, B., Taylor, M. C., Warden, A. C., Afroze, S., Russell, R. J., et al. (2016). The redox cofactor F420 protects mycobacteria from diverse antimicrobial compounds and mediates a reductive detoxification system. *Appl. Environ. Microbiol.* 82, 6810–6818. doi: 10.1128/AEM.02500-16
- Lapalika, G. V., Taylor, M. C., Warden, A. C., Onagi, H., Hennessy, J. E., Mulder, R. J., et al. (2012a). Cofactor promiscuity among F420-dependent reductases enables them to catalyze both oxidation and reduction of the same substrate. *Catal. Sci. Technol.* 2, 1560–1567. doi: 10.1039/c2cy20129a
- Lapalika, G. V., Taylor, M. C., Warden, A. C., Scott, C., Russell, R. J., and Oakeshott, J. G. (2012b). F420H2-dependent degradation of aflatoxin and other furanocoumarins is widespread throughout the Actinomycetales. *PLoS ONE* 7:e30114. doi: 10.1371/journal.pone.0030114
- Mohamed, A. E., Ahmed, F. H., Arulmozhiraja, S., Lin, C. Y., Taylor, M. C., Krausz, E. R., et al. (2016a). Protonation state of F420H2 in the prodrug-activating deazaflavin dependent nitroreductase (Ddn) from *Mycobacterium tuberculosis*. *Mol. Biosyst.* 12, 1110–1113. doi: 10.1039/c6mb00033a
- Mohamed, A. E., Condic-Jurkic, K., Ahmed, F. H., Yuan, P., O'Mara, M. L., Jackson, C. J., et al. (2016b). Hydrophobic shielding drives catalysis of hydride transfer in a family of F420H2-dependent enzymes. *Biochemistry* 55, 6908–6918.
- Morris, G. M., Huey, R., Lindstrom, W., Sanner, M. F., Belew, R. K., Goodsell, D. S., et al. (2009). AutoDock4 and AutoDockTools4: automated docking with selective receptor flexibility. *J. Comput. Chem.* 30, 2785–2791. doi: 10.1002/jcc.21256
- Nestl, B. M., Nebel, B. A., and Hauer, B. (2011). Recent progress in industrial biocatalysis. *Curr. Opin. Chem. Biol.* 15, 187–193. doi: 10.1016/j.cbpa.2010.11.019
- Ney, B., Ahmed, F. H., Carere, C. R., Biswas, A., Warden, A. C., Morales, S. E., et al. (2017). The methanogenic redox cofactor F420 is widely synthesized by aerobic soil bacteria. *ISME J.* 11, 125–137. doi: 10.1038/ismej.2016.100
- Nguyen, Q.-T., Trinco, G., Binda, C., Mattevi, A., and Fraaije, M. W. (2017). Discovery and characterization of an F420-dependent glucose-6-phosphate

- dehydrogenase (Rh-FGD1) from *Rhodococcus jostii* RHA1. *Appl. Microbiol. Biotechnol.* 101, 2831–2842. doi: 10.1007/s00253-016-8038-y
- Pettersen, E. F., Goddard, T. D., Huang, C. C., Couch, G. S., Greenblatt, D. M., Meng, E. C., et al. (2004). UCSF Chimera—a visualization system for exploratory research and analysis. *J. Comput. Chem.* 25, 1605–1612. doi: 10.1002/jcc.20084
- Purwantini, E., and Daniels, L. (1996). Purification of a novel coenzyme F420-dependent glucose-6-phosphate dehydrogenase from *Mycobacterium smegmatis*. *J. Bacteriol.* 178, 2861–2866. doi: 10.1128/jb.178.10.2861-2866.1996
- Stuermer, R., Hauer, B., Hall, M., and Faber, K. (2007). Asymmetric bioreduction of activated C=C bonds using enoate reductases from the old yellow enzyme family. *Curr. Opin. Chem. Biol.* 11, 203–213. doi: 10.1016/j.cbpa.2007.02.025
- Taylor, M. C., Jackson, C. J., Tattersall, D. B., French, N., Peat, T. S., Newman, J., et al. (2010). Identification and characterization of two families of F420H₂-dependent reductases from Mycobacteria that catalyze aflatoxin degradation. *Mol. Microbiol.* 78, 561–575. doi: 10.1111/j.1365-2958.2010.07356.x
- Walsh, C. (1986). Naturally occurring 5-deazaflavin coenzymes: biological redox roles. *Acc. Chem. Res.* 19, 216–221. doi: 10.1021/ar00127a004
- Wang, P., Bashiri, G., Gao, X., Sawaya, M. R., and Tang, Y. (2013). Uncovering the enzymes that catalyze the final steps in oxytetracycline biosynthesis. *J. Am. Chem. Soc.* 135, 7138–7141. doi: 10.1021/ja403516u
- Williams, R. E., and Bruce, N. C. (2002). “New uses for an old enzyme”—the old yellow enzyme family of flavoenzymes. *Microbiology* 148, 1607–1614. doi: 10.1099/00221287-148-6-1607

Conflict of Interest Statement: The authors declare that the research was conducted in the absence of any commercial or financial relationships that could be construed as a potential conflict of interest.

Copyright © 2017 Greening, Jirapanjawat, Afroze, Ney, Scott, Pandey, Lee, Russell, Jackson, Oakeshott, Taylor and Warden. This is an open-access article distributed under the terms of the Creative Commons Attribution License (CC BY). The use, distribution or reproduction in other forums is permitted, provided the original author(s) or licensor are credited and that the original publication in this journal is cited, in accordance with accepted academic practice. No use, distribution or reproduction is permitted which does not comply with these terms.



Cofactor Tail Length Modulates Catalysis of Bacterial F₄₂₀-Dependent Oxidoreductases

Blair Ney^{1,2}, Carlo R. Carere³, Richard Sparling^{3,4}, Thanavit Jirapanjawat¹, Matthew B. Stott³, Colin J. Jackson⁵, John G. Oakeshott², Andrew C. Warden^{2*} and Chris Greening^{1,2*}

¹ School of Biological Sciences, Monash University, Clayton, VIC, Australia, ² Land and Water Flagship, The Commonwealth Scientific and Industrial Research Organisation, Acton, ACT, Australia, ³ GNS Science, Wairakei Research Centre, Lower Hutt, New Zealand, ⁴ Department of Microbiology, University of Manitoba, Winnipeg, MB, Canada, ⁵ Research School of Chemistry, Australian National University, Acton, ACT, Australia

OPEN ACCESS

Edited by:

Dirk Tischler,
Freiburg University of Mining
and Technology, Germany

Reviewed by:

Alberto A. Iglesias,
National University of the Littoral,
Argentina
Matthias Boll,
Albert Ludwigs University of Freiburg,
Germany

*Correspondence:

Chris Greening
chris.greening@monash.edu
Andrew C. Warden
andrew.warden@csiro.au

Specialty section:

This article was submitted to
Microbial Physiology and Metabolism,
a section of the journal
Frontiers in Microbiology

Received: 21 July 2017

Accepted: 15 September 2017

Published: 27 September 2017

Citation:

Ney B, Carere CR, Sparling R,
Jirapanjawat T, Stott MB,
Jackson CJ, Oakeshott JG,
Warden AC and Greening C (2017)
Cofactor Tail Length Modulates
Catalysis of Bacterial F₄₂₀-Dependent
Oxidoreductases.
Front. Microbiol. 8:1902.
doi: 10.3389/fmicb.2017.01902

F₄₂₀ is a microbial cofactor that mediates a wide range of physiologically important and industrially relevant redox reactions, including in methanogenesis and tetracycline biosynthesis. This deazaflavin comprises a redox-active isoalloxazine headgroup conjugated to a lactyloligoglutamyl tail. Here we studied the catalytic significance of the oligoglutamate chain, which differs in length between bacteria and archaea. We purified short-chain F₄₂₀ (two glutamates) from a methanogen isolate and long-chain F₄₂₀ (five to eight glutamates) from a recombinant mycobacterium, confirming their different chain lengths by HPLC and LC/MS analysis. F₄₂₀ purified from both sources was catalytically compatible with purified enzymes from the three major bacterial families of F₄₂₀-dependent oxidoreductases. However, long-chain F₄₂₀ bound to these enzymes with a six- to ten-fold higher affinity than short-chain F₄₂₀. The cofactor side chain also significantly modulated the kinetics of the enzymes, with long-chain F₄₂₀ increasing the substrate affinity (lower K_m) but reducing the turnover rate (lower k_{cat}) of the enzymes. Molecular dynamics simulations and comparative structural analysis suggest that the oligoglutamate chain of F₄₂₀ makes dynamic electrostatic interactions with conserved surface residues of the oxidoreductases while the headgroup binds the catalytic site. In conjunction with the kinetic data, this suggests that electrostatic interactions made by the oligoglutamate tail result in higher-affinity, lower-turnover catalysis. Physiologically, we propose that bacteria have selected for long-chain F₄₂₀ to better control cellular redox reactions despite tradeoffs in catalytic rate. Conversely, this suggests that industrial use of shorter-length F₄₂₀ will greatly increase the rates of bioremediation and biocatalysis processes relying on purified F₄₂₀-dependent oxidoreductases.

Keywords: F₄₂₀, redox, biocatalysis, biodegradation, mycobacterium, actinobacteria, cofactor

INTRODUCTION

Diverse enzymes employ flavins and similar cofactors to mediate biological redox reactions (Leys and Scrutton, 2016). In addition to using the universal flavin cofactors FAD and FMN, some bacteria and archaea employ the deazaflavin cofactor F₄₂₀ (Ney et al., 2017). In its enzyme-unbound state, this redox cofactor has unique redox properties compared to free FMN and FAD, namely a

lower standard redox potential (−340 mV) and exclusive two-electron reactivity (Walsh, 1986; Greening et al., 2016). Due to these properties, F₄₂₀ can mediate a wide range of otherwise challenging redox transformations, including the one-carbon reactions of methanogenesis (Thauer et al., 2008; Greening et al., 2016). In mycobacteria and streptomycetes, the cofactor has been shown to be important for central metabolism (Bashiri et al., 2008; Ahmed et al., 2015), secondary metabolite biosynthesis (Ikeno et al., 2006; Wang et al., 2013), cell wall production (Purwantini and Mukhopadhyay, 2013; Purwantini et al., 2016), and biodegradation pathways (Taylor et al., 2010; Jirapanjawat et al., 2016). Beyond its physiological importance, F₄₂₀ has received recent attention for its potential industrial applications. Notably, actinobacterial F₄₂₀H₂-dependent reductases catalyze the penultimate step of tetracycline antibiotic biosynthesis (Wang et al., 2013), the reductive activation of the clinically approved antituberculosis prodrug delamanid (Cellitti et al., 2012), and the biodegradation of environmental contaminants such as nitroaromatic explosives (Ebert et al., 1999) and arylmethane dyes (Jirapanjawat et al., 2016). F₄₂₀ has also been identified as a promising next-generation cofactor to mediate *in vitro* and *in vivo* biocatalytic cascades (Taylor et al., 2013; Greening et al., 2017).

Nevertheless, there remains an incomplete understanding of how the chemical structure of F₄₂₀ relates to its physiological function and industrial application. Structurally, the cofactor comprises two major components (**Figure 1A**): (i) a redox-active headgroup comprising a modified isoalloxazine tricycle and (ii) a catalytically-inactive side chain comprising a ribitylphospholactyl moiety and an oligoglutamate chain of variable length (Eirich et al., 1978; Ashton et al., 1979). F₀ (8-hydroxy-5-deazaflavin), a chromophore used by DNA photolyases, serves as the biosynthetic precursor to F₄₂₀ (Graupner and White, 2001). The phospholactyl and oligoglutamate constituents are added to this precursor by three dedicated biosynthetic enzymes (CofC, CofD, CofE) (Nocek et al., 2007; Forouhar et al., 2008; Grochowski et al., 2008; Bashiri et al., 2016). It is well-established that key chemical substitutions in the isoalloxazine group confer the unique redox properties of deazaflavins over flavins (Walsh, 1986; Greening et al., 2016). However, it remains to be understood why organisms have selected to incorporate the lacylologlutamate side chain. It also remains elusive why the length of the oligoglutamate chain varies between organisms: two to three residues in methanogens without cytochromes, three to six in Proteobacteria and methanogens with cytochromes (Methanosarcinales), and five to eight in Actinobacteria and Chloroflexi (Gorris and van der Drift, 1994; Bair et al., 2001; Ney et al., 2017). The side chain does not significantly affect the chemical reactivity or redox properties of F₄₂₀ relative to its precursor F₀ (Greening et al., 2016); indeed, previous studies have shown that the redox potential of F₄₂₀ is the same as F₀ (−340 mV) and hence is not modulated by the oligoglutamate tail (Jacobson and Walsh, 1984). Moreover, while the charged nature of F₄₂₀ ensures it does not diffuse from the cell in contrast to its precursor F₀ (Ney et al., 2017), this does not explain why organisms selected to synthesize a polyanionic rather than monoanionic cofactor.

We recently hypothesized that catalytic constraints may have driven the synthesis of the side chain in F₄₂₀ (Ney et al., 2017). Specifically, the oligoglutamate chain may facilitate higher-affinity electrostatic interactions between enzyme and cofactor. We propose that, in addition to driving specific F₄₂₀-dependent reactions, such high-affinity interactions may be crucial for maintaining redox homeostasis and discriminating between cofactor pools (Ney et al., 2017). In support of this observation, two cofactor-bound crystal structures suggest that the oligoglutamate chain can interact with surface cationic residues of F₄₂₀-dependent oxidoreductases (Cellitti et al., 2012; Ahmed et al., 2016), though the significance of this has not been considered. Other structural analyses have proposed that, while the ribityl and phosphate groups of F₄₂₀ make hydrogen bonds with surrounding residues, the oligoglutamate tail instead extends into the solvent phase without contributing to binding (Bashiri et al., 2008). In this work, we addressed the effect of the oligoglutamate side chain on the catalytic activity of F₄₂₀-dependent oxidoreductases. To do this, we purified F₄₂₀ from two sources: short-chain F₄₂₀ from a methanogen and long-chain F₄₂₀ from a mycobacterium. We subsequently studied the cofactor binding affinities and substrate consumption kinetics of mycobacterial F₄₂₀-dependent oxidoreductases in the presence of these different F₄₂₀ variants. We focused on a representative from each of the three main superfamilies of F₄₂₀-dependent oxidoreductases found in bacteria (Selengut and Haft, 2010), namely the luciferase-like hydride transferases (LLHTs; TIM barrel fold) (Bashiri et al., 2008; Greening et al., 2016) and flavin/deazaflavin oxidoreductase superfamilies A (FDOR-As; monomeric split β -barrel proteins) and B (FDOR-Bs; dimeric split β -barrel proteins) (Ahmed et al., 2015; Greening et al., 2016).

MATERIALS AND METHODS

F₄₂₀ Production

Long-chain F₄₂₀ was recombinantly overproduced in *Mycobacterium smegmatis* mc²4517 cells harboring an inducible pYUDDuet shuttle vector encoding the F₄₂₀ biosynthesis genes *cofC*, *cofD*, and *cofE* (Bashiri et al., 2010). Cultures were grown in twenty 2 L Erlenmeyer flasks each containing 500 mL LB broth supplemented with 0.05% Tween 80 (LBT), 50 μ g mL^{−1} hygromycin B and 20 μ g mL^{−1} kanamycin. The cultures were grown to stationary-phase in a rotary incubator (200 rpm) at 37°C for 5 days before harvesting. Short-chain F₄₂₀ was extracted from a thermophilic methanogen strain, *Methanothermobacter marburgensis* A60. We isolated the strain by repeated serial dilution of geothermally heated sediments from Ngatamariki, New Zealand. 16S rRNA gene sequencing of genomic DNA extracts (NucleoSpin Tissue Kit, Macherey-Nagel) using the archaeal-specific primer set 109f/912r confirmed the strain shared 99% sequence identity with the well-studied laboratory strain *Methanothermobacter marburgensis* Marburg^T (Liesegang et al., 2010). For F₄₂₀ production, the strain was cultured in thirty 1 L bottles each containing 400 mL of a previously defined media supplemented with 29 mM sodium formate (Sparling et al., 1993) and a H₂/CO₂ atmosphere (80:20 v/v). Cultures were grown to

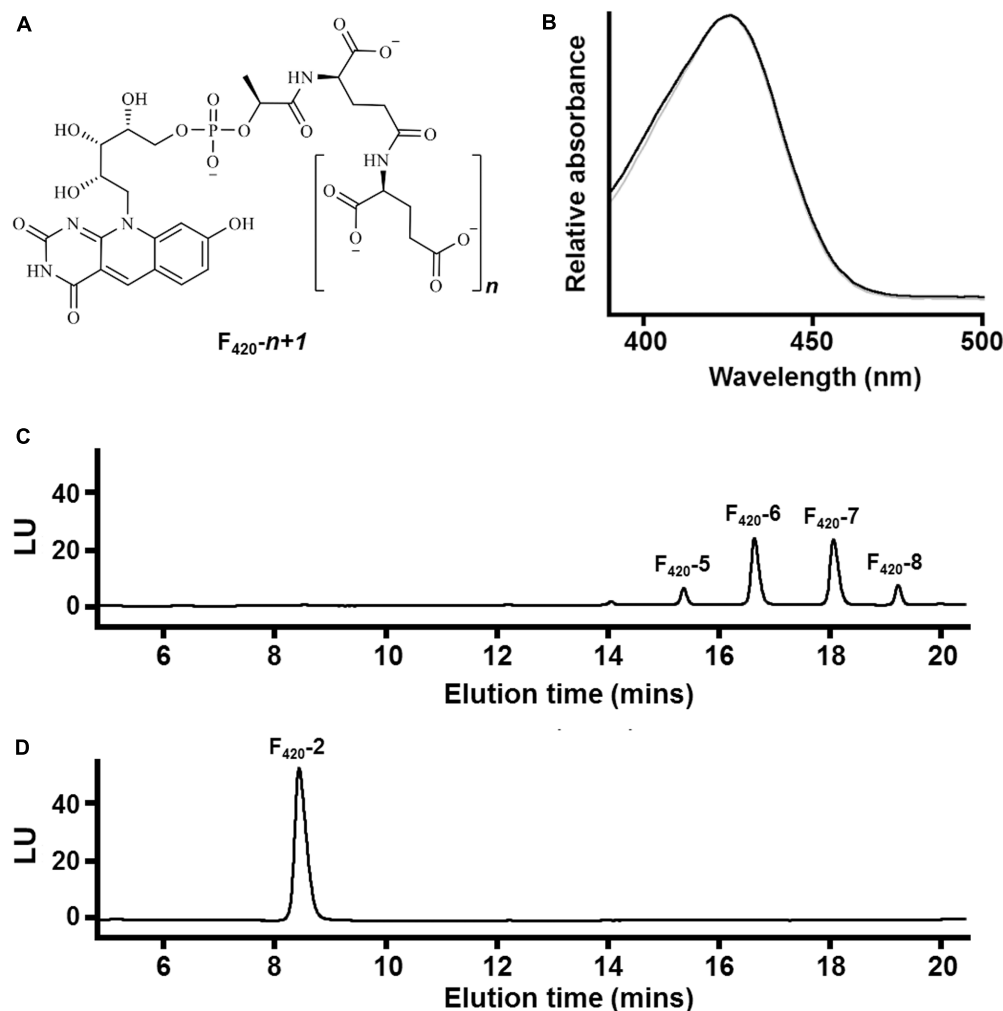


FIGURE 1 | Chemical composition of F₄₂₀ purified from different sources. **(A)** Chemical structure of F₄₂₀ showing the redox-active isalloxazine headgroup and lacylloglutamyl tail. The number of glutamate residues (n) varies between bacteria and archaea. **(B)** Absorbance spectrum of F₄₂₀ purified from *Mycobacterium smegmatis* mc²4517 (black) and *Methanothermobacter marburgensis* A60 (gray). **(C)** HPLC trace showing F₄₂₀ purified from *M. smegmatis* mc²4517 varies in chain length between five to eight glutamates. **(D)** HPLC trace showing F₄₂₀ purified from *Mtb. marburgensis* A60 predominantly contains two glutamate residues.

stationary-phase in a rotary incubator (100 rpm) at 60°C for 3 days with periodic gas feeding before harvesting.

F₄₂₀ Purification

F₄₂₀ was harvested from the mycobacterial and methanogen cultures through variations on an existing protocol (Isabelle et al., 2002). The cells were harvested by centrifugation at 10,000 × g for 20 min, the resultant pellets were washed, and the cultures were resuspended in 20 mM TrisHCl (pH 7.5) at a ratio of 1 g per 10 mL. The cells were autoclaved at 121°C to release F₄₂₀, a heat-stable cofactor, into the buffer. The cell debris was removed by centrifugation at 18,000 × g for 20 min and the supernatant was decanted and vacuum-filtrated through 0.45 μ m filter paper. The F₄₂₀ was isolated by FPLC (fast protein liquid chromatography) with a Macro-prep High Q Resin anion exchange column (Bio-Rad). A gradient of buffer A (20 mM TrisHCl, 100 mM NaCl, pH 7.5) and buffer B (20 mM

TrisHCl, 1 M NaCl, pH 7.5) was applied, with buffer B increasing from 0 to 100% over 10 column volumes. Fractions containing F₄₂₀ were identified *via* analysis of absorbance spectra on a SpectraMax® M3 Multi-Mode Microplate Reader (Bio-Strategy, Australia). Fractions containing F₄₂₀ were pooled. The F₄₂₀ solution was further purified and concentrated by hydrophobic interaction chromatography through a high capacity C18 column equilibrated in H₂O. F₄₂₀ was eluted in 2 mL fractions in 20% methanol, dried by rotary evaporation, and stored at −20°C.

HPLC and LC/MS Analysis

An ion-paired reverse phase HPLC (high-performance liquid chromatography) protocol was used to determine the oligoglutamate chain length of F₄₂₀ purified from mycobacterial and methanogen sources. An Agilent 1200 series system equipped with an Agilent Poroshell 120 EC-C18 2.1 × 50 mm 2.7 μ m column and diode array detector was used. The F₄₂₀ species

were separated at a flow rate of 0.3 mL min⁻¹ using a gradient of two buffers, namely A (20 mM ammonium phosphate, 10 mM tetrabutylammonium phosphate, pH 7.0) and B (100% acetonitrile). A gradient was run from 25 to 40% buffer B as follows: 0–1 min 25%, 1–10 min 25–35%, 10–13 min 35%, 13–16 min 35–40%, 16–19 min 40–25%. F₄₂₀ absorbance was measured at 420 nm using a diode array detector. This system was also used to execute an absorbance scan from 400 to 600 nm on the sole F₄₂₀-2 peak of the methanogen F₄₂₀ and the prominent F₄₂₀-6 peak of the mycobacterial F₄₂₀. The length of the F₄₂₀ oligoglutarate tails were verified by a reverse phase LC/MS (liquid chromatography / mass spectrometry) protocol with an Agilent 1100 series LC/MSD TOF equipped with a Poroshell 120 EC-C18 2.1 × 100 mm 2.7 μm column. A gradient protocol comprising of Buffer A (20 mM ammonium acetate pH 6.8) and Buffer B (100% acetonitrile) was applied as follows: Held from 0 – 1 min at 5% B; 1 – 10 min from 5 – 20% B. Negative mode ESI was used with a capillary voltage of 2500 V and gas temperature of 300°C. The system was run at a flow rate of 0.2 mL min⁻¹ and chemical species were scanned from 150 – 1500 m/z.

Enzymatic Assays

The F₄₂₀-reducing glucose 6-phosphate dehydrogenase (Fgd; MSMEG locus 0777) and two F₄₂₀H₂-dependent reductases (FDORs; MSMEG loci 2027, 3380) from *M. smegmatis* mc²155 were recombinantly overexpressed in *Escherichia coli* BL21(DE3) using previously described vectors and protocols (Taylor et al., 2010; Ahmed et al., 2015). Cells were harvested by centrifugation, resuspended in lysis buffer, and lysed in an EmulsiFlex-C3 homogenizer (ATA Scientific, Australia) according to previously described protocols (Greening et al., 2017). Enzymes were purified from soluble extracts by Ni-nitrilotriacetic acid (NTA) affinity chromatography using gravity columns as previously described (Taylor et al., 2010; Ahmed et al., 2015) and stored in elution buffer (50 mM NaH₂PO₄ 300 mM NaCl, 250 mM imidazole, pH 8.0) until use in assays. The high purity of the proteins was confirmed by running the fractions on NuPAGE Novex 10% Bis-Tris gels (Invitrogen, Australia) and staining with Coomassie Brilliant Blue. We measured the activities of the enzymes by monitoring the rates of F₄₂₀ reduction or F₄₂₀H₂ oxidation in the presence of different substrate concentrations; this serves as a reliable measure of substrate transformation given F₄₂₀-dependent oxidoreductases directly mediate hydride transfer between cofactor and substrate in an equimolar manner (Greening et al., 2016; Jirapanjawat et al., 2016). Enzyme activities were measured in 96-well plates containing degassed TrisHCl buffer [200 mM TrisHCl, 0.1% (w/v) Triton X-100, pH 8.0] sequentially supplemented with substrate at the specified concentration, 50 μM of the relevant cofactor, and 100 nM of the relevant enzyme. Reaction rates were measured by monitoring the initial linear change of absorbance of the reaction mixture at 420 nm using a SpectraMax® M3 Multi-Mode Microplate Reader (Molecular Devices); loss of absorbance was observed due to Fgd-mediated reduction of F₄₂₀, whereas gain of absorbance occurred due to FDOR-mediated reoxidation of F₄₂₀H₂. Prior to measurement of FDOR

activity, F₄₂₀ was enzymatically reduced with 1 μM Fgd in a nitrogen glovebox for 4 h and purified by spin filtration as previously described (Ahmed et al., 2015). Reaction velocities were calculated by subtracting rates of no-enzyme controls from the initial linear rates of F₄₂₀ reduction or F₄₂₀H₂ reoxidation measured.

Intrinsic Tryptophan Fluorescence Quenching

F₄₂₀ dissociation constants were calculated by monitoring the decrease of intrinsic tryptophan fluorescence upon gradual titration of F₄₂₀ as previously described (Ahmed et al., 2015). A SpectraMax® M3 Multi-Mode Microplate Reader (Molecular Devices) with a quartz cuvette containing 500 nM of protein in 20 mM TrisHCl, pH 8.0 at 24°C was used. Samples were excited at 290 nm and emission was monitored at 340 nm. One microliter aliquots of F₄₂₀ standards in the same buffer were added to produce a solution with final concentrations ranging from 0 to 12.3 μM F₄₂₀, with the concentration recalculated for the incremental increase in volume. The fractional saturation (F/F_{max}) was plotted against the concentration of free F₄₂₀, and the K_d derived from fitting the data points to the function: $F/F_{\max} = F_{\max} * [\text{Free F}_{420}] / (K_d + [\text{Free F}_{420}])$.

Molecular Dynamics Simulations

Molecular dynamics simulations used the 1.5 Å resolution crystal structure of MSMEG_2027 [PDB: 4Y91 (Ahmed et al., 2015)] and 1.2 Å resolution structure of MSMEG_3380 [PDB: 3F7E (Taylor et al., 2010)]. The structure of the 26 residues missing from the MSMEG_2027 crystal structure was predicted by homology modeling in Phyre2 (intensive mode) (Kelley et al., 2015) using *M. tuberculosis* Rv3547/Ddn [PDB: 3RZ (Cellitti et al., 2012)] as the template. Simulations were visualized in the VMD: Visual Molecular Dynamics software (Humphrey et al., 1996) and calculations were performed using Amber16 (University of California San Francisco) employing the ff14SB forcefield (Maier et al., 2015). The Antechamber module within Amber16 was used to parameterize the F₄₂₀-2 and F₄₂₀-6 moieties with the GAFF2 forcefield and mulliken charges, and ionsjc_TIP3P parameters were used for the Na⁺ counterions. F₄₂₀-2 and F₄₂₀-6 were modeled into the structure of MSMEG_3380 and docked into the structure of MSMEG_2027 using AutoDock Vina (Morris et al., 2009). For MSMEG_3380, the positions of the cofactor up to the first glutamate residue were based on the cofactor position in the homologous protein Rv1155 [PDB: 4QVB (Mashalidis et al., 2015)]. Diglutamate and hexaglutamate tails were manually constructed and initial geometry optimisations were performed in Discovery Studio 3.5 (Accelrys). The headgroup was constructed in its deprotonated F₄₂₀H⁻ form (Mohamed et al., 2016a) and all carboxylate groups were modeled in deprotonated form. Protein-cofactor complexes were solvated in an octahedral TIP3P water box with a minimum periodic boundary distance of 10.0 Å from the solute. Each system was relaxed for a maximum of 25,000 steps of steepest descent and 25,000 steps of conjugate gradient whilst constraining the protein atoms, after which a production run of 400 ns was

performed at 298 K and 1 bar with a pressure relaxation time of 2.0 ps. Langevin dynamics was employed with a collision frequency of 5.0 and SHAKE constraints were applied to all hydrogen atoms. The ribityl-bearing nitrogen of the headgroup of each F₄₂₀ moiety had light positional restraints enforced (10 kcal mol⁻¹ Å²) to prevent the headgroup from leaving the active site and to allow maximal rotational freedom within the active site so as minimize bias on the interaction energy. MMPBSA (Molecular Mechanics Poisson Boltzmann Surface Area) calculations were carried out on 2,000 frames of each 400 ns simulation employing an ionic strength of 0.15 mM and fillratio setting of 4.0.

Comparative Structural Analysis

For comparative structural analysis, protein sequences of F₄₂₀-dependent oxidoreductases from different subgroups within the LLHT, FDOR-A, and FDOR-B superfamilies were retrieved from the NCBI database. Multiple sequence alignments were constructed with Clustal Omega (Sievers et al., 2011). Homology models of MSMEG_0777 and Rv0132c were constructed in RaptorX (Källberg et al., 2012) using *M. tuberculosis* Rv0407/Fgd as the template (Bashiri et al., 2008). Protein structures were visualized in UCSF Chimera (Pettersen et al., 2004).

RESULTS

The F₄₂₀ Oligoglutamate Chain Influences Cofactor-Binding Affinity and Reaction Kinetics of F₄₂₀-Dependent Oxidoreductases

At present, no chemical syntheses or enzymatic cascades have been developed for cell-free production of F₄₂₀. We therefore obtained sufficient F₄₂₀ for this study through large-scale cultivation of two F₄₂₀-producing strains, namely the new methanogen isolate *Methanothermobacter marburgensis* A60 and a previously described F₄₂₀ overproduction strain of *Mycobacterium smegmatis* mc²4517 (Bashiri et al., 2010), under conditions that would promote high-level F₄₂₀ production. F₄₂₀ was purified from these strains through a sequence of anion-exchange chromatography, hydrophobic interaction chromatography, and rotary evaporation. We detected the eponymous absorbance peak of F₄₂₀ in the purified fractions (Figure 1B). To confirm chain length, we separated the purified F₄₂₀ on a HPLC equipped with an anion-exchange column and detected the cofactor at 420 nm using a diode array detector. F₄₂₀ purified from *M. smegmatis* contained between five to eight glutamates (Figure 1C), consistent with previous mass validation (Bashiri et al., 2010; Ney et al., 2017). In contrast, HPLC traces showed that all detectable F₄₂₀ purified from *Mtb. marburgensis* contained two glutamate residues (Figure 1D). The mass of the dominant chemical species was validated by LC/MS (Supplementary Figure S1).

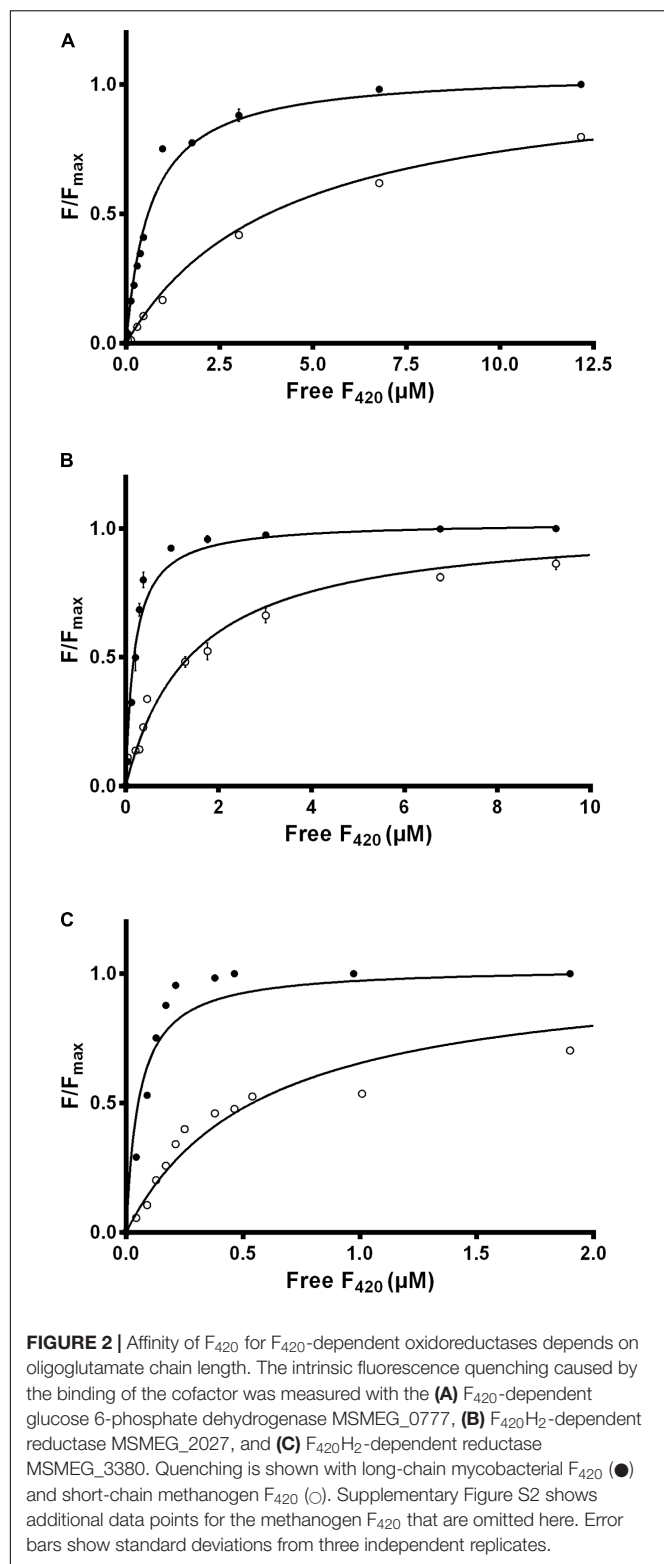
We used intrinsic fluorescence quenching to determine the binding affinities of the two purified F₄₂₀ variants for three

F₄₂₀-dependent oxidoreductases from *M. smegmatis*: the F₄₂₀-dependent glucose 6-phosphate dehydrogenase MSMEG_0777 (LLHT family), the F₄₂₀H₂-dependent quinone reductase MSMEG_2027 (FDOR-A family), and a promiscuous F₄₂₀H₂-dependent reductase of unknown function MSMEG_3380 (FDOR-B family). We observed that long-chain mycobacterial F₄₂₀ bound the enzymes with nanomolar affinities (*K_d* values) of 650 nM, 190 nM, and 54 nM respectively (Figure 2 and Supplementary Figure S2), similar to values derived from previous enzymatic studies (Bashiri et al., 2008; Ahmed et al., 2015). In contrast, short-chain methanogen F₄₂₀ bound with six- to ten-fold lower affinities, i.e., 4.1 μM, 1.4 μM, and 570 nM respectively (Figure 2 and Supplementary Figure S2). We observed no significant binding of the biosynthetic precursor F₆₀, at concentrations up to 50 μM, for any of the three enzymes. This finding suggests that interactions between the F₄₂₀ oligoglutamate chain and mycobacterial F₄₂₀-dependent oxidoreductases are crucial for high-affinity cofactor-enzyme associations.

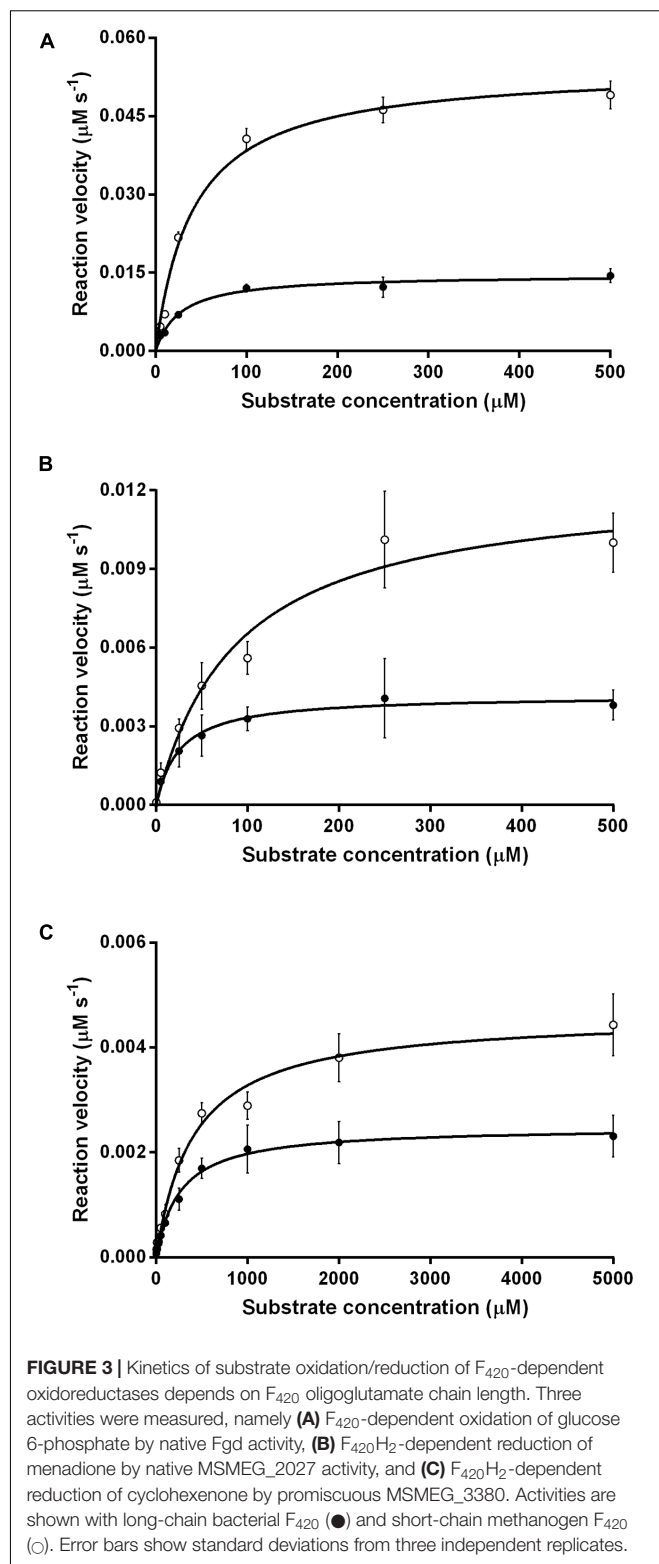
We compared the reaction kinetics of the three enzymes in the presence of the different F₄₂₀ variants. The enzymes were catalytically active in the presence of F₄₂₀ purified from both sources. Consistent with previous findings (Bashiri et al., 2008; Taylor et al., 2010; Ahmed et al., 2015), reaction kinetics of all three enzymes followed Michaelis–Menten models (Figure 3), though the kinetic parameters differed depending on the length of the F₄₂₀ oligoglutamate chain. Observed substrate turnover rates (*k_{cat}*) were between 1.9 and 3.7 times greater in the presence of short-chain F₄₂₀ compared to long-chain F₄₂₀ (Table 1); such enhancements of initial rate were observed irrespective of the F₄₂₀ concentration used (Supplementary Figure S3). A decrease in *K_m* was also observed in the presence of the long-chain species, with differences ranging from 3.5-fold for MSMEG_2027 to a modest 1.5-fold for MSMEG_0777 and MSMEG_3380 (Table 1). Hence, high-affinity cofactor binding results in both enhanced substrate binding and decreased reaction turnover.

The Oligoglutamate Chain Makes Multiple Electrostatic Interactions with Surface Anionic Residues of FDORs

To determine the structural and mechanistic basis for these differences, we used molecular dynamics simulations to compare the binding of long-chain (F₄₂₀-6) and short-chain (F₄₂₀-2) variants of F₄₂₀ to the available crystal structures of the FDOR-A MSMEG_2027 (Ahmed et al., 2015) and the FDOR-B MSMEG_3380 (Taylor et al., 2010). An overarching characteristic of all simulations was that, following equilibration of the position of the cofactor tail, the glutamate residues made multiple transient electrostatic contacts with specific arginine and lysine residues on the surfaces of the oxidoreductases. The first two glutamates of both F₄₂₀-2 and F₄₂₀-6 made interactions with residues Lys73, Arg49, Lys44, and sporadically Lys68 of MSMEG_2027 (Figures 4A,B). These glutamate residues also interacted with Arg205, Arg23, and Arg54 of MSMEG_3380, but these interactions were more transient (Figures 4C,D). In both cases, the terminal four glutamates



of F₄₂₀-6 made multiple transient electrostatic interactions with surface cationic residues, but these residues were highly dynamic and displayed little specificity in the various interactions they formed. These additional interactions also appeared to

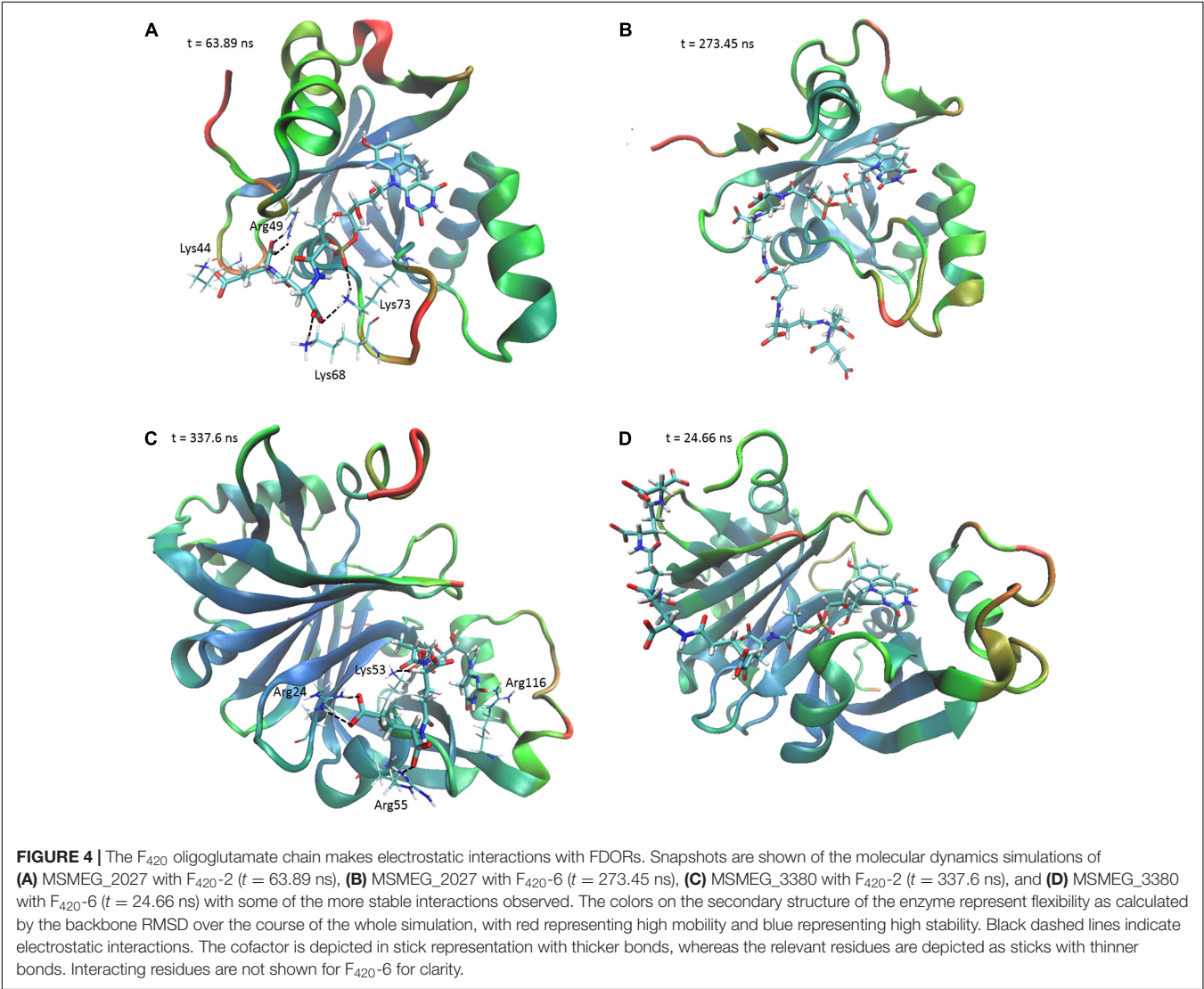


stabilize the core interactions made by the cofactor, for example between the phosphate group and Lys53 of MSMEG_3380 (Figures 4B,D). The multiple alternative tail conformations observed remained favorable even though the headgroup was

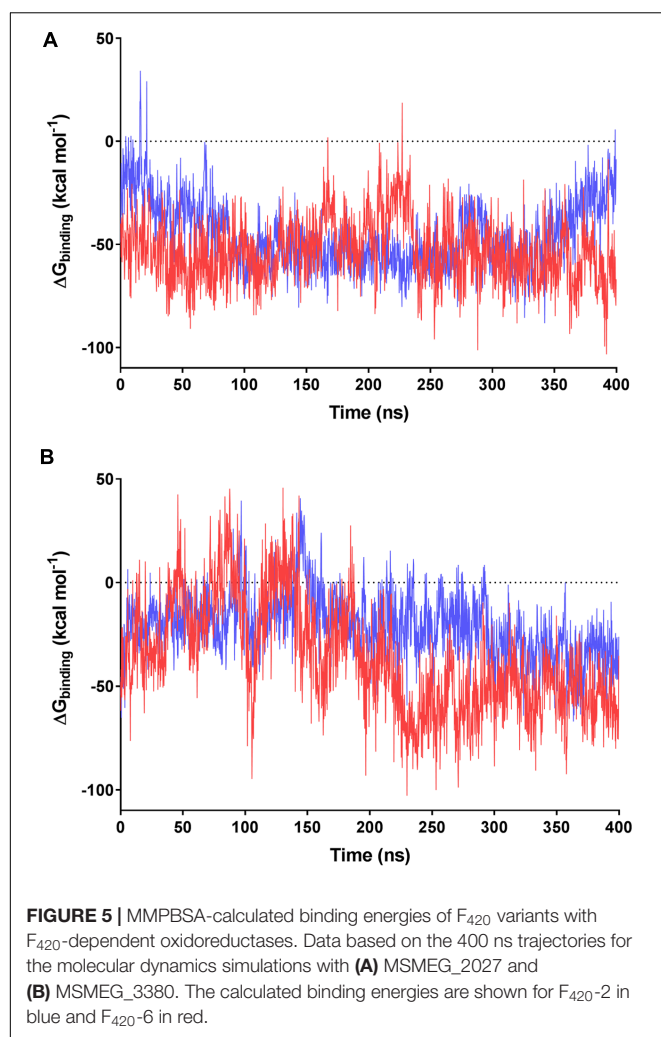
TABLE 1 | Kinetic parameters of F₄₂₀-dependent oxidoreductases in the presence of long-chain F₄₂₀ and short-chain F₄₂₀.

Enzyme	F ₄₂₀ K _d (μM)	K _M (μM)	K _{cat} (s ⁻¹)	K _{cat} /K _M (M ⁻¹ s ⁻¹)
Fgd: Glucose 6-phosphate oxidation				
F ₄₂₀ -long	0.65 ± 0.05	26.8 ± 4.4	0.292 ± 0.012	10900
F ₄₂₀ -short	4.18 ± 0.29	41.3 ± 4.3	1.086 ± 0.029	26300
MSMEG_2027: Menadione reduction				
F ₄₂₀ -long	0.19 ± 0.02	25.6 ± 9.2	0.084 ± 0.007	3280
F ₄₂₀ -short	1.43 ± 0.12	88.2 ± 18.4	0.244 ± 0.018	2770
MSMEG_3380: Cyclohexenone reduction				
F ₄₂₀ -long	0.054 ± 0.010	259 ± 41	0.025 ± 0.001	96
F ₄₂₀ -short	0.57 ± 0.05	407 ± 52	0.046 ± 0.002	177

The dissociation constants (K_d) of the different F₄₂₀ species is shown in the second column. The kinetic parameters of substrate oxidation or reduction by the enzymes is shown in the subsequent four columns. Error margins show standard deviations from three independent replicates.



weakly restrained within the active site (Supplementary Figure S4). We subsequently evaluated the cofactor-enzyme binding energies for the trajectories using MMPBSA analysis, which confirmed that the oligoglutarate chain modulated binding. While the cofactor-enzyme contacts reduced solvation energy, this was offset by the combined energies from 1 to 4 electrostatic and other non-bonded interactions, resulting in a lower total



$\Delta G_{\text{binding}}$ for the complex. Consistent with the additional dynamic interactions observed, F₄₂₀-6 reached lower $\Delta G_{\text{binding}}$ values than F₄₂₀-2 in simulations with both MSMEG_2027 and MSMEG_3380 (**Figures 5A,B**). Such observations are consistent with the lower K_d values determined in the tryptophan fluorescence quenching experiments (**Figure 2** and Supplementary Figure S2). Loss of multiple electrostatic interactions between the enzyme and cofactor tail increased the solvation energy and often pushed $\Delta G_{\text{binding}}$ into positive territory (**Figure 5B**). The internal bond, angle, and dihedral energies of the cofactor were essentially unaffected by the various binding modes (Supplementary Figure S4), emphasizing that most binding energy changes occur due to flexibility of the oligoglutarate chain rather than the isoalloxazine ring. These findings in turn suggest that there are no combinations of interactions that would release the headgroup from the active site and instead cofactor dissociation may be driven by tail solvation.

Interestingly, we observed that the monomeric enzyme MSMEG_2027 exhibited markedly different cofactor binding modes compared to the dimeric enzyme MSMEG_3380. While most of the interacting positive charges were accommodated

on the flexible loop regions of MSMEG_2027 (Lys44, Lys68, Lys73), the main contacting residues of MSMEG_3380 (Arg205, Arg23, Arg54) all lie on highly stable β -sheet and helical secondary structural regions. Multiple sequence alignments and comparative structural analysis suggest that these cationic residues were highly conserved within their respective FDOR-A and FDOR-B superfamilies (Supplementary Figures S5, S6). Most notably, the sequence motif Gx[KR]xG[QKE]xR occurs in all enzymes in the FDOR-A superfamily, among them enzymes sharing less than 25% identity. This sequence forms a loop joining two β -strands (Ahmed et al., 2015); the Gly residues likely contribute to the flexibility of the loop and the cationic residues serve as the main site of sustained interaction with the oligoglutarate chain (**Figure 4**). Conserved cationic surface residues are also proximal to the F₄₂₀ oligoglutarate chain in the LLHT superfamily (Supplementary Figures S5, S6), providing further support that electrostatic interactions generally occur between bacterial F₄₂₀-dependent oxidoreductases and the F₄₂₀ oligoglutarate chain.

DISCUSSION

Since the structure of F₄₂₀ was proposed in Eirich et al. (1978), studies on its catalytic behavior have focused on its redox-active headgroup (Walsh, 1986; Greening et al., 2016) and the role of its side chain has not been addressed. In this study, we reveal that the F₄₂₀ oligoglutarate chain modulates catalysis in bacterial F₄₂₀-dependent oxidoreductases. Our experimental findings demonstrate that synthesis of long-chain F₄₂₀ results in higher-affinity enzyme-cofactor interactions. Molecular dynamics simulations focused on FDOR-A and FDOR-B representatives provide a rationale for these findings by showing that the F₄₂₀ tail electrostatically interacts with conserved cationic residues on the surface of mycobacterial F₄₂₀-dependent oxidoreductases; while the diglutamate chain can make sustained electrostatic interactions, the multiple additional transient interactions made by oligoglutarate chain offsets solvation energy and increases binding energy. We made compatible findings across three different protein families in the presence of both physiological and non-physiological substrates. It is therefore probable that the oligoglutarate chain of F₄₂₀ is of general relevance to catalysis of bacterial F₄₂₀-dependent oxidoreductases.

We also observed that higher-affinity cofactor binding modulates reaction kinetics by increasing substrate affinity but decreasing turnover. Such findings likely reflect that mycobacterial F₄₂₀-dependent oxidoreductases mediate catalysis through a ternary complex, with hydride transfer occurring directly between the isoalloxazine headgroup of the cofactor and the substrate (Greening et al., 2016; Mohamed et al., 2016b). If cofactor dissociation is the rate-limiting step in the catalytic cycle of these oxidoreductases, higher-affinity cofactor-enzyme interactions may result in lower cofactor dissociation rates (k_{off}) and hence reduced substrate turnover. It is also plausible that conformational changes caused by the electrostatic interactions are transmitted to the adjoined

isoalloxazine- and substrate-binding sites, thereby modulating substrate affinity; this may be particularly important in FDOR-A proteins, where interactions between the terminal glutamate residues and the lysine-rich loop region may stabilize the split β -barrel fold and in turn the substrate-binding site. The finding that substrate turnover of F₄₂₀-dependent oxidoreductases is accelerated in the presence of short-chain F₄₂₀ is important for biotechnological reasons: it suggests that F₄₂₀ purified from methanogen sources will result in higher turnovers in the various bioremediation and biocatalysis processes for which F₄₂₀-dependent oxidoreductases have been advocated (Taylor et al., 2013; Greening et al., 2016, 2017). A tradeoff would be the reduction in substrate affinity, but this is likely to be negligible for biocatalytic applications given they rely on high substrate concentrations. Obstacles in metabolic engineering must be overcome, however, if short-chain F₄₂₀ is to be heterologously produced at industrially-relevant scales.

Future studies are required to determine whether the observed tradeoffs between affinity and turnover are physiologically relevant. We hypothesize that the oligoglutamate chain ensures the affinity of interactions between cofactor and enzyme remain in the physiologically desirable nanomolar range. In turn, this may increase the substrate specificity of the oxidoreductases that bind the cofactor. In bacterial cells, loss of this chain may compromise specific F₄₂₀-dependent reactions and have wider effects on redox homeostasis and cofactor partitioning. Consistently, studies on nitroimidazole resistance suggest that the enzyme responsible for oligoglutamate chain elongation, CofE (F₄₂₀-O: γ -glutamyl ligase), is required for optimal functionality of F₄₂₀ in mycobacterial cells, though is less important than the other F₄₂₀ biosynthetic enzymes (Haver et al., 2015). In contrast, most methanogens appear to suffice with a diglutamate- rather than oligoglutamate-containing side chain. One explanation is that F₄₂₀-dependent enzymes in such organisms may be less kinetically constrained, given F₄₂₀ serves as the primary catabolic cofactor and is generally present at higher concentrations than in bacterial cells (Thauer et al., 2008). However, further studies are required to understand the significance of the F₄₂₀ diglutamate chain in the catalysis of F₄₂₀-dependent oxidoreductases in methanogens and why Methanosarcinales synthesize longer-chain F₄₂₀ variants (Gorris and van der Drift, 1994).

The observed differences between bacterial and archaeal F₄₂₀ may also be relevant for understanding the evolution of the biosynthesis of deazaflavins. The F₄₂₀ biosynthesis pathway

appears to have undergone a complex evolutionary trajectory, with phylogenetic evidence unable to resolve whether the cofactor originated in bacteria, archaea, or the last universal common ancestor (Nelson-Sathi et al., 2015; Weiss et al., 2016; Ney et al., 2017). We recently proposed that F₀ served as the primordial cofactor in deazaflavin-dependent enzymes, but selective pressure to produce a membrane-impermeable derivative resulted in the evolution of F₄₂₀ biosynthetic enzymes (CofC, CofD, CofE) and in turn the production of short-chain F₄₂₀ (Ney et al., 2017). We propose here that the synthesis of longer-chain derivatives was driven by selection pressure for higher-affinity cofactor-enzyme interactions or more controlled redox homeostasis. This was likely mediated through evolution of the CofE, which is a single-domain enzyme in short-chain F₄₂₀ producers but is fused with an FMN reductase domain in most long-chain producers (Ney et al., 2017); recent structural and kinetic studies on mycobacterial CofE have demonstrated this second domain is essential for elongation of the oligoglutamate chain (Bashiri et al., 2016). It is plausible that the three families of bacterial F₄₂₀-dependent oxidoreductases co-evolved with CofE, resulting in higher-affinity cofactor-enzyme interactions.

AUTHOR CONTRIBUTIONS

CG and AW conceived the study. CG, AW, BN, CC, RS, TJ, JO, and MS designed experiments. BN, TJ, AW, CG, CC, RS, and MS performed experiments. CG and CJ supervised students. CG, AW, BN, JO, TJ, and CJ interpreted data. CG, AW, and BN wrote the paper.

FUNDING

This work was supported by a CSIRO Office of the Chief Executive Postdoctoral Fellowship and an ARC DECRA Fellowship (DE170100310) awarded to CG, a Marsden Grant (GNS-035) awarded to CC, and Australian Research Council grants (DE120102673, DP130102144) awarded to CJ.

SUPPLEMENTARY MATERIAL

The Supplementary Material for this article can be found online at: <http://journal.frontiersin.org/article/10.3389/fmicb.2017.01902/full#supplementary-material>

REFERENCES

- Ahmed, F. H., Carr, P. D., Lee, B. M., Afriat-Jurnou, L., Mohamed, A. E., Hong, N.-S., et al. (2015). Sequence-structure-function classification of a catalytically diverse oxidoreductase superfamily in mycobacteria. *J. Mol. Biol.* 427, 3554–3571. doi: 10.1016/j.jmb.2015.09.021
- Ahmed, F. H., Mohamed, A. E., Carr, P. D., Lee, B. M., Condic-Jurkic, K., O'Mara, M. L., et al. (2016). Rv2074 is a novel F₄₂₀H₂-dependent biliverdin reductase in *Mycobacterium tuberculosis*. *Protein Sci.* 25, 1692–1709. doi: 10.1002/pro.2975
- Ashton, W. T., Brown, R. D., Jacobson, F., and Walsh, C. (1979). Synthesis of 7,8-didemethyl-8-hydroxy-5-deazariboflavin. *J. Am. Chem. Soc.* 101, 4419–4420. doi: 10.1021/ja00509a083
- Bair, T. B., Isabelle, D. W., and Daniels, L. (2001). Structures of coenzyme F₄₂₀ in *Mycobacterium* species. *Arch. Microbiol.* 176, 37–43. doi: 10.1007/s002030100290
- Bashiri, G., Rehan, A. M., Greenwood, D. R., Dickson, J. M. J., and Baker, E. N. (2010). Metabolic engineering of cofactor F₄₂₀ production in *Mycobacterium smegmatis*. *PLOS ONE* 5:e15803. doi: 10.1371/journal.pone.0015803

- Bashiri, G., Rehan, A. M., Sreebhavan, S., Baker, H. M., Baker, E. N., and Squire, C. J. (2016). Elongation of the poly-gamma-glutamate tail of F₄₂₀ requires both domains of the F₄₂₀:gamma-glutamyl ligase (FbiB) of *Mycobacterium tuberculosis*. *J. Biol. Chem.* 291, 6882–6894. doi: 10.1074/jbc.M115.689026
- Bashiri, G., Squire, C. J., Moreland, N. J., and Baker, E. N. (2008). Crystal structures of F₄₂₀-dependent glucose-6-phosphate dehydrogenase FGD1 involved in the activation of the anti-tuberculosis drug candidate PA-824 reveal the basis of coenzyme and substrate binding. *J. Biol. Chem.* 283, 17531–17541. doi: 10.1074/jbc.M801854200
- Cellitti, S. E., Shaffer, J., Jones, D. H., Mukherjee, T., Gurumurthy, M., Bursulaya, B., et al. (2012). Structure of Ddn, the deazaflavin-dependent nitroreductase from *Mycobacterium tuberculosis* involved in bioreductive activation of PA-824. *Structure* 20, 101–112. doi: 10.1016/j.str.2011.11.001
- Ebert, S., Rieger, P.-G., and Knackmuss, H.-J. (1999). Function of coenzyme F₄₂₀ in aerobic catabolism of 2,4,6-trinitrophenol and 2,4-dinitrophenol by *Nocardioides simplex* FJ2-1A. *J. Bacteriol.* 181, 2669–2674.
- Eirich, L. D., Vogels, G. D., and Wolfe, R. S. (1978). Proposed structure for coenzyme F₄₂₀ from *Methanobacterium*. *Biochemistry* 17, 4583–4593. doi: 10.1021/bi00615a002
- Forouhar, F., Abashidze, M., Xu, H., Grochowski, L. L., Seetharaman, J., Hussain, M., et al. (2008). Molecular insights into the biosynthesis of the F₄₂₀ coenzyme. *J. Biol. Chem.* 283, 11832–11840. doi: 10.1074/jbc.M710352200
- Gorris, L. G., and van der Drift, C. (1994). Cofactor contents of methanogenic bacteria reviewed. *Biofactors* 4, 139–145.
- Graupner, M., and White, R. H. (2001). Biosynthesis of the phosphodiester bond in coenzyme F₄₂₀ in the methanoarchaea. *Biochemistry* 40, 10859–10872. doi: 10.1021/bi0107703
- Greening, C., Ahmed, F. H., Mohamed, A. E., Lee, B. M., Pandey, G., Warden, A. C., et al. (2016). Physiology, biochemistry, and applications of F₄₂₀- and F₀-dependent redox reactions. *Microbiol. Mol. Biol. Rev.* 80, 451–493. doi: 10.1128/MMBR.00070-15
- Greening, C., Jirapanjawan, T., Afroze, S., Ney, B., Scott, C., Pandey, G., et al. (2017). Mycobacterial F₄₂₀H₂-dependent reductases promiscuously reduce diverse compounds through a common mechanism. *Front. Microbiol.* 8:1000. doi: 10.3389/fmicb.2017.01000
- Grochowski, L. L., Xu, H., and White, R. H. (2008). Identification and characterization of the 2-phospho-L-lactate guanylyltransferase involved in coenzyme F₄₂₀ biosynthesis. *Biochemistry* 47, 3033–3037. doi: 10.1021/bi702475t
- Haver, H. L., Chua, A., Ghode, P., Lakshminarayana, S. B., Singhal, A., Mathema, B., et al. (2015). Mutations in genes for the F₄₂₀ biosynthetic pathway and a nitroreductase enzyme are the primary resistance determinants in spontaneous *in vitro*-selected PA-824-resistant mutants of *Mycobacterium tuberculosis*. *Antimicrob. Agents Chemother.* 59, 5316–5323. doi: 10.1128/AAC.00308-15
- Humphrey, W., Dalke, A., and Schulten, K. (1996). VMD: visual molecular dynamics. *J. Mol. Graph.* 14, 33–38. doi: 10.1016/0263-7855(96)00018-5
- Ikeno, S., Aoki, D., Hamada, M., Hori, M., and Tsuchiya, K. S. (2006). DNA sequencing and transcriptional analysis of the kasugamycin biosynthetic gene cluster from *Streptomyces kasugaensis* M338-M1. *J. Antibiot.* 59, 18–28. doi: 10.1038/ja.2006.4
- Isabelle, D., Simpson, D. R., and Daniels, L. (2002). Large-scale production of coenzyme F₄₂₀-5,6 by using *Mycobacterium smegmatis*. *Appl. Environ. Microbiol.* 68, 5750–5755. doi: 10.1128/AEM.68.11.5750-5755.2002
- Jacobson, F., and Walsh, C. (1984). Properties of 7,8-didemethyl-8-hydroxy-5-deazaflavins relevant to redox coenzyme function in methanogen metabolism. *Biochemistry* 23, 979–988. doi: 10.1021/bi00300a028
- Jirapanjawan, T., Ney, B., Taylor, M. C., Warden, A. C., Afroze, S., Russell, R. J., et al. (2016). The redox cofactor F₄₂₀ protects mycobacteria from diverse antimicrobial compounds and mediates a reductive detoxification system. *Appl. Environ. Microbiol.* 82, 6810–6818. doi: 10.1128/AEM.02500-16
- Källberg, M., Wang, H., Wang, S., Peng, J., Wang, Z., Lu, H., et al. (2012). Template-based protein structure modeling using the RaptorX web server. *Nat. Protoc.* 7, 1511–1522. doi: 10.1038/nprot.2012.085
- Kelley, L. A., Mezulis, S., Yates, C. M., Wass, M. N., and Sternberg, M. J. E. (2015). The Phyre2 web portal for protein modeling, prediction and analysis. *Nat. Protoc.* 10, 845–858. doi: 10.1038/nprot.2015.053
- Leys, D., and Scrutton, N. S. (2016). Sweating the assets of flavin cofactors: new insight of chemical versatility from knowledge of structure and mechanism. *Curr. Opin. Struct. Biol.* 41, 19–26. doi: 10.1016/j.sbi.2016.05.014
- Liesegang, H., Kaster, A.-K., Wiezer, A., Goenrich, M., Wollherr, A., Seedorf, H., et al. (2010). Complete genome sequence of *Methanothermobacter marburgensis*, a methanoarchaeon model organism. *J. Bacteriol.* 192, 5850–5851. doi: 10.1128/JB.00844-10
- Maier, J. A., Martinez, C., Kasavajhala, K., Wickstrom, L., Hauser, K. E., and Simmerling, C. (2015). ff14SB: improving the accuracy of protein side chain and backbone parameters from ff99SB. *J. Chem. Theory Comput.* 11, 3696–3713. doi: 10.1021/acs.jctc.5b00255
- Mashalidis, E. H., Gittis, A. G., Tomczak, A., Abell, C., Barry, C. E., and Garboczi, D. N. (2015). Molecular insights into the binding of coenzyme F₄₂₀ to the conserved protein Rv1155 from *Mycobacterium tuberculosis*. *Protein Sci.* 24, 729–740. doi: 10.1002/pro.2645
- Mohamed, A. E., Ahmed, F. H., Arulmozhiraja, S., Lin, C. Y., Taylor, M. C., Krausz, E. R., et al. (2016a). Protonation state of F₄₂₀H₂ in the prodrug-activating deazaflavin dependent nitroreductase (Ddn) from *Mycobacterium tuberculosis*. *Mol. Biosyst.* 12, 1110–1113. doi: 10.1039/c6mb00033a
- Mohamed, A. E., Condic-Jurkic, K., Ahmed, F. H., Yuan, P., O'Mara, M. L., Jackson, C. J., et al. (2016b). Hydrophobic shielding drives catalysis of hydride transfer in a family of F₄₂₀H₂-dependent enzymes. *Biochemistry* 55, 6908–6918.
- Morris, G. M., Huey, R., Lindstrom, W., Sanner, M. F., Belew, R. K., Goodsell, D. S., et al. (2009). AutoDock4 and AutoDockTools4: automated docking with selective receptor flexibility. *J. Comput. Chem.* 30, 2785–2791. doi: 10.1002/jcc.21256
- Nelson-Sathi, S., Sousa, F. L., Roettger, M., Lozada-Chavez, N., Thiergart, T., Janssen, A., et al. (2015). Origins of major archaeal clades correspond to gene acquisitions from bacteria. *Nature* 517, 77–80. doi: 10.1038/nature13805
- Ney, B., Ahmed, F. H., Carere, C. R., Biswas, A., Warden, A. C., Morales, S. E., et al. (2017). The methanogenic redox cofactor F₄₂₀ is widely synthesized by aerobic soil bacteria. *ISME J.* 11, 125–137. doi: 10.1038/ismej.2016.100
- Nocek, B., Evdokimova, E., Proudfoot, M., Kudritska, M., Grochowski, L. L., White, R. H., et al. (2007). Structure of an amide bond forming F₄₂₀:γ-glutamyl ligase from *Archaeoglobus fulgidus* - a member of a new family of non-ribosomal peptide synthetases. *J. Mol. Biol.* 372, 456–469. doi: 10.1016/j.jmb.2007.06.063
- Pettersen, E. F., Goddard, T. D., Huang, C. C., Couch, G. S., Greenblatt, D. M., Meng, E. C., et al. (2004). UCSF Chimera—a visualization system for exploratory research and analysis. *J. Comput. Chem.* 25, 1605–1612. doi: 10.1002/jcc.20084
- Purwantini, E., Daniels, L., and Mukhopadhyay, B. (2016). F₄₂₀H₂ is required for phthiocerol dimycocerosate synthesis in mycobacteria. *J. Bacteriol.* 198, 2020–2028. doi: 10.1128/JB.01035-15
- Purwantini, E., and Mukhopadhyay, B. (2013). Rv0132c of *Mycobacterium tuberculosis* encodes a coenzyme F₄₂₀-dependent hydroxymycolic acid dehydrogenase. *PLOS ONE* 8:e81985. doi: 10.1371/journal.pone.0081985
- Selengut, J. D., and Haft, D. H. (2010). Unexpected abundance of coenzyme F₄₂₀-dependent enzymes in *Mycobacterium tuberculosis* and other actinobacteria. *J. Bacteriol.* 192, 5788–5798. doi: 10.1128/JB.00425-10
- Sievers, F., Wilm, A., Dineen, D., Gibson, T. J., Karplus, K., Li, W., et al. (2011). Fast, scalable generation of high-quality protein multiple sequence alignments using Clustal Omega. *Mol. Syst. Biol.* 7, 539. doi: 10.1038/msb.2011.75
- Sparling, R., Blaut, M., and Gottschalk, G. (1993). Bioenergetic studies of *Methanospiraeta stadtmanae*, an obligate H₂-methanol utilising methanogen. *Can. J. Microbiol.* 39, 742–748. doi: 10.1139/m93-109
- Taylor, M. C., Jackson, C. J., Tattersall, D. B., French, N., Peat, T. S., Newman, J., et al. (2010). Identification and characterization of two families of F₄₂₀H₂-dependent reductases from *Mycobacteria* that catalyze aflatoxin

- degradation. *Mol. Microbiol.* 78, 561–575. doi: 10.1111/j.1365-2958.2010.07356.x
- Taylor, M. C., Scott, C., and Grogan, G. (2013). F₄₂₀-dependent enzymes - potential for applications in biotechnology. *Trends Biotechnol.* 31, 63–64. doi: 10.1016/j.tibtech.2012.09.003
- Thauer, R. K., Kaster, A.-K., Seedorf, H., Buckel, W., and Hedderich, R. (2008). Methanogenic archaea: ecologically relevant differences in energy conservation. *Nat. Rev. Microbiol.* 6, 579–591. doi: 10.1038/nrmicro1931
- Walsh, C. (1986). Naturally occurring 5-deazaflavin coenzymes: biological redox roles. *Acc. Chem. Res.* 19, 216–221. doi: 10.1021/ar00127a004
- Wang, P., Bashiri, G., Gao, X., Sawaya, M. R., and Tang, Y. (2013). Uncovering the enzymes that catalyze the final steps in oxytetracycline biosynthesis. *J. Am. Chem. Soc.* 135, 7138–7141. doi: 10.1021/ja403516u
- Weiss, M. C., Sousa, F. L., Mrnjavac, N., Neukirchen, S., Roettger, M., Nelson-Sathi, S., et al. (2016). The physiology and habitat of the last universal common ancestor. *Nat. Microbiol.* 1, 16116. doi: 10.1038/nmicrobiol.2016.116
- Conflict of Interest Statement:** The authors declare that the research was conducted in the absence of any commercial or financial relationships that could be construed as a potential conflict of interest.
- Copyright © 2017 Ney, Carere, Sparling, Jirapanjawat, Stott, Jackson, Oakeshott, Warden and Greening. This is an open-access article distributed under the terms of the Creative Commons Attribution License (CC BY). The use, distribution or reproduction in other forums is permitted, provided the original author(s) or licensor are credited and that the original publication in this journal is cited, in accordance with accepted academic practice. No use, distribution or reproduction is permitted which does not comply with these terms.



OPEN ACCESS

Edited by:

Daniela De Biase,
Sapienza Università di Roma, Italy

Reviewed by:

Hans-Peter Kohler,
Swiss Federal Institute of Aquatic
Science and Technology, Switzerland
Alberto A. Iglesias,
National University of the Littoral,
Argentina

*Correspondence:

Willem J. H. van Berkel
willem.vanberkel@wur.nl

†Present address:

Stefania Montersino,
Adienne Pharma & Biotech, Milan,
Italy;
Evelien te Poele and Lubbert
Dijkhuizen,
CarbExplore Research BV, Groningen,
Netherlands;
Roberto Orru,
Institute of Molecular Biology,
Johannes Gutenberg University,
Mainz, Germany;
Robert van der Geize,
Laboratory of Pathology
East-Netherlands, Hengelo,
Netherlands
‡These authors have contributed
equally to this work.

Specialty section:

This article was submitted to
Microbial Physiology and Metabolism,
a section of the journal
Frontiers in Microbiology

Received: 20 April 2017

Accepted: 31 May 2017

Published: 16 June 2017

Citation:

Montersino S, te Poele E, Orru R,
Westphal AH, Barendregt A,
Heck AJR, van der Geize R,
Dijkhuizen L, Mattevi A and
van Berkel WJH (2017)
3-Hydroxybenzoate 6-Hydroxylase
from *Rhodococcus jostii* RHA1
Contains a Phosphatidylinositol
Cofactor. *Front. Microbiol.* 8:1110.
doi: 10.3389/fmicb.2017.01110

3-Hydroxybenzoate 6-Hydroxylase from *Rhodococcus jostii* RHA1 Contains a Phosphatidylinositol Cofactor

Stefania Montersino^{1†}, Evelien te Poele^{2†}, Roberto Orru^{3†}, Adrie H. Westphal¹,
Arjan Barendregt⁴, Albert J. R. Heck⁴, Robert van der Geize^{2†}, Lubbert Dijkhuizen^{2†},
Andrea Mattevi³ and Willem J. H. van Berkel^{1*}

¹ Laboratory of Biochemistry, Wageningen University and Research, Wageningen, Netherlands, ² Microbial Physiology,
Groningen Biomolecular Sciences and Biotechnology Institute, University of Groningen, Groningen, Netherlands,

³ Department of Biology and Biotechnology, University of Pavia, Pavia, Italy, ⁴ Biomolecular Mass Spectrometry and
Proteomics, Bijvoet Center for Biomolecular Research and Utrecht Institute for Pharmaceutical Research, Utrecht University,
Utrecht, Netherlands

3-Hydroxybenzoate 6-hydroxylase (3HB6H, EC 1.13.14.26) is a FAD-dependent monooxygenase involved in the catabolism of aromatic compounds in soil microorganisms. 3HB6H is unique among flavoprotein hydroxylases in that it harbors a phospholipid ligand. The purified protein obtained from expressing the gene encoding 3HB6H from *Rhodococcus jostii* RHA1 in the host *Escherichia coli* contains a mixture of phosphatidylglycerol and phosphatidylethanolamine, which are the major constituents of *E. coli*'s cytoplasmic membrane. Here, we purified 3HB6H (Rj3HB6H) produced in the host *R. jostii* RHA#2 by employing a newly developed actinomycete expression system. Biochemical and biophysical analysis revealed that Rj3HB6H possesses similar catalytic and structural features as 3HB6H, but now contains phosphatidylinositol, which is a specific constituent of actinomycete membranes. Native mass spectrometry suggests that the lipid cofactor stabilizes monomer-monomer contact. Lipid analysis of 3HB6H from *Pseudomonas alcaligenes* NCIMB 9867 (Pa3HB6H) produced in *E. coli* supports the conclusion that 3HB6H enzymes have an intrinsic ability to bind phospholipids with different specificity, reflecting the membrane composition of their bacterial host.

Keywords: expression strain, flavoprotein, monooxygenase, phospholipid, *Rhodococcus*

INTRODUCTION

Rhodococcus jostii RHA1 is a biotechnologically and environmentally important bacterium from the order Actinomycetales. Together with the genera *Nocardia*, *Corynebacterium* and *Mycobacterium*, *Rhodococcus* forms a distinct group of bacteria called mycolata (Finnerty, 1992; Brennan and Nikaido, 1995; Chun et al., 1996; Gürtler et al., 2004), characterized by a complex

Abbreviations: 3HB6H, recombinant 3-hydroxybenzoate 6-hydroxylase from *Rhodococcus jostii* RHA1 produced in *Escherichia coli*; Pa3HB6H, recombinant 3-hydroxybenzoate 6-hydroxylase from *Pseudomonas alcaligenes* NCIMB 9867 produced in *Escherichia coli*; PE, phosphatidylethanolamine; PG, phosphatidylglycerol; PI, phosphatidylinositol; Rj3HB6H, recombinant 3-hydroxybenzoate 6-hydroxylase from *Rhodococcus jostii* RHA1 produced in *Rhodococcus jostii* RHA1#2.

cell envelope (Sutcliffe, 1998; Guerin et al., 2010; De Carvalho et al., 2014) and an impressive catabolic diversity, allowing adaptation to different carbon sources for growth (van der Geize and Dijkhuizen, 2004). In comparison with other mycolata, *R. jostii* RHA1 is particularly rich in oxygenases (203 putative genes) and ligases (192 putative genes), gained primarily through ancient gene duplications or acquisitions (McLeod et al., 2006; Yam et al., 2010).

We recently reported the crystal structure of *R. jostii* RHA1 3-hydroxybenzoate 6-hydroxylase (3HB6H), produced as a recombinant protein in *Escherichia coli* (MonTERSINO et al., 2013). 3HB6H (EC 1.13.14.26) is a NADH and FAD-dependent monooxygenase that catalyzes the *para*-hydroxylation of 3-hydroxybenzoate to 2,5-dihydroxybenzoate, using a Tyr-His pair for substrate binding and catalysis (Sucharitakul et al., 2015). The crystal structure analysis revealed that 3HB6H has the conserved fold of group A flavoprotein hydroxylases (MonTERSINO et al., 2011; Huijbers et al., 2014), but differs from the other family members in additional binding of phospholipids. The tightly bound phospholipids were identified as a mixture of PG and PE, which are the major constituents of the *E. coli* cytoplasmic membrane (Pulfer and Murphy, 2003; Oursel et al., 2007). The fatty acyl chains of the phospholipid ligands of 3HB6H protrude into the substrate-binding pockets, whereas the surface-exposed hydrophilic headgroups are involved in enzyme dimerization (Figure 1) (MonTERSINO et al., 2013).

To shed more light on the role of these lipid guests, bearing in mind the different lipid compositions of Gram-positive and Gram-negative bacterial membranes (Finnerty, 1992; Sutcliffe, 1998), in the present work we produced Rj3HB6H in a newly developed *R. jostii* RHA1#2 expression strain and, in addition, 3HB6H from *Pseudomonas alcaligenes* NCIMB 9867 (*Pa*3HB6H) in *E. coli*. Biochemical and biophysical characterization revealed that Rj3HB6H possesses similar catalytic and structural features as 3HB6H, but contains PI as glycerophospholipid ligand. Lipid analysis of *Pa*3HB6H indicates that lipid binding is an intrinsic property of prokaryotic 3-hydroxybenzoate 6-hydroxylases.

MATERIALS AND METHODS

Chemicals

Aromatic compounds were purchased from Sigma-Aldrich (St Louis, MO, United States) and Acros Organics (Morris Plains, NJ, United States). Catalase, FAD, FMN, arabinose, antibiotics, Terrific broth (TB) and LB broth (Miller) (LB) were from Sigma-Aldrich (St Louis, MO, United States). Pefabloc SC and DNase I were obtained from Roche Diagnostics GmbH (Mannheim, Germany). Restriction enzymes and *Pfu* DNA polymerase were from Thermo Fischer Scientific (United States). 4-androstene-3,17-dione was from Merck (Oss, Netherlands). Crystallization kits were purchased from New Hampton (Aliso Viejo, CA, United States). Immobilized metal affinity chromatography columns (His GraviTrap) were from GE Healthcare Bioscience AB (Uppsala, Sweden). All other chemicals were from commercial sources and of the purest grade available.

Bacterial Strains and Primers

All bacterial strains and primers used in this study are listed in Tables 1, 2.

Construction of *Rhodococcus* Expression Vector Q2+

The *E. coli*-*Rhodococcus* shuttle vector pRESQ (van der Geize et al., 2002) was modified by insertion of the RP4 *oriT* of pK18*mobsacB* (Schäfer et al., 1994) enabling trans-conjugal transfer of the resulting vector. For this, the *oriT*-region was amplified from pK18*mobsacB* by PCR using forward primer *oriT*-F and reverse primer *oriT*-R (Table 1). The obtained 549 bp PCR-product was cloned into the *Sma*I-site of pRESQ, resulting in pQmob. A duplicate region of 424 bp on pQmob was removed by deleting the 760 bp *Xba*I-*Bsp*HI fragment, yielding pQmobΔd. The *egfp* gene from pIJ8630 (Sun et al., 1999) was amplified by PCR using forward primer *egfp*-*Pci*I-F, containing a *Pci*I restriction site, and reverse primer *egfp*-*Pci*I-R, also containing a *Pci*I restriction site (Table 1). The 744 bp *Pci*I-*Pci*I fragment containing the *egfp* gene was cloned into the *Pci*I-site of pQmobΔd to generate pEGFPQ.

The *R. jostii* strain RHA1 genomic region consisting of gene *ro00440*, its promoter region and the *prmA* promoter (*PprmA*) (here referred to as region *reg1-PprmA*; GenBank accession number CP000431: nt 521345 - nt 523358) was amplified from genomic DNA of *R. jostii* RHA1 by PCR using forward primer *reg1*-*Bgl*II-F, containing a *Bgl*II restriction site, and reverse primer *prmA*-*Nde*I-R, containing an *Nde*I restriction site (Table 1). The 2014 bp *Bgl*II-*Nde*I *reg1-PprmA* fragment was cloned into the *Bgl*II-*Nde*I sites of pEGFPQ, yielding prMOeGFPQ1.

The *R. jostii* RHA1 gene *ro00452* and its promoter region (here referred to as region *reg2*; CP000431: nt 534363 - nt 536227) were amplified by PCR using forward primer *reg2*-*Pci*I-F, containing a *Pci*I restriction site and reverse primer *reg2*-*Pci*I-R, also containing a *Pci*I restriction site (Table 1). The 1880 bp *Pci*I-*Pci*I *reg2* fragment was cloned into the *Pci*I-site of prMOeGFPQ1, resulting in prMOeGFPQ2.

For construction of expression vector Q2+, the *egfp* gene of prMOeGFPQ2 was replaced with a multiple cloning site (MCS). For this, part of the MCS of pBluescript KS was amplified by PCR using forward primer MCS-*Nde*I-F, containing an *Nde*I restriction site and reverse primer MCS-*Pci*I-R, containing a *Pci*I restriction site (Table 1). The 125 bp *Nde*I-*Pci*I MCS fragment was cloned into the *Nde*I-*Pci*I site of prMOeGFPQ2, replacing the *Nde*I-*Pci*I region containing *egfp*, resulting in the expression vector Q2+.

Cloning and Production of 3HB6H in *R. jostii* RHA1#2

The 1321 bp *Nde*I-*Xmn*I fragment of pBAD-3HB6H-His₆ (MonTERSINO and van Berkel, 2012) containing the 3HB6H gene including the His₆-tag, was cloned into the *Nde*I-*Hind*III (Klenow-fragment treated) site of expression vector Q2+ to generate Q2+-3HB6H-His₆.

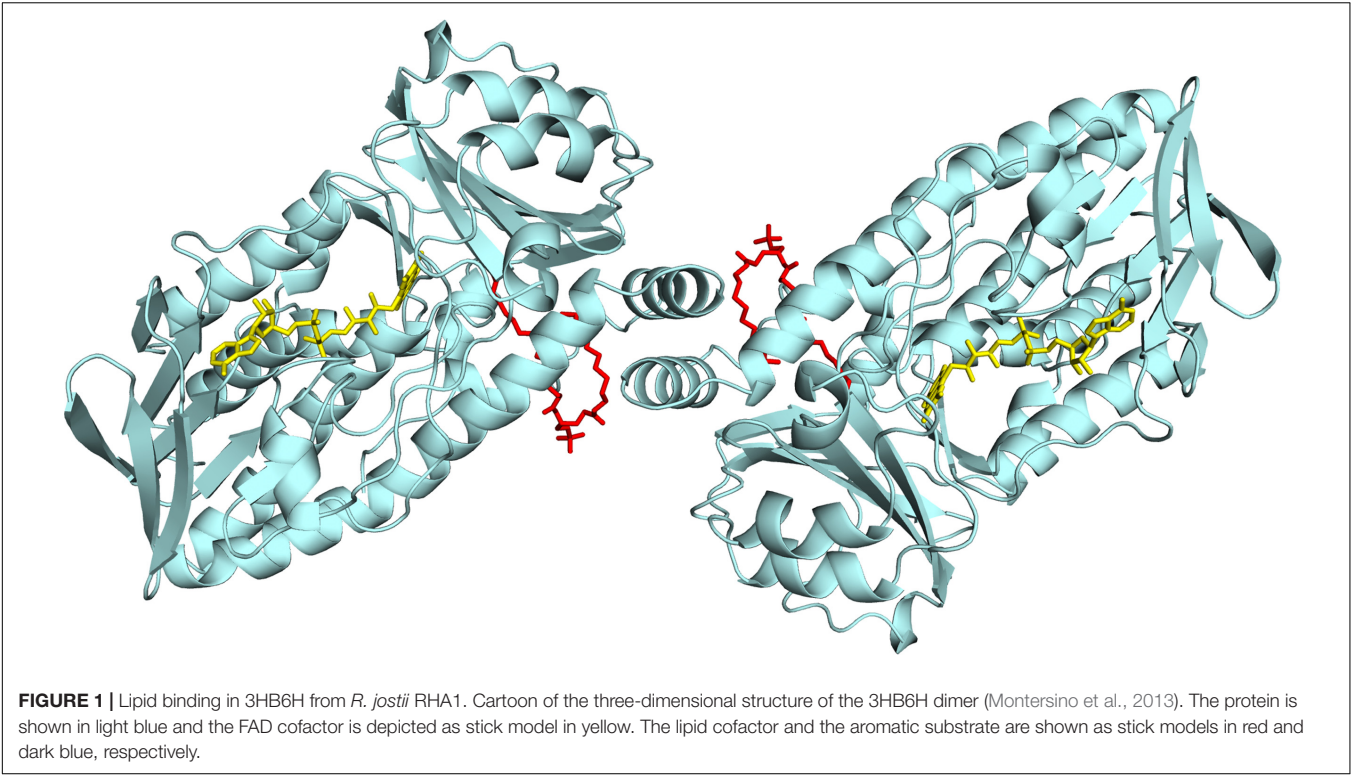


TABLE 1 | List of primers used in PCR.

<i>oriT</i> -F	5'-CATAGTCCACGACGCC-3'
<i>oriT</i> -R	5'-TCTTTGGCATCGTCTCTCG-3'
<i>egfp-Pcil</i> -F	5'-GCACATGTCGGAGGTCCATATGGCCATGGT-3'
<i>egfp-Pcil</i> -R	5'-GCACATGTATTACTTGTACAGCTCGTCCATGC-3'
<i>reg1-BglII</i> -F	5'-GGAGATCTGACATTCGCGGATACG-3'
<i>prmA-NdeI</i> -R	5'-GGCATATGTGCGCTCTCTGGATCG-3'
<i>reg2-Pcil</i> -F	5'-GGACATGTCCGGTCTCCACCACCCGCTCT-3'
<i>reg2-Pcil</i> -R	5'-GGACATGTGCGGTGCGGGCGACGTCATATGTCG-3'
<i>MCS-NdeI</i> -F	5'-TTGCATATGCACCGCGGTGGC-3'
<i>MCS-Pcil</i> -R	5'-GGGAACATGTGCTGGGTACC-3'

TABLE 2 | List of bacterial strains.

<i>R. jostii</i> RHA1	The complete genome of <i>Rhodococcus</i> sp. RHA1 provides insights into a catabolic powerhouse. (McLeod et al., 2006)
<i>R. jostii</i> strain RHA1#2	Used as a host for protein production. This strain is a spontaneous mutant of <i>R. jostii</i> RHA1, carrying deletions of ~0.9 Mb on the 1.12 Mb linear plasmid pRHL1 and ~0.2 Mb on the 0.44 Mb linear plasmid pRHL2. The deletions together comprise ~11.3% of the 9.7 Mb <i>R. jostii</i> genome.
<i>E. coli</i> DH5α	Used as host for cloning procedures.
<i>E. coli</i> TOP10	Used for production of 3HB6H (MonTERSINO and van Berkel, 2012) and <i>Pa</i> 3HB6H.

Rhodococcus cells were electroporated as described previously (van der Geize et al., 2000). Prior to electroporation, plasmid DNA was desalted by dialyzing 10 μL plasmid DNA for 30 min

on a Millipore “V” Series filter disk (0.025 μm) floating on MiliQ water.

Cultures of *R. jostii* RHA1#2 were grown in LB broth supplemented with 50 μg·mL⁻¹ kanamycin at 30°C at 200 rpm. *R. jostii* RHA1#2 cells harboring Q2+3HB6H-His₆ were grown overnight in 3 mL LB broth, diluted 1:300 in 300 mL LB broth in a 3 L Erlenmeyer flask and grown for 20–24 h. Cultures were induced by adding 2 mM 4-androstene-3,17-dione dissolved in acetone. Growth was continued for 48 h after induction. Cells were harvested by centrifugation at 4°C and pellets were washed once with ice-cold 20 mM potassium phosphate, pH 7.2, containing 300 mM NaCl. After centrifugation at 4°C, cells were stored at –20°C.

Cloning and Production of 3HB6H from *Pseudomonas alcaligenes* NCIMB 9867

The *xlnD* gene sequence encoding for *Pa*3HB6H (UniProt: Q9F131) was synthesized and subcloned in a pBAD vector by GeneArt (Invitrogen, Carlsbad, CA, United States). The resulting construct (pBAD-*Pa*3HB6H-His₆) was verified by automated sequencing of both strands and electroporated into *E. coli* TOP10 cells for recombinant expression.

For enzyme production, *E. coli* TOP10 cells, harboring the pBAD-*Pa*3HB6H-His₆ plasmid, were grown in TB medium at 37°C supplemented with 100 μg·mL⁻¹ ampicillin until an optical density (OD_{600 nm}) of 0.8 was reached. Expression was induced by the addition of 0.02% (w/v) arabinose and incubation was continued for 40 h at 17°C. Cells were harvested by centrifugation at 4°C and stored at –20°C.

Enzyme Purification

Rj3HB6H was purified to apparent homogeneity using an Äkta Explorer chromatography system (GE-Healthcare). *R. jostii* RHA1#2 cells containing the recombinant protein were suspended in ice-cold 20 mM potassium phosphate, pH 7.2, containing 300 mM NaCl, 1 mM Pefabloc SC, 1 mg DNase and 100 μ M $MgCl_2$, and subsequently passed twice through a precooled French Pressure cell (SLM Aminco, SLM Instruments, Urbana, IL, United States) at 16,000 psi. The resulting homogenate was centrifuged at $25,000 \times g$ for 45 min at 4°C to remove cell debris, and the supernatant was applied onto a Ni-NTA agarose column (16 mm \times 50 mm) equilibrated with 20 mM potassium phosphate, pH 7.2, containing 300 mM NaCl. After washing with five volumes of equilibration buffer, the enzyme was eluted with 300 mM imidazole in equilibration buffer. The resulting *Rj3HB6H* fraction was supplemented with 100 μ M FAD and loaded onto a Source Q-15 anion exchange column (16 mm \times 90 mm), pre-equilibrated with 50 mM Bis-Tris, 0.1 mM EDTA, pH 7.2. After washing with two volumes of equilibrating buffer, the enzyme was eluted with a linear gradient of 0–1 M NaCl in the same buffer. Active fractions were pooled, concentrated to 10 mg·mL⁻¹ using ultrafiltration (Amicon 30 kDa cutoff filter), and applied onto a Superdex S-200 (26 mm \times 600 mm) column running in 50 mM potassium phosphate, 150 mM NaCl, pH 7.2. Active fractions were concentrated to 10 mg·mL⁻¹ using ultrafiltration (Amicon 30 kDa cutoff filter) and dialyzed at 4°C against 50 mM Bis-Tris, pH 7.2. The final *Rj3HB6H* preparation showed a single band after SDS-PAGE. The specific activity of the purified enzyme was 21 U mg⁻¹ using the standard activity assay (Table 3A).

Pa3HB6H was purified to apparent homogeneity, applying essentially the same procedure as described above for *Rj3HB6H*. The final *Pa3HB6H* preparation showed a single band after SDS-PAGE. The specific activity of the purified enzyme was 34 U·mg⁻¹ using the standard activity assay (Table 3B).

Purified enzymes were flash frozen in 1 mL aliquots in liquid nitrogen and stored at -80°C. Before use, thawed enzyme samples were incubated with 0.1 mM FAD and excess FAD was removed using a gel filtration column (10 mm \times 100 mm) containing Bio-Gel P-6DG.

Biochemical Characterization

Molar absorption coefficients of protein-bound FAD were determined from absorption spectra of *Rj3HB6H* and *Pa3HB6H* recorded in the presence and absence of 0.1% (w/v) SDS, assuming a molar absorption coefficient for free FAD of 11.3 mM⁻¹·cm⁻¹ at 450 nm. The enzyme concentration of *Rj3HB6H* was determined by measuring the absorbance at 453 nm using a molar absorption coefficient for protein-bound FAD of 10.3 mM⁻¹·cm⁻¹. The enzyme concentration of *Pa3HB6H* was determined by measuring the absorbance at 450 nm using a molar absorption coefficient for protein-bound FAD of 11.0 mM⁻¹·cm⁻¹. *Rj3HB6H* and *Pa3HB6H* activity was determined at 25°C by measuring NADH consumption at 360 nm (MonTERSINO and van BERKEL, 2012). The standard assay mixture contained 50 mM Tris-SO₄, pH 8.0, 200 μ M

4-hydroxybenzoate and 250 μ M NADH. Steady-state kinetic parameters were determined from measurements at 25°C in 50 mM Tris-SO₄, pH 8.0. Hydroxylation efficiencies were determined by oxygen consumption experiments, essentially as described before (MonTERSINO and van BERKEL, 2012).

Crystallization and Structure Determination

Crystals of *Rj3HB6H* for structure determination were obtained by the sitting drop vapor diffusion method at 20°C by mixing equal volumes (2 μ L) of protein and reservoir solutions. Protein solutions consisted of 30 mg·mL⁻¹ enzyme in 1 mM FAD, 2 mM 3-hydroxybenzoate, and 50 mM Bis-Tris, pH 7.2, whereas precipitant solutions consisted of 30% PEG 4000, 0.2 M lithium sulfate, and 0.1 M Tris-HCl, pH 8.5. Yellow crystals grew in 1 day.

X-ray diffraction data were collected at Grenoble and processed with the CCP4 package (Winn et al., 2011). The *Rj3HB6H* structure was solved by molecular replacement using the structure of a monomer of 3HB6H (pdb entry: 4BJZ) as search model. Crystallographic computing and model analysis were performed with COOT (Emsley et al., 2010), PHENIX (Adams et al., 2010) and the CCP4 package (Potterton et al., 2004). Pictures were generated with Pymol (Schrodinger, 2015) and CCP4 (Potterton et al., 2004). Data collection parameters and refinement statistics are presented in Table 4.

The atomic coordinates and structure factors of *Rj3HB6H* (code 5HYM) have been deposited in the Protein Data Bank¹.

Lipid Identification and Native ESI-MS Experiments

Extraction and identification of protein-bound lipids from *Rj3HB6H* and *Pa3HB6H* was performed as described for 3HB6H (MonTERSINO et al., 2013). For nanoflow ESI-MS analysis under native conditions, enzyme samples were prepared in 50 mM ammonium acetate, pH 6.8. For analysis under denaturing conditions, enzyme samples were diluted either in 50% acetonitrile with 0.2% formic acid or in 5% formic acid. Native MS analysis was performed using a LC-T nanoflow ESI orthogonal TOF mass spectrometer (Micromass, Manchester, United Kingdom) in positive ion mode with a capillary voltage of 1.3 kV. The cone voltage was varied between 90 and 150 V and source pressure was set to 6.9 mbar to enhance transmission of large ions. Lipid identification was performed using a Quattro Ultima nanoflow triple quadrupole mass spectrometer (Micromass, Manchester, United Kingdom) in negative ion mode, with a capillary voltage of 1.3 kV and a cone voltage of 150 V. For MS/MS analysis, argon was supplied in the collision cell (2.0×10^{-3} bar). Collision energy was adjusted to gain optimal fragmentation. Both mass spectrometers were equipped with a Z-spray nano-electrospray ionization source. Measurements were performed by using gold-coated needles, made from borosilicate glass capillaries (Kwik-Fill; World precision Instruments, Sarasota) on a P-97 puller (from Sutter Instruments, Novato, CA, United States). Needles were coated

¹<http://pdbe.org/5HYM>

with a gold layer using an Edwards Scancoat six Pirani 501 sputter coater (Edwards laboratories, Milpitas, CA, United States). All TOF spectra were mass calibrated by using an aqueous solution of cesium iodide (25 mg·mL⁻¹).

Sequence Comparison

Protein sequences were retrieved using protein resources from the National Centre for Biotechnology Information² and UniProt Database³. Multiple sequence alignments were made using CLUSTALW (Thompson et al., 1994). Phylogenetic plots were made using FigTree⁴.

RESULTS

Biochemical Properties of *Rj3HB6H*

Expression of the 3HB6H gene from *R. jostii* RHA1#2 yielded about 7 mg of purified *Rj3HB6H* protein from 10 g wet cells (Table 3A). *Rj3HB6H* displayed the same absorption spectrum as 3HB6H, with maxima at 274, 383, and 453 nm and a shoulder at 480 nm (Montersino and van Berkel, 2012). A molar absorption coefficient of protein-bound flavin, $\epsilon_{453} = 10.3 \text{ mM}^{-1} \text{ cm}^{-1}$, was used for both proteins.

Determination of steady-state kinetic parameters revealed that *Rj3HB6H* behaves similarly as 3HB6H using 3-hydroxybenzoate as variable substrate and fixed NADH concentration ($k_{\text{cat}} = (20 \pm 1) \text{ s}^{-1}$; $K_M = (35 \pm 3) \mu\text{M}$; $k_{\text{cat}}/K_M = (5.7 \pm 0.8) \times 10^5 \text{ s}^{-1} \cdot \text{M}^{-1}$) and with variable concentration of NADH (preferred coenzyme) and fixed 3-hydroxybenzoate concentration ($k_{\text{cat}} = (20 \pm 1) \text{ s}^{-1}$; $K_M = (68 \pm 5) \mu\text{M}$; $k_{\text{cat}}/K_M = (3.0 \pm 0.4) \times 10^5 \text{ s}^{-1} \cdot \text{M}^{-1}$). *Rj3HB6H* displays a very low NADH oxidase activity ($<1 \text{ U} \cdot \text{mg}^{-1}$). Uncoupling of hydroxylation of 3-hydroxybenzoate occurs to a minor extent (less than 10%), while 2,5-dihydroxybenzoate is a strong non-substrate effector ($k_{\text{cat}} = (6 \pm 0.8) \text{ s}^{-1}$; $K_M = (150 \pm 30) \mu\text{M}$; $k_{\text{cat}}/K_M = (4.0 \pm 1.3) \times 10^4 \text{ s}^{-1} \cdot \text{M}^{-1}$), efficiently stimulating the rate of flavin reduction by NADH (Montersino and van Berkel, 2012; Sucharitakul et al., 2012, 2013; Ni et al., 2016).

Structural Characterization

Rj3HB6H crystals grew in similar conditions as found for 3HB6H, and are isomorphous to those of 3HB6H, where

² www.ncbi.nlm.nih.gov

³ http://www.uniprot.org/www.uniprot.org

⁴ tree.bio.ed.ac.uk

TABLE 3A | Purification of *Rj3HB6H* produced in *R. jostii* RHA1#2.

Step	Protein (mg)	Activity (U)	Specific activity (U·mg ⁻¹)	Yield (%)
Cell extract	208	355	2	100
His GraviTrap	37	300	8	84
Mono-Q	16	230	14	65
His GraviTrap	7	168	21	47

TABLE 3B | Purification of *Pa3HB6H* produced in *E. coli*.

Step	Protein (mg)	Activity (U)	Specific activity (U·mg ⁻¹)	Yield (%)
Cell extract	1080	260	0.2	100
His GraviTrap	45	244	5	94
Mono-Q	12	225	19	87
His GraviTrap	5	170	34	66

TABLE 4 | Crystallographic data collection and refinement statistics of *Rj3HB6H*.

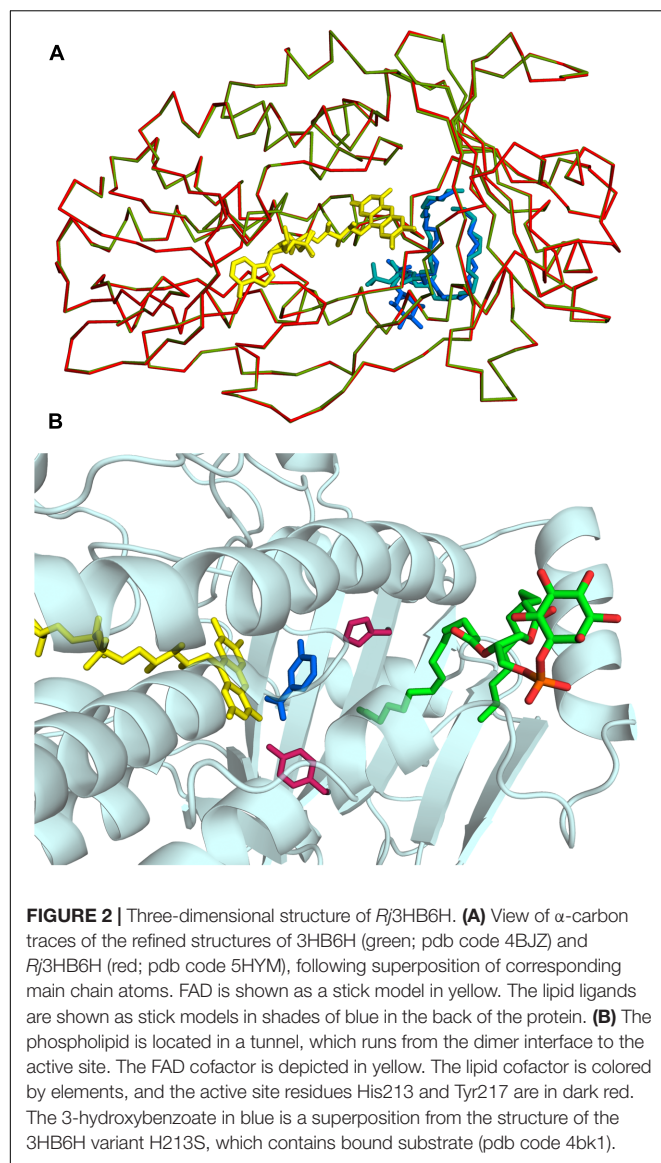
Protein Data Bank Code	5HYM
Unit cell (Å)	$a = b = 106.98 \text{ c} = 143.39$
Space group	$I4_122$
Resolution (Å)	2.30
$R_{\text{sym}}^{\text{a,b}}$ (%)	15.1 (50)
Completeness ^b (%)	99.7 (100)
Unique reflections	18,766
Redundancy ^b	7.5 (5.8)
I/σ^b	8.4 (3.0)
No. of atoms	3,198
Average B value (Å ²)	33.4
$R_{\text{cryst}}^{\text{c}}$ (%)	20.6
$R_{\text{free}}^{\text{c}}$ (%)	26.2
r.m.s. bond length (Å)	0.015
r.m.s. bond angles (°)	1.75

^a $R_{\text{sym}} = \sum |I_i - \bar{I}| / \sum I_i$ where I_i is the intensity of i th observation and \bar{I} is the mean intensity of the reflection. ^bValues in parentheses are for reflections in the highest resolution shell. ^c $R_{\text{cryst}} = \sum |F_{\text{obs}} - F_{\text{calc}}| / \sum F_{\text{obs}}$ where F_{obs} and F_{calc} are the observed and calculated structure factor amplitudes, respectively. R_{cryst} and R_{free} were calculated using the working and test set, respectively. r.m.s., root mean square

lithium sulfate was present instead of sodium acetate. The three-dimensional structure of *Rj3HB6H* was solved at 2.3 Å resolution by molecular replacement (Table 4). The isoalloxazine moiety of FAD was refined with full occupancy in the *in* conformation. Similar to the crystallographic analysis of 3HB6H, no substrate could be detected in the active site of the enzyme, despite presence of excess 3-hydroxybenzoate in the crystallization drop. The protein crystallizes as a dimer, just as 3HB6H (Montersino et al., 2013), and contains a phospholipid molecule in each subunit. The electron density of the phospholipid in the crystal structure was refined as two acyl chains, one of twelve and one of seventeen carbon units. Superimposition of the *Rj3HB6H* and 3HB6H models (root mean square deviation = 0.22 Å) shows minor deviations (Figure 2A). The phospholipid is located in a tunnel, which runs from the dimer interface to the active site (Figure 2B), and interacts with the opposite monomer. The phosphate group resides at the protein surface near Arg350 and Lys385, and the electron density of the headgroup is consistent with the presence of a cyclohexanehexol moiety (Figure 3A).

Identification of Protein-Bound Lipid Molecules

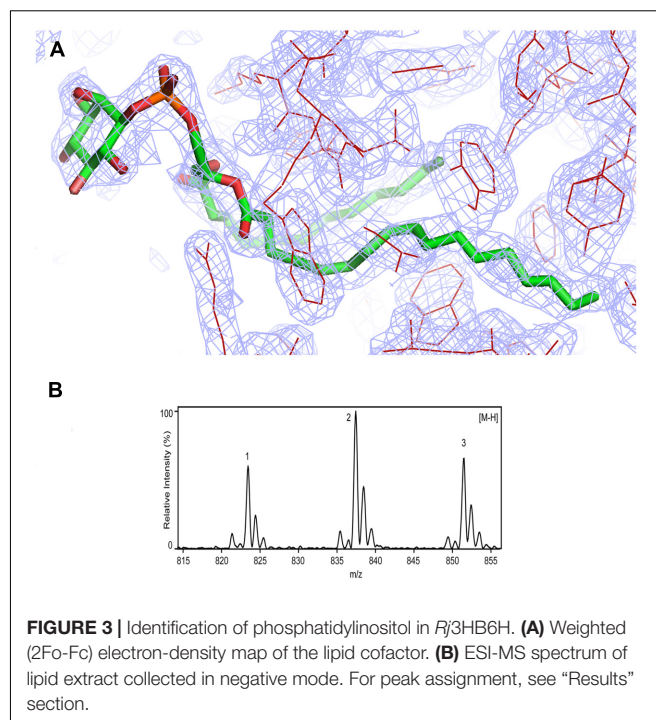
Assignment of protein-bound phospholipids was achieved by ESI-MS analysis of the low molecular weight components



extracted from denatured *Rj3HB6H*. The mass spectrum in negative mode (**Figure 3B**) displayed three main peaks with m/z values of 823, 837, and 851. From the MS pattern it was evident that *Rj3HB6H* binds a phospholipid with a bigger headgroup compared to that of the lipid found in 3HB6H.

Fragmentation analysis and comparison of data to reference lipid MS spectra led to a match of the obtained mass peaks with those of PI, having aliphatic chains containing 15 to 19 carbons. Peak 1 (m/z 823) is assigned to PI (15:0/18:0), peak 2 (m/z 837) is assigned to PI (16:0/18:0) (Sharp et al., 2007; Morita et al., 2011) and peak 3 (m/z 851) is assigned to PI (16:0/19:0) with alternate acylate form (tuberculostearic acid) (Drage et al., 2010).

Typical fragmentation of PI was visible in the MS/MS spectra by signature peaks with m/z values of 153, 223, 241, and 297, representing glycerol phosphate water (m/z 153) and inositol



headgroup fragments (Lang and Philp, 1998; Pulfer and Murphy, 2003; Oursel et al., 2007) (data not shown). Minor peaks at approximately 2 m/z values lower than the identified peaks represent the same PI, containing one unsaturated bond.

Protein Oligomeric Composition

To gain further insight into the enzyme–lipid interaction, we determined the oligomeric protein composition of 3HB6H and *Rj3HB6H* using native MS (Leney and Heck, 2017). As a first step, we determined the experimental masses of the denatured proteins. The measured values ($46,766 \pm 4$ Da for 3HB6H and $46,761 \pm 2$ Da for *Rj3HB6H*) agree with the mass deduced from the primary sequence, lacking the N-terminal methionine.

Native MS of 3HB6H showed eight charge states corresponding to five different protein forms (**Figure 4A** and **Table 5**). The charge state distribution ions +12, +13, and +14 represent the monomeric apoprotein (average mass $46,835 \pm 5$ Da; red stars), the monomeric holoprotein (average mass $47,603 \pm 6$ Da; green stars), and the monomeric holoprotein containing additionally one PG/PE molecule (average mass $48,312 \pm 7$ Da; blue stars). The charge state distribution ions +18, +19, +20, +21, and +22 predominantly represent the dimeric holoprotein with either one or two PG/PE molecules bound (average mass $95,868 \pm 16$ Da; orange stars, and $96,643 \pm 14$ Da; purple stars, respectively). Tandem MS experiments revealed that one, two, three, or four ligands can be expelled from 3HB6H. The assignment of bound ligands was made on the basis of total mass increase and comparison with the mass of the native apoprotein (**Table 5**).

Native MS of *Rj3HB6H* also showed a range of charge state distributions (**Figure 4B** and **Table 5**). The charge state

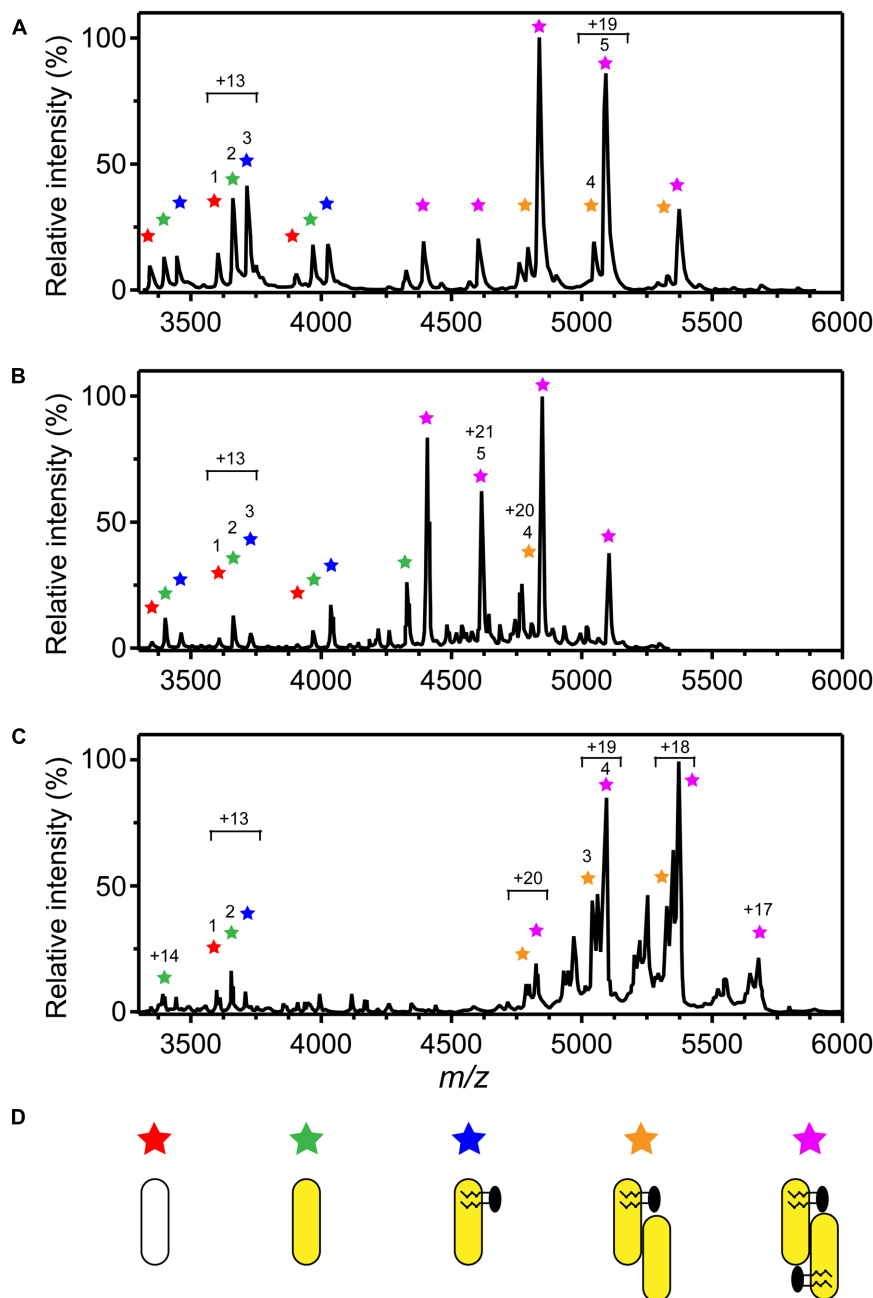


FIGURE 4 | Oligomer distribution and lipid composition of 3HB6H enzymes as determined by native ESI-MS. Mass spectra were recorded in 50 mM ammonium acetate, pH 6.8. **(A)** Mass spectrum of 3HB6H. **(B)** Mass spectrum of *Rj*3HB6H. **(C)** Mass spectrum of *Pa*3HB6H. Masses and intensities of numbered peaks are listed in **Table 5**. **(D)** Cartoons of the various subunit compositions. Apoprotein is indicated in white, holoprotein in yellow and lipid molecules in black.

distribution ions +12, +13, and +14 represent the monomeric apoprotein (average mass $46,829 \pm 1$ Da; red star), the monomeric holoprotein (average mass $47,613 \pm 1$ Da; green stars), and the monomeric holoprotein containing one PI molecule (average mass $48,458 \pm 2$ Da; blue star). The latter species differs from the related 3HB6H species (Figure 4A, blue stars) because it has a bigger lipid headgroup. The major species

in the native mass spectrum of *Rj*3HB6H corresponds to the holo-*Rj*3HB6H dimer with PI bound to both subunits (average mass $96,938 \pm 32$ Da; Figure 4B, yellow stars). Only by magnification it is possible to detect a minor peak representing the holo-*Rj*3HB6H dimer with one PI bound (average mass $96,128 \pm 5$ Da; Figure 4B, orange stars). A cartoon of the different subunit compositions of 3HB6H is presented in Figure 4D.

TABLE 5 | Oligomeric forms of 3HB6H determined by native ESI-MS.

Peak ^a	<i>m/z</i>	Average mass (Da)	Δ mass (Da)
3HB6H			
1	3,603	46,835 ± 5	
2	3,663	47,603 ± 6	767 ^b
3	3,717	48,312 ± 7	1,477 ^b
4	5,048	95,868 ± 16	2,198 ^c
5	5,088	96,643 ± 14	2,973 ^c
Rj3HB6H			
1	3,608	46,829 ± 1	
2	3,663	47,613 ± 1	784 ^b
3	3,728	48,458 ± 2	1,629 ^b
4	4,807	96,128 ± 5	2,470 ^c
5	4,616	96,938 ± 32	3,280 ^c
Pa3HB6H			
1	3,651	47,448 ± 2	790 ^b
2	3,706	48,167 ± 2	1,509 ^b
3	5,035	95,662 ± 7	2,346 ^c
4	5,073	96,738 ± 8	3,062 ^c

^aPeaks are indicated in **Figure 4**. ^bCalculated using apo-monomer. ^cCalculated using apo-dimer.

Conservation of Lipid Binding Site

To analyze whether the lipid-binding site of 3HB6H is conserved among species, we explored the natural diversity of 3HB6H enzymes. 3HB6H activity has been reported for Gram-positive and Gram-negative bacteria and for yeasts. Besides from the *R. jostii* prototype, the enzymes from *Klebsiella pneumonia* M5a1 (Suárez et al., 1995; Liu et al., 2005), *Pseudomonas alcaligenes* NCIMB 9867 (Gao et al., 2005), *Polaromonas naphthalenivorans* CJ2 (Park et al., 2007), *Corynebacterium glutamicum* ATCC 12032 (Yang et al., 2010), *Rhodococcus sp.* NCIMB 12038 (Liu et al., 2011) and *Candida parapsilosis* (Holesova et al., 2011) have been characterized to some extent.

From the structural data of the *R. jostii* 3HB6H enzyme and the multiple sequence alignment presented in **Figure 5** it can be inferred that residues directly involved in lipid binding in Rj3HB6H are not always conserved in the orthologs; among the bacterial enzymes studied, most sequence divergence occurs in 3HB6H from *P. alcaligenes* NCIMB 9867 (Pa3HB6H). This prompted us to study the lipid binding properties of the *Pseudomonas* 3HB6H enzyme.

Expression of the Pa3HB6H gene in *E. coli* TOP10 cells yielded about 10 mg of enzyme from a 1 L batch culture. Purified Pa3HB6H had a specific activity of 34 U·mg⁻¹ (**Table 3B**) and migrated in SDS-PAGE as a single band with an apparent subunit mass of 47 kDa (not shown). ESI-MS established that native Pa3HB6H is a dimer, and not a trimer as suggested earlier (Gao et al., 2005), and that the enzyme indeed contains lipids (**Figure 4C** and **Table 5**). The mass spectrum of extracted lipids showed peaks with *m/z* values characteristic of PG and PE with aliphatic chains ranging from 14 to 19 carbons, similar to the previously identified lipids in 3HB6H from *R. jostii* RHA1 produced in *E. coli* (MonTERSINO et al., 2013).

DISCUSSION

3HB6H is a flavoenzyme that catalyzes the *para*-hydroxylation of 3-hydroxybenzoate to gentisate, a key step in the catabolism of lignin-derived aromatic compounds in the soil (Pérez-Pantoja et al., 2010). Up to now, 3HB6H is the only flavoprotein monooxygenase that has been found to bind phospholipids (MonTERSINO et al., 2013). Structural analysis showed that the hydrophobic tails of the phospholipids deeply penetrate into the substrate-binding domains, whereas the hydrophilic parts are exposed on the protein surface, connecting the dimerization domains (**Figure 1**). Attempts to obtain native lipid-free protein were not successful, indicating that the phospholipids are important to attain a properly folded protein (MonTERSINO et al., 2013).

3HB6H binds a mixture of PG and PE, the major constituents of the *E. coli* inner membrane (MonTERSINO et al., 2013). By expressing its gene in *R. jostii* RHA1#2, we aimed at unraveling the lipid binding abilities of 3HB6H in the original host. Although *E. coli* gives considerable higher yields (MonTERSINO and van Berkel, 2012), significant quantities of soluble His-tagged Rj3HB6H were obtained. The difference in enzyme yield could be linked to the type of induction and promoter strength used in the *R. jostii* RHA1#2 strain, which is based on the propane monooxygenase operon (Sharp et al., 2007). Nevertheless, our results show that the newly developed *R. jostii* RHA1#2 strain opens new prospects for actinomycetes as host cells for production of recombinant proteins (Nakashima et al., 2005).

Rj3HB6H displayed similar catalytic and structural properties as 3HB6H, and the mode of lipid binding was highly conserved (**Figure 2**). Gratifyingly, the crystallographic data and mass spectrometry analysis provided clear evidence that Rj3HB6H contains PI as natural glycerophospholipid cofactor (**Figure 3**). The crystal structure showed that the inositol headgroups of the phospholipids are located at the protein surface, and that the *sn*-2 acyl moieties are in contact with helix 11 of the other subunit (**Figure 1**). Based on MS/MS analysis, we identified the bound phospholipids as a mixture of PIs with carbon chains between 15 and 19 carbons. One of the extracted lipids was identified as tuberculostearic acid, an alternative acylated form of palmitate present in the membranes of *Rhodococcus* and *Mycobacterium* (Drage et al., 2010).

Rj3HB6H is a dimer both in solution and in crystal form, but native MS showed a ratio of monomer to dimer of about 1:3 (**Figure 4B**). Release of only one PI from the dimer resulted in monomerization in the gas phase. A similar observation was made with 3HB6H, but with this enzyme more dimers containing only one bound lipid (PG or PE) were detected (**Figure 4A**). 3HB6H dimers containing two phospholipids seem to be more stable in the gas phase than dimers containing one phospholipid. This strongly supports that lipid binding near the dimer interface stabilizes monomer contacts.

Native MS-analysis showed that Pa3HB6H is a homodimer and not a trimer as postulated earlier (Gao et al., 2005). The dimeric nature is in agreement with the structural properties of 3HB6H and Rj3HB6H. MS-analysis also revealed that

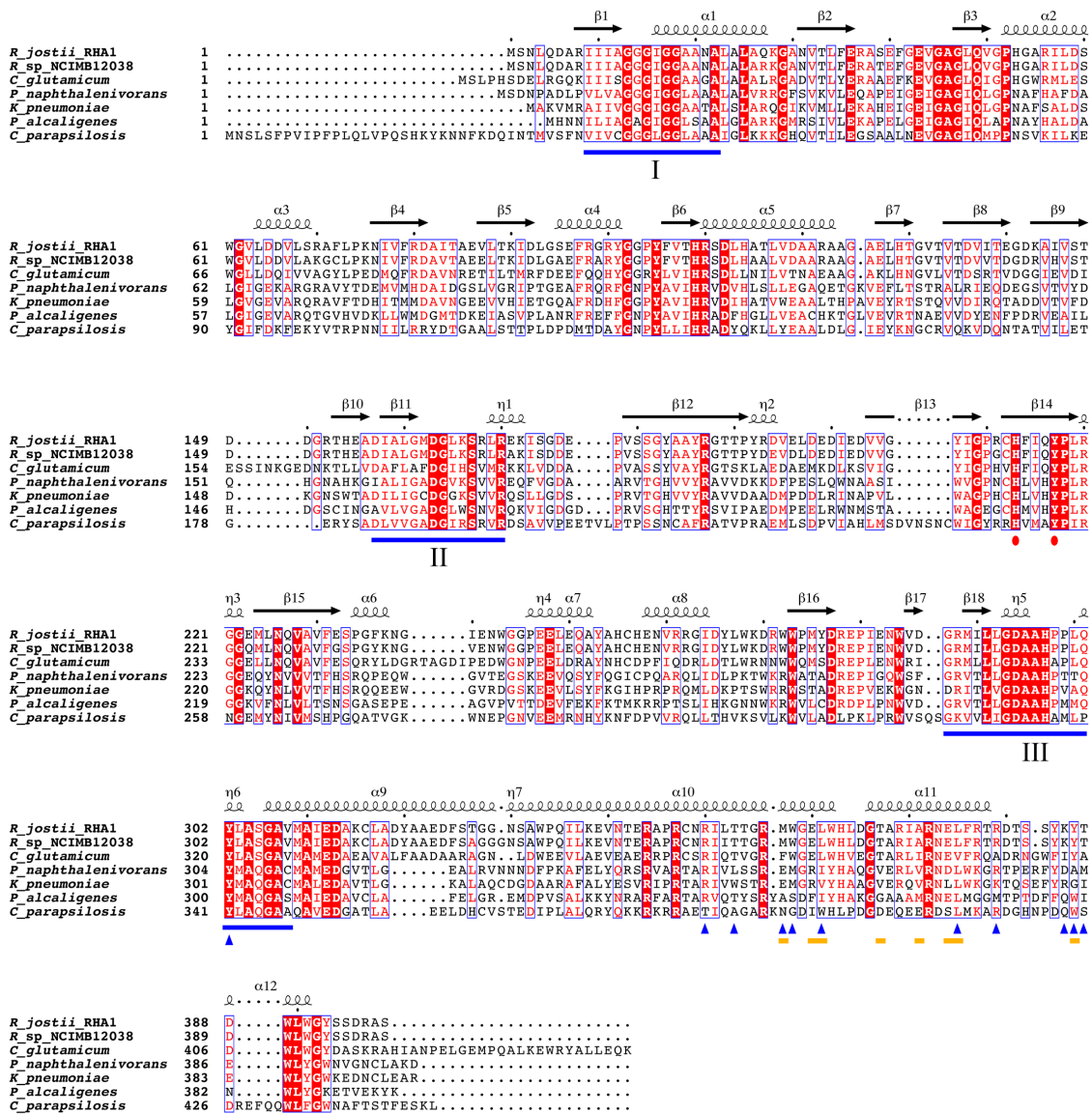


FIGURE 5 | Multiple sequence alignment of known 3HB6H enzymes. UniProt ID numbers: Q05FK6, *R. jostii* RHA1; E7CYP8, *Rhodococcus* sp. NCIMB 12038; Q8NLB6, *C. glutamicum* ATCC 12032; Q3S4B7, *P. naphthalenivorans* CJ2; Q6EXK1, *K. pneumonia* M5a1; Q9F131, *P. alcaligenes* NCIMB 9867; CPAG_03410, *C. parapsilosis*. Identical residues are shown in red. Flavin binding motifs are underlined in blue [I: GXGXXG; II: DG; III: GD (Eppink et al., 1997)]. The His-Tyr pair involved in substrate binding and hydroxylation is marked with red dots. The yellow lines mark residues involved in dimerization contacts. Blue triangles indicate residues involved in lipid binding. Secondary structure assigned from the 3HB6H crystal structure (4BK1). Diagram was produced using ESPript (Robert and Gouet, 2014).

recombinant *Pa*3HB6H binds the same type of phospholipids as 3HB6H. This supports that lipid binding is an intrinsic property of 3HB6Hs. As a main result, it appears that the 3HB6H family uses phospholipids as a common tool to increase their dimerization strength. Phospholipid binding is independent of the type of lipid headgroup, but relies on the presence of hydrophobic tunnels running from the protein surface to the active site.

Like PG/PE in *E. coli* (Oursel et al., 2007), PI is the major lipid membrane component in *Rhodococcus* (Nigou et al., 2003). This

may explain why PG/PE are found as lipid ligands of 3HB6H and *Pa*3HB6H, while PI is found in *Rj*3HB6H. PI is the precursor for lipoarabinomannan and PI-mannoside synthesis. Glycolipid synthesis and reorganization of membrane composition allow *Rhodococcus* to adapt to environmental changes (Lang and Philp, 1998; Sharp et al., 2007; Guerin et al., 2010; Morita et al., 2011; De Carvalho et al., 2014). Binding of PI may localize 3HB6H at the cytoplasmic membrane, via inositol recognition of other proteins or specific phospholipid patching on the inner side of the membrane (Morita et al., 2011). At those specific spots,

uptake of aromatic compounds from the environment may be coupled more efficiently to their catabolism.

Taking together, phospholipids do not have a direct catalytic role in 3HB6H, but are involved in stabilizing the dimer contact and, possibly, substrate orientation (MonTERSINO et al., 2013). At this stage, we cannot exclude that bound phospholipids have some other function, for instance in directing the cytoplasmic membrane localization or in guiding/protecting molecules from entering the active site. In addition, the *R. jostii* RHA1#2 expression strain described here represents a useful alternative for the production of (whole-cell) biocatalysts.

AUTHOR CONTRIBUTIONS

WvB and LD initiated the project; SM, EtP, AW, AB, AH, RvG, LD, AM, and WvB designed experiments and analyzed data; EtP constructed *Rhodococcus* expression vector Q2+; RO crystallized Rj3HB6H and determined the crystal structure; SM, AW, and AB

performed analytical and biochemical experiments; SM, EtP, AM, AW, and WvB wrote the manuscript.

FUNDING

This study was supported by the Integrated Biosynthesis Organic Synthesis program (IBOS; project number 053.63.013) of the Netherlands Organization for Scientific Research (NWO). Additional support from Proteins At Work (project 184.032.201), a program of the Netherlands Proteomics Centre financed by the Netherlands Organization for Scientific Research (NWO) as part of the National Roadmap Large-scale Research Facilities of the Netherlands is acknowledged.

ACKNOWLEDGMENT

Part of the content of this manuscript has been published in the Ph.D. thesis of Dr. Stefania MonTERSINO (MonTERSINO, 2012).

REFERENCES

- Adams, P. D., Afonine, P. V., Bunkóczy, G., Chen, V. B., Davis, I. W., Echols, N., et al. (2010). PHENIX: a comprehensive Python-based system for macromolecular structure solution. *Acta Crystallogr. D Biol.* 66(Pt 2), 213–221. doi: 10.1107/S0907444909052925
- Brennan, P. J., and Nikaido, H. (1995). The envelope of mycobacteria. *Annu. Rev. Biochem.* 64, 29–63. doi: 10.1146/Annurev.Bi.64.070195.000333
- Chun, J., Kang, S. O., Hah, Y. C., and Goodfellow, M. (1996). Phylogeny of mycolic acid-containing actinomycetes. *J. Ind. Microbiol.* 17, 205–213. doi: 10.1007/Bf01574694
- De Carvalho, C. C., Costa, S. S., Fernandes, P., Couto, I., and Viveiros, M. (2014). Membrane transport systems and the biodegradation potential and pathogenicity of genus *Rhodococcus*. *Front. Physiol.* 5:133. doi: 10.3389/fphys.2014.00133
- Drage, M. G., Tsai, H. C., Pecora, N. D., Cheng, T. Y., Arida, A. R., Shukla, S., et al. (2010). *Mycobacterium tuberculosis* lipoprotein LprG (Rv1411c) binds triacylated glycolipid agonists of Toll-like receptor 2. *Nat. Struct. Mol. Biol.* 17, 1088–1095. doi: 10.1038/nsmb.1869
- Emsley, P., Lohkamp, B., Scott, W. G., and Cowtan, K. (2010). Features and development of Coot. *Acta Crystallogr. D Biol.* 66, 486–501. doi: 10.1107/S0907444910007493
- Eppink, M., Schreuder, H., and van Berkel, W. (1997). Identification of a novel conserved sequence motif in flavoprotein hydroxylases with a putative dual function in FAD/NAD(P)H binding. *Protein Sci.* 6, 2454–2458. doi: 10.1002/pro.5560061119
- Finnerty, W. R. (1992). The biology and genetics of the genus *Rhodococcus*. *Annu. Rev. Microbiol.* 46, 193–218. doi: 10.1146/Annurev.Micro.46.1.193
- Gao, X. L., Tan, C. L., Yeo, C. C., and Poh, C. L. (2005). Molecular and biochemical characterization of the *xlnD*-encoded 3-hydroxybenzoate 6-hydroxylase involved in the degradation of 2,5-xyleneol via the gentisate pathway in *Pseudomonas alcaligenes* NCIMB 9867. *J. Bacteriol.* 187, 7696–7702. doi: 10.1128/JB.187.22.7696-7702.2005
- Guerin, M. E., Korduláková, J., Alzari, P. M., Brennan, P. J., and Jackson, M. (2010). Molecular basis of phosphatidyl-myo-inositol mannoside biosynthesis and regulation in mycobacteria. *J. Biol. Chem.* 285, 33577–33583. doi: 10.1074/jbc.R110.168328
- Gürtler, V., Mayall, B. C., and Seviour, R. (2004). Can whole genome analysis refine the taxonomy of the genus *Rhodococcus*? *FEMS Microbiol. Rev.* 28, 377–403. doi: 10.1016/j.femsre.2004.01.001
- Holesova, Z., Jakubkova, M., Zavadikova, I., Zeman, I., Tomaska, L., and Nosek, J. (2011). Gentisate and 3-oxoadipate pathways in the yeast *Candida* *parapsilosis*: identification and functional analysis of the genes coding for 3-hydroxybenzoate 6-hydroxylase and 4-hydroxybenzoate 1-hydroxylase. *Microbiology* 157, 2152–2163. doi: 10.1099/mic.0.048215-0
- Huijbers, M. M. E., MonTERSINO, S., Westphal, A. H., Tischler, D., and van Berkel, W. J. H. (2014). Flavin dependent monooxygenases. *Arch. Biochem. Biophys.* 544, 2–17. doi: 10.1016/j.abb.2013.12.005
- Lang, S., and Philp, J. C. (1998). Surface-active lipids in rhodococci. *Antonie van Leeuwenhoek* 74, 59–70. doi: 10.1023/A:1001799711799
- Leney, A. C., and Heck, A. J. R. (2017). Native mass spectrometry: what is in the name? *J. Am. Soc. Mass Spectrom.* 28, 5–13. doi: 10.1007/s13361-016-1545-3
- Liu, D. Q., Liu, H., Gao, X. L., Leak, D. J., and Zhou, N. Y. (2005). Arg(169) is essential for catalytic activity of 3-hydroxybenzoate 6-hydroxylase from *Klebsiella pneumoniae* M5a1. *Microbiol. Res.* 160, 53–59. doi: 10.1016/j.micres.2004.09.003
- Liu, T. T., Xu, Y., Liu, H., Luo, S., Yin, Y. J., Liu, S. J., et al. (2011). Functional characterization of a gene cluster involved in gentisate catabolism in *Rhodococcus* sp. strain NCIMB 12038. *Appl. Microbiol. Biotechnol.* 90, 671–678. doi: 10.1007/s00253-010-3033-1
- McLeod, M. P., Warren, R. L., Hsiao, W. W. L., Araki, N., Myhre, M., Fernandes, C., et al. (2006). The complete genome of *Rhodococcus* sp RHA1 provides insights into a catabolic powerhouse. *Proc. Natl. Acad. Sci. U.S.A.* 103, 15582–15587. doi: 10.1073/pnas.0607048103
- MonTERSINO, S. (2012). *Structural and Biochemical Characterization of 3-Hydroxybenzoate 6-Hydroxylase*. Doctoral thesis, Wageningen University, Wageningen.
- MonTERSINO, S., Orru, R., Barendregt, A., Westphal, A. H., van Duijn, E., Mattevi, A., et al. (2013). Crystal structure of 3-hydroxybenzoate 6-hydroxylase uncovers lipid-assisted flavoprotein strategy for regioselective aromatic hydroxylation. *J. Biol. Chem.* 288, 26235–26245. doi: 10.1074/jbc.M113.479303
- MonTERSINO, S., Tischler, D., Gassner, G. T., and van Berkel, W. J. H. (2011). Catalytic and structural features of flavoprotein hydroxylases and epoxidases. *Adv. Synth. Catal.* 353, 2301–2319. doi: 10.1002/adsc.201100384
- MonTERSINO, S., and van Berkel, W. J. H. (2012). Functional annotation and characterization of 3-hydroxybenzoate 6-hydroxylase from *Rhodococcus jostii* RHA1. *Biochim. Biophys. Acta* 1824, 433–442. doi: 10.1016/j.bbapap.2011.12.003
- Morita, Y. S., Fukuda, T., Sena, C. B. C., Yamaryo-Butte, Y., McConville, M. J., and Kinoshita, T. (2011). Inositol lipid metabolism in mycobacteria: biosynthesis and regulatory mechanisms. *Biochim. Biophys. Acta* 1810, 630–641. doi: 10.1016/j.bbagen.2011.03.017
- Nakashima, N., Mitani, Y., and Tamura, T. (2005). Actinomycetes as host cells for production of recombinant proteins. *Microb. Cell Fact.* 4:7. doi: 10.1186/1475-2859-4-7

- Ni, Y., Fernandez-Fueyo, E., Baraibar, A. G., Ullrich, R., Hofrichter, M., Yanase, H., et al. (2016). Peroxygenase-catalyzed oxyfunctionalization reactions promoted by the complete oxidation of methanol. *Angew. Chem. Int. Ed. Engl.* 55, 798–801. doi: 10.1002/anie.201507881
- Nigou, J., Gilleron, M., and Puzo, G. (2003). Lipoarabinomannans: from structure to biosynthesis. *Biochimie* 85, 153–166. doi: 10.1016/S0300-9084(03)00048-8
- Oursel, D., Loutelier-Bourhis, C., Orange, N., Chevalier, S., Norris, V., and Lange, C. M. (2007). Lipid composition of membranes of *Escherichia coli* by liquid chromatography/tandem mass spectrometry using negative electrospray ionization. *Rapid Commun. Mass Spectrom.* 21, 1721–1728. doi: 10.1002/rcm.3013
- Park, M., Jeon, Y., Jang, H. H., Ro, H.-S., Park, W., Madsen, E. L., et al. (2007). Molecular and biochemical characterization of 3-hydroxybenzoate 6-hydroxylase from *Pseudomonas naphthalenivorans* CJ2. *Appl. Environ. Microbiol.* 73, 5146–5152. doi: 10.1128/AEM.00782-07
- Pérez-Pantoja, D., González, B., and Pieper, D. H. (2010). “Aerobic Degradation of aromatic hydrocarbons,” in *Handbook of Hydrocarbon and Lipid Microbiology*, ed. K. N. Timmis (Berlin: Springer), 799–837. doi: 10.1007/978-3-540-77587-4_60
- Potterton, L., McNicholas, S., Krissinel, E., Gruber, J., Cowtan, K., Emsley, P., et al. (2004). Developments in the CCP4 molecular-graphics project. *Acta Crystallogr. D Biol.* 60, 2288–2294. doi: 10.1107/S0907444904023716
- Pulfer, M., and Murphy, R. C. (2003). Electrospray mass spectrometry of phospholipids. *Mass Spectrom. Rev.* 22, 332–364. doi: 10.1002/mas.10061
- Robert, X., and Gouet, P. (2014). Deciphering key features in protein structures with the new ENDscript server. *Nucleic Acids Res.* 42, W320–W324. doi: 10.1093/nar/gku316
- Schäfer, A., Tauch, A., Jäger, W., Kalinowski, J., Thierbach, G., and Pühler, A. (1994). Small mobilizable multipurpose cloning vectors derived from the *Escherichia coli* plasmids pK18 and pK19: selection of defined deletions in the chromosome of *Corynebacterium glutamicum*. *Gene* 145, 69–73. doi: 10.1016/0378-1119(94)90324-7
- Schrodinger, L. L. C. (2015). “The PyMOL Molecular Graphics System, Version 1.8”.
- Sharp, J. O., Sales, C. M., LeBlanc, J. C., Liu, J., Wood, T. K., Eltis, L. D., et al. (2007). An inducible propane monooxygenase is responsible for N-nitrosodimethylamine degradation by *Rhodococcus* sp strain RHA1. *Appl. Environ. Microbiol.* 73, 6930–6938. doi: 10.1128/AEM.01697-07
- Suárez, M., Ferrer, E., Garridopertierra, A., and Martín, M. (1995). Purification and characterization of the 3-hydroxybenzoate 6-hydroxylase from *Klebsiella pneumoniae*. *FEMS Microbiol. Lett.* 126, 283–290. doi: 10.1111/J.1574-6968.1995.Tb07431.X
- Sucharitakul, J., Medhanavyn, D., Pakotiprapha, D., van Berkel, W. J., and Chaiyen, P. (2015). Tyr217 and His213 are important for substrate binding and hydroxylation of 3-hydroxybenzoate 6-hydroxylase from *Rhodococcus jostii* RHA1. *FEBS J.* 283, 860–881. doi: 10.1111/febs.13636
- Sucharitakul, J., Tongsook, C., Pakotiprapha, D., van Berkel, W. J. H., and Chaiyen, P. (2013). The reaction kinetics of 3-hydroxybenzoate 6-hydroxylase from *Rhodococcus jostii* RHA1 provide an understanding of the para-hydroxylation enzyme catalytic cycle. *J. Biol. Chem.* 288, 35210–35221. doi: 10.1074/jbc.M113.515205
- Sucharitakul, J., Wongnate, T., MonTERSINO, S., van Berkel, W. J. H., and Chaiyen, P. (2012). Reduction kinetics of 3-hydroxybenzoate 6-hydroxylase from *Rhodococcus jostii* RHA1. *Biochemistry* 51, 4309–4321. doi: 10.1021/bi201823c
- Sun, J. H., Kelemen, G. H., Fernández-Abalos, J. M., and Bibb, M. J. (1999). Green fluorescent protein as a reporter for spatial and temporal gene expression in *Streptomyces coelicolor* A3(2). *Microbiology* 145, 2221–2227. doi: 10.1099/00221287-145-9-2221
- Sutcliffe, I. C. (1998). Cell envelope composition and organisation in the genus *Rhodococcus*. *Antonie van Leeuwenhoek* 74, 49–58. doi: 10.1023/A:1001747726820
- Thompson, J. D., Higgins, D. G., and Gibson, T. J. (1994). Clustal-W - improving the sensitivity of progressive multiple sequence alignment through sequence weighting, position-specific gap penalties and weight matrix choice. *Nucleic Acids Res.* 22, 4673–4680. doi: 10.1093/Nar/22.22.4673
- van der Geize, R., and Dijkhuizen, L. (2004). Harnessing the catabolic diversity of Rhodococci for environmental and biotechnological applications. *Curr. Opin. Microbiol.* 7, 255–261. doi: 10.1016/j.mib.2004.04.001
- van der Geize, R., Hessels, G. L., van Gerwen, R., van der Meijden, R., and Dijkhuizen, L. (2002). Molecular and functional characterization of *kshA* and *kshB*, encoding two components of 3-ketosteroid 1- α -hydroxylase, a class IA monooxygenase, in *Rhodococcus erythropolis* strain SQ1. *Mol. Microbiol.* 45, 1007–1018. doi: 10.1046/j.1365-2958.2002.03069.x
- van der Geize, R., Hessels, G. L., van Gerwen, R., Vrijbloed, J. W., van der Meijden, P., and Dijkhuizen, L. (2000). Targeted disruption of the *kstD* gene encoding a 3-ketosteroid delta(1)-dehydrogenase isoenzyme of *Rhodococcus erythropolis* strain SQ1. *Appl. Environ. Microbiol.* 66, 2029–2036. doi: 10.1128/Aem.66.5.2029-2036.2000
- Winn, M. D., Ballard, C. C., Cowtan, K. D., Dodson, E. J., Emsley, P., Evans, P. R., et al. (2011). Overview of the CCP4 suite and current developments. *Acta Crystallogr. D Biol.* 67, 235–242. doi: 10.1107/S0907444910045749
- Yam, K. C., Geize, R., and Eltis, L. D. (2010). “Catabolism of aromatic compounds and steroids by *Rhodococcus*,” in *Biology of Rhodococcus*, ed. M. H. Alvarez (Berlin: Springer), 133–169.
- Yang, Y. F., Zhang, J. J., Wang, S. H., and Zhou, N. Y. (2010). Purification and characterization of the *ncgl2923*-encoded 3-hydroxybenzoate 6-hydroxylase from *Corynebacterium glutamicum*. *J. Basic Microbiol.* 50, 599–604. doi: 10.1002/jobm.201000053

Conflict of Interest Statement: The authors declare that the research was conducted in the absence of any commercial or financial relationships that could be construed as a potential conflict of interest.

Copyright © 2017 MonTERSINO, te Poele, Orru, Westphal, Barendregt, Heck, van der Geize, Dijkhuizen, Mattevi and van Berkel. This is an open-access article distributed under the terms of the Creative Commons Attribution License (CC BY). The use, distribution or reproduction in other forums is permitted, provided the original author(s) or licensor are credited and that the original publication in this journal is cited, in accordance with accepted academic practice. No use, distribution or reproduction is permitted which does not comply with these terms.



Pyridine Nucleotide Coenzyme Specificity of *p*-Hydroxybenzoate Hydroxylase and Related Flavoprotein Monooxygenases

OPEN ACCESS

Edited by:

Daniela De Biase,
La Sapienza University of Rome, Italy

Reviewed by:

Gianluca Molla,
Università degli Studi dell'Insubria, Italy
Maria Antonietta Vanoni,
University of Milan, Italy
C French,
University of Edinburgh,
United Kingdom

*Correspondence:

Willem J. H. van Berkel
willem.vanberkel@wur.nl

[†]Present Address:

Dirk Tischler,
Microbial Biotechnology, Faculty of
Biology and Biotechnology, Ruhr
University Bochum, Bochum,
Germany
Janosch A. D. Gröning,
Institut für Mikrobiologie der
Universität Stuttgart, Stuttgart,
Germany

Specialty section:

This article was submitted to
Microbial Physiology and Metabolism,
a section of the journal
Frontiers in Microbiology

Received: 05 September 2018

Accepted: 27 November 2018

Published: 18 December 2018

Citation:

Westphal AH, Tischler D, Heinke F,
Hofmann S, Gröning JAD, Labudde D
and van Berkel WJH (2018) Pyridine
Nucleotide Coenzyme Specificity of
p-Hydroxybenzoate Hydroxylase and
Related Flavoprotein
Monooxygenases.
Front. Microbiol. 9:3050.
doi: 10.3389/fmicb.2018.03050

Adrie H. Westphal¹, Dirk Tischler^{2†}, Florian Heinke³, Sarah Hofmann²,
Janosch A. D. Gröning^{2†}, Dirk Labudde³ and Willem J. H. van Berkel^{1*}

¹ Laboratory of Biochemistry, Wageningen University and Research, Wageningen, Netherlands, ² Interdisziplinäres Ökologisches Zentrum, Technische Universität Bergakademie Freiberg, Freiberg, Germany, ³ Bioinformatics Group Mittweida, University of Applied Sciences Mittweida, Mittweida, Germany

p-Hydroxybenzoate hydroxylase (PHBH; EC 1.14.13.2) is a microbial group A flavoprotein monooxygenase that catalyzes the *ortho*-hydroxylation of 4-hydroxybenzoate to 3,4-dihydroxybenzoate with the stoichiometric consumption of NAD(P)H and oxygen. PHBH and related enzymes lack a canonical NAD(P)H-binding domain and the way they interact with the pyridine nucleotide coenzyme has remained a conundrum. Previously, we identified a surface exposed protein segment of PHBH from *Pseudomonas fluorescens* involved in NADPH binding. Here, we report the first amino acid sequences of NADH-preferring PHBHs and a phylogenetic analysis of putative PHBHs identified in currently available bacterial genomes. It was found that PHBHs group into three clades consisting of NADPH-specific, NAD(P)H-dependent and NADH-preferring enzymes. The latter proteins frequently occur in *Actinobacteria*. To validate the results, we produced several putative PHBHs in *Escherichia coli* and confirmed their predicted coenzyme preferences. Based on phylogeny, protein energy profiling and lifestyle of PHBH harboring bacteria we propose that the pyridine nucleotide coenzyme specificity of PHBH emerged through adaptive evolution and that the NADH-preferring enzymes are the older versions of PHBH. Structural comparison and distance tree analysis of group A flavoprotein monooxygenases indicated that a similar protein segment as being responsible for the pyridine nucleotide coenzyme specificity of PHBH is involved in determining the pyridine nucleotide coenzyme specificity of the other group A members.

Keywords: *Actinobacteria*, coenzyme specificity, fingerprint sequence, flavoprotein, monooxygenase, NAD(P)H, phylogenetic analysis, protein evolution

INTRODUCTION

p-Hydroxybenzoate hydroxylase (PHBH; EC 1.14.13.2) is a group A flavoprotein monooxygenase that catalyzes the *ortho*-hydroxylation of 4-hydroxybenzoate to 3,4-dihydroxybenzoate, a common intermediate step in the degradation of aromatic compounds in soil bacteria (Harwood and Parales, 1996):



The structural and mechanistic properties of NADPH-specific *Pseudomonas* PHBH have been studied extensively (Entsch and van Berkel, 1995; Entsch et al., 2005; Palfey and McDonald, 2010; Crozier-Reabe and Moran, 2012; Ballou and Entsch, 2013). As a consequence, this enzyme has emerged as the prototype group A flavoprotein hydroxylase (van Berkel et al., 2006; Suemori and Iwakura, 2007; Montersino et al., 2011; Montersino and van Berkel, 2013; Huijbers et al., 2014).

The isoalloxazine moiety of the flavin cofactor of PHBH is mobile and adopts different positions *in* and *out* the active site (Gatti et al., 1994; Schreuder et al., 1994; **Figure 1**). Reduction of the flavin by NADPH is assumed to take place in the *out* position (van Berkel et al., 1994; Wang et al., 2002; Ballou and Entsch, 2013). After NADP⁺ release, the reduced flavin moves to the *in* position, where the reaction with oxygen and subsequent hydroxylation of the aromatic substrate occurs. A similar mobility of the flavin cofactor has been observed in other group A flavoprotein monooxygenases, including among others phenol hydroxylase (Enroth et al., 1998), 3-hydroxybenzoate 4-monooxygenase (Hiromoto et al., 2006), and 2-hydroxybiphenyl monooxygenase (Kanteev et al., 2015).

Despite their important biological role (Huijbers et al., 2014), relatively little is known about the occurrence of NADH-preferring PHBHs and how PHBH and its relatives interact with the pyridine nucleotide coenzyme. Unlike many other NAD(P)H-dependent oxidoreductases (Scrutton et al., 1990; Ojha et al., 2007; Cahn et al., 2016, 2017; Sellés Vidal et al., 2018), group A flavoprotein monooxygenases lack a canonical pyridine dinucleotide binding domain (van Berkel et al., 2006; Treiber and Schulz, 2008; Huijbers et al., 2014; Mascotti et al., 2016). For PHBH from *Pseudomonas fluorescens* (PHBH_{Pf}), an interdomain binding for NADPH was proposed (Eppink et al., 1998a). Based on this binding mode, a switch in coenzyme specificity was achieved by replacing five amino acid residues of the solvent accessible helix H2 of the FAD domain (**Figure 1**) (Eppink et al., 1999). Support for the interdomain binding of the pyridine nucleotide was obtained from the crystal structure of the R220Q variant of *P. aeruginosa* PHBH in complex with NADPH (Wang et al., 2002). However, this substrate-free complex presented an inactive conformation, which pointed to significant ligand dynamics during the reductive half reaction (Ortiz-Maldonado et al., 2003; Entsch et al., 2005; Westphal et al., 2006; Ballou and Entsch, 2013).

To learn more about the evolutionary relationship of the pyridine nucleotide coenzyme specificity of PHBHs, we here performed a phylogenetic analysis of putative PHBHs and investigated the sequence-function relationship

of actinobacterial and proteobacterial PHBHs. The results were used to predict the structural features that determine the pyridine nucleotide coenzyme specificity of other group A flavoprotein monooxygenases.

MATERIALS AND METHODS

Cloning and Sequencing of *Rhodococcus* PHBH Genes

Cultivation of *Rhodococcus opacus* 557 and *Rhodococcus rhodnii* 135 was performed with 4-hydroxybenzoate as sole source of carbon and energy (Jadan et al., 2001). Genomic DNA from *R. opacus* 557 and *R. rhodnii* 135 was prepared from cells obtained after centrifugation of 50 mL cultures, which were subsequently washed with 50 mM Tris-HCl, pH 7.6 and treated with phenol-chloroform to extract the DNA (Sambrook and Russel, 2001). *Escherichia coli* DH5α (GIBCO BRL) and clones obtained were grown while shaking at 37°C in lysogeny broth (LB) medium (Sambrook and Russel, 2001) containing ampicillin (100 µg per mL).

Oligonucleotides were designed and synthesized according to the *N*-terminal and internal sequences of PHBH_{Ro} and PHBH_{Rr} (Montersino and van Berkel, 2013). In addition, primers were designed using the sequences of conserved regions of PHBH_{Pf} (Weijer et al., 1982), and PHBHs from *Acinetobacter* sp. ADP1 (DiMarco et al., 1993) and *Azotobacter chroococcum* (Quinn et al., 2001).

The constructs pROPOB1 and pRRPOB1 were obtained by cloning the 870 bp PCR products of primers fw-Rh557 [GAA (CT)AC CCA (AG)GT (CG)GG CAT (ACT)GT] and rev-pobA [CGGT(GC)G G(GC)G G(GC)A C(AGT)A T(AG)T G] with *R. opacus* 557 or *R. rhodnii* 135 DNA into the *EcoRV* site of pBS T-tailed as described elsewhere [pBluescript II SK(+), Stratagene; (Marchuk et al., 1991)]. Inserts obtained from *EcoRV* digested plasmid DNA were labeled with digoxigenin by using the DIG DNA Labeling and Detection Kit Nonradioactive (Boehringer, Germany) for the detection of fragments on Southern blots of *EcoRI*-digested *R. opacus* 557 or *R. rhodnii* 135 DNA. Respective DNA-fragments were purified from agarose gels, ligated into *EcoRI*-digested and dephosphorylated pBS. The resulting plasmid was transformed into *E. coli* DH5α and obtained colonies checked by colony hybridization as described elsewhere (Eulberg et al., 1997). Positive clones pRoPOB1-1 contained a 9.8 kb *EcoRI* fragment of *R. opacus* 557 DNA and pRrPOB1-1 a 7.8 kb *EcoRI* fragment of *R. rhodnii* 135 DNA, respectively, comprising the complete *pobA* genes. Subclones containing less flanking DNA regions were obtained by using various restriction endonucleases as shown in **Figure S1**.

DNA sequencing and sequence analysis was performed with common primers such as T3, T7, M13, or rM13 and respective

Abbreviations: PHBH, *p*-hydroxybenzoate hydroxylase; PHBH_{Pf}, PHBH from *Pseudomonas fluorescens*; PHBH_{Ro}, PHBH from *Rhodococcus opacus* 557; PHBH_{Rr}, PHBH from *Rhodococcus rhodnii* 135; PHBH_{Ro1CP}, PHBH from *Rhodococcus opacus* 1CP; PHBH_{Cn1}, PHBH-1 from *Cupriavidus necator* JMP134; PHBH_{Cn2}, PHBH-2 from *Cupriavidus necator* JMP134.

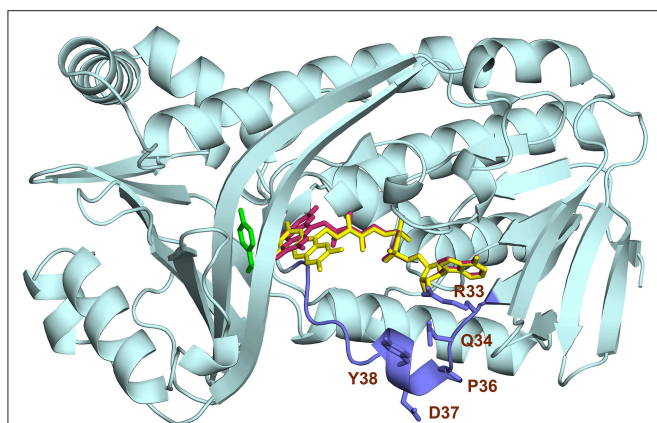


FIGURE 1 | Flavin mobility in *p*-hydroxybenzoate hydroxylase. Cartoon image of the crystal structure of PHBH_{Pr} with the FAD cofactor in the *in* (red; pdb entry 1pbe) and *out* (yellow; pdb entry 1pdh) conformation. The substrate is colored green and the region containing helix H2 is colored blue. The indicated amino acids in the helix H2 region have been replaced by site-directed mutagenesis to alter the pyridine nucleotide coenzyme specificity (Eppink et al., 1999).

software as described previously (Gish and States, 1993; Thiel et al., 2005; Felsenstein, 2009).

Rhodococcus opacus 1CP is a model strain for the degradation of aromatic compounds (Eulberg et al., 1997) and encodes a single PHBH-like protein (accession number ANS30736) which is 99% similar to the other *Rhodococcus* PHBHs reported herein. The corresponding gene *pobA* was amplified by PCR and cloned into pET16bp as described earlier Riedel et al., 2015. Using the primers *pobA*-fw (5'-catatgaacacacaggtcggtatc-3') and *pobA*-rev (5'-gggtacctcagcccagcggtg-3') allowed introducing NdeI/NotI restriction sites for cloning. The subsequent cultivation and expression was done as described below for the *Cupriavidus* enzymes.

Cloning and Expression of *Cupriavidus necator* PHBH Genes

Ralstonia eutropha (also designated as *Cupriavidus necator*) JMP134 harbors a number of enzymes involved in degradation of aromatic compounds and amongst those two PHBH-like proteins (accession numbers KX345395 and KX345396 for PHBH_{Cn1} and PHBH_{Cn2}, respectively; Pérez-Pantoja et al., 2008). The PHBH-encoding genes AOR50758 and AOR50759 were codon optimized according to the codon table of *Acinetobacter* sp. ADP1, synthetically produced, obtained in a pEX-cloning vector and cloned into pET16pb by methods reported earlier Oelschlägel et al., 2015; Riedel et al., 2015. Cloning was performed using *E. coli* DH5α and LB medium (10 g tryptone, 5 g yeast extract and 10 g NaCl per L) was used with ampicillin (100 μg per ml). For gene expression, the pET construct was transferred to *E. coli* BL21 (DE3) pLysS and cultivated in LB medium containing ampicillin (100 μg per ml) and chloramphenicol (34 μg per ml). Fernbach flasks (1 L) were used and the cultures were grown at 37°C until an OD600 of 0.2 and subsequently

cooled to 20°C. At an OD600 of about 0.5 the gene expression was induced by adding IPTG (0.5 mM) and the cultures were continued at 20°C for 20 h. Afterwards cells were harvested by centrifugation (1 h at 5,000 × g, 4°C) and the pellets were stored at −20°C.

Purification of PHBH Enzymes

The cell pellets were resuspended in 50 mM Tris/sulfate buffer (pH 7.5) while adding 8 units DNaseI (AppliChem—BioChemica, Darmstadt). Cells were broken through ultrasonic treatment (15 times 30 s, 70% power using a HD 2070, MS 72, Bandelin Sonoplus) in an ice-bath. Cell debris was removed by centrifugation (20,000 × g for 20 min, 4°C). After filtration through a cellulose membrane (0.2 μm pore size) to remove remaining particles, the crude extracts were subjected to Ni-chelate chromatography using a 1 ml HisTrap FF column (GE Healthcare) mounted in an ÄKTA fast-performance liquid chromatographer (GE Healthcare). The column was pre-equilibrated with 10 mM Tris/sulfate buffer (pH 7.5). After applying the cell extract, the column was washed with 3 ml loading buffer and then with loading buffer containing 25 mM imidazole until no protein eluted anymore (about 6 ml). Next we started a gradient to achieve 500 mM imidazole in the loading buffer within 6 ml. Target protein eluted during this gradient. Fractions were collected in 1 ml size and checked for standard PHBH activity (see section Enzyme Activity Measurements and Product Analysis). Active fractions were pooled and concentrated and buffer exchanged using Amicon Ultra-15 centrifugal filter devices (30 kDa) in 50 mM Tris/sulfate buffer (pH 7.5) containing 45% glycerol. The enzyme samples were stored at −20°C until further use. Protein concentration was determined by means of a Bradford assay.

Enzyme Activity Measurements and Product Analysis

Enzyme activity measurements were performed at 30°C in 50 mM Tris/sulfate buffer (pH 7.5), containing 60 μM FAD, 175 μM NAD(P)H (or 0 to 175 μM if varied) and 500 μM 4-hydroxybenzoate (or 0–500 μM if varied). Reactions were started by adding 20–40 nM of enzyme solution. All assays were performed in triplicate and either followed by the decrease in absorption at 340 nm ($\epsilon_{340} = 6.22 \text{ mM}^{-1} \text{ cm}^{-1}$) or by HPLC analysis of 3,4-dihydroxybenzoate. For HPLC analysis, five samples were taken at 1 min intervals and reactions were stopped adding ice-cold methanol. Before analysis, samples were centrifuged at 17,000 × g for 2 min to remove protein precipitates. HPLC (10 μl sample volume) was performed with a C18 reverse phase column (Knauer) running in a Ultimate3000 (ThermoScientific) UHPLC system. Elution was done isocratically with 0.1% trifluoroacetic acid, containing 30% methanol (flow rate 1 ml per min; 6 min total run time). Authentic standards of 4-hydroxybenzoate, NAD(P)H, NAD(P)⁺ and 3,4-dihydroxybenzoate were used to calibrate the system. Absorption was continuously monitored at 215 nm and spectra of eluting compounds were acquired with a diode array detector.

Phylogenetic Analysis

PHBH protein sequence analyses were performed using the NCBI BlastP-service (Altschul et al., 1990). In total, 70 PHBHs of various bacterial phyla were selected and used for *in silico* analyses. The protein sequences from *P. putida* KT2440 (NP_746074; salicylate hydroxylase), *C. testosterone* TA441 (BAA82878; 3-(3-hydroxyphenyl)propionate hydroxylase), *S. chlorophenolicum* L-1 (AAF15368; pentachlorophenol monooxygenase), and *Acinetobacter* sp. ADP1 (AAF04312; salicylate hydroxylase) served as appropriate out-group, as reported earlier (Suemori et al., 2001; Pérez-Pantoja et al., 2008).

The sequence information was used for a phylogenetic analysis allowing functional annotation of PHBH genes. Several algorithms (Fitch-Margoliash, maximum parsimony, maximum likelihood, and neighbor joining) were applied to obtain reliable sequence alignments and representative distance trees. The following software tools were used: Clustal-X (ver. 1.8) (Higgins and Sharp, 1988; Thompson et al., 1997), GeneDoc (ver. 2.6.003), the PHYLIP 3.66 package (PROTDIST and FITCH) (Felsenstein, 2005), and MEGA5 (Tamura et al., 2011). Bootstraps of 1,000 replicates were calculated from the corresponding alignment by means of the PHYLIP 3.66 package (SEQBOOT, PROTDIST, FITCH, and CONSENSE) (Felsenstein, 2005).

Sequence logos were constructed as follows: the PHBH_{pf} protein sequence was used as input query for a BlastP (NCBI) (Altschul et al., 1990) search using the non-redundant protein sequences database. Only sequences with an E-value smaller than $1e^{-100}$ were selected. After filtering the output sequences for duplicates, crystal structure sequences and cloned protein variants using Sequence Dereplicator and Database Curator (SDDC, ver. 2.0) (Ibrahim et al., 2017), the sequences of the protein segment involved in pyridine nucleotide coenzyme binding were selected and aligned using Clustal Omega (Sievers et al., 2011). The top 200 protein segment sequences were used to generate a sequence logo using the WebLogo server (ver. 2.8.2, Crooks et al., 2004). This process was repeated with the PHBH_{Ro} protein sequence as query input.

Protein Energy Profiling

The phylogenetic analysis and its outcome is of major relevance for the identification of the pyridine nucleotide coenzyme binding sites. The above described methods were validated by the herein described protein energy profiling, which allows for drawing sequence—structure relations (Heinke et al., 2015).

Obtaining energy profiles from protein structures is realized by means of a coarse-grained residue-level pair potential function. Based on the theoretical assumptions elucidated in Wertz and Scheraga (1978), Eisenberg and McLachlan (1986), and Dressel et al. (2007), this energy model approximates the hydrophobic effect by utilizing buried and exposed preferences for each of the 20 canonical amino acids. Given a set of globular protein structures, one can determine the frequencies for each amino acid of being exposed on the outside or buried inside the protein by using the DSSP program (Kabsch and Sander, 1983) as proposed by Ofra and Rost (2003) or by determining residue orientation and local spatial residue packing (Dressel et al., 2007; Heinke and Labudde, 2012). The energy potential (E_i)

is calculated using the following equations:

$$e_i = -\ln\left(\frac{f_{bur,i}}{f_{exp,i}}\right), \quad (1)$$

$$e_{ij} = e_i + e_j, \quad (2)$$

$$E_i = \sum_{j \in \text{Protein}, j \neq i} g(i, j) [e_{ij}]. \quad (3)$$

Given a residue at sequence index i , the single-residue potential e_i is computed using the amino acid-specific buried-exposed frequency ratio (Equation 1). As shown in Equation (2), the pair potential e_{ij} between two residues at indices i and j corresponds to the sum of single-residue potentials in this model. Finally, by iterating over all residues that are in contact with residue i , the potential E_i is derived (Equation 3). A contact between two residues (i and j) is assumed, if the C β - C β atom distance is $<8 \text{ \AA}$ (in case of Gly, C α atom coordinates are used as spatial reference points instead).

The sequence of residue energy potentials ($E_1, \dots, E_i, \dots, E_n$) corresponds to the protein's energy profile (Dressel et al., 2007; Heinke and Labudde, 2012, 2013; Heinke et al., 2015). In addition, an algorithm for aligning two energy profiles has been adapted from Mrozek et al. (2007) which, besides detecting similarities and differences of residue energy potentials, can also give a distance scoring function (referred to as dScore) as a measure of global energy profile similarity of two energy profiles P_1 and P_2 (Heinke and Labudde, 2013; Heinke et al., 2015):

$$\text{dScore}(P_1, P_2) = -\log\left(\frac{x_r - \bar{x}_p}{x_{\text{Opt}} - \bar{x}_p}\right), \quad (4)$$

where

$$x_{\text{Opt}} = \frac{\delta(|P_1| + |P_2|)}{2}. \quad (5)$$

The dScore corresponds to the normalized energy profile alignment raw score x_r with respect to the average score \bar{x}_p obtained from random energy profiles and the highest possible dScore x_{Opt} of two profiles with lengths $|P_1|$ and $|P_2|$. Here, δ acts as an alignment parameter with $\delta > 0$. The negative logarithm leads to a distance-like formulation, with two identical energy profiles yielding a dScore of 0.

Two PHBH structures PDB ID: 1d7l (Ortiz-Maldonado et al., 1999) and PDB ID: 1bgj (Eppink et al., 1998a) were retrieved from the Protein Data Bank (Rose et al., 2011) and used as modeling templates for automated comparative modeling using Modeler (ver. 9.14) (Eswar et al., 2006).

Seventy PHBH sequences (including 15 sequences of biochemically characterized PHBHs and 55 randomly selected PHBH sequences from various bacteria) were used for automated comparative modeling (average sequence identity of $\sim 50\%$). For each PHBH sequence, five comparative models were generated from which the model with the best corresponding DOPE score (Eswar et al., 2006) was selected for energy profile calculation. In the first step of energy profile analyses, energy profile distance trees were generated. As shown recently (Heinke and Labudde, 2013; Heinke et al., 2015) such distance trees can indicate

functional and structural relations and, in case of PHBHs, can support the proposed molecular evolution. To obtain such distance trees, pairwise energy profile alignments were computed as elucidated and, for each energy profile alignment, the corresponding dScore was derived, leading to an energy profile distance matrix. By utilizing the un-weighted pair group method arithmetic mean (Sokal and Michener, 1958) and neighbor joining (Saitou and Nei, 1987) with the derived distance matrix as input, distance trees were generated.

Evolutionary Rate Calculation

The Rate4Site tool (ver. 2.01) (Mayrose et al., 2004) was used for determining conserved amino acids in PHBH proteins specific for NADPH and NADH, respectively. Multiple sequence alignments were made from selections containing only sequences of pseudomonads and rhodococci, which were used as input to calculate evolutionary rates for all amino acids applying default settings of Rate4site. The obtained values for conservation were scaled to b-factors ranging between 0 and 100. These b-factors were used to color the image of the crystal structure of PHBH_{pf} as example of a NADPH-specific protein. In a similar way, the image of the model structure of PHBH_{Ro} as an example of a NADH-preferring protein, was colored. The program Pymol (ver. 1.4) (Schrodinger, 2011) was used to create structure images.

NADPH Docking in PHBH From *Pseudomonas fluorescens*

The three-dimensional structure of the PHBH_{pf} monomer with the FAD cofactor in the *out* conformation (PDB ID: 1pdh) was used to access the mode of NADPH binding. Docking was performed using HADDOCK (ver. 2.0) (de Vries et al., 2010). The solvated docking was carried out with the recommended parameters of HADDOCK. A distance restraint of 9.0 Å was set between C4N of NADPH and C4a of the flavin cofactor. For rigid-body energy minimization, 2,000 structures were generated, and the 200 lowest energy solutions were used for subsequent semi-flexible simulated annealing and water refinement. Resulting structures were sorted according to intermolecular energy and clustered using a 6.5 Å cut-off criterion. Subsequent cluster analysis was performed within a 2.0 Å cut-off criterion. The structure with the lowest score was selected for generating an image showing the NADPH binding mode of PHBH_{pf}.

Accession Numbers

PHBH sequences determined in this study are available from the GenBank/EMBL/DDBJ nucleotide sequence databases under accession numbers KF234626 for *R. opacus* 557 and KF234627 for *R. rhodnii* 135.

RESULTS

Pyridine Nucleotide Coenzyme Specificity of Biochemically Characterized PHBHs

Most biochemically characterized PHBHs with known amino acid sequence are strictly dependent on NADPH (Table 1). However, PHBH from *R. opacus* 557 (PHBH_{Ro}) and PHBH from

R. rhodnii 135 (PHBH_{Rr}) show a clear preference for NADH (Jadan et al., 2001, 2004). This prompted us to determine the amino acid sequences of PHBH_{Ro} and PHBH_{Rr} (see Methods). Genomic *R. opacus* 557 DNA contained a 1,179-bp open reading frame coding for a PHBH polypeptide of 392 amino acids. The amino acid sequence predicted from the open reading frame corresponded with the experimentally determined *N*-terminal sequence of the protein (MNTQVGIVGGGAGLM) and with the *N*-terminal sequence (TDHFRQYPFAWFGILAEAPP) of an internal 25 kDa tryptic fragment. Genomic *R. rhodnii* 135 DNA contained a 1,191-bp open reading frame coding for a PHBH polypeptide of 396 amino acids.

In this paper, amino acid residues are numbered according to the sequence of PHBH_{pf} (CAA48483) to facilitate reference to the 3D-structure. The amino acid sequences of PHBH_{Ro} (accession number KF234626) and PHBH_{Rr} (accession number KF234627) both share 46.7% identical positions with PHBH_{pf} (Figure 2). Their helix H2 regions, proposed to be involved in determining the pyridine nucleotide coenzyme specificity (Eppink et al., 1999), deviate in amino acid sequence from that of NADPH-specific PHBHs (Figure 2). The latter enzymes typically contain the fingerprint sequence 32-ERxxx(D/E)YVLxR, while the NADH-preferring *Rhodococcus* PHBHs contain the sequence 32-E(S/C)RTREEVEGT.

Pyridine Nucleotide Coenzyme Specificity of Newly Produced PHBHs

His₁₀-tagged forms of two putative PHBHs originating from *C. necator* JMP134 were successfully produced by recombinant expression in *E. coli* BL21 (DE3) and purified by nickel-chelate chromatography (see section Materials and Methods). HPLC experiments confirmed that both isoforms produce 3,4-dihydroxybenzoate as sole product from 4-hydroxybenzoate (Figure S2). Activity measurements with either NADH or NADPH established that PHBH_{Cn2} is strictly dependent on NADPH whereas PHBH_{Cn1} can utilize both coenzymes to perform aromatic hydroxylation. Determination of the apparent kinetic parameters *k*_{CAT} and *K*_M (Table 2) through monitoring NAD(P)H consumption as well as 3,4-dihydroxybenzoate production revealed that PHBH_{Cn1} has a slight preference for NADH and that the NADPH-specific PHBH_{Cn2} is about four times more active than PHBH_{Cn1}. These experiments also revealed that both enzymes suffer to some extent from uncoupling of substrate hydroxylation resulting in hydrogen peroxide as by-product, thus yielding aromatic product/NAD⁺ ratios of 0.73 and 0.81 for PHBH_{Cn1} and PHBH_{Cn2}, respectively.

We also determined the pyridine nucleotide coenzyme specificity of the His₁₀-tagged form of a putative PHBH from *R. opacus*-1CP (see section Materials and Methods). Kinetic analysis of this enzyme (PHBH_{Ro1CP}) established a clear preference for NADH (Table 2).

The amino acid sequences of the PHBHs from *C. necator* JMP134 and *R. opacus* 1CP are in agreement with the experimentally determined coenzyme specificities. PHBH_{Cn2} contains the NADPH-preferring sequence motif 32-EQRSPEYVLGR, while PHBH_{Ro1CP} contains

TABLE 1 | Pyridine nucleotide coenzyme specificity of biochemically characterized *p*-hydroxybenzoate hydroxylases.

Source	Accession number	Cofactor preference	References
<i>Pseudomonas fluorescens</i>	CAA48483	NADPH	Howell et al., 1972; Weijer et al., 1982; van Berkel et al., 1992
<i>Pseudomonas putida</i> WCS358	CAB64666	NADPH	Bertani et al., 2001
<i>Pseudomonas fluorescens</i> IFO14160	BAB20910	NADPH	Suemori et al., 1995, 2001
<i>Pseudomonas aeruginosa</i> PAO1	NP_248938	NADPH	Entsch et al., 1988; Entsch and Ballou, 1989
<i>Acinetobacter</i> sp. ADP1	YP_046383	NADPH	DiMarco et al., 1993; Fernandez et al., 1995
<i>Pseudomonas fluorescens</i> ATCC13525	AAA25834	NADPH	Shuman and Dix, 1993
<i>Rhizobium leguminosarum</i> B155	AAA73519	NADPH	Wong et al., 1994
<i>Azotobacter chroococcum</i> ATCC9043	AAB70835	NADPH	Quinn et al., 2001
<i>Corynebacterium glutamicum</i> ATCC 13032	NP_600305	NAD(P)H	Huang et al., 2008
<i>Pseudomonas</i> sp. CBS3	CAA52824	NAD(P)H	Seibold et al., 1996
<i>Rhodococcus opacus</i> 557	KF234626	NADH	Jadan et al., 2001, this paper
<i>Rhodococcus rhodnii</i> 135	KF234627	NADH	Jadan et al., 2001, this paper
<i>Rhodococcus opacus</i> 1CP	ANS30736	NADH	This paper
<i>Cupriavidus necator</i> JMP134	KX345395*	NAD(P)H	This paper
<i>Cupriavidus necator</i> JMP134	KX345396*	NADPH	This paper

*The accession numbers of proteins with N-terminal His₁₀-tags obtained of codon optimized genes are provided and correspond to original sequences from the JMP134 genome as follows: KX345395 to YP_298206, and KX345396 to YP_299212 (see **Figure S3**).

the NADH-preferring sequence motif 32-ESRTREEVEGT. The NAD(P)H-dependent PHBH_{Cn1} contains the sequence 32-EDCTQAHVEAR.

PHBH Distribution Among the Tree of Life

Bacteria capable of degrading various aromatic compounds convert the consecutive degradation products into 4-hydroxybenzoate, which then can be funneled into the protocatechuate pathway. Thus, the PHBH enzyme necessary for this route can be expected to be common among microorganisms capable of degrading these aromatic compounds.

Using the amino acid sequence of the NADPH-specific PHBH_{Pf} as query sequence for a BlastP search, we identified many putative PHBHs among bacterial phyla with an aerobic lifestyle. Most of them are present in proteobacteria, while roughly 10% is present in *Actinobacteria*. In the other domains of life, PHBH is rarely present. In Archaea, a few putative PHBHs are found, while in Eukarya a small number of hypothetical PHBHs are identified in basidiomycetes such as *Ceratitis capitata*, XP_004528594; *Trichosporon oleaginosus* IBC246, KLT40385; and *Trichosporon asahii* var. *asahii* CBS 2479, EJT53028. Some of them are similar to PHBH-like proteins of proteobacteria, while others show a high similarity to PHBH-like proteins encoded by *Streptomyces* species (cf. **Figure S3a**).

By limiting the BlastP output to an E-value smaller than $1e^{-100}$, 6135 sequences were retrieved. From these sequences, 1423 had an unique sequence for the loop-helix H2 region. Taking the first 200 sequences of this group for construction of a sequence motif showed that the previously found motif 32-ERxxx(D/E)YVLxR for NADPH specificity is more accurately described by 32-ERx(S/T)x(D/E)YVL(G/S)R (**Figure 3A**). Similarly, by using the NADH-preferring PHBH_{Ro} protein sequence as BlastP query, we found 6,337 sequences

with an E-value smaller than $1e^{-100}$, having 1564 unique loop-helix H2 regions. Taking the first 200 sequences of this group for construction of a sequence motif showed that the NADH-preferring PHBH motif is represented by 32-ExR(S/T)Rxx(I/V)ExT (**Figure 3B**). After filtering duplicates from the combined total number of 12472 PHBH sequences, 6,482 sequences were unique. Thus, a large overlap exists between the two groups. In the dataset obtained using the PHBH_{Pf} sequence, 145 sequences were not present in the dataset obtained with the PHBH_{Ro} sequence. Vice versa, 347 sequences were not found in the PHBH_{Pf} dataset. The distribution of the sequences not present in each dataset (**Figure S3b**) shows that most of the sequences only present in the *Ro*-dataset are found among the first 2,000 sequences, while those for the sequences only present in the *Pf*-dataset are located in the last 3,000 sequences of each group.

Interestingly, among the actinobacterial sequences presently available, most comprise the NADH-preferring fingerprint. However, *Mycobacteria* have a mixed type motif, often the first or both arginine(s) of the NADH-fingerprint are present but the remaining part is lacking. In addition, many mycobacterial sequences have parts of the NADPH-preferring fingerprint, especially, x(D/E)YVL(G/S)R. Among the *Streptomyces* sequences many have the NADH-preferring fingerprint, but some also have a mixed type like *Mycobacteria*. However, these mixed-type fingerprints do not have larger parts of the NADPH-fingerprint and are more similar to the sequence of *Cupriavidus* PHBH_{Cn1} and thus might accept both NADH and NADPH. Among rhodococci, the NADH-fingerprint is highly conserved and only a few examples of a mixed type were identified, for example among plant pathogens as *Rhodococcus fascians*, which shows a similar sequence to some *Mycobacteria*. Hereafter, we focused on bacterial PHBHs from which 70

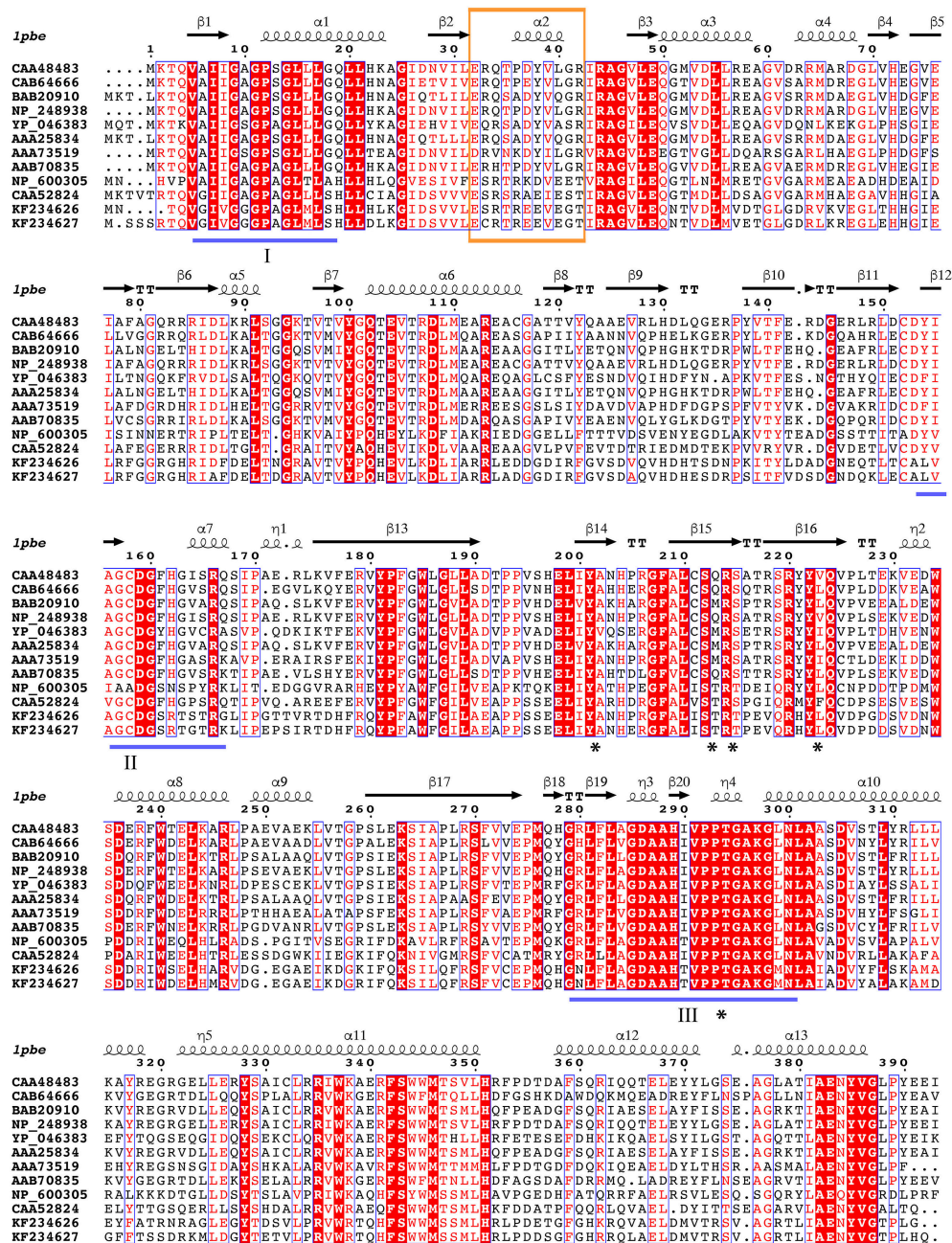
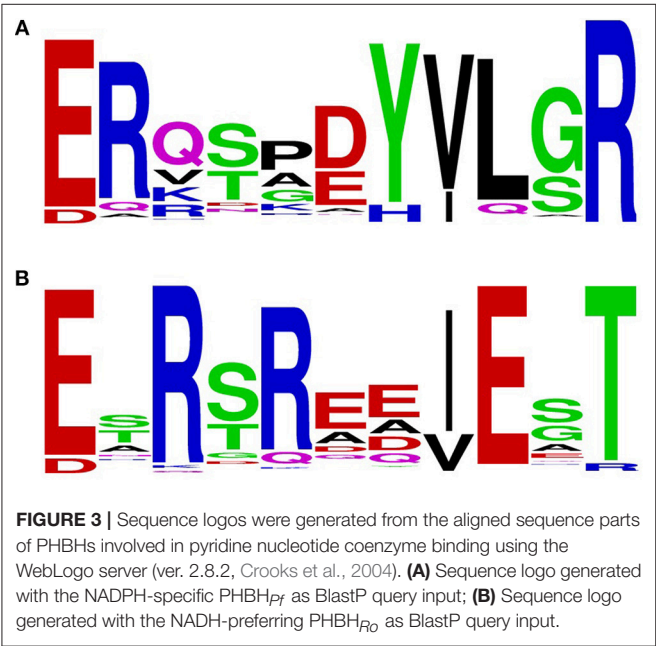


FIGURE 2 | Multiple sequence alignment of selected PHBHs. Accession numbers are given in **Table 1**. PHBH_{Ro} is KF234626 and PHBH_{Ar} is KF234627. Identical residues are shown in red. Flavin binding motifs are underlined in blue (I: “GXGXXG”; II: “DG”; III: “GD”; Eppink et al., 1997). Secondary structure assigned from the PHBH_{Ar} crystal structure (PDB ID: 1pbe) is indicated above the sequences. The pyridine dinucleotide cofactor recognizing fingerprint region is boxed and residues in direct contact with the substrate are marked with an asterisk. The diagram was produced using ESPript (Robert and Gouet, 2014).

TABLE 2 | Apparent steady-state kinetic parameters of newly produced PHBH enzymes.

Enzyme	Method and corresponding results					
	UV/VIS—NAD(P)H consumption			HPLC—product formation		
	V_{MAX} [U mg ^{−1}]	k_{CAT} [s ^{−1}]	K_{M} [μM]	V_{MAX} [U mg ^{−1}]	k_{CAT} [s ^{−1}]	K_{M} [μM]
Variable NADH (0–175 μM), constant 4-hydroxybenzoate (500-μM)						
PHBH _{Cn1}	12.3 ± 0.5	9.4 ± 0.4	49.8 ± 5.6	not determined		
PHBH _{Ro1CP}	20.0 ± 0.9	15.3 ± 0.7	39.7 ± 5.0	not determined		
Constant NADH (175 μM), variable 4-hydroxybenzoate (0–500-μM)						
PHBH _{Cn1}	9.9 ± 0.2	7.6 ± 0.2	20.2 ± 2.3	9.0 ± 0.1	6.8 ± 0.1	19.3 ± 1.4
PHBH _{Cn2}	- no activity measurable -					
PHBH _{Ro1CP}	16.8 ± 0.3	12.9 ± 0.2	30.4 ± 2.4	21.8 ± 1.0	16.8 ± 0.8	49.9 ± 7.3
Variable NADPH (0–175 μM), constant 4-hydroxybenzoate (500-μM)						
PHBH _{Cn2}	49.1 ± 3.7	37.0 ± 2.8	146 ± 20	not determined		
PHBH _{Ro1CP}	19.8 ± 2.0	15.0 ± 1.5	153 ± 16	not determined		
Constant NADPH (175-μM), variable 4-hydroxybenzoate (0–500-μM)						
PHBH _{Cn1}	8.6 ± 0.1	6.5 ± 0.1	19.4 ± 1.2	6.1 ± 0.2	4.6 ± 0.1	20.4 ± 2.5
PHBH _{Cn2}	27.0 ± 1.0	18.0 ± 0.7	26.4 ± 4.4	40.0 ± 1.8	30.4 ± 1.5	30.6 ± 5.6
PHBH _{Ro1CP}	11.3 ± 0.1	8.7 ± 0.1	35.0 ± 1.6	12.5 ± 0.4	9.6 ± 0.3	42.0 ± 4.9



sequences (including the 15 biochemically characterized PHBHs and 55 randomly chosen candidates of various bacteria) were chosen for further analysis of the pyridine nucleotide coenzyme specificity.

Phylogenetic Analysis

The 70 selected PHBH amino acid sequences and 4 distinct proteins (as out-group as reported elsewhere; Pérez-Pantoja et al., 2008) were used to generate an extended multiple sequence alignment (Figure S1). All sequences in the alignment

(except ZP_01743892) harbor the three consensus sequences of flavoprotein hydroxylases involved in FAD binding (Eppink et al., 1997). Furthermore, residues in direct contact with the aromatic substrate are strongly conserved. These residues include Tyr201 and Pro293, which interact with the phenolic moiety, and Ser212, Arg214, and Tyr222, involved in binding the carboxylic group of 4-hydroxybenzoate (Schreuder et al., 1989). With exception of Ser212 (97% Ser, 3% Thr), these residues are 100% conserved.

As already indicated by the pairwise similarity data, the distance tree of bacterial PHBHs (Figure 4) does not reflect the taxonomic relationships, in contrast to what one might expect for a chromosomally encoded enzyme. While some branches in the distance tree represent sequences of only relatively closely related strains, such as various *Burkholderia* strains or various *Rhodococcus* strains, other branches represent relatively closely related PHBHs from taxonomically distant bacteria (e.g., from the phyla of proteobacteria *Acinetobacter* sp. ADP1, *C. necator* JMP134, *Polaromonas* sp. JS666, *Mesorhizobium loti* MAFF303099, and *Rhodospseudomonas palustris* CGA009).

Interestingly, the distance tree clearly reflects the pyridine nucleotide coenzyme preference shown in Table 1. All NADPH-specific PHBHs are located on one side of the tree and on the opposite side the NADH-preferring enzymes are clustered. In between these types we mostly find PHBHs for which a pyridine nucleotide coenzyme preference is not proven yet. However, this preference can be predicted from the phylogenetic tree, and we conclude that representatives closer to the NADH-assigned PHBHs can use both coenzymes, with a preference for NADH. We experimentally confirmed this conclusion by determining the pyridine nucleotide specificity of PHBH_{Cn1}, a newly produced representative of this group (Table 2). In the other part of the tree closer to the NADPH-assigned enzymes, PHBHs may also use both pyridine nucleotides but tend to be stricter or even exclusively dependent on NADPH. The out-group of the

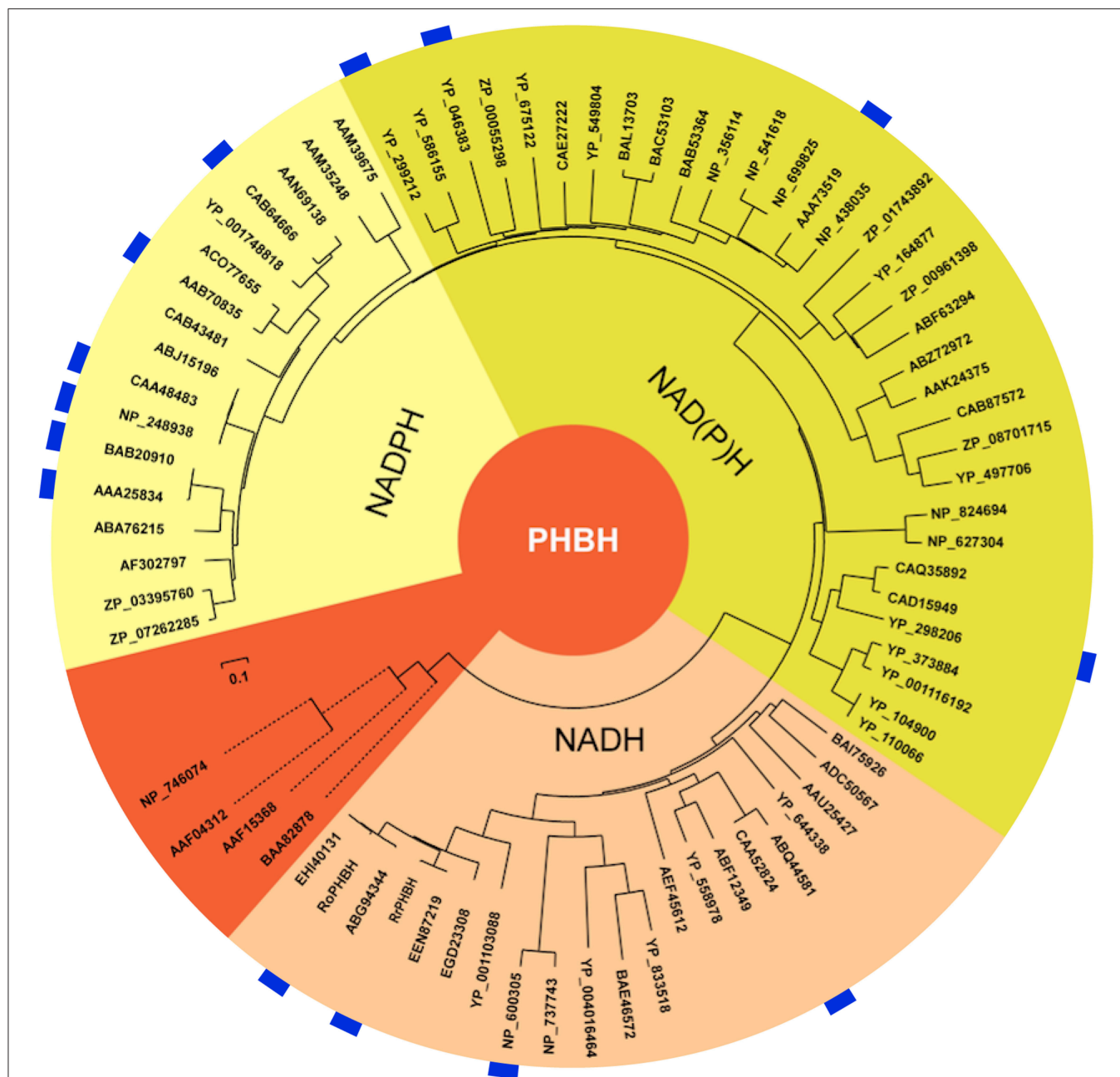


FIGURE 4 | Distance tree illustrating the sequence similarities and predicted pyridine nucleotide coenzyme specificities of PHBHs. The distance tree is based on a similar alignment as that in **Figure 2**, but now with 74 sequences (**Figure S1**). The biochemically characterized PHBHs (**Table 1**) are indicated in blue. The additional accession numbers for (putative) PHBHs are as follows: *Acinetobacter* sp. ADP1, YP_046383; *Agrobacterium tumefaciens* C58, NP_356114; *Arthrobacter* sp. FB24, YP_833518; *Azospirillum* sp. B510, BAI75926; *Azotobacter chroococcum*, AAB70835; *Azotobacter vinelandii* DJ, ACO77655; *Bacillus licheniformis* ATCC 14580, AAU25427; *Bacillus pseudofirmus* OF4, ADC50567; *Bradyrhizobium japonicum* USDA 110, BAC53103; *Bradyrhizobium japonicum* USDA 6, BAL13703; *Brucella melitensis* bv. 1 16M, NP_541618; *Brucella suis* 1330, NP_699825; *Burkholderia mallei* ATCC 23344, YP_104900; *Burkholderia pseudomallei* K96243, YP_110066; *Burkholderia* sp. 383, YP_373884; *Burkholderia vietnamiensis* G4, YP_001116192; *Burkholderia xenovorans* LB400, YP_558978; *Caulobacter crescentus* CB15, AAK24375; *Caulobacter* sp. K31, ABZ72972; *Chelatovans* sp. BNC1, YP_675122; *Citromicrobium* sp. JLT1363, ZP_08701715; *Corynebacterium efficiens* YS-314, NP_737743; *Corynebacterium* sp. ATCC 13032, NP_600305; *Corynebacterium* sp. ATCC 51369, BAE46572; *Cupriavidus metallidurans* CH34, YP_586155; *Cupriavidus metalliredurans* CH34, ABF12349; *Frankia* sp. Eu1c, YP_004016464; *Magnetospirillum* sp. MS-1, ZP_00055298; *Mesorhizobium loti* MAFF303099, BAB53364; *Novosphingobium* sp. DSM 12444, YP_497706; *Polaromonas* sp. JS666, YP_549804; *Pseudomonas aeruginosa* PAO1, NP_248938; *Pseudomonas aeruginosa* UCBPP-PA14, ABJ15196; *Pseudomonas fluorescens* IFO14160, BAB20910; *Pseudomonas fluorescens* Pf0-1, ABA76215; *Pseudomonas fluorescens*, CAA48483; *Pseudomonas putida* KT2440, AAN69138; *Pseudomonas putida* W619, YP_001748818; *Pseudomonas putida* WCS358, CAB64666; *Pseudomonas* sp. ATCC 13525, AAA25834; *Pseudomonas* sp. CBS-3, ABQ44581; *Pseudomonas* sp. CBS3, CAA52824; *Pseudomonas* sp. IMT40, AF302797; *Pseudomonas* sp.

(Continued)

FIGURE 4 | strain HR199, CAB43481; *Pseudomonas syringae* syringae 642, ZP_07262285; *Pseudomonas syringae* tomato T1, ZP_03395760; *Ralstonia eutropha* JMP134, YP_298206; *Ralstonia eutropha* JMP134, YP_299212; *Ralstonia solanacearum* GMI1000, CAD15949; *Ralstonia solanacearum* MolK2, CAQ35892; *Rhizobium leguminosarum* B155, AAA73519; *Rhodococcus equi* ATCC 33707, EGD23308; *Rhodococcus erythropolis* SK121, EEN40131; *Rhodococcus jostii*, ABG94344; *Rhodococcus opacus* 557, KF234626; *Rhodococcus opacus* PD630, EHI40131; *Rhodococcus rhodnii* 135, KF234627; *Rhodopseudomonas palustris* CGA009, CAE27222; *Roseovarius nubinihibens* ISM, ZP_00961398; *Rubrobacter xylanophilus* DSM 9941, YP_644338; *Rugeria pomeroyi* DSS-3, YP_164877; *Rugeria* sp. TM1040, ABF63294; *Saccharopolyspora erythraea* sp. NRRL 2338, WP_009944246.1; *Sagittula stellata* E-37, ZP_01743892; *Serratia plymuthica* AS9, AEF45612; *Sinorhizobium meliloti* 1021, NP_438035; *Sphingomonas* sp. LB126, CAB87572; *Streptomyces avermitilis* MA-4680, NP_824694; *Streptomyces coelicolor* A3(2), NP_627304; *Xanthomonas axonopodis citri* 306, AAM35248; *Xanthomonas campestris* ATCC 33913, AAM39675. Some of the PHBH-like hypothetical proteins have been annotated as putative 2-polyphenyl-6-methoxyphenol hydroxylases. The start codons of the sequences of *Rubrobacter xylanophilus* DSM 9941, YP_644338, and *Cupriavidus metallidurans* CH34, YP_586155, were set manually in accordance to the other sequences in the alignment. Sequences from *P. putida* KT2440 (NP_746074; salicylate hydroxylase), *C. testosterone* TA441 [BAA82878; 3-(3-hydroxyphenyl) propionate hydroxylase], *S. chlorophenolicum* L-1 (AAF15368; pentachlorophenol monooxygenase), and *Acinetobacter* sp. ADP1 (AAF04312; salicylate hydroxylase) were used as out-groups (orange).

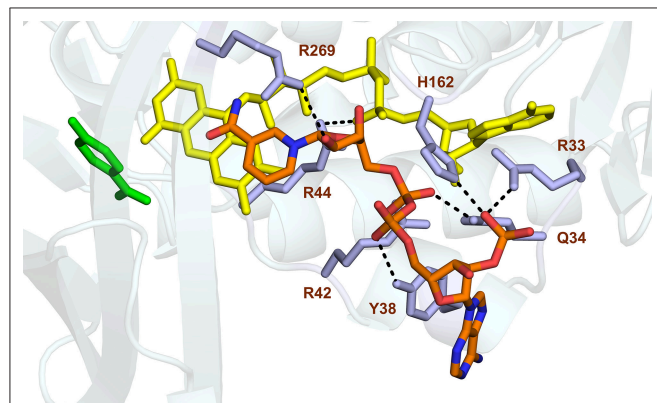


FIGURE 5 | Model of NADPH binding in PHBH_{pf}. Cartoon image of the PHBH protein chain in light blue, substrate in green, FAD cofactor (in the out position) in yellow and the docked NADPH colored by element. Amino acid residues Arg33, Gln34, Tyr38, Arg42, Arg44, His162, and Arg269, putatively involved in NADPH binding, are shaded in mauve. Hydrogen bonds are indicated by black dashes.

distance tree includes NAD(P)H-dependent enzymes (Pérez-Pantoja et al., 2008) and intersects the NAD(P)H using putative PHBHs close to the NADH-preferring PHBH type. From an evolutionary point of view this makes sense since a PHBH-predecessor protein might have used both nicotinamide cofactors or even had a preference for NADH. However, more questions on the PHBH evolution need to be answered, e.g., has the pyridine nucleotide coenzyme preference happened by chance or by adaptation, and why does it seem to be stable among certain bacteria, especially among *Actinobacteria*? Most *Actinobacteria* show a NADH-preferring fingerprint or a slightly altered one with the exception of *Mycobacteria*. This might be related to lifestyle and environment of those bacteria, which needs further investigations.

Energy Potentials of Residues Determining the Pyridine Nucleotide Coenzyme Specificity of PHBH

To get more insight into the evolutionary relationship of the pyridine nucleotide coenzyme specificity, we extracted energy potentials of residues located in the PHBH coenzyme fingerprint motifs from energy profile datasets. Pairwise alignments of these

sub-energy profiles have been computed and used for deriving dScores which, similar to the strategies elucidated in the Materials and Methods section, have been processed by un-weighted pair group method arithmetic mean clustering (Figures S4, S5) or neighbor joining hierarchical clustering (Figures S6, S7). A multiple sequence alignment-like representation of these energy potentials (Figures S8, S9) illustrates a strong relationship between residue composition, pyridine nucleotide coenzyme specificity, and energetic properties. First, it becomes clear that conserved residues in these motifs yield a conservation of their energetic state, with most energy potentials being relatively low. It can be proposed that these energetically conserved residues serve as fold stabilizing elements in these motifs as well as in the intra-molecular environment of helix H2. Compared to NADPH-specific and NAD(P)H-dependent PHBHs, NADH-preferring PHBHs yield a high-energetic, unstable environment (Figure S10), which is energetically determined by the presence of two conserved Glu-residues and variable positions which are predominantly occupied by destabilizing residues, such as Asp, Glu and Arg (Zhou and Zhou, 2004). In contrast to these findings, residues in the coenzyme fingerprint motif of NADPH-specific and NAD(P)H-dependent PHBHs yield comparatively low energy potentials and thus are partly stabilizing the binding moiety. It can be concluded that this deviation in molecular stability can contribute to the pyridine nucleotide coenzyme specificity and is an important driver of PHBH evolution.

Evolutionary Rate of NADPH-Specific and NADH-Preferring PHBHs

We used the Rate4site program (Materials and Methods section) to assess the evolutionary rate of NADPH-specific and NADH-preferring PHBHs. Figure S11 shows that the NADH-enzymes have more regions (colored red) susceptible to mutation compared to the NADPH-enzymes. Indeed, also the loop region with the coenzyme-binding motif is a little more mutation sensitive in the NADH-preferring enzymes, indicative of a strong selection favoring specific amino acids in the NADPH-specific enzymes.

Pyridine Nucleotide Coenzyme Binding

Studies from PHBH variants generated using site-directed mutagenesis support the idea that Tyr38 and Arg42 of helix H2 confer the specificity of PHBH_{pf} for NADPH (Eppink et al., 1998b, 1999; Huang et al., 2008). Based on these findings

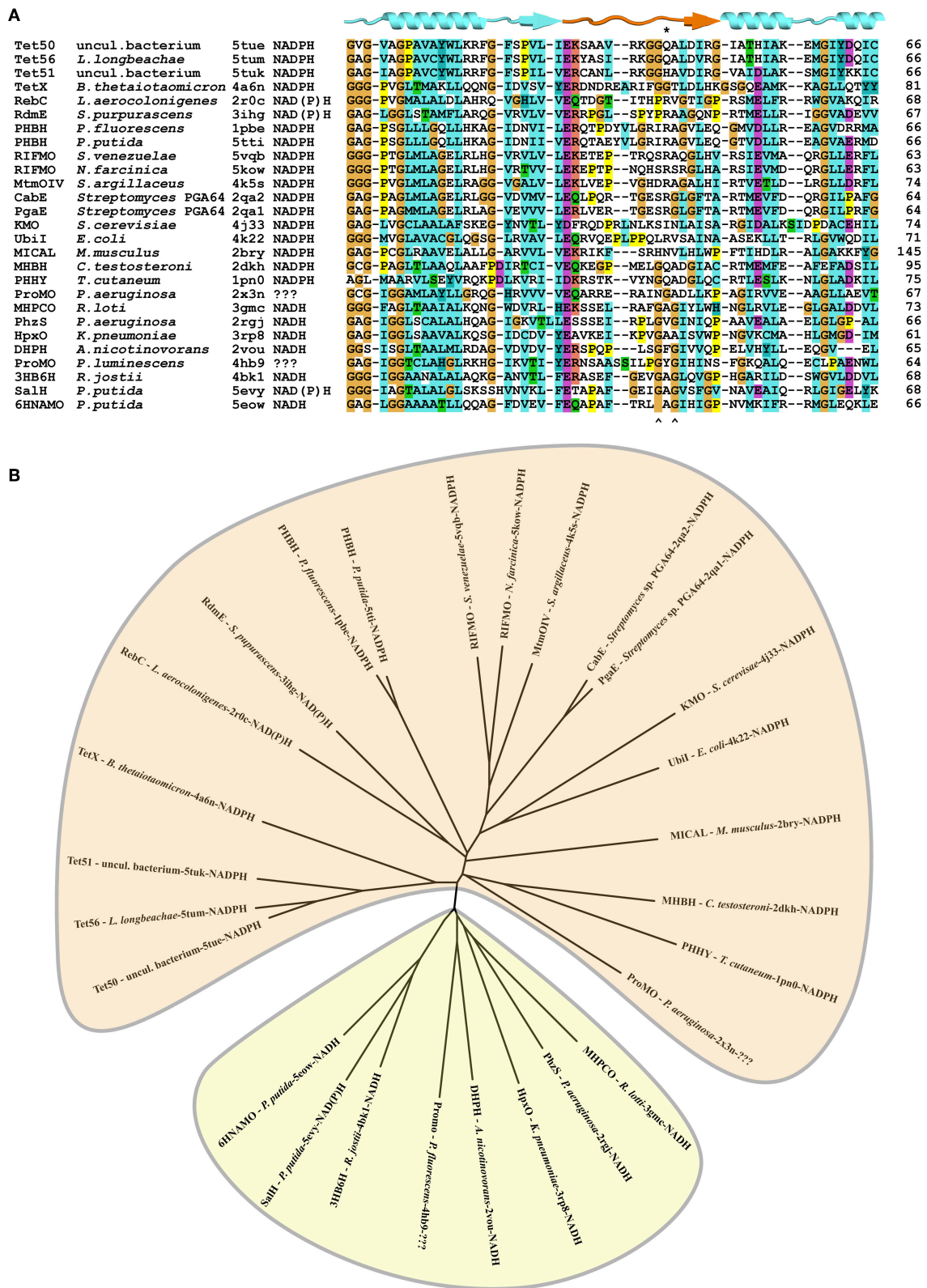


FIGURE 6 | Conservation of loop segment putatively involved in determining the pyridine nucleotide coenzyme specificity of group A flavoprotein monooxygenases. (A) Alignment of the sequences forming the loop structures putatively involved in NAD(P)H binding. Alignment of sequences was made using Clustal-X. PDB-entry (Continued)

FIGURE 6 | codes of the sequences used: 5tue, uncultured bacterium, tetracycline destructase (Tet50); 5tum, *Legionella longbeachae*, tetracycline destructase (Tet56); 5tuk, uncultured bacterium, tetracycline destructase (Tet51); 4a6n, *Bacteroides thetaiotaomicron*, tetracycline degrading monooxygenase (TetX); 2r0c, *Lechevalieria aerocolonigenes*, rebeccamycin biosynthetic enzyme (RebC); 3ihg, akalavione-11-hydroxylase (RdmE); 1pbe, *Pseudomonas fluorescens*, 4-hydroxybenzoate-3-hydroxylase (PHBH); 5tti, *Pseudomonas putida*, 4-hydroxybenzoate-3-hydroxylase (PHBH); 5vqb, *Streptomyces venezuelae*, rifampicin monooxygenase (RIFMO); 5kow, *Nocardia farcinica*, rifampicin monooxygenase (RIFMO); 4k5s, *Streptomyces argillaceus*; Baeyer-Villiger monooxygenase (MtmOIV); 2qa2, *Streptomyces* sp. PGA64, aromatic hydroxylase (CabE); 2qa1, *Streptomyces* sp. PGA64, aromatic hydroxylase (PgaE); 4j31, *Saccharomyces cerevisiae*; kynurenine monooxygenase (KMO); 4k22, *Escherichia coli*, 3-octaprenylphenol 2-monooxygenase (Ubil); 2bry, *Mus musculus*, catalytic region of molecule interacting with CasL (MICAL); 2dkh, *Comamonas testosteroni*, 3-hydroxybenzoate hydroxylase (MHBH); 1pn0, *Trichosporon cutaneum*, phenol hydroxylase (PHHY); 2x3n, *Pseudomonas aeruginosa*, probable FAD-dependent monooxygenase (ProMO); 3gmc, *Mesorhizobium loti*, 2-methyl-3-hydroxypyridine-5-carboxylic acid oxygenase (MHPCO); 2rgj, *Pseudomonas aeruginosa*, phenazine-modifying monooxygenase (PhzS); 3rp8, *Klebsiella pneumoniae* MGH 78578, urate oxidase (HpxO); 2vou, *Arthrobacter nicotinovorans*, 2,6-dihydroxypyridine-3-hydroxylase (DHPH); 4hb9, *Photobacterium luminescens*, probable FAD dependent monooxygenase (ProMO); 4bk1, *Rhodococcus jostii* RHA1, 3-hydroxybenzoate 6-hydroxylase (3HB6H); 5evy, *Pseudomonas putida*, salicylate hydroxylase (SalH); 5eow, *Pseudomonas putida* KT2440, 6-hydroxynicotinic acid 3-monooxygenase (6HNAMO). Secondary structure elements are indicated above the alignment, with the loop segment colored orange and the amino acid residue number of the last element in the alignment is listed for each sequence. The asterisk (*) indicates the position of R44 of Pf-PHBH and the circumflexes (^) indicate the glycine residues of the GxG motif in other sequences. The secondary structural elements above the sequences refer to the structure shown in **Figure 1**. **(B)** Distance tree related to the alignment of the sequences forming the loop structures putatively involved in determining the coenzyme specificity of group A flavoprotein monooxygenases. Enzymes in the beige area (top) prefer NADPH, those in the yellowish area (bottom) prefer NADH as coenzyme.

and the fact that the nicotinamide ring of NADPH binds at the *re*-side of the flavin (Manstein et al., 1986), we docked the NADPH in the enzyme-substrate complex of PHBH_{pf} with the isoalloxazine moiety of the FAD cofactor oriented in the *out* conformation. As can be seen from **Figure 5**, the docking predicts that His162 and Arg269 interact with the pyrophosphate moiety of NADPH (Eppink et al., 1998a; Wang et al., 2002) and that Arg33, Tyr38 and Arg42 of the NADPH-specific fingerprint sequence 32-ERx(S/T)x(D/E)YVL(G/S)R are involved in orienting the adenosine 2'-phosphate part of NADPH (Eppink et al., 1999).

Pyridine Nucleotide Coenzyme Specificity in Related Enzymes

At present, crystal structures of 28 different group A flavoprotein monooxygenases are available in the Protein Data Bank, and for most of these enzymes, the preference for the nicotinamide cofactor is known. Structural alignment of the subfamily members showed similar folds for the FAD and substrate binding domains, which is indicative for a conserved interdomain binding mode of the NAD(P)H coenzyme (Treiber and Schulz, 2008). We aligned the loop segments of these enzymes, putatively involved in NAD(P)H binding, based on the structural position of the adenine moiety of the FAD cofactor and the N- and C-termini of these loops. The alignment obtained from the loop segment sequences (**Figure 6A**) suggests that the proteins can indeed be grouped in NADPH- or NADH-dependent enzymes and the associated distance tree shows this feature as two separate clusters (**Figure 6B**). The NAD(P)H-dependent enzymes are located in both the NADH- and NADPH-cluster. Based on type of cluster, the “putative monooxygenase” from *P. luminescens* (PDB ID: 4hb9) is likely NADH-dependent, whereas the “putative monooxygenase” from *P. aeruginosa* (PDB ID: 2x3n) is likely NADPH-dependent.

Within the whole subfamily, there is no clear consensus motif present for NADH- or NADPH-dependency. However, most NADPH-dependent enzymes have an arginine at position 44 (PHBH_{pf} numbering), which is capable of H-bond formation, in contrast to the corresponding residue in the NADH-group. The

NADH-group has instead a 'GxG' motif near the end of the loop, with x being mostly a hydrophobic residue.

The loop segments do not show a clear consensus structure (**Figure 7**). Those from PHBH enzymes contain a small helix, but none of the others structures have this feature. A few structures are missing some amino acid residues in the loop segment, due to low electron density in the diffraction dataset, which indicates that here the loop is flexible. This flexibility might change upon NAD(P)H binding, which could be essential to allow for the isoalloxazine moiety movement of FAD (i.e., “in/out” conformation).

DISCUSSION

This paper provides new insights into the pyridine nucleotide coenzyme specificity and evolutionary relationship of PHBH. Based on the known coenzyme preferences of a limited amount of biochemically characterized PHBHs and phylogenetic analysis of putative PHBHs, sequence logos for NADPH-specific and NADH-preferring enzymes could be inferred. The pyridine nucleotide coenzyme specificities of newly produced proteobacterial and actinobacterial PHBHs are in agreement with our phylogenetic analysis, which shows that PHBHs group into three clades comprising sequences of NADPH-specific, NAD(P)H-dependent and NADH-preferring enzymes. The present findings also support that the 2'-phosphate of NADPH does not interact with the side chain of Arg44 (Wang et al., 2002), but binds more close to Tyr38 and Arg42 (Eppink et al., 1999).

Energy profiling established that NADH-preferring PHBHs yield a high-energetic unstable environment around helix H2. This supports that this environment is a predominant site for evolutionary adaptations and leads us to suggest that the pyridine nucleotide coenzyme specificity linked to this sequence has evolved differently according to the evolutionary pressure in the host cell.

It has been estimated that the FAD-binding domain of flavoprotein monooxygenases appeared in coincidence with the emergence of aerobic metabolism, around 2.9 billion

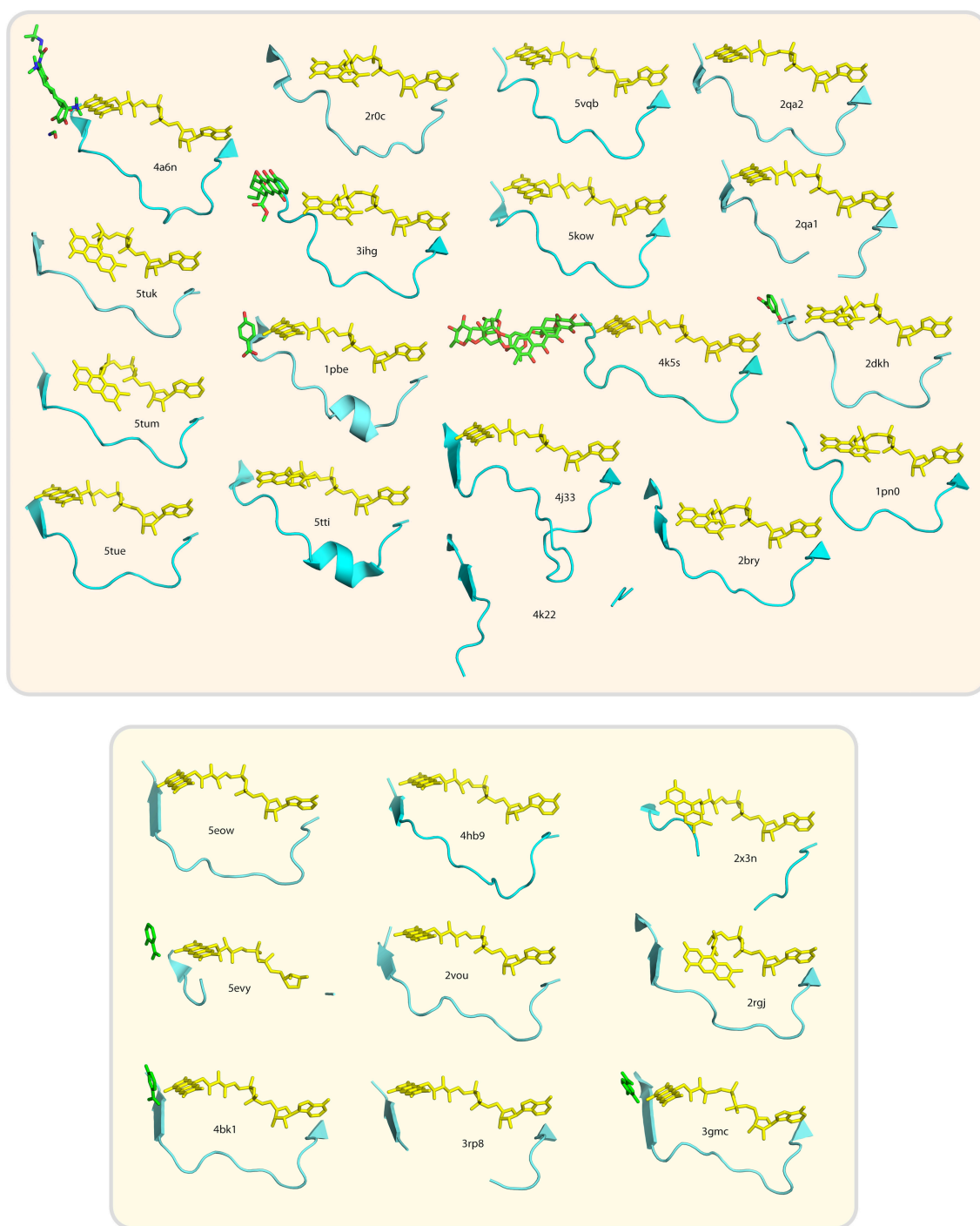


FIGURE 7 | Cartoon images of loop segment structures putatively involved in NAD(P)H binding of group A flavoprotein monooxygenases. Structures in the beige box (top) are NADPH-prefering enzymes, those in the yellowish box (bottom) are NADH-prefering enzymes. Substrates or inhibitors present in the used crystal structures are sketched in green.

years ago (Mascotti et al., 2016). Because both nicotinamide cofactors were already present, the pyridine nucleotide coenzyme specificity of PHBH must have evolved later. What can we learn from the present study regarding the evolutionary

history of the pyridine nucleotide coenzyme specificity of PHBH?

First, we raised the question on convergent or divergent evolution. Especially, since NADH is mainly involved in catabolic

and NADPH in anabolic pathways, one might argue that two different ancestor proteins arose from different pathways, which led by convergent evolution to PHBH-like proteins but with different nicotinamide cofactor dependency. However, the extensive phylogenetic analysis and alignments made herein do not support this theory since all (putative) PHBHs have highly similar sequences, a comparable length, conserved secondary structure elements and thus a similar fold. Therefore, a divergent evolution of PHBHs from one predecessor must have led to the differences in nicotinamide cofactor dependency. The phylogenetic distance tree suggests that the PHBH ancestor could use both nicotinamide co-substrates and the NADH-preferring PHBHs are supposed to be closer related to this predecessor and therewith the older enzymes (**Figure 4**). Thus NADPH-specific PHBHs have likely evolved more recently.

Next, we asked ourselves if this evolutionary event occurred by chance or by adaptation (Zhu et al., 2005). As noted above, most of the NADH-preferring (putative) PHBH enzymes are harbored by *k*-strategists as actinobacterial *Rhodococcus*, *Corynebacterium*, or *Streptomyces* species (Juteau et al., 1999; Margesin et al., 2003; Singer et al., 2011). These microorganisms can handle nutrient limited and highly populated environments, known to be stress tolerant, have a huge catabolic power, and are slow in reproducing. On the other hand, *r*-strategists such as proteobacterial *Pseudomonas* and *Acinetobacter* species (Margesin et al., 2003), reproduce fast, colonize quickly nutrient rich environments, form less stable populations and are attractive prey for other organisms. They need to adapt to a certain environment very fast; thus, they can reproduce in a sufficient manner to ensure survival of their species. Interestingly, all NADPH-specific PHBH proteins are harbored by those *r*-strategists. Moreover, some of these pseudomonads are known to need high levels of NADPH for generating a reductive environment (Singh et al., 2007, 2008). The prevalence of NADPH in such organisms could have caused an adaptive, stepwise evolution toward NADPH-dependence of PHBH enzymes. This is also in agreement with the fact that mutations of few amino acids already change the nicotinamide cofactor preference (Eppink et al., 1999).

Based on phylogeny and lifestyle of various PHBH harboring bacteria we propose that the pyridine nucleotide coenzyme specificity of PHBH has emerged through adaptive evolution. It can be assumed that the PHBH ancestor could use both nicotinamide cofactors with a preference for NADH as source of reducing equivalents. In rhodococci, which are *k*-strategists characterized by slow doubling times (Kurosawa et al., 2010) and in general a high stress tolerance, the NADH-dependent PHBHs retained. These enzymes are the older versions of PHBH. In case of *r*-strategists, which possess a high energy-consuming lifestyle, the available NADPH acted likely as a driving force to evolve strictly NADPH-dependent PHBHs. These enzymes are supposed to have evolved more recently. Thus, we can state that NADPH converting PHBHs have evolved by adaptation to their host and therewith present the youngest PHBH enzymes.

Our data indicate that group A flavoprotein monooxygenases all share with PHBH a similar mode of NAD(P)H binding. However, the here identified pyridine nucleotide coenzyme recognition motifs are specific for PHBH enzymes. Other group A flavoprotein monooxygenases (Huijbers et al., 2014); (Mascotti et al., 2016) likely contain similar motifs, but the sparse availability of biochemical data on the pyridine nucleotide coenzyme specificity of these enzymes does not allow for a reliable prediction of these motifs.

CONCLUSION

In this paper, we have described new insights into the pyridine nucleotide coenzyme specificity of *p*-hydroxybenzoate hydroxylase (PHBH) and related group A flavoprotein monooxygenases. By integrating data from phylogeny, structural modeling and enzyme kinetics, it was established that PHBHs group into three clades consisting of NADPH-specific, NAD(P)H-dependent and NADH-preferring enzymes. Furthermore, the results suggest that the NADPH-specific enzymes evolved through an adaptive process from NADH-preferring enzymes and that the loop segment responsible for the pyridine nucleotide coenzyme specificity of PHBH is also involved in the pyridine nucleotide coenzyme specificity of the other group A members. The present work might stimulate future studies directed at understanding the pyridine nucleotide coenzyme specificity of group A flavoprotein monooxygenases in molecular detail.

AUTHOR CONTRIBUTIONS

AW and DT carried out the phylogenetic analysis. AW performed the structural alignments and docking experiments. FH and DL carried out the energy potential profiling and evolutionary rate analysis. The cloning and expression of *pob* genes was performed by SH and JG. Purification and biochemical characterization of enzymes was done by AW and SH. AW, DT, FH, and WB wrote the manuscript. All authors read and approved the final manuscript.

FUNDING

DT and WB were supported by a grant from the European Social Fund (ESF) and the Saxonian Government (GETGEOWEB: 100101363).

ACKNOWLEDGMENTS

This paper is dedicated to Monika Thiel.

SUPPLEMENTARY MATERIAL

The Supplementary Material for this article can be found online at: <https://www.frontiersin.org/articles/10.3389/fmicb.2018.03050/full#supplementary-material>

REFERENCES

- Altschul, S. F., Gish, W., Miller, W., Myers, E. W., and Lipman, D. J. (1990). Basic local alignment search tool. *J. Mol. Biol.* 215, 403–410. doi: 10.1016/S0022-2836(05)80360-2
- Ballou, D. P., and Entsch, B. (2013). “The reaction mechanisms of Groups A and B flavoprotein monooxygenases,” in *Handbook of Flavoproteins: Complex Flavoproteins, Dehydrogenases and Physical Methods*, eds R. Hille, S. Miller, and B. A. Palfey (Berlin: De Gruyter), 1–28.
- Bertani, I., Kojic, M., and Venturi, V. (2001). Regulation of the *p*-hydroxybenzoic acid hydroxylase gene (*pobA*) in plant-growth-promoting *Pseudomonas putida* WCS358. *Microbiology* 147(Pt 6), 1611–1620. doi: 10.1099/00221287-147-6-1611
- Cahn, J. K., Baumschlager, A., Brinkmann-Chen, S., and Arnold, F. H. (2016). Mutations in adenine-binding pockets enhance catalytic properties of NAD(P)H-dependent enzymes. *Prot. Eng. Des. Sel.* 29, 31–38. doi: 10.1093/protein/gzv057
- Cahn, J. K., Werlang, C. A., Baumschlager, A., Brinkmann-Chen, S., Mayo, S. L., and Arnold, F. H. (2017). A general tool for engineering the NAD/NADP cofactor preference of oxidoreductases. *ACS Synth. Biol.* 6, 326–333. doi: 10.1021/acssynbio.6b00188
- Crooks, G. E., Hon, G., Chandonia, J. M., and Brenner, S. E. (2004). WebLogo: a sequence logo generator. *Genome Res.* 14, 1188–1190. doi: 10.1101/gr.849004
- Crozier-Reabe, K., and Moran, G. R. (2012). Form follows function: structural and catalytic variation in the class A flavoprotein monooxygenases. *Int. J. of Mol. Sci.* 13, 15601. doi: 10.3390/ijms131215601
- de Vries, S. J., van Dijk, M., and Bonvin, A. M. (2010). The HADDOCK web server for data-driven biomolecular docking. *Nat. Protoc.* 5, 883–897. doi: 10.1038/nprot.2010.32
- DiMarco, A. A., Averhoff, B., Kim, E. E., and Ornston, L. N. (1993). Evolutionary divergence of *pobA*, the structural gene encoding *p*-hydroxybenzoate hydroxylase in an *Acinetobacter calcoaceticus* strain well-suited for genetic analysis. *Gene* 125, 25–33. doi: 10.1016/0378-1119(93)90741-K
- Dressel, F., Marsico, A., Tuukkanen, A., Schroeder, M., and Labudde, D. (2007). “Understanding of SMFS barriers by means of energy profiles,” in *Proceedings of German Conference on Bioinformatics* (Potsdam).
- Eisenberg, D., and McLachlan, A. D. (1986). Solvation energy in protein folding and binding. *Nature* 319, 199–203.
- Enroth, C., Neujahr, H., Schneider, G., and Lindqvist, Y. (1998). The crystal structure of phenol hydroxylase in complex with FAD and phenol provides evidence for a concerted conformational change in the enzyme and its cofactor during catalysis. *Structure* 6, 605–617. doi: 10.1016/S0969-2126(98)00062-8
- Entsch, B., and Ballou, D. P. (1989). Purification, properties, and oxygen reactivity of *p*-hydroxybenzoate hydroxylase from *Pseudomonas aeruginosa*. *Biochim. Biophys. Acta* 999, 313–322. doi: 10.1016/0167-4838(89)90014-9
- Entsch, B., Cole, L. J., and Ballou, D. P. (2005). Protein dynamics and electrostatics in the function of *p*-hydroxybenzoate hydroxylase. *Arch. Biochem. Biophys.* 433, 297–311. doi: 10.1016/j.abb.2004.09.029
- Entsch, B., Nan, Y., Weach, K., and Scott, K. F. (1988). Sequence and organization of *pobA*, the gene coding for *p*-hydroxybenzoate hydroxylase, an inducible enzyme from *Pseudomonas aeruginosa*. *Gene* 71, 279–291. doi: 10.1016/0378-1119(88)90044-3
- Entsch, B., and van Berkel, W. J. H. (1995). Structure and mechanism of *para*-hydroxybenzoate hydroxylase. *FASEB J.* 9, 476–483. doi: 10.1096/fasebj.9.7.7737455
- Eppink, M. H. M., Overkamp, K. M., Schreuder, H. A., and Van Berkel, W. J. H. (1999). Switch of coenzyme specificity of *p*-hydroxybenzoate hydroxylase. *J. Mol. Biol.* 292, 87–96. doi: 10.1006/jmbi.1999.3015
- Eppink, M. H. M., Schreuder, H. A., and van Berkel, W. J. H. (1997). Identification of a novel conserved sequence motif in flavoprotein hydroxylases with a putative dual function in FAD/NAD(P)H binding. *Protein Sci.* 6, 2454–2458. doi: 10.1002/pro.5560061119
- Eppink, M. H. M., Schreuder, H. A., and van Berkel, W. J. H. (1998a). Interdomain binding of NADPH in *p*-hydroxybenzoate hydroxylase as suggested by kinetic, crystallographic and modeling studies of histidine 162 and arginine 269 variants. *J. Biol. Chem.* 273, 21031–21039.
- Eppink, M. H. M., Schreuder, H. A., and van Berkel, W. J. H. (1998b). Lys42 and Ser42 variants of *p*-hydroxybenzoate hydroxylase from *Pseudomonas fluorescens* reveal that Arg42 is essential for NADPH binding. *Eur. J. Biochem.* 253, 194–201.
- Eswar, N., Webb, B., Marti-Renom, M. A., Madhusudhan, M. S., Eramian, D., Shen, M. Y., et al. (2006). Comparative protein structure modeling using MODELLER. *Curr. Protoc. Bioinformatics* Chapter 5, Unit-5.6. doi: 10.1002/0471250953.bi0506s15
- Eulberg, D., Golovleva, L. A., and Schlömann, M. (1997). Characterization of catechol catabolic genes from *Rhodococcus erythropolis* ICP. *J. Bacteriol.* 179, 370–381. doi: 10.1128/jb.179.2.370-381.1997
- Felsenstein, J. (2005). Using the quantitative genetic threshold model for inferences between and within species. *Philos. Trans. R. Soc. Lond. B. Biol. Sci.* 360, 1427–1434. doi: 10.1098/rstb.2005.1669
- Felsenstein, J. (2009). *PHYMLIP (Phylogeny Inference Package) Version 3.7a*. Department of Genome Sciences; University of Washington.
- Fernandez, J., Dimarco, A. A., Ornston, L. N., and Harayama, S. (1995). Purification and characterization of *Acinetobacter calcoaceticus* 4-hydroxybenzoate 3-hydroxylase after its overexpression in *Escherichia coli*. *J. Biochem.* 117, 1261–1266. doi: 10.1093/oxfordjournals.jbchem.a124853
- Gatti, D. L., Palfey, B. A., Lah, M. S., Entsch, B., Massey, V., Ballou, D. P., et al. (1994). The mobile flavin of 4-OH benzoate hydroxylase. *Science* 266, 110–114.
- Gish, W., and States, D. J. (1993). Identification of protein coding regions by database similarity search. *Nat. Genet.* 3, 266–272. doi: 10.1038/ng0393-266
- Harwood, C. S., and Parales, R. E. (1996). The β -ketoadipate pathway and the biology of self-identity. *Annu. Rev. Microbiol.* 50, 553–590. doi: 10.1146/annurev.micro.50.1.553
- Heinke, F., and Labudde, D. (2012). Membrane protein stability analyses by means of protein energy profiles in case of nephrogenic diabetes insipidus. *Comput. Math. Meth. Med.* 2012, 11. doi: 10.1155/2012/790281
- Heinke, F., and Labudde, D. (2013). Functional analyses of membrane protein mutants involved in nephrogenic diabetes insipidus: An energy-based approach,” in *Research on Diabetes I* (Hong Kong: iConcept Press), 133–152.
- Heinke, F., Stockmann, D., Schildbach, S., Langer, M., and Labudde, D. (2015). “eProS – A bioinformatics knowledgebase, toolbox and database for characterizing protein function,” in *Beyond Databases, Architectures and Structures*, eds S. Kozielski, D. Mrozek, P. Kasprowski, B. Malysiak-Mrozek, and D. Kozrzewa (Cham: Springer International Publishing), 575–584.
- Higgins, D. G., and Sharp, P. M. (1988). CLUSTAL: a package for performing multiple sequence alignment on a microcomputer. *Gene* 73, 237–244. doi: 10.1016/0378-1119(88)90330-7
- Hiromoto, T., Fujiwara, S., Hosokawa, K., and Yamaguchi, H. (2006). Crystal structure of 3-hydroxybenzoate hydroxylase from *Comamonas testosteroni* has a large tunnel for substrate and oxygen access to the active site. *J. Mol. Biol.* 364, 878–896. doi: 10.1016/j.jmb.2006.09.031
- Howell, L. G., Spector, T., and Massey, V. (1972). Purification and properties of *p*-hydroxybenzoate hydroxylase from *Pseudomonas fluorescens*. *J. Biol. Chem.* 241, 2453–2460.
- Huang, Y., Zhao, K., Shen, X. H., Jiang, C. Y., and Liu, S. J. (2008). Genetic and biochemical characterization of a 4-hydroxybenzoate hydroxylase from *Corynebacterium glutamicum*. *Appl. Microbiol. Biotechnol.* 78, 75–83. doi: 10.1007/s00253-007-1286-0
- Huijbers, M. M. E., Montersino, S., Westphal, A. H., Tischler, D., and van Berkel, W. J. H. (2014). Flavin dependent monooxygenases. *Arch. Biochem. Biophys.* 544, 2–17. doi: 10.1016/j.abb.2013.12.005
- Ibrahim, E. S., Kashef, M. T., Essam, T. M., and Ramadan, M. A. (2017). A degradome-based polymerase chain reaction to resolve the potential of environmental samples for 2,4-dichlorophenol biodegradation. *Curr. Microbiol.* 74, 1365–1372. doi: 10.1007/s00284-017-1327-6
- Jadan, A. P., Moonen, M. J. H., Boeren, S., Golovleva, L. A., Rietjens, I. M. C. M., and van Berkel, W. J. H. (2004). Biocatalytic potential of *p*-hydroxybenzoate hydroxylase from *Rhodococcus rhodnii* 135 and *Rhodococcus opacus* 557. *Adv. Synth. Catal.* 346, 367–375. doi: 10.1002/adsc.200303146
- Jadan, A. P., van Berkel, W. J. H., Golovleva, L. A., and Golovlev, E. L. (2001). Purification and properties of *p*-hydroxybenzoate hydroxylases from *Rhodococcus* strains. *Biochemistry* 66, 898–903. doi: 10.1023/A:1011908920472
- Juteau, P., Larocque, R., Rho, D., and LeDuy, A. (1999). Analysis of the relative abundance of different types of bacteria capable of toluene degradation in a compost biofilter. *Appl. Microbiol. Biotechnol.* 52, 863–868. doi: 10.1007/s002530051604

- Kabsch, W., and Sander, C. (1983). Dictionary of protein secondary structure: pattern recognition of hydrogen-bonded and geometrical features. *Biopolymers* 22, 2577–2637. doi: 10.1002/bip.360221211
- Kanteev, M., Bregman-Cohen, A., Deri, B., Shahar, A., Adir, N., and Fishman, A. (2015). A crystal structure of 2-hydroxybiphenyl 3-monoxygenase with bound substrate provides insights into the enzymatic mechanism. *Biochim. Biophys. Acta* 1854, 1906–1930. doi: 10.1016/j.bbapap.2015.08.002
- Kurosawa, K., Boccazzi, P., de Almeida, N. M., and Sinskey, A. J. (2010). High-cell-density batch fermentation of *Rhodococcus opacus* PD630 using a high glucose concentration for triacylglycerol production. *J. Biotechnol.* 147, 212–218. doi: 10.1016/j.jbiotec.2010.04.003
- Manstein, D. J., Pai, E. F., Schopfer, L. M., and Massey, V. (1986). Absolute stereochemistry of flavins in enzyme-catalyzed reactions. *Biochemistry* 25, 6807–6816. doi: 10.1021/bi00370a012
- Marchuk, D., Drumm, M., Saulino, A., and Collins, F. S. (1991). Construction of T-vectors, a rapid and general system for direct cloning of unmodified PCR products. *Nucleic Acids Res.* 19:1154. doi: 10.1093/nar/19.5.1154
- Margesin, R., Labbé, D., Schinner, F., Greer, C. W., and Whyte, L. G. (2003). Characterization of hydrocarbon-degrading microbial populations in contaminated and pristine alpine soils. *Appl. Environ. Microbiol.* 69, 3085–3092. doi: 10.1128/AEM.69.6.3085-3092.2003
- Mascotti, M. L., Juri Ayub, M., Furnham, N., Thornton, J. M., and Laskowski, R. A. (2016). Chopping and changing: the evolution of the flavin-dependent monooxygenases. *J. Mol. Biol.* 428, 3131–3146. doi: 10.1016/j.jmb.2016.07.003
- Mayrose, I., Graur, D., Ben-Tal, N., and Pupko, T. (2004). Comparison of site-specific rate-inference methods for protein sequences: empirical Bayesian methods are superior. *Mol. Biol. Evol.* 21, 1781–1791. doi: 10.1093/molbev/msh194
- Monterino, S., Tischler, D., Gassner, G. T., and van Berkel, W. J. H. (2011). Catalytic and structural features of flavoprotein hydroxylases and epoxidases. *Adv. Synth. Catal.* 353, 2301–2319. doi: 10.1002/adsc.201100384
- Monterino, S., and van Berkel, W. J. H. (2013). “The flavin monooxygenases,” in *Handbook of Flavoproteins: Complex Flavoproteins, Dehydrogenases and Physical Methods*, eds R. Hille, S. Miller, and B.A. Palfey (Berlin: De Gruyter), 51–72.
- Mrozek, D., Malysiak, B., and Kozielski, S. (2007). “An optimal alignment of proteins energy characteristics with crisp and fuzzy similarity awards,” in *IEEE International Conference on Fuzzy Systems (FUZZ-IEEE)* (London: IEEE).
- Oelschlägel, M., Heiland, C., Schlömann, M., and Tischler, D. (2015). Production of a recombinant membrane protein in an *Escherichia coli* strain for the whole cell biosynthesis of phenylacetic acids. *Biotechnol. Rep.* 7, 38–43. doi: 10.1016/j.btre.2015.05.002
- Ofran, Y., and Rost, B. (2003). Analysing six types of protein-protein interfaces. *J. Mol. Biol.* 325, 377–387. doi: 10.1016/S0022-2836(02)01223-8
- Ojha, S., Meng, E. C., and Babbitt, P. C. (2007). Evolution of function in the “two dinucleotide binding domains” flavoproteins. *PLoS Comput. Biol.* 3:e121. doi: 10.1371/journal.pcbi.0030121
- Ortiz-Maldonado, M., Entsch, B., and Ballou, D. P. (2003). Conformational changes combined with charge-transfer interactions are essential for reduction in catalysis by *p*-hydroxybenzoate hydroxylase. *Biochemistry* 42, 11234–11242. doi: 10.1021/bi030114y
- Ortiz-Maldonado, M., Gatti, D. L., Ballou, D. P., and Massey, V. (1999). Structure-function correlations of the reaction of reduced nicotinamide analogues with *p*-hydroxybenzoate hydroxylase substituted with a series of 8-substituted flavins. *Biochemistry* 38, 16636–16647. doi: 10.1021/bi991603u
- Palfey, B. A., and McDonald, C. A. (2010). Control of catalysis in flavin-dependent monooxygenases. *Arch. Biochem. Biophys.* 493, 26–36. doi: 10.1016/j.abb.2009.11.028
- Pérez-Pantoja, D., de la Iglesia, R., Pieper, D. H., and González, B. (2008). Metabolic reconstruction of aromatic compounds degradation from the genome of the amazing pollutant-degrading bacterium *Cupriavidus necator* JMP134. *FEMS Microbiol. Rev.* 32, 736–794. doi: 10.1111/j.1574-6976.2008.00122.x
- Quinn, J. A., McKay, D. B., and Entsch, B. (2001). Analysis of the *pobA* and *pobR* genes controlling expression of *p*-hydroxybenzoate hydroxylase in *Azotobacter chroococcum*. *Gene* 264, 77–85. doi: 10.1016/S0378-1119(00)00599-0
- Riedel, A., Heine, T., Westphal, A. H., Conrad, C., Rathack, P., van Berkel, W. J., et al. (2015). Catalytic and hydrodynamic properties of styrene monooxygenases from *Rhodococcus opacus* 1CP are modulated by cofactor binding. *AMB Express* 5:112. doi: 10.1186/s13568-015-0112-9
- Robert, X., and Gouet, P. (2014). Deciphering key features in protein structures with the new ENDSript server. *Nucleic Acids Res.* 42, 320–324. doi: 10.1093/nar/gku316
- Rose, P. W., Beran, B., Bi, C., Bluhm, W. F., Dimitropoulos, D., Goodsell, D. S., et al. (2011). The RCSB Protein Data Bank: redesigned web site and web services. *Nucleic Acids Res.* 39(Database issue), D392–D401. doi: 10.1093/nar/gkq1021
- Saitou, N., and Nei, M. (1987). The neighbor-joining method: a new method for reconstructing phylogenetic trees. *Mol. Biol. Evol.* 4, 406–425.
- Sambrook, J., and Russel, D. W. (2001). *Molecular Cloning: A Laboratory Manual*. Cold Spring Harbor, NY: Cold Spring Harbour Laboratory Press.
- Schreuder, H. A., Mattevi, A., Obmolova, G., Kalk, K. H., Hol, W. G. J., van der Bolt, F. J. T., et al. (1994). Crystal structures of wild-type *p*-hydroxybenzoate hydroxylase complexed with 4-aminobenzoate, 2,4-dihydroxybenzoate and 2-hydroxy-4-aminobenzoate and the Tyr222Ala mutant, complexed with 2-hydroxy-4-aminobenzoate. Evidence for a proton channel and a new binding mode of the flavin ring. *Biochemistry* 33, 10161–10170. doi: 10.1021/bi00199a044
- Schreuder, H. A., Prick, P. A., Wierenga, R. K., Vriend, G., Wilson, K. S., Hol, W. G. J., et al. (1989). Crystal structure of the *p*-hydroxybenzoate hydroxylase-substrate complex refined at 1.9 Å resolution. Analysis of the enzyme-substrate and enzyme-product complexes. *J. Mol. Biol.* 208, 679–696. doi: 10.1016/0022-2836(89)90158-7
- Schreudinger, L. (2011). “The PyMol Molecular Graphics System, Version 1.4”. Schrödinger, LLC.
- Scrutton, N. S., Berry, A., and Perham, R. N. (1990). Redesign of the coenzyme specificity of a dehydrogenase by protein engineering. *Nature* 343:38. doi: 10.1038/343038a0
- Seibold, B., Matthes, M., Eppink, M. H. M., Lingens, F., Van Berkel, W. J. H., and Müller, R. (1996). 4-Hydroxybenzoate hydroxylase from *Pseudomonas* sp. CBS3. Purification, characterization, gene cloning, sequence analysis and assignment of structural features determining the coenzyme specificity. *Eur. J. Biochem.* 239, 469–478. doi: 10.1111/j.1432-1033.1996.0469u.x
- Sellés Vidal, L., Kelly, C. L., Mordaka, P. M., and Heap, J. T. (2018). Review of NAD(P)H-dependent oxidoreductases: Properties, engineering and application. *Biochim. Biophys. Acta* 1866, 327–347. doi: 10.1016/j.bbapap.2017.11.005
- Shuman, B., and Dix, T. A. (1993). Cloning, nucleotide sequence, and expression of a *p*-hydroxybenzoate hydroxylase isozyme gene from *Pseudomonas fluorescens*. *J. Biol. Chem.* 268, 17057–17062.
- Sievers, F., Wilm, A., Dineen, D., Gibson, T. J., Karplus, K., Li, W., et al. (2011). Fast, scalable generation of high-quality protein multiple sequence alignments using CLUSTAL Omega. *Mol. Syst. Biol.* 7:539. doi: 10.1038/msb.2011.75
- Singer, E., Webb, E. A., Nelson, W. C., Heidelberg, J. F., Ivanova, N., Pati, A., et al. (2011). Genomic potential of *Marinobacter aquaeolei*, a biogeochemical “opportunistic”. *Appl. Environ. Microbiol.* 77, 2763–2771. doi: 10.1128/AEM.01866-10
- Singh, R., Lemire, J., Mailloux, R. J., and Appanna, V. D. (2008). A novel strategy involved in anti-oxidative defense: the conversion of NADH into NADPH by a metabolic network. *PLoS ONE* 3:e2682. doi: 10.1371/annotation/5fac086b-3806-4aa9-a5c5-2611b3355f8f
- Singh, R., Mailloux, R. J., Puiseux-Dao, S., and Appanna, V. D. (2007). Oxidative stress evokes a metabolic adaptation that favors increased NADPH synthesis and decreased NADH production in *Pseudomonas fluorescens*. *J. Bacteriol.* 189, 6665–6675. doi: 10.1128/JB.00555-07
- Sokal, R., and Michener, C. (1958). *A Statistical Method for Evaluating Systematic Relationships*. Lawrence: Kansas University Science Bulletin.
- Suemori, A., and Iwakura, M. (2007). A systematic and comprehensive combinatorial approach to simultaneously improve the activity, reaction specificity, and thermal stability of *p*-hydroxybenzoate hydroxylase. *J. Biol. Chem.* 282, 19969–19978. doi: 10.1074/jbc.M610320200
- Suemori, A., Nakajima, K., Kurane, R., and Nakamura, Y. (1995). Physicochemical and immunochemical characterization of salicylate 5-hydroxylase, *m*-hydroxybenzoate 6-hydroxylase and *p*-hydroxybenzoate 3-hydroxylase from *Rhodococcus erythropolis*. *Biotechnol. Lett.* 17, 1063–1068. doi: 10.1007/BF00143101

- Suemori, A., Ozawa, M., and Iwakura, M. (2001). Engineering of histidine tail in the N-terminal region of *p*-hydroxybenzoate hydroxylase from *Pseudomonas fluorescens*. *Biotechnol. Lett.* 23, 489–495. doi: 10.1023/A:1010345807073
- Tamura, K., Peterson, D., Peterson, N., Stecher, G., Nei, M., and Kumar, S. (2011). MEGA5: molecular evolutionary genetics analysis using maximum likelihood, evolutionary distance, and maximum parsimony methods. *Mol. Biol. Evol.* 28, 2731–2739. doi: 10.1093/molbev/msr121
- Thiel, M., Kaschabek, S. R., Gröning, J., Mau, M., and Schlömann, M. (2005). Two unusual chlorocatechol catabolic gene clusters in *Sphingomonas* sp. TFD44. *Arch. Microbiol.* 183, 80–94. doi: 10.1007/s00203-004-0748-3
- Thompson, J. D., Gibson, T. J., Plewniak, F., Jeanmougin, F., and Higgins, D. G. (1997). The CLUSTAL-X windows interface: flexible strategies for multiple sequence alignment aided by quality analysis tools. *Nucleic Acids Res.* 25, 4876–4882. doi: 10.1093/nar/25.24.4876
- Treiber, N., and Schulz, G. E. (2008). Structure of 2,6-dihydroxypyridine 3-hydroxylase from a nicotine-degrading pathway. *J. Mol. Biol.* 379, 94–104. doi: 10.1016/j.jmb.2008.03.032
- van Berkel, W. J. H., Eppink, M. H. M., and Schreuder, H. A. (1994). Crystal structure of *p*-hydroxybenzoate hydroxylase reconstituted with the modified FAD present in alcohol oxidase from methylotrophic yeasts: evidence for an arabinoflavin. *Protein Sci.* 3, 2245–2253. doi: 10.1002/pro.5560031210
- van Berkel, W. J. H., Kamerbeek, N. M., and Fraaije, M. W. (2006). Flavoprotein monooxygenases, a diverse class of oxidative biocatalysts. *J. Biotechnol.* 124, 670–689. doi: 10.1016/j.jbiotec.2006.03.044
- van Berkel, W. J. H., Westphal, A. H., Eschrich, K., Eppink, M. H. M., and de Kok, A. (1992). Substitution of Arg214 at the substrate-binding site of *p*-hydroxybenzoate hydroxylase from *Pseudomonas fluorescens*. *Eur. J. Biochem.* 210, 411–419. doi: 10.1111/j.1432-1033.1992.tb17436.x
- Wang, J., Ortiz-Maldonado, M., Entsch, B., Massey, V., Ballou, D. P., and Gatti, D. L. (2002). Protein and ligand dynamics in 4-hydroxybenzoate hydroxylase. *Proc. Natl. Acad. Sci. U.S.A.* 99, 608–613. doi: 10.1073/pnas.022640199
- Weijer, W. J., Hofsteenge, J., Vereijken, J. M., Jekel, P. A., and Beintema, J. J. (1982). Primary structure of *p*-hydroxybenzoate hydroxylase from *Pseudomonas fluorescens*. *Biochim. Biophys. Acta* 704, 385–388. doi: 10.1016/0167-4838(82)90170-4
- Wertz, D. H., and Scheraga, H. A. (1978). Influence of water on protein structure. An analysis of the preferences of amino acid residues for the inside or outside and for specific conformations in a protein molecule. *Macromolecules* 11, 9–15. doi: 10.1021/ma60061a002
- Westphal, A. H., Matorin, A., Hink, M. A., Borst, J. W., van Berkel, W. J. H., and Visser, A. J. W. G. (2006). Real-time enzyme dynamics illustrated with fluorescence spectroscopy of *p*-hydroxybenzoate hydroxylase. *J. Biol. Chem.* 281, 11074–11081. doi: 10.1074/jbc.M600609200
- Wong, C. M., Dilworth, M. J., and Glenn, A. R. (1994). Cloning and sequencing show that 4-hydroxybenzoate hydroxylase (*PobA*) is required for uptake of 4-hydroxybenzoate in *Rhizobium leguminosarum*. *Microbiology* 140, 2775–2786. doi: 10.1099/00221287-140-10-2775
- Zhou, H., and Zhou, Y. (2004). Quantifying the effect of burial of amino acid residues on protein stability. *Proteins* 54, 315–322. doi: 10.1002/prot.10584
- Zhu, G., Golding, G. B., and Dean, A. M. (2005). The selective cause of an ancient adaptation. *Science* 307, 1279–1282. doi: 10.1126/science.1106974

Conflict of Interest Statement: The authors declare that the research was conducted in the absence of any commercial or financial relationships that could be construed as a potential conflict of interest.

Copyright © 2018 Westphal, Tischler, Heinke, Hofmann, Gröning, Labudde and van Berkel. This is an open-access article distributed under the terms of the Creative Commons Attribution License (CC BY). The use, distribution or reproduction in other forums is permitted, provided the original author(s) and the copyright owner(s) are credited and that the original publication in this journal is cited, in accordance with accepted academic practice. No use, distribution or reproduction is permitted which does not comply with these terms.



Mining the Genome of *Streptomyces leeuwenhoekii*: Two New Type I Baeyer–Villiger Monooxygenases From Atacama Desert

Alejandro Gran-Scheuch^{1,2}, Milos Trajkovic¹, Loreto Parra^{2,3*} and Marco W. Fraaije^{1*}

¹ Molecular Enzymology Group, University of Groningen, Groningen, Netherlands, ² Department of Chemical and Bioprocesses Engineering, School of Engineering, Pontificia Universidad Católica de Chile, Santiago, Chile, ³ Schools of Engineering, Medicine and Biological Sciences, Institute for Biological and Medical Engineering, Pontificia Universidad Católica de Chile, Santiago, Chile

OPEN ACCESS

Edited by:

Christian Sohlenkamp,
Universidad Nacional Autónoma
de México, Mexico

Reviewed by:

Pablo Cruz-Morales,
Lawrence Berkeley National
Laboratory (LBNL), United States
Martha Sophia Smit,
University of the Free State,
South Africa

*Correspondence:

Loreto Parra
lparra@uc.cl;
lparra@ing.puc.cl
Marco W. Fraaije
m.w.fraaije@rug.nl

Specialty section:

This article was submitted to
Microbial Physiology and Metabolism,
a section of the journal
Frontiers in Microbiology

Received: 23 January 2018

Accepted: 27 June 2018

Published: 18 July 2018

Citation:

Gran-Scheuch A, Trajkovic M,
Parra L and Fraaije MW (2018)
Mining the Genome of *Streptomyces*
leeuwenhoekii: Two New Type I
Baeyer–Villiger Monooxygenases
From Atacama Desert.
Front. Microbiol. 9:1609.
doi: 10.3389/fmicb.2018.01609

Actinobacteria are an important source of commercial (bio)compounds for the biotechnological and pharmaceutical industry. They have also been successfully exploited in the search of novel biocatalysts. We set out to explore a recently identified actinomycete, *Streptomyces leeuwenhoekii* C34, isolated from a hyper-arid region, the Atacama desert, for Baeyer–Villiger monooxygenases (BVMOs). Such oxidative enzymes are known for their broad applicability as biocatalysts by being able to perform various chemical reactions with high chemo-, regio-, and/or enantioselectivity. By choosing this specific Actinobacterium, which comes from an extreme environment, the respective enzymes are also expected to display attractive features by tolerating harsh conditions. In this work, we identified two genes in the genome of *S. leeuwenhoekii* (*sle_13190* and *sle_62070*) that were predicted to encode for Type I BVMOs, the respective flavoproteins share 49% sequence identity. The two genes were cloned, overexpressed in *E. coli* with phosphite dehydrogenase (PTDH) as fusion partner and successfully purified. Both flavin-containing proteins showed NADPH-dependent Baeyer–Villiger oxidation activity for various ketones and sulfoxidation activity with some sulfides. Gratifyingly, both enzymes were found to be rather robust by displaying a relatively high apparent melting temperature (45°C) and tolerating water-miscible cosolvents. Specifically, *Sle_62070* was found to be highly active with cyclic ketones and displayed a high regioselectivity by producing only one lactone from 2-phenylcyclohexanone, and high enantioselectivity by producing only normal (-)-1*S*,5*R* and abnormal (-)-1*R*,5*S* lactones (ee > 99%) from bicyclo[3.2.0]hept-2-en-6-one. These two newly discovered BVMOs add two new potent biocatalysts to the known collection of BVMOs.

Keywords: Atacama, actinobacteria, Baeyer–Villiger monooxygenase, flavoprotein, biocatalysis

INTRODUCTION

Enzymes are attractive catalysts for several industrial processes by being biodegradable, non-toxic, efficient, and selective. These biocatalysts can offer a high level of safety, low energy consumption, and a global environmentally friendly process (Santiago et al., 2016). Enzyme-based approaches often fulfill all the requirements for ecological and economical viable processes

(Dijkman et al., 2013; Reetz, 2013; Woodley, 2017; Pellis et al., 2018). The recognition that enzymes can be used in industrially relevant processes is reflected in a predicted growing market for biocatalysts (Dewan, 2014; Research and Markets, 2017). Particular examples of enzymes that show industrial potential are Baeyer–Villiger monooxygenases (BVMOs). BVMOs are well-studied enzymes (EC. 1.14.13.XX) that can be used for the production of (enantiopure) esters, lactones, and sulfoxides by incorporating an atom of oxygen in an organic substrate releasing a molecule of water using NADPH as cofactor (Bučko et al., 2016). These enzymes typically display a high chemo-, regio-, and enantioselectivity while operating at mild reaction conditions (Leisch et al., 2011). In the last years some new Type I BVMOs have been discovered and characterized from different organisms, such as YMOB (*Yarrowia lipolytica*, which shows activity on some ketones and sulfoxides (Bordewick et al., 2018), the BVMO_{AFL706} and BVMO_{AFL334} from the fungus *Aspergillus flavus*, which showed a broad substrate acceptance including substituted cyclic, aliphatic, and aromatic ketones (Mthethwa et al., 2017), BVMO_{Lepto} from *Leptospira biflexa*, which was used in whole-cell reactions conversions of various ketones (Ceccoli et al., 2014) and PockeMO from *Thermothelomyces thermophila*, which displays a high thermostability and shows activity on bulky substrates (Füerst et al., 2016). However, the BVMOs require special conditions that challenge the application of these biocatalysts on a large scale, like the expensive nicotinamide adenine dinucleotide phosphate (NADPH) as coenzyme. To reduce the costs related to the coenzyme usage, efficient external regeneration systems have been developed. For example, the thermostable phosphite dehydrogenase (PTDH) from *Pseudomonas stutzeri* WM88 can be used to regenerate NAD(P)H (Johannes et al., 2005; Torres Pazmiño et al., 2009). Another major issue concerning the application of BVMOs is the poor stability they often display at industrial conditions, like the presence of cosolvent, high temperature and, in some cases, high salinity (Woodley, 2017; Pellis et al., 2018). Generally, enzymes isolated from mesophilic organisms do not tolerate such conditions. Extremozymes, which are enzymes derived from extremophilic organisms, are typically more suited to withstand harsh environments (Karan et al., 2012). Currently, there is only one BVMO that can tolerate harsh conditions: phenylacetone monooxygenase (PAMO) from *Thermobifida fusca* (Fraaije et al., 2005). This biocatalyst was obtained by a genome mining approach specifically targeting this mesothermophilic actinobacterium. PAMO was found to be rather thermostable while tolerating cosolvents (de Gonzalo et al., 2006; Rodríguez et al., 2008). Recently, other moderately stable BVMOs, isolated from mesothermophilic microbes, were reported (Füerst et al., 2016; Romero et al., 2016). Inspired by these, we considered performing genome mining to another extremophilic actinobacterium to search for novel BVMOs.

The Atacama desert is a hyper-arid area in the north of Chile, characterized by: (a) a large daily temperature variation, where in some areas it ranges from -8 to 50°C (Pulschen et al., 2015); (b) low water availability, the area is considered the driest desert in the world (Azua-Bustos et al., 2012); (c) exposition to high ultraviolet (UV) light, this zone is

characterized by its high altitude, prevalent cloudless conditions and relatively low total ozone column, making this desert one of the highest UV radiation sites on Earth (Paulino-Lima et al., 2013; Pulschen et al., 2015) and; (d) high salinity, the desert contains extremely large natural deposits of anions (as Cl , ClO_3^- , SO_4^{2-} , ClO_4^- , and others). These geographic and environmental characteristics make the microorganisms thriving in the Atacama desert unique, comprising a genetic and molecular treasure that could lead to novel (bio)chemistry (Bull and Asenjo, 2013; Bull et al., 2016; Idris et al., 2017). Several microorganisms have been isolated from the Atacama desert, being an interesting environment to search bacteria with different adaptive qualities to be exploited for biotechnological applications. Among the microorganisms isolated, numerous Actinomycetes have been characterized, including a particular species, *Streptomyces leeuwenhoekii* C34, found to produce novel natural products (Okoro et al., 2009). This actinobacterium is a Gram-positive mycelial bacterium rich in novel pharmaceutical compounds (Busarakam et al., 2014). *S. leeuwenhoekii* was found in a soil sample, grows from 4 to 50°C , optimally at 30°C , from pH 6.0–11, optimally at 7.0, and in the presence of 10% w/v sodium chloride. Because of its highly biotechnological potential, this bacterium was sequenced after its discovery (Gomez-Escribano et al., 2015). Genomic analysis revealed a 72% G+C content, the presence of a linear chromosome (8 Mb) and two extrachromosomal replicons, the circular pSLE1 (86 kb) and the linear pSLE2 (132 kb). The *S. leeuwenhoekii* genome contains 35 gene clusters apparently encoding for the biosynthesis of specialized metabolites with potent antibiotic activity such as chaxamycins and chaxalactins (Rateb et al., 2011; Busarakam et al., 2014). Genome mining in *Streptomyces* isolates has already been reported for the identification and characterization of novel BVMOs, including: (i) MtmOIV, a BVMO isolated from *S. argillaceus* which is a key enzyme in the mithramycin biosynthesis pathway (Gibson et al., 2005), (ii) the BVMOs PenE and PntE forming pentalenolactone precursors in the pathway of antibiotic biosynthesis in *S. exfoliates* and *S. arenae*, respectively (Seo et al., 2011), (iii) two BVMOs from *S. coelicolor* acting on thioanisole and a heptanone (Park et al., 2007), and (iv) PtlE from *S. avermitilis* has also been described to be involved in a pentalenolactone biosynthetic pathway (Jiang et al., 2009). We performed a search in the predicted proteome of *S. leeuwenhoekii* using the sequence motifs described for Type I BVMOs (Fraaije et al., 2002; Riebel et al., 2012). In this work, we report the discovery, expression and characterization of two novel Type I BVMOs fused to PTDH.

MATERIALS AND METHODS

Genome Analysis

The GenomeNet server¹ was used for searching proteins that harbor specific sequence motifs (Rossmann fold G-x-G-x-x-[GA] and the Type I BVMOs fingerprints [AG]-G-x-W-x-x-x-x-[FY]-[GM]-x-x-x-x-D and F-x-G-x-x-x-H-x-x-x-W-[PD]) using

¹www.genome.jp/tools/motif/MOTIF2.html

the predicted proteome of *S. leeuwenhoekii* (code: Actinobacteria, *Streptomyces*, sle). The UniProt server was used for the identification of the proteins² and the NCBI server for the BLAST searches and identity sequence confirmation³. Multiple sequence alignments were prepared using 45 protein sequences in MUSCLE software (v3.8.31) configured with default settings for highest accuracy and employing the UPGMB clustering method. The phylogenetic tree was reconstructed using the maximum likelihood (ML) method implemented in MEGA 7.0 (500 bootstrap replications). The default substitution model was selected assuming an estimated proportion of invariant sites and 4 gamma-distributed rate categories to account for rate heterogeneity across sites (WAG model). Nearest-Neighbor Interchange (NNI) ML heuristic method was chosen. Initial tree(s) for the heuristic search were obtained by applying the BioNJ method to a matrix of pairwise distances estimated using a JTT model (Whelan and Goldman, 2001; Kumar et al., 2016).

Reagents, Bacterial Strains, and Plasmids

All chemical reagents were purchased from Sigma-Aldrich, Difco or Merck, unless otherwise stated. Oligonucleotide primers synthesis and DNA sequencing were performed by Macrogen. The genes were amplified by PCR from genomic DNA isolated from *S. leeuwenhoekii* C34. *Escherichia coli* TOP10 (Thermo Fisher Scientific) and *E. coli* NEB 10 β (New England Biolabs) were used as host strain for recombinant DNA. The pCRE2 vector was used for expressing the target proteins fused to PTDH equipped with an N-terminal His-tag (Torres Pazmiño et al., 2009). Lysogenic broth (LB), terrific broth (TB), and mannitol soya flour media (SFM) were used for bacterial growth (Hobbs, 1989). PTDH-PAMO (phenylacetone monooxygenase fused to PTDH) and PTDH-TmCHMO (*Thermocrispum municipale* cyclohexanone monooxygenase fused to PTDH) were from GECCO-Biotech.

Cloning, Expression, and Purification

Streptomyces leeuwenhoekii was grown in SFM and its genomic DNA was isolated and purified using Purelink® Genomic DNA kit (Invitrogen) according to the recommendations of the manufacturer. Genes encoding the putative enzymes were amplified by PCR using Phusion High-Fidelity DNA Polymerase with the same program: 95°C-420 s, [95°C-40 s, 59°C-40 s-73°C-120 s] \times 35 cycles, 73°C-600 s and 4°C-overnight. For the *sle_13190* gene the forward and reverse primers were: 5'-CCT GCG GCT GAC TCG AGA TCT GCA GCT GGT ATG GCC CGC GCC GAA and 5'-TTT TGT TCG GGC CCA AGC TTG GTA ATC TAT GTA TCC TGG TCA GCG CAG TTC GAG GCC, respectively. For the *sle_62070* gene the forward and reverse primers were 5'-CCT GCG GCT GAC TCG AGA TCT GCA GCT GGT ATG ACA CAA GGT CAG ACG TTG TCC and 5'-TTT TGT TCG GGC CCA AGC TTG GTA ATC TAT GTA TCC TGG TCA GCT CAC CGT GGA GCC, respectively. For the *sle_41160* gene the forward and

reverse primers were: 5'-CCT GCG GCT GAC TCG AGA TCT GCA GCT GGT ATG GCC GAG CAC GAG CAT and 5'-TTT TGT TCG GGC CCA AGC TTG GTA ATC TAT GTA TCC TGG TCA CGC GGT CAC CCC. For the pCRE2 amplification the primers were 5'-CCA GGA TAC ATA GAT TAC CAA GCT TGG GCC CGA ACA AAA AC and 5'-ACC AGC TGC AGA TCT CGA GT. The PCR conditions were optimized to a final concentration of 3% DMSO and 125 nM of each primer. Purified PCR products were cloned into the pCRE2 vector by Gibson assembly (Gibson et al., 2009). Products were used directly for transformation of competent *E. coli* TOP10 cells. Colonies were grown on LB-agar plates supplemented with ampicillin at 37°C. Plasmids were isolated (Wizard®Plus SV Minipreps DNA Purification System) and sequenced for cloning confirmation (Macrogen). Verified plasmids were transformed in competent *E. coli* NEB 10 β used for protein expression. For purification, a single colony was taken for growing a preculture in LB at 37°C overnight. An aliquot of the preculture (1:100) was used to inoculate fresh TB medium supplemented with 50 μ g mL⁻¹ ampicillin. Cultures were incubated at 37°C with shaking until an OD₆₀₀ of 0.7 was reached after which expression was induced by adding L-arabinose. To optimize the expression, different inducer concentrations (0.002, 0.02, and 0.2%) and temperatures (17, 24, 30, and 37°C) for 16, 24, and 48 h were tested. Cells were harvested by centrifugation (6,000 \times 20' at 4°C using a JLA-9100 rotor, Beckman Coulter) and suspended in lysis buffer (50 mM Tris-HCl pH 7.0, 10% w/v glycerol, 1.5 mg mL⁻¹ lysozyme, 10 μ M FAD and 1 mM PMSF). Cell extracts (CE) were obtained by sonication (Vibra cell, Sonics, and materials) for 10' (amplitude 70%, 7 s on and 7 s off). The cleared cell extracts (CCEs) were obtained by centrifugation at 10,000 rpm for 1 h at 4°C (Centrifuge 5810R, Eppendorf). CCE, CE, and insoluble fraction were analyzed by SDS-PAGE to verify expression of the respective BVMOs. After establishing proper expression conditions, CCE was prepared, filtered (0.45 μ M) and loaded on 3 mL of nickel sepharose HP (GE Health Care) pre-equilibrated with buffer and incubated for 1 h at 4°C in a rotating system. Then, the column was washed with ten column volumes of buffer (50 mM Tris-HCl pH 7.0, 10% glycerol, 0.5 M NaCl) followed by two column volumes of 50 mM Tris-HCl pH 7.0, 10% glycerol, 0.5 M NaCl and 5 mM imidazole. The protein was eluted using buffer with 500 mM imidazole. Fractions containing yellow protein were loaded on a pre-equilibrated Econo-Pac 10DG desalting columns (Bio-Rad). The final sample was flash frozen with liquid nitrogen and stored at -80°C. The purity of each purified enzyme batch was confirmed by SDS-PAGE analysis.

Fluorescence and Spectrophotometric Analysis

To determine the protein concentration based on FAD content, samples were diluted until an absorbance of around 0.5 at 440 nm. After collecting a full UV-vis spectrum, sodium dodecyl sulfate (SDS) was added to a final concentration of 0.1% w/v. An UV-vis spectrum was recorded again after 10 min. The spectrum obtained with SDS was used to determine the FAD concentration (ϵ = 11,300 M⁻¹ cm⁻¹), and the extinction coefficient for the

²www.uniprot.org

³blast.ncbi.nlm.nih.gov/Blast.cgi

protein by comparison with the spectrum of the native protein (Fraaije et al., 2005).

The apparent melting temperatures (T_M') were determined by using the ThermoFAD method (Forneris et al., 2009). For this, 20 μ L samples were prepared in a 96-well PCR plate. The samples contained 1 mg mL⁻¹ enzyme in different buffered solutions: 50 mM Bis-Tris HCl, 50 mM Tris-HCl, or 10 mM CAPS NaOH buffer adjusted at desired pH, cosolvents, and other additives. The plate was heated from 20 to 99°C, increasing the temperature by 0.5°C every 10 s, using an RT-PCR instrument (CFX96-Touch, Bio-Rad). By measuring fluorescence using a 450–490 nm excitation filter and a 515–530 nm emission filter, the T_M' or unfolding temperature was determined as the maximum of the derivative of the sigmoidal curve.

Enzyme activity was screened by measuring the oxidation of NADPH at 340 nm ($\epsilon = 62,220 \text{ M}^{-1} \text{ cm}^{-1}$) in 96-well F-bottom plates (Greiner Bio-One GmbH) at 25°C using a SynergyMX micro-plate reader (BioTek). The reactions were performed in 200 μ L containing 10% glycerol, 50 mM Bis-Tris HCl, 50 mM Tris HCl or 10 mM CAPS at the desired pH, cosolvent concentration, and additive, 0.45 μ M of purified BVMO, 150 μ M NADPH, 10 μ M FAD, and 5.0 mM phenylacetone. As a control, to measure NADPH consumption in the absence of substrate (uncoupling activity), phenylacetone was omitted. For determining kinetic parameters, activity was analyzed using a V-660 spectrophotometer (Jasco) using a 100 μ L quartz cuvette at 25°C, and NADPH oxidation at 340 nm was followed. The reaction mixture contained 50 mM Tris-HCl pH 8.0, 10% glycerol, 100 mM NaCl, 0.45 μ M of purified BVMO, 150 μ M NADPH, 10 μ M FAD, and substrate solubilized in 1,4-dioxane (2.5% v/v final concentration). The control reaction contained no substrate and the same concentration of cosolvent. The reaction was started by adding the nicotinamide cofactor and mixing, after which the absorbance was measured for 60 s.

Biotransformation Studies

The substrate scope analysis was performed using 6 different substrate mixtures (400 μ M final concentration of each substrate and 2.5% v/v 1,4-dioxane). For transformations, the reaction mixture was prepared in 500 μ L containing Tris-HCl pH 7.0, 10% glycerol, 100 mM NaCl, 30 μ M FAD, 10 mM Na₂PO₃·5H₂O, 150 μ M NADPH, and 2.7 μ M of purified enzyme in a 20 mL glass vial. The mixture was subsequently shaken at 150 rpm and 24°C for 24 h. The mixture was extracted three times by mixing one volume of ethyl acetate for 60 s. Subsequently, anhydrous sulfate magnesium was added to the organic solution to remove residual water. Analysis was carried out using a GCMS-QP2010 Ultra (Shimadzu) with electron ionization and quadrupole separation with a HP-1 column. The temperature program, column data and injection volumes are in the Supplementary Table S1.

After identifying the positive substrates and optimizing the conditions, biotransformations with single substrates were carried out in buffer Tris-HCl pH 8.0 using the same concentration for the additives, enzyme, cofactor and phosphite described above. The conversion of racemic bicyclo[3.2.0]hept-2-en-6-one, phenylacetone, 2-phenylcyclohexanone, and 4-phenylcyclohexanone was performed using a final substrate

concentration of 5.0 mM. For benzoin, a concentration of 1.0 mM was used. The reaction mixtures were incubated at 24°C and 150 rpm for 2 and 24 h. After incubation, samples were extracted three times with one volume of tert-butyl methyl ether containing 0.1% v/v mesitylene as an external standard and vortexed for 1 min. Then, the GC analysis was performed in the same instrument described above, for chiral analysis of bicyclo[3.2.0]hept-2-en-6-one, 2-phenylcyclohexanone and 4-phenylcyclohexanone the substrates were analyzed using a 7890A GC System (Agilent Technologies) equipped with a CP-Chirasil-Dex CB column. The enantiomers were identified by comparing with reported retention times and biocatalytic preference (Alphand et al., 1996; Vogel and Schwarz-Linek, 1999; Bocola et al., 2005; Romero et al., 2016).

¹H-NMR Analysis

For ¹H-NMR analysis, the reactions were carried out at 4 mL for 2-phenylcyclohexanone (10 mM) and 10 mL for benzoin (1.0 mM). Extraction was performed three times with ethyl acetate, dried over anhydrous sulfate magnesium and concentrated by rota-evaporation. The extracts were suspended in 1 mL CDCl₃ and NMR analysis was performed in a 400 MHz Varian Unity Plus spectrometer.

Statistical Analysis

All analyses were performed using GraphPad Prism v6.05 for Windows (GraphPad Software, La Jolla, CA, United States). To assess statistical significant differences between more than two groups of data, a two-way ANOVA test was used, with the Tukey post-test used to compare each different group, using a $p < 0.05$. Kinetic parameters were obtained by fitting the obtained data to the Michaelis–Menten equation. Chromatograms and MS spectra were analyzed using GCMSsolution Postrun Analysis 4.11 (Shimadzu). The library for the MS spectra was NIST11.

RESULTS

Genome Analysis and Molecular Cloning

By using the sequence motif for Rossmann fold (GxGxxG/A) and two previously described Type I BVMO-specific sequence motifs ([A/G]GxWxxxx[F/Y]P[G/M]xxxD and FxGxxxHxxxWP/D) (Fraaije et al., 2002; Riebel et al., 2012), we could identify three putative BVMOs in the predicted proteome of *S. leeuwenhoekii* C34: Sle_41160, Sle_13190 and Sle_62070 (UniProt codes A0A0F7VV32, A0A0F7VUW7, and A0A0F7W6X7, respectively) (Supplementary Table S2). A sequence alignment analysis revealed that Sle_13190 displays 92% sequence identity with PntE (pentalenolactone D synthase from *S. arenae*) (Seo et al., 2011) while, Sle_62070 only has 50% sequence identity with PntE. Another known BVMO that is closely related in sequence with Sle_62070 is PockeMO (Polycyclic Ketone Monooxygenase, 39% sequence identity) from the fungus *T. thermophila* (Fürst et al., 2016). These two putative BVMOs share 49% of sequence identity. On the other hand, Sle_41160, has 36% sequence identity with HAPMO (4-hydroxyacetophenone monooxygenase from *P. fluorescens*) (Kamerbeek et al., 2001) and shares around

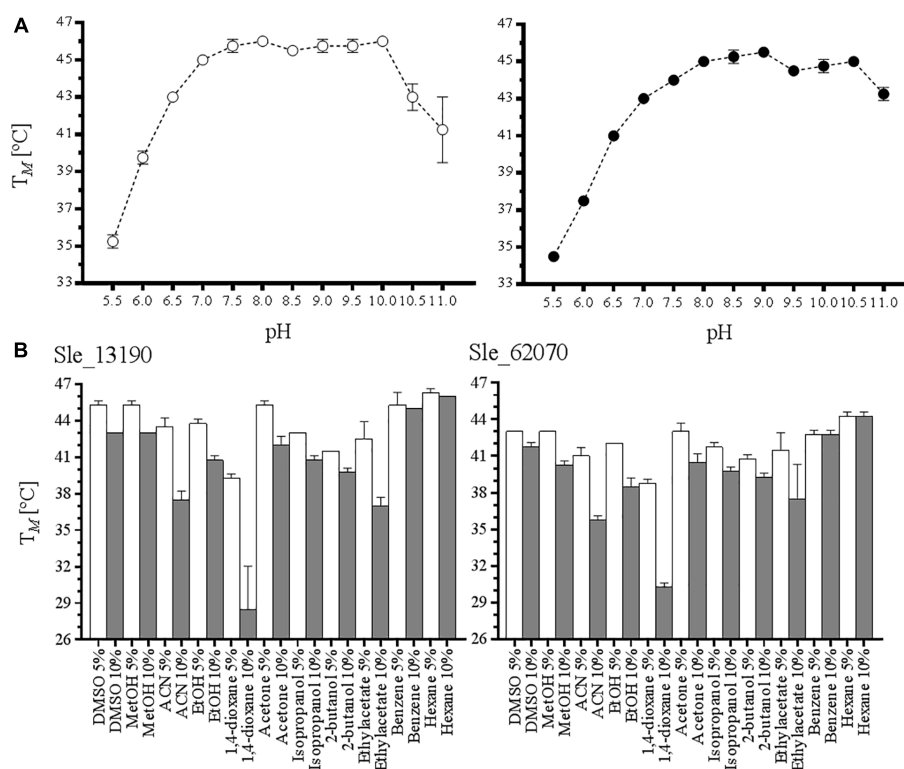


FIGURE 1 | Determination of apparent melting temperature of *S. leeuwenhoekii* Type I BVMOs. **(A)** The thermostability of Sle_13190 (white dots) and Sle_62070 (black dots) were measured at different pH (5.0–11.0). **(B)** The effect in the T_M by the presence of cosolvents at 5% v/v (white column) and 10% v/v (black column) was analyzed for Sle_13190 and Sle_62070 in Tris–HCl pH 7.0.

30% sequence identity with the other two predicted BVMOs. A phylogenetic molecular analysis was inferred using ML (Whelan and Goldman, 2001). The resultant tree revealed that Sle_13190 and Sle_62070 belong to a distinct clade of Type I BVMOs (Supplementary Figure S1). Based on the recently elucidated crystal structure of PockeMO, it has been reported that this group of BVMOs have a special structure feature in common that allows them to accommodate relatively large substrates in their active site (Fürst et al., 2016). This suggests that Sle_13190 and Sle_62070 should have the capacity to deal with bulky compounds. On the other hand, Sle_41160 was clustered close to HAPMO, a Type I BVMO described to catalyze the reaction of 4-hydroxyacetophenone to the corresponding acetate ester (Kamerbeek et al., 2001).

The *sle_13190*, *sle_62070*, and *sle_41160* genes have 69, 71, and 73% of G+C% content which is similar to the chromosomal DNA of *S. leeuwenhoekii* (Gomez-Escribano et al., 2015). We amplified the three genes from the isolated genomic DNA after optimizing PCR conditions. Thereupon, we cloned them into a pCRE2 vector that harbors a NADPH-recycling PTDH as a N-terminal fusion partner with a N-terminal histidine tag. The generated expression plasmids were used to transform *E. coli* TOP10, the subsequent expression of soluble protein was tested at various temperatures. The best results for Sle_13190 and Sle_62070 were obtained when expression was performed at 17°C for 48 h using 0.02% of L-arabinose. For Sle_41160, no expression

could be obtained at any of the tested conditions and therefore was discarded for further experiments. The proteins were purified through Ni²⁺-affinity chromatography in one step, a clear yellow color was indicative of proper folding and FAD binding. The purified proteins displayed UV-vis spectra that are characteristic for flavin-containing proteins displaying a maxima absorbance at 385 and 440 nm (Supplementary Figure S2). Using SDS as unfolding agent, the extinction coefficient at 450 nm of each flavoprotein was determined: 14.1 and 15.7 mM⁻¹ cm⁻¹ for Sle_13190 and Sle_62070, respectively.

Characterization of the Atacama BVMOs

To obtain a better view on the biochemical properties of the two purified flavoenzymes, their thermostability and tolerance toward cosolvents were studied. The ThermoFAD method was used to probe their thermostability. This method determines the apparent melting temperature (T_M) of a flavoprotein based on the increase in flavin fluorescence when the flavin cofactor is released upon protein unfolding (Forneris et al., 2009). First, we determined the T_M of the enzymes at various pH values using different buffers (Tris–HCl, Bis–Tris HCl, or CAPS) in the presence of 100 mM NaCl and 10% w/v glycerol. Interestingly, both flavoproteins display a similar pH-dependent unfolding profile (Figure 1A). For Sle_13190 and Sle_62070, the T_M was around 45°C between pH 7.5 and 10.0, showing that the two enzymes are relatively thermostable. To discard a possible buffer

TABLE 1 | Substrate scope analysis of Type I BVMOs.

Mix	Substrate	CAS number		Sle_13190	Sle_62070
1	2-hexylcyclopentanone	13074	65-2	+++++	++++
1	3-methyl-2,4-pentanedione	815	57-6	–	–
1	benzylphenyl sulfide	831	91-4	–	+++
1	Cycloundecanone	878	13-7	–	–
1	Indole	120	72-9	–	–
1	Phenylacetone	103	79-7	+++++	+++++
2	2-propylcyclohexanone	94	65-5	+++++	++
2	3-octanone	106	68-3	–	++
2	bicyclo[3.2.0]hept-2-en-6-one	13173	09-6	+++++	+++++
2	Cyclododecanone	830	13-7	–	–
2	Cyclopentanone	120	92-3	–	–
2	methyl-p-tolyl sulfide	1519	39-7	++++	++++
3	2-phenylcyclohexanone	1444	65-1	++++	+++++
3	androsta-1,4-diene-3,17-dione	897	06-3	–	–
3	Cyclopentadecanone	502	72-7	+	+
3	Nicotin	54	11-5	–	–
3	Vanillylacetone	122	48-5	–	–
4	4-hydroxyacetophenone	99	93-4	–	–
4	4-phenylcyclohexanone	4894	75-1	+++++	+++++
4	androst-4-ene-3,17-dione	63	05-8	++++	++
5	4-octanone	589	63-9	–	+
5	Acetophenone	98	86-2	–	–
5	Cyclohexanone	108	94-1	+++	+
5	Pregnenolone	145	13-1	–	–
5	Thioanisole	100	68-5	+++	++++
6	2-octanone	111	13-7	+	–
6	4-methylcyclohexanone	589	92-4	++	+++
6	Benzoin	119	53-9	++	+++++
6	Cyclooctanone	502	49-8	–	–
6	Stanolone	521	18-6	++	+++++

The 30 compounds tested in the substrate scope analysis are shown with their respective CAS number. Conversion was determined semi-quantitatively for each substrate by analysis of the peak areas in the GC chromatograms normalized by the compound(s) of the mixture that were not accepted by the enzyme. The results are categorized by the observed degree of conversion as 100–81%, +++++; 80–61%, +++++; 60–41%, ++++; 40–21%, ++; <20%, +; or <1%, –.

composition effect, HEPES at pH 7.0–7.5 and citrate buffer at pH 6 were also tested, resulting in highly similar T_M ' values. Subsequently, the effect of several commonly used cosolvents on the thermostability was explored by analyzing samples containing 5 and 10% v/v of DMSO, methanol, acetonitrile (ACN), ethanol, 1,4-dioxane, acetone, isopropanol, 2-butanol, ethyl acetate, benzene or hexane (Figure 1B). Again, both flavoenzymes displayed similar patterns of solvent tolerance. For both enzymes, a major deleterious effect was observed with 10% ACN, ethyl acetate and 1,4-dioxane, resulting in a drop of 7–8°C with ACN and ethyl acetate, and a drop of >10°C with 1,4-dioxane. The data suggest that the enzymes can be employed in the presence of various solvents.

The effect of increasing concentrations of NaCl, ectoine, 5-hydroxyectoine and proline was also analyzed. These additives were chosen because the BVMOs may have evolved to operate in the presence of high concentrations of these compounds as *S. leeuwenhoekii* thrives in a highly salty environment. While Sle_13190 was rather insensitive to increasing amounts of NaCl, Sle_62070 was more stable at lower concentrations

(Supplementary Figure S3). For the other additives, no significant differences in effects on the T_M ' values were observed. While increasing amounts of ectoine resulted in lower T_M ' values, 5-hydroxyectoine (0–200 mM) and proline (0–4 mM) did not have a significant effect (Supplementary Figure S3).

Substrate Profiling of the Atacama's BVMOs

After the thermostability analysis, the substrate scopes for both flavoenzymes were studied through a high-throughput GC-MS analysis approach by verifying product formation for each potential substrate. Each enzyme was incubated with six different mixtures containing 3–6 distinct ketones and thioethers at a final concentration of 400 μ M each and 2.5% 1,4-dioxane as cosolvent. In this way, a total of 30 different potential substrates were tested with each BVMO (Supplementary Figure S4). For regeneration of the nicotinamide coenzyme, the fusion partner of the recombinant enzymes, PTDH, was exploited by including phosphite and a catalytic amount of the coenzyme.

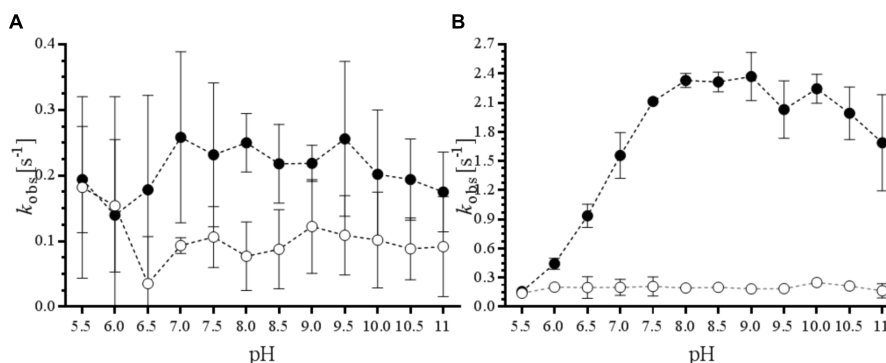


FIGURE 2 | Effects of pH on BVMO and NADPH oxidase activities. The ratio of k_{obs} in the presence (black dots) and absence of 5.0 mM phenylacetone (white dots) was analyzed at pH 5.0–11.0 for Sle_13190 (A) and Sle_62070 (B).

The conversions were incubated for 24 h at 24°C and after extraction the analysis revealed a broad substrate acceptance for both enzymes. For Sle_13190, 15 compounds were identified as substrate through detection of formed substrate, while Sle_62070 was found to convert 17 of the 30 tested compounds (Table 1). The substrate profiles include several cyclic aliphatic ketones, aromatic ketones, and sulfides, linear aliphatic ketones and also a steroid, stanolone. The two BVMOs shared most of the uncovered substrates but also some striking differences were noted. For example, of the tested octanones, Sle_13190 converted 2-octanone, and Sle_62070 converted 3- and 4-octanone (the predicted products are included in the Supplementary Figure S5).

To determine the optimal conditions and robustness of the potential biocatalysts, phenylacetone was selected as model substrate as it was found to be well-accepted substrate (Table 1). We measured the rate of NADPH consumption in the absence or presence of 5.0 mM of this ketone at various pH values (Figure 2). The data confirm that Sle_62070 has a good activity with phenylacetone as substrate, and a significantly higher activity with the substrate over the uncoupling activity (consumption of NADPH in absence of substrate). The highest activity (around 2.4 s^{-1}) was observed at pH 7.5–10. Sle_13190 has a relatively low activity on phenylacetone (around 0.24 s^{-1} at pH 7–9.5), which is only slightly higher when compared with its uncoupling activity. Based on these activity results we chose a pH value of 8.0 for the subsequent experiments. We also compared the effect of seven water-miscible solvents at 2.5, 5, and

10% v/v (Supplementary Figure S6). This revealed that DMSO is probably a substrate for both BVMOs. For Sle_62070 the rate of NADPH consumption increased significantly at higher DMSO concentrations while for Sle_13190 the observed rate with DMSO were even equal to the rates in the presence phenylacetone. BVMO activity on DMSO has also been noted before and therefore is not a suitable cosolvent (Bordewick et al., 2018). Interestingly, up to 10% v/v of the other six cosolvents seem to be compatible with both BVMOs, even at the highest concentration these cosolvents did not significantly affect the observed activities. While the BVMO activities were in the same range when compared in buffer, only some modest increase in uncoupling activity was seen in the presence of ACN, methanol and isopropanol. This demonstrates that both biocatalysts are rather tolerant toward regularly used cosolvents.

In order to test the effects of known microbial osmoprotectants we studied their effects on Sle_62070 because this BVMO seemed to exhibit better kinetic properties. We chose 1,4-dioxane (2.5% v/v) as cosolvent. The effect of increasing concentrations of ectoin, 5-hydroxyectoine (0–200 mM) and proline (0–4 M) on BVMO activity of Sle_62070 was studied (Supplementary Figure S7). None of the osmoprotectants exerted a dramatic effect on the BVMO or uncoupling activities. A slight boost (20%) on BVMO activity was observed with 200 mM ectoin, while 4 M proline decreased the BVMO activity by 30%. To have a better view on the kinetic properties of Sle_62070, the initial rates of NADPH consumption with a set of ketones and sulfides were determined (Supplementary Figure S8A). These kinetic data revealed a relatively high k_{obs} with bicyclo[3.2.0]hept-2-en-6-one, phenylacetone, 2-phenylcyclohexanone and 4-phenylcyclohexanone, and a lower activity with the thioethers methyl p-tolyl sulfide, benzylphenyl sulfide and thioanisole and the cyclic ketones 2-hexylcyclopentanone and cyclopentadecanone. The other tested compounds did not show a significant difference in activity when compared with the uncoupling rate. The steady-state kinetic parameters for four substrates on which Sle_62070 displayed a relatively high activity were determined (Table 2). As it was found for

TABLE 2 | Kinetic parameters of Sle_62070.

Substrate	k_{cat} [s^{-1}]	K_M [mM]	$k_{\text{cat}} K_M^{-1}$ [$\text{s}^{-1} \text{mM}^{-1}$]
bicyclo[3.2.0]hept-2-en-6-one	4.0 ± 0.06	0.20 ± 0.01	20
Phenylacetone	4.1 ± 0.2	3.0 ± 0.3	1.3
2-phenylcyclohexanone	>4.0	>3.0	1.3
4-phenylcyclohexanone	>4.0	>3.0	1.3

NADPH oxidation rates were spectrophotometrically followed in 50 mM Tris-HCl at pH 8.0, 10% glycerol and 100 mM NaCl at 25°C (enzyme 0.45 μM , NADPH 150 μM) with four ketones in increasing concentrations. The data obtained were fit using a Michaelis–Menten equation in GraphPad Prism.

TABLE 3 | Biocatalysis performance of Sle_62070.

Bicyclo[3.2.0]hept-2-en-6-one	ee _N	ee _A	Phenylacetone	2-phenylcyclohexanone	4-phenylcyclohexanone	Benzoin	Thioanisole
>99%	>99%	>99%	>99%	69%	>99%	>99%	18%

Biotransformation assays were carried out for 2 h at 24°C for six different substrates, consumption percentages are shown. Enantioselectivity was determined for bicyclo[3.2.0]hept-2-en-6-one. N:A, ratio normal and abnormal product, ee, enantiomeric excess of the product calculated as $ee = \frac{(A_{\text{major}} - A_{\text{minor}})}{(A_{\text{major}} + A_{\text{minor}})} \times 100$.

other Type I BVMOs, Sle_62070 displays a relatively high activity with bicyclo[3.2.0]hept-2-en-6-one and phenylacetone, showing a k_{cat} of 4.0 s^{-1} for both compounds, and K_M values of 0.2 and 3 mM, respectively (Supplementary Figures S8B,C). In addition, Sle_62070 shows high activity with 2-phenylcyclohexanone and 4-phenylcyclohexanone, displaying k_{cat} values of $>4.0 \text{ s}^{-1}$ and K_M values of $>3.0 \text{ mM}$ for both phenylcyclohexanones (Supplementary Figures S8D,E). We also attempted to determine kinetic parameters for Sle_13190, but the observed rates were too low for an accurate kinetic analysis. Clearly, using the applied conditions, Sle_62070 is a superior biocatalyst concerning its kinetic properties.

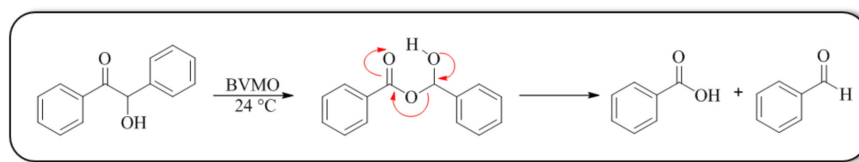
After establishing the substrate profiles and kinetic properties of the two newly discovered BVMOs, some substrates were selected as candidates to perform conversions at a larger scale. Racemic bicyclo[3.2.0]hept-2-en-6-one was chosen as a hallmark BVMO substrate for enantio- and regioselectivity, phenylacetone as a well described ketone for BVMOs, and thioanisole to include a thioether for testing a sulfoxidation reaction. 2-Phenylcyclohexanone, 4-phenylcyclohexanone and benzoin were selected as relatively unexplored BVMO substrates. All the compounds were tested at 5.0 mM except for the conversion of benzoin; due its poor solubility it was used at a concentration of 1.0 mM. Upon incubating the substrates with $2.7 \mu\text{M}$ Sle_62070-PTDH for 2 h, complete conversion was observed with most targeted compounds (Table 3). For 2-phenylcyclohexanone merely 69% was converted and for thioanisole only 18% conversion was obtained. Extending the incubation to 24 h only resulted in a minor improvement (83 and 22% conversion for 2-phenylcyclohexanone and thioanisole, respectively). Sle_13190 was only tested for the conversion of benzoin, resulting in 40% conversion after 2 h incubation. By GC-MS analysis it was found that both enzymes produce benzaldehyde when converting benzoin. NMR analysis revealed that, except for benzaldehyde, also benzoic acid is formed upon conversion of benzoin (Supplementary Figure S9A). Also the conversion of 2-phenylcyclohexanone was subjected to ^1H -NMR analysis. The NMR spectral

data revealed the production of the proximal lactone when 2-phenylcyclohexanone was converted by Sle_62070 (Supplementary Figure S9B).

To probe the enantioselectivity of Sle_62070, chiral GC analyses were performed. First, the conversion of 4-phenylcyclohexanone was studied. As reference the conversion of 4-phenylcyclohexanone with TmCHMO-PTDH was performed. The reaction using CHMOs is described to produce preferably the S lactone (Vogel and Schwarz-Linek, 1999; Rial et al., 2008). The results revealed that Sle_62070 is highly enantioselective toward this ketone as only the S lactone was formed (Supplementary Figure S10). Using 2-phenylcyclohexanone as racemic substrate, Sle_62070 was found to be highly enantioselective for convert the R enantiomer substrate. The reaction was compared with TmCHMO-PTDH which is described to display a higher preference for the same enantiomer (Alphand et al., 1996; Bocola et al., 2005; Supplementary Figure S10). The enantioselective properties of Sle_62070 with racemic bicyclo[3.2.0]hept-2-en-6-one as substrate was also analyzed. As reference reaction, the biotransformation of the racemic prochiral cyclic ketone was also performed with PAMO-PTDH resulting in the formation of all four possible lactone products (Romero et al., 2016). After 2 h conversion, two of the four possible lactone products, in equal amounts, were observed when using Sle_62070: the (-)-1S,5R normal lactone and the (-)-1R,5S abnormal lactone. The enantiomeric excess for both products were determined as $>99\%$ (Supplementary Figure S11). Finally, the reaction was analyzed in time (Supplementary Figures S12A,B) which revealed that Sle_62070 has no preference for one of the two substrate enantiomers.

DISCUSSION

By genome sequence analysis, we have identified two new actinobacterial BVMOs. As far as we know, these are the first BVMOs described from an Atacama desert's microorganism. Both BVMOs were shown to be rather robust by tolerating

**FIGURE 3** | Proposed reaction of benzoin oxidation by Sle_62070. Mechanism of the hydrolysis of oxidation product to benzaldehyde and benzoic acid.

cosolvents up to 10% v/v and by displaying relatively high melting temperatures. Compared with CHMO from *Acinetobacter* sp. or STMO from *Rhodococcus rhodochrous* (both having a T_M' of 39°C), these two new BVMOs showed a higher T_M' (5–6°C higher). The two BVMOs are similar in thermostability when compared with the recently reported PockeMO (T_M' of 47°C) which was identified from a thermophilic fungus (Fürst et al., 2016). Both uncovered enzymes showed activity on a wide variety of ketones and sulfides, a typical feature of Type I BVMOs. As already can be deduced from the clustering of the sequences based on sequence homology with other BVMOs that are known to act on bulky compounds, Sle_13190 and Sle_62070 also accept rather complex compounds as substrate, including biphenyls and a steroid. Remarkably, even though the substrate scope is similar between these two enzymes, Sle_62070 showed to be more promising by acting on more compounds and by exhibiting higher activities. Sle_62070 also revealed to be highly enantio- and regioselective in converting bicyclo[3.2.0]hept-2-en-6-one into two enantiopure lactones. Interestingly, it is also efficient in converting benzoin which, as far we know, was only reported as substrate for CPMO without any product identification (Riebel et al., 2012). We have identified for the first time the products formed by BVMO-catalyzed benzoin oxidation: benzaldehyde and benzoic acid. For the production of these compounds, we suggest the formation of a labile ester product which decomposes to from the two aromatic products (Figure 3). Overall, this work has delivered two new BVMOs to complement the available collection of known BVMOs. The extreme environment of the Atacama desert may develop as an interesting source for new robust enzymes. Using metagenomic approaches it should become feasible to tap novel biocatalysts from this rich source of actinobacterial “biosynthetic dark matter,” which is unique due to the special soil subsurface geochemistry, ecological diversity, and environmental conditions

REFERENCES

- Alphand, V., Furstoss, R., Pedragosa-Moreau, S., Roberts, S. M., and Willetts, A. J. (1996). Comparison of microbiologically and enzymatically mediated Baeyer–Villiger oxidations: synthesis of optically active caprolactones. *J. Chem. Soc. Perkin Trans. 1*, 1867–1872. doi: 10.1039/P19960001867
- Azua-Bustos, A., Urrejola, C., and Vicuña, R. (2012). Life at the dry edge: microorganisms of the Atacama Desert. *FEBS Lett.* 586, 2939–2945. doi: 10.1016/j.febslet.2012.07.025
- Bocola, M., Schulz, F., Leca, F., Vogel, A., Fraaije, M. W., and Reetz, M. T. (2005). Converting phenylacetone monooxygenase into phenylcyclohexanone monooxygenase by rational design: towards practical Baeyer–Villiger monooxygenases. *Adv. Synth. Catal.* 347, 979–986. doi: 10.1002/adsc.200505069
- Bordewick, S., Beier, A., Balke, K., and Bornscheuer, U. T. (2018). Baeyer–Villiger monooxygenases from *Yarrowia lipolytica* catalyze preferentially sulfoxidations. *Enzyme Microb. Technol.* 109, 31–42. doi: 10.1016/j.enzmictec.2017.09.008
- Bučko, M., Gemeiner, P., Schenkmyerová, A., Krajčovič, T., Rudroff, F., and Mihovilović, M. D. (2016). Baeyer–Villiger oxidations: biotechnological approach. *Appl. Microbiol. Biotechnol.* 100, 6585–6599.
- Bull, A. T., and Asenjo, J. A. (2013). Microbiology of hyper-arid environments: recent insights from the Atacama Desert, Chile. *Antonie Van Leeuwenhoek* 103, 1173–1179. doi: 10.1007/s10482-013-9911-7
- Bull, A. T., Asenjo, J. A., Goodfellow, M., and Gómez-Silva, B. (2016). The Atacama Desert: technical resources and the growing importance of novel microbial diversity. *Annu. Rev. Microbiol.* 70, 215–234. doi: 10.1146/annurev-micro-102215-095236
- Busarakam, K., Bull, A. T., Girard, G., Labeda, D. P., van Wezel, G. P., and Goodfellow, M. (2014). *Streptomyces leeuwenhoekii* sp. nov., the producer of chaxalactins and chaxamycins, forms a distinct branch in *Streptomyces* gene trees. *Antonie Van Leeuwenhoek* 105, 849–861. doi: 10.1007/s10482-014-0139-y
- Ceccoli, R. D., Bianchi, D. A., and Rial, D. V. (2014). Flavoprotein monooxygenases for oxidative biocatalysis: recombinant expression in microbial hosts and applications. *Front. Microbiol.* 5:25. doi: 10.3389/fmicb.2014.00025
- de Gonzalo, G., Ottolina, G., Zambianchi, F., Fraaije, M. W., and Carrea, G. (2006). Biocatalytic properties of Baeyer–Villiger monooxygenases in aqueous–organic media. *J. Mol. Catal. B Enzym.* 39, 91–97. doi: 10.1016/j.molcatb.2006.01.010
- Dewan, S. S. (2014). *Global Markets for Enzymes in Industrial Applications*. Wellesley, MA: BCC Research.
- Dijkman, W. P., De Gonzalo, G., Mattevi, A., and Fraaije, M. W. (2013). Flavoprotein oxidases: classification and applications. *Appl. Microbiol. Biotechnol.* 97, 5177–5188. doi: 10.1007/s00253-013-4925-7
- Forneris, F., Orru, R., Bonivento, D., Chiarelli, L. R., and Mattevi, A. (2009). ThermoFAD, a ThermoFluor-adapted flavin *ad hoc* detection system for protein folding and ligand binding. *FEBS J.* 276, 2833–2840. doi: 10.1111/j.1742-4658.2009.07006.x
- Fraaije, M. W., Kamerbeek, N. M., van Berkel, W. J. H., and Janssen, D. B. (2002). Identification of a Baeyer–Villiger monooxygenase sequence motif. *FEBS Lett.* 518, 43–47. doi: 10.1016/S0014-5793(02)02623-6
- of this hyper-arid desert (Bull et al., 2016; Idris et al., 2017).

AUTHOR CONTRIBUTIONS

AG-S, LP, and MF conceived and designed the study, analyzed the data, and prepared the manuscript. AG-S performed the experiments. MT analyzed the ¹H-NMR results.

FUNDING

This work was supported by the Institute for Biological and Medical Engineering from Pontificia Universidad Católica de Chile and CORFO 14ENI2-26862. A Ph.D. fellowship from CONICYT (Comisión Nacional de Investigación Científica y Tecnológica de Chile) and a scholarship from Pontificia Universidad Católica de Chile to AG-S was also acknowledged.

ACKNOWLEDGMENTS

We would like to thank to Prof. Dr. Juan Asenjo De Leuze from Universidad de Chile for kindly providing the *S. leeuwenhoekii* C34 strain.

SUPPLEMENTARY MATERIAL

The Supplementary Material for this article can be found online at: <https://www.frontiersin.org/articles/10.3389/fmicb.2018.01609/full#supplementary-material>

- Fraaije, M. W., Wu, J., Heuts, D. P., van Hellemond, E. W., Spelberg, J. H., and Janssen, D. B. (2005). Discovery of a thermostable Baeyer–Villiger monooxygenase by genome mining. *Appl. Microbiol. Biotechnol.* 66, 393–400.
- Fürst, M. J. L. J., Savino, S., Dudek, H. M., Rúbén Gómez, Castellanos, J., Gutiérrez, et al. (2016). Polycyclic ketone monooxygenase from the thermophilic fungus *Thermothelomyces thermophila*: a structurally distinct biocatalyst for bulky substrates. *J. Am. Chem. Soc.* 139, 627–630. doi: 10.1021/jacs.6b12246
- Gibson, D. G., Young, L., Chuang, R.-Y., Venter, J. C., Hutchison, C. A., and Smith, H. O. (2009). Enzymatic assembly of DNA molecules up to several hundred kilobases. *Nat. Methods* 6, 343–345. doi: 10.1038/nmeth.1318
- Gibson, M., Nur-e-alam, M., Lipata, F., Oliveira, M. A., and Rohr, J. (2005). Characterization of kinetics and products of the Baeyer–Villiger oxygenase MtmOIV, the key enzyme of the biosynthetic pathway toward the natural product anticancer drug mithramycin from *Streptomyces argillaceus*. *J. Am. Chem. Soc.* 127, 17594–17595. doi: 10.1021/ja055750t
- Gomez-Escribano, J. P., Castro, J. F., Razmilic, V., Chandra, G., Andrews, B., Asenjo, J. A., et al. (2015). The *Streptomyces leeuwenhoekii* genome: *de novo* sequencing and assembly in single contigs of the chromosome, circular plasmid pSLE1 and linear plasmid pSLE2. *BMC Genomics* 16:485. doi: 10.1186/s12864-015-1652-8
- Hobbs, G. (1989). Dispersed growth of *Streptomyces* in liquid culture. *Appl. Microbiol. Biotechnol.* 31, 272–277. doi: 10.1007/BF00258408
- Idris, A., Goodfellow, M., Sanderson, R., Asenjo, J. A., and Bull, A. T. (2017). Actinobacterial rare biospheres and dark matter revealed in habitats of the Chilean Atacama desert. *Sci. Rep.* 7:8373. doi: 10.1038/s41598-017-08937-4
- Jiang, J., Tetzlaff, C. N., Takamatsu, S., Iwatsuki, M., Komatsu, M., Ikeda, H., et al. (2009). Genome mining in *Streptomyces avermitilis*: a biochemical Baeyer–Villiger reaction and discovery of a new branch of the pentalenolactone family tree. *Biochemistry* 48, 6431–6440. doi: 10.1021/bi900766w
- Johannes, T. W., Woodyer, R. D., and Zhao, H. (2005). Directed evolution of a thermostable phosphite dehydrogenase for NAD(P)H regeneration. *Appl. Environ. Microbiol.* 71, 5728–5734. doi: 10.1128/AEM.71.10.5728-5734.2005
- Kamerbeek, N. M., Moonen, M. J., Van Der Ven, J. G., Van Berkel, W. J. H., Fraaije, M. W., and Janssen, D. B. (2001). 4-Hydroxyacetophenone monooxygenase from *Pseudomonas fluorescens* ACB. A novel flavoprotein catalyzing baeyer-villiger oxidation of aromatic compounds. *Eur. J. Biochem.* 268, 2547–2557. doi: 10.1046/j.1432-1327.2001.02137.x
- Karan, R., Capes, M. D., and DasSarma, S. (2012). Function and biotechnology of extremophilic enzymes in low water activity. *Aquat. Biosyst.* 8:4. doi: 10.1186/2046-9063-8-4
- Kumar, S., Stecher, G., and Tamura, K. (2016). MEGA7: molecular evolutionary genetics analysis version 7.0 for bigger datasets. *Mol. Biol. Evol.* 33, 1870–1874. doi: 10.1093/molbev/msw054
- Leisch, H., Morley, K., and Lau, P. C. K. (2011). Baeyer–Villiger monooxygenases: more than just green chemistry. *Chem. Rev.* 111, 4165–4222. doi: 10.1021/cr1003437
- Mthethwa, K. S., Kassier, K., Engel, J., Kara, S., Smit, M. S., and Opperman, D. J. (2017). Fungal BVMOs as alternatives to cyclohexanone monooxygenase. *Enzyme Microb. Technol.* 106, 11–17. doi: 10.1016/j.enzmictec.2017.06.017
- Okoro, C. K., Brown, R., Jones, A. L., Andrews, B. A., Asenjo, J. A., Goodfellow, M., et al. (2009). Diversity of culturable actinomycetes in hyper-arid soils of the Atacama Desert, Chile. *Antonie Van Leeuwenhoek* 95, 121–133. doi: 10.1007/s10482-008-9295-2
- Park, J., Kim, D., Kim, S., Kim, J., Bae, K., and Lee, C. (2007). The analysis and application of a recombinant monooxygenase library as a biocatalyst for the Baeyer–Villiger reaction. *J. Microbiol. Biotechnol.* 17, 1083–1089.
- Paulino-Lima, I. G., Azua-Bustos, A., Vicuña, R., González-Silva, C., Salas, L., Teixeira, L., et al. (2013). Isolation of UVC-tolerant bacteria from the hyperarid Atacama Desert, Chile. *Microb. Ecol.* 65, 325–335. doi: 10.1007/s00248-012-0121-z
- Pellis, A., Cantone, S., Ebert, C., and Gardossi, L. (2018). Evolving biocatalysis to meet bioeconomy challenges and opportunities. *New Biotechnol.* 40, 154–169. doi: 10.1016/j.nbt.2017.07.005
- Pulschen, A. A., Rodrigues, F., Duarte, R. T. D., Araujo, G. G., Santiago, I. F., Paulino-Lima, I. G., et al. (2015). UV-resistant yeasts isolated from a high-altitude volcanic area on the Atacama Desert as eukaryotic models for astrobiology. *Microbiologyopen* 4, 574–588. doi: 10.1002/mbo3.262
- Rateb, M. E., Houssen, W. E., Harrison, W. T. A., Deng, H., Okoro, C. K., Asenjo, J. A., et al. (2011). Diverse metabolic profiles of a *Streptomyces* strain isolated from a hyper-arid environment. *J. Nat. Prod.* 74, 1965–1971. doi: 10.1021/np200470u
- Reetz, M. T. (2013). Biocatalysis in organic chemistry and biotechnology: past, present, and future. *J. Am. Chem. Soc.* 135, 12480–12496. doi: 10.1021/ja405051f
- Research and Markets (2017). *Global Biocatalysis and Biocatalysts Market 2017–2021: Analysis by Application, Source & Type*. Dublin: Research and Markets.
- Rial, D. V., Bianchi, D. A., Kapitanova, P., Lengár, A., van Beilen, J. B., and Mihovilovic, M. D. (2008). Stereoselective desymmetrizations by recombinant whole cells expressing the Baeyer–Villiger monooxygenase from *Xanthobacter* sp. ZL5: a new biocatalyst accepting structurally demanding substrates. *Eur. J. Org. Chem.* 2008, 1203–1213. doi: 10.1002/ejoc.200700872
- Riebel, A., Dudek, H. M., de Gonzalo, G., Stepniak, P., Rychlewski, L., and Fraaije, M. W. (2012). Expanding the set of rhodococcal Baeyer–Villiger monooxygenases by high-throughput cloning, expression and substrate screening. *Appl. Microbiol. Biotechnol.* 95, 1479–1489. doi: 10.1007/s00253-011-3823-0
- Rodríguez, C., de Gonzalo, G., Torres Pazmiño, D. E., Fraaije, M. W., and Gotor, V. (2008). Selective Baeyer–Villiger oxidation of racemic ketones in aqueous–organic media catalyzed by phenylacetone monooxygenase. *Tetrahedron Asymmetry* 19, 197–203. doi: 10.1016/j.tetasy.2007.12.008
- Romero, E., Gómez Castellanos, J. R., Mattevi, A., and Fraaije, M. W. (2016). Characterization and crystal structure of a robust cyclohexanone monooxygenase. *Angew. Chem. Int. Ed. Engl.* 55, 15852–15855. doi: 10.1002/anie.201608951
- Santiago, M., Ramírez-Sarmiento, C. A., Zamora, R. A., and Parra, L. P. (2016). Discovery, molecular mechanisms, and industrial applications of cold-active enzymes. *Front. Microbiol.* 7:1408. doi: 10.3389/fmicb.2016.01408
- Seo, M.-J., Zhu, D., Endo, S., Ikeda, H., and Cane, D. E. (2011). Genome mining in *Streptomyces*. Elucidation of the role of Baeyer–Villiger monooxygenases and non-heme iron-dependent dehydrogenase/oxygenases in the final steps of the biosynthesis of pentalenolactone and neopentalenolactone. *Biochemistry* 50, 1739–1754. doi: 10.1021/bi1019786
- Torres Pazmiño, D. E., Riebel, A., de Lange, J., Rudroff, F., Mihovilovic, M. D., and Fraaije, M. W. (2009). Efficient biooxidations catalyzed by a new generation of self-sufficient Baeyer–Villiger monooxygenases. *ChemBioChem* 10, 2595–2598. doi: 10.1002/cbic.200900480
- Vogel, M., and Schwarz-Linek, U. (1999). *Bioorganic Chemistry: Highlights and New Aspects*, ed. U. Diederichsen. Weinheim: Wiley-VCH, 102–110.
- Whelan, S., and Goldman, N. (2001). A general empirical model of protein evolution derived from multiple protein families using a maximum-likelihood approach. *Mol. Biol. Evol.* 18, 691–699. doi: 10.1093/oxfordjournals.molbev.a003851
- Woodley, J. M. (2017). Integrating protein engineering with process design for biocatalysis. *Philos. Trans. A Math. Phys. Eng. Sci.* 376:20170062. doi: 10.1098/rsta.2017.0062

Conflict of Interest Statement: The authors declare that the research was conducted in the absence of any commercial or financial relationships that could be construed as a potential conflict of interest.

Copyright © 2018 Gran-Scheuch, Trajkovic, Parra and Fraaije. This is an open-access article distributed under the terms of the Creative Commons Attribution License (CC BY). The use, distribution or reproduction in other forums is permitted, provided the original author(s) and the copyright owner(s) are credited and that the original publication in this journal is cited, in accordance with accepted academic practice. No use, distribution or reproduction is permitted which does not comply with these terms.



Catalytic Performance of a Class III Old Yellow Enzyme and Its Cysteine Variants

Anika Scholtissek¹, Eric Gädke^{1,2}, Caroline E. Paul^{3,4}, Adrie H. Westphal⁵, Willem J. H. van Berkel⁵ and Dirk Tischler^{2*}

¹ Environmental Microbiology Group, Interdisciplinary Ecological Center, Institute of Biosciences, Technical University Bergakademie Freiberg, Freiberg, Germany, ² Microbial Biotechnology, Department of Biology and Biotechnology, Ruhr-University Bochum, Bochum, Germany, ³ Laboratory of Organic Chemistry, Wageningen University and Research, Wageningen, Netherlands, ⁴ Department of Biotechnology, Delft University of Technology, Delft, Netherlands, ⁵ Laboratory of Biochemistry, Wageningen University and Research, Wageningen, Netherlands

OPEN ACCESS

Edited by:

Daniela De Biase,
Università degli Studi di Roma La
Sapienza, Italy

Reviewed by:

Loredano Pollegioni,
Università degli Studi dell'Insubria, Italy
Alberto A. Iglesias,
National University of the Littoral,
Argentina

*Correspondence:

Dirk Tischler
dirk.tischler@rub.de

Specialty section:

This article was submitted to
Microbial Physiology and Metabolism,
a section of the journal
Frontiers in Microbiology

Received: 05 July 2018

Accepted: 20 September 2018

Published: 12 October 2018

Citation:

Scholtissek A, Gädke E, Paul CE,
Westphal AH, van Berkel WJH and
Tischler D (2018) Catalytic
Performance of a Class III Old Yellow
Enzyme and Its Cysteine Variants.
Front. Microbiol. 9:2410.
doi: 10.3389/fmicb.2018.02410

Class III old yellow enzymes (OYEs) contain a conserved cysteine in their active sites. To address the role of this cysteine in OYE-mediated asymmetric synthesis, we have studied the biocatalytic properties of OYERo2a from *Rhodococcus opacus* 1CP (WT) as well as its engineered variants C25A, C25S and C25G. OYERo2a in its redox resting state (oxidized form) is irreversibly inactivated by *N*-methylmaleimide. As anticipated, inactivation does not occur with the Cys variants. Steady-state kinetics with this maleimide substrate revealed that C25S and C25G doubled the turnover frequency (k_{cat}) while showing increased K_M values compared to WT, and that C25A performed more similar to WT. Applying the substrate 2-cyclohexen-1-one, the Cys variants were less active and less efficient than WT. OYERo2a and its Cys variants showed different activities with NADPH, the natural reductant. The variants did bind NADPH less well but k_{cat} was significantly increased. The most efficient variant was C25G. Replacement of NADPH with the cost-effective synthetic cofactor 1-benzyl-1,4-dihydronicotinamide (BNAH) drastically changed the catalytic behavior. Again C25G was most active and showed a similar efficiency as WT. Biocatalysis experiments showed that OYERo2a, C25S, and C25G converted *N*-phenyl-2-methylmaleimide equally well (81–84%) with an enantiomeric excess (ee) of more than 99% for the *R*-product. With cyclic ketones, the highest conversion (89%) and ee (>99%) was observed for the reaction of WT with *R*-carvone. A remarkable poor conversion of cyclic ketones occurred with C25G. In summary, we established that the generation of a cysteine-free enzyme and cofactor optimization allows the development of more robust class III OYEs.

Keywords: biocatalysis, ene reductase, flavoprotein, inactivation, actinobacteria, protein engineering, *Rhodococcus opacus* 1CP, cysteine modification

INTRODUCTION

Protein engineering is a powerful tool to improve the catalytic properties of enzymes. Through inducing subtle changes in amino acid side chains, it is possible to optimize binding of specific ligands, thermostability, reaction rates and catalytic efficiency (Balke et al., 2017). Also, the enantioselectivity can be switched (van Den Heuvel et al., 2000). An encouraging enzyme class

in the focus of biocatalysis is the flavin-dependent ene reductase (ER) from the Old Yellow Enzyme family (OYEs, EC 1.6.99.1). The FMN-containing OYEs catalyze the selective reduction of activated α,β -unsaturated alkenes yielding valuable alkanes containing one or two chiral carbon centers (**Scheme 1**). Capable of catalyzing the asymmetric *trans*-hydrogenation of various alkene substrates such as cyclic enones, maleimides, aldehydes, or (di)-carboxylic acids (Swiderska and Stewart, 2006a; Nivinskas et al., 2008; Toogood et al., 2008; Fryszkowska et al., 2009; Gao et al., 2012; Fu et al., 2013; Riedel et al., 2015; Scholtissek et al., 2017b; Toogood and Scrutton, 2018), ERs promise potential applications in industrial processes due to their exquisite *regio*-, stereo- and enantioselectivity. The FMN cofactor receives electrons from NAD(P)H, but ERs also accept nicotinamide coenzyme biomimetics (NCBs) (Knaus et al., 2016; Scholtissek et al., 2017a).

A detailed summary of protein engineering studies on OYEs was reported earlier (Amato and Stewart, 2015; Toogood and Scrutton, 2018). OYE1 from *Saccharomyces pastorianus* (Saito et al., 1991) is the most investigated OYE toward mutagenesis so far. Due to the small size of the active pocket, OYE1 is limited to smaller substrates and to a strict enantioselectivity (Swiderska and Stewart, 2006b). Replacement of Trp116 by Ile or Phe led to an opposite binding of several substrates, which induced an inverted stereochemical outcome (Padhi et al., 2009; Pompeu et al., 2013; Walton et al., 2014). Further amino acid replacements of OYE1 conserved residues Tyr196 (Kohli and Massey, 1998), Thr37 (Xu et al., 1999), and His191/Asn194 (Fox and Karplus, 1994), affecting both the oxidative as well as reductive half-reaction.

OYEs from class III (Scholtissek et al., 2017a) were engineered to improve stability or to modulate their reduction potential (Spiegelhauer et al., 2010; Riedel et al., 2015). Introduction of a characteristic salt bridge in OYERo2 generated a protein variant (OYERo2a) with similar catalytic properties as the wildtype enzyme (Riedel et al., 2015). However, thermal stability and tolerance toward organic solvents were highly improved. In subsequent studies, we observed that several substrates, especially maleimides, have an inhibitory effect on OYERo2a (discussed as wild type (WT) here). Considering the presence of a cysteine residue near the *N*-terminus of the protein—only conserved for class III OYEs—it was assumed that this cysteine might form a thioether due to a Michael addition reaction with

maleimides (Gregory, 1955). This cysteine was already the subject of a previous study on xenobiotic reductase A (XenA) and was found to modulate the FMN/FMNH[−] reduction potential (Spiegelhauer et al., 2010). Structural investigations of XenA and two Cys variants revealed that the cysteine residue determines whether the oxidation of NADPH (reduction of FMN) or the reduction of the alkene substrate (oxidation of FMNH[−]) is rate-limiting.

In this study, we produced C25A, C25S, and C25G variants of OYERo2a and studied their kinetic and biocatalytic properties. Interestingly, we found that the Cys replacements result in substrate-dependent catalytic efficiencies and enantioselectivities. Moreover, we established that the natural electron donor NADPH can be cost-effectively replaced by the synthetic cofactor BNAH.

EXPERIMENTAL

Chemicals and Enzymes

All chemicals and substrates used for buffers and biotransformations were purchased from Sigma-Aldrich (Steinheim, Germany), Carl Roth (Karlsruhe, Germany) and Merck Chemicals GmbH (Darmstadt, Germany) and of the purest grade available. Nicotinamide adenine dinucleotide phosphate (NADPH) was purchased from ProZomix (Northumberland, UK). 1-Benzyl-1,4-dihydronicotinamide (BNAH) was synthesized as described previously (Paul et al., 2013).

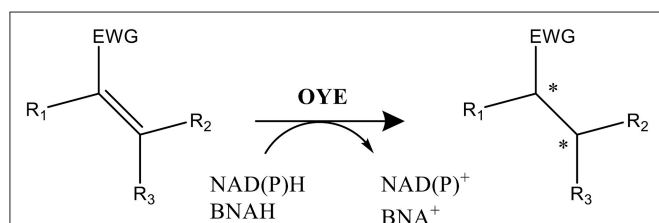
Site-Directed Mutagenesis, Expression, and Purification

All plasmids, primers and mutant megaprimers used in this study are presented in **Table 1**. Site directed mutagenesis of *oyeRo2a* was performed in two steps (**Scheme S1**, Supplementary Material).

(1) Synthesis of the mutant megaprimer by template mutation. Single-site mutated *oyeRo2a* genes were amplified by PCR from pET16bp_oyeRo2a DNA solution (100 ng μl^{-1}) applying the respective primers (**Table 1**). The received PCR products served as mutant megaprimers oyeRo2a-C25S, oyeRo2a-C25A and oyeRo2a-C25G. (2) Annealing of the mutated megaprimer (500 ng) and the original pET16bp_oyeRo2a vector (50 ng) using the GeneMorph[®] EzClone Reaction (Agilent Technologies) for a novel PCR reaction. Add-on DpnI digestion was applied in order to remove the *E. coli* template DNA. Resulting recombinant plasmids pSRoOYE2a_P02, pSRoOYE2a_P03 and pSRoOYE2a_P04 were transformed into *E. coli* BL21 (DE3) pLysS. Expression and purification of the protein variants was performed as described earlier for OYERo2a (Riedel et al., 2015).

Enzyme Activity and Kinetic Characterization

Specific activities of ERs were determined spectrophotometrically by following the consumption of NADPH or BNAH at 340 nm as described earlier (Riedel et al., 2015). However, the enzyme, buffer and substrate concentrations were slightly modified to achieve best performance. In a pre-screen it



SCHEME 1 | Reaction catalyzed by FMN-containing OYEs. NAD(P)H or BNAH serve as the electron donor and the substrate (α,β -unsaturated alkene) is activated by an electron withdrawing group (EWG; e.g., aldehyde, ketone, or nitro among others). Two potential stereo centers are indicated by an *.

TABLE 1 | Plasmids and primers used in this study.

Plasmids	Relevant characteristic(s)	Source
PLASMIDS		
pSRoOYE2a_P01	<i>oyeRo2a</i> of <i>R. opacus</i> 1CP (1.098-kb <i>NdeI</i> / <i>NotI</i> fragment) cloned into pET16bP	Riedel et al., 2015
pSRoOYE2a_P02	<i>oyeRo2a_C25S</i> of <i>R. opacus</i> 1CP (1.098-kb <i>NdeI</i> / <i>NotI</i> fragment) cloned into pET16bP	This study
pSRoOYE2a_P03	<i>oyeRo2a_C25A</i> of <i>R. opacus</i> 1CP (1.098-kb <i>NdeI</i> / <i>NotI</i> fragment) cloned into pET16bP	This study
pSRoOYE2a_P04	<i>oyeRo2a_C25G</i> of <i>R. opacus</i> 1CP (1.098-kb <i>NdeI</i> / <i>NotI</i> fragment) cloned into pET16bP	This study
PRIMER		
C25S_fw	5'-ATGGCTCCTATGTCTCAATACTCAGCAGATG-3'	This study
C25A_fw	5'-ATGGCTCCTATGGCTCAATACTCAGCAGATG-3'	This study
C25G_fw	5'-ATGGCTCCTATGGGTCAATACTCAGCAGATG-3'	This study
pET_check_rev	5'-CAGCTTCCTTTGGGCTTTGTTAG-3'	Qi et al., 2016
MEGAPRIMER		
<i>oyeRo2a_C25S</i>	<i>oyeRo2a</i> gene of <i>R. opacus</i> 1CP (1.098-kb fragment) containing the substitution guanine77→cysteine77	This study
<i>oyeRo2a_C25A</i>	<i>oyeRo2a</i> gene of <i>R. opacus</i> 1CP (1.098-kb fragment) containing the substitutions thymine76→guanine76 and guanine77→cysteine77	This study
<i>oyeRo2a_C25G</i>	<i>oyeRo2a</i> gene of <i>R. opacus</i> 1CP (1.098-kb fragment) containing the substitution thymine76→guanine76	This study

turned out that *N*-methylmaleimide served as best substrate to generate reproducible kinetics (data not shown) and thus it was used herein as the major substrate. The molar absorption coefficients $6.22 \text{ mM}^{-1}\text{cm}^{-1}$ and $4.75 \text{ mM}^{-1}\text{cm}^{-1}$ were used for NADPH and BNAH, respectively. Standard assays (1.0 mL) were performed at 25°C in 50 mM phosphate buffer ($\text{KH}_2\text{PO}_4/\text{Na}_2\text{HPO}_4$; pH 7.1) containing 180 μM NADPH and 1 mM of the respective substrate.

Steady-state kinetic parameters for the electron donor were determined using a fixed concentration of *N*-methylmaleimide (1 mM) and varying the concentration of NADPH or BNAH in a range from 0 to 350 μM . The reaction was started through the addition of enzyme in a final concentration of 36 nM. Steady-state kinetic parameters for the substrate were determined using a fixed concentration of NADPH (180 μM) and varying the concentration of *N*-methylmaleimide in a range from 0 to 350 μM or 2-cyclohexen-1-one in a range from 0 to 20 mM. The reaction was started through the addition of enzyme in a final concentration of 36–72 nM. All activity assays were performed in triplicates and the calculated mean values and respective standard deviation are given as results later.

Cofactor Analysis and Enzyme Stability

Flavin content of the Cys variants was determined spectrophotometrically from absorption scans (300–600 nm) as described earlier for OYERo2a (Riedel et al., 2015) using the molar absorption coefficient for free FMN ($\epsilon_{445} = 12.5 \text{ mM}^{-1}\text{cm}^{-1}$) (Whitby, 1953). Free flavin was obtained from incubating the protein sample (25 μM) for 20 min at 95°C either in the dark (closed water bath) or under exposure to light (open thermomixer), respectively. After a centrifugation step (20 min; $16,000 \times g$), a spectral analysis was performed on the supernatant.

Long-time stability of the proteins was investigated at 4°C in 50 mM $\text{KH}_2\text{PO}_4/\text{Na}_2\text{HPO}_4$ buffer (pH 7.1) using enzyme concentrations of 7–36 μM . Eppendorf tubes, containing the

enzyme solution, were kept either in the dark or under exposure to light. Specific activity was followed for 8 days at intervals of 24 h applying the standard assay with 1 mM *N*-methylmaleimide as the substrate.

Covalent Enzyme Modification and Determination of Cysteine Content

In order to monitor enzyme inactivation caused by maleimides for OYERo2a as well as mutant proteins, specific activity of untreated enzyme (0.3 mg mL^{-1}) was compared with that of enzyme pre-incubated for 120 min in 50 mM $\text{KH}_2\text{PO}_4/\text{Na}_2\text{HPO}_4$ buffer pH 7.1 at 4°C with 10 mM *N*-methylmaleimide. The specific activity was measured as described above using 1 mM *N*-methylmaleimide as a substrate and pre-incubated or untreated protein in a final concentration of 3 $\mu\text{g mL}^{-1}$.

The Ellman's test was used to quantify the cysteine residues (Ellman, 1959; Riener et al., 2002). The enzymes (2.2 mg mL^{-1}) were diluted 1:50 with the working solution (2.5 mM sodium acetate, 0.1 mM DTNB, 8 M urea, 50 mM phosphate buffer pH 7.5) and incubated for 3 min at 20°C. Extinctions were measured at 412 nm ($\epsilon_{412} = 14,150 \text{ M}^{-1}\text{cm}^{-1}$) (Riddles et al., 1979). To obtain a proper blank, OYERo2a and C25S variant (2.2 mg mL^{-1}) were pre-incubated with 5 mM *N*-methylmaleimide for 3 h to mask all cysteine residues and extinctions were measured as described above. The measured blank value (corrected for DTNB and for the FAD absorbance of the enzyme) was subtracted from the normal extinction. Cysteine concentration was calculated from the calibration $y = 73.942 x$, whereas y is the cysteine concentration in μM and x is the extinction. All assays (enzyme samples and blanks) were performed at least 3-times.

Biotransformation Reactions and Stereochemistry

Conversion of cyclic enones and maleimides was performed using 1.5-mL sealed glass vials containing the following components in a final volume of 1 mL: 25 mM

$\text{KH}_2\text{PO}_4/\text{Na}_2\text{HPO}_4$ buffer (pH 7.1), 10 mM substrate, 12 mM NADPH, and $2\text{ }\mu\text{M}$ enzyme. BNAH, used as a nicotinamide cofactor mimic, was dissolved in methanol and added in a final concentration of 16.7 mM. Reactions were performed for 4 h at 18°C in vials constantly shaken at 650 rpm in the dark. Extractions followed for 10 min with ethyl acetate (1:2) containing dodecane as an internal standard. Extracts were dried with MgSO_4 and stored at 7°C prior to gas chromatography (GC) and HPLC analyses.

Product concentrations were calculated based on calibration curve equations using 5 mM dodecane as an internal standard. Enantiomeric excess was measured via GC or HPLC with chiral columns. GC analyses were carried out on a Shimadzu GC-2010 gas chromatograph equipped with an FID on the assigned column (see **Table S1**). The calibration curves using 5 mM dodecane as an internal standard were linear in the range of product detection ($R^2 > 0.99$). Authentic samples were used to determine the absolute configuration of the product enantiomers. Specific column information, temperature programs and retention times are listed in the Supplemental Material (**Tables S1, S2**).

Structural Modeling

An amino acid sequence alignment based on previously published work (Scholtissek et al., 2017a) was used to generate a sub-alignment of class III OYEs. This served as a template for the subsequent modeling efforts. The following sequences with respective available structural data were used to generate dimeric homology models of OYERo2a and Cys variants including FMN in their oxidized forms: TOYE (OYE from *Thermoanaerobacter* sp.; pdb: 3KRZ; Adalbjörnsson et al., 2010), XenA (pdb: 3L5L; Spiegelhauer et al., 2010), and YqjM (ene reductase from *Bacillus subtilis*; pdb: 1Z41; Kitzing et al., 2005). For this, the following tools were employed: MEGA7-mac for the sequence alignment (Kumar et al., 2016), Modeler version 9.15 for comparative homology modeling, and PyMol V1.1r1 for

visualization (Sali and Blundell, 1993; Eswar et al., 2006; Riedel et al., 2015).

RESULTS

Structural Modeling of Active Site Wild-Type OYERo2a and Cys Variants

The OYERo2a structure was modeled as a dimer according to the template structures of TOYE (3KRZ; Adalbjörnsson et al., 2010), XenA (3L5L; Spiegelhauer et al., 2010), and YqjM (1Z41; Kitzing et al., 2005). This is in congruence with our previously made observations from structural modeling as well as from analytical gel filtration of OYERo2a (Riedel et al., 2015). The FMN cofactor was positioned into the active site by using the structure of YqjM (1Z41) as the building template (**Figure 1A**). A closer look into the active site of OYERo2a (**Figure 1B**) showed that all catalytically important amino acid residues are in a similar position as in the template structures (Scholtissek et al., 2017a). The class III conserved residue Arg364 points into the active site of the respective adjacent monomer. The mutations introduced at Cys25 did not change the model and thus the active site construction, which is in accordance with results obtained for XenA, where no structural perturbations were observed upon changing Cys25 (Spiegelhauer et al., 2010). However, it is clear that substitution of Cys with Ser at position 25 does nearly perfectly match the OYERo2a structure, while the substitutions with Ala or Gly yields a more open active site.

Cofactor Analysis and Stability

A protein-flavin ratio of 1:1 was obtained for all proteins (WT, C25S, C25A, and C25G), which is in analogy to our previous study on OYERo2 (Riedel et al., 2015). RP-HPLC analysis confirmed that the Cys variants contain FMN as prosthetic group. Protein-bound flavin showed two maxima at 370 and 460 nm and also a characteristic shoulder at around 485 nm

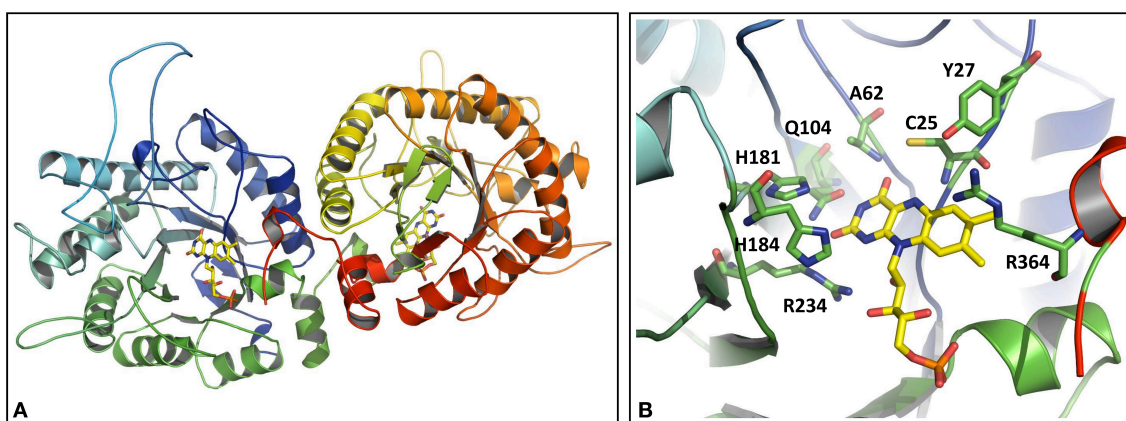


FIGURE 1 | Homology model of OYERo2a. **(A)** Three-dimensional model of the dimeric protein structure. The FMN prosthetic group is indicated in yellow. **(B)** Active site model. The side chains interacting with the flavin are shown in stick models (green) and colored by elements (red = oxygen-containing group; blue = nitrogen-containing group). The FMN cofactor is shown as stick model and colored by elements with carbons in yellow. Note that R364 belongs to the adjacent subunit. C25 is in hydrogen bonding distance to the O4-atom of the isoalloxazine ring of the flavin.

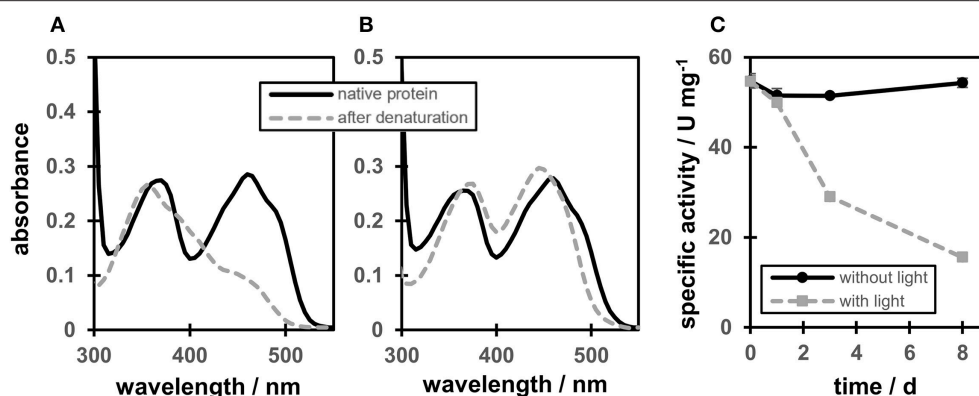


FIGURE 2 | Degradation of the flavin cofactor and stability of OYERo2a (WT). **(A)** OYERo2a (WT) before denaturation (black line) and free flavin after denaturation at 95°C for 20 min while protein was exposed to light. **(B)** OYERo2a (WT) before denaturation (black line) and after denaturation at 95°C for 20 min while stored in a dark water bath. **(C)** Specific activity of OYERo2a over a time interval of 8 days while stored at 4°C in 50 mM KH₂PO₄/Na₂HPO₄ buffer pH 7.1 in the dark (black line) or under exposure to light (gray line).

(Figures 2A,B, black lines). However, depending on the presence of a light source, the flavin cofactor revealed two different spectra after denaturation of the protein at 95°C. When protein denaturation was performed in a thermomixer under exposure to light, a maximum in absorption of the flavin was observed around 355 nm, while a strong decrease in absorption occurred around 450 nm (Figure 2A, gray line). Denaturation in the dark revealed the expected FMN cofactor with maxima at 374 and 446 nm (Figure 2B, gray line).

These observations are in congruence with long time protein stability tests. Incubating the WT protein at 4°C in 50 mM KH₂PO₄/Na₂HPO₄ buffer pH 7.1 in the dark and determination of the specific activity over a time interval of 8 days, showed no significant activity drop (Figure 2C, black line). However, under exposure to light, only 10% residual activity remained after the same time (Figure 2C, gray line). These observations are referred to a light-mediated photoreduction of the FMN cofactor as it was published before for Xena (Spiegelhauer et al., 2009, 2010). The previous study described photoreduction as a two-step mechanism ensuring single electron transfer. In a first step a red anionic flavin-semiquinone is formed, followed by the formation of a flavin-hydroquinone (Spiegelhauer et al., 2009). However, while Xena was completely reoxidized after exposure to air, OYERo2a and variants could not be regenerated. Instead, using RP-HPLC and as reference the ribityl side-chain lacking lumichrome (Holzer et al., 2005) revealed that under the conditions applied here, OYERo2 bound flavin is degraded to lumichrome.

Inactivation of WT by Covalent Binding of Maleimides

The amino acid sequence of OYERo2a comprises a single Cys residue at position 25 (Riedel et al., 2015). Quantitative determination of the cysteine residues applying Ellman's test confirmed that the WT enzyme contains one cysteine (ratio of mol cys per mol protein: 1.33 ± 0.14) whereas the Cys variants did

not possess any cysteine (C25A: 0.21 ± 0.02 ; C25G: 0.07 ± 0.15 ; C25S: 0.08 ± 0.09) (see Table S3 in Supplementary Material).

Interestingly, using maleimide as a substrate, the specific activity for the Cys variants was 192% (C25G), 191% (C25S), and 117% (C25A) of that of OYERo2a (Figure 3A). When the enzyme was incubated over 2 h in the dark, relative activity remained between 90 and 100% for each variant (Figure 3B). However, when the enzymes were pre-incubated with 10 mM *N*-methylmaleimide for 120 min, the activity of the Cys variants remained stable (80–100% relative activity), while the OYERo2a became almost completely inactivated (Figure 3C). This inactivation of the enzyme is a strong indication that Cys25 plays an important role in the binding of OYERo2a substrates.

Steady-State Kinetics Cofactor Preference

The activity of OYERo2a and Cys variants with the natural nicotinamide cofactor NADPH was compared with that of the synthetic nicotinamide cofactor BNAH using *N*-methylmaleimide as the fixed substrate (Figure 4). The OYERo2a and Cys variants followed Michaelis-Menten kinetics and respective kinetic parameters were determined. From Table 2 it can be noticed that OYERo2a has similar k_{cat} values for NADPH and BNAH. However, the Cys variants have much lower k_{cat} values with BNAH, while a remarkable increase is observed with NADPH. An exception represents C25G which has a high turnover frequency with both NADPH and BNAH. Nevertheless, the catalytic efficiencies (k_{cat}/K_m values) of OYERo2a and Cys variants with NADPH are in the same range. This is due to a lower K_m^{NADPH} value ($34.8 \mu\text{M}$) for OYERo2a compared to the variants ($55\text{--}121 \mu\text{M}$). For all four proteins the catalytic efficiency is higher when using NADPH. However, with OYERo2a the catalytic efficiency ratio between NADPH and BNAH is 2.5:1, while with each of the three variants the ratio is at least 10:1. Highest catalytic efficiency was shown for C25G using NADPH. To conclude, the Cys variants have a strong preference for NADPH over BNAH.

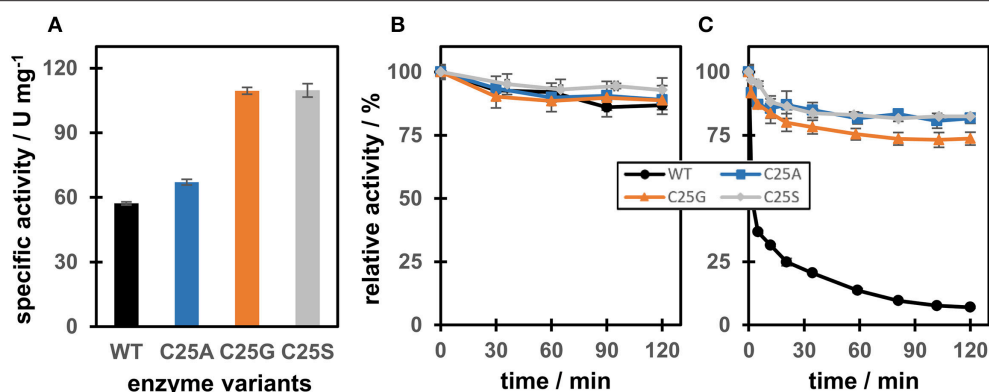


FIGURE 3 | Specific activity and time-dependent inactivation of OYERo2a WT and Cys variants with *N*-methylmaleimide. **(A)** Specific activities using *N*-methylmaleimide as a substrate. **(B)** Relative activity of WT and variants after incubation for 120 min in 50 mM KH₂PO₄/Na₂HPO₄ buffer pH 7.1 at 4°C (in the dark). Samples were taken at several time points to measure enzyme activity. **(C)** Relative activity of WT and variants after incubation for 120 min with 10 mM *N*-methylmaleimide in 50 mM KH₂PO₄/Na₂HPO₄ buffer pH 7.1 at 4°C (in the dark). Samples were taken at several time points to measure enzyme activity.

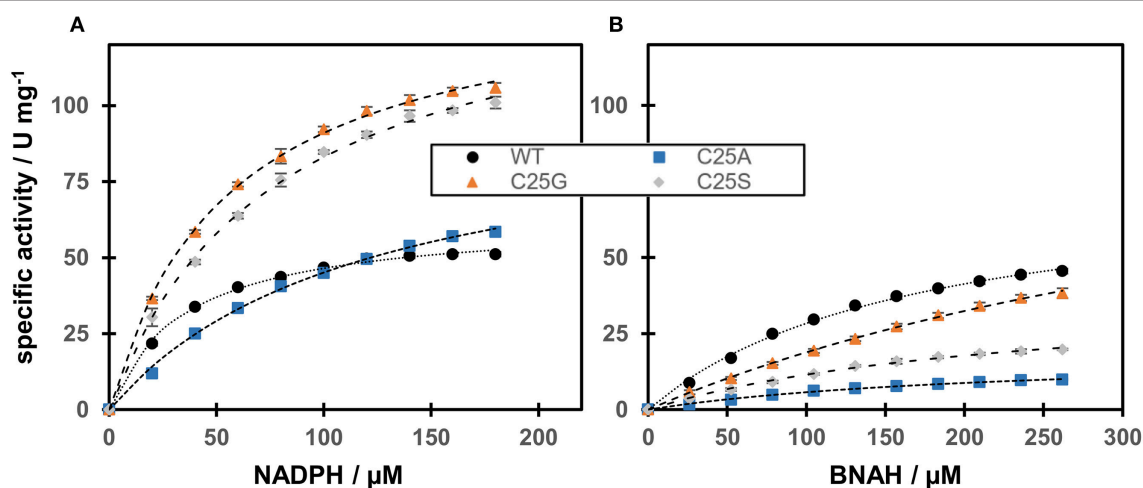


FIGURE 4 | Steady-state kinetics of OYERo2a (WT) and Cys variants regarding cofactor preference. The assay contained different amounts of nicotinamide cofactors NADPH **(A)** and BNAH **(B)**. The Michaelis-Menten model has been used to fit the data.

TABLE 2 | Steady-state kinetic parameters of OYERo2a (WT) and Cys variants regarding cofactor preference.

	WT		C25S		C25A		C25G	
	NADPH	BNAH	NADPH	BNAH	NADPH	BNAH	NADPH	BNAH
V_{\max} (U mg ⁻¹)	62.6 ± 1.0	76.3 ± 2.8	147.0 ± 3.2	38.9 ± 2.3	99.5 ± 3.7	18.9 ± 0.8	141.1 ± 2.1	116.4 ± 7.4
K_m (μM)	34.8 ± 2.0	169.0 ± 12.4	76.9 ± 4.1	238.7 ± 24.3	120.7 ± 8.7	230.2 ± 17.8	55.2 ± 2.3	516.9 ± 45.0
k_{cat} (s ⁻¹)	44.6 ± 0.7	54.3 ± 2.0	104.6 ± 2.3	27.7 ± 1.6	70.8 ± 2.6	13.4 ± 0.6	100.4 ± 1.5	82.8 ± 5.3
k_{cat}/K_m (μM ⁻¹ s ⁻¹)	1.28	0.32	1.36	0.12	0.59	0.06	1.82	0.16

Assays were performed in triplicates. Data (mean values and standard deviation) were analyzed by means of Kaleidagraph (Synergy Software). The given values are calculated from the fits of Michaelis-Menten kinetics following either NADPH or BNAH consumption according to **Figure 4**. The standard error derived of the best fit is provided.

Substrate Dependence

The catalytic efficiency of WT and Cys variants with *N*-methylmaleimide and 2-cyclohexen-1-one as substrates was studied using NADPH as the fixed co-substrate (**Figure 5**).

Regarding *N*-methylmaleimide, the apparent k_{cat} of WT is comparable with the turnover frequency of C25A (**Figure 5A**). Both these enzymes share a low K_m (around 10 μM), resulting in a high catalytic efficiency in the range of 4600–5700 mM⁻¹ s⁻¹.

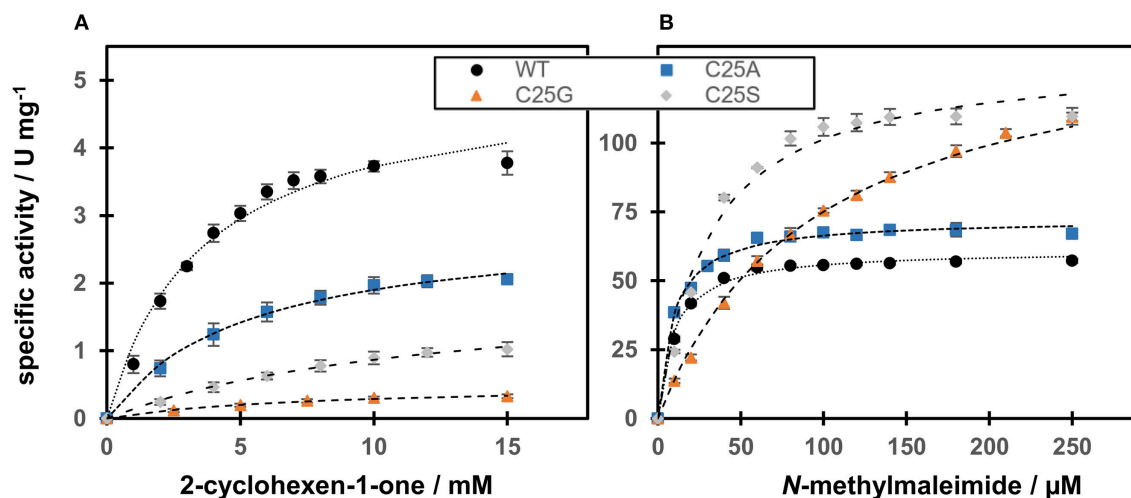


FIGURE 5 | Steady-state kinetics of OYERo2a WT and Cys variants regarding substrate dependence. The assay contained excess NADPH and different amounts of the substrates **(A)** 2-cyclohexen-1-one or **(B)** *N*-methylmaleimide. The Michaelis-Menten model has been used to fit the data.

(Table 3). Compared to WT and C25A, C25S has a doubled k_{cat} with *N*-methylmaleimide but a tripled K_m (30 μ M) resulting in a lower catalytic efficiency (Table 3). C25G shows the highest K_m for *N*-methylmaleimide, and therefore a catalytic efficiency 4 times lower than that of WT (Table 3).

With respect to 2-cyclohexen-1-one, WT showed the highest catalytic efficiency (Figure 5B). However, compared to *N*-methylmaleimide the catalytic efficiencies of all four proteins are reduced by a factor of 400 (WT) to 2500 (C25S) (Table 3). This is due to 70–520 times increase of the Michaelis constant and a 10–340 times decrease of the turnover frequency.

Biocatalysis Applying NADPH and BNAH as Electron Donors

Regarding conversion rates and enantioselectivities, 2-methyl-*N*-phenylmaleimide **1** as well as *R*- and *S*-carvones (**6** and **7**) are preferred substrates for all four enzymes (Table 4). Especially maleimide-like substrates seem to be favored in terms of kinetics (Table 3) since they show a higher specific activity and efficient coupling of NADPH-consumption with ene reduction. Application of NADPH or BNAH (done for **1** and **2**) showed no significant differences, neither in conversion nor in stereochemistry. Comparing WT with the three protein variants brought no significant differences for substrate **1**. For ketosiphorone **5** and 2-methyl-cyclopentenone **3**, WT enzyme and C25A variant generally performed best. C25G variant showed very low conversions on all substrates, except of 2-methyl-*N*-phenylmaleimide **1**. Because C25G is highly active with *N*-methylmaleimide, but poorly active with cyclic ketones, it appears that residue 25 is critical for determining the substrate specificity of OYERo2 catalysis. This effect was shown with C25G variants of *Rm*OYE and *Ts*OYE where lower conversions were found for *R*-carvone with respect to WT (Nett et al., 2017).

TABLE 3 | Steady-state kinetic parameters of OYERo2a WT and Cys variants regarding substrate dependence.

	WT	C25S	C25A	C25G
N-METHYLMALEIMIDE				
V_{max} (U mg ⁻¹)	61.0	132.2	72.3	145.9
K_m (μ M)	9.6	30.4	9.1	94.4
k_{cat} (s ⁻¹)	42.3	91.7	50.1	101.2
k_{cat}/K_m (μ M ⁻¹ s ⁻¹)	4.4	3.0	5.5	1.1
coupling efficiency (%) [*]	97.4	89.9	72.7	100.0
2-CYCLOHEXEN-1-ONE				
V_{max} (U mg ⁻¹)	5.0	1.6	2.9	0.5
K_m (mM)	3.5	8.9	5.2	6.2
k_{cat} (s ⁻¹)	3.5	1.1	2.0	0.3
k_{cat}/K_m (mM ⁻¹ s ⁻¹)	1.0	0.12	0.38	0.05

The values are calculated from the fits of Michaelis-Menten kinetics according to Figure 5. All assays were performed in triplicates and the values have a maximal error of 10% (standard deviation).

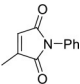
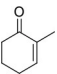
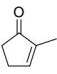
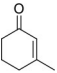
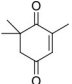
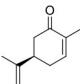
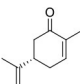
^{*}The coupling efficiency (percentage of alkene reduced per NADPH consumed) is calculated from the NADPH-oxidation (see Table 2) and *N*-methylmaleimide-reducing activity.

DISCUSSION

An *N*-terminal cysteine residue was found to function in the binding of the FMN cofactor of class III OYEs thereby modulating the flavin reduction potential (Spiegelhauer et al., 2010). Additionally, cysteine residues are known for Michael addition reactions with maleimides, forming thioethers (Gregory, 1955). To study its role in further detail, the cysteine residue of OYERo2a was replaced by alanine (A), glycine (G) or serine (S) through site-directed mutagenesis.

Structural modeling of OYERo2a indicated that the replacement of Cys25 is not inducing a general structural

TABLE 4 | Conversion and stereochemistry of OYERo2a (WT) and Cys variants with α,β -unsaturated alkenes.

Substrate	WT		C25S		C25A		C25G	
	Conversion [%]	ee (%)	Conversion [%]	ee (%)	Conversion [%]	ee (%)	Conversion [%]	ee (%)
1 	72/84 (NADPH/BNAH)	>99/>99 (<i>R</i>)	71/81	>99/>99 (<i>R</i>)	65/60	>99/>99 (<i>R</i>)	87/81	>99/>99 (<i>R</i>)
2 	64/49 (NADPH/BNAH)	>99/99 (<i>R</i>)	27/17	>99/99 (<i>R</i>)	n.d./27	n.d./95 (<i>R</i>)	n.d./1	n.a.
3 	19	>99 (<i>S</i>)	4	>99 (<i>S</i>)	30	91 (<i>S</i>)	<1	n.a.
4 	<1	n.a.	<1	n.a.	n.d.	n.d.	n.d.	n.d.
5 	26	93 (<i>R</i>)	2	82 (<i>R</i>)	34	65 (<i>R</i>)	1	71 (<i>R</i>)
6 	89	>99 (<i>R</i>)	70	>99 (<i>R</i>)	77	>99 (<i>R</i>)	6	>99 (<i>R</i>)
7 	78	96 (<i>R</i>)	30	93 (<i>R</i>)	n.d.	n.d.	n.d.	n.d.

n.d. not determined; n.a. not accessible due to low conversion or lack of a chiral center; value < 1 = no observable peak detected. All assays were performed in triplicates and the standard deviation was less than 5% regarding the conversions.

rearrangement of the active pocket. However, while Ser isosterically replaces the Cys, more space is created when Ala or Gly is inserted. These three variants (C25 substitutions) were successfully generated and confirmed by gene sequencing as well as by the Ellman's test. The substitutions of Cys25 increased the initial rates with *N*-methylmaleimide, but gave rise to somewhat higher K_m values for C25S and C25G. As a result, catalytic efficiencies decreased by about 32% (C25S) and 75% (C25G), respectively. Due to a comparable Michaelis constant and a slightly increased turnover frequency, replacement with alanine gave a catalytic efficiency increase of about 25%. However, it seems that the cysteine plays an important role for catalysis of the substrate 2-cyclohexen-1-one leading to the hypothesis that 2-cyclohexen-1-one is structurally closely related to the natural substrate of class III OYEs. The results with 2-cyclohexen-1-one suggest that Cys25 is important for substrate coordination and positioning properly with respect to the FMN cofactor since this residue is an essential part of the substrate binding pocket interacting not only with the O4-atom of the FMN cofactor but also with Tyr27 (Kitzing et al., 2005; Spiegelhauer et al., 2010).

In contrast to the WT enzyme, the variants C25A, C25G, and C25S did not show a time-dependent inactivation with *N*-methylmaleimide in the oxidized resting state (Figure 3). The covalent modification reaction with this maleimide was

completely prevented when Ser/Ala/Gly protein variants were applied. Because this property is of benefit for biocatalytic applications, we addressed the catalytic performance of the OYERo2a Cys variants. It appeared that, under the conditions applied, the active site cysteine is not affecting the degree of conversion of *N*-phenyl-2-methylmaleimide. For conversion of 2-cyclohexen-1-one, the cysteine is required. For all other cyclic ketones tested, the WT is also favored, since conversion yield and enantioselectivity is better in most cases.

Besides ene-reducing activity, also the cofactor-dependent FMN reduction needs to be discussed for WT and Cys variants. The following observations can be summarized from this study. WT does most efficiently bind NADPH as well as BNAH, but the variants show an increased turnover frequency only with NADPH. Thus more flexibility of the protein structure might yield a higher turnover frequency for the initial reductant (here NADPH) but this not necessarily leads to a higher ene-reductase activity (Table 3). Only in case of *N*-methylmaleimide a highly efficient transfer of electrons was achieved, which is expressed as coupling efficiency. Therefore, it can be reasoned that the mutual orientation of both cofactor and substrate with respect to the flavin influence the overall catalysis as it was discussed above (Kitzing et al., 2005; Spiegelhauer et al., 2010). With respect to NADPH/BNAH turnover the C25G variant was most

efficient and in combination with above mentioned catalytic properties it may be a valuable starting point to further evolve succinimide producing biocatalysts. Especially, this variant showed the highest conversion rates of the pro-chiral *N*-phenyl-2-methylmaleimide at highest enantiomeric excess (Table 4). Further, the BNAH cofactor mimic can replace effectively NADPH in this biotransformation.

Regarding cofactor choice, catalytic efficiency with BNAH is lower in all cases compared to NADPH. Despite that, BNAH seems a reasonable alternative electron donor for OYERo2a biotransformations since it has no inhibitory effects and compared to the natural cofactor NADPH it is more economical (Paul et al., 2013, 2014).

So far, we did not study the operational stability of the enzyme (incubations with gram amounts of substrate and a cofactor-regenerating system, using an immobilized form of the enzyme). We only looked at the inactivation of the oxidized enzyme (the resting state). Nevertheless, this study is a valuable indication to make use of the Cys variants when upscaling the reaction for maleimides for industrial purposes.

CONCLUSION

An *N*-terminal cysteine residue, occurring only in class III OYEs, was found to be involved in the catalytic functioning of OYERo2a. We show that the substrate *N*-methylmaleimide inactivates OYERo2a through covalent modification. The cysteine-lacking variants C25S and C25G are not inactivated by *N*-methylmaleimide and show high specific activities with this substrate (up to 147 U mg⁻¹) using NADPH as a cofactor.

Interestingly, the choice of cofactor seems to play a major role in OYERo2a catalysis. More precisely, an efficient catalysis was observed for OYERo2a with the cofactor mimic BNAH and *N*-methylmaleimide as the pyrrole-dione substrate.

REFERENCES

- Adalbjörnsson, B. V., Toogood, H. S., Fryszkowska, A., Pudney, C. R., Jowitt, T. A., Leys, D., et al. (2010). Biocatalysis with thermostable enzymes: structure and properties of a thermophilic ene-reductase related to old yellow enzyme. *Chembiochem* 11, 197–207. doi: 10.1002/cbic.200900570
- Amato, E. D., and Stewart, J. D. (2015). Applications of protein engineering to members of the old yellow enzyme family. *Biotechnol. Adv.* 33, 624–631. doi: 10.1016/j.biotechadv.2015.04.011
- Balke, K., Beier, A., and Bornscheuer, U. T. (2017). Hot spots for the protein engineering of Baeyer-Villiger monooxygenases. *Biotechnol. Adv.* 36, 247–263. doi: 10.1016/j.biotechadv.2017.11.007
- Ellman, G. L. (1959). Tissue sulfhydryl groups. *Arch. Biochem. Biophys.* 82, 70–77. doi: 10.1016/0003-9861(59)90090-6
- Eswar, N., Webb, B., Marti-Renom, M. A., Madhusudhan, M. S., Eramian, D., Shen, M. Y., et al. (2006). Comparative protein structure modeling using Modeller. *Curr. Protoc. Bioinformatics* Chapter 5:Unit-5.6. doi: 10.1002/0471250953.bi0506s15
- Fox, K. M., and Karplus, P. A. (1994). Old yellow enzyme at 2 Å resolution: overall structure, ligand binding, and comparison with related flavoproteins. *Structure* 2, 1089–1105. doi: 10.1016/S0969-2126(94)00111-1
- Fryszkowska, A., Toogood, H., Sakuma, M., Gardiner, J. M., Stephens, G. M., and Scrutton, N. S. (2009). Asymmetric reduction of activated alkenes by pentaerythritol tetranitrate reductase: specificity and control of stereochemical

AUTHOR CONTRIBUTIONS

AS carried out the cloning and site-directed mutagenesis. Spectral analysis, kinetic characterization (data acquisition and analysis), stability analysis and inhibition studies were established and carried out by EG, AW, and AS. Substrate specificity, product analysis and stereochemistry was carried out by EG and CP. DT carried out the structural modeling. AS, CP, AW, WB, and DT drafted the manuscript, which was critically revised by all authors. All authors read and approved the final manuscript.

FUNDING

This project was supported by the European Social Fund (ESF) and the Saxonian Government (GETGEOWEB: 100101363). We acknowledge support by the DFG Open Access Publication Funds of the Ruhr-Universität Bochum.

ACKNOWLEDGMENTS

We thank Mr. Ringo Schwabe for development of the mutagenesis strategy by combination of the synthesis of the mutant megaprimer and application of this primer to the GeneMorph® EzClone Reaction kit (Agilent Technologies). We thank Mr. Arne Scholtissek for his support on the mathematical equations regarding inhibition kinetics as well as preparing the kinetic plots. Part of the content of this manuscript has been published in the Ph.D. thesis of Dr. AS (Scholtissek, 2017c).

SUPPLEMENTARY MATERIAL

The Supplementary Material for this article can be found online at: <https://www.frontiersin.org/articles/10.3389/fmicb.2018.02410/full#supplementary-material>

outcome by reaction optimisation. *Adv. Synth. Catal.* 351, 2976–2990. doi: 10.1002/adsc.200900574

- Fu, Y., Castiglione, K., and Weuster-Botz, D. (2013). Comparative characterization of novel ene-reductases from cyanobacteria. *Biotechnol. Bioeng.* 110, 1293–1301. doi: 10.1002/bit.24817
- Gao, X., Ren, J., Wu, Q., and Zhu, D. (2012). Biochemical characterization and substrate profiling of a new NADH-dependent enoate reductase from *Lactobacillus casei*. *Enzyme Microb. Technol.* 51, 26–34. doi: 10.1016/j.enzmictec.2012.03.009
- Gregory, J. D. (1955). The stability of *N*-ethylmaleimide and its reaction with sulfhydryl groups. *J. Am. Chem. Soc.* 77, 3922–3923. doi: 10.1021/ja01619a073
- Holzer, W., Shirdel, J., Zirak, P., Penzkofer, A., Hegemann, P., Deutzmann, R., et al. (2005). Photo-induced degradation of some flavins in aqueous solution. *Chem. Phys.* 308, 69–78. doi: 10.1016/j.chemphys.2004.08.006
- Kitzing, K., Fitzpatrick, T. B., Wilken, C., Sawa, J., Bourenkov, G. P., Macheroux, P., et al. (2005). The 1.3 Å crystal structure of the flavoprotein YqjM reveals a novel class of old yellow enzymes. *J. Biol. Chem.* 280, 27904–27913. doi: 10.1074/jbc.M502587200
- Knaus, T., Paul, C. E., Levy, C. W., de Vries, S., Mutti, F. G., Hollmann, F., et al. (2016). Better than nature: nicotinamide biomimetics that outperform natural coenzymes. *J. Am. Chem. Soc.* 138, 1033–1039. doi: 10.1021/jacs.5b12252
- Kohli, R. M., and Massey, V. (1998). The oxidative half-reaction of old yellow enzyme. the role of tyrosine 196. *J. Biol. Chem.* 273, 32763–32770. doi: 10.1074/jbc.273.49.32763

- Kumar, S., Stecher, G., and Tamura, K. (2016). MEGA7: molecular evolutionary genetics analysis version 7.0 for bigger datasets. *Mol. Biol. Evol.* 33, 1870–1874. doi: 10.1093/molbev/msw054
- Nett, N., Duewel, S., Richter, A. A., and Hoebeinreich, S. (2017). Revealing additional stereocomplementary pairs of old yellow enzymes by rational transfer of engineered residues. *ChemBiochemistry* 18, 685–691. doi: 10.1002/cbic.201600688
- Nivinskas, H., Sarlauskas, J., Anusevicius, Z., Toogood, H. S., Scrutton, N. S., and Cenas, N. (2008). Reduction of aliphatic nitroesters and N-nitramines by *Enterobacter cloacae* PB2 pentaerythritol tetranitrate reductase: quantitative structure-activity relationships. *FEBS J.* 275, 6192–6203. doi: 10.1111/j.1742-4658.2008.06744.x
- Padhi, S. K., Bougioukou, D. J., and Stewart, J. D. (2009). Site-saturation mutagenesis of tryptophan 116 of *Saccharomyces pastorianus* old yellow enzyme uncovers stereocomplementary variants. *J. Am. Chem. Soc.* 131, 3271–3280. doi: 10.1021/ja8081389
- Paul, C. E., Arends, I. W. C. E., and Hollmann, F. (2014). Is simpler better? synthetic nicotinamide cofactor analogues for redox chemistry. *ACS Catal.* 4, 788–797. doi: 10.1021/cs4011056
- Paul, C. E., Gargiulo, S., Opperman, D. J., Lavandera, I., Gotor-Fernández, V., Gotor, V., et al. (2013). Mimicking nature: synthetic nicotinamide cofactors for C-C bioreduction using enoate reductases. *Org. Lett.* 15, 180–183. doi: 10.1021/ol303240a
- Pompeu, Y. A., Sullivan, B., and Stewart, J. D. (2013). X-ray crystallography reveals how subtle changes control the orientation of substrate binding in an alkene reductase. *ACS Catal.* 3, 2376–2390. doi: 10.1021/cs400622e
- Qi, J., Schlömann, M., and Tischler, D. (2016). Biochemical characterization of an azoreductase from *Rhodococcus opacus* 1CP possessing methyl red degradation ability. *J. Mol. Catal. B Enzym.* 130, 9–17. doi: 10.1016/j.molcatb.2016.04.012
- Riddles, P. W., Blakeley, R. L., and Zerner, B. (1979). Ellman's reagent: 5,5'-dithiobis(2-nitrobenzoic acid)—a reexamination. *Anal. Biochem.* 94, 75–81.
- Riedel, A., Mehnert, M., Paul, C. E., Westphal, A. H., van Berkel, W. J. H., and Tischler, D. (2015). Functional characterization and stability improvement of a thermophilic-like ene-reductase from *Rhodococcus opacus* 1CP. *Front. Microbiol.* 6:1073. doi: 10.3389/fmicb.2015.01073
- Riener, C. K., Kada, G., and Gruber, H. J. (2002). Quick measurement of protein sulfhydryls with Ellman's reagent and with 4,4'-dithiodipyridine. *Anal. Bioanal. Chem.* 373, 266–276. doi: 10.1007/s00216-002-1347-2
- Saito, K., Thiele, D. J., Davio, M., Lockridge, O., and Massey, V. (1991). The cloning and expression of a gene encoding Old yellow enzyme from *Saccharomyces carlsbergensis*. *J. Biol. Chem.* 266, 20720–20724.
- Sali, A., and Blundell, T. L. (1993). Comparative protein modelling by satisfaction of spatial restraints. *J. Mol. Biol.* 234, 779–815. doi: 10.1006/jmbi.1993.1626
- Scholtissek, A. (2017c). *Classification and Characterization of Novel 'Yellow Enzymes' For Biocatalysis*. Dissertation, Freiberg: Technical University Bergakademie Freiberg.
- Scholtissek, A., Tischler, D., Westphal, A., van Berkel, W., and Paul, C. (2017a). Old yellow enzyme-catalysed asymmetric hydrogenation: linking family roots with improved catalysis. *Catalysts* 7:130. doi: 10.3390/catal7050130
- Scholtissek, A., Ullrich, S. R., Mühling, M., Schlömann, M., Paul, C. E., and Tischler, D. (2017b). A thermophilic-like ene-reductase originating from an acidophilic iron oxidizer. *Appl. Microbiol. Biotechnol.* 101, 609–619. doi: 10.1007/s00253-016-7782-3
- Spiegelhauer, O., Dickert, F., Mende, S., Niks, D., Hille, R., Ullmann, M., et al. (2009). Kinetic characterization of xenobiotic reductase A from *Pseudomonas putida* 86. *Biochemistry* 48, 11412–11420. doi: 10.1021/bi901370u
- Spiegelhauer, O., Mende, S., Dickert, F., Knauer, S. H., Ullmann, G. M., and Dobbek, H. (2010). Cysteine as a modulator residue in the active site of xenobiotic reductase A: a structural, thermodynamic and kinetic study. *J. Mol. Biol.* 398, 66–82. doi: 10.1016/j.jmb.2010.02.044
- Swiderska, M. A., and Stewart, J. D. (2006a). Asymmetric bioreductions of beta-nitro acrylates as a route to chiral beta2-amino acids. *Org. Lett.* 8, 6131–6133. doi: 10.1021/ol062612f
- Swiderska, M. A., and Stewart, J. D. (2006b). Stereoselective enone reductions by *Saccharomyces carlsbergensis* old yellow enzyme. *J. Mol. Catal. B Enzym.* 42, 52–54. doi: 10.1016/j.molcatb.2006.06.023
- Toogood, H. S., Fryszkowska, A., Hare, V., Fisher, K., Roujeinikova, A., Leys, D., et al. (2008). Structure-based insight into the asymmetric bioreduction of the C=C double bond of α,β -unsaturated nitroalkenes by pentaerythritol tetranitrate reductase. *Adv. Synth. Catal.* 350, 2789–2803. doi: 10.1002/adsc.200800561
- Toogood, H. S., and Scrutton, N. S. (2018). Discovery, characterization, engineering, and applications of ene-reductases for industrial biocatalysis. *ACS Catal.* 8, 3532–3549. doi: 10.1021/acscatal.8b00624
- van Den Heuvel, R. H., Fraaije, M. W., Ferrer, M., Mattevi, A., and van Berkel, W. J. (2000). Inversion of stereospecificity of vanillyl-alcohol oxidase. *Proc. Natl. Acad. Sci. U.S.A.* 97, 9455–9460. doi: 10.1073/pnas.160175897
- Walton, A. Z., Sullivan, B., Patterson-Orazem, A. C., and Stewart, J. D. (2014). Residues controlling facial selectivity in an alkene reductase and semirational alterations to create stereocomplementary variants. *ACS Catal.* 4, 2307–2318. doi: 10.1021/cs500429k
- Whitby, L. G. (1953). A new method for preparing flavin-adenine dinucleotide. *Biochem. J.* 54, 437–442.
- Xu, D., Kohli, R. M., and Massey, V. (1999). The role of threonine 37 in flavin reactivity of the old yellow enzyme. *Proc. Natl. Acad. Sci. U.S.A.* 96, 3556–3561. doi: 10.1073/pnas.96.7.3556

Conflict of Interest Statement: The authors declare that the research was conducted in the absence of any commercial or financial relationships that could be construed as a potential conflict of interest.

Copyright © 2018 Scholtissek, Gädke, Paul, Westphal, van Berkel and Tischler. This is an open-access article distributed under the terms of the Creative Commons Attribution License (CC BY). The use, distribution or reproduction in other forums is permitted, provided the original author(s) and the copyright owner(s) are credited and that the original publication in this journal is cited, in accordance with accepted academic practice. No use, distribution or reproduction is permitted which does not comply with these terms.



Development of a Novel *Escherichia coli*–*Kocuria* Shuttle Vector Using the Cryptic pKPAL3 Plasmid from *K. palustris* IPUFS-1 and Its Utilization in Producing Enantiopure (S)-Styrene Oxide

Hiroshi Toda and Nobuya Itoh*

Department of Biotechnology, Biotechnology Research Center, Toyama Prefectural University, Imizu, Japan

OPEN ACCESS

Edited by:

Dirk Tischler,
Freiburg University of Mining
and Technology, Germany

Reviewed by:

Toru Matsui,
University of the Ryukyus, Japan
Pablo Ivan Nikel,
The Novo Nordisk Foundation Center
for Biosustainability (DTU Biosustain),
Denmark

*Correspondence:

Nobuya Itoh
nbito@pu-toyama.ac.jp;
itohnobuya123@gmail.com

Specialty section:

This article was submitted to
Microbial Physiology and Metabolism,
a section of the journal
Frontiers in Microbiology

Received: 02 September 2017

Accepted: 09 November 2017

Published: 27 November 2017

Citation:

Toda H and Itoh N (2017)
Development of a Novel *Escherichia coli*–*Kocuria* Shuttle Vector Using
the Cryptic pKPAL3 Plasmid from
K. palustris IPUFS-1 and Its Utilization
in Producing Enantiopure (S)-Styrene
Oxide. *Front. Microbiol.* 8:2313.
doi: 10.3389/fmicb.2017.02313

The novel cryptic pKPAL3 plasmid was isolated from the Gram-positive microorganism *Kocuria palustris* IPUFS-1 and characterized in detail. pKPAL3 is a circular plasmid that is 4,443 bp in length. Open reading frame (ORF) and homology search analyses indicated that pKPAL3 possesses four ORFs; however, there were no replication protein coding genes predicted in the plasmid. Instead, there were two nucleotide sequence regions that showed significant identities with untranslated regions of *K. rhizophila* DC2201 (NBRC 103217) genomic sequences, and these sequences were essential for autonomous replication of pKPAL3 in *Kocuria* cells. Based on these findings, we constructed the novel *Escherichia coli*–*Kocuria* shuttle vectors pKITE301 (kanamycin resistant) and pKITE303 (thiostrepton resistant) from pKPAL3. The copy numbers of the constructed shuttle vectors were estimated to be 20 per cell, and they exhibited low segregation stability in *Kocuria* transformant cells in the absence of antibiotics. Moreover, constructed vectors showed compatibility with the other *K. rhizophila* shuttle vector pKITE103. We successfully expressed multiple heterologous genes, including the styrene monooxygenase gene from *Rhodococcus* sp. ST-10 (*rhsmo*) and alcohol dehydrogenase gene from *Leifsonia* sp. S749 (*lsadh*), in *K. rhizophila* DC2201 using the pKITE301P and pKITE103P vectors under the control of the glyceraldehyde 3-phosphate dehydrogenase (*gapdh*) promoter. The RhSMO–LSADH co-expressing *K. rhizophila* was used as a biocatalyst in an organic solvent–water biphasic reaction system to efficiently convert styrene into (S)-styrene oxide with 99% ee in the presence of 2-propanol as a hydrogen donor. The product concentration of the reaction in the organic solvent reached 235 mM after 30 h under optimum conditions. Thus, we demonstrated that this novel shuttle vector is useful for developing biocatalysts based on organic solvent-tolerant *Kocuria* cells.

Keywords: *Kocuria rhizophila*, *Kocuria palustris*, styrene monooxygenase, styrene oxide, biphasic reaction system, organic solvent-tolerant biocatalyst

INTRODUCTION

Enantiopure epoxides are useful building blocks for synthesizing various chiral materials, including pharmaceuticals, agrochemicals, and fine chemicals (Farina et al., 2006; Patel, 2008). Direct enantioselective epoxidation of prochiral alkenes is a straightforward strategy for producing chiral epoxides, and many chemical approaches have been developed to achieve this objective (Shi, 2004). Sharpless epoxidation is an efficient procedure for oxidizing allylic alcohols using a titanium/tartrate/*tert*-butyl hydroperoxide system to yield corresponding chiral epoxides. Many chemical catalysts that contain transition metals, such as metal-salen complexes and chiral metalloporphyrins, have been developed for the enantioselective epoxidation of alkenes (Katsuki and Sharpless, 1980; Hanson and Sharpless, 1986; Irie et al., 1991; Chang et al., 1994; Tu et al., 1996). Furthermore, the biological synthesis of epoxides using monooxygenases has also been studied (Panke et al., 1998; Martinez and Stewart, 2000; Hollmann et al., 2003; Farinas et al., 2004; Champreda et al., 2006). Biological synthesis of epoxides has several advantages over chemical synthesis, including superior chemoselectivity, regioselectivity, and enantioselectivity, as well as improved environmental sustainability.

The genomes of several styrene-degrading microorganisms contain styrene monooxygenase (SMO) genes, which are involved in the first step of styrene degradation and allow them to catalyze the epoxidation of styrene to enantiopure (*S*)-styrene oxide (Hartmans et al., 1990; Beltrametti et al., 1997; Panke et al., 1998). SMOs consist of two enzymes: flavin adenine dinucleotide (FAD)-dependent monooxygenase (StyA) and NAD(H)-dependent flavin oxidoreductase (StyB). SMOs convert styrene to (*S*)-styrene oxide with high enantioselectivity using NADH as an electron donor (Panke et al., 1999; Hollmann et al., 2003). Many SMOs are well characterized, and their enzymatic properties and substrate specificities have been investigated (Marconi et al., 1996; Panke et al., 1998; Velasco et al., 1998; Lin et al., 2010; Tischler et al., 2012). We have also reported the isolation and characterization of SMO genes from *Rhodococcus* sp. ST-10 (RhSMO; Toda and Itoh, 2012; Toda et al., 2012a) and the development of biocatalysis reactions for producing enantiopure epoxides from various aryl- and aliphatic alkenes using RhSMO (Toda et al., 2012b, 2014).

Escherichia coli is the microorganism most frequently used as biocatalyst host cells owing to its ease of use and abundant molecular tools for genetic manipulation. However, *E. coli* cells are unsuitable for long-term biocatalysis reactions using organic solvents and toxic compounds because they are easily inactivated by these substances. To overcome this problem, organic solvent-tolerant microorganisms, especially *Pseudomonas putida*, have been assessed as host cells for biocatalysis (Heipieper et al., 2007; Park et al., 2007; Verhoef et al., 2009; Siriphongphaew et al., 2012; Nikel et al., 2014). Recently, we also reported the construction of a biocatalysis system possessing RhSMO that uses the organic

solvent-tolerant microorganism *K. rhizophila* DC2201 as a host cell and demonstrated the bioproduction of various enantiopure (*S*)-epoxyalkanes in an organic solvent–water biphasic reaction (Toda et al., 2015). *K. rhizophila* DC2201 is a Gram-positive microorganism belonging to the family *Micrococcaceae* in the order *Actinomycetales*, and its whole genomic DNA sequence was previously determined (Takarada et al., 2008). This microorganism has several advantages for utilization as a biocatalysis host cell, including its organic solvent tolerance, high halotolerance, robust cell structure, and small genome size. Furthermore, it was reported that several *Kocuria* species produce important natural pigments, including astaxanthin and β -carotene, which are widely used as food additives and health supplements (Goodwin, 1980; Porter and Spurgeon, 1981; Dufosse, 2006). It is expected that development of genetic modification tools for these bacteria may contribute to the efficient production of various useful materials such as pharmaceutical and functional food components.

Thus, *Kocuria* species are expected to be useful host cells for biocatalysis. However, only a few genetic tools are available for *Kocuria* cells (Matsumura et al., 2012; Ohta et al., 2014) and little is known about gene transcription, protein expression, and metabolite flux in *Kocuria* cells. Such tools and information are important for increasing the potential uses of host cells by controlling recombinant protein expression and modification of the metabolite pathways of host cells. Therefore, we aimed to both construct genetic tools for use in the genus *Kocuria* and apply them to a biocatalysis system for producing a wide variety of organic compounds.

In our previous study, we reported the isolation and characterization of the two cryptic plasmids pKPAL1 and pKPAL2 from *K. palustris* IPUFS-1 and the construction of the *E. coli*-*Kocuria* shuttle vector pKITE101 series based on pKPAL1 (Toda et al., 2017). These plasmids were inferred to be theta-replicating plasmids with copy numbers of 60 per chromosome in *Kocuria* cells. The constructed shuttle vector was stably maintained in *K. rhizophila* DC2201 cells, and it was available for heterologous gene expression under control of the *gapdh* promoter.

In this study, we isolated and characterized pKPAL3, another novel cryptic plasmid from *K. palustris* IPUFS-1. The whole nucleotide sequence of pKPAL3 was determined, and four putative open reading frames (ORFs) and two regions homologous to *K. rhizophila* DC2201 genomic DNA sequences were confirmed. The copy numbers of *E. coli*-*Kocuria* shuttle vectors pKITE301 and pKITE303 were assayed, and their segregation stability and compatibility with other *E. coli*-*Kocuria* shuttle vectors were examined. Moreover, we constructed a biocatalyst co-expressing RhSMO and LSADH (alcohol dehydrogenase from *Leifsonia* sp. S749) using pKITE301 and pKITE103, and the bioproduction of enantiopure (*S*)-styrene oxide from styrene in an organic solvent–water biphasic reaction system using 2-propanol as a hydrogen donor was demonstrated.

MATERIALS AND METHODS

Chemicals

Styrene and styrene oxide were purchased from Nacalai Tesque, Inc. (Kyoto, Japan). Bis-(2-ethylhexyl) phthalate (DEHP) and other chemicals were purchased from Wako Pure Chemical Industries (Osaka, Japan).

Culture Strains and Vectors

Kocuria palustris IPUFS-1 (Toda et al., 2017) was used as a source of cryptic plasmids. *K. rhizophila* DC2201 (NBRC 103217), *K. kristinae* NBRC 15354, *K. varians* NBRC15358, *K. palustris* NBRC 16318, *K. rhizophila* NBRC 16319, *K. polaris* NBRC 103063, *K. flava* HO-9041 (NBRC 107626), and *K. turfanensis* HO-9042 (NBRC 107627) were used as transformation hosts for the constructed shuttle vectors, while *E. coli* JM109 and EC100D *pir*-116 were used for cloning. pHSG298 and pUC118 were used to construct the *E. coli*-*Kocuria* shuttle vectors. pGEM-T Easy Vector (Promega Corp., Fitchburg, WI, United States) was used to construct control plasmids for quantitative polymerase chain

reaction (qPCR). The bacterial strains and plasmids used in this study are listed in Table 1.

Isolation and Characterization of pKPAL3 from *K. palustris* IPUFS-1

Standard techniques were used for DNA manipulation (Sambrook and Russell, 2001). Cryptic plasmids were extracted from *K. palustris* IPUFS-1 cells using a previously described method (Toda et al., 2017). To obtain pure plasmid samples, extracted plasmids were purified by CsCl density-gradient ultracentrifugation and separated by agarose gel electrophoresis. Plasmids were then extracted from agarose gel and purified using the Wizard SV Gel and PCR Clean-Up System (Promega Corp.). Transposons were inserted into the purified plasmid with the EZ-Tn5TM <R6K γ ori/KAN-2: kanamycin resistant> Insertion Kit (AR Brown, Tokyo, Japan) according to the manufacture's protocol. Plasmids with transposons inserted were introduced into *E. coli* EC100D *pir*-116 competent cells, and transformed cells were selected on LB agar plates containing 100 μ g/mL kanamycin. Selected transformants were cultured in 4 mL of

TABLE 1 | Bacterial strains and plasmids in this study.

Bacterial strain/Plasmid	Description	Source
Bacterial strain		
<i>Escherichia coli</i> JM109	F'[traD36, proAB ⁺ , lac Iq, lacZ Δ M15]/ Δ (lac-proAB) recA1, relA1, endA1, gyrA96, thi-1, hsdR17(r _K ⁻ m _K ⁺), e14 ⁻ (mcrA ⁻), supE44,	TaKaRa
<i>E. coli</i> EC100D <i>pir</i> -116	F ⁻ mcrA Δ (mrr-hsdRMS-mcrBC) Δ 80dlacZ Δ M15 Δ lacX74 recA1 endA1 araD139 Δ (ara, leu)7697 galU galK λ -rpsL nupG <i>pir</i> -116(DHFR)	AR Brown
<i>Kocuria palustris</i> IPUFS-1	Wild-type	Toda et al., 2017
<i>K. rhizophila</i> DC2201	Wild-type	NBRC
Plasmid		
pHSG298	<i>E. coli</i> cloning vector	
pUC118	<i>E. coli</i> cloning vector	
pKPAL3	4.4 kbp wild-type plasmid from <i>K. palustris</i> IPUFS-1	This study
pKES3300	<i>E. coli</i> - <i>Kocuria</i> shuttle vector harboring 4.4 kbp fragment from pKPAL3; Km ^r	This study
pKES3301	<i>E. coli</i> - <i>Kocuria</i> shuttle vector harboring 3.4 kbp fragment from pKPAL3; Km ^r	This study
pKES3302	<i>E. coli</i> - <i>Kocuria</i> shuttle vector harboring 2.4 kbp fragment from pKPAL3; Km ^r	This study
pKES3303	<i>E. coli</i> - <i>Kocuria</i> shuttle vector harboring 1.4 kbp fragment from pKPAL3; Km ^r	This study
pKES3305	<i>E. coli</i> - <i>Kocuria</i> shuttle vector harboring 3.4 kbp fragment from pKPAL3; Km ^r	This study
pKES3306	<i>E. coli</i> - <i>Kocuria</i> shuttle vector harboring 2.5 kbp fragment from pKPAL3; Km ^r	This study
pKES3307	<i>E. coli</i> - <i>Kocuria</i> shuttle vector harboring 1.5 kbp fragment from pKPAL3; Km ^r	This study
pKES3309	<i>E. coli</i> - <i>Kocuria</i> shuttle vector harboring 1.4 kbp fragment from pKPAL3; Km ^r	This study
pKES3310	<i>E. coli</i> - <i>Kocuria</i> shuttle vector harboring 1.0 kbp fragment from pKPAL3; Km ^r	This study
pKES3311	<i>E. coli</i> - <i>Kocuria</i> shuttle vector harboring 0.6 kbp fragment from pKPAL3; Km ^r	This study
pKES3312	<i>E. coli</i> - <i>Kocuria</i> shuttle vector harboring 0.8 kbp fragment from pKPAL3; Km ^r	This study
pKES3300 Δ orf1	<i>E. coli</i> - <i>Kocuria</i> shuttle vector harboring 3.7 kbp fragment from pKPAL3; Km ^r	This study
pKES3300 Δ orf2	<i>E. coli</i> - <i>Kocuria</i> shuttle vector harboring 3.4 kbp fragment from pKPAL3; Km ^r	This study
pKES3300 Δ orf12	<i>E. coli</i> - <i>Kocuria</i> shuttle vector harboring 2.4 kbp fragment from pKPAL3; Km ^r	This study
pKES3300 Δ orf3	<i>E. coli</i> - <i>Kocuria</i> shuttle vector harboring 4.0 kbp fragment from pKPAL3; Km ^r	This study
pKES3300 Δ orf4	<i>E. coli</i> - <i>Kocuria</i> shuttle vector harboring 3.5 kbp fragment from pKPAL3; Km ^r	This study
pKITE301	<i>E. coli</i> - <i>Kocuria</i> shuttle vector harboring 1.0 kbp fragment from pKPAL3; Km ^r	This study
pKITE301P	Lac promoter of pKITE301 is replaced by <i>gapdh</i> promoter of <i>K. rhizophila</i> DC2201	This study
pKITE303	<i>E. coli</i> - <i>Kocuria</i> shuttle vector harboring 1.0 kbp fragment from pKPAL3; Thio ^r	This study
pKITE103P-LSADH	LSADH expression vector	Toda et al., 2017

LB liquid medium containing 100 µg/mL kanamycin, and the plasmids were prepared using the Wizard Plus SV Minipreps DNA purification system (Promega Corp.). DNA sequencing was conducted using a 3130 capillary DNA sequencer (Applied Biosystems, Foster City, CA, United States) to determine the nucleotide sequences of the obtained plasmid. The primers used for the determination of the nucleotide sequences are shown in Supplementary Table S1.

Construction of *E. coli*–*Kocuria* Shuttle Vectors

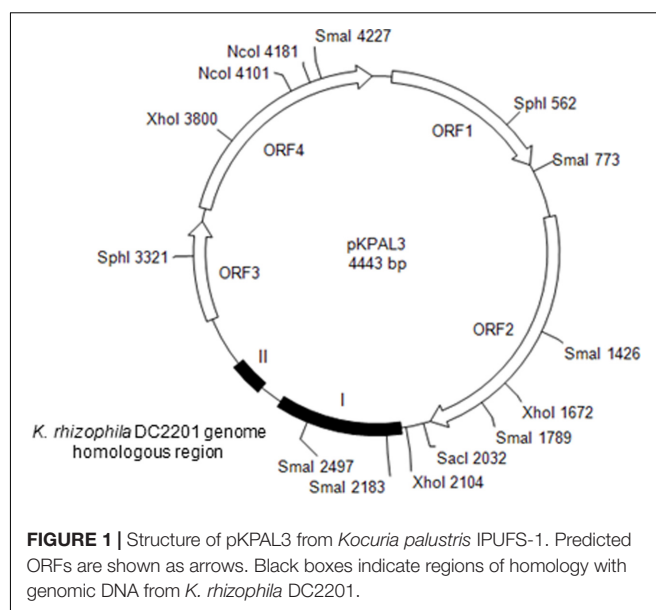
To determine the minimum region of pKPAL3 required for autonomous replication in *Kocuria* cells, deletion clones were derived from pKPAL3 (Figure 1). Various pKPAL3 DNA fragments were obtained by PCR using the primers listed in Supplementary Table S1. The amplified DNA fragments were treated with the restriction endonucleases *Bam*HI and *Sal*I and ligated with pHSG298 that had been amplified by PCR and incubated with *Bgl*II and *Sal*I. Ligated plasmids were then transformed into *E. coli* JM109 and selected on LB agar plates containing 100 µg/mL kanamycin. *K. rhizophila* DC2201 cells were transformed with pKPAL3 derivatives (pKES3300 to pKES3312 and pKES3300Δorf1 to pKES3300Δorf4) according to methods detailed in our previous report (Toda et al., 2017), and transformants were selected on SOB agar (2% [w/v] tryptone, 0.5% [w/v] yeast extract, 10 mM NaCl, 2.5 mM KCl, 10 mM MgSO₄, 10 mM MgCl₂, pH 7.0) containing 400 µg/mL kanamycin.

To construct the pKITE301 vector (Figure 2), the PCR-amplified fragment of pKPAL3 (amplified using primers pKPAL3Fdel5nco and pKPAL3Rdel2bgl) was incubated with the restriction endonucleases *Nco*I and *Bgl*II and ligated with a portion of pHSG298 that was PCR amplified using primers pHSG298Fbgl and pHSG298Rnco and incubated with the same restriction endonucleases. The ligated plasmid was transformed into *E. coli* JM109 to yield pKITE301. Similarly, the PCR fragment of pKPAL3 described above was ligated with a portion of pUC118 PCR amplified using primer pHSG298Fbgl and pHSG298Rnco and incubated with *Nco*I and *Bgl*II, and it was then transformed into *E. coli* JM109. The obtained plasmid was cut with *Bgl*II and ligated with the thiostrepton resistance gene (*tsr*) amplified by PCR to yield pKITE303. All transformation experiments were performed three times, and transformation efficiencies were expressed as means and standard deviations (SDs).

Plasmid copy number was estimated using real-time qPCR, and plasmid stability in *Kocuria* cells was determined according to the methods described in a previous study (Toda et al., 2017). The primers used for estimating copy number by real-time qPCR are shown in Supplementary Table S1.

Transformation of Various *Kocuria* Species

Competent *Kocuria* spp. cells were prepared by washing cells with glycerol solution as described previously (Toda et al., 2017). Each microorganism was grown on LB medium

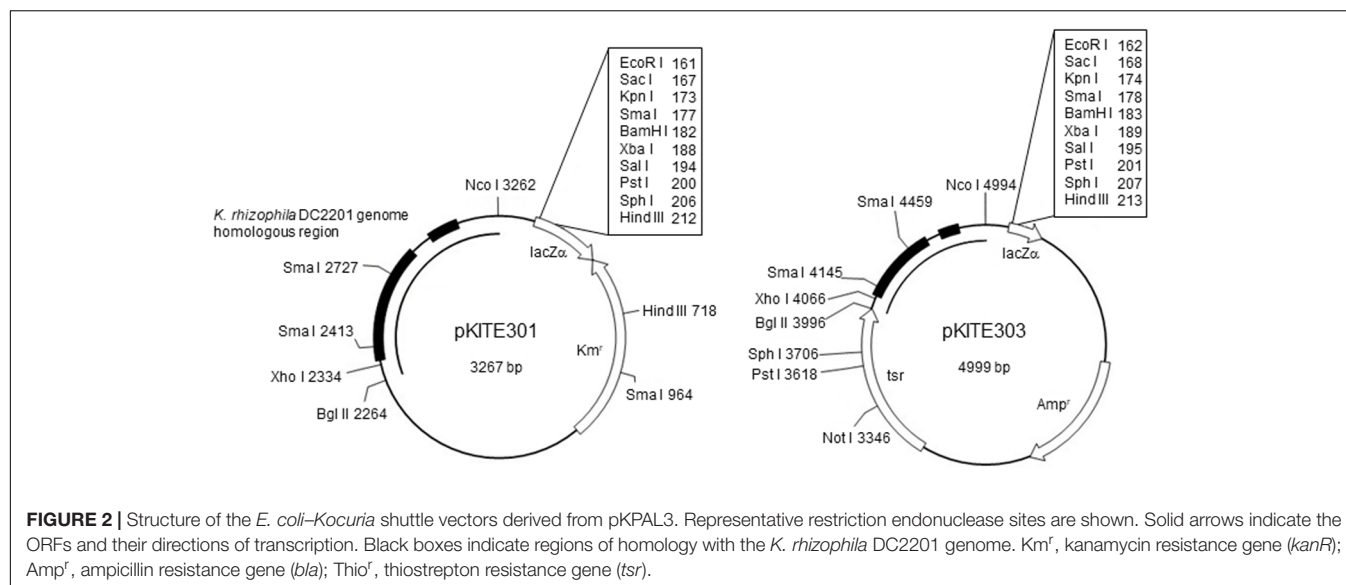


supplemented with 1.5% (w/v) glycine, except *K. polaris* NBRC 103063, to an OD₆₆₀ of 0.7 at 30°C with shaking. The harvested cells were washed twice with sterilized water and resuspended in 10% (v/v) glycerol with OD₆₆₀ adjusted to 50. Electroporation was conducted with 0.5 µg of the pKITE301 plasmid, and cells were cultured on a selection plate (SOB medium containing 100 or 200 µg/mL kanamycin). All transformation experiments using *Kocuria* spp. were performed three times, and transformation efficiencies were expressed as means and SDs.

Development of a RhSMO and LSADH Co-expressing Biocatalyst

To develop a *K. rhizophila* DC2201 biocatalyst that expresses both RhSMO and LSADH genes, the two plasmids pKITE301P-RhSMO and pKITE103P-LSADH were constructed as follows. First, to construct a pKITE301P plasmid in which the *lac* promoter was replaced with the *gapdh* promoter from *K. rhizophila* DC2201, an *Nde*I restriction site was introduced into multicloning sites of pKITE301 using a PrimeSTAR Mutagenesis Basal Kit (Takara, Shiga, Japan) according to the manufacturer's protocol to yield pKITE301nde. The promoter sequence of *gapdh* was amplified by PCR using *K. rhizophila* DC2201 genomic DNA as a template and introduced into the pKITE301nde vector using the *Nde*I and *Nco*I restriction sites. The obtained plasmid was designated pKITE301P. The RhSMO gene was amplified by PCR using *Rhodococcus* sp. ST-10 genomic DNA as a template, and the PCR product was inserted into pKITE103P using *Nde*I and *Bam*HI sites. A PCR fragment of the LSADH gene from *Leifsonia* sp. S749 was inserted into pKITE103P (Toda et al., 2017) using the *Nde*I and *Bam*HI restriction sites.

The constructed plasmids were used to transform *K. rhizophila* DC2201 cells, and transformants were grown on DC2201 agar medium (0.5% [w/v] glucose, 1% [w/v] tryptone, 1% [w/v]



yeast extract, 0.5% [w/v] NaCl, 0.3% [w/v] bonito extract, pH 7.0) containing 400 µg/mL kanamycin and 10 µg/mL thiostrepton. The transformants harboring both pKITE301P-RhSMO and pKITE103P-LSADH were selected and used for further experiments.

Bioproduction of (S)-Styrene Oxide in a Bi-phasic System

The *K. rhizophila* DC2201 cells expressing RhSMO and LSADH were grown on 50 mL DC2201 medium containing 400 µg/mL kanamycin and 10 µg/mL thiostrepton at 30°C with shaking. After cultivation, the culture medium (50 mL) was supplemented with 2.5 mL of 1 M MOPS buffer (pH 7.5) to stabilize its pH and 25 mL of DEHP containing 400 mM styrene and an appropriate amount of 2-propanol (5% to 20% [v/v] in DEHP). Bioconversion was conducted at 30°C with shaking, and an aliquot of the organic layer (500 µL) was collected after centrifugation for 5 min. The collected samples were dried with anhydrous Na₂SO₄ and dissolved in ethyl acetate. Then, gas chromatography analysis was performed to determine the concentrations of styrene and (S)-styrene oxide in the reaction mixture.

Gas Chromatography

Products in the reaction mixture were analyzed using an HP 6890 GC system (Agilent Technologies, Tokyo, Japan) equipped with a Chrompack CP-cyclodextrin-β-2,3,6-M19 chiral capillary column (0.25 mm × 25 m, 0.25 µm film; Valian, Palo Alto, CA, United States). Helium gas was used as the carrier at 15 psi, and the split ratio was 50. Both the injector and detector temperatures were 250°C. Measurement of the product was performed isothermally (at a column temperature of 105°C) with a flame ionization detector. The retention times of styrene, (R)-styrene oxide, and (S)-styrene oxide were 2.90, 7.50, and 7.69 min, respectively.

Nucleotide Sequence Accession Numbers

The determined nucleotide sequences of pKPAL3 from *K. palustris* IPUFS-1, pKITE301, pKITE303, and pKITE301P were registered with the DNA Data Bank Japan (DDBJ) under accession numbers LC317093, LC317094, LC317095, and LC317096, respectively. The nomenclatures of the constructed vectors should be standardized in the future, according to the 'Standard European Vector Architecture' database (SEVA-DB) for a coherent platform of molecular tools that are subject to a concise, and standardized format and nomenclature (Silva-Rocha et al., 2013).

RESULTS

Isolation and Characterization of pKPAL3

We isolated the novel cryptic plasmid pKPAL3 from *K. palustris* IPUFS-1 by using a transposon insertion kit in a manner similar to that described in a previous report (Toda et al., 2017). The isolated plasmid was designated pKPAL3, and its whole nucleotide sequence was determined. pKPAL3 consisted of 4,443 bp with a GC content of 63.5%, and it possessed four estimated ORFs (Figure 1). BLAST searches indicated that ORF1, ORF2, and ORF3 showed approximately 40–50% amino acid sequence identity with hypothetical proteins from other organisms, but their physiological functions remain unclear (Table 2). ORF4 exhibited an amino acid sequence identity of 48.8% with bacterial integrase/recombinase XerD from *Nocardiacae bacterium* Broad-1. However, we were unable to identify genes encoding replication proteins in pKPAL3. There were two nucleotide sequence regions that showed significant identities with untranslated genomic regions of *K. rhizophila* DC2201 (black boxes in Figure 1). Region I consisted of 504 nucleotides and showed 76% identity with the *K. rhizophila* DC2201 genome (positions 61704–62167).

TABLE 2 | BLAST search analysis of putative ORFs of pKPAL3 from *Kocuria palustris* IPUFS-1.

ORF	Position	BLAST search	Identity (%)	Accession no.
ORF1	63-743	Hypothetical protein from <i>Streptococcus pneumoniae</i> PCS70012	53.5	ELU61146
ORF2	966-2003	Hypothetical protein from <i>Corynebacterium epidermidicantis</i>	50.0	AKK03111
ORF3	3061-3459	Hypothetical protein from <i>Cellulomonas cellasea</i> DSM 20118	41.7	KGM01696
ORF4	3512-4426	Putative integrase/recombinase XerD from <i>Nocardioideaceae bacterium</i> Broad-1	48.8	EGD42648
Region	Position	Homologous sequence (positions)	Identity (%)	Accession no.
Region I	2123-2626	<i>K. rhizophila</i> DC2201, complete genome (61704 to 62167)	76	AP009152.1
Region II	2721-2854	<i>K. rhizophila</i> DC2201, complete genome (799495 to 799629; 790542 to 790676; 1921252 to 1921379)	77–84	AP009152.1
		<i>K. turfanensis</i> strain HO-9042 genome (2647231 to 2647361; 3417000 to 3417130; 380434 to 380564; 1459868 to 1459991; 3357701 to 3357842; 2547137 to 2547259)	80–81	CP014480.1
		<i>K. turfanensis</i> strain HO-9042 plasmid unnamed1 (103019 to 103143; 1885 to 2014; 33792 to 33917; 109507 to 109631)	79–80	CP014481.1
		<i>K. turfanensis</i> strain HO-9042 plasmid unnamed4 (28066 to 28195)	79	CP014483.1
		<i>Micrococcus luteus</i> NCTC2665 complete genome (2439192 to 2439324; 344175 to 344304; 2304461 to 2304592; 577570 to 577702; 1526931 to 1527030; 1558046 to 1558175)	77–82	CP001628.1
		<i>Micrococcus</i> sp. A7 plasmid pLMA7 (65195 to 65324; 79792 to 79924)	78–81	KJ599675.1
		<i>Micrococcus</i> sp. 28 plasmid pSD10 (12672 to 12802; 16904 to 17034)	80	AY034092.1
		<i>Micrococcus</i> sp. A1 plasmid pLMA1 (3973 to 4104)	78	LK056645.1
		<i>Micrococcus</i> sp. V7 plasmid pLMV7 (61981 to 62111)	79	KF577591.1

Region II consisted of 134 nucleotides, and it showed 77–84% identities with three homologous regions in the *K. rhizophila* DC2201 genome (positions 790542–790676, 799495–799629, and 1921252–1921379). Furthermore, microorganisms belonging to *Micrococcaceae* such as *K. turfanensis* and *Micrococcus luteus* possessed chromosomal or endogenous plasmid sequences that were homologous to portions of region II (Table 2).

Minimum Sequence Region Required for Autonomous Replication in *K. rhizophila* DC2201

We determined the minimum nucleotide sequence required for self-replication of pKPAL3 in *K. rhizophila* DC2201 through the construction of pKPAL3 deletion plasmids. Positive transformant cells were obtained that had plasmids containing both regions I and II; however, predicted ORFs encoding hypothetical proteins or the predicted recombinase (XerD) were unnecessary for autonomous replication (Figure 3).

Transformation Efficiency

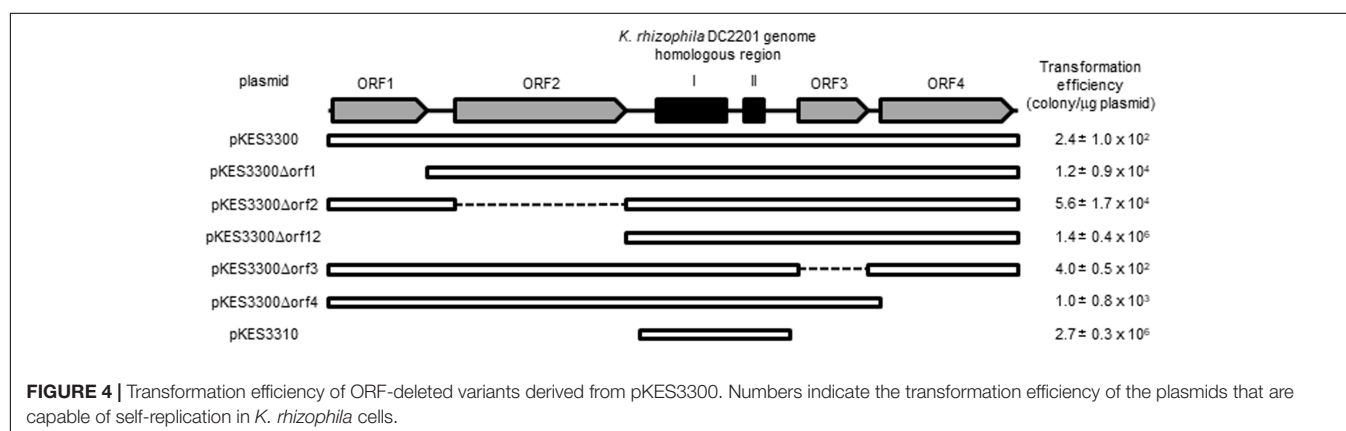
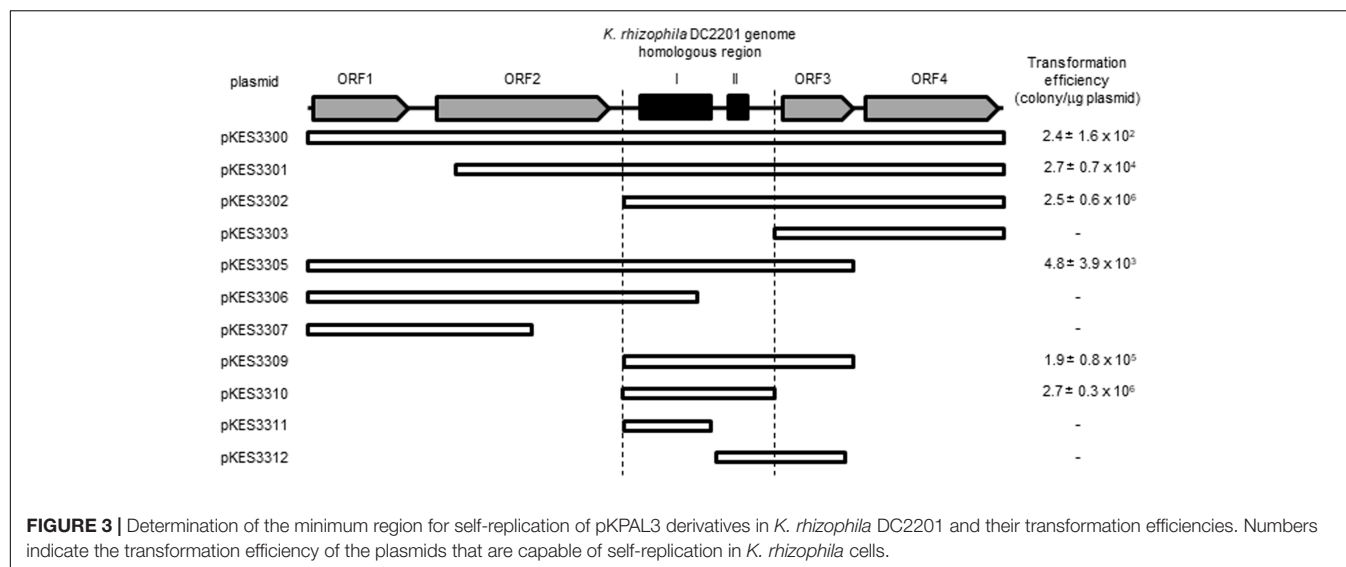
As shown in Figure 3, there were significant differences in transformation efficiencies for *K. rhizophila* DC2201 among the various deletion plasmids. For example, pKES3310 consisted of the minimum region for replication and exhibited a transformation efficiency that was four orders of magnitude higher than that of pKES3300 possessing the entire pKPAL3 plasmid. To investigate the effect of each ORF on transformation efficiency, we constructed deletion plasmids that lacked each

of the predicted ORFs and examined the transformation efficiency of host *K. rhizophila* DC2201 cells with each deletion plasmid (Figure 4). ORF1 and ORF2 were revealed to have a negative effect on transformation efficiency. As expected, the elimination of these ORFs from the plasmid increased the transformation efficiency of constructed plasmids by more than 100-fold compared with that of pKES3300. On the other hand, deletion of ORF3 and/or ORF4 showed much less effect on the transformation efficiency relative to the deletion of ORF1 or ORF2.

Plasmid Copy Number and Segregation Stability

To estimate the copy number of pKITE301 in *K. rhizophila* DC2201, qPCR analysis was conducted on transformed *K. rhizophila* DC2201 using an approach that was similar to that described in a previous report that targeted *tpi*, *pgk*, and *eno* genes in chromosomal DNA and *kanR* in plasmid DNA (Toda et al., 2017). The copy number of pKITE301 was calculated to be 20 per chromosome by the ratio of the mean copy number of *kanR* gene to those of *tpi*, *pgk*, and *eno*.

We examined the segregation stability of pKITE301, pKES3300 and the pKES3300 deletion plasmids (pKES3300 Δ orf1 to pKES3300 Δ orf4; Figure 4) in *K. rhizophila* DC2201 transformant cells. As shown in Figure 5, pKITE301 exhibited much lower segregation stability than pKITE101, and the number of antibiotic-resistant cells harboring plasmids decreased to about



2% of that of the original population after 10 subculture passages. Furthermore, a substantial decrease of segregation stability was observed only for pKES3300Δorf4 and pKITE101, while other deletion plasmids were stably maintained in *K. rhizophila* DC2201 cells (Supplementary Figure S1).

Compatibility of pKITE301 and pKITE103 in *Kocuria* Cells

To confirm the compatibility of the novel shuttle vector pKITE301 (Km^r), the vector was transformed into *K. rhizophila* DC2201 cells harboring pKITE103 (Thio^r), and transformant cells that demonstrated resistance to both kanamycin and thioestrepton were selected. *K. rhizophila* cells harboring both plasmids were then confirmed by agarose gel electrophoresis analysis. Both plasmids were compatible with each other, and they were able to simultaneously replicate in *K. rhizophila* transformant cells in the presence of antibiotics. We also confirmed that pKITE301 and pKITE103 derivatives are able to coexist with the *Kocuria*-*E. coli* shuttle vector pCK-PSD1 developed by Matsumura et al. (2012) in *K. rhizophila*, indicating they are compatible with each other (data not shown).

Transformation of *Kocuria* Species with pKITE301

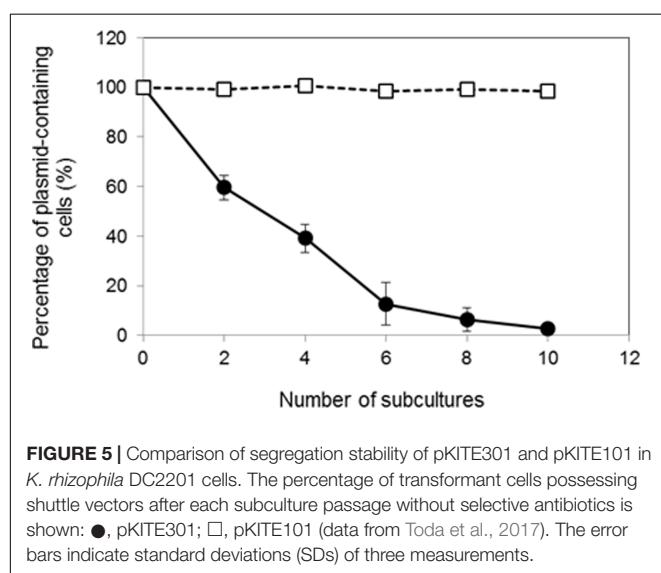
The self-replication of the constructed shuttle vectors was tested in other *Kocuria* species (Table 3). pKITE301 showed a broad range of compatibility with various *Kocuria* species, and the transformation efficiencies for these microorganisms were two to four orders of magnitude higher than those for pKITE101 except for *K. rhizophila* NBRC 16319. However, no successful transformant was observed for *K. kristinae* NBRC 15354 and *K. polaris* NBRC 103063. We also attempted transformation of *M. luteus* NBRC3333 cells using pKITE301, but no transformant was observed (data not shown).

Bioproduction of (S)-Styrene Oxide Using a *K. rhizophila* RhSMO-LSADH Co-expression Biocatalyst

To develop biocatalysis systems for producing enantiopure epoxides, the RhSMO-coding gene was heterologously expressed in *K. rhizophila* DC2201 cells under the control of a *gapdh* promoter using pKITE301P. LSADH, an alcohol dehydrogenase from *Leifsonia* sp. S749, was also expressed in *K. rhizophila* cells

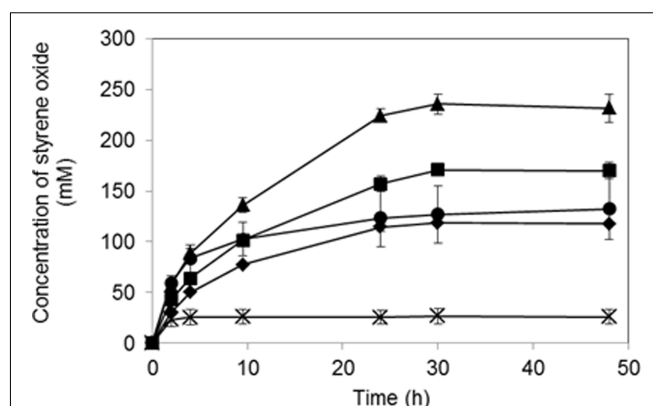
TABLE 3 | Transformation efficiencies of pKITE301 and pKITE101 for *Kocuria* species.

Strain	Transformation efficiency of pKITE301 (cfu/ μ g DNA)	Transformation efficiency of pKITE101 (cfu/ μ g DNA) ^a
<i>K. rhizophila</i> DC2201	$2.7 \pm 0.3 \times 10^6$	5.3×10^2
<i>K. kristinae</i> NBRC 15354	ND ^b	ND
<i>K. varians</i> NBRC 15358	$4.7 \pm 1.1 \times 10^5$	2.8×10^3
<i>K. palustris</i> NBRC 16318	$1.1 \pm 0.2 \times 10^4$	1.5×10^2
<i>K. rhizophila</i> NBRC 16319	$8 \pm 1.4 \times 10$	5×10^2
<i>K. polaris</i> NBRC 103063	ND	ND
<i>K. flava</i> NBRC 107626	$2.5 \pm 1.4 \times 10^6$	ND
<i>K. turfanensis</i> NBRC 107627	$3.1 \pm 0.3 \times 10^5$	1×10^2

^aData from Toda et al. (2017).^bND, not detected.**FIGURE 5** | Comparison of segregation stability of pKITE301 and pKITE101 in *K. rhizophila* DC2201 cells. The percentage of transformant cells possessing shuttle vectors after each subculture passage without selective antibiotics is shown: ●, pKITE301; □, pKITE101 (data from Toda et al., 2017). The error bars indicate standard deviations (SDs) of three measurements.

using pKITE103P for regenerating NADH by using 2-propanol as a hydrogen donor. Bioconversion of styrene to (S)-styrene oxide was conducted in the organic solvent–water biphasic system because the produced epoxide is unstable under aqueous conditions. Table 4 shows that the biocatalyst expressing both RhSMO and LSADH genes successfully produced (S)-styrene oxide in the presence of 2-propanol. Under the same conditions, a negligible amount of product was obtained by *Kocuria* cells possessing pKITE301P-RhSMO/pKITE103P. The control biocatalyst harboring pKITE301P/pKITE103P-LSADH showed no production of styrene oxide.

To optimize the bioconversion, the effect of 2-propanol concentration in the organic solvent was investigated. As shown in Figure 6, the product concentration generally increased in accordance with the increased 2-propanol concentration, and the highest production level of (S)-styrene oxide was obtained in the presence of 15% (v/v) 2-propanol in the organic solvent. Under this condition, the product concentration reached 235 mM in a 30-h reaction. However, styrene oxide production decreased

**FIGURE 6** | Bioproduction of (S)-styrene oxide using *K. rhizophila* DC2201 biocatalysts co-expressing the RhSMO and LSADH genes. Symbols indicate 2-propanol concentrations in the bis-(2-ethylhexyl) phthalate (DEHP) organic solvent phase: ◆, 5% (v/v); ■, 10% (v/v); ▲, 15% (v/v); ●, 20% (v/v); ×, 25% (v/v). The errors bars indicate SDs of three measurements.

at a 2-propanol concentration of 20% (v/v), and a low yield of (S)-styrene oxide was obtained at a 25% (v/v) 2-propanol concentration.

DISCUSSION

Recently, we demonstrated that *K. rhizophila* DC2201 was a suitable host cell strain for producing aliphatic epoxyalkanes because they have robust cell structure and organic solvent tolerance (Toda et al., 2015). Developing genetic tools for *Kocuria* spp. is important for increasing the availability of this microorganism for industrial use to produce various organic compounds.

In our previous study, we isolated the two cryptic plasmids pKPAL1 and pKPAL2 from *K. palustris* IPUFS-1 using the transposon-plasmid rescue method (Toda et al., 2017). Unfortunately, we were unable to generate shuttle vectors from pKPAL2. In that study, other plasmids were detected in the extracted plasmid sample. Thus, *K. palustris* IPUFS-1 was assumed to have more than three cryptic plasmids in their cells. In order to construct a biocatalyst, a combination of compatible plasmid vectors expressing multiple genes in one microorganism cell is often required. In this study, we successfully identified the cryptic plasmid pKPAL3 from *K. palustris* IPUFS-1 and constructed a novel *E. coli*-*Kocuria* shuttle vector that is compatible with the pKITE101 plasmid previously constructed.

pKPAL3 possesses four putative ORFs, which showed high sequence identity with hypothetical proteins from Gram-positive bacteria, although the physiological roles of all ORFs remain unclear except for that of ORF4 (Table 2). The amino acids sequence of ORF4 showed high sequence identity with the putative recombinase/integrase XerD from *N. bacterium* Broad-1. Blakely et al. (1993) reported that the XerC/D recombinase system is involved in the stable inheritance of the ColE1-related circular plasmid, and it also maintains a portion of

TABLE 4 | Comparison of styrene oxide production by *K. rhizophila* DC2201 biocatalysts.

Plasmid	Hydrogen source ^a	Gene	Styrene oxide (mM) ^b
pKITE301P-RhSMO/pKITE103P	2-propanol	RhSMO	1.1 ± 0.8
pKITE301P-RhSMO/pKITE103P-LSADH	2-propanol	RhSMO, LSADH	47.0 ± 2.7
pKITE301P/pKITE103P-LSADH	2-propanol	LSADH	0

^aReactions were performed in the presence of 5% (w/v) 2-propanol in the organic solvent phase with 100 mM styrene. ^bProduct concentration in the organic phase.

chromosomal DNA from *E. coli* (Blakely and Sherratt, 1994). Furthermore, the *resU* gene, which is a member of the XerD recombinase gene family in the cryptic plasmid pUE10 from *Deinococcus radiodurans*, is involved in the stable replication and inheritance of pUE10 derivatives, and Δ *resU* derivatives decreased in segregation stability in *D. radiodurans* cells (Meima and Lidstrom, 2000). These findings suggest that ORF4 may be involved in stabilizing segregation and inheritance of pKPAL3 in *Kocuria* cells. Indeed, segregation stability significantly decreased only in pKES3300 Δ orf4 compared with original pKES3300 and other ORF-deleted derivatives as shown in Supplementary Figure S1. This result supported our speculation.

Notably, pKPAL3 contained two nucleotide sequence regions (regions I and II; **Figure 1**) that showed significant sequence identities with genomic DNA from *K. rhizophila* DC2201. At least one and three conserved nucleotide sequences corresponding to regions I and II of pKPAL3 were confirmed in *K. rhizophila* DC2201 genomic DNA, respectively. These nucleotide sequences are located upstream of the IS 1380 family transposase (region I) and the IS481 family transposase (region II), and neither codes for a polypeptide. Additionally, several *Kocuria* and *Micrococcus* species, including *K. turfanensis* and *M. luteus*, have sequences that are homologous to regions I and II in their chromosomal and plasmid sequences (**Table 2**). Most of these sequences are located upstream of transposases as observed in *K. rhizophila* DC2201. These findings suggested that such nucleotide sequences have been horizontally transferred from the same origin via the transposase gene.

To determine the minimum sequence region required for autonomous replication of pKPAL3 in *Kocuria* cells, deletion plasmids of pKPAL3 were constructed and used to transform a series of *K. rhizophila* DC2201 cells. **Figure 3** shows that no predicted ORFs are required for autonomous replication, whereas regions I and II are essential for self-replication of pKPAL3 in *Kocuria* cells. Furthermore, we found that transformation efficiency varied among plasmid derivatives. Therefore, we investigated the effect of each ORF on transformation frequency using a deletion series. The results shown in **Figure 4** revealed that the deletion of each ORF except ORF3 increased transformation efficiency of pKPAL3 plasmids. Particularly, the deletion of ORF1 and/or ORF2 substantially increased transformation efficiency, whereas the effect of ORF4 deletion was less than that of ORF1 or ORF2 deletion. Maier et al. (2004) also reported that a deletion derivative of an *E. coli*-*Francisella* shuttle vector lacking several ORFs exhibited higher transformation frequency than did the native plasmid. It is generally known that transformation efficiency is affected by modifications of plasmids by methylation in host cells and the

configuration of plasmid DNA with respect to oligomerization and catenation (Ehrlich, 1977; Gryczan et al., 1978; Mottes et al., 1979; Canosi et al., 1981). Therefore, we deduced that differences in transformation efficiency of pKPAL3 derivatives were a consequence of the configurations or modifications caused by the deletion of ORFs in each plasmid, although the specific mechanism of this effect remains unclear.

To estimate the copy number of pKITE301 in culture, qPCR was performed using whole DNA extracted from *K. rhizophila* DC2201 harboring pKITE301 as a DNA template. In culture, pKITE301 showed lower copy number than pKITE101 (Toda et al., 2017), and it was calculated to be 20 per chromosome. In comparison with pKITE101, pKITE301 exhibited lower segregation stability and disappeared during culture in the absence of antibiotics (**Figure 5**). Several reports have indicated that theta-replicating plasmids are stably maintained in Gram-positive bacteria cultures (Kiewiet et al., 1993; Zhang et al., 1994; Seegers et al., 1995; Lee and O'Sullivan, 2006), and pKITE101 is also stably maintained in *Kocuria* cells (Toda et al., 2017). In contrast, pKITE301 exhibited poor stability in *Kocuria* cells in the absence of antibiotics. These results suggest that the replicating mechanism of pKPAL3 is different from that of the highly stable theta-type plasmid. As described earlier, the low stability of pKITE301 may be restored by the addition of ORF4 into pKITE301, although further experiments are necessary to confirm this conclusion.

The transformation of various *Kocuria* species by the constructed shuttle vectors was tested. As shown in **Table 3**, several *Kocuria* species, including *K. rhizophila* NBRC 16319, *K. varians* NBRC 15358, *K. palustris* NBRC 16318, *K. flava* NBRC 107626, and *K. turfanensis* NBRC 107627, were successfully transformed with pKITE301 at transformation efficiencies of 8×10 to 2.5×10^6 cfu/mg DNA; however, no transformants were observed for *K. kristinae* NBRC 15354 or *K. polaris* NBRC 103063. Further optimization of conditions to prepare competent cells may be needed for these species and/or strains. Additionally, it is generally known that most bacteria have restriction modification (RM) systems that prevent the entry of foreign DNA into the host cell (Wilson and Murray, 1991). Two host cells, *K. kristinae* and *K. polaris*, are likely to have eliminated pKITE301 via their RM systems, or these strains were not competent under the general cell-transformation procedure; either of these conclusions requires confirmation. In most cases, the transformation efficiencies of pKITE301 for *Kocuria* species exceeded those of pKITE101, except for *K. rhizophila* NBRC 16319. These results indicate that the constructed shuttle vectors can be used for genetic modification of various *Kocuria* species.

To confirm the utility of constructed plasmids for heterologous gene expression, we constructed the RhSMO-expression plasmid pKITE301P-RhSMO and the LSADH-expression plasmid pKITE103P-LSADH (Toda et al., 2017), and both plasmids were simultaneously transformed into *K. rhizophila* DC2201 cells. Under the control of the *gapdh* promoter from *K. rhizophila*, both RhSMO and LSADH genes were successfully expressed in transformed cells (data not shown). Using *K. rhizophila* cells (i.e., pKITE301P-RhSMO and pKITE103P-LSADH) as a biocatalyst, we conducted bioconversion of styrene to (S)-styrene oxide in an organic solvent–water biphasic reaction system. The biocatalyst harboring both RhSMO and LSADH successfully converted styrene to (S)-styrene oxide using 2-propanol as a hydrogen donor, whereas negligible amounts of product were obtained in the absence of 2-propanol (Table 4). Furthermore, no product was observed when a biocatalyst possessing only LSADH was used. These results indicate that both RhSMO and LSADH were successfully expressed and that LSADH functioned as a NADH regenerator in *Kocuria* cells. These results suggest that these shuttle vectors are more broadly applicable for constructing multi-enzymatic cascade systems for producing various compounds in *Kocuria* cells.

The concentration of 2-propanol (the hydrogen donor for NADH regeneration by LSADH) in the organic solvent phase is an important factor for producing styrene oxide because it affects not only the solubility of the substrate in the aqueous phase but also the inactivation of the biocatalyst. When 15% (v/v) 2-propanol was added to the organic solvent (i.e., DEHP) phase, the highest product concentration (235 mM) was achieved after a 30-h reaction (Figure 6). On the other hand, styrene oxide production significantly decreased at a 2-propanol concentration

of 20% (v/v), and the lowest production level was observed for 25% (v/v) 2-propanol. Thus, *K. rhizophila* biocatalysts possessing the RhSMO–LSADH enzyme system exhibited the maximum epoxidation rate in the presence of 15% (v/v) 2-propanol and showed resistance to 20% (v/v) 2-propanol. In corresponding *E. coli* recombinant biocatalyst systems, the optimum 2-propanol concentration was 6% (v/v), and the reaction was greatly inhibited at concentrations exceeding 10% (v/v), although the conditions were slightly different (Toda et al., 2012a). Thus, the *K. rhizophila* biocatalyst system had higher 2-propanol resistance than the corresponding *E. coli* system and achieved higher yields of (S)-styrene oxide (235 mM) than that of the *E. coli* biocatalyst system (150 mM).

We expect that the shuttle vectors developed in this study will be a powerful tool for modification of some *Kocuria* spp. and developing *K. rhizophila* biocatalysis systems to produce various useful water-insoluble compounds via organic synthesis.

AUTHOR CONTRIBUTIONS

HT performed the construction of the plasmid vectors from pKPAL3 and characterization of these plasmid vectors for *Kocuria* sp. and wrote those sections. NI planned the experimental design and wrote some parts of the manuscript.

SUPPLEMENTARY MATERIAL

The Supplementary Material for this article can be found online at: <https://www.frontiersin.org/articles/10.3389/fmicb.2017.02313/full#supplementary-material>

REFERENCES

- Beltrametti, F., Marconi, A. M., Bestetti, G., Colombo, C., Galli, E., Ruzzi, M., et al. (1997). Sequencing and functional analysis of styrene catabolism genes from *Pseudomonas fluorescens* ST. *Appl. Environ. Microbiol.* 63, 2232–2239.
- Blakely, G., May, G., McCulloch, R., Arciszewska, L. K., Burke, M., Lovett, S. T., et al. (1993). Two related recombinases are required for site-specific recombination at dif and cer in *E. coli* K12. *Cell* 75, 351–361. doi: 10.1016/0092-8674(93)80076-Q
- Blakely, G. W., and Sherratt, D. J. (1994). Interactions of the site-specific recombinases XerC and XerD with the recombination site dif. *Nucleic Acids Res.* 22, 5613–5620. doi: 10.1093/nar/22.25.5613
- Canosi, U., Iglesias, A., and Trautner, T. A. (1981). Plasmid transformation in *Bacillus subtilis*: effects of insertion of *Bacillus subtilis* DNA into plasmid pC194. *Mol. Gen. Genet.* 181, 434–440. doi: 10.1007/BF00428732
- Champreda, V., Choi, Y. J., Zhou, N. Y., and Leak, D. J. (2006). Alternation of the stereo- and regioselectivity of alkene monooxygenase based on coupling protein interaction. *Appl. Microbiol. Biotechnol.* 71, 840–847. doi: 10.1007/s00253-005-0208-2
- Chang, S., Galvin, J. M., and Jacobsen, E. N. (1994). Effect of chiral quaternary ammonium salts on (salen)Mn-catalyzed epoxidation of cis-olefins. a highly enantioselective, catalytic route to trans-epoxides. *J. Am. Chem. Soc.* 116, 6937–6938. doi: 10.1021/ja00094a059
- Dufosse, L. (2006). Microbial production of food grade pigments. *Food Technol. Biotechnol.* 44, 313–321.
- Ehrlich, S. D. (1977). Replication and expression of plasmids from *Staphylococcus aureus* in *Bacillus subtilis*. *Proc. Natl. Acad. Sci. U.S.A.* 74, 1680–1682. doi: 10.1073/pnas.74.4.1680
- Farina, V., Reeves, J. T., Senanayake, C. H., and Song, J. J. (2006). Asymmetric synthesis of active pharmaceutical ingredients. *Chem. Rev.* 106, 2734–2793. doi: 10.1021/cr040700c
- Farinas, E. T., Alcalde, M., and Arnold, F. (2004). Alkene epoxidation catalyzed by cytochrome P450 BM-3 139-3. *Tetrahedron* 60, 525–528. doi: 10.1016/j.tet.2003.10.099
- Goodwin, T. W. (1980). “Functions of carotenoids,” in *The Biochemistry of the Carotenoids*, Vol. 1, ed. T. W. Goodwin (New York, NY: Chapman and Hall), 77–95. doi: 10.1007/978-94-009-5860-9_3
- Gryczan, T. J., Contente, S., and Dubnau, D. (1978). Characterization of *Staphylococcus aureus* plasmids introduced by transformation into *Bacillus subtilis*. *J. Bacteriol.* 134, 318–329.
- Hanson, R. M., and Sharpless, K. B. (1986). Procedure for the catalytic asymmetric epoxidation of allylic alcohols in the presence of molecular sieves. *J. Org. Chem.* 51, 1922–1925. doi: 10.1021/jo00360a058
- Hartmans, S., van der Werf, M. J., and de Bont, J. A. (1990). Bacterial degradation of styrene involving a novel flavin adenine dinucleotide-dependent styrene monooxygenase. *Appl. Environ. Microbiol.* 56, 1347–1351.
- Heipieper, H. J., Neumann, G., Cornelissen, S., and Meinhardt, F. (2007). Solvent-tolerant bacteria for biotransformations in two-phase fermentation systems. *Appl. Microbiol. Biotechnol.* 74, 961–973. doi: 10.1007/s00253-006-0833-4
- Hollmann, F., Lin, P. C., Witholt, B., and Schmid, A. (2003). Stereospecific biocatalytic epoxidation: the first example of direct regeneration of a FAD-dependent monooxygenase for catalysis. *J. Am. Chem. Soc.* 125, 8209–8217. doi: 10.1021/ja034119u
- Irie, R., Noda, K., Ito, Y., and Katsuki, T. (1991). Enantioselective epoxidation of unfunctionalized olefins using chiral (salen)manganese(III)

- complexes. *Tetrahedron Lett.* 32, 1055–1058. doi: 10.1016/S0040-4039(00)74486-8
- Katsuki, T., and Sharpless, K. B. (1980). The first practical method for asymmetric epoxidation. *J. Am. Chem. Soc.* 102, 5974–5976. doi: 10.1021/ja00538a077
- Kiewiet, R., Kok, J., Seegers, J. F., Venema, G., and Bron, S. (1993). The mode of replication is a major factor in segregational plasmid instability in *Lactococcus lactis*. *Appl. Environ. Microbiol.* 59, 358–364.
- Lee, J.-H., and O'Sullivan, D. J. (2006). Sequence analysis of two cryptic plasmids from *Bifidobacterium longum* DJO10A and construction of a shuttle cloning vector. *Appl. Environ. Microbiol.* 72, 527–535. doi: 10.1128/AEM.72.1.527-535.2006
- Lin, H., Qiao, J., Liu, Y., and Wu, Z. L. (2010). Styrene monooxygenase from *Pseudomonas* sp. LQ26 catalyzes the asymmetric epoxidation of both conjugated and unconjugated alkenes. *J. Mol. Catal. B Enzym.* 67, 236–241. doi: 10.1016/j.molcatb.2010.08.012
- Maier, T. M., Havig, A., Casey, M., Nano, F. E., Frank, D. W., and Zahrt, T. C. (2004). Construction and characterization of a highly efficient *Francisella* shuttle plasmid. *Appl. Environ. Microbiol.* 70, 7511–7519. doi: 10.1128/AEM.70.12.7511-7519.2004
- Marconi, A. M., Beltrametti, F., Bestetti, G., Solinas, F., Ruzzi, M., and Galli, E. (1996). Cloning and characterization of styrene catabolism genes from *Pseudomonas fluorescens* ST. *Appl. Environ. Microbiol.* 62, 121–127.
- Martinez, C. A., and Stewart, J. D. (2000). Cytochrome P450s potential catalysts for asymmetric olefin epoxidations. *Curr. Org. Chem.* 4, 263–282. doi: 10.2174/1385272003376265
- Matsumura, E., Hamasaki, M., and Matsuyama, A. (2012). Novel expression vector. U.S. Patent No 0,142,050. Washington, DC: U.S. Patent and Trademark Office.
- Meima, R., and Lidstrom, M. E. (2000). Characterization of the minimal replicon of a cryptic *Deinococcus radiodurans* SARK plasmid and development of versatile *Escherichia coli*-*D. radiodurans* shuttle vectors. *Appl. Environ. Microbiol.* 66, 3856–3867. doi: 10.1128/AEM.66.9.3856-3867.2000
- Mottes, M., Grandi, G., Sgarabella, V., Canosi, U., Morelli, G., and Trautner, T. A. (1979). Different specific activities of the monomeric and oligomeric forms of plasmid DNA in transformation of *B. subtilis* and *E. coli*. *Mol. Gen. Genet.* 174, 281–286. doi: 10.1007/BF00267800
- Nikel, P. I., Martínez-García, E., and de Lorenzo, V. (2014). Biotechnological domestication of pseudomonads using synthetic biology. *Nat. Rev. Microbiol.* 12, 368–379. doi: 10.1038/nrmicro3253
- Ohta, Y., Hatada, Y., Mori, K., and Nakamura, N. (2014). Plasmid vector. U.S. Patent No 8,809,048. Washington, DC: U.S. Patent and Trademark Office.
- Panke, S., de Lorenzo, V., Kaiser, A., Witholt, B., and Wubbolts, M. G. (1999). Engineering of a stable whole-cell biocatalyst capable of (S)-styrene oxide formation for continuous two-liquid-phase applications. *Appl. Environ. Microbiol.* 65, 5619–5623.
- Panke, S., Witholt, B., Schmid, A., and Wubbolts, M. G. (1998). Towards a biocatalyst for (S)-styrene oxide production: characterization of the styrene degradation pathway of *Pseudomonas* sp. strain VLB120. *Appl. Environ. Microbiol.* 64, 2032–2043.
- Park, J. B., Buhler, B., Panke, S., Witholt, B., and Schmid, A. (2007). Carbon metabolism and product inhibition determine the epoxidation efficiency of solvent-tolerant *Pseudomonas* sp. strain VLB120DeltaC. *Biotechnol. Bioeng.* 98, 1219–1229. doi: 10.1002/bit.21496
- Patel, R. N. (2008). Synthesis of chiral pharmaceutical intermediates by biocatalysis. *Coord. Chem. Rev.* 252, 659–701. doi: 10.1016/j.ccr.2007.10.031
- Porter, J. W., and Spurgeon, S. L. (eds). (1981). "Biosynthesis of carotenoids," in *Biosynthesis of Isoprenoid Compounds* (New York, NY: Wiley), 1–122.
- Sambrook, J., and Russell, W. D. (2001). *Molecular Cloning, a Laboratory Manual*, 3rd Edn. Cold Spring, NY: Harbor Laboratory Press.
- Seegers, J. F., Franke, C. M., Kiewiet, R., Venema, G., and Bron, S. (1995). Use of continuous culture for the selection of plasmids with improved segregational stability. *Plasmid* 33, 71–77. doi: 10.1006/plas.1995.1009
- Shi, Y. (2004). Organocatalytic asymmetric epoxidation of olefins by chiral ketones. *Acc. Chem. Res.* 37, 488–496. doi: 10.1021/ar030063x
- Silva-Rocha, R., Martínez-García, E., Calles, B., Chavarría, M., Arce-Rodríguez, A., de las Heras, A., et al. (2013). The Standard European Vector Architecture (SEVA): a coherent platform for the analysis and deployment of complex prokaryotic phenotypes. *Nucleic Acids Res.* 41, D666–D675. doi: 10.1093/nar/gks1119
- Siriphongphaew, A., Pisnupong, P., Wongkongkatep, J., Inprakhon, P., Vangnai, A., Honda, K., et al. (2012). Development of a whole-cell biocatalyst co-expressing P450 monooxygenase and glucose dehydrogenase for synthesis of epoxyhexane. *Appl. Microbiol. Biotechnol.* 95, 357–367. doi: 10.1007/s00253-012-4039-7
- Takarada, H., Sekine, M., Kosugi, H., Matsuo, Y., Fujisawa, T., Omata, S., et al. (2008). Complete genome sequence of the soil actinomycete *Kocuria rhizophila*. *J. Bacteriol.* 190, 4139–4146. doi: 10.1128/JB.01853-07
- Tischler, D., Gröning, J. D., Kaschabek, S., and Schlömann, M. (2012). One-component styrene monooxygenases: an evolutionary view on a rare class of flavoproteins. *Appl. Biochem. Biotechnol.* 167, 931–944. doi: 10.1007/s12010-012-9659-y
- Toda, H., Imae, R., and Itoh, N. (2012a). Efficient biocatalysis for the production of enantiopure (S)-epoxides using a styrene monooxygenase (SMO) and *Leifsonia* alcohol dehydrogenase (LSADH) system. *Tetrahedron Asymmetry* 23, 1542–1549. doi: 10.1016/j.tetasy.2012.09.017
- Toda, H., Imae, R., and Itoh, N. (2014). Bioproduction of chiral epoxyalkanes using styrene monooxygenase from *Rhodococcus* sp. ST-10 (RhSMO). *Adv. Synth. Catal.* 356, 3443–3450. doi: 10.1002/adsc.201400383
- Toda, H., Imae, R., Komio, T., and Itoh, N. (2012b). Expression and characterization of styrene monooxygenases of *Rhodococcus* sp. ST-5 and ST-10 for synthesizing enantiopure (S)-epoxides. *Appl. Microbiol. Biotechnol.* 96, 407–418. doi: 10.1007/s00253-011-3849-3
- Toda, H., and Itoh, N. (2012). Isolation and characterization of styrene metabolism genes from styrene-assimilating soil bacteria *Rhodococcus* sp. ST-5 and ST-10. *J. Biosci. Bioeng.* 113, 12–19. doi: 10.1016/j.jbiosc.2011.08.028
- Toda, H., Koyanagi, T., Enomoto, T., and Itoh, N. (2017). Characterization of two cryptic plasmids from *Kocuria palustris* IPUFS-1 and construction of novel *Escherichia coli*-*Kocuria* shuttle vector for biocatalysis. *J. Biosci. Bioeng.* 124, 255–262. doi: 10.1016/j.jbiosc.2017.03.018
- Toda, H., Ohuchi, T., Imae, R., and Itoh, N. (2015). Microbial production of aliphatic (S)-epoxyalkanes by using *Rhodococcus* sp. strain ST-10 styrene monooxygenase expressed in organic-solvent-tolerant *Kocuria rhizophila* DC2201. *Appl. Environ. Microbiol.* 81, 1919–1925. doi: 10.1128/AEM.03405-14
- Tu, Y., Wang, Z.-X., and Shi, Y. (1996). An efficient asymmetric epoxidation method for trans-olefins mediated by a fructose-derived ketone. *J. Am. Chem. Soc.* 118, 9806–9807. doi: 10.1021/ja962345g
- Velasco, A., Alonso, S., Garcia, J. L., Perera, J., and Diaz, E. (1998). Genetic and functional analysis of the styrene catabolic cluster of *Pseudomonas* sp strain Y2. *J. Bacteriol.* 180, 1063–1071.
- Verhoef, S., Wierckx, N., Westerhof, R. G. M., de Winde, J. H., and Ruijsenaars, H. J. (2009). Bioproduction of p-hydroxystyrene from glucose by the solvent-tolerant bacterium *Pseudomonas putida* S12 in a two-phase water-decanol fermentation. *Appl. Environ. Microbiol.* 75, 931–936. doi: 10.1128/AEM.02186-08
- Wilson, G. G., and Murray, N. E. (1991). Restriction and modification systems. *Annu. Rev. Genet.* 25, 585–627. doi: 10.1146/annurev.gen.25.120191.003101
- Zhang, Y., Praszkie, J., Hodgson, A., and Pittard, A. J. (1994). Molecular analysis and characterization of a broad-host-range plasmid, pEP2. *J. Bacteriol.* 176, 5718–5728. doi: 10.1128/jb.176.18.5718-5728.1994

Conflict of Interest Statement: The authors declare that the research was conducted in the absence of any commercial or financial relationships that could be construed as a potential conflict of interest.

Copyright © 2017 Toda and Itoh. This is an open-access article distributed under the terms of the Creative Commons Attribution License (CC BY). The use, distribution or reproduction in other forums is permitted, provided the original author(s) or licensor are credited and that the original publication in this journal is cited, in accordance with accepted academic practice. No use, distribution or reproduction is permitted which does not comply with these terms.



Real Time Monitoring of NADPH Concentrations in *Corynebacterium glutamicum* and *Escherichia coli* via the Genetically Encoded Sensor mBFP

Oliver Goldbeck¹, Alexander W. Eck² and Gerd M. Seibold^{1,2*}

¹ Institute of Microbiology and Biotechnology, Ulm University, Ulm, Germany, ² Institute for Biochemistry, University of Cologne, Cologne, Germany

OPEN ACCESS

Edited by:

Dirk Tischler,
Ruhr-Universität Bochum, Germany

Reviewed by:

Peter Neubauer,
Technische Universität Berlin,
Germany
Juan Carlos Aon,
GlaxoSmithKline, United States

*Correspondence:

Gerd M. Seibold
gerd.seibold@uni-ulm.de

Specialty section:

This article was submitted to
Microbial Physiology and Metabolism,
a section of the journal
Frontiers in Microbiology

Received: 03 July 2018

Accepted: 08 October 2018

Published: 24 October 2018

Citation:

Goldbeck O, Eck AW and
Seibold GM (2018) Real Time
Monitoring of NADPH Concentrations
in *Corynebacterium glutamicum*
and *Escherichia coli* via
the Genetically Encoded Sensor
mBFP. *Front. Microbiol.* 9:2564.
doi: 10.3389/fmicb.2018.02564

Analyses of intracellular NADPH concentrations are prerequisites for the design of microbial production strains and process optimization. mBFP was described as metagenomics derived, blue fluorescent protein showing NADPH-dependent fluorescence. Characterization of mBFP showed a high specificity for binding of NADPH (K_D 0.64 mM) and no binding of NADH, the protein exclusively amplified fluorescence of NADPH. mBFP catalyzed the NADPH-dependent reduction of benzaldehyde and further aldehydes, which fits to its classification as short chain dehydrogenase. For *in vivo* NADPH analyses a codon-optimized gene for mBFP was introduced into *Corynebacterium glutamicum* WT and the phosphoglucosyltransferase-deficient strain *C. glutamicum* Δpgi , which accumulates high levels of NADPH. For determination of intracellular NADPH concentrations by mBFP a calibration method with permeabilized cells was developed. By this means an increase of intracellular NADPH concentrations within seconds after the addition of glucose to nutrient-starved cells of both *C. glutamicum* WT and *C. glutamicum* Δpgi was observed; as expected the internal NADPH concentration was significantly higher for *C. glutamicum* Δpgi (0.31 mM) when compared to *C. glutamicum* WT (0.19 mM). Addition of paraquat to *E. coli* cells carrying mBFP led as expected to an immediate decrease of intracellular NADPH concentrations, showing the versatile use of mBFP as intracellular sensor.

Keywords: *Corynebacterium glutamicum*, *Escherichia coli*, NADPH, redox state, biosensor, short chain dehydrogenase

INTRODUCTION

The redox state of cells is represented by the ratio of the internal concentrations of the pyridine nucleotides NADH and NADPH and their corresponding oxidized forms NAD^+ and $NADP^+$ (Blacker et al., 2014). These ubiquitous cofactors are present in cells only in catalytic amounts, therefore efficient recycling is required for the maintenance of viability and antioxidant protection

Abbreviations: CTAB, cetyl trimethylammonium bromide; IPTG, isopropyl β -D-1-thiogalactopyranoside; TF, transcription factor.

(Krömer et al., 2008; Agledal et al., 2010; Mailloux et al., 2011). Intracellular availability of NADPH is of special relevance for microbial production processes like the biosynthesis of medicinal compounds, alcohols, biopolymers, and especially amino acids like L-lysine and L-valine (Weckbecker and Hummel, 2004; Sanchez et al., 2006; Bartek et al., 2010; Chemler et al., 2010; Kocharin et al., 2013; Lindner et al., 2013; Zhao et al., 2017). *Escherichia coli* and *Corynebacterium glutamicum*, two workhorses for the production of commodity chemicals (Becker and Wittmann, 2015), maintain their NADPH supply mainly via the pentose phosphate pathway (PPP) and the tricarboxylic acid cycle (Marx et al., 1996; Sauer et al., 2004; Spaans et al., 2015). To increase productivity and yields of microbial production strains current metabolic engineering strategies aim at an improved NADPH availability such as the redirection of the metabolism toward the PPP or introduction of transhydrogenases (Kabus et al., 2007; Lindner et al., 2013; Wang et al., 2017). Analyses of intracellular NADPH concentrations and their changes provide the basis for rational strain design and optimization and serve also for the detailed understanding of physiological roles of NADPH (Blacker et al., 2014; Ng et al., 2015; Liu and Wang, 2017). However, research is limited due to the technically challenging and labor-intensive analysis of internal NADPH concentrations (Lu et al., 2018).

Genetically encoded biosensors provide non-invasive optical readouts for internal concentrations of many different metabolites (Bolbat and Schultz, 2017; Lin et al., 2017). These sensors allow high throughput analyses of intracellular metabolite levels in microorganisms as a novel approach for strain selection and can also be employed to monitor metabolite levels in the course of cultivations (Schallmeyer et al., 2014; Eggeling et al., 2015; Bolbat and Schultz, 2017). For latter application transcription factor (TF) based sensors and the commonly used auto-fluorescent GFP derivatives come along with the drawback of poor dynamic behaviors (Liu et al., 2015; Liu and Wang, 2017), caused by their oxygen dependency and slow response times. For analysis of intracellular NADPH availability, only few biosensors have been described: The [2Fe-2S]-cluster containing transcriptional regulator SoxR of *E. coli*, was recently used for the design of a NADPH biosensor. Depending on the redox status of SoxR expression of the fluorescent protein eYFP is activated (Siedler et al., 2014). SoxR remains reduced and inactive as long as NADPH-dependent reductases are not limited in their substrate. Lack of NADPH leads to activation of SoxR and thus expression of eYFP. The SoxR-dependent NADPH biosensor was successfully applied to screen *E. coli* strains harboring gene bank derived variants of an NADPH consuming alcohol dehydrogenase (Siedler et al., 2014). A second NADPH sensor named iNAP recently described by Tao et al. (2017) reduces the probability of false positive readouts due to its ratiometric signal. The synthetic iNAP sensor consists of circularly permuted eYFP fused to the NADH binding domain of Rex from *Thermus aquaticus* (Zhao et al., 2015), of which the nucleotide binding pocket was subsequently mutated for NADPH-specificity by switching conserved residues (Tao et al., 2017). The iNAP sensor offers a fast, non-TF-based response to changes in the NADPH/NADP⁺

ratio in various types of cells (Zhao et al., 2016; Tao et al., 2017).

The protein mBFP was recently described as NADPH-dependent, metagenomics derived, blue fluorescent protein: upon binding of NADPH mBFP amplifies the intrinsic fluorescence of NADPH in an oxygen independent manner (Hwang et al., 2012), and produces more fluorescence when supplied with more NADPH (Ng et al., 2015). Oxygen independent fluorescent proteins such as mBFP, whose fluorescent properties rely on the binding of the metabolite of interest, are generally ideal candidates for *in vivo* analytics of metabolite concentrations in the course of cultivation (Lin et al., 2017). The NADPH dependent fluorescence of mBFP were exploited to screen a series of *E. coli* strains for improved NADPH regeneration (Ng et al., 2015). Based on its amino acid sequence mBFP is classified as short chain dehydrogenase (SDR), however, no experiments were conducted in this direction so far. The analysis of fast variations of intracellular NADPH concentrations by the use of genetically encoded biosensors was to our knowledge hitherto not reported.

In this study, we characterized NADPH binding, fluorescence properties, and enzymatic activities of purified mBFP. Based on this knowledge of its biochemical parameters, we optimized application of this highly specific NADPH sensor for the *in vivo* analysis of fast changes in intracellular NADPH concentrations in both *C. glutamicum* and *E. coli*. The results of these experiments demonstrate that mBFP is a versatile tool for the quantitative determination of internal NADPH concentrations and their fast alterations in bacteria.

MATERIALS AND METHODS

Bacterial Strains, Plasmids, and Culture Conditions

Bacterial strains and plasmids used in this study are listed in **Table 1**. Pre-cultures of *E. coli* and *C. glutamicum* were carried out in 2xTY medium in baffled Erlenmeyer flasks on a rotary shaker (130 rpm) at 30 and 37°C, respectively. CgXII was used as minimal medium for *C. glutamicum* (Eggeling and Bott, 2005) with 10 g L⁻¹ glucose as carbon source. Strains carrying plasmids were cultivated in the presence of kanamycin (50 µg/mL) and IPTG (1 mM) for mBFP expression. Growth of *E. coli* and of *C. glutamicum* was followed by measuring the optical density (OD) at 600 nm in an Ultrospec 2100 pro spectrophotometer (GE Healthcare Life Sciences GmbH, Freiburg, Germany).

Construction of Plasmid pEKEx2_mBFPopt

For plasmid construction, transformation and plasmid isolation from *E. coli* DH5α standard cloning and molecular biology procedures were employed (Sambrook et al., 2001), transformation of *C. glutamicum* strains by electroporation was conducted as described (Tauch et al., 2002). Recombinant strains were selected using 2xTY-agar plates containing kanamycin

TABLE 1 | Strains and plasmids used in this study.

Strains and plasmids	Relevant properties and applications	Sources and reference
Strains		
<i>E. coli</i> DH5 α	F ⁻ <i>thi-1 endA1 hsdR17</i> (r ⁻ m ⁻) <i>supE44 ΔlacU169</i> (ϕ 80 <i>lacZ</i> Δ M15) <i>recA1 gyrA96</i> <i>relA1 F⁻ λ-<i>ilvG rfb-50 rph-1</i></i>	Hanahan, 1983
<i>E. coli</i> BL21 (DE3)	F ⁻ <i>ompT gal dcm lon</i> <i>hsdSB</i> (rB–mB–) [<i>malB</i> + JK–12(λ S)]	Studier and Moffatt, 1986
<i>C. glutamicum</i> ATCC13032	Wild type	American Type Culture Collection
<i>C. glutamicum</i> Δ <i>pgi</i>	In-frame deletion of <i>pgi</i> gene (cg0973) of <i>C. glutamicum</i> ATCC13032	Lindner et al., 2013
Plasmids		
pEKEx2	Ptac, <i>lacI^q</i> , Km ^r	Eikmanns et al., 1991
pCN_mBFP	Expression plasmid carrying mBFP under constitutive promoter	Ng et al., 2015
pEKEx2_mBFPopt	Expression plasmid carrying the codon-optimized gene for mBFP under the control of the IPTG inducible Ptac promoter	This work

(50 μ g/mL). Eurofins MWG (Ebersberg, Germany) carried out synthesis of the mBFPopt gene fragment for a *C. glutamicum* codon-optimized mBFP gene (Supplementary Table S1). The optimized gene was amplified via PCR using the primers mBFPopt_fw and mBFPopt_rev (Supplementary Table S1) resulting in a 780 bp amplicon, which was subsequently digested with the restriction endonucleases *SacI* and *SalI*. Ligation of the 766 bp fragment into *SacI* and *SalI* linearized pEKEx2 (8,130 bp) resulted in the final construct pEKEx2_mBFPopt (8,896 bp). The plasmid pEKEx2_mBFPopt was controlled by restriction digestions and DNA sequencing (MWG Eurofins).

Fluorescence Analysis

Fluorescence measurements were carried out in black 96-well plates (Sarstedt, Nümbrecht, Germany) in a TECAN infinite M200 plate reader (Tecan Group, Männedorf, Switzerland) equipped with an injection module. NADPH, NADH and mBFP holoenzyme fluorescence was recorded at an emission of 451 nm and excitation at 390 nm. For fluorescence kinetic measurements cells were harvested after overnight cultivation by centrifugation (4,000 rpm, 8 min, 4°C), washed twice with PBS (137 mM NaCl, 10 mM Na₂HPO₄, 1.8 mM NaH₂PO₄, pH 7.4) and suspended in PBS to an OD₆₀₀ of 1. Fluorescence kinetic measurements were performed using read intervals of 1–2 s and automatic injection of substrate (100 mM glucose final concentration) at indicated time points. For kinetic measurements of the effects of paraquat first glucose (final concentration 100 mM) was added after 30 s of pre-incubation to cells suspended in PBS and then at the indicated time point paraquat (8–16 mM final

concentration) was added. For analysis of mBFP fluorescence during cultivation of *C. glutamicum*, cultures were sampled after 2 h of cultivation, and the OD₆₀₀ of the sample set to 1 with CgXII minimal medium before the fluorescence was measured in the plate reader.

Fluorescence microscopy was performed with an Axio Observer Z1 microscope (Zeiss, Oberkochen, Germany) using Zen software. For the visualization of mBFP fluorescence, cells were cultivated and treated as described above for kinetic measurements; 2% (w/v) glucose (final concentration) were added immediately before immobilization on agarose pads (1% w/v of agarose in PBS). For detection of mBFP fluorescence the Zeiss filter set 49 (Excitation 365 nm, Emission 445/50 nm) was used. To analyze permeabilization of *E. coli* and *C. glutamicum* cell membranes by CTAB treatment, the LIVE/DEADTM BacLightTM Bacterial Viability Kit was used according to the manufacturer's instructions (Thermo Scientific, Waltham, MA, United States) and the AF microscope filter to analyze propidium iodide staining of the permeabilized cell (excitation at 545 \pm 30 nm, emission at 610 \pm 75 nm). Cells were cultivated and washed as described above for kinetic fluorescence measurements, CTAB was added to the washed cells at concentrations indicated in results 5 min prior before samples were analyzed by microscopy.

For *in situ* calibration of the sensor signals, cells were harvested and washed with PBS as described above for kinetic fluorescence measurements. The washed cells were transferred to black 96-well plates and 0.05% (w/v) CTAB (final concentration) were added. After 2 min of incubation at room temperature, NADPH at concentrations from 0.01 to 1 mM was added to the CTAB treated cells and subsequently fluorescence was measured at 395 and 451 nm for excitation and emission, respectively. Thereby obtained fluorescence values were plotted against the NADPH concentrations and the resulting calibration curve was then used for the quantification of the intracellular NADPH concentrations in the fluorescence kinetic measurements described above.

In vitro Characterization of mBFP

For purification of mBFP *E. coli* (pCN_mBFP) cells were cultivated in TB-medium (Hobbs and Tartoff, 1987) to an OD₆₀₀ of 12. Cells were harvested by centrifugation (20 min, 3,200 \times g, 4°C, Eppendorf 5804 R Centrifuge), washed twice with start buffer (50 mM KH₂PO₄, pH 7), suspended in start buffer, and disrupted using a Branson Sonifier 250 (Branson Ultrasonics, Danbury, CT, United States). Amplitude was set to 90%, cycle 0.5 and 10 times 30 s burst intervals with intermittent cooling on ice were performed. After removal of cell debris by centrifugation (16,000 \times g, 4°C, 15 min, Eppendorf 5804 R Centrifuge) the supernatant was centrifuged at 60,000 \times g, 4°C, 1 h (Beckmann XPN 100 ultracentrifuge) to remove the membrane fraction. The cytosolic fraction was diluted 1:3 with start buffer and applied to a HiScreen Capto Blue column (GE Healthcare) equilibrated with start buffer on an Äkta Purifier chromatography system (GE Healthcare). After washing the column with 40 mL start buffer to remove unspecific bound proteins, bound proteins were eluted using a gradient step with elution buffer (1.5 M KCl, 50 mM

KH₂PO₄, pH 7). Fractions were collected, screened by activity and fluorescence analysis, and analyzed by SDS-PAGE according to Laemmli (1970).

Thermoshift assays were done in a CFX96™ real-time PCR detection system (BioRad Laboratories, Hercules, CA, United States) using SYPRO orange fluorescent dye (Sigma Aldrich, St. Louis, MO, United States) as described (Niesen et al., 2007).

Fluorescence of the purified mBFP in absence and presence of NADPH was determined as described above in an TECAN infinite M200 plate reader at an emission of 451 nm and excitation at 390 nm.

Enzymatic activity of mBFP with different substrates and cofactors was determined using an Ultrospec 2100pro photometer (GE Healthcare). The reaction was performed at 30°C in phosphate buffer (0.4 g/L KH₂PO₄, 12.6 g/L K₂HPO₄, pH 8). NADPH and NADH were used in concentrations of 200 μM for the determination of benzaldehyde dependent activity (or other substrates, see **Supplementary Material**). Varying benzaldehyde concentrations were used for the determination of kinetic parameters (K_M , k_{cat}). Protein concentrations were determined with the Roti-Nanoquant kit (Carl Roth, Karlsruhe, Germany) using a BSA standard.

RESULTS AND DISCUSSION

The NADPH Sensor Protein mBFP Possesses Benzaldehyde Reductase Activity

Genetically encoded biosensors offer various opportunities for analysis of intracellular metabolites in microorganisms in the course of cultivation and the development of novel strain selection strategies (Eggeling et al., 2015; Cheng et al., 2018). Fluorescent proteins such as mBFP, whose fluorescent properties exclusively rely on the binding of the metabolite of interest, are good candidates for *in vivo* analytics. The metagenome derived blue fluorescent protein mBFP exhibits blue fluorescence upon binding of NADPH independently of the availability of oxygen (Hwang et al., 2012). mBFP was here produced with *E. coli* (pCN_mBFP), which carries the plasmid pCN_mBFP for constitutive high expression of mBFP in *E. coli* strains (Spaans et al., 2015). After cell growth, harvest and disruption the mBFP protein was purified from cell free extracts of *E. coli* (pCN_mBFP) to apparent homogeneity by affinity chromatography using a HiScreen Capto Blue column (**Supplementary Figure S1**). Previous studies on mBFP disregarded the possibility that mBFP may possess an enzymatic function (Polizzi et al., 2007; Buysschaert et al., 2013) albeit it shares high sequence similarities with other, well characterized, enzymatically active SDR (**Supplementary Figure S2**). We tested purified mBFP with different known substrates of SDRs thereby using either NADPH or NADH as coenzyme. Benzaldehyde in combination with NADPH as cofactor was found to be the preferred substrate of mBFP (**Supplementary Table S2**). Minor enzyme activities were also detected for mBFP with a series of different other aldehydes

as substrates (**Supplementary Table S2**), however, activities of mBFP with different substrates were detected exclusively with NADPH as a cofactor. Further analysis of mBFP activity with different amounts of the substrate benzaldehyde and the cofactor NADPH revealed saturation kinetics for both compounds. The activity data were fitted to Michaelis–Menten kinetics and resulted in a K_M value of 3.1 mM of mBFP for benzaldehyde (**Figure 1A**) and a k_{cat} of 4.5 1/s. Analysis of the mBFP activity data with different NADPH concentrations resulted in a K_M value of 41 μM for NADPH and a k_{cat} of 11.85 1/s (**Figure 1B**). With NADH as co-factor, no enzymatic activity of mBFP was detected. From these results, we conclude that mBFP is an active reductase with a preference for NADPH as cofactor.

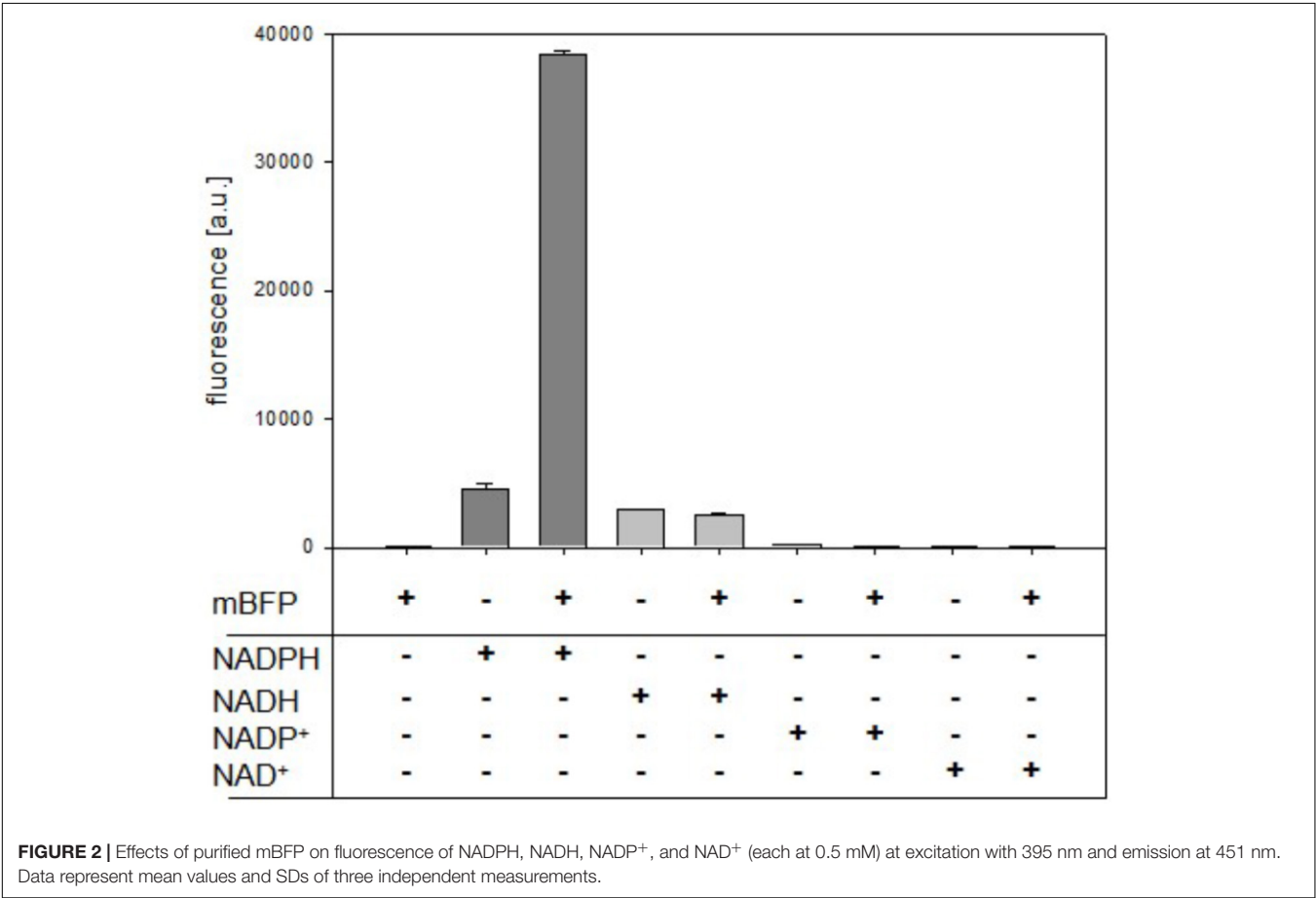
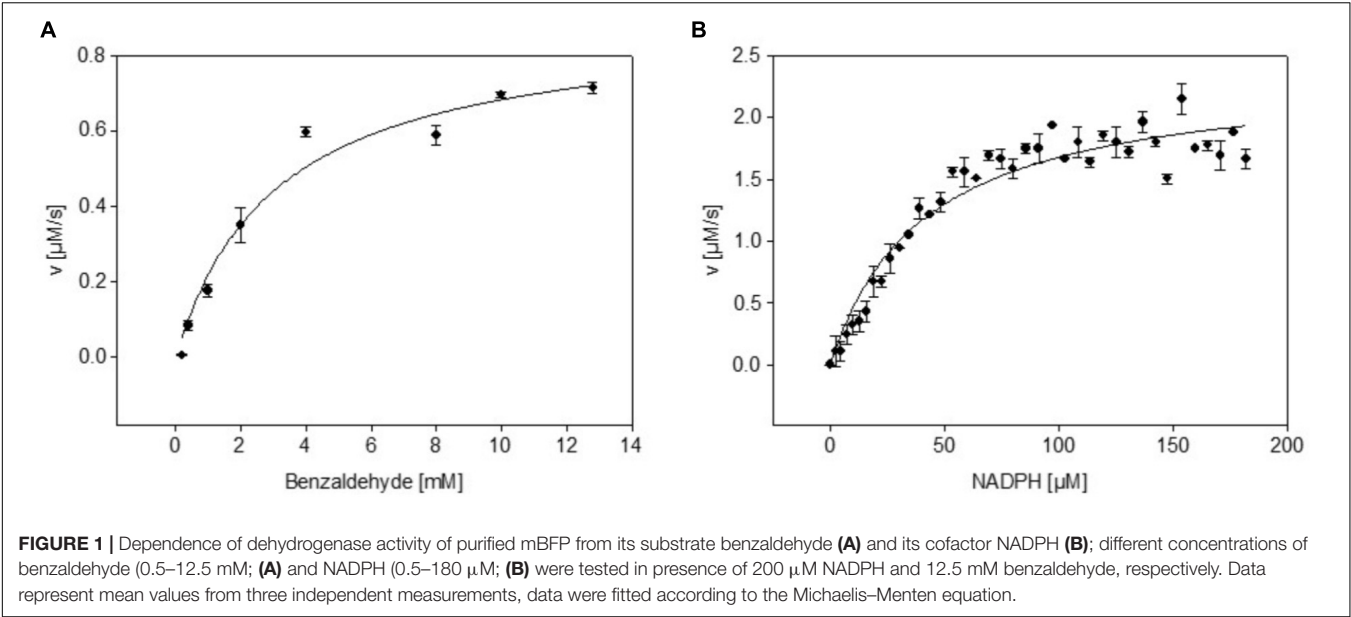
mBFP Exclusively Binds NADPH

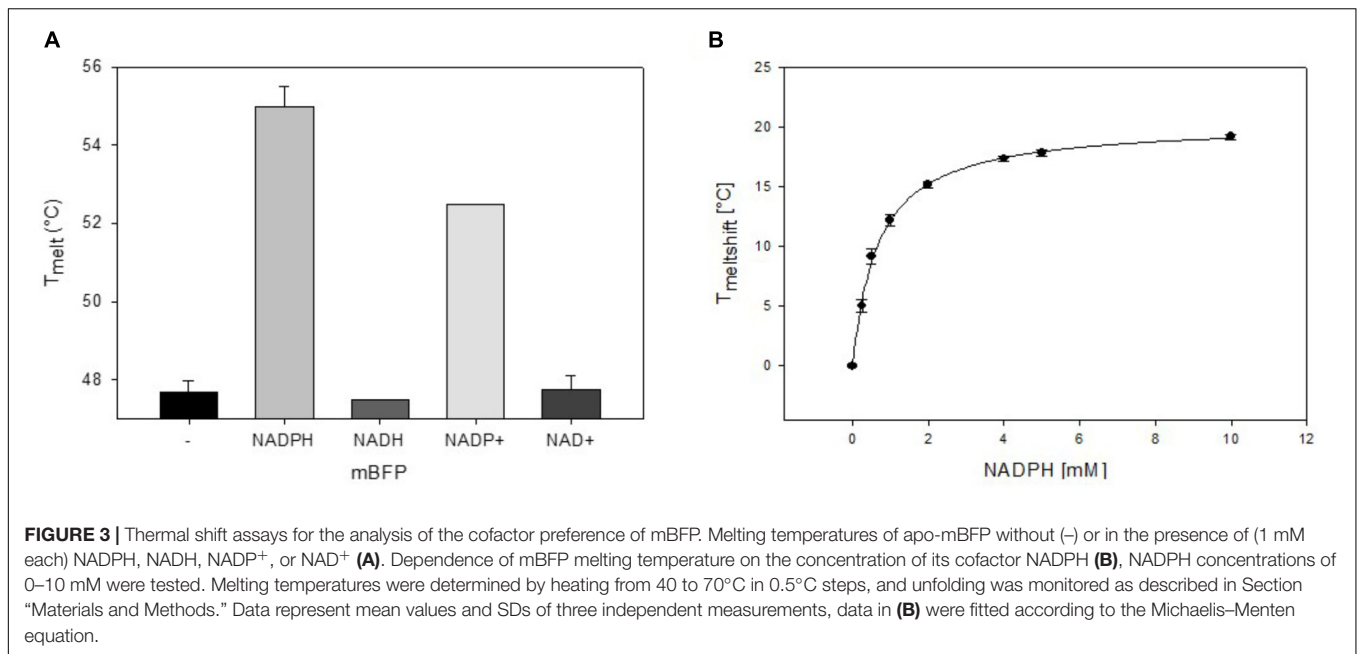
The quality of a metabolite sensor stands or falls with the specificity of the signal induced by the detected molecule. Noticeable, mBFP amplifies the intrinsic fluorescence of NADPH upon binding as it is described for other SDRs (Polizzi et al., 2007; Buysschaert et al., 2012). As expected purified mBFP apoenzyme shows no emission at 451 nm when excited at 395 nm, but its presence lead to an increase of the emission signal for 0.5 mM NADPH about 8.5 fold from $4,532 \pm 408$ (pure NADPH) to $38,402 \pm 277$ (NADPH + mBFP) (**Figure 2**). For NADH no amplification of its intrinsic fluorescence by addition of mBFP was detected (**Figure 2**), demonstrating the specificity of the mBFP for NADPH.

To analyze mBFPs affinity for different cofactors, thermal degradation assays (thermofluor) were performed. In these experiments binding of a cofactor leads to a shift in melting temperature (T_{Melt}) of the protein under investigation (Niesen et al., 2007). The T_{Melt} of 47.5°C determined for the mBFP apoenzyme was shifted to 55°C upon addition of 1 mM NADPH and 52°C upon addition of 1 mM NADP⁺ (**Figure 3A** and **Supplementary Figure S3A**), which implies a higher affinity of mBFP toward NADPH than NADP⁺. Binding of mBFP to NADPH and NADP is plausible as redox enzymes often catalyze reversible reactions. For further characterization, effects of different NADPH concentrations (0–10 mM) on T_{Melt} of mBFP were analyzed (**Figure 3B**). Non-linear regression of the resulting data revealed a saturation kinetics with a dissociation constant (K_D) of 0.64 mM (**Figure 3B** and **Supplementary Figure S3B**). Interestingly only presence of phosphorylated cofactors led to an increase in T_{Melt} of mBFP, whereas T_{Melt} determined in presence of the non-phosphorylated cofactors NADH (47°C) and NAD⁺ (47.5°C) were identical to T_{Melt} of the apoenzyme (**Figure 3A**). This result indicates that mBFP does not bind to NADH and NAD⁺. The broad dynamic range of fluorescence amplification in combination with the high specificity for NADPH makes mBFP a suitable candidate to be used as NADPH biosensor for *in vivo* applications.

Use of the Genetically Encoded NADPH Sensor mBFP in *C. glutamicum*

Large-scale microbial production of amino acids such as L-lysine heavily relies on efficient recycling of the cofactor





NADPH (Eggeling and Bott, 2015; Xu et al., 2018), which has therefore been a well-studied target for the engineering of *C. glutamicum* strains (Blombach and Seibold, 2010; Wang et al., 2016). For analysis of NADPH levels in *C. glutamicum* via mBFP as a genetically encoded sensor, the plasmid pKEEx2_mBFPopt was constructed. For this purpose, an mBFP gene was synthesized with codon-optimization for *C. glutamicum* and cloned into the plasmid pKEEx2. The sensor plasmid was introduced in *C. glutamicum* WT and the phosphoglucosyltransferase-deficient mutant strain *C. glutamicum* Δ pgi. Deletion of *pgi* results in the redirection of the carbon flux from glycolysis to the pentose-phosphate pathway, which brings about the generation of high NADPH concentrations in this strain (Marx et al., 2003). To analyze NADPH concentrations with the sensor mBFP, cells of *C. glutamicum* WT (pKEEx2_mBFPopt) and *C. glutamicum* Δ pgi (pKEEx2_mBFPopt) were cultivated in CgXII medium with 100 mM glucose as substrate, sampled after 4 h of cultivation, and their fluorescence analyzed in a plate reader. A significantly higher fluorescence of $2,125 \pm 551$ FLU/OD at excitation 395 nm with and emission at 451 nm was detected for *C. glutamicum* Δ pgi (pKEEx2_mBFPopt) when compared to *C. glutamicum* (pKEEx2_mBFPopt), for which a fluorescence of 613 ± 167 FLU/OD was determined.

Analyses of these cells by fluorescence microscopy revealed besides the overall increased fluorescence of *C. glutamicum* Δ pgi (pKEEx2_mBFPopt) when compared to *C. glutamicum* (pKEEx2_mBFPopt) that the fluorescence showed only minor cell-cell variations for each strain (Supplementary Figure S4). As for *C. glutamicum* Δ pgi an increased NADPH concentration is expected during cultivation with glucose when compared to *C. glutamicum* WT, the observed higher overall fluorescence for *C. glutamicum* Δ pgi (pKEEx2_mBFPopt) indicates that

by the use of mBFP NADPH levels can be monitored in *C. glutamicum*.

mBFP Enables Detection of Fast Alterations of NADPH Concentrations in *C. glutamicum* and *E. coli*

Current techniques for analyses of intracellular NADPH concentrations are mostly employed to study steady state levels but have a limited capacity for analyses of dynamic changes. However, the latter are the key for the understanding of sensing and adaptive mechanisms, drug modes of action, and homeostasis mechanisms (Zampieri et al., 2017). In bacteria, levels of metabolites often change upon perturbations within seconds (Chubukov et al., 2014; Wegner et al., 2015). These fast changes cannot be observed in real-time by the use of genetically encoded sensors requiring transcription and translation of a fluorescent reporter, but the properties of protein based sensors are matching this task (Liu et al., 2015; Lin et al., 2017). The protein sensor mBFP binds and enhances specifically the fluorescence of NADPH and was above shown to be suited for measurements of intracellular NADPH concentrations in *C. glutamicum*.

To test utilization of mBFP for the detection of fast changes of NADPH levels, the response to fast changes of nutrient availability was analyzed in *C. glutamicum* strains carrying mBFP. *C. glutamicum* WT (pKEEx2_mBFPopt) and *C. glutamicum* Δ pgi (pKEEx2_mBFPopt) were cultivated for 12 h in 2xTY complex medium with 1 mM IPTG to induce synthesis of mBFP. The derived nutrient-starved cells of *C. glutamicum* WT (pKEEx2_mBFPopt) and *C. glutamicum* Δ pgi (pKEEx2_mBFPopt) were washed twice with PBS, suspended in PBS and transferred into single wells of a 96-well plate.

Kinetic assays were performed in a Tecan M200 plate reader equipped with an injector module: mBFP fluorescence was read in 2 s intervals for 2 min and glucose was injected automatically into the wells after the first 15 s of the kinetic assay. As depicted in **Figure 4A**, a very fast increase of the mBFP fluorescence within 30–40 s after the addition of glucose to 658 FLU and 1,374 FLU can be seen for *C. glutamicum* WT (pEKEx2_mBFPopt) and *C. glutamicum* Δ pgi (pEKEx2_mBFPopt), respectively. As the addition of glucose and its metabolism via glycolysis and tricarboxylic acid cycle besides NADPH probably also causes formation of the redox intermediates NADH and FADH (Blombach and Seibold, 2010), which both also show fluorescence at an emission wavelength of 451 nm when excited at 390 nm, changes of fluorescence upon glucose addition were also analyzed for cells of the control strains *C. glutamicum* WT (pEKEx2) and *C. glutamicum* Δ pgi (pEKEx2). As depicted in **Supplementary Figure S5** the fluorescence increased after the addition of glucose from initially 14 FLU to 19 FLU and from 10 FLU to 50 FLU in *C. glutamicum* WT (pEKEx2) and *C. glutamicum* Δ pgi (pEKEx2), respectively. As fluorescence values obtained for the two mBFP carrying strains *C. glutamicum* WT (pEKEx2_mBFPopt) and *C. glutamicum* Δ pgi (pEKEx2_mBFPopt) are about 30 times higher than the fluorescence values measured for the mBFP-deficient control strain, the amplification of NADPH fluorescence by mBFP effectively masks the fluorescence derived from other redox intermediates such as NADH and FADH in the mBFP carrying strains.

For determination of intracellular NADPH concentrations we calibrated the sensor *in situ* in cells of *C. glutamicum* WT (pEKEx2_mBFPopt) and *C. glutamicum* Δ pgi (pEKEx2_mBFPopt), which were permeabilized by addition of 0.05% (w/v) of CTAB (final concentration). At this CTAB concentration small pores are formed in the membrane, which allow the fast diffusion of small molecules, however, the cell's superstructure remains intact (**Supplementary Figure S6**). As depicted in **Figure 4B**, different slopes were observed for the linear regression lines based NADPH dependent mBFP fluorescence of permeabilized cells of *C. glutamicum* WT (pEKEx2_mBFPopt) and *C. glutamicum* Δ pgi (pEKEx2_mBFPopt), which is probably brought about different levels of mBFP formed in course of the pre-cultivation. Based on the *in situ* calibration for *C. glutamicum* WT (pEKEx2_mBFPopt) an increase of the NADPH concentration from initially 0.127 to 0.185 mM after the addition of glucose was determined (**Figure 4C**). The initial NADPH concentration of 0.175 mM determined for starved cells of *C. glutamicum* Δ pgi (pEKEx2_mBFPopt) is higher than the initial concentration determined for *C. glutamicum* WT (pEKEx2_mBFPopt), and after glucose addition the NADPH concentration in *C. glutamicum* Δ pgi (pEKEx2_mBFPopt) increased up to 0.313 mM. The intracellular concentrations already reached within 1 min after the addition of the substrate in both *C. glutamicum* WT (pEKEx2_mBFPopt) and *C. glutamicum* Δ pgi (pEKEx2_mBFPopt) are in the same concentration range as the NADPH concentrations

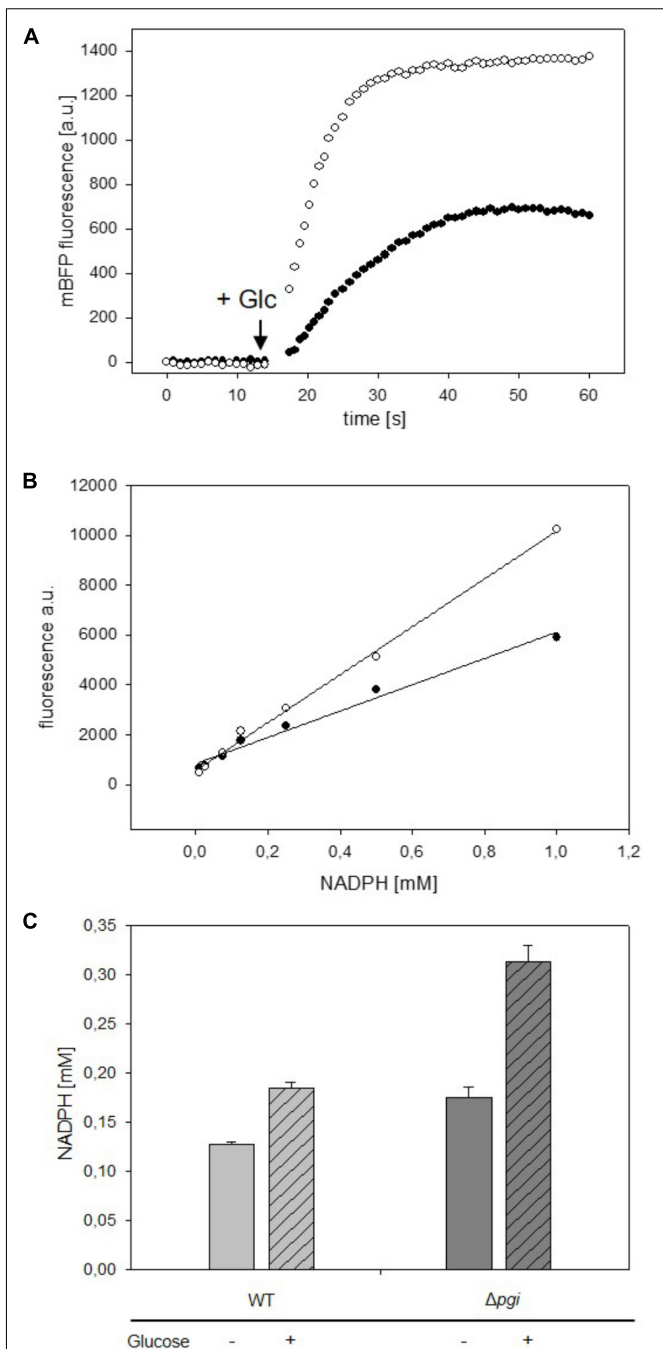


FIGURE 4 | Analyses of changes of mBFP fluorescence in starved cells of *C. glutamicum* WT (pEKEx2-mBFPopt) [filled circles] and *C. glutamicum* Δ pgi (pEKEx2-mBFPopt) [open circles] upon addition of the substrate glucose (indicated by the arrow) **(A)**. *In situ* calibration of mBFP derived signals by the use CTAB permeabilized cells from *C. glutamicum* WT (pEKEx2-mBFPopt) [filled circles] and *C. glutamicum* Δ pgi (pEKEx2-mBFPopt) [open circles] **(B)** in presence of different amounts of added NADPH. Steady state levels of intracellular NADPH concentrations calculated based on *in situ* calibrations in *C. glutamicum* WT (pEKEx2-mBFPopt) and *C. glutamicum* Δ pgi (pEKEx2-mBFPopt) before and after glucose addition **(C)**. For panels **(A,B)** one representative experiment of a series of three independent experiments is shown. Data in **(C)** represent mean values and SDs of three independent experiments.

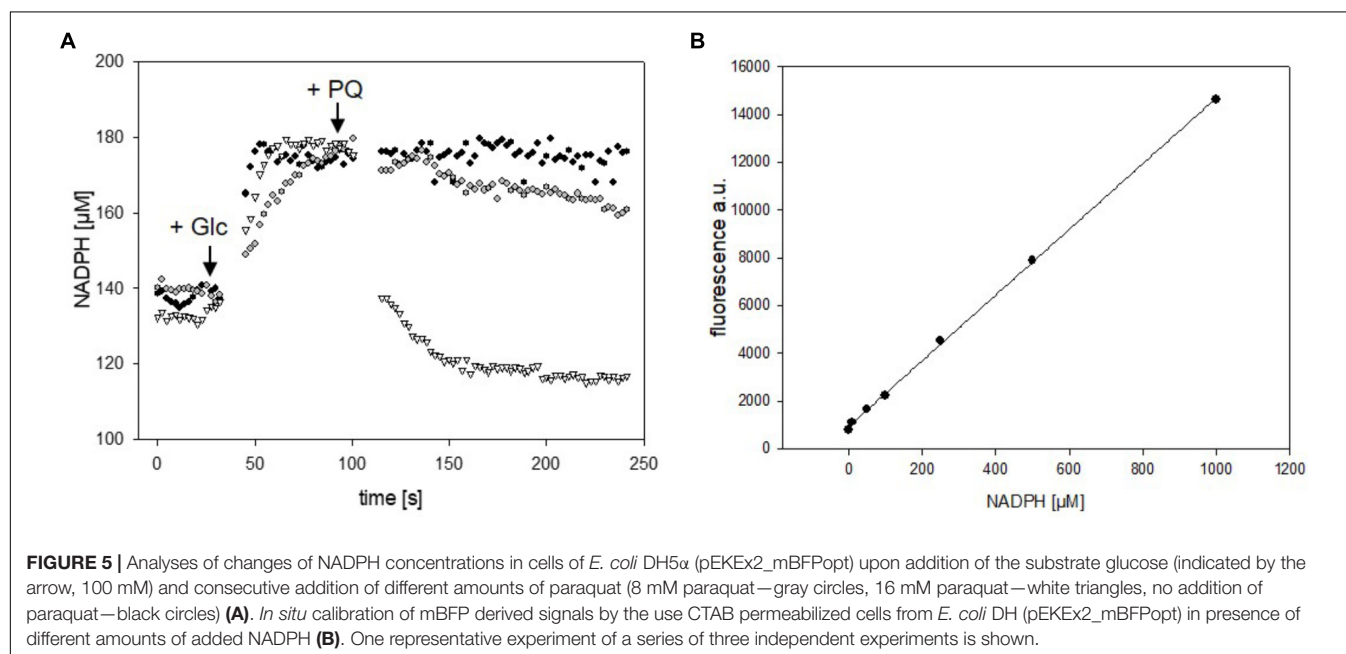
determined via metabolite extraction and subsequent HPLC-MS analyses for WT and Pgi-deficient *C. glutamicum* cells, respectively, in previous studies (Marx et al., 2003; Bartek et al., 2010).

Versatility of the mBFP-based method for observation of fast variations of NADPH concentrations was also tested in *E. coli* DH5 α (pEKEx2_mBFPopt). For this purpose, cells of *E. coli* DH5 α (pEKEx2_mBFPopt) cultivated in 2xTY medium and induced with 1 mM IPTG for 12 h were harvested by centrifugation and carefully washed with PBS. One aliquot of the washed *E. coli* DH5 α (pEKEx2_mBFPopt) cells was permeabilized by addition of 0.05% CTAB (**Supplementary Figure S7**) and then used for an *in situ* calibration of the mBFP sensor signal response to different NADPH concentrations (**Figure 5B**). Further aliquots of *E. coli* DH5 α (pEKEx2_mBFPopt) were transferred to wells of a 96-well plate and used for kinetic assays. Within 30 s upon addition of 100 mM glucose (final concentration) the intracellular NADPH concentration increased in *E. coli* DH5 α (pEKEx2_mBFPopt) from 140 to 180 μ M, which shows that in both *E. coli* and *C. glutamicum* NADPH accumulates fast in response to increases of nutrient availability. Protein based sensors like mBFP should also enable the observation of fast decreases in their analytes concentrations. Addition of paraquat initiates antioxidative mechanisms in *E. coli*, which lead to the depletion of the NADPH pool (Gu and Imlay, 2011). Indeed, upon addition of paraquat to glucose-fed cells of *E. coli* DH5 α (pEKEx2_mBFPopt) the intracellular NADPH concentrations decreased in dependence of the added paraquat concentration (**Figure 5A**). As expected addition of water did not lead to a change of the intracellular NADPH concentration in control experiments (**Figure 5A**). These results demonstrate the functionality of mBFP in two different hosts and show that it is highly suitable for the fast dynamic measurements of intracellular NADPH

concentrations required to understand redox mechanisms of cells.

CONCLUSION

mBFP was here shown to specifically bind to and amplify fluorescence of NADPH, which are essential prerequisites for its use as a genetically encoded biosensor for the analysis of intracellular NADPH concentrations. Plasmid encoded mBFP allowed to measure fast changes of NADPH concentrations in both *C. glutamicum* and *E. coli* strains and most importantly it allowed to analyze increases as well as decreases of NADPH concentrations in real time. It has to be denoted, that each use of mBFP requires calibration of the signals by permeabilization of the cell and incubation with different NADPH concentrations as the mBFP derived fluorescence signal depends both on the internal NADPH concentration as well as the amount of mBFP, which also varies. For short time intervals variations of mBFP amounts can be neglected but to monitor intracellular NADPH levels in the course of fermentations regular sampling to perform calibrations with permeabilized cells is probably necessary. The development of a ratiometric sensor based on mBFP will probably allow to easily monitor NADPH levels also during longtime experiments. The monitoring of NADPH levels in *C. glutamicum* and *E. coli* during cultivations is interesting as NADPH is the redox cofactor limiting production of bulk chemicals synthesized via anabolic pathways such as amino acids (Hirasawa and Shimizu, 2016; Xu et al., 2018), but for this purpose conventional, sampling dependent techniques can be easily employed (Liu et al., 2018). The general advantage of a genetically encoded metabolite sensors for NADPH like mBFP is the site specific analyses of metabolite concentrations, e.g., in to monitor compartment-specific transient changes of



intracellular balances of NADPH in eukaryotic cells (Ying, 2008; Wiederkehr and Demaurex, 2017). These measurements are currently performed via analyses of autofluorescence (Blacker et al., 2012; Blacker and Duchen, 2016), which unfortunately coincidences in the case of NADH and NADPH. The specificity of mBFP for NADPH over NADH, the masking of NADH fluorescence by the strong amplification of the NADPH fluorescence signal, and the possibility to monitor fast changes without sampling indicate that mBFP might be a suitable molecular tool for cell biologist. In its present state, the sensor protein mBFP is already well suited to observe fast changes of intracellular NADPH concentrations in bacteria, which provides a new insight into the kinetics of microbial metabolism.

AUTHOR CONTRIBUTIONS

GS and OG designed and coordinated the study. OG and AE carried out the experiments. GS, AE, and OG analyzed the results and wrote the manuscript.

REFERENCES

- Agledal, L., Niere, M., and Ziegler, M. (2010). The phosphate makes a difference: cellular functions of NADP. *Redox Rep.* 15, 2–10. doi: 10.1179/174329210X12650506623122
- Bartek, T., Blombach, B., Zonnchen, E., Makus, P., Lang, S., Eikmanns, B. J., et al. (2010). Importance of NADPH supply for improved L-valine formation in *Corynebacterium glutamicum*. *Biotechnol. Prog.* 26, 361–371. doi: 10.1002/btpr.345
- Becker, J., and Wittmann, C. (2015). Advanced biotechnology: metabolically engineered cells for the bio-based production of chemicals and fuels, materials, and health-care products. *Angew. Chem. Int. Ed. Engl.* 54, 3328–3350. doi: 10.1002/anie.201409033
- Blacker, T. S., and Duchen, M. R. (2016). Investigating mitochondrial redox state using NADH and NADPH autofluorescence. *Free Radic. Biol. Med.* 100, 53–65. doi: 10.1016/j.freeradbiomed.2016.08.010
- Blacker, T. S., Mann, Z. F., Gale, J. E., Ziegler, M., Bain, A. J., and Duchen, M. R. (2012). Separation of NADPH and NADH fluorescence emission in live cells using flim. *Biophys. J.* 102, 196a. doi: 10.1016/j.bpj.2011.11.1067
- Blacker, T. S., Mann, Z. F., Gale, J. E., Ziegler, M., Bain, A. J., Szabadkai, G., et al. (2014). Separating NADH and NADPH fluorescence in live cells and tissues using FLIM. *Nat. Commun.* 5:3936. doi: 10.1038/ncomms4936
- Blombach, B., and Seibold, G. M. (2010). Carbohydrate metabolism in *Corynebacterium glutamicum* and applications for the metabolic engineering of L-lysine production strains. *Appl. Microbiol. Biotechnol.* 86, 1313–1322. doi: 10.1007/s00253-010-2537-z
- Bolbat, A., and Schultz, C. (2017). Recent developments of genetically encoded optical sensors for cell biology. *Biol. Cell* 109, 1–23. doi: 10.1111/boc.2016.00040
- Buysschaert, G., Verstraete, K., Savvides, S. N., and Vergauwen, B. (2012). Crystallization of an atypical short-chain dehydrogenase from *Vibrio vulnificus* lacking the conserved catalytic tetrad. *Acta Crystallogr. Sect. F Struct. Biol. Cryst. Commun.* 68, 771–774. doi: 10.1107/S1744309112018672
- Buysschaert, G., Verstraete, K., Savvides, S. N., and Vergauwen, B. (2013). Structural and biochemical characterization of an atypical short-chain dehydrogenase/reductase reveals an unusual cofactor preference. *FEBS J.* 280, 1358–1370. doi: 10.1111/febs.12128
- Chemler, J. A., Fowler, Z. L., Mchugh, K. P., and Koffas, M. A. (2010). Improving NADPH availability for natural product biosynthesis in *Escherichia coli* by metabolic engineering. *Metab. Eng.* 12, 96–104. doi: 10.1016/j.ymben.2009.07.003
- Cheng, F., Tang, X. L., and Kardashliev, T. (2018). Transcription factor-based biosensors in high-throughput screening: advances and applications. *Biotechnol. J.* 13:e1700648. doi: 10.1002/biot.201700648
- Chubukov, V., Gerosa, L., Kochanowski, K., and Sauer, U. (2014). Coordination of microbial metabolism. *Nat. Rev. Microbiol.* 12, 327–340. doi: 10.1038/nrmicro3238
- Eggeling, L., and Bott, M. (2005). *Handbook of Corynebacterium glutamicum*. Boca Raton, FL: CRC Press. doi: 10.1201/9781420039696
- Eggeling, L., and Bott, M. (2015). A giant market and a powerful metabolism: L-lysine provided by *Corynebacterium glutamicum*. *Appl. Microbiol. Biotechnol.* 99, 3387–3394. doi: 10.1007/s00253-015-6508-2
- Eggeling, L., Bott, M., and Marienhagen, J. (2015). Novel screening methods—biosensors. *Curr. Opin. Biotechnol.* 35, 30–36. doi: 10.1016/j.copbio.2014.12.021
- Eikmanns, B. J., Kleinertz, E., Liebl, W., and Sahm, H. (1991). A family of *Corynebacterium glutamicum*/*Escherichia coli* shuttle vectors for cloning, controlled gene expression, and promoter probing. *Gene* 102, 93–98. doi: 10.1016/0378-1119(91)90545-M
- Gu, M., and Imlay, J. A. (2011). The SoxRS response of *Escherichia coli* is directly activated by redox-cycling drugs rather than by superoxide. *Mol. Microbiol.* 79, 1136–1150. doi: 10.1111/j.1365-2958.2010.07520.x
- Hanahan, D. (1983). Studies on transformation of *Escherichia coli* with plasmids. *J. Mol. Biol.* 166, 557–580. doi: 10.1016/S0022-2836(83)80284-8
- Hirasawa, T., and Shimizu, H. (2016). Recent advances in amino acid production by microbial cells. *Curr. Opin. Biotechnol.* 42, 133–146. doi: 10.1016/j.copbio.2016.04.017
- Hobbs, K. T. C., and Tartoff, K. (1987). Improved media for growing plasmid and cosmid clones. *Focus* 9, 9–12.
- Hwang, C. S., Choi, E. S., Han, S. S., and Kim, G. J. (2012). Screening of a highly soluble and oxygen-independent blue fluorescent protein from metagenome. *Biochem. Biophys. Res. Commun.* 419, 676–681. doi: 10.1016/j.bbrc.2012.02.075
- Kabus, A., Georgi, T., Wendisch, V. F., and Bott, M. (2007). Expression of the *Escherichia coli* pntAB genes encoding a membrane-bound transhydrogenase in *Corynebacterium glutamicum* improves L-lysine formation. *Appl. Microbiol. Biotechnol.* 75, 47–53. doi: 10.1007/s00253-006-0804-9
- Kocharin, K., Siewers, V., and Nielsen, J. (2013). Improved polyhydroxybutyrate production by *Saccharomyces cerevisiae* through the use of the phosphoketolase pathway. *Biotechnol. Bioeng.* 110, 2216–2224. doi: 10.1002/bit.24888
- Krömer, J. O., Bolten, C. J., Heinzle, E., Schröder, H., and Wittmann, C. (2008). Physiological response of *Corynebacterium glutamicum* to oxidative stress induced by deletion of the transcriptional repressor McbR. *Microbiology* 154, 3917–3930. doi: 10.1099/mic.0.2008/021204-0

FUNDING

We thank the German Ministry of Education and Research for financial funding in the frame of the e:Bio initiative (Contract No. 031A302D).

ACKNOWLEDGMENTS

We thank Bernhard Eikmanns and Reinhard Kärmer for continuous support. We are very grateful to Howard Salis for the generous gift of the plasmid pCN-mBFP (Addgene plasmid #63847).

SUPPLEMENTARY MATERIAL

The Supplementary Material for this article can be found online at: <https://www.frontiersin.org/articles/10.3389/fmicb.2018.02564/full#supplementary-material>

- Laemmli, U. K. (1970). Cleavage of structural proteins during the assembly of the head of bacteriophage T4. *Nature* 227, 680–685. doi: 10.1038/227680a0
- Lin, J.-L., Wagner, J. M., and Alper, H. S. (2017). Enabling tools for high-throughput detection of metabolites: metabolic engineering and directed evolution applications. *Biotechnol. Adv.* 35, 950–970. doi: 10.1016/j.biotechadv.2017.07.005
- Lindner, S. N., Petrov, D. P., Hagmann, C. T., Henrich, A., Krämer, R., Eikmanns, B. J., et al. (2013). Phosphotransferase system-mediated glucose uptake is repressed in phosphoglucose isomerase-deficient *Corynebacterium glutamicum* strains. *Appl. Environ. Microbiol.* 79, 2588–2595. doi: 10.1128/AEM.03231-12
- Liu, D., Evans, T., and Zhang, F. (2015). Applications and advances of metabolite biosensors for metabolic engineering. *Metab. Eng.* 31, 35–43. doi: 10.1016/j.ymben.2015.06.008
- Liu, J., Li, H., Zhao, G., Caiyin, Q., and Qiao, J. (2018). Redox cofactor engineering in industrial microorganisms: strategies, recent applications and future directions. *J. Ind. Microbiol. Biotechnol.* 45, 313–327. doi: 10.1007/s10295-018-2031-7
- Liu, Y., and Wang, M. (2017). Design, optimization and application of small molecule biosensor in metabolic engineering. *Front. Microbiol.* 8:2012. doi: 10.3389/fmicb.2017.02012
- Lu, W., Wang, L., Chen, L., Hui, S., and Rabinowitz, J. D. (2018). Extraction and quantitation of nicotinamide adenine dinucleotide redox cofactors. *Antioxid. Redox Signal.* 28, 167–179. doi: 10.1089/ars.2017.7014
- Mailloux, R. J., Lemire, J., and Appanna, V. D. (2011). Metabolic networks to combat oxidative stress in *Pseudomonas fluorescens*. *Antonie Van Leeuwenhoek* 99, 433–442. doi: 10.1007/s10482-010-9538-x
- Marx, A., De Graaf, A. A., Wiechert, W., Eggeling, L., and Sahm, H. (1996). Determination of the fluxes in the central metabolism of *Corynebacterium glutamicum* by nuclear magnetic resonance spectroscopy combined with metabolite balancing. *Biotechnol. Bioeng.* 49, 111–129. doi: 10.1002/(SICI)1097-0290(19961020)49:2<111::AID-BIT1>3.0.CO;2-T
- Marx, A., Hans, S., Mockel, B., Bathe, B., De Graaf, A. A., McCormack, A. C., et al. (2003). Metabolic phenotype of phosphoglucose isomerase mutants of *Corynebacterium glutamicum*. *J. Biotechnol.* 104, 185–197. doi: 10.1016/S0168-1656(03)00153-6
- Ng, C. Y., Farasat, I., Maranas, C. D., and Salis, H. M. (2015). Rational design of a synthetic entner-doudoroff pathway for improved and controllable NADPH regeneration. *Metab. Eng.* 29, 86–96. doi: 10.1016/j.ymben.2015.03.001
- Niesen, F. H., Berglund, H., and Vedadi, M. (2007). The use of differential scanning fluorimetry to detect ligand interactions that promote protein stability. *Nat. Protoc.* 2, 2212–2221.
- Polizzi, K. M., Moore, D. A., and Bommaris, A. S. (2007). A short-chain dehydrogenase/reductase from *Vibrio vulnificus* with both blue fluorescence and oxidoreductase activity. *Chem. Commun.* 18, 1843–1845.
- Sambrook, J., Russel, D. W., Irwin, N., and Janssen, U. A. (2001). *Molecular Cloning: A Laboratory Manual*. Cold Spring Harbor, NY: Cold Spring Harbor Laboratory Press.
- Sanchez, A. M., Andrews, J., Hussein, I., Bennett, G. N., and San, K. Y. (2006). Effect of overexpression of a soluble pyridine nucleotide transhydrogenase (UdhA) on the production of poly(3-hydroxybutyrate) in *Escherichia coli*. *Biotechnol. Prog.* 22, 420–425. doi: 10.1021/bp050375u
- Sauer, U., Canonaco, F., Heri, S., Perrenoud, A., and Fischer, E. (2004). The soluble and membrane-bound transhydrogenases UdhA and PntAB have divergent functions in NADPH metabolism of *Escherichia coli*. *J. Biol. Chem.* 279, 6613–6619. doi: 10.1074/jbc.M311657200
- Schallmeyer, M., Frunzke, J., Eggeling, L., and Marienhagen, J. (2014). Looking for the pick of the bunch: high-throughput screening of producing microorganisms with biosensors. *Curr. Opin. Biotechnol.* 26, 148–154. doi: 10.1016/j.copbio.2014.01.005
- Siedler, S., Schendzielorz, G., Binder, S., Eggeling, L., Bringer, S., and Bott, M. (2014). SoxR as a single-cell biosensor for NADPH-consuming enzymes in *Escherichia coli*. *ACS Synth. Biol.* 3, 41–47. doi: 10.1021/sb400110j
- Spaans, S. K., Weusthuis, R. A., Van Der Oost, J., and Kengen, S. W. (2015). NADPH-generating systems in bacteria and archaea. *Front. Microbiol.* 6:742. doi: 10.3389/fmicb.2015.00742
- Studier, F. W., and Moffatt, B. A. (1986). Use of bacteriophage T7 RNA polymerase to direct selective high-level expression of cloned genes. *J. Mol. Biol.* 189, 113–130. doi: 10.1016/0022-2836(86)90385-2
- Tao, R., Zhao, Y., Chu, H., Wang, A., Zhu, J., Chen, X., et al. (2017). Genetically encoded fluorescent sensors reveal dynamic regulation of NADPH metabolism. *Nat. Methods* 14, 720–728. doi: 10.1038/nmeth.4306
- Tauch, A., Kirchner, O., Löffler, B., Gotker, S., Pühler, A., and Kalinowski, J. (2002). Efficient electrotransformation of *Corynebacterium diphtheriae* with a mini-replicon derived from the *Corynebacterium glutamicum* plasmid pGA1. *Curr. Microbiol.* 45, 362–367. doi: 10.1007/s00284-002-3728-3
- Wang, C., Zhou, Z., Cai, H., Chen, Z., and Xu, H. (2017). Redirecting carbon flux through pgi-deficient and heterologous transhydrogenase toward efficient succinate production in *Corynebacterium glutamicum*. *J. Ind. Microbiol. Biotechnol.* 44, 1115–1126. doi: 10.1007/s10295-017-1933-0
- Wang, Z., Chan, S. H. J., Sudarsan, S., Blank, L. M., Jensen, P. R., and Solem, C. (2016). Elucidation of the regulatory role of the fructose operon reveals a novel target for enhancing the NADPH supply in *Corynebacterium glutamicum*. *Metab. Eng.* 38, 344–357. doi: 10.1016/j.ymben.2016.08.004
- Weckbecker, A., and Hummel, W. (2004). Improved synthesis of chiral alcohols with *Escherichia coli* cells co-expressing pyridine nucleotide transhydrogenase, NADP⁺-dependent alcohol dehydrogenase and NAD⁺-dependent formate dehydrogenase. *Biotechnol. Lett.* 26, 1739–1744. doi: 10.1007/s10529-004-3746-2
- Wegner, A., Meiser, J., Weindl, D., and Hiller, K. (2015). How metabolites modulate metabolic flux. *Curr. Opin. Biotechnol.* 34, 16–22. doi: 10.1016/j.copbio.2014.11.008
- Wiederkehr, A., and Demareux, N. (2017). Illuminating redox biology using NADH- and NADPH-specific sensors. *Nat. Methods* 14, 671–672. doi: 10.1038/nmeth.4336
- Xu, J.-Z., Yang, H.-K., and Zhang, W.-G. (2018). NADPH metabolism: a survey of its theoretical characteristics and manipulation strategies in amino acid biosynthesis. *Crit. Rev. Biotechnol.* 38, 1061–1076. doi: 10.1080/07388551.2018.1437387
- Ying, W. (2008). NAD⁺/NADH and NADP⁺/NADPH in cellular functions and cell death: regulation and biological consequences. *Antioxid. Redox Signal.* 10, 179–206. doi: 10.1089/ars.2007.1672
- Zampieri, M., Sekar, K., Zamboni, N., and Sauer, U. (2017). Frontiers of high-throughput metabolomics. *Curr. Opin. Chem. Biol.* 36, 15–23. doi: 10.1016/j.cbpa.2016.12.006
- Zhao, C., Zhao, Q., Li, Y., and Zhang, Y. (2017). Engineering redox homeostasis to develop efficient alcohol-producing microbial cell factories. *Microb. Cell Fact.* 16:115. doi: 10.1186/s12934-017-0728-3
- Zhao, Y., Hu, Q., Cheng, F., Su, N., Wang, A., Zou, Y., et al. (2015). SoNar, a highly responsive NAD⁺/NADH sensor, allows high-throughput metabolic screening of anti-tumor agents. *Cell Metab.* 21, 777–789. doi: 10.1016/j.cmet.2015.04.009
- Zhao, Y., Wang, A., Zou, Y., Su, N., Loscalzo, J., and Yang, Y. (2016). In vivo monitoring of cellular energy metabolism using SoNar, a highly responsive sensor for NAD⁺/NADH redox state. *Nat. Protoc.* 11, 1345–1359. doi: 10.1038/nprot.2016.074

Conflict of Interest Statement: The authors declare that the research was conducted in the absence of any commercial or financial relationships that could be construed as a potential conflict of interest.

Copyright © 2018 Goldbeck, Eck and Seibold. This is an open-access article distributed under the terms of the Creative Commons Attribution License (CC BY). The use, distribution or reproduction in other forums is permitted, provided the original author(s) and the copyright owner(s) are credited and that the original publication in this journal is cited, in accordance with accepted academic practice. No use, distribution or reproduction is permitted which does not comply with these terms.



Efficient Production of the Dicarboxylic Acid Glutarate by *Corynebacterium glutamicum* via a Novel Synthetic Pathway

Fernando Pérez-García¹, João M. P. Jorge^{1†}, Annika Dreyszas¹, Joe Max Risse² and Volker F. Wendisch^{1*}

¹ Chair of Genetics of Prokaryotes, Faculty of Biology and CeBiTec, Bielefeld University, Bielefeld, Germany, ² Fermentation Technology, Technical Faculty and CeBiTec, Bielefeld University, Bielefeld, Germany

OPEN ACCESS

Edited by:

Dirk Tischler,
Ruhr-Universität Bochum, Germany

Reviewed by:

Stefan Junne,
Technische Universität Berlin,
Germany
Dae-Hee Lee,
Korea Research Institute
of Bioscience and Biotechnology
(KRIBB), South Korea

*Correspondence:

Volker F. Wendisch
volker.wendisch@uni-bielefeld.de

† Present address:

João M. P. Jorge,
Instituto de Investigação e Inovação
em Saúde, Universidade do Porto,
Porto, Portugal

Specialty section:

This article was submitted to
Microbial Physiology and Metabolism,
a section of the journal
Frontiers in Microbiology

Received: 21 August 2018

Accepted: 10 October 2018

Published: 30 October 2018

Citation:

Pérez-García F, Jorge JMP, Dreyszas A, Risse JM and Wendisch VF (2018) Efficient Production of the Dicarboxylic Acid Glutarate by *Corynebacterium glutamicum* via a Novel Synthetic Pathway. *Front. Microbiol.* 9:2589. doi: 10.3389/fmicb.2018.02589

The dicarboxylic acid glutarate is an important building-block gaining interest in the chemical and pharmaceutical industry. Here, a synthetic pathway for fermentative production of glutarate by the actinobacterium *Corynebacterium glutamicum* has been developed. The pathway does not require molecular oxygen and operates via lysine decarboxylase followed by two transamination and two NAD-dependent oxidation reactions. Using a genome-streamlined L-lysine producing strain as basis, metabolic engineering was performed to enable conversion of L-lysine to glutarate in a five-step synthetic pathway comprising lysine decarboxylase, putrescine transaminase and γ -aminobutyraldehyde dehydrogenase from *Escherichia coli* and GABA/5AVA amino transferase and succinate/glutarate semialdehyde dehydrogenase either from *C. glutamicum* or from three *Pseudomonas* species. Loss of carbon via formation of the by-products cadaverine and N-acetylcadaverine was avoided by deletion of the respective acetylase and export genes. As the two transamination reactions in the synthetic glutarate biosynthesis pathway yield L-glutamate, biosynthesis of L-glutamate by glutamate dehydrogenase was expected to be obsolete and, indeed, deletion of its gene *gdh* increased glutarate titers by 10%. Glutarate production by the final strain was tested in bioreactors ($n = 2$) in order to investigate stability and reliability of the process. The most efficient glutarate production from glucose was achieved by fed-batch fermentation ($n = 1$) with a volumetric productivity of $0.32 \text{ g L}^{-1} \text{ h}^{-1}$, an overall yield of 0.17 g g^{-1} and a titer of 25 g L^{-1} .

Keywords: lysine, cadaverine, 5-aminovalerate, glutarate, *Corynebacterium glutamicum*, *Escherichia coli*, *Pseudomonas*, fed-batch

INTRODUCTION

With an expected global market of 6.1 million tons in 2021, bio-based plastic is in the spotlight as suitable and environmental-friendly alternative to petro-based plastic¹. Polyamides (also called nylons) are important plastics well known for fiber applications. Polyamides can be produced by ring-opening polycondensation of lactams as well as via condensation of dicarboxylic acids with diamines (Shen et al., 2010). For instance, condensation of the diamine putrescine with the

¹ www.european-bioplastics.org/market

dicarboxylate sebacic acid yields the polyamide Nylon-4,10 (Shen et al., 2010). In general, aliphatic dicarboxylic acids such as succinate, glutarate, adipate, pimelate, and sebacate are important monomeric building blocks for production of polymers such as polyamides, but also polyurethanes and polycarbonates (Jambunathan and Zhang, 2014; Chung et al., 2015; Gobin et al., 2015). Glutarate is a C5 dicarboxylic acid and a building block in the chemical industry. For example, hydrogenation of glutarate yields 1,5-pentanediol, which is a plasticizer and precursor of polyesters (Mishra et al., 2013). With respect to polyamides, copolymerization of glutarate with the diamine putrescine yields nylon-4,5 and its copolymerization with the diamine cadaverine yields nylon-5,5 (Park et al., 2013; Wang et al., 2017).

Chemically, the most common way to synthesize glutarate involves ring-opening of butyrolactone with potassium cyanide and hydrolysis (Vafaezadeh and Hashemi, 2016). However, due to the cost and the environmental impact of these chemical methods it is desirable to establish an effective bio-based glutarate synthesis. Microbial production of glutarate was achieved but not optimized in *Escherichia coli* by using the L-lysine degradation pathway or 5-aminovalerate (5AVA) pathway from *Pseudomonas putida* KT2440 (Adkins et al., 2013; Park et al., 2013), and in *Corynebacterium glutamicum* glutarate was synthesized as a by-product of a 5AVA production process (Rohles et al., 2016). *P. putida* converts L-lysine to glutarate, which is then catabolized via the tricarboxylic acid cycle (TCA). Lysine monooxygenase (DavB) and 5-aminovaleramidase (DavA) convert L-lysine to 5AVA (Adkins et al., 2013). Next, the intermediate 5AVA is transaminated to glutarate semialdehyde by GABA/5AVA aminotransferase (GabT), which subsequently is oxidized to glutarate by succinate/glutarate semialdehyde dehydrogenase (GabD). Independently, an alternative pathway for the production of 5AVA from L-lysine has been described and established for *C. glutamicum* (Jorge et al., 2017b). In this pathway, L-lysine decarboxylase, putrescine transaminase and γ -aminobutyraldehyde dehydrogenase from *E. coli* catabolize L-lysine to 5AVA without the requirement for molecular oxygen (Jorge et al., 2017b).

Since glutarate production initiates with L-lysine it is desirable to use L-lysine overproducing strains as basis for efficient glutarate production. Since decades *C. glutamicum* is used industrially for fermentative production of L-lysine, a process operated at a scale of 2.4 million tons L-lysine produced annually (Lee and Wendisch, 2017). Rational metabolic engineering and genome reduction of *C. glutamicum* has been applied enhancing L-lysine productivity and/or yield (Becker et al., 2011; Baumgart et al., 2013; Pérez-García et al., 2016). The resulting L-lysine producers have proven to be suitable base strains for the production of L-lysine-derived chemicals such as cadaverine, L-pipecolic acid and 5AVA (Kind et al., 2014; Jorge et al., 2017b; Pérez-García et al., 2017a). In this way, the *C. glutamicum* strain GRLys1 was chosen as initial platform for the production of glutarate here. GRLys1, also called DM1933 Δ CGP123 (Unthan et al., 2015), is a L-lysine producer which carries several genome modifications allowing L-lysine overproduction from glucose with a product yield of 0.20 – 0.25 g g⁻¹ (Pérez-García et al., 2016).

In this work, the dicarboxylic acid glutarate was produced from L-lysine by heterologous expression of the “cadaverine” pathway for the synthesis of 5AVA in combination with different *gabTD* operons, one from *C. glutamicum* and three from *Pseudomonas* species. Production was optimized by reducing formation of by-products and by enhancing glucose consumption. Additionally, in order to couple glutarate overproduction with biosynthesis of L-glutamate *gdh* coding for glutamate dehydrogenase was deleted, thus, the resulting strain required transamination reactions of glutarate overproduction yielding L-glutamate to compensate for the absence of glutamate dehydrogenase (Figure 1). Finally, glutarate overproduction was tested in a glucose-based fed-batch fermentation.

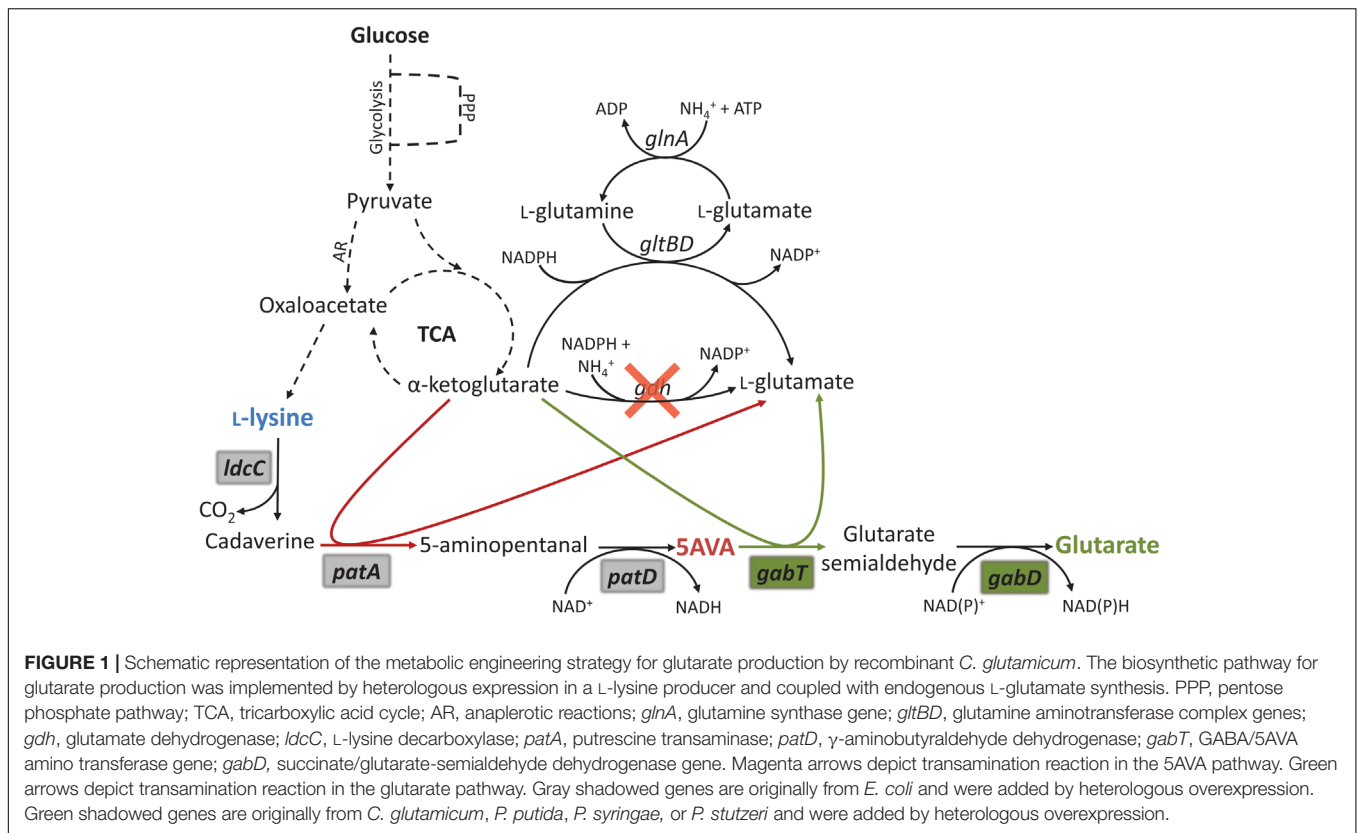
MATERIALS AND METHODS

Bacterial Strains, Vectors and Growth Conditions

Corynebacterium glutamicum and *Escherichia coli* strains and plasmids used in this work are listed in Table 1. The primers used were obtained from Metabion (Planegg/Steinkirchen, Germany) and they are listed in Table 2. *E. coli* DH5 α was routinely cultivated in LB medium or on LB agar plates at 37°C. *C. glutamicum* strains were routinely precultivated in brain heart infusion (BHI, ROTH®) plates or liquid medium overnight at 30°C. For *C. glutamicum* main cultures CGXII medium (Eggeling and Bott, 2005) was inoculated to an OD₆₀₀ of 1 and with glucose as sole-carbon source at the concentration of 4% (w/v). For the determination of the amino acids and glutarate production, samples were withdrawn from the cultures when glucose was depleted. When needed, kanamycin, tetracycline and/or spectinomycin were used at a concentration of 25, 25 and 100 μ g/mL respectively.

Molecular Biology Techniques

E. coli DH5 α was used as host for gene cloning. Transformation of *E. coli* was performed by heat shock at 42°C for 90 s following the rubidium chloride method (Hanahan, 1983), while *C. glutamicum* was transformed by electroporation at 2.5 kV, 200 Ω , and 25 μ F (Eggeling and Bott, 2005). The pair of primers AG01/AG02 and AG03/AG04 were used to amplified *gabT* and *gabD* respectively from genomic DNA of *C. glutamicum* ATCC 13032. The pair of primers AG05/AG06 and AG07/AG08 were used to amplified *gabT* and *gabD* respectively from genomic DNA of *P. putida* KT2440. The pair of primers AG09/AG10 and AG11/AG12 were used to amplified *gabT* and *gabD* respectively from genomic DNA of *Pseudomonas stutzeri* ATCC 17588. The pair of primers AG13/AG14 and AG15/AG16 were used to amplified *gabT* and *gabD* respectively from genomic DNA of *Pseudomonas syringae* DSM 50281. The *gabTD* operons were cloned by Gibson assembly (Gibson, 2011) into the vector pECXT99A (Kirchner and Tauch, 2003) digested with BamHI, yielding the vectors pECXT99A-*gabTD*^{Cg}, pECXT99A-*gabTD*^{Ppu}, pECXT99A-*gabTD*^{Pstu}, and pECXT99A-*gabTD*^{Psy}. Positive clones were verified by colony PCR using the pair of primers



X1FW/X1RV. The up- and downstream regions of the *gdh* gene were amplified by PCR from genomic DNA of *C. glutamicum* ATCC 13032 using the pair of primers GDHA/GDHB and GDHC/GDHD. The up and down PCR fragments were fused by cross-over PCR with primer pair GDHA/GDHD and cloned by ligation (Eggeling and Bott, 2005) into the vector pK19mobsacB (Schäfer et al., 1994) digested with SmaI. Positive clones were verified by colony PCR using the pair of primers 196F/197R. The resulting vector pK19mobsacB-*gdh* was transferred to *E. coli* S17-1. In-frame deletion of the *sugR*, *ldhA*, *snaA*, *cgmA*, and *gdh* genes from *C. glutamicum* was performed via a two-step homologous recombination method (Eggeling and Bott, 2005). All the pK19mobsacB vectors were transferred to *C. glutamicum* strains via conjugation using *E. coli* S17-1 (Simon et al., 1983). The deletions of *sugR*, *ldhA*, *snaA*, *cgmA*, and *gdh* were verified by colony PCR using the pair of primers SUGE/SUGE, LDHE/LDHE, SNAE/SNAE, CGME/CGME, and GDHE/GDHE respectively.

Transcriptome Analysis

To understand the genome expression response due to the addition of glutarate to the growth medium, *C. glutamicum* wild-type was grown in minimal medium with 4% (w/v) glucose and either 200 mM glutarate or 200 mM sodium chloride. Exponentially growing cells were harvested by centrifugation (4000 × g, 10 min, 4°C) and kept at −80°C. RNA isolation was performed as described (Wendisch, 2003) and the RNA was kept at −80°C until further use. DNA microarray analysis, synthesis

of fluorescently labeled cDNA from total RNA, DNA microarray hybridization, and gene expression analysis were performed as described previously (Netzer et al., 2004; Polen et al., 2007). The data are available as Gene Expression Omnibus GSE117175 data set at <http://www.ncbi.nlm.nih.gov/geo/>.

Enzymatic Assay for GabT and GabD

The apparent activities of GABA/5AVA transaminase GabT and succinate/glutarate semialdehyde oxidoreductase GabD were assayed together (NAD(P)H formation when started with GABA or 5AVA. The pellet from a 50 mL BHI culture in exponential phase was washed in 20 mL 50 mM phosphate buffer pH 7.0, centrifuged for 10 min at 4000 rpm and 4°C, resuspended in 1 mL of lysis buffer (50 mM phosphate buffer pH 7.0 with 9% glycerol and 1 mM DTT), and disrupted by sonication (10 min, cycle 0.5, amplitude of 55%, on ice). Centrifugation was done for 1 h at 14000 rpm and 4°C to remove cells debris and the supernatant was used for measuring apparent enzyme activities. The 1 mL assay mixture contained 150 mM phosphate buffer (pH 7.0 or pH 9.0), 15 mM α-ketoglutarate, 0.1 mM pyridoxal 5'-phosphate, 1 mM NAD⁺ or NADP⁺, 20 mM 5AVA or GABA and 0.5 mg/mL of proteins (crude extract). Protein concentrations were determined with the Bradford assay kit (Bio-Rad Laboratories, Hercules, CA, United States) using BSA (bovine serum albumin) as standard. The formation of NADH or NADPH was monitored photometrically at 340 nm and 30°C for 3 min using a Shimadzu UV-1202 spectrophotometer (Shimadzu, Duisburg, Germany).

TABLE 1 | Strains and plasmids used in this work.

Strains and plasmids	Description	Source
Strains		
GRLys1	<i>C. glutamicum</i> ATCC13032 with the following modifications: Δpck , pyc^{P458S} , hom^{Y59A} , 2 copies of $lysC^{T311I}$, 2 copies of asd , 2 copies of $dapA$, 2 copies of $dapB$, 2 copies of ddh , 2 copies of $lysA$, 2 copies of $lysE$, in-frame deletion of prophages CGP1 (cg1507-cg1524), CGP2 (cg1746-cg1752) and CGP3 (cg1890-cg2071). Also called DM1933 Δ CGP123.	Unthan et al., 2015
GRLys1 Δ sugR Δ ldhA Δ snaA Δ cgmA	In-frame deletion of <i>sugR</i> (cg2115), <i>ldhA</i> (cg3219), <i>snaA</i> (cg1722) and <i>cgmA</i> (cg2893) in GRLys1	This work
GRLys1 Δ sugR Δ ldhA Δ snaA Δ cgmA Δ gdh	In-frame deletion of <i>sugR</i> (cg2115), <i>ldhA</i> (cg3219), <i>snaA</i> (cg1722), <i>cgmA</i> (cg2893), and <i>gdh</i> (cg2280) in GRLys1	This work
<i>E. coli</i> DH5 α	F [−] <i>thi-1 endA1 hsdR17</i> (r [−] , m [−]) <i>supE44 ΔlacU169</i> (Φ 80 <i>lacZ</i> Δ M15) <i>recA1 gyrA96 relA1</i>	Hanahan, 1983
<i>E. coli</i> S17-1	<i>recA</i> , <i>thi</i> , <i>pro</i> , <i>hsd</i> R–M+ (RP4: 2–Tc:Mu–:Km, integrated into the chromosome)	Simon et al., 1983
Plasmids		
pECXT99A	Tet ^R , <i>E. coli</i> / <i>C. glutamicum</i> shuttle vector for regulated gene expression (Ptrc, <i>lacI</i> , pGA1 <i>oriVc_G</i>)	Kirchner and Tauch, 2003
pECXT99A- <i>gabTD</i> ^{Cg}	pECXT99A derivative for the IPTG-inducible expression of <i>gabTD</i> operon from <i>C. glutamicum</i> ATCC 13032	This work
pECXT99A- <i>gabTD</i> ^{Ppu}	pECXT99A derivative for the IPTG-inducible expression of <i>gabTD</i> operon from <i>Pseudomonas putida</i> KT2440	This work
pECXT99A- <i>gabTD</i> ^{Psy}	pECXT99A derivative for the IPTG-inducible expression of <i>gabTD</i> operon from <i>Pseudomonas syringae</i> DSM 50281	This work
pECXT99A- <i>gabTD</i> ^{Pstu}	pECXT99A derivative for the IPTG-inducible expression of <i>gabTD</i> operon from <i>Pseudomonas stutzeri</i> ATCC 17588	This work
pVWEx1- <i>ldcC</i>	pVWEx1 derivative for IPTG-inducible expression of <i>ldcC</i> from <i>E. coli</i> MG1655	Jorge et al., 2016
pEKEx3- <i>patDA</i>	pEKEx3 derivative for IPTG-inducible expression of <i>patD</i> and <i>patA</i> from <i>E. coli</i> MG1655	Jorge et al., 2016
pK19 <i>mobsacB</i>	Km ^R ; <i>E. coli</i> / <i>C. glutamicum</i> shuttle vector for construction of insertion and deletion mutants in <i>C. glutamicum</i> (pK18 <i>oriVEc sacB lacZα</i>)	Schäfer et al., 1994
pK19 <i>mobsacB</i> - Δ sugR	pK19 <i>mobsacB</i> with a <i>sugR</i> (cg2115) deletion construct	Engels and Wendisch, 2007
pK19 <i>mobsacB</i> - Δ ldhA	pK19 <i>mobsacB</i> with a <i>ldhA</i> (cg3219) deletion construct	Blombach et al., 2011
pK19 <i>mobsacB</i> - Δ snaA	pK19 <i>mobsacB</i> with a <i>snaA</i> (cg1722) deletion construct	Nguyen et al., 2015
pK19 <i>mobsacB</i> - Δ cgmA	pK19 <i>mobsacB</i> with a <i>cgmA</i> (cg2893) deletion construct	Jorge et al., 2017a
pK19 <i>mobsacB</i> - Δ gdh	pK19 <i>mobsacB</i> with a <i>gdh</i> (cg2280) deletion construct	This work

Quantitation of Carbohydrates, Organic Acids and Amino Acids by HPLC

For the quantification of extracellular carbohydrates, organic acids and amino acids a high-pressure liquid chromatography system was used (1200 series, Agilent Technologies Deutschland GmbH, Böblingen, Germany). 1 mL cell cultures were centrifuged at 14000 rpm for 10 min and the supernatant were used for analysis or stored at −20°C. The quantification of carbohydrates and organic acids was done using a column for organic acids (300 × 8 mm, 10 μm particle size, 25 Å pore diameter, CS Chromatographie Service GmbH) and detected by a refractive index detector (RID G1362A, 1200 series, Agilent Technologies) and a diode array detector (DAD G1315B, 1200 series, Agilent Technologies) (Schneider et al., 2011). For the detection of amino acids and the diamine cadaverine, the samples were derivatized with OPA (ortho-phthaldialdehyde) and separated with a spherical silica sorbent column [LiChrospher 100 RP18 EC-5 μ (125 × 4 mm), CS Chromatographie Service GmbH]. Detection then was performed by a fluorescence

detector (FLD G1321A, 1200 series, Agilent Technologies) (Schneider et al., 2011).

Glucose-Based Fed-Batch Fermentation

A baffled bioreactor with total a volume of 3.6 L was used (KLF, Bioengineering AG, Switzerland). Three six-bladed rushton turbines were placed in the stirrer axis with a distance from the bottom of the reactor of 6, 12, and 18 cm. The aspect ratio of the reactor was 2.6:1.0 and the stirrer to reactor diameter ratio was 0.39. Automatic control of the stirrer speed kept the relative dissolved oxygen saturation at 30%. 2. The feeding started when the pO2 value raised from 30 to 60% for the first time. A pH of 7.0 was established and controlled by automatic addition of phosphoric acid (10% (w/w)) and potassium hydroxide (4 M). The temperature was maintained constant at 30°C. The fermentation was performed under head space overpressure conditions at 0.4 bar. A constant 2.0 NL min^{−1} of air/O2 flow with the ratio 5:1 was applied from the top of the bioreactor, preventing foaming and, therefore, antifoam was not needed.

TABLE 2 | List of primers used in this work.

Name	Sequence (5' -> 3')
AG01	CATGGAATTCGAGCTCGGTACCCGGGAAAGGAGGCCCTTCAG ATGGAAGATCTCTCATACCGC
AG02	GGGGCGTTTCAATTAGCCACCTTCTGGTGCGC
AG03	GAAGGTGGGCTAATTCGAACGCCCGAAAGGAGGCCCTTCAGA TGCTTTTGACCTTCCAGTAATC
AG04	GCCTGCAGGTCGACTCTAGAGGATCTCACGGCAAAGCGAGGT AACG
AG05	CATGGAATTCGAGCTCGGTACCCGGGAAAGGAGGCCCTTCAG ATGAGCAAAACCAACGAATCC
AG06	GGGGCGTTTCAATCAGCGGATTTCAGCGAAGCAC
AG07	TGAAATCGCCTGATTTCGAACGCCCGAAAGGAGGCCCTTCAGAT GCAGCTCAAAGACGCTCAG
AG08	GCCTGCAGGTCGACTCTAGAGGATCTCAGACGCTGATGCACAGG
AG09	CATGGAATTCGAGCTCGGTACCCGGGAAAGGAGGCCCTTCAGA TGAGCAAGACCAACGAATCC
AG10	GGGGCGTTTCAATCAGGTCAGCTCGTCAAACAC
AG11	CGAGCTGACCTGATTTCGAACGCCCGAAAGGAGGCCCTTCAGAT GACTCTGCAACTTGGGCAAC
AG12	GCCTGCAGGTCGACTCTAGAGGATCTCAGATGCCGCCAGG CACAG
AG13	CATGGAATTCGAGCTCGGTACCCGGGAAAGGAGGCCCTTCAGA TGAGCAAGACTAACAATCC
AG14	GGGGCGTTTCAATTACGCGATTTCAGCAAAGC
AG15	TGAAATCGCGTAATTCGAACGCCCGAAAGGAGGCCCTTCAGA TGCAGCTCAAAGATTCCACAC
AG16	GCCTGCAGGTCGACTCTAGAGGATCTCAGACCGACAGGCAGAGG
X1FW	CATCATAACGGTTCTGGC
X1RV	ATCTTCTCTCATCGCCA
GDHA	AAAACCCGGGCTTCATGCAGTTACCGCG
GDHB	CCCATCCACTAACTTAAACACTGCTCATCAACTGTCTAT
GDHC	TGTTTAAAGTTAGTGATGGGGTAGCTGACGCGATGCTGGCACAG GGCGTCACTAA
GDHD	AAAACCCGGGCTGCTTTAGAGCAAGCG
GDHE	CGGTGCGCCAATTGAGGAGTGG
GDHF	CAGGTTACGCGATAGCAACAG
196F	CGCCAGGGTTTTCCAGTCAAGAC
197R	AGCGGATAACAATTCACACAGGA
SUGE	GTTCTGTCGCGGCAATGATTGACG
SUGF	CTCACCACATCCACAACCACGCG
LDHE	TGATGGCACCAGTTGCGATGT
LDHF	CCATGATGCAGGATGGAGTA
SNAE	GAGCTCGAAAGGAGGCCCTTCAGATGAGTCCACCGTTTTG
SNAF	GAATTCCTAAACAGTTGGCATCGCTG
CGME	CCGACGTCTTAAATCGCC
CGMF	CATATGTTAAGTCTGGCTTGGTATC

The initial working volume of 2 L was inoculated to an OD₆₀₀ of 1.5 – 2 from an overnight shake flask pre-culture in complex medium BHI. Samples were collected by an autosampler and cooled down to 4°C until use. The fermentation medium composition was described previously in Pérez-García et al. (2017b). Per liter of medium it contains: 40 g (NH₄)₂SO₄, 1.25 g KH₂PO₄, 1.125 mL H₃PO₄ [85% (w/w)], 1 mL PKS-solution (30 mg mL⁻¹ of 3,4-dihydroxybenzoic acid), 0.55 mL of filtered FeSO₄-citrate solution (20 g L⁻¹ FeSO₄ heptahydrate and 20.2 g

L⁻¹ citrate monohydrate), 7 mL of filtered vitamin solution (0.3 g L⁻¹ biotin, 0.5 g L⁻¹ thiamin hydrochloride, 2 g L⁻¹ calcium pantothenate, and 0.6 g L⁻¹ nicotinamide) and 1 mM of IPTG. As carbon source 100 g L⁻¹ of D-glucose monohydrate was used. The feed-medium contained per liter: 40 g L⁻¹ (NH₄)₂SO₄, 0.4 mL L⁻¹ of vitamin solution, 1 mM of IPTG, and D-glucose monohydrate in the concentration of 150 g L⁻¹.

RESULTS

Physiological and Genome-Wide Expression Response of *C. glutamicum* to Glutarate

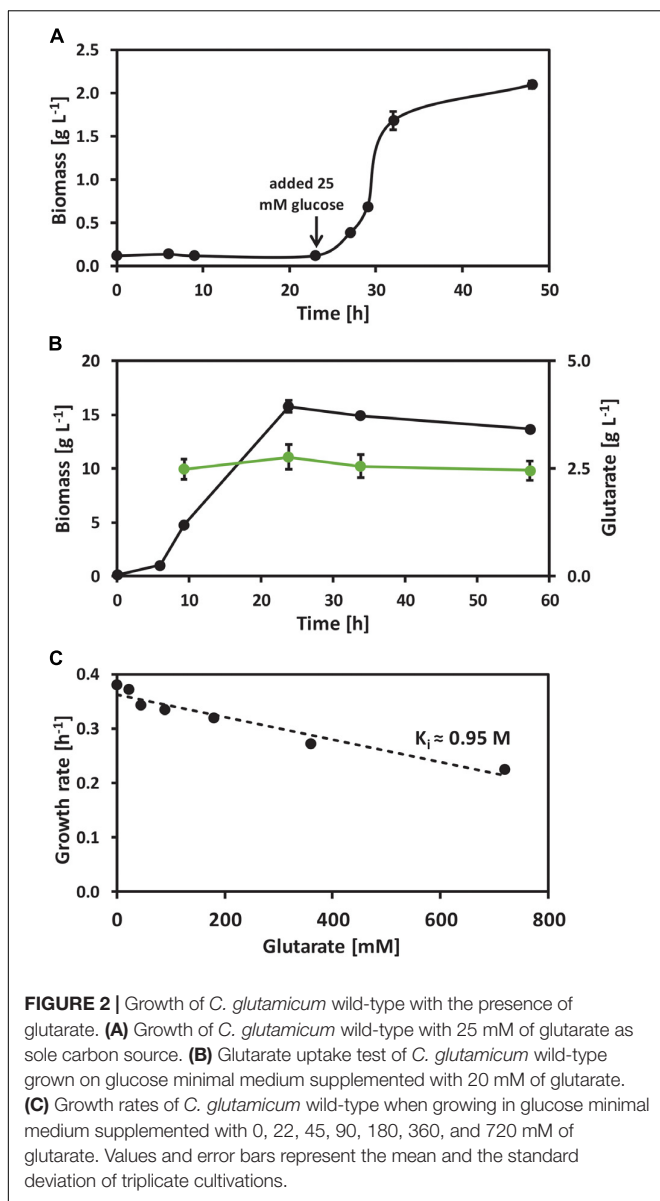
In order to test if *C. glutamicum* is a suitable production host for glutarate, its response to glutarate as carbon source or as potential inhibitor of growth was determined by growth and microarrays analysis. *C. glutamicum* wild-type was grown in CGXII minimal medium with 25 mM glutarate as sole carbon source. No growth was observed until 25 mM of the preferred carbon source glucose was added to the medium (**Figure 2A**). Thus, glutarate is not a carbon source for *C. glutamicum*. When present in a blend with glucose, glutarate was not consumed while glucose was completely consumed (**Figure 2B**). Thus, glutarate is not utilized as co-substrate to glucose. At very high concentrations glutarate inhibited growth in glucose minimal medium and the inhibitory constant (K_i) for *C. glutamicum* wild-type was extrapolated to be about 0.95 M, i.e., the concentration of glutarate that reduced the maximum growth rate to half (**Figure 2C**).

The effect of glutarate on global gene expression in *C. glutamicum* was determined by microarrays analysis. For the preparation of RNA, *C. glutamicum* wild-type cells growing exponentially in glucose minimal medium supplemented with 200 mM of either glutarate or sodium chloride were harvested. Ten genes showed significantly ($p < 0.05$) increased RNA levels by a factor of two or more, 9 genes significantly decreased RNA levels (**Table 3**). Among the genes showing increased RNA levels were *capD* (dTDP-glucose 4,6-dehydratase), *mrcB* (carboxypeptidase), *cysI* (ferredoxin sulfite reductase), and *asd* encoding aspartate-semialdehyde dehydrogenase (Eikmanns et al., 1991). Genes with reduced RNA levels included *uspA1* (stress protein UspA) and *ufaA* (cyclopropane fatty acid synthase). Genes coding for dicarboxylate uptake systems such as *dccT* or *dctA* (Youn et al., 2008, 2009) were not affected. Overall, the response to glutarate on the transcription level was weak and did not indicate candidate genes for uptake, metabolism or export of glutarate.

Taken together, *C. glutamicum* appears as a suitable host for production of glutarate since it tolerates extracellularly added glutarate well.

Metabolic Engineering for Efficient Provision of 5AVA for Glutarate Biosynthesis

The glutarate precursor 5AVA can be generated from lysine by a monooxygenase (Fothergill and Guest, 1977) or by a



transaminase-oxidoreductase pathway (Jorge et al., 2017b). Since the latter does not require molecular oxygen (Jorge et al., 2017b), a possible bottleneck in batch fermentations, we followed the transaminase-oxidoreductase pathway option.

Production of 5AVA via this route was achieved by heterologous overexpression of *ldcC* (L-lysine decarboxylase gene), *pata* (putrescine transaminase gene) and *patD* (γ -aminobutyraldehyde dehydrogenase gene) from *E. coli* in the L-lysine producer GRLys1. The resulting strain produced 3.3 ± 0.1 g L⁻¹ of 5AVA and 0.5 ± 0.1 g L⁻¹ of glutarate in 4% glucose minimal medium with the by-products L-lysine (0.1 ± 0.0 g L⁻¹), cadaverine (0.3 ± 0.0 g L⁻¹) and N-acetylcadaverine (0.5 ± 0.1 g L⁻¹) (Figure 3). To increase 5AVA, glucose consumption was enhanced via the deletion of the transcriptional repressor gene *sugR* (Pérez-García et al., 2016), formation of L-lactate and N-acetylcadaverine as by-products was

avoided via the deletion of *ldhA* (L-lactate dehydrogenase) and *snaA* (N-acetyltransferase) as described previously (Engels et al., 2008; Nguyen et al., 2015). Third, cadaverine export was disrupted via the deletion of *cgmA* (diamine export system) (Lubitz et al., 2016). The resulting GRLys1 Δ *sugR* Δ *ldhA* Δ *snaA* Δ *cgmA* strain was transformed with the vectors pVWEx1-*ldcC* and pEKEx3-*patDA*. In 4% glucose minimal medium, the strain GRLys1 Δ *sugR* Δ *ldhA* Δ *snaA* Δ *cgmA*(pVWEx1-*ldcC*)(pEKEx3-*patDA*) produced 4.9 ± 0.2 g L⁻¹ of 5AVA and 1.5 ± 0.1 g L⁻¹ of glutarate and 0.1 ± 0.0 g L⁻¹ of L-lysine as by-products (Figure 3). Thus, in comparison to the parental strain production of 5AVA and glutarate was increased by 45 and 200%. Moreover, GRLys1 Δ *sugR* Δ *ldhA* Δ *snaA* Δ *cgmA* (pVWEx1-*ldcC*) (pEKEx3-*patDA*) showed better 5AVA yield (0.12 ± 0.10 g g⁻¹) and volumetric productivity (0.10 ± 0.00 g L⁻¹ h⁻¹) (Table 4). The good 5AVA production parameters made this strain a starting point for further metabolic engineering toward glutarate production.

Establishment of Glutarate Production Using Different *gabTD* Operons

Conversion of 5AVA to glutarate involves transamination by aminovalerate aminotransferase GabT and subsequent oxidation by succinate/glutarate semialdehyde dehydrogenase GabD. To identify an *gabTD* operon suitable for efficient conversion of 5AVA to glutarate, several *gabTD* operons from different microorganisms were cloned in the vector pECXT99A and tested in the strain GRLys1 Δ *sugR* Δ *ldhA* Δ *snaA* Δ *cgmA*(pVWEx1-*ldcC*)(pEKEx3-*patDA*) for glutarate production.

Since the *gabTD* operon from *P. putida* KT2440 was shown to support glutarate production (Park et al., 2013) and deletion of the endogenous *gabTD* operon from *C. glutamicum* improved 5AVA formation (Rohles et al., 2016; Jorge et al., 2017b), these operons were overexpressed in the 5AVA overproducing strain (see above). The *gabTD* genes from *P. syringae* and *P. stutzeri* have never been tested before with the purpose of producing glutarate. The GabT (accession number AEJ03917) and GabD (accession number AEJ03916) from *P. stutzeri* ATCC17588 showed identities of 81 and 73%, respectively, compared with GabT (accession number NP_742382.1) and GabD (accession number NP_742381.1) from *P. putida* KT2440. The GabT (accession number YP_233202.1) and GabD (accession number YP_233203.1) from *P. syringae* DSM 50281 showed identities of 86 and 89%, respectively, compared with GabT and GabD from *P. putida* KT2440. Therefore, also these operons were assayed with respect to glutarate production by *C. glutamicum*. The generated vectors pECXT99A-*gabTD*^{Cg} (operon from *C. glutamicum*), pECXT99A-*gabTD*^{Ppu} (operon from *P. putida*), pECXT99A-*gabTD*^{Syr} (operon from *P. syringae*), and pECXT99A-*gabTD*^{Stu} (operon from *P. stutzeri*) as well as the empty vector pECXT99A were used to transform 5AVA producing strain GRLys1 Δ *sugR* Δ *ldhA* Δ *snaA* Δ *cgmA*(pVWEx1-*ldcC*)(pEKEx3-*patDA*).

To test if these operons are functionally expressed in *C. glutamicum*, the combined apparent activities of GabT and GabD were assayed using 5AVA (or GABA) as substrate for

TABLE 3 | Genes differentially expressed in *C. glutamicum* grown in glucose minimal medium in the presence of glutarate as compared to sodium chloride^a.

Gene ID ^b	Gene Name ^b	Gene Description ^b	Ratio of mRNA level (Glutarate/NaCl) ^c
cg0307	<i>asd</i>	Aspartate-semialdehyde dehydrogenase	2.2
cg0417	<i>capD</i>	Putative dTDP-glucose 4,6-dehydratase, transmembrane protein	4.3
cg0544	–	Putative membrane protein	2.3
cg1248	–	Putative GTPase, probably involved in stress response	3.0
cg2337	–	Hypothetical protein	2.8
cg2523	<i>malQ</i>	4-Alpha-glucanotransferase	2.6
cg3021	–	Putative peptidase M20/M25/M40 family	2.8
cg3027	<i>mrpE</i>	Putative secondary Na ⁺ /H ⁺ antiporter, monovalent cation:proton antiporter-3 (CPA3) family	2.4
cg3118	<i>cysI</i>	Ferredoxin-sulfite reductase	3.4
cg3313	<i>mrcB</i>	Putative membrane carboxypeptidase	3.9
cg0980	–	Putative secreted protein, related to metalloendopeptidases	0.5
cg1221	–	Conserved hypothetical protein	0.4
cg1291	–	Putative membrane protein	0.3
cg1551	<i>uspA1</i>	Universal stress protein UspA	0.4
cg1657	<i>ufaA</i>	Putative cyclopropane-fatty-acyl-phospholipid synthase	0.3
cg1831	–	Putative transcriptional regulator, ArsR-family	0.3
cg1966	–	Hypothetical protein	0.4
cg2375	<i>ftsI</i>	Penicillin-binding protein	0.5
cg2507	–	Putative membrane protein	0.3

^aGenes are sorted according to their identifiers and whether they are up- or downregulated. ^bGene ID, name and description are according to GSE117175. ^cDifferential gene expression. Values listed were selected for $P < 0.05$ and at least mRNA level 2-fold.

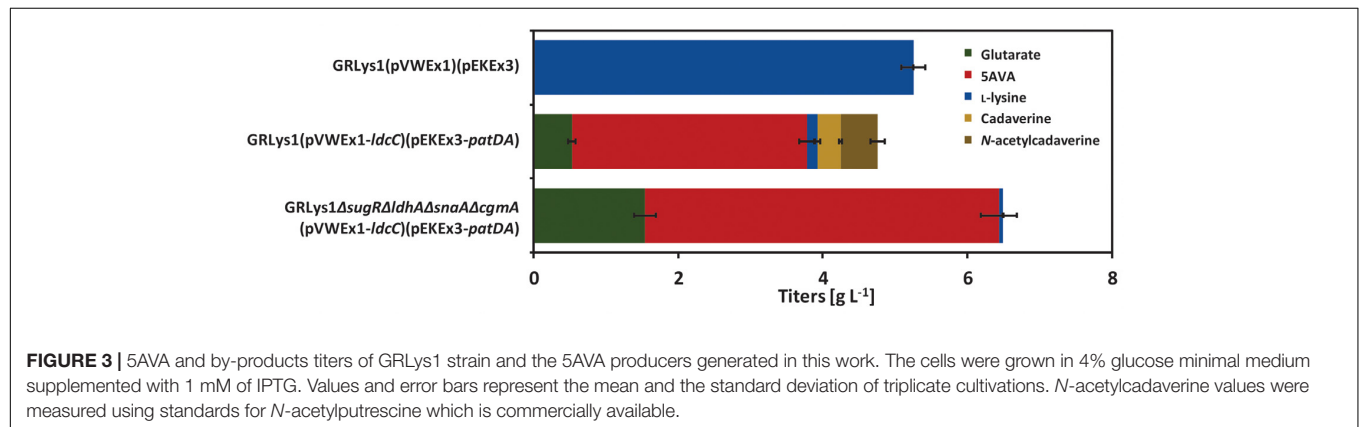


FIGURE 3 | 5AVA and by-products titers of GRLys1 strain and the 5AVA producers generated in this work. The cells were grown in 4% glucose minimal medium supplemented with 1 mM of IPTG. Values and error bars represent the mean and the standard deviation of triplicate cultivations. *N*-acetylcadaverine values were measured using standards for *N*-acetylputrescine which is commercially available.

TABLE 4 | Growth and 5AVA production data of recombinant *C. glutamicum* strains.

Strain	Growth rate [h ⁻¹]	Biomass [g L ⁻¹]	5AVA titer [g L ⁻¹]	5AVA yield [g g ⁻¹]	5AVA vol. prod. [g L ⁻¹ h ⁻¹]	References
GRLys1(pVWEx1)(pEKEx3)	0.25 ± 0.02	11.6 ± 0.3	–	–	–	Jorge et al., 2017b
GRLys1(pVWEx1-ldcC)(pEKEx3-patDA)	0.16 ± 0.01	12.0 ± 0.4	3.3 ± 0.1	0.08 ± 0.00	0.07 ± 0.00	Jorge et al., 2017b
GRLys1ΔsugRΔldhAΔsnaAΔcgmA (pVWEx1-ldcC)(pEKEx3-patDA)	0.13 ± 0.02	9.0 ± 0.3	4.9 ± 0.2	0.12 ± 0.10	0.10 ± 0.00	This work

Samples were harvested and analyzed after glucose depletion. Values represent means and standard deviations of triplicate cultivations.

transamination of α -ketoglutarate and NADP⁺ or NAD⁺ as cofactor for semialdehyde oxidation. Ideally, NAD⁺-dependent 5AVA oxidation at the near-physiological pH 7.5 combined with little side activity with GABA resulted from *gabTD* overexpression. The empty vector carrying strain only showed

activity at pH 9.0 (1.0 ± 0.1 U/mg) with 5AVA when the assay mix contained NAD⁺, but GABA was preferred (1.6 ± 0.9 U/mg with NAD⁺ at pH 9.0; **Table 5**). This activity is due to the native expression level from the chromosomal *gabTD*. Plasmid-borne overexpression of the endogenous *gabTD*^{Cg} increased apparent

activities with NADP^+ at both pH values and at pH 7.5 the activity with NAD^+ and 5AVA was 1.9 ± 0.2 U/mg (Table 5). Differences in the apparent activities may be due to different characteristics of the encoded enzymes and/or different gene expression/protein levels. Characterization of the encoded enzymes and optimization of gene expression may help to guide further metabolic engineering. As consequence of overexpression of the *gabTD^{Ppu}* and *gabTD^{Syr}* operon, preferential transamination and NADP^+ -dependent oxidation of GABA with high apparent activities (93.3 ± 10.0 and 67.5 ± 5.0 U/mg, respectively) resulted (Table 5). However, upon overexpression of *gabTD^{Stu}*, the operon from *P. stutzeri*, preferential NAD^+ -dependent transamination and oxidation of 5AVA was observed (Table 5). At pH 7.5, the combined transamination/semialdehyde oxidation activity with NAD^+ of 18.4 ± 0.9 U/mg was about 10-fold higher than those with GABA or with NADP^+ (Table 5). Thus, overexpression of *gabTD^{Stu}* appeared most useful for fermentative glutarate production.

Growth and glutarate production of all strains were compared in 4% glucose minimal medium (Figure 4 and Table 6). Overexpression of the native *gabTD^{Cg}* operon improved glutarate formation by 75% (Table 6). The overexpression of *gabTD^{Ppu}*, *gabTD^{Syr}* and *gabTD^{Stu}* operons improved glutarate formation from 5AVA by 230, 210, and 250% respectively as compared with the empty vector strain (Table 6). Although the tested *gabTD* operons from pseudomonads improved glutarate production, we cannot exclude that better *gabTD* operons exist in nature. The strain overexpressing *gabTD^{Stu}* showed the best performance regarding glutarate production reaching a titer of 4.7 ± 0.1 g L⁻¹, a yield of 0.12 ± 0.00 g g⁻¹, and a volumetric productivity of 0.10 ± 0.00 g L⁻¹ h⁻¹ (Table 6). Moreover, this strain produced little 5AVA (0.8 ± 0.0 g L⁻¹) and L-lysine (0.2 ± 0.0 g L⁻¹) as byproducts (Figure 4).

Enforced Glutarate Production Upon Deletion of Glutamate Dehydrogenase gene *gdh*

The two transaminases PatA and GabT involved in glutarate biosynthesis use α -ketoglutarate as acceptor and yield L-glutarate. Partially, L-glutarate is converted to α -ketoglutarate

in the transamination reactions of L-lysine biosynthesis (aspartate transaminase Asd as part of the succinylase and the dehydrogenase pathways and *N*-succinyldiaminopimelate transaminase DapC as part only of the succinylase pathway). In addition, reductive amination of α -ketoglutarate yielding L-glutamate is catalyzed by glutamate dehydrogenase (encoded by *gdh*; Figure 1), the major enzyme of nitrogen assimilation of *C. glutamicum*. The ATP consuming GS/GOGAT system (encoded by the genes *gltBD* and *glnA*) only operates under nitrogen concentrations below 5 mM (Tesch et al., 1998; Nolden et al., 2001). In the nitrogen-rich minimal medium CgXII, we expected that the transaminases of glutarate biosynthesis would compensate for the absence of reductive amination of α -ketoglutarate due to *gdh* deletion and, thus, that glutarate production would be increased as consequence of *gdh* deletion.

To test this hypothesis, *gdh* was deleted in the *C. glutamicum* strain GRLys1 Δ sugR Δ ldhA Δ snaA Δ cgmA. Transformation of the resulting strain GRLys1 Δ sugR Δ ldhA Δ snaA Δ cgmA Δ gdh with the vectors pVWEx1, pEKEx3, pECXT99A, pVWEx1-ldcC, pEKEx3-patDA, pECXT99A-*gabTD^{Cg}*, pECXT99A-*gabTD^{Ppu}*, pECXT99A-*gabTD^{rmSyr}*, and pECXT99A-*gabTD^{Stu}* yielded the second set of glutarate producer strains. Growth and production parameters obtained after growth in 4% glucose minimal medium are listed in Table 7. As expected, the *gdh* positive parent strain GRLys1 Δ sugR Δ ldhA Δ snaA Δ cgmA carrying vectors pVWEx1-ldcC, pEKEx3-patDA, and pECXT99A grew faster (0.10 ± 0.01 h⁻¹, Table 6) than the isogenic strain lacking *gdh* (0.05 ± 0.00 h⁻¹; Table 7). This growth perturbation was enhanced when neither *patA* nor *gabT* were overexpressed as is the case in the *gdh* deletion strain carrying only empty vectors (0.03 ± 0.00 h⁻¹; Table 7). All *gdh* deletion strains overexpressing *gabTD* operons grew faster than this strain (Table 7). However, none of the *gdh* deletion strains grew as fast as its *gdh* positive parent strain (compare Tables 6, 7).

Deletion of *gdh* reduced the biomass concentration in each case (compare Tables 6, 7). For example, the biomass concentrations reached by all *gdh* deletion strains overexpressing *gabTD* operons was lower (4.0 – 4.6 g L⁻¹, Table 7) than those of the isogenic *gdh* positive parents strains (5.7 – 7.2 g L⁻¹, Table 6).

TABLE 5 | Combined enzyme activity assays for transaminase GabT and semialdehyde dehydrogenase GabD in crude extracts of various recombinant *C. glutamicum* strains.

GabTD:	Phosphate buffer pH 7.5				Phosphate buffer pH 9.0			
	5AVA		GABA		5AVA		GABA	
	NADP ⁺	NAD ⁺	NADP ⁺	NAD ⁺	NADP ⁺	NAD ⁺	NADP ⁺	NAD ⁺
Endogenous-	nd	nd	0.5 ± 0.2	0.7 ± 0.3	nd	1.0 ± 0.1	1.6 ± 0.9	0.8 ± 0.2
Endogenous overexpressed	nd	1.9 ± 0.2	1.2 ± 0.2	3.1 ± 0.9	2.4 ± 0.9	5.2 ± 0.4	8.1 ± 2.3	6.6 ± 1.6
from <i>P. putida</i>	30.8 ± 5.1	2.8 ± 1.1	37.7 ± 5.5	7.3 ± 1.5	45.2 ± 7.9	21.3 ± 1.5	93.3 ± 10.0	15.3 ± 1.8
from <i>P. stutzeri</i>	1.3 ± 0.4	18.4 ± 0.9	1.6 ± 0.6	2.0 ± 0.0	1.2 ± 0.5	27.3 ± 2.5	13.5 ± 1.4	10.8 ± 3.7
from <i>P. syringae</i>	16.9 ± 5.5	9.4 ± 2.7	23.5 ± 2.0	18.9 ± 1.7	12.8 ± 2.3	21.9 ± 0.6	67.5 ± 5.0	21.7 ± 4.2

The apparent activities expressed as U per mg protein in crude extracts were assayed at pH 7.5 and pH 9.0 for the substrates 5AVA and GABA and the cofactors NADP^+ and NAD^+ . Values represent means and standard deviations of triplicate cultivations.

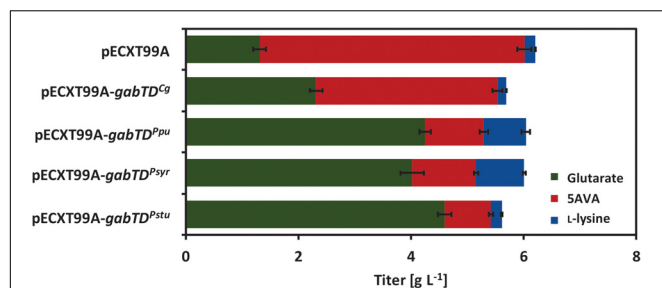


FIGURE 4 | Glutamate and by-products titers of the first round of glutarate producers generated in this work. The strain GRLys1 Δ sugR Δ ldhA Δ snaA Δ cgmA (pVWEx1-ldcC)(pEKEx3-patDA) harboring the vectors pECXT99A, pECXT99A-*gabTD^{Cg}*, pECXT99A-*gabTD^{Ppu}*, pECXT99A-*gabTD^{Psr}* or pECXT99A-*gabTD^{Pstu}* was grown in 4% glucose minimal medium supplemented with 1 mM of IPTG. Values and error bars represent the mean and the standard deviation of triplicate cultivations.

This may be due at least in part to alteration of the redox balance in the absence of NADPH-dependent Gdh.

As consequence of *gdh* deletion, increased glutarate titers resulted (compare **Tables 6, 7**). For example, the *gdh* deletion strain overexpressing *gabTD^{Cg}* produced $3.3 \pm 0.1 \text{ g L}^{-1}$ with a yield of $0.08 \pm 0.00 \text{ g g}^{-1}$ (**Table 7**) whereas its *gdh* positive isogenic parent overexpressing *gabTD^{Cg}* produced $2.3 \pm 0.1 \text{ g L}^{-1}$ with a yield of $0.06 \pm 0.00 \text{ g g}^{-1}$ (**Table 6**).

The best glutarate producer strain GRLys1 Δ sugR Δ ldhA Δ snaA Δ cgmA Δ gdh (pVWEx1-ldcC)(pEKEx3-patDA)(pECXT99A-*gabTD^{Pstu}*) was *gdh* negative and reached a titer, yield and volumetric productivity of $5.2 \pm 0.1 \text{ g L}^{-1}$, $0.13 \pm 0.00 \text{ g g}^{-1}$ and $0.09 \pm 0.00 \text{ g L}^{-1} \text{ h}^{-1}$, respectively (**Table 7**).

Bioreactor-Based Production of Glutarate in Fed-Batch Mode

C. glutamicum is a robust microorganism, which typically performs well in fed-batch fermentations. This fact was shown, for instance, for the production of the L-lysine or L-glutamate derivatives L-pipecolic acid, GABA and 5AVA (Rohles et al., 2016; Jorge et al., 2017a; Pérez-García et al., 2017a).

To test if glutarate production can be enhanced at maximal cell density by feeding glucose, two fed-batch cultivations in 2 L scale (initial volume) were performed. The best producer strain GRLys1 Δ sugR Δ ldhA Δ snaA Δ cgmA Δ gdh (pVWEx1-ldcC)(pEKEx3-patDA)(pECXT99A-*gabTD^{Pstu}*) was used to inoculate glucose minimal medium with an initial glucose concentration of 100 g L^{-1} . By the end of the process (80 h) the glutarate titer reached 25.2 g L^{-1} ($n = 1$) (**Figure 5**), which corresponds to a volumetric productivity of $0.32 \text{ g L}^{-1} \text{ h}^{-1}$. At the end of the batch-phase 7.3 g L^{-1} of glutarate were produced, hence most of the glutarate accumulated was formed during the feeding-phase. The overall yield for glutarate under the present conditions was 0.17 g g^{-1} . The by-products 5AVA and L-lysine were produced along the whole fermentation process, with a small boost in the feeding-phase. The final titers for 5AVA and L-lysine were 2.4 and 3.8 g L^{-1} (**Figure 5**). No L-glutamate was observed as by-product.

DISCUSSION

Corynebacterium glutamicum is a suitable host for production of L-lysine-derived compounds (Lee and Wendisch, 2017) and, thus, was used as basis for fermentative glutarate production here. *C. glutamicum* cannot catabolize L-lysine

TABLE 6 | Growth and glutarate production data of recombinant *C. glutamicum* strains.

GRLys1 Δ sugR Δ ldhA Δ snaA Δ cgmA +	Growth rate [h ⁻¹]	Biomass [g L ⁻¹]	Glutarate titer [g L ⁻¹]	Glutarate yield [g g ⁻¹]	Glutarate vol. prod. [g L ⁻¹ h ⁻¹]
(pVWEx1-ldcC)(pEKEx3-patDA)(pECXT99A)	0.10 ± 0.01	7.4 ± 0.3	1.3 ± 0.2	0.03 ± 0.00	0.03 ± 0.00
(pVWEx1-ldcC)(pEKEx3-patDA)(pECXT99A- <i>gabTD^{Cg}</i>)	0.11 ± 0.00	6.8 ± 0.8	2.3 ± 0.1	0.06 ± 0.00	0.05 ± 0.00
(pVWEx1-ldcC)(pEKEx3-patDA)(pECXT99A- <i>gabTD^{Ppu}</i>)	0.10 ± 0.01	7.2 ± 0.8	4.3 ± 0.2	0.11 ± 0.00	0.09 ± 0.00
(pVWEx1-ldcC)(pEKEx3-patDA)(pECXT99A- <i>gabTD^{Psr}</i>)	0.12 ± 0.01	6.2 ± 0.7	4.0 ± 0.2	0.10 ± 0.01	0.08 ± 0.00
(pVWEx1-ldcC)(pEKEx3-patDA)(pECXT99A- <i>gabTD^{Pstu}</i>)	0.10 ± 0.00	5.7 ± 0.9	4.7 ± 0.1	0.12 ± 0.00	0.10 ± 0.00

Samples were harvested and analyzed after glucose depletion. Values represent means and standard deviations of triplicate cultivations.

TABLE 7 | Growth and glutarate production data of recombinant *C. glutamicum* strains that lack glutamate dehydrogenase.

GRLys1 Δ sugR Δ ldhA Δ snaA Δ cgmA Δ gdh +	Growth rate [h ⁻¹]	Biomass [g L ⁻¹]	Glutarate titer [g L ⁻¹]	Glutarate yield [g g ⁻¹]	Glutarate vol. prod. [g L ⁻¹ h ⁻¹]
(pVWEx1)(pEKEx3)(pECXT99A)	0.03 ± 0.00	3.7 ± 0.2	–	–	–
(pVWEx1-ldcC)(pEKEx3-patDA)(pECXT99A)	0.05 ± 0.00	4.3 ± 0.4	1.7 ± 0.0	0.04 ± 0.00	0.03 ± 0.00
(pVWEx1-ldcC)(pEKEx3-patDA)(pECXT99A- <i>gabTD^{Cglu}</i>)	0.05 ± 0.00	4.1 ± 0.3	3.3 ± 0.1	0.08 ± 0.00	0.05 ± 0.00
(pVWEx1-ldcC)(pEKEx3-patDA)(pECXT99A- <i>gabTD^{Ppu}</i>)	0.05 ± 0.01	4.3 ± 0.2	5.0 ± 0.1	0.12 ± 0.01	0.08 ± 0.00
(pVWEx1-ldcC)(pEKEx3-patDA)(pECXT99A- <i>gabTD^{Psr}</i>)	0.06 ± 0.00	4.0 ± 0.4	4.7 ± 0.2	0.12 ± 0.00	0.08 ± 0.00
(pVWEx1-ldcC)(pEKEx3-patDA)(pECXT99A- <i>gabTD^{Pstu}</i>)	0.07 ± 0.00	4.6 ± 0.3	5.2 ± 0.1	0.13 ± 0.00	0.09 ± 0.00

Samples were harvested and analyzed after glucose depletion. Values represent means and standard deviations of triplicate cultivations.

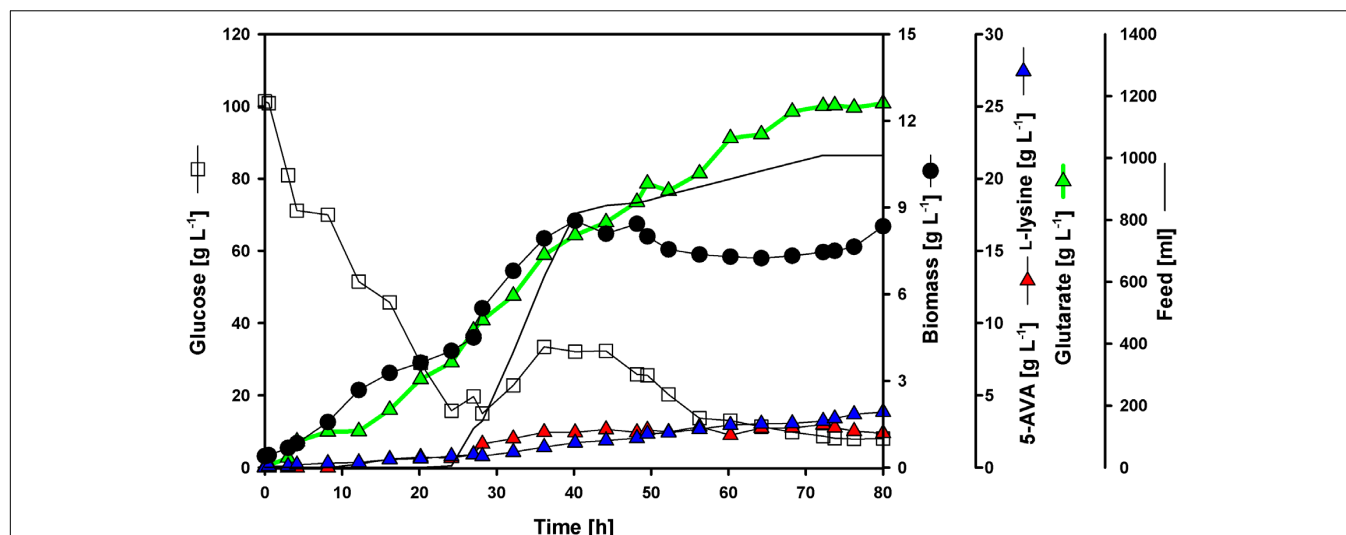


FIGURE 5 | Fed-batch glutarate production. The *C. glutamicum* strain GRLys1 Δ sugR Δ dhA Δ snaA Δ cgmA Δ gdh(pVWEx1-ldcC)(pKEEx3-patDA) (pECXT99A-gabTD^{Stu}) was tested under industrial relevant conditions using glucose as sole carbon source. The data given include glucose consumption in g L⁻¹ (opened squares); L-lysine (blue triangles), 5-AVA (red triangles) and glutarate (green triangles) titers in g L⁻¹; biomass formation (closed circles) in g L⁻¹; and feeding profile in mL depicted as a line. The initial culture volume was 2 l plus 1 l of feed media.

(Eggeling and Bott, 2005) and was shown here not to be able to catabolize glutarate. By contrast, L-lysine can be used by some microorganisms in the secondary metabolism as precursor of antibiotics and alkaloids (Clevenstine et al., 1979; Shima et al., 1984). L-Lysine is used as carbon and/or nitrogen source by a number of bacterial species. For example, *Pseudomonas* sp. can use both D- and L-enantiomers of lysine as sole carbon and nitrogen source (Chang and Adams, 1974; Fothergill and Guest, 1977). *P. putida* catabolizes L-lysine through the 5AVA pathway forming NH₄⁺ and glutarate, which is oxidized in the TCA cycle (Fothergill and Guest, 1977). Since *C. glutamicum* cannot utilize glutarate as carbon source for growth, it may lack the ability to activate glutarate to glutaryl-CoA. Activation of acetate and propionate occur via the acetate kinase/phosphotransacetylase pathway and CoA transferase interconverts acetyl-CoA, propionyl-CoA and succinyl-CoA, but lacks acetyl-CoA synthetase (Veit et al., 2007). Besides acetate and propionate only one further fatty acid (Jolkver et al., 2009; Veit et al., 2009) has been shown to support growth of *C. glutamicum*. Utilization of the dicarboxylates succinate, malate, and fumarate requires overexpression of the genes coding for the uptake systems DccT and/or DctA (Youn et al., 2008, 2009). *C. glutamicum* responds to externally added glutarate (see Table 3), indicating that glutarate may be imported into the cell, however, the relevant import system remains unknown under the tested conditions. Also, *C. glutamicum* showed no growth with glutarate as sole carbon source, which may change be overexpressing *dccT* and/or *dctA* (Youn et al., 2008, 2009).

To achieve glutarate production, a new synthetic pathway was designed: conversion of L-lysine to 5AVA via cadaverine using *E. coli* enzymes (Jorge et al., 2017b) followed by transamination and oxidation to glutarate by *Pseudomonas* enzymes. An alternative pathway to 5AVA involved the enzymes

L-lysine monooxygenase (DavB) and 5-aminovaleramidase (DavA) from *P. putida* to convert L-lysine to 5AVA (Fothergill and Guest, 1977; Adkins et al., 2013; Rohles et al., 2016; Shin et al., 2016). This pathway is characterized by the requirement of molecular oxygen for decarboxylation of L-lysine to the amide 5-aminovaleramidate followed by deamination, thus, ammonium is not assimilated by transamination (Fothergill and Guest, 1977). The pathway to 5AVA used here involves decarboxylation of L-lysine to the diamine cadaverine, followed by transamination of cadaverine to 5-aminopentanal by putrescine transaminase PatA and oxidation to 5AVA by 4-aminobutyraldehyde dehydrogenase PatD (Jorge et al., 2017b). Thus, this pathway does not require molecular oxygen, but the transamination reaction yields L-glutamate and the oxidation reaction yields NADH. By bypassing molecular oxygen in the pathway, the problems that may arise due to low dissolved oxygen are avoided with regard to glutarate production.

Both, the new pathway to 5AVA (Jorge et al., 2017b) and the DavAB pathway to 5AVA (Fothergill and Guest, 1977) were combined with subsequent transamination and oxidation to glutarate. Heterologous expression of the full 5AVA pathway from *P. putida* in an *E. coli* L-lysine producer led to 0.8 g L⁻¹ of glutarate within 48 h. In a *C. glutamicum* L-lysine producer, overexpression *davBA* from *P. putida* led to co-production of 5AVA and glutarate, and deletion of endogenous *gabT* reduced production of glutarate as by-product (Rohles et al., 2016; Shin et al., 2016). This indicated a) that residual glutarate formation is likely due to (side)activity of (a) further transaminase(s), and (b) that the endogenous *gabTD* operon codes for enzymes able to convert not only GABA to succinate, but also 5AVA to glutarate. Deletion of *gabTD* abrogated glutarate formation completely indicating that GabD is the only succinate/glutarate semialdehyde dehydrogenase active in *C. glutamicum*

(Jorge et al., 2017b). However, while overexpression of the endogenous *gabTD^{Cg}* operon improved glutarate formation and reduced 5AVA accumulation, heterologous expression of the *gabTD* operons from *Pseudomonas* sp. performed better. A coupled assay of the GabT and GabD reactions revealed that upon overexpression of the endogenous *gabTD^{Cg}* activity with the substrate GABA always exceeded activity with the substrate 5AVA (Table 5). On the other hand, heterologous expression of *gabTD^{Stu}* from *Pseudomonas stutzeri* revealed the highest activity with 5AVA, the cofactor NAD⁺ and pH7.5. Thus, the enzymes encoded by *gabTD^{Stu}* preferred 5AVA over GABA, and their properties were compatible with the intracellular pH of *C. glutamicum* (Jakob et al., 2007), although apparent activities at pH 9.0 were generally higher than at pH7.5 (Table 5) as has been described for *Pseudomonas* sp. F-126 (Yonaha and Toyama, 1980). Since cellular metabolism, in general, operates via NADPH-dependent reduction and NAD⁺-dependent oxidation reactions, the preferred use of NAD⁺ by the enzymes encoded by *gabTD^{Stu}* was ideal for efficient oxidation of glutarate semialdehyde to glutarate.

C. glutamicum strain GRLys1 Δ sugR Δ ldhA Δ snaA Δ cgmA Δ gdh is a genome-reduced L-lysine overproducing strain that shows fast glucose utilization under aerobic conditions due to the deletions Δ sugR and Δ ldhA (Pérez-García et al., 2016). SugR represses genes of the sugar phosphotransferase systems, glycolysis as well as *ldhA* encoding fermentative L-lactate dehydrogenase, which has to be deleted to avoid lactate formation (Engels et al., 2008; Teramoto et al., 2011). *C. glutamicum* GRLys1 Δ sugR Δ ldhA Δ snaA Δ cgmA Δ gdh does neither form cadaverine nor N-acetylcadaverine due to deletions of the genes for diamine acetyltransferase SnaA (Nguyen et al., 2015) and CgmA, the export system for L-arginine and diamines (Lubitz et al., 2016). Importantly, production of glutarate was coupled to biosynthesis of L-glutamate due to the deletion of glutamate dehydrogenase gene *gdh*. As consequence, glutarate production with its two transamination reactions catalyzed by PatA and GabT was enforced in order to provide sufficient L-glutamate for growth. *C. glutamicum* lacks other amino acid dehydrogenase and assimilates nitrogen either via glutamate dehydrogenase or via the GOGAT/GS system. Ammonium assimilation via glutamate dehydrogenase has high capacity, but low affinity. The high affinity GOGAT/GS system operates when nitrogen concentrations are below 5 mM and ammonium assimilation via GS/GOGAT requires ATP (Tesch et al., 1998; Nolden et al., 2001). The strategy was successful as it increased glutarate production, however, reduced biomass yields due to Δ gdh were only partially restored upon overexpression of *patA* and *gabT* (compare Tables 6, 7). This may be due to the fact that in transamination reactions catalyzed by PatA and GabT no net ammonium assimilation occurs. A comparable strategy has been used to improve

L-lysine production by coupling of the TCA cycle to the succinylase branch of L-lysine biosynthesis by deletion of the gene for succinyl-CoA synthetase, which competes with lysine biosynthesis for succinyl-CoA (Kind et al., 2013). Although the L-lysine yield was increased by 60%, slower growth resulted and the conversion of succinyl-CoA to succinate was not completely restored [the sum of the fluxes for conversion of succinyl-CoA to succinate was reduced by about 30% in the absence of succinyl-CoA synthase; (Kind et al., 2013)]. Coupling production to reactions or pathways important for growth bears the potential to select improved strains by laboratory evolution. This strategy has been successful for selecting faster growing *C. glutamicum* strains (Pfeifer et al., 2017; Radek et al., 2017; Wang Z. et al., 2018) or strains more tolerant to methanol (Leßmeier and Wendisch, 2015), lignocellulose derived inhibitors (Wang X. et al., 2018) or thermal stress (Oide et al., 2015).

Taken together, the metabolic engineering strategy described here led to a glutarate fed-batch cultivation. During this process and due to the high feed rate within 24 and 40 h, both biomass and glutarate concentration increases significantly. When the maximum biomass concentration was reached the demand of nutrients was reduced. Therefore, the feed rate was decelerated until depletion of feed medium after 71 h of cultivation. The same shift from biomass formation to product formation was observed previously in similar fed-batch fermentations using *C. glutamicum* strains (Rohles et al., 2016; Pérez-García et al., 2017a,b). With a volumetric productivity of 0.32 g L⁻¹ h⁻¹, an overall product yield of 0.17 g g⁻¹ and a titer of 25 g L⁻¹. To the best of our knowledge, these are the highest titers, yields and productivities for fermentative glutarate production published to date.

AUTHOR CONTRIBUTIONS

FP-G, JJ, and VW designed the study. FP-G, JJ, and AD performed the experiments. FP-G, JJ, AD, JR, and VW analyzed the data. FP-G and JJ drafted the manuscript. VW finalized the manuscript. All authors read and approved the final version of the manuscript.

ACKNOWLEDGMENTS

The authors thank Thomas Schäffer from the Department of Fermentation Technology at Bielefeld University for his support during the fed-batch fermentations. They acknowledge support for the Article Processing Charge by the Deutsche Forschungsgemeinschaft and the Open Access Publication Fund of Bielefeld University.

REFERENCES

- Adkins, J., Jordan, J., and Nielsen, D. R. (2013). Engineering *Escherichia coli* for renewable production of the 5-carbon polyamide building-blocks 5-aminovaleate and glutarate. *Biotechnol. Bioeng.* 110, 1726–1734. doi: 10.1002/bit.24828
- Baumgart, M., Unthan, S., Rückert, C., Sivalingam, J., Grünberger, A., Kalinowski, J., et al. (2013). Construction of a prophage-free variant of *Corynebacterium glutamicum* ATCC 13032 for use as a platform strain for basic research and industrial biotechnology. *Appl. Environ. Microbiol.* 79, 6006–6015. doi: 10.1128/AEM.01634-13

- Becker, J., Zelder, O., Häfner, S., Schröder, H., and Wittmann, C. (2011). From zero to hero—design-based systems metabolic engineering of *Corynebacterium glutamicum* for L-lysine production. *Metab. Eng.* 13, 159–168. doi: 10.1016/j.ymben.2011.01.003
- Blombach, B., Riester, T., Wieschalka, S., Ziert, C., Youn, J. W., Wendisch, V. F., et al. (2011). *Corynebacterium glutamicum* tailored for efficient isobutanol production. *Appl. Environ. Microbiol.* 77, 3300–3310. doi: 10.1128/AEM.02972-10
- Chang, Y. F., and Adams, E. (1974). D-lysine catabolic pathway in *Pseudomonas putida*: interrelations with L-lysine catabolism. *J. Bacteriol.* 117, 753–764.
- Chung, H., Yang, J. E., Ha, J. Y., Chae, T. U., Shin, J. H., Gustavsson, M., et al. (2015). Bio-based production of monomers and polymers by metabolically engineered microorganisms. *Curr. Opin. Biotechnol.* 36, 73–84. doi: 10.1016/j.copbio.2015.07.003
- Clevenstine, E. C., Walter, P., Harris, T. M., and Broquist, H. P. (1979). Biosynthesis of slaframine, (1S,6S,8aS)-1-acetoxy-6-aminooctahydroindolizine, a parasymphomimetic alkaloid of fungal origin. 4. Metabolic fate of ethyl pipercolylacetate, 1,3-dioxooctahydroindolizine, and 1-hydroxyoctahydroindolizine in *Rhizoctonia leguminicola*. *Biochemistry* 18, 3663–3667.
- Eggeling, L., and Bott, M. (2005). *Handbook of Corynebacterium glutamicum*. Boca Raton, FL: CRC Press.
- Eikmanns, B. J., Metzger, M., Reinscheid, D., Kircher, M., and Sahm, H. (1991). Amplification of three threonine biosynthesis genes in *Corynebacterium glutamicum* and its influence on carbon flux in different strains. *Appl. Microbiol. Biotechnol.* 34, 617–622.
- Engels, V., Lindner, S. N., and Wendisch, V. F. (2008). The global repressor SugR controls expression of genes of glycolysis and of the L-lactate dehydrogenase LdhA in *Corynebacterium glutamicum*. *J. Bacteriol.* 190, 8033–8044. doi: 10.1128/JB.00705-08
- Engels, V., and Wendisch, V. F. (2007). The DeoR-type regulator SugR represses expression of ptsG in *Corynebacterium glutamicum*. *J. Bacteriol.* 189, 2955–2966. doi: 10.1128/JB.01596-06
- Fothergill, J. C., and Guest, J. R. (1977). Catabolism of L-lysine by *Pseudomonas aeruginosa*. *J. Gen. Microbiol.* 99, 139–155. doi: 10.1099/00221287-99-1-139
- Gibson, D. G. (2011). Enzymatic assembly of overlapping DNA fragments. *Methods Enzymol.* 498, 349–361. doi: 10.1016/B978-0-12-385120-8.00015-2
- Gobin, M., Loulergue, P., Audic, J. L., and Lemiègre, L. (2015). Synthesis and characterisation of bio-based polyester materials from vegetable oil and short to long chain dicarboxylic acids. *Ind. Crops Prod.* 70, 213–220. doi: 10.1016/j.indcrop.2015.03.041
- Hanahan, D. (1983). Studies on transformation of *Escherichia coli* with plasmids. *J. Mol. Biol.* 166, 557–580.
- Jakob, K., Satorhelyi, P., Lange, C., Wendisch, V. F., Silakowski, B., Scherer, S., et al. (2007). Gene expression analysis of *Corynebacterium glutamicum* subjected to long-term lactic acid adaptation. *J. Bacteriol.* 189, 5582–5590. doi: 10.1128/JB.00082-07
- Jambunathan, P., and Zhang, K. (2014). Novel pathways and products from 2-keto acids. *Curr. Opin. Biotechnol.* 29, 1–7. doi: 10.1016/j.copbio.2014.01.008
- Jolkver, E., Emer, D., Ballan, S., Krämer, R., Eikmanns, B. J., and Marin, K. (2009). Identification and characterization of a bacterial transport system for the uptake of pyruvate, propionate, and acetate in *Corynebacterium glutamicum*. *J. Bacteriol.* 191, 940–948. doi: 10.1128/JB.01155-08
- Jorge, J. M. P., Leggewie, C., and Wendisch, V. F. (2016). A new metabolic route for the production of gamma-aminobutyric acid by *Corynebacterium glutamicum* from glucose. *Amino Acids* 48, 2519–2531. doi: 10.1007/s00726-016-2272-6
- Jorge, J. M. P., Nguyen, A. Q. D., Pérez-García, F., Kind, S., and Wendisch, V. F. (2017a). Improved fermentative production of gamma-aminobutyric acid via the putrescine route: systems metabolic engineering for production from glucose, amino sugars, and xylose. *Biotechnol. Bioeng.* 114, 862–873. doi: 10.1002/bit.26211
- Jorge, J. M. P., Pérez-García, F., and Wendisch, V. F. (2017b). A new metabolic route for the fermentative production of 5-aminovalerate from glucose and alternative carbon sources. *Bioresour. Technol.* 245, 1701–1709. doi: 10.1016/j.biortech.2017.04.108
- Kind, S., Becker, J., and Wittmann, C. (2013). Increased lysine production by flux coupling of the tricarboxylic acid cycle and the lysine biosynthetic pathway—metabolic engineering of the availability of succinyl-CoA in *Corynebacterium glutamicum*. *Metab. Eng.* 15, 184–195. doi: 10.1016/j.ymben.2012.07.005
- Kind, S., Neubauer, S., Becker, J., Yamamoto, M., Völkert, M., Abendroth, G., et al. (2014). From zero to hero - production of bio-based nylon from renewable resources using engineered *Corynebacterium glutamicum*. *Metab. Eng.* 25, 113–123. doi: 10.1016/j.ymben.2014.05.007
- Kirchner, O., and Tauch, A. (2003). Tools for genetic engineering in the amino acid-producing bacterium *Corynebacterium glutamicum*. *J. Biotechnol.* 104, 287–299.
- Lee, J. H., and Wendisch, V. F. (2017). Production of amino acids - Genetic and metabolic engineering approaches. *Bioresour. Technol.* 245(Pt B), 1575–1587. doi: 10.1016/j.biortech.2017.05.065
- Leßmeier, L., and Wendisch, V. F. (2015). Identification of two mutations increasing the methanol tolerance of *Corynebacterium glutamicum*. *BMC Microbiol.* 15:216. doi: 10.1186/s12866-015-0558-6
- Lubitz, D., Jorge, J. M. P., Pérez-García, F., Taniguchi, H., and Wendisch, V. F. (2016). Roles of export genes cgmA and lysE for the production of L-arginine and L-citrulline by *Corynebacterium glutamicum*. *Appl. Microbiol. Biotechnol.* 100, 8465–8474. doi: 10.1007/s00253-016-7695-1
- Mishra, M. K., Varughese, S., Ramamurthy, U., and Desiraju, G. R. (2013). Odd-even effect in the elastic moduli of α,ω -alkanedicarboxylic acids. *J. Am. Chem. Soc.* 135, 8121–8124. doi: 10.1021/ja402290h
- Netzer, R., Peters-Wendisch, P., Eggeling, L., and Sahm, H. (2004). Cometabolism of a nongrowth substrate: L-serine utilization by *Corynebacterium glutamicum*. *Appl. Environ. Microbiol.* 70, 7148–7155. doi: 10.1128/AEM.70.12.7148-7155.2004
- Nguyen, A. Q. D., Schneider, J., and Wendisch, V. F. (2015). Elimination of polyamine N-acetylation and regulatory engineering improved putrescine production by *Corynebacterium glutamicum*. *J. Biotechnol.* 201, 75–85. doi: 10.1016/j.jbiotec.2014.10.035
- Nolden, L., Farwick, M., Krämer, R., and Burkovski, A. (2001). Glutamine synthetases of *Corynebacterium glutamicum*: transcriptional control and regulation of activity. *FEMS Microbiol. Lett.* 201, 91–98.
- Oide, S., Gunji, W., Moteki, Y., Yamamoto, S., Suda, M., Jojima, T., et al. (2015). Adaptive laboratory evolution conferred cross-tolerance to thermal and solvent stress to *Corynebacterium glutamicum*. *Appl. Environ. Microbiol.* 81, 2284–2298. doi: 10.1128/AEM.03973-14
- Park, S. J., Kim, E. Y., Noh, W., Park, H. M., Oh, Y. H., Lee, S. H., et al. (2013). Metabolic engineering of *Escherichia coli* for the production of 5-aminovalerate and glutarate as C5 platform chemicals. *Metab. Eng.* 16, 42–47. doi: 10.1016/j.ymben.2012.11.011
- Pérez-García, F., Max Risse, J., Friehs, K., and Wendisch, V. F. (2017a). Fermentative production of L-pipecolic acid from glucose and alternative carbon sources. *Biotechnol. J.* 12:1600646. doi: 10.1002/biot.201600646
- Pérez-García, F., Ziert, C., Risse, J. M., and Wendisch, V. F. (2017b). Improved fermentative production of the compatible solute ectoine by *Corynebacterium glutamicum* from glucose and alternative carbon sources. *J. Biotechnol.* 258, 59–68. doi: 10.1016/j.jbiotec.2017.04.039
- Pérez-García, F., Peters-Wendisch, P., and Wendisch, V. F. (2016). Engineering *Corynebacterium glutamicum* for fast production of L-lysine and L-pipecolic acid. *Appl. Microbiol. Biotechnol.* 100, 8075–8090. doi: 10.1007/s00253-016-7682-6
- Pfeifer, E., Gärgens, C., Polen, T., and Frunzke, J. (2017). Adaptive laboratory evolution of *Corynebacterium glutamicum* towards higher growth rates on glucose minimal medium. *Sci. Rep.* 7:16780. doi: 10.1038/s41598-017-17014-9
- Polen, T., Schluesener, D., Poetsch, A., Bott, M., and Wendisch, V. F. (2007). Characterization of citrate utilization in *Corynebacterium glutamicum* by transcriptome and proteome analysis. *FEMS Microbiol. Lett.* 273, 109–119. doi: 10.1111/j.1574-6968.2007.00793.x
- Radek, A., Tenhaef, N., Müller, M. F., Brüsseler, C., Wiechert, W., Marienhagen, J., et al. (2017). Miniaturized and automated adaptive laboratory evolution: Evolving *Corynebacterium glutamicum* towards an improved d-xylose utilization. *Bioresour. Technol.* 245, 1377–1385. doi: 10.1016/j.biortech.2017.05.055
- Rohles, C. M., Gießelmann, G., Kohlstedt, M., Wittmann, C., and Becker, J. (2016). Systems metabolic engineering of *Corynebacterium glutamicum* for the

- production of the carbon-5 platform chemicals 5-aminovalerate and glutarate. *Microb. Cell Fact.* 15:154. doi: 10.1186/s12934-016-0553-0
- Schäfer, A., Tauch, A., Jäger, W., Kalinowski, J., Thierbach, G., and Pühler, A. (1994). Small mobilizable multi-purpose cloning vectors derived from the *Escherichia coli* plasmids pK18 and pK19: selection of defined deletions in the chromosome of *Corynebacterium glutamicum*. *Gene* 145, 69–73.
- Schneider, J., Niermann, K., and Wendisch, V. F. (2011). Production of the amino acids L-glutamate, L-lysine, L-ornithine and L-arginine from arabinose by recombinant *Corynebacterium glutamicum*. *J. Biotechnol.* 154, 191–198. doi: 10.1016/j.jbiotec.2010.07.009
- Shen, B., Makley, D. M., and Johnston, J. N. (2010). Umpolung reactivity in amide and peptide synthesis. *Nature* 465, 1027–1032. doi: 10.1038/nature09125
- Shima, S., Matsuoka, H., Iwamoto, T., and Sakai, H. (1984). Antimicrobial action of epsilon-poly-L-lysine. *J. Antibiot.* 37, 1449–1455.
- Shin, J. H., Park, S. H., Oh, Y. H., Choi, J. W., Lee, M. H., Cho, J. S., et al. (2016). Metabolic engineering of *Corynebacterium glutamicum* for enhanced production of 5-aminovaleric acid. *Microb. Cell Fact.* 15:174. doi: 10.1186/s12934-016-0566-8
- Simon, R., Priefer, U., and Pühler, A. (1983). A broad host range mobilization system for in vivo genetic engineering: transposon mutagenesis in gram negative bacteria. *Nat. Biotechnol.* 1, 784–791. doi: 10.1038/nbt1183-784
- Teramoto, H., Inui, M., and Yukawa, H. (2011). Transcriptional regulators of multiple genes involved in carbon metabolism in *Corynebacterium glutamicum*. *J. Biotechnol.* 154, 114–125. doi: 10.1016/j.jbiotec.2011.01.016
- Tesch, M., Eikmanns, B. J., Graaf, A. A., and de Sahm, H. (1998). Ammonia assimilation in *Corynebacterium glutamicum* and a glutamate dehydrogenase-deficient mutant. *Biotechnol. Lett.* 20, 953–957. doi: 10.1023/A:1005406126920
- Unthan, S., Baumgart, M., Radek, A., Herbst, M., Siebert, D., Brühl, N., et al. (2015). Chassis organism from *Corynebacterium glutamicum*—a top-down approach to identify and delete irrelevant gene clusters. *Biotechnol. J.* 10, 290–301. doi: 10.1002/biot.201400041
- Vafaezadeh, M., and Hashemi, M. M. (2016). A non-cyanide route for glutaric acid synthesis from oxidation of cyclopentene in the ionic liquid media. *Process Saf. Environ. Prot.* 100, 203–207. doi: 10.1016/j.psep.2016.01.011
- Veit, A., Polen, T., and Wendisch, V. F. (2007). Global gene expression analysis of glucose overflow metabolism in *Escherichia coli* and reduction of aerobic acetate formation. *Appl. Microbiol. Biotechnol.* 74, 406–421. doi: 10.1007/s00253-006-0680-3
- Veit, A., Rittmann, D., Georgi, T., Youn, J.-W., Eikmanns, B. J., and Wendisch, V. F. (2009). Pathway identification combining metabolic flux and functional genomics analyses: acetate and propionate activation by *Corynebacterium glutamicum*. *J. Biotechnol.* 140, 75–83. doi: 10.1016/j.jbiotec.2008.12.014
- Wang, J., Wu, Y., Sun, X., Yuan, Q., and Yan, Y. (2017). De novo biosynthesis of glutarate via α -keto acid carbon chain extension and decarboxylation pathway in *Escherichia coli*. *ACS Synth. Biol.* 6, 1922–1930. doi: 10.1021/acssynbio.7b00136
- Wang, X., Khushk, I., Xiao, Y., Gao, Q., and Bao, J. (2018). Tolerance improvement of *Corynebacterium glutamicum* on lignocellulose derived inhibitors by adaptive evolution. *Appl. Microbiol. Biotechnol.* 102, 377–388. doi: 10.1007/s00253-017-8627-4
- Wang, Z., Liu, J., Chen, L., Zeng, A.-P., Solem, C., and Jensen, P. R. (2018). Alterations in the transcription factors GntR1 and RamA enhance the growth and central metabolism of *Corynebacterium glutamicum*. *Metab. Eng.* 48, 1–12. doi: 10.1016/j.ymben.2018.05.004
- Wendisch, V. F. (2003). Genome-wide expression analysis in *Corynebacterium glutamicum* using DNA microarrays. *J. Biotechnol.* 104, 273–285.
- Yonaha, K., and Toyama, S. (1980). gamma-Aminobutyrate:alpha-ketoglutarate aminotransferase from *Pseudomonas* sp. F-126: purification, crystallization, and enzymologic properties. *Arch. Biochem. Biophys.* 200, 156–164.
- Youn, J.-W., Jolkver, E., Krämer, R., Marin, K., and Wendisch, V. F. (2008). Identification and characterization of the dicarboxylate uptake system DccT in *Corynebacterium glutamicum*. *J. Bacteriol.* 190, 6458–6466. doi: 10.1128/JB.00780-08
- Youn, J.-W., Jolkver, E., Krämer, R., Marin, K., and Wendisch, V. F. (2009). Characterization of the dicarboxylate transporter DctA in *Corynebacterium glutamicum*. *J. Bacteriol.* 191, 5480–5488. doi: 10.1128/JB.00640-09

Conflict of Interest Statement: The authors declare that the research was conducted in the absence of any commercial or financial relationships that could be construed as a potential conflict of interest.

Copyright © 2018 Pérez-García, Jorge, Dreyszas, Risse and Wendisch. This is an open-access article distributed under the terms of the Creative Commons Attribution License (CC BY). The use, distribution or reproduction in other forums is permitted, provided the original author(s) and the copyright owner(s) are credited and that the original publication in this journal is cited, in accordance with accepted academic practice. No use, distribution or reproduction is permitted which does not comply with these terms.



Expression and Characteristics of Two Glucose-Tolerant GH1 β -glucosidases From *Actinomadura amylolytica* YIM 77502^T for Promoting Cellulose Degradation

Yi-Rui Yin^{1†}, Peng Sang^{2†}, Wen-Dong Xian¹, Xin Li¹, Jian-Yu Jiao¹, Lan Liu¹, Wael N. Hozzein^{3,4}, Min Xiao^{1*} and Wen-Jun Li^{1,5*}

¹ State Key Laboratory of Biocontrol and Guangdong Provincial Key Laboratory of Plant Resources, School of Life Sciences, Sun Yat-sen University, Guangzhou, China, ² College of Agriculture and Biological Science, Dali University, Dali, China, ³ Bioproducts Research Chair, Department of Zoology, College of Science, King Saud University, Riyadh, Saudi Arabia, ⁴ Department of Botany and Microbiology, Faculty of Science, Beni-Suef University, Beni-Suef, Egypt, ⁵ Key Laboratory of Biogeography and Bioresource in Arid Land, Xinjiang Institute of Ecology and Geography, Chinese Academy of Sciences, Ürümqi, China

OPEN ACCESS

Edited by:

Dirk Tischler,
Ruhr-Universität Bochum, Germany

Reviewed by:

Jack Christopher Leo,
University of Oslo, Norway
Biswarup Sen,
Tianjin University, China

*Correspondence:

Min Xiao
xiaomin8@mail.sysu.edu.cn
Wen-Jun Li
liwenjun3@mail.sysu.edu.cn

[†]These authors have contributed
equally to this work

Specialty section:

This article was submitted to
Microbial Physiology and Metabolism,
a section of the journal
Frontiers in Microbiology

Received: 18 October 2018

Accepted: 04 December 2018

Published: 18 December 2018

Citation:

Yin Y-R, Sang P, Xian W-D, Li X,
Jiao J-Y, Liu L, Hozzein WN, Xiao M
and Li W-J (2018) Expression
and Characteristics of Two
Glucose-Tolerant GH1
 β -glucosidases From *Actinomadura*
amylolytica YIM 77502^T for Promoting
Cellulose Degradation.
Front. Microbiol. 9:3149.
doi: 10.3389/fmicb.2018.03149

The bioconversion of lignocellulose in various industrial processes, such as biofuel production, requires the degradation of cellulose. *Actinomadura amylolytica* YIM 77502^T is an aerobic, Gram-positive actinomycete that can efficiently degrade crystalline cellulose by extracellular cellulases. Genomic analysis of *A. amylolytica* identified 9 cellulase and 11 β -glucosidase genes that could potentially encode proteins that digest cellulose. Extracellular proteome characterization of *A. amylolytica* cell-free culture supernatant by liquid chromatography tandem mass spectrometry analysis revealed that 4 of these cellulases and 2 of these β -glucosidases functioned during cellulose hydrolysis. Thin-layer chromatography analysis revealed extracellular β -glucosidases play a major role in carboxyl methyl cellulose (CMC) degradation of products in culture supernatants. In this study, 2 of the identified secreted β -glucosidases, AaBGL1 and AaBGL2, were functionally expressed in *Escherichia coli* and found to have β -glucosidase activity with wide substrate specificities, including for *p*-nitrophenyl β -D-glucopyranoside (pNPG), *p*-nitrophenyl-beta-D-cellobioside (pNPC), and cellobiose. Moreover, AaBGL1 and AaBGL2 had high tolerances for glucose. After adding these β -glucosidases to commercial cellulases, the degradation rates of CMC, Avicel, birch sawdust, and corncob powder increased by 37, 42, 33, and 9%, respectively. Overall, this work identifies an alternative potential source of β -glucosidases with potential applications in commercial cellulose utilization and the bioenergy industry.

Keywords: *Actinomadura amylolytica*, glucose tolerance, β -glucosidase, GH1, cellulose degradation

INTRODUCTION

Cellulose is an ecologically friendly material, the main component of lignocellulosic materials, especially agro-industrial residues, such as wheat straw, rice straw, corn stover, bagasse, and wood chips, and comprises 35–50% of a plant's dry weight (Khandeparker and Numan, 2008; Brinchi et al., 2013). Cellulose is a polysaccharide consisting of a backbone of β -1,4-glucose units. A series

of enzymes is essential for the complete degradation of cellulose into glucose, including endo-1,4- β -glucanases (endoglucanase, EC 3.2.1.4), exo-1,4- β -glucanases (i.e., cellobiohydrolases; EC 3.2.1.91), and β -glucosidases (EC 3.2.1.21). Endoglucanases and cellobiohydrolases act on internal cellulose chains and cellulose chain ends to release smaller fragments and cellobiose, respectively, and then the cello-oligosaccharides are ultimately degraded to glucose by β -glucosidases. The accumulation of cello-oligosaccharides, such as cellobiose and cellotriose, inhibits the functioning of both endoglucanases and cellobiohydrolases during simultaneous saccharification and, therefore, β -glucosidases play a crucial role in enzymatic degradation of cellulose by relieving product inhibition of cello-oligosaccharides for cellulases (Chauve et al., 2010).

A variety of microorganisms, including filamentous fungi, bacteria, and archaea, have the ability to produce cellulases (Jayant et al., 2011; Thomas et al., 2017). The filamentous fungus *Trichoderma reesei* (i.e., anamorph of *Hypocrea jecorina*) is a cellulase overproducer widely used in commercial and industrial lignocellulose degradation and bioethanol production (Henrissat et al., 1985; Huang et al., 2014). It secretes various endoglucanases, exoglucanases and beta-glucosidases to break down and convert cellulose into glucose (Ouyang et al., 2006; Peterson and Nevalainen, 2012). However, the β -glucosidase activity of these cellulase mixtures is too low to prevent inhibition by cellobiohydrolase following cellobiose accumulation (Saloheimo et al., 2002; Zhang et al., 2010). The low β -glucosidase activity of the extracellular secretions of *T. reesei* limits their application in degradation of cellulosic biomass (Nieves et al., 1998; Rahman et al., 2009). Therefore, the discovery of additional β -glucosidases is necessary to enhance the efficiency of cellulose hydrolysis.

Based on analysis of sequences, enzymatic properties, and three-dimensional protein structures, β -glucosidases that hydrolyze substrates through double displacement mechanisms, which also permit enzymes to transglycosylate, are classified as members of glycoside hydrolase (GH) families 1, 3, 5, 9, 16, 30, and 116 (Thongpoo et al., 2013)¹. A large number of β -glucosidases from the GH1 and GH3 families have been purified from microorganisms and characterized (Wang et al., 2005). Most bacterial β -glucosidases employed in cellulose hydrolysis belong to the GH1 family (Cantarel et al., 2009). A majority of these bacterial β -glucosidases are sensitive to glucose, with only a few being glucose tolerant (Bohlin et al., 2010; Datta, 2016), which is a major barrier to efficient utilization of cellulose (Mallerman et al., 2014). To effectively hydrolyze cellulose and accumulate high levels of monosaccharides during enzymatic hydrolysis of lignocelluloses, the GH1 β -glucosidase should have a high glucose tolerance.

In the work presented here, two secreted GH1 β -glucosidases, AaBGL1 and AaBGL2, were identified by secretome and genomic analyses of *Actinomadura amylolytica* YIM 77502^T. AaBGL1 and AaBGL2 were then functionally expressed in *Escherichia coli* BL21 and the resulting recombinant proteins were purified and characterized. Both AaBGL1 and AaBGL2

can degrade cellobiose and *p*-nitrophenyl β -D-glucopyranoside (pNPG). AaBGL1 can also effectively degrade *p*-nitrophenyl β -D-cellobioside (pNPC). Furthermore, AaBGL1 and AaBGL2 are highly tolerant of glucose. After adding these β -glucosidases to commercial cellulase, the degradation rate of carboxyl methyl cellulose (CMC), Avicel, corncob powder, and birch sawdust increased. The demand for β -glucosidases that are insensitive to glucose is increasing with commercial cellulase utilization. Compared with other β -glucosidases, both AaBGL1 and AaBGL2 had high K_i values. These results suggest GH1 β -glucosidases secreted from *A. amylolytica* have potential applications in industrial cellulose utilization.

MATERIALS AND METHODS

Strains, Plasmid, and Culture Conditions

Actinomadura amylolytica YIM 77502^T (i.e., DSM 45822^T and CCTCC AA 2012024^T) was stored in our laboratory (Jiao et al., 2015). The *E. coli* DH5 α strain (Invitrogen, United States) was used for cloning and the *E. coli* BL21 DE3 strain (Invitrogen, United States) was utilized as the host for expression of proteins. The pET28a vector (Invitrogen, United States) was used to construct recombinant plasmids. *A. amylolytica* YIM 77502^T was cultured on R2A medium (0.5 g/l yeast extract, 0.5 g/l peptone, 0.5 g/l glucose, 0.5 g/l soluble starch, 0.5 g/l casein acid hydrolysates, 0.5 g/l sodium pyruvate, 0.3 g/l K₂HPO₄, and 0.024 g/l MgSO₄) at 40°C. Recombinant *E. coli* strains were grown at 37°C in lysogeny broth (LB) medium (1% tryptone, 0.5% yeast extract, and 1% sodium chloride; pH 7.0) containing kanamycin (50 μ g/ml).

Genome Sequencing and Assembly and Gene Functions

Actinomadura amylolytica YIM 77502^T was cultured in R2A and then genomic DNA was extracted using a MasterPure Gram-positive DNA Purification kit (Epicentre MGP04100) following the standard DNA isolation procedure recommended by the manufacturer with modifications (Wu et al., 2009). Whole-genome sequencing was performed on the Illumina HiSeq 2500-PE125 platform with massively parallel sequencing Illumina technology at the Beijing Novogene Bioinformatics Technology Co., Ltd. All high-quality paired reads were assembled using the SOAP *de novo*² into a number of scaffolds (Gu et al., 2013). Glimmer v3.0 (Chen et al., 2011) was used for gene prediction in assembled sequences of *A. amylolytica* YIM 77502^T. The sequence data described here have been deposited in GenBank (Accession number: CP032402). Proteins encoded by *A. amylolytica* were annotated using cluster of orthologous groups (COG) protein functional classification (Tatusov et al., 2003). Carbohydrate-active enzymes (CAZymes) of *A. amylolytica* YIM 77502^T were identified using the CAZyme Analysis Toolkit³ (Petit et al., 2015). The glycoside hydrolase

¹<http://www.cazy.org/>

²<http://soap.genomics.org.cn/soapdenovo.html>

³<http://allie.dbcls.jp/cooccur/CAT;CAZymes+Analysis+Toolkit.html>

families were analyzed using HMMER software based on the Pfam database⁴ (Finn et al., 2011).

Determination of Cellulose Degradation Activity of *A. amyloxyticus* Fermentation Broth

Degradation of filter paper was assessed by inoculating strain *A. amyloxyticus* YIM 77502^T into a test tube containing filter paper basic medium (NaH₂PO₄, KNO₃, and MgSO₄) after static culture at 40°C for 1 month. *A. amyloxyticus* was cultured in cellulose basic medium (NaH₂PO₄, KNO₃, MgSO₄, and Avicel 2 g/l) at 40°C with shaking at 180 rpm for 14 days. The supernatant was harvested by centrifuging for 10 min at 12,000 \times g at 4°C.

The cellulose degradation activity of the above fermentation broth was measured using CMC (Sigma, United States), Avicel (Sigma, United States), and cellobiose (Sigma, United States). Fermentation broth (100 μ l) was added to 400 μ l PBS buffer (pH 7) containing 1% (w/v) CMC or Avicel to test cellulase activity. This mixture was incubated at different temperatures (25–90°C) for 1 h. The release of reducing sugar from CMC was determined using the 3,5-dinitrosalicylic acid assay and measuring the absorbance at 540 nm (Miller, 1959). One unit (IU) of CMCase activity was defined as the volume of fermentation broth required to release 1 μ mol of reducing sugar from CMC per minute. Hydrolytic products of the fermentation broth from CMC were identified by thin-layer chromatography (TLC) using silica gel 60 plates (Merck, Darmstadt, Germany) developed with 1-butanol/acetic acid/water (2:1:1, v/v/v). Sugars were detected by heat treatment at 120°C for 10 min after spraying the plates with freshly prepared 5% (v/v) H₂SO₄ in ethanol (Yin et al., 2015). Glucose (G1), cellobiose (G2), cellotriose (G3), and cellotetraose (G4) were used as sugar standards. The sugar standards was purchased from Sigma, United States.

The β -glucosidase activity of the fermentation broth was measured using cellobiose. Fermentation broth (100 μ l) was added to 400 μ l PBS buffer (pH 7) containing 1% (w/v) cellobiose at different temperatures (25–80°C) for 30 min to test β -glucosidase activity. The release of glucose from cellobiose was determined based on the absorbance at 490 nm of the mixture using a Glucose Oxidase Assay Kit (Abnova, China). One unit (IU) of β -glucosidase activity was defined as the volume of fermentation broth required to release 2 μ mol glucose from cellobiose per minute.

LC-MS/MS Analysis of Secreted Glycoside Hydrolases

The above fermentation broth was transferred into 5 kD ultra-filter concentrators (Sartorius, Germany) and centrifuged for 30 min at 4°C in a swing bucket rotor, resulting in the medium become concentrated by 30-fold. Extracellular protein was precipitated overnight by ammonium sulfate precipitation. The precipitate was resuspended in 150 μ l supernatant. Proteins were isolated and digested as described by Hornburg et al. (2014). Peptides were desalted on C18 StageTips as previously

described and subjected to liquid chromatography tandem mass spectrometry (LC-MS/MS) analysis (Schwanhäusser et al., 2013). The peptides were then separated using a nano high-performance liquid chromatography (HPLC; Thermo Fisher Scientific) with a C18 column. HPLC was directly coupled to a quadrupole-Orbitrap mass spectrometer via a nano electrospray ion source (Q ExactiveTM, Thermo Fisher Scientific). The mass spectrometry (MS) raw data was processed by MaxQuant (v. 1.3.8.2; Cox and Mann, 2008). MS/MS spectra were searched against the *A. amyloxyticus* YIM 77502^T genomic database.

Gene Cloning and Plasmid Construction

The putative β -glucosidase genes *aabgl1* (1335 bp) and *aabgl2* (1431 bp) from the genomic sequences of *A. amyloxyticus* were amplified via polymerase chain reaction (PCR) with the four designed primers listed in **Table 1** using TransStarFastPfu Fly DNA Polymerase (TransGen Biotech, China). The PCR cycle consisted of denaturation at 98°C for 3 min, followed by 34 cycles at 98°C for 10 s, 65°C for 20 s, and 72°C for 45 s, and then a final incubation at 72°C for 5 min for the final extension. The PCR products were cloned into the *pET28a* plasmid, which had been digested with *Bam*H I and *Hind* III, using the *pEASY*-Uni Seamless Cloning and Assembly Kit (TransGen Biotech, China). Recombinant plasmids with the correct size fragments were sequenced. Subsequently, the DNA from the correct recombinant plasmids were transformed into *E. coli* BL21 (DE3) for protein expression.

Sequence Analysis

DNA and protein sequences were aligned using the BLASTx and BLASTp programs (Madden, 2002)⁵, respectively. Signal peptides were predicted using SignalP (Bendtsen et al., 2004)⁶. The primary structures of the amino acid sequences were deduced and analyzed using EXPASY tools⁷. Multiple alignments with protein sequences of the closely related AaBGL1 and AaBGL2

⁵<http://blast.ncbi.nlm.nih.gov/Blast.cgi>

⁶<http://www.cbs.dtu.dk/services/SignalP/>

⁷<http://web.expasy.org/protparam/>

TABLE 1 | Primer sets used in this study.

Primer name	Sequence (5' \rightarrow 3')	Primer length (bp)
Aabgl1-F	<u>GACAGCAAATGGGT</u> <u>CGCGGAATGAACCTT</u> CCCGCCGACT	39
Aabgl1-R	TGCTCGAGTGCGGCC <u>GCATCATGGGGCT</u> CCTCTGTGG	37
Aabgl2-F	<u>GACAGCAAATGGGT</u> <u>CGCGGAATGACAG</u> CACACGAGACGC	39
Aabgl2-R	TGCTCGAGTGCGGCC <u>GCATCAGTCCGG</u> CAGTCCGCC	36

All primers were designed by Primer Premier 5. The underlined region represents the homologous recombinant fragment with the vector.

⁴<http://pfam.xfam.org/>

(retrieved from NCBI database) were carried out using Clustal X (Thompson et al., 1997). Phylogenetic analyses were performed using the MEGA 5 software package (Tamura et al., 2011). Trees were constructed using the maximum likelihood (ML) method with a Poisson correction model. Structural models of AaBGL1 and AaBGL2 were generated with the MODELLER package (Sali and Blundell, 1993) using the β -glucosidase BglM-G1 mutant H75R (PDB ID, 5NS7; sequence identity, 47%) from a marine metagenome and β -xylosidase (PDB ID, 1GNX; sequence identity, 52%) from *Streptomyces* sp. as templates.

Expression, Production, and Purification of Recombinant β -glucosidases

To express the recombinant AaBGL1 and AaBGL2 proteins, the above transformants were cultured overnight in LB medium containing 100 μ g/ml kanamycin at 37°C and with shaking at 220 rpm. One ml of overnight culture was inoculated into 100 ml fresh LB medium containing 100 μ g/ml kanamycin and incubated at 37°C with shaking at 220 rpm. To induce expression of the recombinant β -glucosidases, 0.1 ml of 100 mM IPTG was added to the cell suspension until the cells reached mid-exponential phase ($OD_{600} \approx 0.6$) and incubated at 25°C with shaking at 220 rpm for 6 h. Cell pellets were harvested by centrifuging at $8,000 \times g$ at 4°C for 10 min and resuspended in 20 ml buffer A (20 mM sodium phosphate, 300 mM NaCl, and 10 mM Tris; pH 8.0).

The resuspended cells were disrupted by ultrasonication. The lysates were centrifuged at $12,000 \times g$ for 30 min at 4°C. Cell-free extracts were transferred onto a Ni-chelating affinity column (GE, United States) as the recombinant proteins possessed an N-terminal His-tag. The column was then washed with ten column volumes of buffer A and then ten column volumes of buffer A containing 20 mM imidazole (pH 8.0) and eluted with buffer A containing 300 mM imidazole (pH 8.0). The eluted proteins were desalted using disposable PD-10 Desalting Columns (GE, United States) and the desalted proteins were used for enzyme characterization. Sodium dodecyl sulfate polyacrylamide gel electrophoresis (SDS-PAGE) was performed using a 10% polyacrylamide gel that was then stained with Coomassie brilliant blue dye R-250 (Liu et al., 2010). Protein concentrations were determined with Bradford Protein Assay Kit (Order NO. C503031, Sangon Biotech, China) using bovine serum albumin as the standard.

Enzymatic Characterization of Recombinant β -glucosidases AaBGL1 and AaBGL2

Assays of Enzymatic Activity

β -glucosidase activity was assayed using cellobiose and *p*-nitrophenyl- β -D-glucopyranoside (pNPG). Activity against cellobiose was determined by adding 10 μ g of purified protein to a 200- μ l reaction mixture containing 2% (w/v) cellobiose. After 10 min, the activity was tested using a Glucose Oxidase Assay Kit (Abnova, China). One unit (U) of β -glucosidase activity was defined as the amount of enzyme required to release 2 μ mol glucose from cellobiose per minute. When using

pNPG as the substrate, 10 μ g protein was added to a 200- μ l reaction mixture containing 2.5 mM pNPG (Sigma, St. Louis, MO, United States). After 5 min of incubation at the optimal temperature, the reaction was stopped by adding 0.6 ml of 1 M Na_2CO_3 (Yang et al., 2015). The pNP was measured by monitoring the absorbance at 405 nm (Harnpicharnchai et al., 2009). One unit of β -glucosidase activity was equivalent to 1 μ mol of pNP released from the pNPG in 1 min.

Optimal Temperatures and Thermostabilities

The optimal temperatures for AaBGL1 and AaBGL2 were determined by measuring β -glucosidases activity at different temperatures (10–80°C) at the optimal pH according to the activity assay method. For thermostability analysis, purified β -glucosidases were incubated in buffer A at temperatures ranging between 10 to 80°C for 30, 60, and 120 min. The samples were rapidly cooled in an ice-water bath and residual activity was measured by the standard method.

Optimal pHs and Stabilities at These pHs

The optimal pHs for purified recombinant AaBGL1 and AaBGL2 were investigated in pHs ranging from 2.0 to 11 in buffer (50 mM Na_2HPO_4 -citric acid, pH 2.0–8.0; 50 mM Tris-HCl, pH 8.0–9.0; and 50 mM glycine-NaOH, pH 9.0–11.0). The stabilities of purified AaBGL1 and AaBGL2 at different pHs were assessed by incubating these enzymes in buffers with different pHs as described above at 4°C for 12 and 24 h. The amount of residual activity at the optimal temperature was then determined according to the activity assay method.

Effect of Metal Ions and Chemical Reagents on Enzymatic Activity

To evaluate the effects of metal ions and chemical reagents on enzymatic activity, 10 mM of various metal ions and chemical reagents (K^+ , Na^+ , Fe^{3+} , Mg^{2+} , Mn^{2+} , Ca^{2+} , Cu^{2+} , Co^{2+} , Zn^{2+} , Ni^{2+} , SDS, and EDTA) were added individually to the reaction system. The control was tested using the same process described above without any additive in the reaction mixture.

Effect of Glucose Concentration on Enzymatic Activity

To investigate the effect of the end product glucose on catalytic activity, the reaction was carried out in the presence of glucose concentrations ranging from 0 to 3000 mM. The concentration of the initial substrate pNPG was 1 mM. For the control, the same reaction system was used, but glucose was not added.

Determination of Substrate Specificity

To determine the substrate specificity of AaBGL1 and AaBGL2, cellobiose, beechwood xylan, CMC, Avicel, and different *p*-nitrophenyl derivatives, such as *p*-nitrophenyl- β -D-glucopyranoside (pNPG), *p*-nitrophenyl- α -D-glucopyranoside (pNP- α -G), *p*-nitrophenyl β -D-xylopyranoside (pNPX), and *p*-nitrophenyl- β -D-cellobioside (pNPC), were used as substrates to measure enzymatic activity. All these substrates were purchased from Sigma, United States. The release of pNP was determined by measuring the absorbance at 405 nm of the mixture using pNP as the standard. One unit (U) of activity

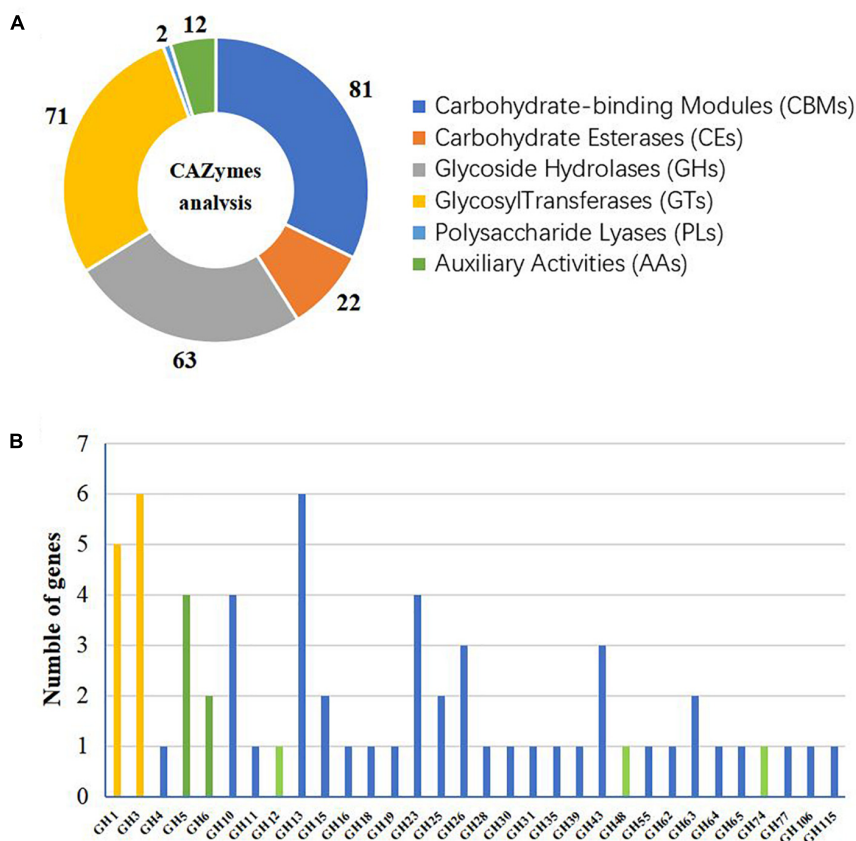


FIGURE 1 | Glycoside hydrolase (GH) families of *Actinomadura amyolytica* YIM 77502^T. **(A)** CAZyme analysis. **(B)** Number of GH genes. Histogram colors indicate different functions: yellow indicates predicted β -glucosidase, green indicates predicted cellulase, and blue indicates other predicted functions.

was defined as the amount of enzyme released from 1 μ mol pNP/min. β -glucosidase activity for cellobiose was tested using the Glucose Oxidase Assay Kit (Abnova, China). One unit (U) of β -glucosidase activity was defined as the amount of enzyme required to release 2 μ mol glucose/min from cellobiose. Beechwood xylan, glucan, CMC, and Avicel were measured using the 3,5-dinitrosalicylic acid assay (Miller, 1959). One unit (U) of enzymatic activity was defined as the amount of enzyme required to release 1 μ mol glucose or xylose-equivalent reducing sugars per minute. All the substrates were purchased from Sigma (St. Louis, MO, United States).

Determination of Kinetic Constants

The kinetic constants (V_{max} and K_m) of AaBGL1 and AaBGL2 were determined using different concentrations of cellobiose (0.2–2 mg/ml) and pNPG (0.5–5.0 mg/ml) at the optimal pH and temperature for 5 min. The V_{max} and K_m of the β -glucosidases for cellobiose and pNPG were calculated using Lineweaver-Burk plots.

Enzymatic Hydrolysis

Enzymatic hydrolysis of different lignocellulosic materials, such as CMC, Avicel, birch sawdust, and corncob, was performed by

adding the appropriate cellulases (Sangon Biotech, China) and/or AaBGL1 and AaBGL2 to a 0.5 ml reaction system containing 50 mM Na_2HPO_4 -citric acid buffer (pH 6.0) and 0.5 ml of 1% (w/v) substrate at 40 and 50°C for 24 h. The dosages of cellulases and β -glucosidases (AaBGL1 and AaBGL2) were 0.2 and 0.02 U/mg, respectively, based on the dry weight of substrate (Ye et al., 2017). Pretreatment of birch sawdust and corncob with ionic liquid (1-ethyl-3-methylimidazolium acetate) was carried out according to the method described in previous studies (Cheng et al., 2012). After enzymatic hydrolysis, the reactions were terminated by boiling for 10 min. The supernatants were collected by centrifugation at 4°C at 10000 $\times g$ for 10 min. The glucose contents of the hydrolysis liquors were measured using the Glucose Oxidase Assay Kit (Abnova, China).

RESULTS

Features of the *A. amyolytica* YIM 77502^T Genome

The complete genome of *A. amyolytica* YIM 77502^T consisted of a single circular 6.8 Mbp chromosome, and a G+C content of 73.28%. The genome contained 6,373 coding sequences with

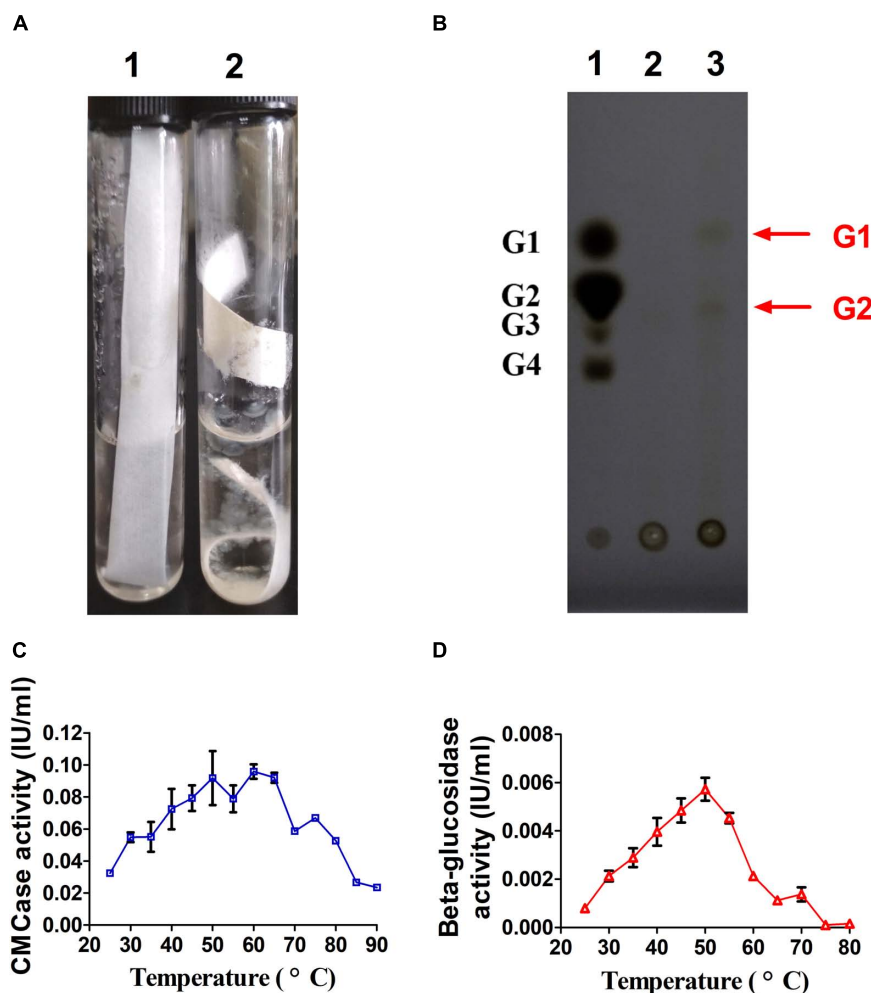


FIGURE 2 | Cellulase activity of *A. amylytica* YIM strain 77502^T. **(A)** Hydrolysis experiment using filter paper. **(B)** Thin-layer chromatography plate analysis of hydrolytic products of carboxyl methyl cellulose (CMC) in fermentation broth of *A. amylytica*, which was cultured with microcrystalline cellulose. **(C)** CMCase activity of fermentation broth. **(D)** β -glucosidase activity of fermentation broth.

an average length of 922 bp. The general genomic features of *A. amylytica* are listed in **Supplementary Table S1**. Among the predicted genes, 95.8% (6,105 genes) were assigned a function and 4.2% (268 genes) had unknown functions. In addition, 86.4% of the sequence encoded genes, while 13.6% belonged to internal sequences. The functions of these genes were mainly gene transcription (590), signal transduction (373), amino acid transport and metabolism (354), carbohydrate transport and metabolism (344), lipid transport and metabolism (324), energy production and conversion (289), coenzyme transport and metabolism (284), and cell wall/membrane/envelope biogenesis (273), as shown in **Supplementary Figure S1**.

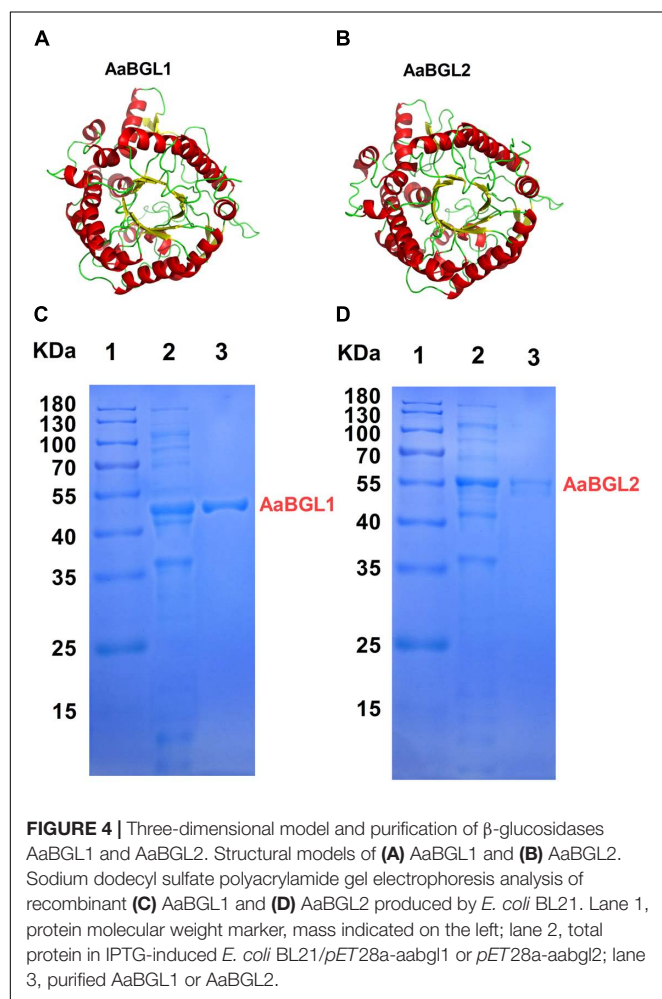
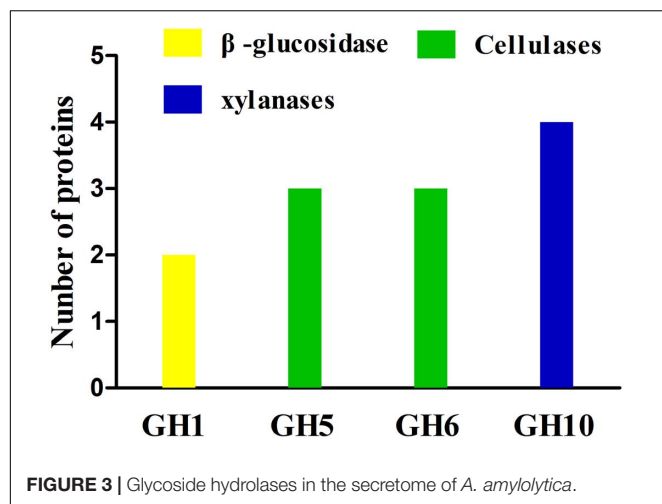
Genes Encoding Carbohydrate-Active Enzymes

A CAZyme analysis was conducted to identify potential enzymes with plant cell-wall degradation ability. Through this analysis, 81 carbohydrate-binding modules (CBMs) distributed in 12

families, 63 glycoside hydrolases (GHs) in 32 families, 2 polysaccharide lyases (PLs) in 2 families, 22 carbohydrate esterases (CEs) in 5 families, 71 glycosyl transferases (GTs) in 14 families, and 12 auxiliary activities (AAs) in 4 families were found to be encoded in the genome of *A. amylytica* (**Figure 1A**). GH1 (glycoside hydrolase family 1) and GH3 were predicted to function as β -glucosidases and GH5, GH6, GH12, GH48 and GH74 were predicted cellulases. Altogether, 11 β -glucosidase genes and 9 cellulase genes were predicted in the genome of *A. amylytica* (**Figure 1B**).

Cellulase Activity of *A. amylytica* YIM 77502^T

As shown in **Figure 2A**, filter paper was degraded by *A. amylytica* YIM 77502^T after culturing 1 month. TLC demonstrated the hydrolytic products of fermentation broth from CMC were mainly glucose and cellobiose (**Figure 2B**). Fermentation broths from cultures in microcrystalline cellulose



basic medium for 2 weeks exhibited CMC and cellobiose activity under test conditions. High CMCase activity was found from 50 to 65°C, where the highest β -glucosidase activity was observed at 50°C (Figures 2C,D).

Glycoside Hydrolases in the Secretome

The secretome of *A. amylytica* was examined by MS. Secretome analysis revealed 209 proteins produced by *A. amylytica*, which were mainly involved in carbohydrate transport and metabolism (43), amino acid transport and metabolism (23), protein turnover (18), cell wall/membrane/envelope biogenesis (16), energy production and conversion (10), and signal transduction (10), as shown in **Supplementary Figure S2**. Among these secreted proteins, 4 cellulases belonging to GH5 and GH6, 4 xylanases belonging to GH10, and two β -glucosidases belonging to GH1 were identified among the secretion proteins (Figure 3). These two β -glucosidases were designated AaBGL1 and AaBGL2.

Cloning and Sequence Analysis of Genes *aabgl1* and *aabgl2*

According to the genome sequences of *A. amylytica* YIM 77502^T, two putative genes encoding β -glucosidases AaBGL1A (GenBank: MH974516) and AaBGL2 (GenBank: MH974517) were amplified by PCR and introduced into the *pET28a* vector to construct recombinant plasmids *pET28a-aabgl1* and *pET28a-aabgl2*. AaBGL1 and AaBGL2 consisted of 444 and 476 residues with theoretical molecular weights of 48.47 and 52.61 KDa, respectively. Signal peptides were not predicted at the N-termini of AaBGL1 and AaBGL2 based on analysis with Signal P 4.1 Server⁸. Sequence analysis revealed AaBGL1 and AaBGL2 contained distinct catalytic modules of glycosyl hydrolase family 1 (GH1) in the predicted enzyme proteins. The deduced amino acid sequence of AaBGL1 had the highest amino acid sequence identity (89%) to β -glucosidase (NCBI: WP 103938629.1) from *Actinomadura echinospora*. AaBGL2 had 84% similarity with β -glucosidases from *Thermomonospora curvata* (NCBI: WP 012852091.1) and *Actinomadura echinospora* (NCBI: WP 103937196.1). As shown in **Figures 4A,B**, the predicted three-dimensional model structures of AaBGL1 and AaBGL2 were very similar to other GH1 β -glucosidases with known structures. The monomeric subunit of GH1 β -glucosidase adopts the expected topology of a single (α/β)₈ barrel, with additional units of quite well-conserved secondary structures inserted between the α/β units. A phylogenetic analysis of the protein sequences revealed AaBGL1 and AaBGL2 also clustered with β -glucosidases (**Supplementary Figures S3, S4**).

Expression and Purification of β -glucosidases AaBGL1 and AaBGL2

The β -glucosidase genes were successfully expressed in *E. coli* BL21 (DE3) and the resulting recombinant proteins with His-tagged N-termini were purified by Ni-NTA affinity chromatography. SDS-PAGE analysis indicated the molecular masses of the recombinant β -glucosidase proteins were in good agreement with the theoretical ones (Figures 4C,D).

⁸<http://www.cbs.dtu.dk/services/SignalP/>

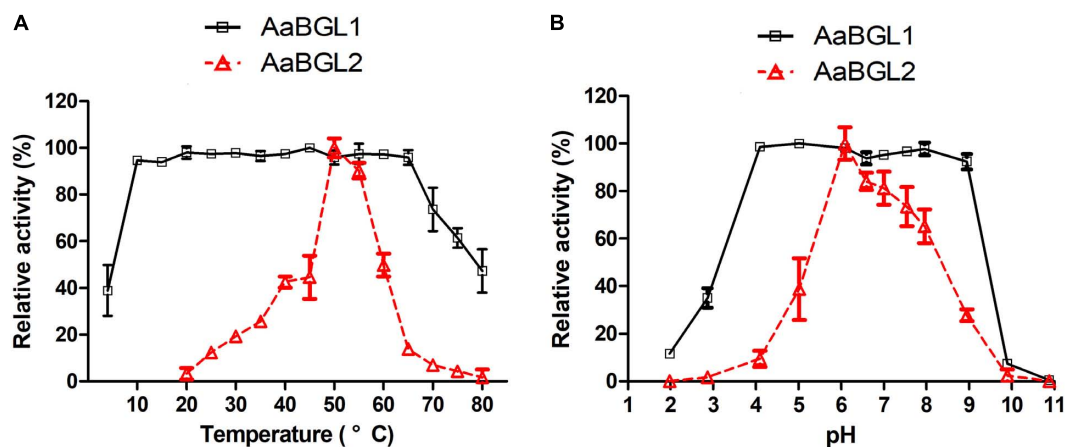


FIGURE 5 | Effects of temperature and pH on the activity and stability of the recombinant AaBGL1 and AaBGL2. **(A,B)** Effect of **(A)** temperature and **(B)** pH on the activity of the recombinant β -glucosidases. The primary activity was designated 100%. Each value in the figure represents the mean \pm standard deviation ($n = 3$). AaBGL1: 100% = 6.2 U/mg. AaBGL2 100% = 5.6 U/mg.

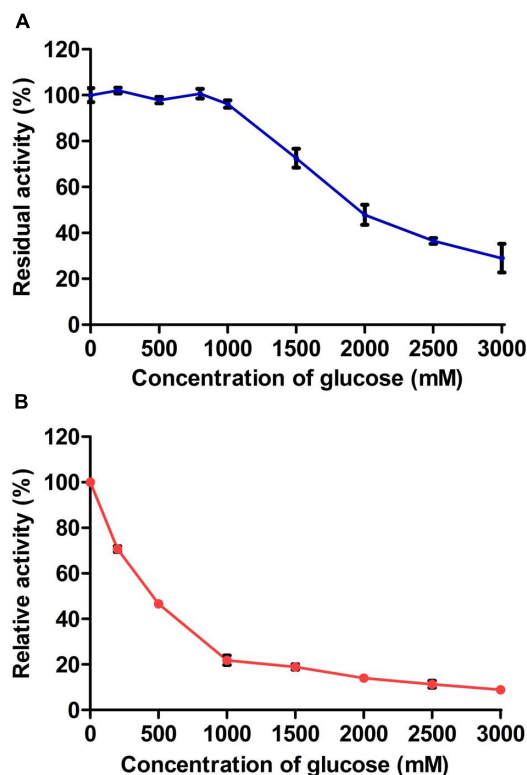


FIGURE 6 | Effect of glucose concentration on recombinant **(A)** AaBGL1 and **(B)** AaBGL2.

Enzymatic Characteristics of Purified Recombinant AaBGL1 and AaBGL2

Optimal Temperatures and Thermostabilities

AaBGL1 exhibited high activity at 10–65°C at the optimal pH of 6.0. AaBGL2 exhibited the highest activity at 50°C and a pH of 6.0

(Figure 5A). Within 2 h, AaBGL1 and AaBGL2 were stable below 50°C, but their activity rapidly decreased when the temperature rose above 50°C (Supplementary Figures S5A, S6A). The thermostabilities of AaBGL1 and AaBGL2 were similar to reported β -glucosidases from fungi and bacteria, which were lost most activity when the temperature above 50°C (Santos et al., 2016; Florindo et al., 2018).

Optimal pHs and Stability at These pHs

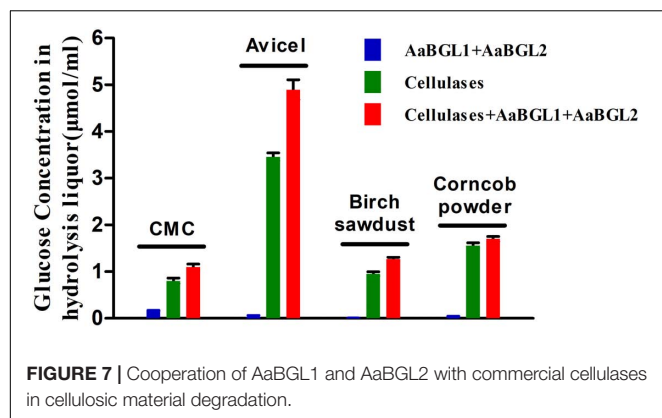
The effects of pH on the activity of the β -glucosidases AaBGL1 and AaBGL2 were assessed. AaBGL1 functioned in a broad optimum pH, retaining more than 95% of the catalytic activity at pHs ranging from 4.0 to 9.0. The optimum pH of AaBGL2 was 6 (Figure 5B). As shown in Supplementary Figures S5B, S6B, AaBGL1 was stable in the pH range of 4.0–9.0, retaining 100%

TABLE 2 | Substrate specificities of AaBGL1 and AaBGL2.

Substrates	AaBGL1 (U/mg)	AaBGL2 (U/mg)
Cellobiose	6.2 \pm 0.3	5.6 \pm 0.2
pNPG	4 \pm 0.2	1.3 \pm 0.1
pNP- α -G	0.56 \pm 0.05	0
pNPX	0	0
pNPC	0.75 \pm 0.1	0.1 \pm 0.02
CMC	0	0
Avicel	0	0
Beechwood xylan	0	0

TABLE 3 | Kinetic parameters of AaBGL1 and AaBGL2.

	Vmax (μ mol/min/mg)		Km (μ mol/ml)		Kcat (s^{-1})	
	Cellobiose	pNPG	Cellobiose	pNPG	Cellobiose	pNPG
AaBGL1	13.2	6.8	95.3	3.3	10.7	5.5
AaBGL2	18.9	1.9	187.7	0.73	16.6	1.7



residual activity after incubating for 12 h in pH buffer at 25°C. AaBGL2 was relatively pH stable, retaining more than 60% residual activity after incubation for 24 h at pH 4–10 at 25°C.

Effects of Metal Ions and Chemical Reagents on Activity

The influence of various metal ions and chemical reagents on the activity of AaBGL1 and AaBGL2 was also investigated and the results are shown in **Supplementary Figure S7**. The enzymatic activity of AaBGL1 was $102 \pm 0.3\%$ and $100 \pm 1.2\%$ by K^+ and Mg^{2+} , respectively. Na^+ , Ca^{2+} , Co^{2+} , Ni^{2+} , and SDS ions at a concentration of 10 mM did not affect AaBGL1 activity. Fe^{3+} and Mn^{2+} slightly inhibited both AaBGL1 and AaBGL2 activity, while Cu^{2+} , Co^{2+} , Zn^{2+} , Ni^{2+} , and EDTA severely inhibited AaBGL1 activity. The enzymatic activity of AaBGL2 was not influenced by K^+ , Na^+ , Mg^{2+} , or Ca^{2+} ; however, the addition of Cu^{2+} , Co^{2+} , Zn^{2+} , Ni^{2+} , SDS, and EDTA strongly inhibited AaBGL2 activity.

Effect of Glucose Concentration on Enzymatic Activity

The glucose tolerances of AaBGL1 and AaBGL2 were determined using 1 mM pNPG as a substrate. The activity of AaBGL1 and AaBGL2 measured in the absence of exogenous glucose was set as 100%. As shown in **Figure 6**, glucose had no effect on AaBGL1 activity when the added glucose concentration was less than 1000 mM. Even when the added glucose concentration was 2000 times greater than the pNPG concentration, AaBGL1 still retained more than 40% activity, suggesting AaBGL1 is highly tolerant of glucose. AaBGL2 also retained 40% activity when the added glucose concentration was 500 times greater than the pNPG concentration (**Figure 6**). This suggests AaBGL2 is also a glucose-tolerant β -glucosidase.

Substrate Specificities and Kinetic Constants of AaBGL1 and AaBGL2

Analysis of substrate specificity revealed AaBGL1 hydrolyzed pNPG, cellobiose, pNP- α -G, and pNPC, but not pNPX, beechwood xylan, CMC, or Avicel (**Table 2**). AaBGL2 exhibited activity for pNPG and cellobiose, but not other tested substrates. Based on Lineweaver-Burk plots (**Supplementary Figures S8, S9**), the K_{cat} , K_m , and V_{max} of AaBGL1 and

AaBGL2 calculated using the pNPG and cellobiose as substrates are shown in **Table 3**.

Potential Use of AaBGL1 and AaBGL2 for Enzymatic Hydrolysis of CMC, Avicel, and Ionic Liquid-Pretreated Birch Sawdust and Corncob Powder

To evaluate the potential use of AaBGL1 and AaBGL2 in degradation of lignocellulose, enzymatic hydrolysis of various lignocellulosic materials, including CMC, Avicel, and ionic liquid-pretreated birch sawdust and corncob powder, were performed. As shown in **Figure 7**, the glucose concentrations in the hydrolysis liquors were ordered Avicel > corncob > birch sawdust > CMC. After adding the β -glucosidases AaBGL1 and AaBGL2 to commercial cellulases, the degradation rates of CMC, Avicel, birch sawdust, and corncob powder increased by 37, 42, 33, and 9%, respectively. This suggests AaBGL1 and AaBGL2 cooperated with commercial cellulases in cellulose degradation.

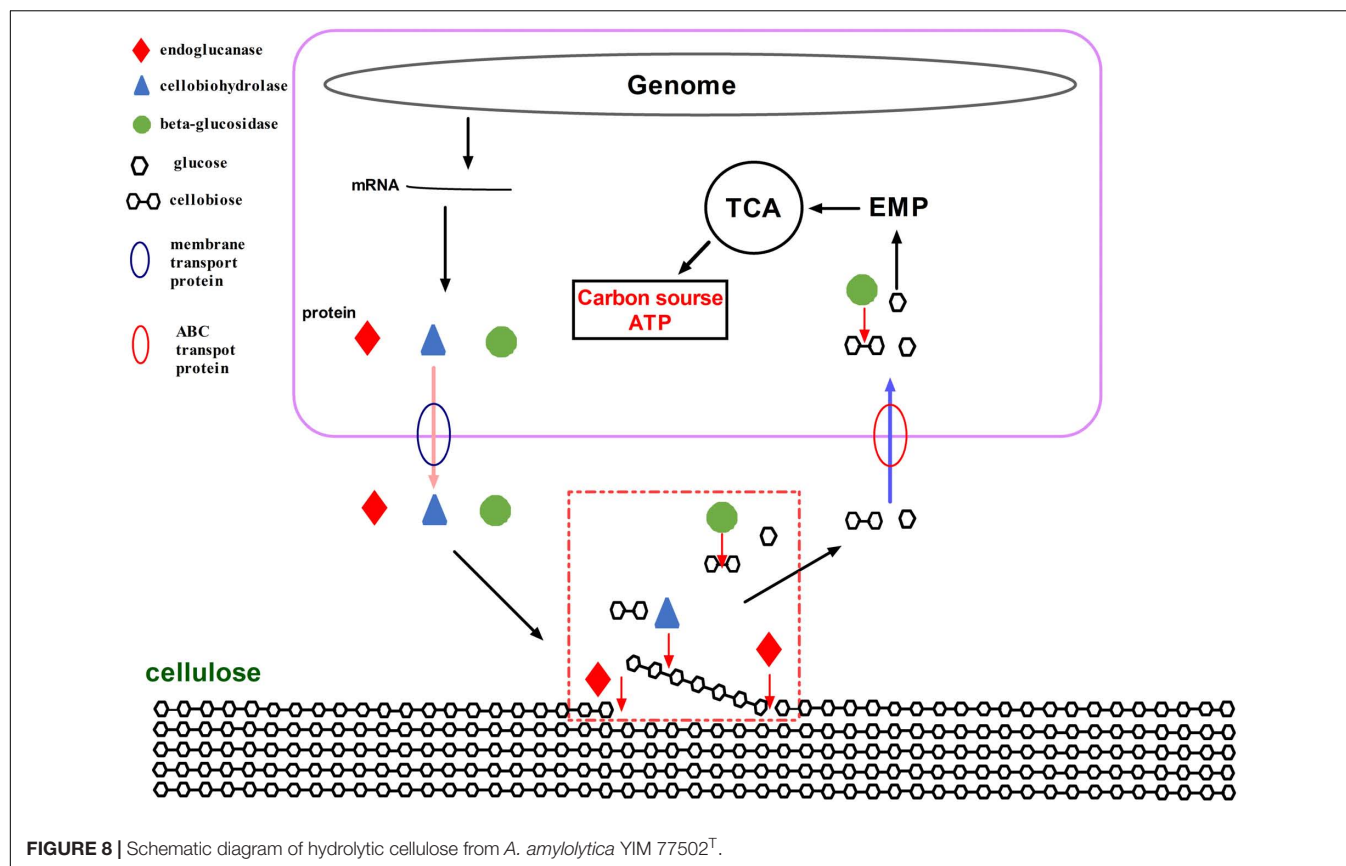
DISCUSSION

A. amyloxyticus Is a Potential Source of Cellulose Hydrolases

An aerobic Gram-positive actinomycete, *A. amyloxyticus* YIM 77502^T can digest cellulose rapidly and efficiently. A large number of glycosidase enzymes, including 9 cellulase genes and 11 β -glucosidase genes, have been predicted in the genome of *A. amyloxyticus*. Other actinomycetes, such as *Thermobifida fusca* (Wilson, 2010), *Thermobifida halotolerans* YIM 90462^T (Yin et al., 2015), *Thermoactinospira rubra* YIM 77501^T (Yin et al., 2017), and *Streptomyces* strains (Ventorino et al., 2016), also display highly lignocellulose-degrading activities. To date, many cellulose-degrading enzymes have been identified from cellulolytic actinomycetes (Vanev et al., 2017), indicating cellulolytic actinomycetes, such as *A. amyloxyticus*, are good potential sources of cellulose hydrolases.

In this research, 4 cellulases and 2 β -glucosidases were identified from the secretome of *A. amyloxyticus* YIM 77502^T cultured with microcrystalline cellulose. These enzymes may be involved in the degradation of cellulose, but no signal peptides were found in the 2 identified β -glucosidases, AaBGL1 and AaBGL2. Broeker et al. (2018) also found 32 proteins lacking signal peptides in the secretome of *Clostridium stercoarum*. These 2 β -glucosidases of *A. amyloxyticus* found in the secretome may be secreted through the release of proteins from cells through cell lysis or alternative secretion pathways. The sequence similarity, tertiary structures, and ML phylogenetic trees of AaBGL1 and AaBGL2 suggest GH1 β -glucosidases are conserved. Discovery of AaBGL1 and AaBGL2 in the secretome of *A. amyloxyticus* indicates LC-MS/MS is potentially a highly useful method of discovering new proteins with specific functions.

During cellulose degradation, cellulolytic microorganisms secrete some hydrolytic enzymes, including free cellulases (endoglucanase, cellobiohydrolases, and β -glucosidases) and



cellulosome, which consist of a wide variety of polysaccharide-degrading enzymes (e.g., cellulases, hemicellulases, and pectinases) (Wilson, 2009; Artzi et al., 2017). Most bacteria and fungi hydrolyze cellulose by secreting free cellulases (Cavedon et al., 1990; Ja'afaru, 2013). Meanwhile, a cellulosome is a supramolecular multienzyme complex that can efficiently degrade lignocellulose and is found in just a few bacterial species, including *Clostridium* (*Ruminiclostridium*) *clariflavum* and *Clostridium* (*Ruminiclostridium*) *thermocellum* (Bayer et al., 2004; Shiratori et al., 2009; Shinoda et al., 2018). As described above, *A. amylytica* YIM 77502^T secreted cellulases extracellularly to hydrolyze cellulose. A total of 344 and 38 genes in the genome of *A. amylytica* were found to potentially be involved in carbohydrate transport and secretory transport of proteins, respectively (Supplementary Figure S1). Of these genes, membrane transporters are membrane proteins associated with transportation of macromolecules, such as proteins, across biological membranes (Saier et al., 2006). ATP-binding cassette transporters (ABC transporters) are members of a transport system superfamily and involved in the translocation of various substrates, such as glucose, cellobiose, and galactose, across membranes (Kemner et al., 1997; Petit et al., 2015).

Membrane transporters and ABC transporters from *A. amylytica* possibly transfer cellulose-degrading enzymes and carbohydrates. Through the activity of *A. amylytica* extracellular enzymes, secretome and TLC plate analyses of CMC hydrolysis products, including endoglucanase,

cellobiohydrolases, and β -glucosidases, revealed hydrolysis of cellulose to oligosaccharides (cellobiose as the main product) and monosaccharide (glucose). As shown in a schematic diagram (Figure 8), cellulose-degrading enzymes are secreted into the extracellular medium and the cellulosic substrate is degraded by synergistic hydrolysis of these free glycosidolytic enzymes. The cellulose hydrolyze these products (cellobiose and glucose), which are then transported to the cytoplasm across the cell membrane through ABC transporters. The oligosaccharides are eventually hydrolyzed to monosaccharides by intracellular β -glucosidases. Finally, glucose entrance into the Embden-Meyerhof-Parnas pathway and tricarboxylic acid cycle provided material (carbon source) and energy (ATP) required for the growth and reproduction of *A. amylytica*. This is the process of cellulose hydrolysis in pure culture in the laboratory simulation, but cellulose does not exist in a pure state in nature. Besides cellulose, there are also large amounts of hemicellulose, lignin, and pectin in plant biomass. Xylan, one of the main components of hemicellulose, can be hydrolyzed by xylanases. As shown in Figures 3, 4 GH10 xylanases were identified in the secretome of *A. amylytica*, indicating they were also induced by cellulose. Robison reported that *Trichoderma reesei* Rut C-30 produces extracellular xylanases when grown on cellulose (Robison, 1984). The complete hydrolysis of lignocellulose requires the synergistic cooperation of cellulases, xylanase, pectinase, laccase, and other enzymes (Van Dyk and Pletschke, 2012). Therefore, for *A. amylytica*, the collaborative expression of cellulases and

xylanases may be a functional adaptation for hydrolysing plant biomass to be used as a carbon source.

Two β -glucosidases (AaBGL1 and AaBGL2) secreted by *A. amylytica* exhibited synergistic cooperation with commercial cellulases. After adding AaBGL1 and AaBGL2, the decomposition rate of Avicel (40%), CMC (37%), and ionic liquid-pretreated birch sawdust (33%) increased by more than 30%. Meanwhile, the degradation rate of ionic liquid-pretreated corncob improved only 9%. Compared to wood, such as birch sawdust, corncob contains more hemicellulose as it is more than one-third of the dry matter of the corncob (Sun et al., 2014). This indicates degradation of substrate by the synergistic action of different kinds of cellulases is related to the purity or amount of cellulose in the substrate. It was also suggested that cellulases need to cooperate with other enzymes, such as hemicellulases (e.g., xylanase) and pectinase, when lignocellulose is degraded. The importance of the cocktail method for degradation of lignocellulosic materials also indicates that more new enzyme resources need to be found to enhance this synergistic degradation (Ibrahim, 2011).

The enzymatic properties of AaBGL1 and AaBGL2 include that, like other β -glucosidases, their activities were completely inhibited by Cu^{2+} (Chen et al., 2010; Wu et al., 2018). However, the activity of AaBGL1 was not affected by 10 mM SDS. A strong denaturant of proteins, SDS can inactivate most enzymes (Joo and Chang, 2010). The SDS stability of AaBGL1 suggests it is suitable for application in industrial purposes. During cellulose hydrolysis by cellulases, the hydrolysis products inhibit the activity of the enzymes. Most β -glucosidases are sensitive to the final product of glucose, which limits the use of β -glucosidase and efficient degradation of cellulose. The inhibition constants (K_i) of AaBGL1 and AaBGL2 were 1502 and 193.5 mM glucose, respectively. Meanwhile, the K_i of most fungal β -glucosidases, such as β -glucosidases from *Penicillium citrinum* UFV1, *Chaetomium globosum*, and *Neurospora crassa*, are between 0.1 and 10 mM (Bohlin et al., 2010; Da Costa et al., 2016). This indicates AaBGL1 and AaBGL2 are glucose-tolerant β -glucosidases. The glucose-tolerances of β -glucosidases are of great significance due to increases in glucose concentration and the conversion rates of soluble fermentable sugars from cellulose degradation.

CONCLUSION

Actinomadura amylytica YIM 77502^T exhibited CMCase and β -glucosidase activity when cultivated at 40°C using Avicel as the sole carbon source. Two GH1 β -glucosidases, designated AaBGL1 and AaBGL2, were identified in the secretome of *A. amylytica* by LC-MS/MS. AaBGL1 and AaBGL2 were successfully expressed in *E. coli* BL21, and the recombinant proteins were purified and characterized. Both AaBGL1 and AaBGL2 were highly glucose-tolerant β -glucosidases and exhibited synergistic cooperation with commercial cellulases. Overall, the β -glucosidases studied in this work (AaBGL1 and AaBGL2) had different specificities and characteristics and could be used in different biotechnological applications, such as bioethanol production.

AUTHOR CONTRIBUTIONS

Y-RY, MX, and W-JL conceived the study. PS and WH were responsible for bioinformatics analysis of the genome and secretome. W-DX and XL cultured strains and collected samples. Y-RY and J-YJ separated proteins. LL and MX measured enzymatic activity. Y-RY and PS performed the data analysis and mapping. Y-RY, PS, MX, and W-JL wrote the manuscript. All authors discussed the results and commented on the manuscript. All authors read and approved the final manuscript.

FUNDING

This research was supported by the Infrastructure work project of the China Ministry of Science and Technology (No. 2015FY110100), Guangzhou Municipal People's Livelihood Science and Technology Plan (No. 201803030030), and China Postdoctoral Science Foundation (Grant No. 2017M622861). The authors are grateful to the Deanship of Scientific Research, King Saud University for funding through Vice Deanship of Scientific Research Chairs. W-JL was supported by the Guangdong Province Higher Vocational Colleges & Schools Pearl River Scholar Funded Scheme (2014).

SUPPLEMENTARY MATERIAL

The Supplementary Material for this article can be found online at: <https://www.frontiersin.org/articles/10.3389/fmicb.2018.03149/full#supplementary-material>

FIGURE S1 | Clusters of orthologous groups (COG) functional classification of *Actinomadura amylytica* genome-encoded proteins.

FIGURE S2 | COG functional classification of secretome of *A. amylytica*.

FIGURE S3 | Phylogenetic dendrogram obtained by maximum likelihood (ML) analysis based on amino acid sequences showing the phylogenetic position of AaBGL1 with related β -glucosidases. Bootstrap values (expressed as a percentage of 1000 replications) are given at nodes.

FIGURE S4 | Phylogenetic dendrogram obtained by maximum likelihood (ML) analysis based on amino acid sequences showing the phylogenetic position of AaBGL2 with related β -glucosidases. Bootstrap values (expressed as a percentage of 1000 replications) are given at nodes.

FIGURE S5 | Effects of temperature and pH on the stability of recombinant AaBGL1. (A,B) The effect of (A) temperature and (B) pH on stability.

FIGURE S6 | Effects of temperature and pH on the stability of recombinant AaBGL2. (A,B) The effect of (A) temperature and (B) pH on stability.

FIGURE S7 | Effects of metal ions and reagents on the activity of (A) AaBGL1 and (B) AaBGL2. Statistical analysis was performed using one-way ANOVA followed by Tukey's test for comparison of multiple treatment groups. Data marked with * and ** were statistically significant different at the $p < 0.05$ and $p < 0.001$ cut-off values, respectively.

FIGURE S8 | Lineweaver-Burk plots of AaBGL1 for pPNG (A) and cellobiose (B).

FIGURE S9 | Lineweaver-Burk plots of AaBGL2 for pPNG (A) and cellobiose (B).

TABLE S1 | The general genomic features of *A. amylytica*.

REFERENCES

- Artzi, L., Bayer, E. A., and Morais, S. (2017). Cellulosomes: bacterial nanomachines for dismantling plant polysaccharides. *Nat. Rev. Microbiol.* 15, 83–95. doi: 10.1038/nrmicro.2016.164
- Bayer, E. A., Belaich, J. P., Shoham, Y., and Lamed, R. (2004). The cellulosomes: multienzyme machines for degradation of plant cell wall polysaccharides. *Annu. Rev. Microbiol.* 58, 521–554. doi: 10.1146/annurev.micro.57.030502.091022
- Bendtsen, J. D., Nielsen, H., Heijne, G. V., and Brunak, S. (2004). Improved prediction of signal peptides: signalp 3.0. *J. Mol. Biol.* 340, 783–795. doi: 10.1016/j.jmb.2004.05.028
- Bohlin, C., Olsen, S. N., Morant, M. D., Patkar, S., Borch, K., and Westh, P. (2010). A comparative study of activity and apparent inhibition of fungal beta-glucosidases. *Biotechnol. Bioeng.* 107, 943–952. doi: 10.1002/bit.22885
- Brinchi, L., Cotana, F., Fortunati, E., and Kenny, J. M. (2013). Production of nanocrystalline cellulose from lignocellulosic biomass: technology and applications. *Carbohydr. Polym.* 94, 154–169. doi: 10.1016/j.carbpol.2013.01.033
- Broeker, J., Mechelke, M., Baudrexel, M., Mennerich, D., Hornburg, D., Mann, M., et al. (2018). The hemicellulose-degrading enzyme system of the thermophilic bacterium *Clostridium stercorarium*: comparative characterisation and addition of new hemicellulolytic glycoside hydrolases. *Biotechnol. Biofuels* 11:229. doi: 10.1186/s13068-018-1228-3
- Cantarel, B. L., Coutinho, P. M., Rancurel, C., Bernard, T., Lombard, V., and Henrissat, B. (2009). The carbohydrate-active enzymes database (CAZy): an expert resource for glycogenomics. *Nucleic Acids Res.* 37, D233–D238. doi: 10.1093/nar/gkn663
- Cavedon, K., Leschine, S. B., and Canale-Parola, E. (1990). Cellulase system of a free-living, mesophilic clostridium (strain C7). *J. Bacteriol.* 172, 4222–4230. doi: 10.1128/jb.172.8.4222-4230.1990
- Chauve, M., Mathis, H., Huc, D., Casanave, D., Monot, F., and Lopes Ferreira, N. (2010). Comparative kinetic analysis of two fungal beta-glucosidases. *Biotechnol. Biofuels* 3:3. doi: 10.1186/1754-6834-3-3
- Chen, S., Hong, Y., Shao, Z., and Liu, Z. (2010). A cold-active β -glucosidase (Bgl1C) from a sea bacteria *Exiguobacterium oxidotolerans* A011. *World J. Microbiol. Biotechnol.* 26, 1427–1435. doi: 10.1007/s11274-010-0317-7
- Chen, Y., He, Y., Zhang, B., Yang, J., Li, W., Dong, Z., et al. (2011). Complete genome sequence of *Alicyclobacillus acidocaldarius* strain Tc-4-1. *J. Bacteriol.* 193, 5602–5603. doi: 10.1128/JB.05709-11
- Cheng, G., Varanasi, P., Arora, R., Stavila, V., Simmons, B. A., Kent, M. S., et al. (2012). Impact of ionic liquid pretreatment conditions on cellulose crystalline structure using 1-ethyl-3-methylimidazolium acetate. *J. Phys. Chem. B* 116, 10049–10054. doi: 10.1021/jp304538v
- Cox, J., and Mann, M. (2008). Maxquant enables high peptide identification rates, individualized p.p.b.-range mass accuracies and proteome-wide protein quantification. *Nat. Biotechnol.* 26, 1367–1372. doi: 10.1038/nbt.1511
- Da Costa, S. G., Pereira, O. L., Teixeira-Ferreira, A., Valente, R. H., da Rezende, S. T., Guimarães, V. M., et al. (2018). *Penicillium citrinum* UFV1 β -glucosidases: purification, characterization, and application for biomass saccharification. *Biotechnol. Biofuels* 11:226. doi: 10.1186/s13068-018-1226-5
- Datta, S. (2016). Recent strategies to overexpress and engineer cellulases for biomass degradation. *Curr. Metabolomics* 4, 14–22. doi: 10.2174/2213235X03666150702155845
- Finn, R. D., Clements, J., and Eddy, S. R. (2011). HMMER web server: interactive sequence similarity searching. *Nucleic Acids Res.* 39, 29–37. doi: 10.1093/nar/gkr367
- Florindo, R. N., Souza, V. P., Manzone, L. R., Camilo, C. M., Marana, S. R., Polikarpov, I., et al. (2018). Structural and biochemical characterization of a GH3 B-glucosidase from the probiotic bacteria, *Bifidobacterium adolescentis*. *Biochimie* 148, 107–115. doi: 10.1016/j.biochi.2018.03.007
- Gu, S., Fang, L., and Xu, X. (2013). Using SOAPaligner for short reads alignment. *Curr. Protoc. Bioinformatics* 44, 11.11.1–11.11.17. doi: 10.1002/0471250953.bi1111s44
- Harnpicharnchai, P., Champreda, V., Sornlake, W., and Eurwilaichitr, L. (2009). A thermotolerant beta-glucosidase isolated from an endophytic fungi, *Periconia* sp., with a possible use for biomass conversion to sugars. *Protein Expr. Purif.* 67, 61–69. doi: 10.1016/j.pep.2008.05.022
- Henrissat, B., Driguez, H., Viet, C., and Schülein, M. (1985). Synergism of cellulases from *Trichoderma reesei* in the degradation of cellulose. *Nat. Biotechnol.* 3, 722–726. doi: 10.1038/nbt0885-722
- Hornburg, D., Drepper, C., Butter, F., Meissner, F., Sendtner, M., and Mann, M. (2014). Deep proteomic evaluation of primary and cell line motoneuron disease models delineates major differences in neuronal characteristics. *Mol. Cell. Proteomics* 13, 3410–3420. doi: 10.1074/mcp.M113.037291
- Huang, J., Dong, C., Wei, Y., Wang, Q., Li, Z., Ying, C., et al. (2014). Direct ethanol production from lignocellulosic sugars and sugarcane bagasse by a recombinant *Trichoderma reesei* strain HJ48. *Sci. World J.* 2014:798683. doi: 10.1155/2014/798683
- Ibrahim, M. F. (2011). *Crude Cellulase Cocktail for Lignocellulosic Materials Degradation*. Available at: <https://www.researchgate.net/publication/2596779>
- Ja'afaru, M. I. (2013). Screening of fungi isolated from environmental samples for xylanase and cellulase production. *ISRN Microbiol.* 2013:283423. doi: 10.1155/2013/283423
- Jayant, M., Rashmi, J., Shailendra, M., and Deepesh, Y. (2011). Production of cellulase by different co-culture of *Aspergillus niger* and *Penicillium chrysogenum* from waste paper, cotton waste and bagasse. *J. Yeast Fungal Res.* 2, 24–27.
- Jiao, J. Y., Liu, L., Zhou, E. M., Wei, D. Q., Ming, H., Xian, W. D., et al. (2015). *Actinomadura amylolytica* sp. nov. and *Actinomadura cellulolytica* sp. nov., isolated from geothermally heated soil. *Antonie van Leeuwenhoek* 108, 75–83. doi: 10.1007/s10482-015-0465-8
- Joo, H., and Chang, C. (2010). Oxidant and SDS-stable alkaline protease from a halo-tolerant *Bacillus clausii* I-52: enhanced production and simple purification. *J. Appl. Microbiol.* 98, 491–497. doi: 10.1111/j.1365-2672.2004.02464.x
- Kemner, J. M., Liang, X., and Nester, E. W. (1997). The *Agrobacterium tumefaciens* virulence gene *chvE* is part of a putative ABC-type sugar transport operon. *J. Bacteriol.* 179, 2452–2458. doi: 10.1128/jb.179.7.2452-2458.1997
- Khandeparker, R., and Numan, M. T. (2008). Bifunctional xylanases and their potential use in biotechnology. *J. Ind. Microbiol. Biotechnol.* 35, 635–644. doi: 10.1007/s10295-008-0342-9
- Liu, S. Y., Shibu, M. A., Jhan, H. J., Lo, C. T., and Peng, K. C. (2010). Purification and characterization of novel glucanases from *Trichoderma harzianum* ETS 323. *J. Agric. Food Chem.* 58, 10309–10314. doi: 10.1021/jf1029338
- Madden, T. (2002). “The BLAST sequence analysis tool,” in *The NCBI Handbook Internet*, ed. J. McEntyre (Bethesda, MD: National Library of Medicine).
- Mallerman, J., Papinutti, L., and Levin, L. (2014). Characterization of β -glucosidase produced by the white rot fungus *flamulinula velutipes*. *J. Microbiol. Biotechnol.* 25, 57–65. doi: 10.4014/jmb.1401.01045
- Miller, G. L. (1959). Use of dinitrosalicylic acid reagent for determination of reducing sugar. *Anal. Biochem.* 31, 426–428. doi: 10.1021/ac60147a030
- Nieves, R. A., Ehrman, C. I., Adney, W. S., Elander, R. T., and Himmel, M. E. (1998). Technical communication: survey and analysis of commercial cellulase preparation suitable for biomass conversion to ethanol. *World J. Microbiol. Biotechnol.* 14, 301–304. doi: 10.1023/A:1008871205580
- Ouyang, J., Yan, M., Kong, D., and Xu, L. (2006). A complete protein pattern of cellulase and hemicellulase genes in the filamentous fungus *Trichoderma reesei*. *Biotechnol. J.* 1, 1266–1274. doi: 10.1002/biot.200600103
- Peterson, R., and Nevalainen, H. (2012). *Trichoderma reesei* RUT-C30—thirty years of strain improvement. *Microbiology* 158, 58–68. doi: 10.1099/mic.0.054031-0
- Petit, E., Coppi, M. V., Hayes, J. C., Tolonen, A. C., Warnick, T., Latouf, W. G., et al. (2015). Genome and transcriptome of clostridium phytofermentans, catalyst for the direct conversion of plant feedstocks to fuels. *PLoS One* 10:e0118285. doi: 10.1371/journal.pone.0118285
- Rahman, Z., Shida, Y., Furukawa, T., Suzuki, Y., Okada, H., Ogasawara, W., et al. (2009). Application of *Trichoderma reesei* cellulase and xylanase promoters through homologous recombination for enhanced production of extracellular beta-glucosidase I. *Biosci. Biotechnol. Biochem.* 73, 1083–1089. doi: 10.1271/bbb.80852
- Robison, P. D. (1984). Cellulase and xylanase production by *Trichoderma reesei* rut C-30. *Biotechnol. Lett.* 6, 119–122. doi: 10.1007/BF00127301
- Saier, M. H. Jr., Tran, C. V., and Barabote, R. D. (2006). TCDB: the transporter classification database for membrane transport protein analyses and information. *Nucleic Acids Res.* 34, D181–D186. doi: 10.1093/nar/gkj001

- Sali, A., and Blundell, T. L. (1993). Comparative protein modelling by satisfaction of spatial restraints. *Mol. Med. Today* 1, 270–277.
- Saloheimo, M., Kujapanula, J., Ylösmäki, E., Ward, M., and Penttilä, M. (2002). Enzymatic Properties and intracellular localization of the novel *Trichoderma reesei* β -glucosidase BGLII (Cel1A). *Appl. Environ. Microbiol.* 68, 4546–4553. doi: 10.1128/AEM.68.9.4546-4553.2002
- Santos, C. A., Zanthorlin, L. M., Crucello, A., Tonoli, C. C. C., Ruller, R., Horta, M. A. C., et al. (2016). Crystal structure and biochemical characterization of the recombinant ThBgl, a GH1 β -glucosidase overexpressed in *Trichoderma harzianum* under biomass degradation conditions. *Biotechnol. Biofuels* 9:71. doi: 10.1186/s13068-016-0487-0
- Schwanhäusser, B., Busse, D., Li, N., Dittmar, G., Schuchhardt, J., Wolf, J., et al. (2013). Global quantification of mammalian gene expression control. *Nature* 495, 126–127. doi: 10.1038/nature11848
- Shinoda, S., Kurosaki, M., Kokuzawa, T., Hirano, K., Takano, H., Ueda, K., et al. (2018). Comparative biochemical analysis of cellulosomes isolated from *Clostridium clariflavum* DSM 19732 and *Clostridium thermocellum* ATCC 27405 grown on plant biomass. *Appl. Biochem. Biotechnol.* doi: 10.1007/s12010-018-2864-6 [Epub ahead of print].
- Shiratori, H., Sasaya, K., Ohiwa, H., Ikeno, H., Ayame, S., Kataoka, N., et al. (2009). *Clostridium clariflavum* sp. nov. and *Clostridium caenicola* sp. nov., moderately thermophilic, cellulose-/cellobiose-digesting bacteria isolated from methanogenic sludge. *Int. J. Syst. Evol. Microbiol.* 59, 1764–1770. doi: 10.1099/ijs.0.003483-0
- Sun, S. N., Cao, X. F., Xu, F., Sun, R. C., Jones, G. L., and Baird, M. (2014). Structure and thermal property of alkaline hemicelluloses from steam exploded *Phyllostachys pubescens*. *Carbohydr. Polym.* 101, 1191–1197. doi: 10.1016/j.carbpol.2013.09.109
- Tamura, K., Peterson, D., Peterson, N., Stecher, G., Nei, M., and Kumar, S. (2011). MEGA5: molecular evolutionary genetics analysis using maximum likelihood, evolutionary distance, and maximum parsimony methods. *Mol. Biol. Evol.* 28, 2731–2739. doi: 10.1093/molbev/msr121
- Tatusov, R. L., Fedorova, N. D., Jackson, J. D., Jacobs, A. R., Kiryutin, B., Koonin, E. V., et al. (2003). The COG database: an updated version includes eukaryotes. *BMC Bioinformatics* 4:41. doi: 10.1186/1471-2105-4-41
- Thomas, L., Ram, H., and Singh, V. P. (2017). Evolutionary relationships and taxon-specific conserved signature indels among cellulases of archaea, bacteria, and eukarya. *J. Comput. Biol.* 24, 1029–1042. doi: 10.1089/cmb.2016.0161
- Thompson, J. D., Gibson, T. J., Plewniak, F., Jeanmougin, F., and Higgins, D. G. (1997). The Clustal_X windows interface: flexible strategies for multiple sequence alignment aided by quality analysis tools. *Nucleic Acids Res.* 25, 4876–4882. doi: 10.1093/nar/25.24.4876
- Thongpoo, P., McKee, L. S., Araujo, A. C., Kongsaree, P. T., and Brumer, H. (2013). Identification of the acid/base catalyst of a glycoside hydrolase family 3 (GH3) β -glucosidase from *Aspergillus niger* ASKU28. *Biochim. Biophys. Acta* 1830, 2739–2749. doi: 10.1016/j.bbagen.2012.11.014
- Van Dyk, J. S., and Pletschke, B. I. (2012). A review of lignocellulose bioconversion using enzymatic hydrolysis and synergistic cooperation between enzymes—factors affecting enzymes, conversion and synergy. *Biotechnol. Adv.* 30, 1458–1480. doi: 10.1016/j.biotechadv.2012.03.002
- Vanee, N., Brooks, J. P., and Fong, S. S. (2017). Metabolic profile of the cellulolytic industrial actinomycete *Thermobifida fusca*. *Metabolites* 7:57. doi: 10.3390/metabo7040057
- Ventorino, V., Ionata, E., Birolo, L., Montella, S., Marcolongo, L., De Chiaro, A., et al. (2016). Lignocellulose-adapted endo-cellulase producing streptomyces strains for bioconversion of cellulose-based materials. *Front. Microbiol.* 7:2061. doi: 10.3389/fmicb.2016.02061
- Wang, L., Ridgway, D., Gu, T., and Moo-Young, M. (2005). Bioprocessing strategies to improve heterologous protein production in filamentous fungal fermentations. *Biotechnol. Adv.* 23, 115–129. doi: 10.1016/j.biotechadv.2004.11.001
- Wilson, D. B. (2009). The first evidence that a single cellulase can be essential for cellulose degradation in a cellulolytic microorganism. *Mol. Microbiol.* 74, 1287–1288. doi: 10.1111/j.1365-2958.2009.06889.x
- Wilson, D. B. (2010). Studies of *Thermobifida fusca* plant cell wall degrading enzymes. *Chem. Rec.* 4, 72–82. doi: 10.1002/tcr.20002
- Wu, D., Hugenholtz, P., Mavromatis, K., Pukall, R., Dalin, E., Ivanova, N. N., et al. (2009). A phylogeny-driven genomic encyclopaedia of bacteria and archaea. *Nature* 462, 1056–1060. doi: 10.1038/nature08656
- Wu, J., Geng, A., Xie, R., Wang, H., and Sun, J. (2018). Characterization of cold adapted and ethanol tolerant β -glucosidase from *Bacillus cellulosilyticus* and its application for directed hydrolysis of cellobiose to ethanol. *Int. J. Biol. Macromol.* 109, 872–879. doi: 10.1016/j.ijbiomac.2017.11.072
- Yang, F., Yang, X., Li, Z., Du, C., Wang, J., and Li, S. (2015). Overexpression and characterization of a glucose-tolerant beta-glucosidase from *T. aotearoense* with high specific activity for cellobiose. *Appl. Microbiol. Biotechnol.* 99, 8903–8915. doi: 10.1007/s00253-015-6619-9
- Ye, Y., Li, X., and Zhao, J. (2017). Production and characteristics of a novel xylose- and alkali-tolerant GH 43 beta-xylosidase from *Penicillium oxalicum* for promoting hemicellulose degradation. *Sci. Rep.* 7:11600. doi: 10.1038/s41598-017-11573-7
- Yin, Y. R., Meng, Z. H., Hu, Q. W., Jiang, Z., Xian, W. D., Li, L. H., et al. (2017). The hybrid strategy of *Thermoactinospira rubra* YIM 77501(T) for utilizing cellulose as a carbon source at different temperatures. *Front. Microbiol.* 8:942. doi: 10.3389/fmicb.2017.00942
- Yin, Y. R., Zhang, F., Hu, Q. W., Xian, W. D., Hozzein, W. N., Zhou, E. M., et al. (2015). Heterologous expression and characterization of a novel halotolerant, thermostable, and alkali-stable GH6 endoglucanase from *Thermobifida halotolerans*. *Biotechnol. Lett.* 37, 857–862. doi: 10.1007/s10529-014-1742-8
- Zhang, J., Zhong, Y., Zhao, X., and Wang, T. (2010). Development of the cellulolytic fungus *Trichoderma reesei* strain with enhanced β -glucosidase and filter paper activity using strong artificial cellobiohydrolase 1 promoter. *Bioresour. Technol.* 101, 9815–9818. doi: 10.1016/j.biortech.2010.07.078

Conflict of Interest Statement: The authors declare that the research was conducted in the absence of any commercial or financial relationships that could be construed as a potential conflict of interest.

Copyright © 2018 Yin, Sang, Xian, Li, Jiao, Liu, Hozzein, Xiao and Li. This is an open-access article distributed under the terms of the Creative Commons Attribution License (CC BY). The use, distribution or reproduction in other forums is permitted, provided the original author(s) and the copyright owner(s) are credited and that the original publication in this journal is cited, in accordance with accepted academic practice. No use, distribution or reproduction is permitted which does not comply with these terms.



Whole Cell Actinobacteria as Biocatalysts

Yitayal Shiferaw Anteneh^{1,2} and Christopher Milton Mathew Franco^{1*}

¹ College of Medicine and Public Health, Medical Biotechnology, Flinders University, Bedford Park, SA, Australia,

² Department of Medical Microbiology, College of Medicine, Addis Ababa University, Addis Ababa, Ethiopia

Production of fuels, therapeutic drugs, chemicals, and biomaterials using sustainable biological processes have received renewed attention due to increasing environmental concerns. Despite having high industrial output, most of the current chemical processes are associated with environmentally undesirable by-products which escalate the cost of downstream processing. Compared to chemical processes, whole cell biocatalysts offer several advantages including high selectivity, catalytic efficiency, milder operational conditions and low impact on the environment, making this approach the current choice for synthesis and manufacturing of different industrial products. In this review, we present the application of whole cell actinobacteria for the synthesis of biologically active compounds, biofuel production and conversion of harmful compounds to less toxic by-products. Actinobacteria alone are responsible for the production of nearly half of the documented biologically active metabolites and many enzymes; with the involvement of various species of whole cell actinobacteria such as *Rhodococcus*, *Streptomyces*, *Nocardia* and *Corynebacterium* for the production of useful industrial commodities.

Keywords: Actinobacteria, biocatalysts, nitriles, biotransformation, biofuel, ethylene glycol

OPEN ACCESS

Edited by:

Dirk Tischler,
Ruhr-Universität Bochum, Germany

Reviewed by:

Jan Bobek,
Charles University, Czechia
Damjan Franjevic,
University of Zagreb, Croatia
Diego Fabian Gomez-Casati,
National University of Rosario,
Argentina

*Correspondence:

Christopher Milton Mathew
Franco
Chris.franco@flinders.edu.au

Specialty section:

This article was submitted to
Microbial Physiology and Metabolism,
a section of the journal
Frontiers in Microbiology

Received: 07 October 2018

Accepted: 15 January 2019

Published: 18 February 2019

Citation:

Anteneh YS and Franco CMM
(2019) Whole Cell Actinobacteria as
Biocatalysts. *Front. Microbiol.* 10:77.
doi: 10.3389/fmicb.2019.00077

INTRODUCTION

Biotransformation is the process by which substrates are converted into useful products using biocatalysts either in the form of whole cells or their enzymes (Ward and Köhler, 2015; Bezborodov and Zagustina, 2016). The classical chemical based transformation of substrates is prone to several disadvantages, including ecologically unfavorable conditions and associated undesirable by-products (Lin and Tao, 2017). Unlike chemical methods, biocatalysts provide several benefits such as their availability from renewable resources, they work at low temperature and pH, are easy to degrade biologically and are selective in both substrate and product stereochemistry (Jemli et al., 2016). Enzyme based biotransformations, however, are also not free of drawbacks including their high cost, higher susceptibility to changes in operating conditions and substrate or product toxicity (Garzón-Posse et al., 2018). In contrast to other catalytic reactions, whole cell biocatalysts allow transformation of substrates via multiple cascades of reactions, help generation of cofactors, have high regio- and stereo-selectivity, work under mild operational, environmentally-friendly conditions, and help selective hydroxylation of non-activated carbon atoms. The latter is not possible with chemical catalysts (de Carvalho, 2017). In addition to these advantages, compounds produced by microorganisms are considered to be safe, which attract many health-conscious consumers (de Carvalho, 2017).

To meet the growing call for efficient and economically feasible biocatalysts, researchers are testing different groups of microorganisms, including actinobacteria (Mukhtar et al., 2017), *Escherichia coli* (Lin et al., 2013; Ladkau et al., 2014; de Carvalho, 2017), *Pseudomonas putida* (Gehring et al., 2016), *Bacillus cereus* (Banerjee and Ghoshal, 2010), *Enterococcus faecalis* and

Saccharomyces cerevisiae (Whited et al., 2010; Lin and Tao, 2017). Actinobacteria are widely distributed in nature, with several phenotypes including anaerobes, aerobes, spore formers, unicellular, and filamentous forms (Lewin et al., 2016). They are one of the most diverse, well characterized and metabolically versatile group of microorganisms. They play an essential role in maintaining soil structure and carbon recycling through decomposition of various organic matter such as cellulose, chitin, and pectin (Priyadharsini and Dhanasekaran, 2015; Kim et al., 2016). Furthermore, they produce several enzymes (amylases, cellulases, proteases, chitinases, xylanases, and pectinase) (Mukhtar et al., 2017), antibiotics, antitumor agents, plant growth regulators, and vitamins (Prakash et al., 2013; Kamjam et al., 2017).

Over 22,000 biologically active microbial metabolites reported and actinobacteria alone represented 45% of them which are followed by fungi (38%) and unicellular bacteria, especially *Bacillus* sp. and *Pseudomonas* sp. (17%) (Bérdy, 2005; Demain and Sanchez, 2009). Among the described 140 genera of actinobacteria, only few of them produce the majority of active compounds (Jensen et al., 2005; Bull and Stach, 2007; Pimentel-Elardo et al., 2010; Adegboye and Babalola, 2013). *Streptomyces* alone represents three fourth of the total active metabolites produced by actinobacteria (Lam, 2007; Solecka et al., 2012; Barka et al., 2015; Chater, 2016). **Table 1** below highlights the approximate share of each microbial group for active metabolite production.

Apart from the above contributions, actinobacteria play a vital part in the development of a sustainable bioenergy industry, predominantly through their cellulolytic enzymes which decompose plant biomass to produce simple sugars that serve as raw materials for biofuel production. Furthermore, their diverse biosynthetic capacity allow them to mediate various environmental interactions which lead to synthesis of various biologically active products (Lewin

et al., 2016). Here, we review the application of whole cells actinobacteria for biotransformation of various substrates in a way to produce more active and less toxic compounds as well as biofuels.

BIOTRANSFORMATION OF HARMFUL COMPOUNDS

Nitrile Biotransformation

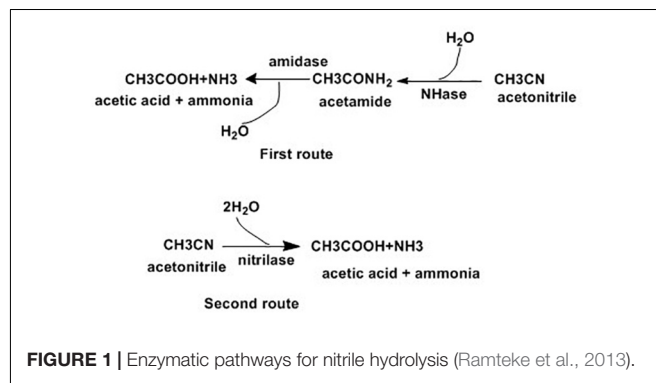
Microbial or enzymatic biotransformation of nitriles result the conversion of these toxic compounds into industrially important compounds like acids and amides. Nitriles constitute a group of chemicals widely used in drugs, rubbers, and plastic industries. These compounds contain a cyano group in their backbone which is highly correlated with toxicity (Ramteke et al., 2013). Their high rate of manufacture and continuous usage make them an important source of environmental pollution and have been detected in different environmental samples including sediments of water-treatment plants, in marinas and beach areas (Baxter and Cummings, 2006). Clinically, nitrile toxicity has been associated with cancer and different health problems such as bronchial irritation, respiratory disorders, convulsions, coma, and skeletal deformities (Ramteke et al., 2013). Some researchers highlighted the link with psycho-behavioral abnormalities including learning, memory, motor nerve anomalies in rats treated with aliphatic nitriles such as acetonitrile, acrylonitrile and crotononitrile (Boadas-Vaello et al., 2007; Ramteke et al., 2013).

The removal of nitrile compounds from the environment is possible using microbial methods, due to their associated low cost and user-friendly approach (Fang et al., 2015). Microorganisms degrade nitrile compounds through the hydrolytic route, which comprises two enzymatic systems as indicated in **Figure 1**. In the first route, nitrile hydratase (NHase, EC 4.2.1.84) catalyzes the formation of amides from nitriles, which are later changed to ammonia and carboxylic acids by amidase (EC 3.5.1.4). Alternatively, nitrilase (EC 3.5.5.1) catalyzes for the direct conversion of nitriles into carboxylic acids and ammonia (Ramteke et al., 2013).

The production of acids and amides from nitriles is possible using chemical catalysts. However, this approach is only achieved

TABLE 1 | Microbial share of active bioactive metabolites (Bérdy, 2005).

Source	Total bioactive metabolites	Antibiotics	Other bioactive metabolites
Bacteria	3800	2900	900
<i>Eubacteriales</i>	2750		
<i>Bacillus</i> sp.	860		
<i>Pseudomonas</i> sp.	795		
<i>Myxobacter</i>	410		
<i>Cyanobacter</i>	640		
Actinobacteria	10100	8700	1400
<i>Streptomyces</i> sp.	7630		
Other genera	2470		
Fungi	8600	4900	3700
Microscopic fungi	6450		
<i>Penicillium/Aspergillus</i>	1950		
<i>Basidiomycetes</i>	2000		
Yeasts	140		
Slime molds	60		
Total	22500	16500	6000



under harsh conditions like extreme temperature, acidity or alkalinity (Nigam et al., 2009). Currently, many microorganisms having either of the two nitrile degradation enzymatic systems have been reported. These microorganisms can be categorized into two groups. The first is made up of bacteria like *Mesorhizobium* sp. F28 (Feng and Lee, 2009), *Klebsiella oxytoca* (Kao et al., 2006), *Rhodococcus erythropolis* A4 and *Rhodococcus rhodochrous* PA-34 (Vesela et al., 2012), which only contain a single enzyme system of NHase/amidase and *Streptomyces* sp. MTCC 7546 only contains nitrilase (Nigam et al., 2009). The other group contain bacteria such as *Nocardia globerula* NHB-2 (Bhalla and Kumar, 2005), *Amycolatopsis* sp. IITR215 (Babu et al., 2010), *Bacillus subtilis* ZJB-063 (Zheng et al., 2008) and *R. rhodochrous* BX2 (Fang et al., 2015), which have both NHase/amidase and nitrilase.

Variation among nitrile degrading microorganisms also exists in terms of the end products of nitrile degradation. Bacteria in the single enzyme system like *R. rhodochrous* PA-34 convert nitrile only into amides while *K. oxytoca* and *Mesorhizobium* sp. F28 convert nitriles into corresponding amides and carboxylic acids. Those bacteria which utilize the two enzyme system result in amides and carboxylic acids. Among these group of bacteria, *R. rhodochrous* BX2, *B. subtilis* AJB-063 and *Paracoccus* sp. SKG (Santoshkumar et al., 2011) displayed completed degradation of carboxylic acids with final end product of ammonia. As indicated above nitrile degradation systems vary among different bacterial genera as well as with in the same genus such as *Rhodococcus*. Unlike others, *Streptomyces* sp. MTCC 7546 in the immobilized as well as Free State biotransforms acrylonitrile into acrylic acid without the formation of amides. The authors suggested that due to several reasons such as operational stability (allow to reuse the system several times), and ease of production on a large scale, the conversion of acrylonitrile using immobilized cells is better than cells in the free state (Nigam et al., 2009).

Biotransformation of Aromatic Ring Containing Compounds

Phthalate esters and phenols are the two most common chemicals used in industry for stabilization and modification of the characteristics and performance of polymers (He Z. et al., 2014). Di-n-butyl phthalate (DBP), a type of phthalate ester, is a component of different merchandises including pesticides, wrapping materials, makeups, wrappers, wears, and insulators in electric disposals (Dargnat et al., 2009). Similarly, phenol can be applied for the manufacturing of drugs, rubbers, polycarbonate resins, and nylon (Christen et al., 2011).

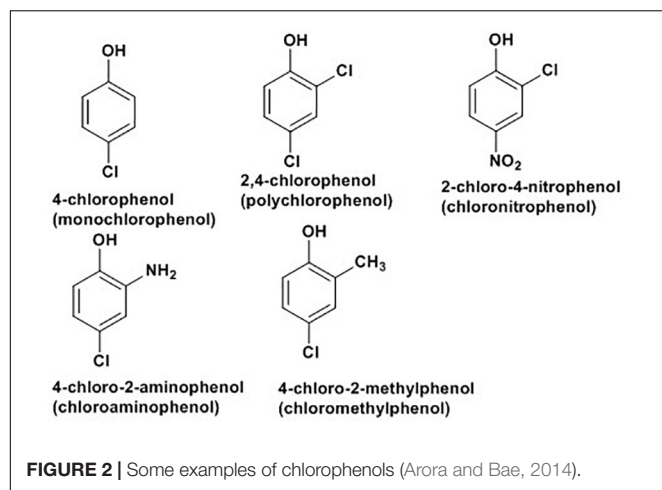
Phthalates are major environmental pollutants which come into contact with humans and animals through contaminated water systems (He Z. et al., 2014). The European community listed these compounds among the 33 dangerous substances to be controlled in surface water (Dargnat et al., 2009). As they are a constituent of plastics which are now ubiquitous in diverse environments phthalates are now present almost everywhere (Fang et al., 2010). Phthalate toxicity is associated with endocrine

system disruption in different species of fish and mammals. These compounds were also observed to interfere with the reproductive system and in human and animal development (Lottrup et al., 2006; Li et al., 2010). Concurrent observation of phenols and phthalate esters has been reported in the Selangor River basin in Malaysia (Santhi and Mustafa, 2013) and induction of lactate dehydrogenase release from Sertoli cells, which is associated with infertility, coexist compared to individual chemical effects (Li et al., 2010).

Different approaches have been documented for removal of DBP from natural environments. These are hydrolysis, photo degradation and biodegradation (Lau et al., 2005; Jonsson et al., 2006; Chen et al., 2009). Two of the former approaches were not effective due to the structural nature of DBP and microbial mediated metabolic transformation of DBP is the current choice. Microbial mediated degradation of DBP involves initial conversion of DBP into phthalic acid and which is further transformed with the help of two dioxygenase pathways into 4,5-dihydroxyphthalate and 4,5-dihydroxyphthalate in gram negative and gram positive bacteria, respectively. Finally, these two compounds are transformed into a common intermediate protocatechuate under aerobic conditions (Wu et al., 2011). For the degradation of phenols the first step is hydroxylation of phenol to catechol followed by ring cleavage of catechol into 2-hydroxymuconic semialdehyde for the meta-pathway aided by catechol-2, 3-dioxygenase and into cis, cis-muconate with the help of catechol-1, 2-dioxygenase for ortho pathway. Finally 2-hydroxymuconic semialdehyde oxidized 4-oxalocrotonate or hydrolyzed it to 2-oxopent-4-enoate and cis, cis-muconate into muconolactone (Banerjee and Ghoshal, 2010).

Several bacteria strains have the ability to degrade DBP, such as *Rhodococcus* sp. (Yu et al., 2009; Jin et al., 2010), *Gordonia* sp. (Wu et al., 2011), *Agrobacterium* sp. (Wu et al., 2011) and *Enterobacter* sp. (Fang et al., 2010). Members of the *Rhodococcus* genus, have been demonstrated for degradation of Phenol in addition to DBP (Saa et al., 2010), individually as well as via simultaneously mineralization of DBP and phenol (Lu et al., 2009; He et al., 2013). Individual or synchronous biodegradation of DBP and phenol by *Rhodococcus ruber* strain DP-2 was also reported in similar study (He Y.C. et al., 2014).

Chlorophenols (CPs) are aromatic compounds which contain a minimum of one chlorine and a hydroxyl group on the benzene rings. Five types of CPs, as indicated in **Figure 2** below, based on chemical structures include monochlorophenols, polychlorophenols, chloronitrophenols, chloroaminophenols, and chloromethylphenols (Arora and Bae, 2014). They are largely used as fungicidal, germicidal and wood preservatives agents. They are also important for synthesis of dyes and drugs (Arora and Bae, 2014). CPs and their derivatives rank among the top environmental pollutants where industrial wastes, pesticides, herbicides, and complex chlorinated hydrocarbons are major sources of contamination (Olaniran and Igbinosa, 2011). Direct skin contact and eating or drinking of contaminated substances are major sources of people exposure (Arora and Bae, 2014). Cellular exposure to CPs are associated with cytotoxic,



mutagenic and carcinogenic properties, with several types of polychlorophenols labeled as potential human carcinogens by the World Health Organization and the International Agency for Research on Cancers (Igbinosa et al., 2013).

Different possible mechanisms are reported for bacterial degradation of CPs and their derivatives. In the first mechanism, hydroxylation of chlorophenolic rings at ortho-positions with the help of monooxygenases results in formation of chlorocatechols which are further degraded (Hollender et al., 1997; Solyanikova and Golovleva, 2011) or hydroxylated prior to ring cleavage (Nordin et al., 2005). In the second mechanism, with the same enzyme, hydroxylation of chlorophenolic rings at meta position results in chlorocatechols which degrade via hydroxylation (Nordin et al., 2005) or dehalogenation (Xun et al., 1992) prior to ring cleavage. The third mechanism applicable for degradation of chloronitrophenols where the degradation may be initiated by hydroxylation (Arora and Jain, 2012), reductive dehalogenation (Pandey et al., 2011), or reduction of the nitro group (Arora and Jain, 2012). Finally, in case of chloroaminophenols degradation, the pathway may start with removal of ammonium ions by the enzyme deaminase followed by the ring cleavage (Arora and Bae, 2014) or the dehalogenation (Arora and Bae, 2014). The detail mechanisms of different routes of biodegradation of chlorophenols and its derivatives with various bacteria, such as *Pseudomonas knackmussii* B-13, *Rhodococcus opacus* 1G, *Arthrobacter chlorophenolicus* A6, *Streptomyces rochei* 303, *Pseudomonas* sp. NCIB9340, *Bacillus insolitus*, *Nocardioides* sp. K44, *Mycobacterium chlorophenolicum* PCP1 and *Mycobacterium fortuitum* CG-2 are well documented in a recent review by Arora and Bae (2014); and the following **Figure 3** presents degradation of 4-chlorophenol as an example of the process.

Hou and his colleagues reported for the first time magnetically immobilized *R. rhodochrous* cells for biodegradation of CPs. Their study demonstrated that *R. rhodochrous* DSM6263 depends on constitutively expressed enzymes for hydroxylation of CPs resulting in chlorocatechol formation and complete degradation. Their observation was consistent with another study where *Rhodococcus* sp. AN-22 (an aniline-assimilating bacterium)

produced *cis, cis*-muconic acid from catechol (Matsumura et al., 2006) and highlighted how these compounds could also be metabolized with immobilized cells of *R. rhodochrous* DSM6263 (Hou et al., 2016). Researchers advocated the use of immobilized cells, over free cells, to degrade toxic chemicals due to many reasons such as long-term stability of the catalyst and the immobilization also protects cells from harmful effects of toxic pollutants (Jianlong et al., 2002). Immobilization of cells can be done using a number of techniques including surface adsorption, natural or artificial flocculation, covalent or electrostatic binding to carriers, and encapsulation in a polymer-gel (Hou et al., 2016).

Atrazine (2-chloro-4-(ethylamino)-6-(isopropylamino)-1, 3, 5-triazine) was first introduced in 1950s as an emergent herbicide and they are among widely used pesticides in different countries such as United States, Canada, Africa, and Asia Pacific region (Huang et al., 2003; Jablonowski et al., 2011). Usage of atrazine banned in European countries in 2004 as atrazine concentrations in water surpassed or were estimated to surpass allowable limits (Jablonowski et al., 2011). Due to factors like its widespread utilization as a herbicide and its persistence in the environment, it is common to observe traces of atrazine both in surface and ground water bodies (Gilliom et al., 2006). Traces of atrazine were detected in widely dispersed areas which are far from urban and agricultural areas such as in rainwater in different places (Brun et al., 2008) in fog, arctic ice and seawater.

Contact with atrazine is associated with a serious threat to human and ecosystem health. One of the most notable effects of exposure is endocrine (Solomon et al., 2008; Rohr and McCoy, 2010). Many studies link atrazine with harmful effects on the health of animals and humans, such as sexual abnormalities (demasculinization) in frogs, low testosterone production in rats and higher levels of prostate cancer in workers at an atrazine manufacturing factory (Hecker et al., 2005; Liu and Parales, 2009), and it is also categorized as a group 3 carcinogen according to the International Agency for research on cancer¹. The above observations indicated that there is cause for concern regarding atrazine residues in soil, groundwater, and surface waters.

Due to its persistence in the environment and being highly toxic, it is very important to develop approaches to degrade and remove atrazine deposits from the environment. Microbial-degradation is one of the methods for elimination of atrazine from soil (Tappe et al., 2002). Different species of microorganisms associated with degradation of atrazine with various degree of biodegradation where some undergo complete mineralization while others produce various intermediates including hydroxyatrazine, deethylatrazine, deisopropylatrazine, *n*-isopropylammilide, *n*-ethylammilide, and cyanuric acid (Mandelbaum et al., 1995; Ralebits et al., 2002; Ghosh and Philip, 2004; Getenga et al., 2009). Specifically, atrazine degradation was documented with the help of *Rhodococcus* sp. BCH2 (Kolekar et al., 2014), *Arthrobacter* sp. (Getenga et al., 2009), *Nocardioides* sp. (Topp et al., 2000). *Pseudomonas* sp. strain ADP (Rousseaux et al., 2001; Liu and Parales, 2009) was the first bacterium reported that could completely mineralize atrazine; with most of the degradation studies based on study

¹<https://monographs.iarc.fr/agents-classified-by-the-iarc/>

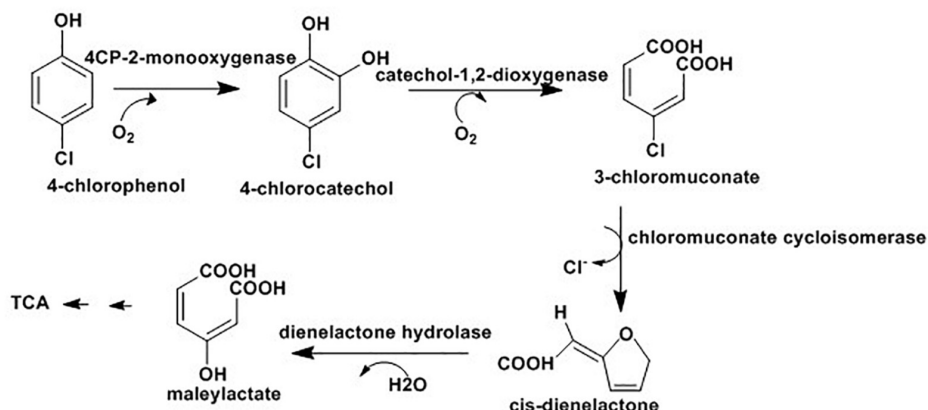


FIGURE 3 | 4-chlorophenol degradation via ortho position where the final intermediate, maleylactate, enters the TCA cycle for complete mineralization (Arora and Bae, 2014).

this strain. As indicated in **Figure 4** (below) atrazine degradation is achieved because of the presence of the genes, *atzA*, *atzB* and *atzC*, which code for enzymes such as chlorohydrolase (*AtzA*), hydroxyatrazine ethylaminohydrolase (*AtzB*) and *N*-isopropylammelide isopropylaminohydrolase (*AtzC*), respectively which convert atrazine sequentially to cyanuric acid (Neumann et al., 2004). Some strains of *Pseudomonas* can further degrade cyanuric acid into CO_2 and NH_3 .

1, 4-Dioxane is a cyclic ether with many applications including components of deodorants, detergents and various types of paints. The process for manufacturing of polyesters also results in 1,4-dioxane production. Various factors including illegal dumping of industrial wastes contribute to 1, 4-dioxane associated water contamination. High level of 1, 4-Dioxane can cause liver and nasal cancers in rats (Dourson et al., 2014) and are listed as group 2B human carcinogen (Inoue et al., 2016). These compounds are soluble in water with low volatility and have a lower chance of absorbance in solids (Stepien et al., 2014). Therefore, once 1, 4-dioxane appears in the environment

it can persist for many days and a high degree of 1, 4-dioxane pollution was observed in surface water, groundwater, and landfill leachate (Stepien et al., 2014).

Their removal from water bodies is an important public concern, especially as the routine physical and chemical methods for water decontamination are not effective for removal of 1, 4-dioxane (Adams et al., 1994). Advanced procedures such as the combination of ozone and hydrogen peroxide treatments are expensive to use (Adams et al., 1994; Kishimoto et al., 2008). Thus, cost effective as well as reliable methods for cleaning of 1, 4-dioxane from water lead to nocardioform actinobacteria such as *Pseudonocardia* (Matsui et al., 2016) and *Rhodococcus* (Deeb and Alvarez-Cohen, 1999) which account for the major portion of capable microorganisms. Inoue et al. (2016) tested various species of *Pseudonocardia* and *Rhodococcus* for their ability to degrade 1, 4-dioxane. Their findings indicated *P. dioxanivorans* JCM 13855T (also known as *P. dioxanivorans* CB1190) (Parales et al., 1994) was the only *Pseudonocardia* sp. tested that used 1,4-dioxane as a carbon source and degraded it. In contrast, they observed the inability of *R. ruber* JCM 3205T to degrade 1, 4-dioxane. However, there are reports on the ability of *Rhodococcus* spp. such as *R. ruber* 219 (Bernhardt and Diekmann, 1991) and *R. ruber* T1 and T5 (Oyama et al., 2013) to biodegrade 1,4-dioxane. This highlighted species variation among *Rhodococcus* in relation to effective degradation and utilization of 1, 4-dioxane.

PRODUCTION OF IMPORTANT COMPOUNDS

Ethylene Glycol Synthesis

Due to the continuing concern about climate change and depletion of fossil energy, expansion of biological processes using renewable biological resources to produce different chemical feed stocks and energy has become an attractive approach for the chemical industry. Ethylene glycol is a feedstock which serves as a starting material for the manufacture of several items including polymers, anti-freeze agents, and coolants (Zhang and

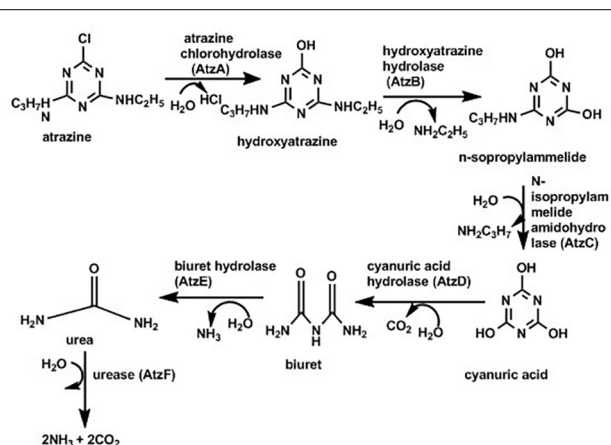
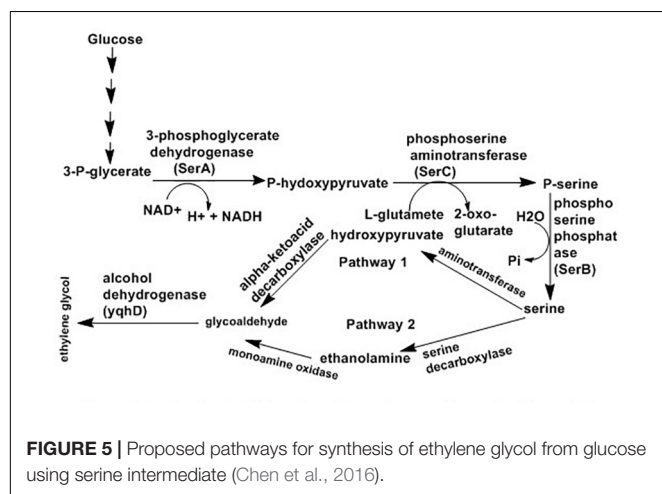


FIGURE 4 | Pathway for atrazine degradation (Liu and Parales, 2009).

Yu, 2013). Routinely, ethylene glycol is produced through a costly chemical process using ethylene derived from the petrochemical industry as a starting material. Therefore, there is a preference for biological synthesis of ethylene glycol over chemical methods as the former has a low impact on the environment and the reaction is selective (Mattam et al., 2013).

Fermentation of carbohydrates is an economical process for production of ethylene glycol from biofeed stock. *Corynebacterium glutamicum*, an actinobacterium, has been designed for manufacture of ethylene glycol directly from glucose via extension of the serine synthesis pathway. Serine is produced by most microorganisms from 3-phosphoglycerate (a glycolysis intermediate) using three enzymatic steps: 3-phosphoglycerate converted into P-hydroxypyruvate with the help of 3-phosphoglycerate dehydrogenase (PGDH; *serA*), followed by conversion of P-hydroxypyruvate to P-serine by phosphoserine aminotransferase (PSAT; *serC*) and P-serine to serine with the help of phosphoserine phosphatase (PSP; *serB*) (Peters-Wendisch et al., 2005). Chen et al. (2016) proposed two ways for ethylene glycol synthesis via the extension of the serine synthesis pathway where serine is the starting material for both systems with the end product glycoaldehyde (Chen et al., 2016). The first route involves deamination of serine with aminotransferase or amino acid dehydrogenase resulting in hydroxypyruvate. Finally, glycoaldehyde is produced from hydroxypyruvate with the help of α -ketoacid decarboxylase. Similarly, the other route also has two steps where ethanolamine produced from serine with decarboxylation and then converted to glycoaldehyde following oxidation by monoamine oxidase. Finally, glycoaldehyde can be reduced to ethylene glycol by alcohol dehydrogenase such as *yqhD* as indicated in **Figure 5**.

In addition to glucose, *C. glutamicum* uses several substrates such as sugars present in molasses (sucrose and fructose), pentose sugars present in lignocellulosic (Zahoor et al., 2012), *n*-acetyl-D-glucosamine and *n*-acetyl-D-muramic acid (Sgobba et al., 2018) for manufacturing of various amino acids (Bommareddy et al., 2014). Production of other compounds such as isobutanol, cadaverine, and succinate are possible with *C. glutamicum* (Blombach et al., 2011; Buschke et al., 2011; Litsanov et al., 2012).



Rhodococcus sp. are also associated with production of Ethylene glycol. *Rhodococcus* sp. CGMCC 4911 converted 1, 3-propanediol cyclic sulfate and its derivatives into corresponding diols. The growing cells of *Rhodococcus* successfully hydrolyzed ethylene sulfate, glycol sulfide, 1, 3-propanediol cyclic sulfate, and 1, 2-propanediol cyclic sulfate with different conversion rates (He et al., 2015).

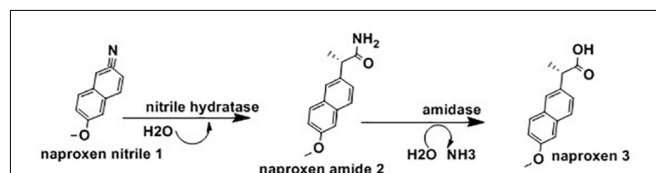
Cyclic sulfates and its derivatives are very important compounds that serve as starting materials for the synthesis of various useful intermediates (Steinmann et al., 2001). Sulfatases hydrolyse organic sulfate esters into primary or secondary alkyl alcohols (Gadler and Faber, 2007). Microbial transformation of cyclic sulfates into diols can be achieved under mild reaction conditions. He et al. (2013) reported for the first time that *Rhodococcus* sp. CCZU10-1 can convert 1, 3-propanediol cyclic sulfate and its derivatives into diols, where factors like pH, temperature, and cells dose affect rate of biotransformation.

Production of Less Toxic and Biologically Active Drugs

The absolute configuration of chiral centers in molecules determine the biological activities of the compounds as these molecules bind with receptors made of enantiomerically pure protein (Kato et al., 2003). Most of the available chiral carbon containing drugs are racemic which contain equal concentration of S (+) and R (+) enantiomers. Since only one of the two is active and the other associated with toxicity, the current drug development gives priority to compounds only with a single enantiomer.

Ibuprofen [(R,S)-2-(4'-isobutylphenyl)propionic acid] are a group of effective, orally active, nonsteroidal, anti-inflammatory agents which include drugs such as naproxen, fenoprofen, and flurbiprofen (Sen and Anliker, 1996). Even though the S-(+)-ibuprofen form is more than 100 times more effective than the R-(-)-ibuprofen, the racemic form of ibuprofen is widely used (Kumaresan, 2010). The (R)-ibuprofen form can be converted to its enantiomer in the livers and kidneys of pigs and rats, though this process is not free of toxicity (Liu et al., 2009). **Figure 6** below highlighted the application of whole cells *N. corallina* to biocatalyse the enantioselective hydrolysis of racemic ibuprofen nitrile [2-(4-isobutylphenyl) propanenitrile, 1] to optically active ibuprofen amide [2-(4-isobutylphenyl) propanamide, 2], a prodrug using nitrile hydratase (NHase) and hydrolyse this amide into optically active ibuprofen (3) using amidase.

The results of the above observation indicated *N. corallina* B-276 displayed nitrile hydratase and amidase activities having



low stereo-selectivity (**Figure 6**). This finding also revealed that *N. corallina* catalyzed deracemisation of racemic ibuprofen to (R)-ibuprofen enantiomer with an efficiency of >99%. This is the first observation where *N. corallina* B-276 catalyzed deracemisation processes. Currently, the (R)-enantiomer form of non-steroidal anti-inflammatory agents are the center of studies and research focus on resolving rac-ibuprofen (Pignatello et al., 2008); and due to this, recent efforts have been directed at resolving rac-ibuprofen (Trung et al., 2006).

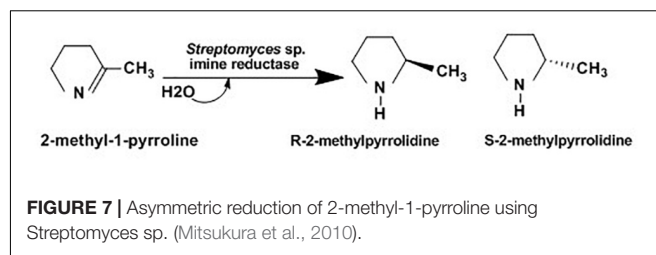
A high percentage of optical active S-(+)-ibuprofen was reported from hydrolysis of ibuprofen amide and four related 2-phenylpropionamides using whole cell *Rhodococcus* AJ270 (Snell and Colby, 1999). This high purity was achieved through partial hydrolysis as complete hydrolysis of (R, S)-(+)-2-(4'-isobutylphenyl) propionamide (ibuprofen amide) results in a racemic mixture of ibuprofen enantiomers. The findings of this study suggested that prolonged hydrolysis of ibuprofen amide resulted in both ibuprofen amide and an optical purity of 90-94% of s-(+)-ibuprofen if the reaction is stopped before completion.

Due to its huge production and wide usage, ibuprofen is one of the most commonly detected compounds in wastewater (Buser et al., 1999). In addition to production of active ibuprofen, different species of actinobacteria including *Patulibacter* sp. strain I11 (Almeida et al., 2013) and *Nocardia* sp. NRRL 5646 (Chen and Rosazza, 1994; Cy et al., 2018) are involved in its biodegradation to the level where there is no more risk the community.

Carvedilol is a non-selective, β -adrenergic receptor antagonist and α 1-adrenoceptor blocker, and it exists in two enantiomeric forms (Gagyi et al., 2008). The overall cardio-protective action of Carvedilol is due to its (S)-(-)-enantiomer, which is less hepatotoxic than the racemic mixture, and (R)-(+)- enantiomer (Hao and Kim, 2010). Ettireddy et al. (2017) tested *Streptomyces halstedii* and other bacteria for their ability to biotransform racemic carvedilol to its (S)-(-)-enantiomer. The result indicated some bacteria including *S. halstedii* exhibited incubation time dependence enantioselective conversion of carvedilol where the conversion rate increased up to 10 days of incubation and then after the rate is reduced and finally become zero.

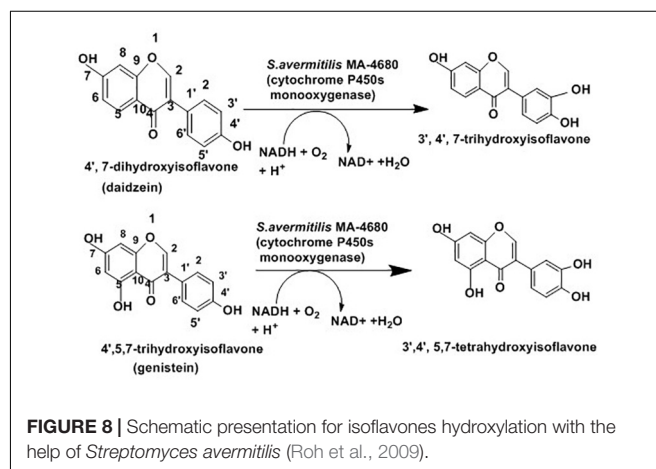
Chiral amines have been widely used for manufacturing of several therapeutics such as codeine (pain relief), zolof / sertraline (anti-depression), lariam (anti-malaria) and ethambuto (anti tuberculosis) and agrochemical intermediates including insecticides (imiprothrin, nornicotine), herbicides (imazapyr, imazapic) and fungicides (cyprofuram, fenbuconazole) (Ulrich et al., 2012). Several syntheses of optically active amines have been studied for many years. Asymmetric synthesis of chiral cyclic amine from cyclic imine achieved using whole-cell *Streptomyces* sp. GF3587 and 3546. As showed in **Figure 7**, these strains produced novel imine reductase enzymes which facilitate enantioselective reduction of cyclic 2-methyl-1-pyrroline into R-2-methylpyrrolidine and S-2-methylpyrrolidine in the presence of glucose.

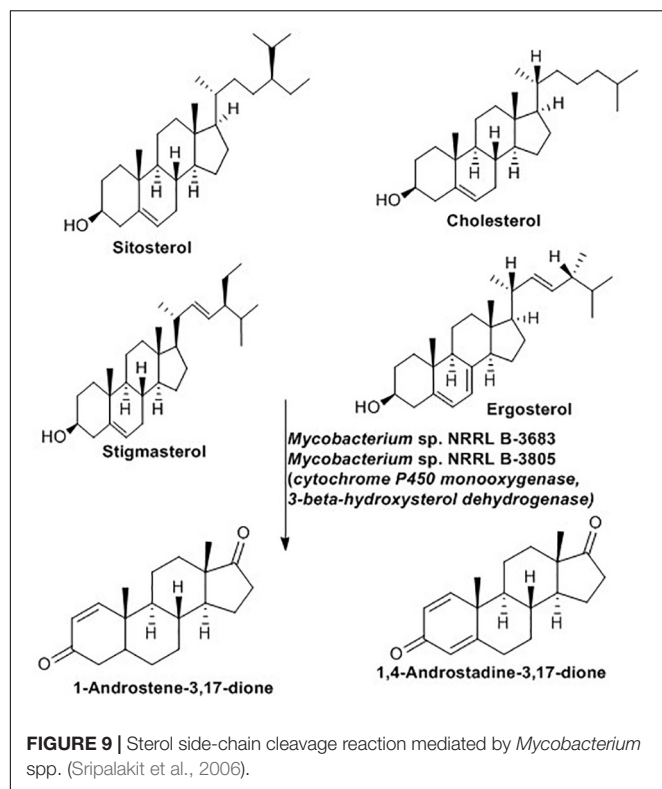
In addition to enantioselective production of active drugs, regioselective addition or substitution of functional groups can also produce active drugs. Actinobacteria play a role in regioselective hydroxylation which mediates the conversion



into more active forms. The hydroxylated form of isoflavones such as daidzein (4', 7-dihydroxyisoflavone) and genistein (4',5,7-trihydroxyisoflavone) are associated with lowering blood cholesterol and preventing cardiovascular diseases and cancer (Foti et al., 2005). As presented in **Figure 8** below, some cytochrome P450 monooxygenases of *Streptomyces avermitilis* MA-4680 catalyze 3'-specific hydroxylation of daidzein and genistein to 3',4',7-trihydroxyisoflavone and 3',4',5,7-tetrahydroxyisoflavone, respectively (Roh et al., 2009).

Microbial biotransformation of natural steroids into pharmaceutically active intermediates has been practiced for many years (Fernandes et al., 2003). These active intermediates play a role in the manufacturing of all type I aromatase inhibitors (Lombardi, 2002) and several high-value steroidal drugs (Wadhwa and Smith, 2000). The bioconversion reaction proceeds with removal of the C-17 side chain of the steroid without any modification of the steroid nucleus (Szentirmai, 1990; Murohisa and Iida, 1993). As indicated in **Figure 9**, *Mycobacterium* sp. NRRL B-3683 and *Mycobacterium* sp. NRRL B-3805 facilitate a single step C-17 side chain cleavage of sitosterol, cholesterol, stigmasterol and ergosterol to produce C-19 steroids such as 1-androstene-3,17-dione and 1,4-androstadiene-3,17-dione (Sripalakit et al., 2006). The initial step of the side-chain oxidation of sterols is hydroxylation at C-17. The reaction is catalyzed by cytochrome P450 monooxygenase, then several dehydrogenase including 3- β -hydroxysterol dehydrogenase remove hydrogen to introduced a double bound at various points (Donova and Egorova, 2012).





Amino Acid Production

Amino acids alone or in combination with other molecules can be used as drugs, food supplements, agriculture chemicals, and polymers. Ever year the annual production of amino acids has increased and is currently estimated to be about 3.7 million metric tons (Ikeda and Takeno, 2013). The global market for amino acids is estimated to be about US\$6.6 billion and expected to increase by 8-10% each year (Leuchtenberger et al., 2005; Ikeda and Takeno, 2013). Amino acids including L-lysine, DL-methionine, L-threonine, and L-tryptophan account for the largest share in terms of production followed by L-glutamate, L-aspartate, and L-phenylalanine (Ikeda and Takeno, 2013).

Microbial fermentation is the primary source of most of the available amino acids in the market. The L-glutamate-producing bacterium, *C. glutamicum*, has been the cornerstone for the introduction of fermentation in industrial manufacturing of amino acids (Udaka, 1960). This bacterium is still the most widely utilized strain for manufacturing of important amino acids, mainly L-glutamate and L-lysine (Leuchtenberger et al., 2005). Manipulation of metabolic pathways of this bacterium allowed for the an improved product range including L-phenylalanine, L-aspartate, L-tryptophan, L-arginine, L-valine, nucleic acids such as purines, vitamins such as riboflavin and pantothenic acid (Burkovski, 2008; Gopinath et al., 2012) and significant amounts of organic acids such as acetic, lactic and succinic acid (Inui et al., 2004). **Figure 10** highlights the biotechnological role of *C. glutamicum*. As indicated, *C. glutamicum* utilizes different starting materials for manufacturing of amino acids and other chemical commodities.

Apart from the above mentioned biologically active compounds, different species of actinobacteria are involved in the synthesis of active compounds. **Table 2** below summarizes some of these compounds.

PRODUCTION OF BIOFUELS

A recent report indicated 80% of the world's energy is obtained from fossil fuels such as petroleum, coal, and natural gas (Biro, 2017) with huge consequences for all living systems. Therefore, the search for environmentally benign sustainable energy from renewable sources continues. Plant biomass is considered the most promising feedstock to meet the global demand for sustainable energy and chemicals (Jojima et al., 2013). Lignocellulosic biomass hydrolysates are the primary polymers of plant biomass ideal for biofuel production. Glucose and xylose are the major components of this biomass followed by minor sugars, such as arabinose, and galactose (Elander et al., 2009).

Microbial conversion of plant biomass to sugars and their transformation into a wide array of important compounds, contribute in a major way to the development of a sustainable biofuel industry (Van Hamme et al., 2003; Fulton et al., 2015). Unlike other bacteria phyla, actinobacteria are equipped with the necessary enzymes for degradation of plant biomass (Berlemont and Martiny, 2013) and form the choice of biocatalysts in the biofuel industry (Lewin et al., 2016). Several species of actinobacteria including *Streptomyces*, *Cellulomonas*, *Mycobacterium*, *Propionibacterium*, *Nocardia*, *Corynebacterium*, *Rhodococcus*, and *Micromonospora* are rich in carbohydrate-degrading enzymes (glycoside hydrolase, endo/exo glucanases, cellulases, esterases) (Lombard et al., 2013).

The above mentioned enzymes are used to produce several types of simple sugars, which are further converted into biofuels and other compounds. The widespread utilization of bioethanol from corn and sugarcane and biodiesel from plant oil suffers

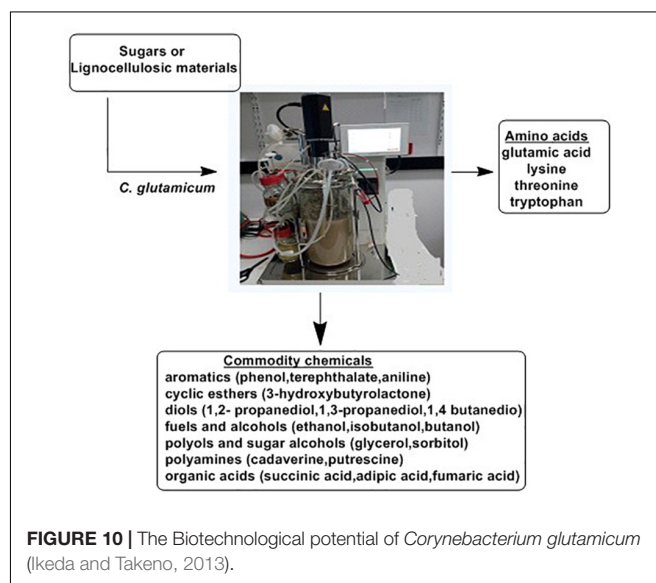


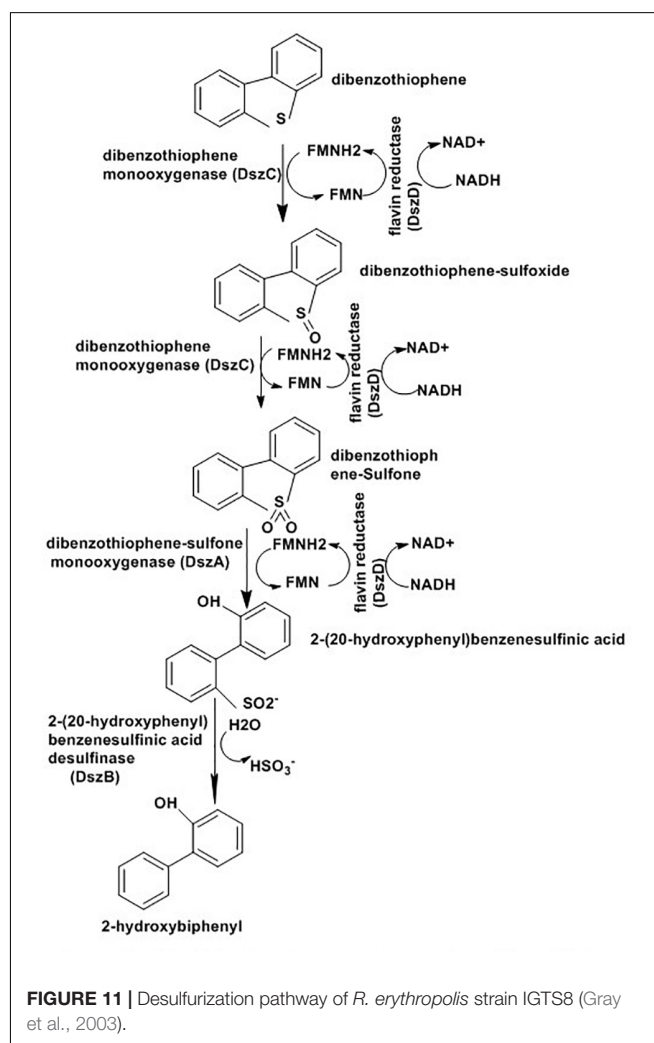
TABLE 2 | Industrial production of bioactive molecules using whole cells as biocatalysts.

Compound	Microorganism	Biological activity	Reference
nicotinamide	<i>Rhodococcus rhodochrous</i> J1		Meyer and Ruesing, 2008
L-lysine	<i>Corynebacterium glutamicum</i>	Amino acids	Burkovski, 2015
L-glutamate	<i>Corynebacterium glutamicum</i>	Amino acids	Burkovski, 2015
carboxylic acids	<i>Rhodococcus</i> sp. MTB5	Various application	Ismailsab et al., 2017
phenylpropanoic acid	<i>Nocardia diaphanozonaria</i> JCM3208	Non-steroidal anti-inflammatory drugs	Mitsukura et al., 2002
aromatic dicarboxylic acids	<i>Rhodococcus jostii</i> RHA1	Aromatic chemicals synthesis	Mycroft et al., 2015
ammonium acrylate	<i>Rhodococcus ruber</i> NCIMB 40757	Raw materials for water-soluble polymers	Webster et al., 2001
L-malic Acid	<i>Nocardia</i> sp.	Metabolites	Hronska et al., 2015
butyramide	<i>Rhodococcus rhodochrous</i>	Drugs	Raj et al., 2007
daptomycin	<i>Streptomyces roseosporus</i>	Antibiotics	Boeck et al., 1988
hydroxylated adamantane (1-adamantanol)	<i>Streptomyces griseoplanus</i>	Pharmaceutical intermediate	Mitsukura et al., 2006

from several disadvantages (Atsumi et al., 2008; Atabani et al., 2012; Caspeta and Nielsen, 2013). Therefore, alternative biofuels including microbially produced specialty biofuels with similar properties to traditional fuels have increased (Atsumi et al., 2008). These specialty biofuels which encompasses higher-alcohol biofuels, fatty acid alkyl esters and various isoprenoid compounds can be used directly as an energy source or fuel precursors (Peralta-Yahya et al., 2012; Beller et al., 2015). *C. glutamicum* is used for the production of specialty biofuels as this bacterium inherently resists the effect of isobutanol and synthesizes several amino acids like glutamate which are important for production of branched-chain alcohols. Genetic engineering of *C. glutamicum* was employed to produce similar amount of isobutanol as *E. coli* strains, the known producers of isobutanol (Smith et al., 2010; Blombach et al., 2011; Yamamoto et al., 2013). For the past few years, *R. opacus* PD630 has been the center of studies as they were capable of depositing up to 80% lipid in their biomass (Alvarez et al., 2000). The substrates used were alkanes, phenylalkanes, or non-hydrocarbons as the only source of carbon (Hong et al., 2011). Moreover, production of long chain fatty acid alkyl esters (biodiesel) were observed using a *Streptomyces* strain isolated from sheep feces (Lu et al., 2013); bisabolene, another alternative to diesel fuel (Phelan et al., 2014) produced by *Streptomyces venezuelae*; also produced 1-Propanol, an industrially relevant solvent with good fuel properties from *Thermobifida fusca* (Deng and Fong, 2011).

In addition to direct involvement in biofuels production, actinobacteria play a significant role in detoxifying fuel-associated toxic compounds. Starting from formation to maturation, microorganisms have been in contact with crude oil in different reservoirs which contribute for their adaptation to use and modify nearly all chemical categories in crude oil (Mohamed Mel et al., 2015). 85% of fossil fuels contain polycyclic aromatic hydrocarbons (PAHs) and about 13% of these PAHs contain nitrogen, oxygen or sulfur (hetero-PAHs) (Brinkmann et al., 2014). Burning of these fuels results different pollutants such as the oxides of carbon (COx), nitrogen (NOx), and sulfur (SOx) (Ma et al., 2006). Oxides of nitrogen and sulfur combine with water vapor in cloud and result acid rain of sulfuric and nitric acids, which become part of rain and snow (Gupta et al., 2005).

Among PAHs, sulfur (hetero-PAHs) in the form of thiophenic compounds such as benzothiophene (BT), dibenzothiophene (DBT), and their alkylated homologs (Khedkar and Shanker, 2015) have attracted increasingly stringent regulations due to their harmful effects on the environment and human health



(Brinkmann et al., 2014; Sousa et al., 2016). The harmful effects of PAHs, particularly hetero-PAHs well documented (Brinkmann et al., 2014) and associated with mutagenic effects, chromosome aberrations, toxicity to daphnia and green algae, embryotoxicity of the zebrafish, and respiratory system irritations.

The concentration of sulfur compounds in crude oil ranges from 0.1 to 8% (w/w) (Müller et al., 2012) and their combustion associated with toxic pollution, most countries developed legislation which demands low level of sulfur in oils, and this in turn forces companies to produce ultra-low sulfur oil, which is currently a challenge (Kawaguchi et al., 2012; Khedkar and Shanker, 2015). Traditionally, reduction of sulfur from crude oil has been achieved with hydrodesulfurization (Gupta et al., 2005), a method that depends on high energy and pressure, which mostly reduces the quality of fuel in terms of energy (Shafi and Hutchings, 2000).

Biodesulfurization depends on whole microbes or their enzymes to eliminate sulfur atom selectively from various refractory compounds present in the fossil fuels. Several strains of *Rhodococcus* sp. (Khairy et al., 2015), *Mycobacterium* sp. (Kawaguchi et al., 2012), *Brevibacterium* sp. (van Afferden et al., 1990), *Corynebacterium* sp. (Maghsoudi et al., 2001), *Paenibacillus* sp. (Izumi and Ohshiro, 2001), *Pseudomonas* sp. (Van Keulen et al., 1998), *Gordonia* sp. (Chang et al., 2000), and *Bacillus* sp. (Kirimura et al., 2001) have been studied for their ability to metabolize various polyaromatic sulfur heterocycles (PASHs) including BT and DBT (Aggarwal et al., 2013). The process adopted by this organism is known as the 4S pathway and involves four enzymes: DszA, DszB, DszC, and DszD (Wang et al., 2013; Sousa et al., 2016). DszA and DszC are monooxygenases that insert oxygen into the sulfur compounds, while DszB is a desulphinase that removes sulfur in the form of sulfite. DszD supplies FMNH₂ to the two monooxygenases and is responsible for reduction of FMN to FMNH₂ through NADH oxidation to NAD⁺. The complete reaction as indicated in **Figure 11** result in a phenolic product and SO₃²⁻ (Gray et al., 2003; Kawaguchi et al., 2012).

Most desulfurization studies in the literature have used DBT as the model compound. While several rhodococci strains exhibit non-destructive desulfurization of DBT, *R. erythropolis* IGTS8 (Kilbane and Jackowski, 1992) was the first to be identified and has received the most attention. Even recent study highlighted their potential to desulfurization and denitrogenation of heavy gas oil by *R. erythropolis* ATCC 4277 (Maass et al., 2015). However, most rhodococci are unable to show high activity for the alkyl derivatives of DBT and show no activity for BT and other thiophenic compounds. Various *Gordonia* species demonstrated greater desulfurization potential against broader range of PASHs compared to rhodococci (Alves et al., 2005). Of them, *G. alkanivorans* desulfurized DPT with a 4S enzyme system similar to *R. erythropolis*. Besides DBT, it can also specifically cleave the C-S bond in BT and other thiophenes with a reaction rate 2-10 times higher when compared to *R. erythropolis* (Mohebbi et al., 2007; Aggarwal et al., 2013).

Microbial mechanisms also operate for degradation of N and O heterocycles. Carbazole is representative N heterocycles and bacteria such as *pseudomonas* sp. and *Rhodococcus* sp. (Maass

et al., 2015) reported for mineralization of this compound. Metabolic pathways employed by most microorganisms for carbazole degradation are similar which involve ring cleavage of heterocycles to produce anthranilic acid as intermediates before their complete mineralization. In this pathway, carbazole is first degraded to 2'-aminobiphenyl-2, 3-diol by carbazole 1,9a-dioxygenase which breaks the first C-N bond. This process allow for the selective removal of refractory organonitrogen compounds from petroleum. Unlike other dioxygenases active against aromatic compound carbazole 1,9a-dioxygenase can catalyze cis-dihydroxylation, monooxygenation and angular dioxygenation on diverse aromatic compounds (Xu et al., 2006).

Dibenzofuran is representative of an O heterocyclic pollutant and microbes also developed mechanisms for biodegradation of these O heterocycles. The detail mechanisms were reviewed by Xu et al. (2006) and different monooxygenase and dioxygenases participate in angular dioxygenation, lateral dioxygenation and lateral oxygenation.

CONCLUSION

Unlike the traditional chemical based production of biologically active compounds, biocatalysts, particularly whole cell microbial biocatalysts, provide a cost effective and environmentally sound approach. Several candidate microorganisms displayed their ability to catalyze a range of substrates either to change them into usable compounds or to make them less toxic to the general community. Compared to other microorganisms, species in the phylum Actinobacteria are a priority for whole cell biocatalysts as this group of bacteria produce the highest percentage of biologically active compounds compared to any other and they are abundant in a range of environmental conditions. These inherent characteristics of actinobacteria encourage screening of various species in this phylum for their metabolic potential with the discovery of metabolic pathways applicable into different industries, including pharmaceuticals, food and bioenergy sectors. While most screening studies for whole cell actinobacteria as biocatalysts targeted only common species such as *Rhodococcus*, *Streptomyces* and *Corynebacterium*, future evaluation should consider other uncommon species such as *Gordonia* which has demonstrated promising biocatalytic activities. Furthermore, most recent studies of whole cell actinobacteria as biocatalysts did not show the detailed mechanisms behind biotransformation such as what genes and enzymes are involved in the process. Future studies should focus on the investigation of the mechanisms behind the biotransformation of certain substrate to product, as this will help to manipulate each system to maximize the yield.

AUTHOR CONTRIBUTIONS

CF provided the guidelines and wrote the outline and guided YA in the development of the review, sought a number of research papers on the topic, and did the Tables and the final proofreading. YA did most of the drafting of the manuscript and also sought relevant research papers.

REFERENCES

- Adams, C. D., Scanlan, P. A., and Secrist, N. D. (1994). Oxidation and biodegradability enhancement of 1,4-dioxane using hydrogen peroxide and ozone. *Environ. Sci. Technol.* 28, 1812–1818. doi: 10.1021/es00060a010
- Adegbeye, M., and Babalola, O. (2013). “Actinomycetes: a yet inexhaustive source of bioactive secondary metabolites,” in *Microbial Pathogens and Strategies for Combating Them: Science, Technology and Education, Microbiology Book Series*, ed. A. Mendez-Vilas (Badajoz: Formatex), 786–795.
- Aggarwal, S., Karimi, I., and Ivan, G. R. (2013). In silico modeling and evaluation of *Gordonia alkanivorans* for biodesulfurization. *Mol. Biosyst.* 9, 2530–2540. doi: 10.1039/c3mb70132h
- Almeida, B., Kjeldal, H., Lolas, I., Knudsen, A. D., Carvalho, G., Nielsen, K. L., et al. (2013). Quantitative proteomic analysis of ibuprofen-degrading *Patulibacter* sp. strain I11. *Biodegradation* 24, 615–630. doi: 10.1007/s10532-012-9610-5
- Alvarez, H., Kalscheuer, R., and Steinbüchel, A. (2000). Accumulation and mobilization of storage lipids by *Rhodococcus opacus* PD630 and *Rhodococcus ruber* NCIMB 40126. *Appl. Microbiol. Biotechnol.* 54, 218–223. doi: 10.1007/s002530000395
- Alves, L., Salgueiro, R., Rodrigues, C., Mesquita, E., Matos, J., and Giro, F. M. (2005). Desulfurization of dibenzothiophene, benzothiophene, and other thiophene analogs by a newly isolated bacterium, *Gordonia alkanivorans* strain 1B. *Appl. Biochem. Biotechnol.* 120, 199–208. doi: 10.1385/ABAB:120:3:199
- Arora, P. K., and Bae, H. (2014). Bacterial degradation of chlorophenols and their derivatives. *Microb Cell Fact.* 13:31. doi: 10.1186/1475-2859-13-31
- Arora, P. K., and Jain, R. K. (2012). Metabolism of 2-chloro-4-nitrophenol in a Gram negative bacterium, *Burkholderia* sp. RKJ 800. *PLoS One* 7:e38676. doi: 10.1371/journal.pone.0038676
- Atabani, A. E., Silitonga, A. S., Badruddin, I. A., Mahlia, T., Masjuki, H., and Mekhilef, S. (2012). A comprehensive review on biodiesel as an alternative energy resource and its characteristics. *Renew. Sustain. Energy Rev.* 16, 2070–2093. doi: 10.1016/j.biortech.2014.10.030
- Atsumi, S., Hanai, T., and Liao, J. C. (2008). Non-fermentative pathways for synthesis of branched-chain higher alcohols as biofuels. *Nature* 451, 86–89. doi: 10.1038/nature06450
- Babu, V., Shilpi, and Choudhury, B. (2010). Nitrile-metabolizing potential of *Amycolatopsis* sp. IITR215. *Process Biochem.* 45, 866–873. doi: 10.1016/j.procbio.2010.02.008
- Banerjee, A., and Ghoshal, A. K. (2010). Phenol degradation by *Bacillus cereus*: pathway and kinetic modeling. *Bioresour. Technol.* 101, 5501–5507. doi: 10.1016/j.biortech.2010.02.018
- Barka, E. A., Vatsa, P., Sanchez, L., Gaveau-Vaillant, N., Jacquard, C., Meier-Kolthoff, J. P., et al. (2015). Taxonomy, physiology, and natural products of Actinobacteria. *Microbiol. Mol. Biol. Rev.* 80, 1–43. doi: 10.1128/MMBR.00019-15
- Baxter, J., and Cummings, S. P. (2006). The current and future applications of microorganism in the bioremediation of cyanide contamination. *Antonie Van Leeuwenhoek* 90, 1–17. doi: 10.1007/s10482-006-9057-y
- Beller, H. R., Lee, T. S., and Katz, L. (2015). Natural products as biofuels and bio-based chemicals: fatty acids and isoprenoids. *Nat. Prod. Rep.* 32, 1508–1526. doi: 10.1039/c5np00068h
- Bérdy, J. (2005). Bioactive microbial metabolites. *J. Antibiot.* 58, 1–26. doi: 10.1038/ja.2005.1
- Berlemont, R., and Martiny, A. C. (2013). Phylogenetic distribution of potential cellulases in bacteria. *Appl. Environ. Microbiol.* 79, 1545–1554. doi: 10.1128/AEM.03305-12
- Bernhardt, D., and Diekmann, H. (1991). Degradation of dioxane, tetrahydrofuran and other cyclic ethers by an environmental *Rhodococcus* strain. *Appl. Microbiol. Biotechnol.* 36, 120–123. doi: 10.1007/BF00164711
- Bezborodov, A., and Zagustina, N. (2016). Enzymatic biocatalysis in chemical synthesis of pharmaceuticals. *Appl. Biochem. Microbiol.* 52, 237–249. doi: 10.1134/S0003683816030030
- Bhalla, T. C., and Kumar, H. (2005). *Nocardia globerula* NHB-2: a versatile nitrile-degrading organism. *Can. J. Microbiol.* 51, 705–708. doi: 10.1139/w05-046
- Birol, F. (2017). *Key World Energy Statistics*. Paris: International Energy Agency.
- Blombach, B., Riester, T., Wieschalka, S., Ziert, C., Youn, J. W., Wendisch, V. F., et al. (2011). *Corynebacterium glutamicum* tailored for efficient isobutanol production. *Appl. Environ. Microbiol.* 77, 3300–3310. doi: 10.1128/aem.02972-10
- Boadas-Vaello, P., Jover, E., Diez-Padrisa, N., Bayona, J. M., and Llorens, J. (2007). Differential role of CYP2E1-mediated metabolism in the lethal and vestibulotoxic effects of cis-crotononitrile in the mouse. *Toxicol. Appl. Pharmacol.* 225, 310–317. doi: 10.1016/j.taap.2007.07.014
- Boeck, L. D., Fukuda, D. S., Abbott, B. J., and Debono, M. (1988). Deacylation of A21978C, an acidic lipopeptide antibiotic complex, by *Actinoplanes utahensis*. *J. Antibiot.* 41, 1085–1092. doi: 10.7164/antibiotics.41.1085
- Bommarreddy, R. R., Chen, Z., Rappert, S., and Zeng, A. P. (2014). A de novo NADPH generation pathway for improving lysine production of *Corynebacterium glutamicum* by rational design of the coenzyme specificity of glyceraldehyde 3-phosphate dehydrogenase. *Metab. Eng.* 25, 30–37. doi: 10.1016/j.ymben.2014.06.005
- Brinkmann, M., Blenkle, H., Salowsky, H., Bluhm, K., Schiw, S., Tiehm, A., et al. (2014). Genotoxicity of heterocyclic PAHs in the micronucleus assay with the fish liver cell line RTL-W1. *PLoS One* 9:e85692. doi: 10.1371/journal.pone.0085692
- Brun, G. L., MacDonald, R. M., Verge, J., and Aubé, J. (2008). Long-term atmospheric deposition of current-use and banned pesticides in Atlantic Canada; 1980–2000. *Chemosphere* 71, 314–327. doi: 10.1016/j.chemosphere.2007.09.003
- Bull, A. T., and Stach, J. E. (2007). Marine Actinobacteria: new opportunities for natural product search and discovery. *Trends Microbiol.* 15, 491–499. doi: 10.1016/j.tim.2007.10.004
- Burkovski, A. (2008). *Corynebacteria: Genomics and Molecular Biology*. Poole: Horizon Scientific Press.
- Burkovski, A. (ed.). (2015). “Trends in *Corynebacterium glutamicum* research and application,” in *Corynebacterium glutamicum: From Systems Biology to Biotechnological Applications*, (Poole: Caister Academic Press), 1–9. doi: 10.21775/9781910190050.01
- Buschke, N., Schroder, H., and Wittmann, C. (2011). Metabolic engineering of *Corynebacterium glutamicum* for production of 1,5-diaminopentane from hemicellulose. *Biotechnol. J.* 6, 306–317. doi: 10.1002/biot.201000304
- Buser, H.-R., Poiger, T., and Müller, M. D. (1999). Occurrence and environmental behavior of the chiral pharmaceutical drug ibuprofen in surface waters and in wastewater. *Environ. Sci. Technol.* 33, 2529–2535. doi: 10.1021/es981014w
- Caspeta, L., and Nielsen, J. (2013). Economic and environmental impacts of microbial biodiesel. *Nat. Biotechnol.* 31, 789–793. doi: 10.1038/nbt.2683
- Chang, J. H., Chang, Y. K., Ryu, H. W., and Chang, H. N. (2000). Desulfurization of light gas oil in immobilized-cell systems of *Gordonia* sp. CYKS1 and *Nocardia* sp. CYKS2. *FEMS Microbiol. Lett.* 182, 309–312. doi: 10.1111/j.1574-6968.2000.tb08913.x
- Chater, K. F. (2016). Recent advances in understanding *Streptomyces*. *F1000Res.* 5:2795. doi: 10.12688/f1000research.9534.1
- Chen, Y., and Rosazza, J. P. (1994). Microbial transformation of ibuprofen by a *Nocardia* species. *Appl. Environ. Microbiol.* 60, 1292–1296.
- Chen, Y.-H., Chen, L.-L., and Shang, N.-C. (2009). Photocatalytic degradation of dimethyl phthalate in an aqueous solution with Pt-doped TiO₂-coated magnetic PMMA microspheres. *J. Hazard. Mater.* 172, 20–29. doi: 10.1016/j.jhazmat.2009.06.122
- Chen, Z., Huang, J., Wu, Y., and Liu, D. (2016). Metabolic engineering of *Corynebacterium glutamicum* for the de novo production of ethylene glycol from glucose. *Metab. Eng.* 33, 12–18. doi: 10.1016/j.ymben.2015.10.013
- Christen, P., Davidson, S., Combet-Blanc, Y., and Auria, R. (2011). Phenol biodegradation by the thermoacidophilic archaeon *Sulfolobus solfataricus* 98/2 in a fed-batch bioreactor. *Biodegradation* 22, 475–484. doi: 10.1007/s10532-010-9420-6
- Cy, H., Lh, F., Mh, S., Cf, H., Jp, W., and Hw, K. (2018). Ibuprofen biodegradation by hospital, municipal, and distillery activated sludges. *Environ. Technol.* doi: 10.1080/09593330.2018.1493146 [Epub ahead of print].
- Dargnat, C., Teil, M. J., Chevreuil, M., and Blanchard, M. (2009). Phthalate removal throughout wastewater treatment plant: case study of Marne Aval station (France). *Sci. Total Environ.* 407, 1235–1244. doi: 10.1016/j.scitotenv.2008.10.027

- de Carvalho, C. C. (2017). Whole cell biocatalysts: essential workers from Nature to the industry. *Microb. Biotechnol.* 10, 250–263. doi: 10.1111/1751-7915.12363
- Deeb, R. A., and Alvarez-Cohen, L. (1999). Temperature effects and substrate interactions during the aerobic biotransformation of BTEX mixtures by toluene-enriched consortia and *Rhodococcus rhodochrous*. *Biotechnol. Bioeng.* 62, 526–536. doi: 10.1002/(SICI)1097-0290(19990305)62:5<526::AID-BIT4>3.0.CO;2-8
- Demain, A. L., and Sanchez, S. (2009). Microbial drug discovery: 80 years of progress. *J. Antibiot.* 62, 5–16. doi: 10.1038/ja.2008.16
- Deng, Y., and Fong, S. S. (2011). Metabolic engineering of *Thermobifida fusca* for direct aerobic bioconversion of untreated lignocellulosic biomass to 1-propanol. *Metab. Eng.* 13, 570–577. doi: 10.1016/j.ymben.2011.06.007
- Donova, M. V., and Egorova, O. V. (2012). Microbial steroid transformations: current state and prospects. *Appl. Microbiol. Biotechnol.* 94, 1423–1447. doi: 10.1007/s00253-012-4078-0
- Dourson, M., Reichard, J., Nance, P., Burleigh-Flayer, H., Parker, A., Vincent, M., et al. (2014). Mode of action analysis for liver tumors from oral 1, 4-dioxane exposures and evidence-based dose response assessment. *Regul. Toxicol. Pharmacol.* 68, 387–401. doi: 10.1016/j.yrtph.2014.01.011
- Elander, R. T., Dale, B. E., Holtzapfel, M., Ladisch, M. R., Lee, Y., Mitchinson, C., et al. (2009). Summary of findings from the biomass refining consortium for applied fundamentals and innovation (CAFI): corn stover pretreatment. *Cellulose* 16, 649–659. doi: 10.1007/s10570-009-9308-y
- Ettireddy, S., Chandupatla, V., and Veeresham, C. (2017). Enantioselective resolution of (R,S)-Carvedilol to (S)-(-)-Carvedilol by biocatalysts. *Nat. Prod. Bioprospect.* 7, 171–179. doi: 10.1007/s13659-016-0118-2
- Fang, C.-R., Yao, J., Zheng, Y.-G., Jiang, C.-J., Hu, L.-F., Wu, Y.-Y., et al. (2010). Dibutyl phthalate degradation by *Enterobacter* sp. T5 isolated from municipal solid waste in landfill bioreactor. *Int. Biodeterior. Biodegradation* 64, 442–446. doi: 10.1016/j.ibiod.2010.04.010
- Fang, S., An, X., Liu, H., Cheng, Y., Hou, N., Feng, L., et al. (2015). Enzymatic degradation of aliphatic nitriles by *Rhodococcus rhodochrous* BX2, a versatile nitrile-degrading bacterium. *Bioresour. Technol.* 185, 28–34. doi: 10.1016/j.biortech.2015.02.078
- Feng, Y. S., and Lee, C. M. (2009). The potential of the acetonitrile biodegradation by *Mesorhizobium* sp. F28. *J. Hazard. Mater.* 164, 646–650. doi: 10.1016/j.jhazmat.2008.08.039
- Fernandes, P., Cruz, A., Angelova, B., Pinheiro, H., and Cabral, J. (2003). Microbial conversion of steroid compounds: recent developments. *Enzyme Microb. Technol.* 32, 688–705. doi: 10.1016/S0141-0229(03)00029-2
- Foti, P., Erba, D., Riso, P., Spadafranca, A., Criscuoli, F., and Testolin, G. (2005). Comparison between daidzein and genistein antioxidant activity in primary and cancer lymphocytes. *Arch. Biochem. Biophys.* 433, 421–427. doi: 10.1016/j.abb.2004.10.008
- Fulton, L. M., Lynd, L. R., Körner, A., Greene, N., and Tonachel, L. R. (2015). The need for biofuels as part of a low carbon energy future. *Biofuel. Bioprod. Biorefin.* 9, 476–483. doi: 10.1021/ic3008848
- Gadler, P., and Faber, K. (2007). New enzymes for biotransformations: microbial alkyl sulfatases displaying stereo- and enantioselectivity. *Trends Biotechnol.* 25, 83–88. doi: 10.1016/j.tibtech.2006.11.006
- Gagyi, L., Gyeresi, A., and Kilar, F. (2008). Role of chemical structure in stereoselective recognition of beta-blockers by cyclodextrins in capillary zone electrophoresis. *J. Biochem. Biophys. Methods* 70, 1268–1275. doi: 10.1016/j.jbbm.2007.10.004
- Garzón-Posse, F., Becerra-Figueroa, L., Hernández-Arias, J., and Gamba-Sánchez, D. (2018). Whole cells as biocatalysts in organic transformations. *Molecules* 23:1265. doi: 10.3390/molecules23061265
- Gehring, C., Wessel, M., Schaffer, S., and Thum, O. (2016). The power of biocatalysis: a one-pot total synthesis of rhamnolipids from butane as the sole carbon and energy source. *ChemistryOpen* 5, 513–516. doi: 10.1002/open.201600127
- Getenga, Z., Dorfner, U., Iwobi, A., Schmid, M., and Schroll, R. (2009). Atrazine and terbutylazine mineralization by an *Arthrobacter* sp. isolated from a sugarcane-cultivated soil in Kenya. *Chemosphere* 77, 534–539. doi: 10.1016/j.chemosphere.2009.07.031
- Ghosh, P. K., and Philip, L. (2004). Atrazine degradation in anaerobic environment by a mixed microbial consortium. *Water Res.* 38, 2276–2283. doi: 10.1016/j.watres.2003.10.059
- Gilliom, R. J., Barbash, J. E., Crawford, C. G., Hamilton, P. A., Martin, J. D., Nakagaki, N., et al. (2006). *Pesticides in the Nation's Streams and Ground Water, 1992–2001*. Reston, VA: US Geological Survey.
- Gopinath, V., Murali, A., Dhar, K. S., and Nampoothiri, K. M. (2012). *Corynebacterium glutamicum* as a potent biocatalyst for the bioconversion of pentose sugars to value-added products. *Appl. Microbiol. Biotechnol.* 93, 95–106. doi: 10.1007/s00253-011-3686-4
- Gray, K. A., Mrachko, G. T., and Squires, C. H. (2003). Biodesulfurization of fossil fuels. *Curr. Opin. Microbiol.* 6, 229–235. doi: 10.1016/S1369-5274(03)00065-1
- Gupta, N., Roychoudhury, P., and Deb, J. (2005). Biotechnology of desulfurization of diesel: prospects and challenges. *Appl. Microbiol. Biotechnol.* 66, 356–366. doi: 10.1007/s00253-004-1755-7
- Hao, J., and Kim, C.-H. (2010). Comparing the effects of carvedilol enantiomers on regression of established cardiac hypertrophy induced by pressure overload. *Lab. Anim. Res.* 26, 75–82. doi: 10.5625/lar.2010.26.1.75
- He, Y. C., Ma, C. L., Zhang, X., Li, L., Xu, J. H., and Wu, M. X. (2013). Highly enantioselective oxidation of racemic phenyl-1,2-ethanediol to optically pure (R)-(-)-mandelic acid by a newly isolated *Brevibacterium lutescens* CCZU12-1. *Appl. Microbiol. Biotechnol.* 97, 7185–7194. doi: 10.1007/s00253-013-4989-4
- He, Y. C., Tao, Z. C., Zhang, D. P., Yang, Z. X., Gao, S., and Ma, C. L. (2015). Biotransformation of 1,3-propanediol cyclic sulfate and its derivatives to diols by *Rhodococcus* sp. *Biotechnol. Lett.* 37, 183–188. doi: 10.1007/s10529-014-1670-7
- He, Y. C., Tao, Z. C., Zhang, X., Yang, Z. X., and Xu, J. H. (2014). Highly efficient synthesis of ethyl (S)-4-chloro-3-hydroxybutanoate and its derivatives by a robust NADH-dependent reductase from *E. coli* CCZU-K14. *Bioresour. Technol.* 161, 461–464. doi: 10.1016/j.biortech.2014.03.133
- He, Z., Niu, C., and Lu, Z. (2014). Individual or synchronous biodegradation of di-n-butyl phthalate and phenol by *Rhodococcus ruber* strain DP-2. *J. Hazard. Mater.* 273, 104–109. doi: 10.1016/j.jhazmat.2014.03.033
- Hecker, M., Park, J. W., Murphy, M. B., Jones, P. D., Solomon, K. R., Van Der Kraak, G., et al. (2005). Effects of atrazine on CYP19 gene expression and aromatase activity in testes and on plasma sex steroid concentrations of male African clawed frogs (*Xenopus laevis*). *Toxicol. Sci.* 86, 273–280. doi: 10.1093/toxsci/kfi203
- Hollender, J., Hopp, J., and Dott, W. (1997). Degradation of 4-Chlorophenol via the meta cleavage pathway by *Comamonas testosteroni* JH5. *Appl. Environ. Microbiol.* 63, 4567–4572.
- Hong, W.-K., Rairakhwada, D., Seo, P.-S., Park, S.-Y., Hur, B.-K., Kim, C. H., et al. (2011). Production of lipids containing high levels of docosahexaenoic acid by a newly isolated microalga, *Aurantiochytrium* sp. KRS101. *Appl. Biochem. Biotechnol.* 164, 1468–1480. doi: 10.1007/s12010-011-9227-x
- Hou, J., Liu, F., Wu, N., Ju, J., and Yu, B. (2016). Efficient biodegradation of chlorophenols in aqueous phase by magnetically immobilized aniline-degrading *Rhodococcus rhodochrous* strain. *J. Nanobiotechnology* 14:5. doi: 10.1186/s12951-016-0158-0
- Hronská, H., Tokosova, S., Pilnikova, A., Kristofikova, L., and Rosenberg, M. (2015). Bioconversion of fumaric acid to L-malic acid by the bacteria of the genus *Nocardia*. *Appl. Biochem. Biotechnol.* 175, 266–273. doi: 10.1007/s12010-014-1251-1
- Huang, G., Li, Q., and Zhang, X. (2003). Adsorption and desorption of atrazine by three soils. *Bull. Environ. Contam. Toxicol.* 71, 655–659. doi: 10.1007/s00128-003-0183-1
- Igbinsola, E. O., Odjadjare, E. E., Chigor, V. N., Igbinsola, I. H., Emoghene, A. O., Ekhaie, F. O., et al. (2013). Toxicological profile of chlorophenols and their derivatives in the environment: the public health perspective. *Sci. World J.* 2013:460215. doi: 10.1155/2013/460215
- Ikeda, M., and Takeno, S. (2013). “Amino acid production by *Corynebacterium glutamicum*,” in *Corynebacterium glutamicum*. *Microbiology Monographs*, Vol. 23, eds H. Yukawa and M. Inui (Berlin: Springer), 107–147.
- Inoue, D., Tsunoda, T., Sawada, K., Yamamoto, N., Saito, Y., Sei, K., et al. (2016). 1,4-Dioxane degradation potential of members of the genera *Pseudonocardia* and *Rhodococcus*. *Biodegradation* 27, 277–286. doi: 10.1007/s10532-016-9772-7
- Inui, M., Murakami, S., Okino, S., Kawaguchi, H., Vertès, A. A., and Yukawa, H. (2004). Metabolic analysis of *Corynebacterium glutamicum* during lactate and succinate productions under oxygen deprivation conditions. *J. Mol. Microbiol. Biotechnol.* 7, 182–196. doi: 10.1159/000079827

- Ismailsab, M., Reddy, P. V., Nayak, A. S., and Karegoudar, T. B. (2017). Biotransformation of aromatic and heterocyclic amides by amidase of whole cells of *Rhodococcus* sp. MTB5: biocatalytic characterization and substrate specificity. *Biocatal. Biotransformation* 35, 74–85. doi: 10.1080/10242422.2017.1282467
- Izumi, Y., and Ohshiro, T. (2001). Purification and characterization of enzymes involved in desulfurization of dibenzothiophene in fossil fuels. *J. Mol. Catal. B Enzym.* 11, 1061–1064. doi: 10.1016/S1381-1177(00)00063-1
- Jablonowski, N. D., Schaffer, A., and Burael, P. (2011). Still present after all these years: persistence plus potential toxicity raise questions about the use of atrazine. *Environ. Sci. Pollut. Res. Int.* 18, 328–331. doi: 10.1007/s11356-010-0431-y
- Jemli, S., Ayadi-Zouari, D., Hlima, H. B., and Bejar, S. (2016). Biocatalysts: application and engineering for industrial purposes. *Crit. Rev. Biotechnol.* 36, 246–258. doi: 10.3109/07388551.2014.950550
- Jensen, P. R., Mincer, T. J., Williams, P. G., and Fenical, W. (2005). Marine actinomycete diversity and natural product discovery. *Antonie Van Leeuwenhoek* 87, 43–48. doi: 10.1007/s10482-004-6540-1
- Jianlong, W., Xiangchun, Q., Liping, H., Yi, Q., and Hegemann, W. (2002). Microbial degradation of quinoline by immobilized cells of *Burkholderia pickettii*. *Water Res.* 36, 2288–2296. doi: 10.1016/S0043-1354(01)00457-2
- Jin, D. C., Liang, R. X., Dai, Q. Y., Zhang, R. Y., Wu, X. L., and Chao, W. L. (2010). Biodegradation of di-n-butyl phthalate by *Rhodococcus* sp. JDC-11 and molecular detection of 3, 4-phthalate dioxygenase gene. *J. Microbiol. Biotechnol.* 20, 1440–1445. doi: 10.4014/jmb.1004.04034
- Jojima, T., Inui, M., and Yukawa, H. (2013). “Biorefinery applications of *Corynebacterium glutamicum*,” in *Corynebacterium glutamicum*. *Microbiology Monographs*, Vol. 23, eds H. Yukawa and M. Inui (Berlin: Springer), 149–172.
- Jonsson, S., Vavilin, V., and Svensson, B. (2006). Phthalate hydrolysis under landfill conditions. *Water Sci. Technol.* 53, 119–127. doi: 10.2166/wst.2006.242
- Kamjam, M., Sivalingam, P., Deng, Z., and Hong, K. (2017). Deep sea actinomycetes and their secondary metabolites. *Front. Microbiol.* 8:760. doi: 10.3389/fmicb.2017.00760
- Kao, C. M., Chen, K. F., Liu, J. K., Chou, S. M., and Chen, S. C. (2006). Enzymatic degradation of nitriles by *Klebsiella oxytoca*. *Appl. Microbiol. Biotechnol.* 71, 228–233. doi: 10.1007/s00253-005-0129-0
- Kato, D.-I., Mitsuda, S., and Ohta, H. (2003). Microbial deracemization of α -substituted carboxylic acids: substrate specificity and mechanistic investigation. *J. Org. Chem.* 68, 7234–7242. doi: 10.1021/jo034253x
- Kawaguchi, H., Kobayashi, H., and Sato, K. (2012). Metabolic engineering of hydrophobic *Rhodococcus opacus* for biodesulfurization in oil-water biphasic reaction mixtures. *J. Biosci. Bioeng.* 113, 360–366. doi: 10.1016/j.jbiosc.2011.10.017
- Khairy, H., Wubbeler, J. H., and Steinbuchel, A. (2015). Biodegradation of the organic disulfide 4,4'-dithiodibutyric acid by *Rhodococcus* spp. *Appl. Environ. Microbiol.* 81, 8294–8306. doi: 10.1128/aem.02059-15
- Khedkar, S., and Shanker, R. (2015). Isolation and classification of a soil actinomycete capable of sulphur-specific biotransformation of dibenzothiophene, benzothiophene and thianthrene. *J. Appl. Microbiol.* 118, 62–74. doi: 10.1111/jam.12665
- Kilbane, J. J., and Jackowski, K. (1992). Biodesulfurization of water-soluble coal-derived material by *Rhodococcus rhodochrous* IGTS8. *Biotechnol. Bioeng.* 40, 1107–1114. doi: 10.1002/bit.260400915
- Kim, S.-K., Toldrá, F., Prihanto, A., Wakayama, M., Trivedi, N., Reddy, C., et al. (2016). *Marine Enzymes Biotechnology: Production and Industrial Applications, Part II-Marine Organisms Producing Enzymes*. New York, NY: Elsevier.
- Kirimura, K., Furuya, T., Nishii, Y., Ishii, Y., Kino, K., and Usami, S. (2001). Biodesulfurization of dibenzothiophene and its derivatives through the selective cleavage of carbon-sulfur bonds by a moderately thermophilic bacterium *Bacillus subtilis* WU-S2B. *J. Biosci. Bioeng.* 91, 262–266. doi: 10.1016/S1389-1723(01)80131-6
- Kishimoto, N., Nakagawa, T., Asano, M., Abe, M., Yamada, M., and Ono, Y. (2008). Ozonation combined with electrolysis of 1,4-dioxane using a two-compartment electrolytic flow cell with solid electrolyte. *Water Res.* 42, 379–385. doi: 10.1016/j.watres.2007.07.029
- Kolekar, P. D., Phugare, S. S., and Jadhav, J. P. (2014). Biodegradation of atrazine by *Rhodococcus* sp. BCH2 to N-isopropylammelide with subsequent assessment of toxicity of biodegraded metabolites. *Environ. Sci. Pollut. Res. Int.* 21, 2334–2345. doi: 10.1007/s11356-013-2151-6
- Kumaresan, C. (2010). Ibuprofen (Dexibuprofen): the superior non-steroidal anti-inflammatory agents for development of pharmaceuticals. *Int. J. Curr. Pharm. Res.* 2, 1–3.
- Ladkau, N., Schmid, A., and Bühler, B. (2014). The microbial cell—functional unit for energy dependent multistep biocatalysis. *Curr. Opin. Biotechnol.* 30, 178–189. doi: 10.1016/j.copbio.2014.06.003
- Lam, K. S. (2007). New aspects of natural products in drug discovery. *Trends Microbiol.* 15, 279–289. doi: 10.1016/j.tim.2007.04.001
- Lau, T., Chu, W., and Graham, N. (2005). The degradation of endocrine disruptor di-n-butyl phthalate by UV irradiation: a photolysis and product study. *Chemosphere* 60, 1045–1053. doi: 10.1016/j.chemosphere.2005.01.022
- Leuchtenberger, W., Huthmacher, K., and Drauz, K. (2005). Biotechnological production of amino acids and derivatives: current status and prospects. *Appl. Microbiol. Biotechnol.* 69, 1–8. doi: 10.1007/s00253-005-0155-y
- Lewin, G. R., Carlos, C., Chevrette, M. G., Horn, H. A., McDonald, B. R., Stankey, R. J., et al. (2016). Evolution and ecology of actinobacteria and their bioenergy applications. *Annu. Rev. Microbiol.* 70, 235–254. doi: 10.1146/annurev-micro-102215-095748
- Li, D., Hu, Y., Shen, X., Dai, X., and Han, X. (2010). Combined effects of two environmental endocrine disruptors nonyl phenol and di-n-butyl phthalate on rat Sertoli cells in vitro. *Reprod. Toxicol.* 30, 438–445. doi: 10.1016/j.reprotox.2010.06.003
- Lievano, R., Perez, H. I., Manjarrez, N., Solis, A., and Solis-Oba, M. (2012). Hydrolysis of ibuprofen nitrile and ibuprofen amide and deracemisation of ibuprofen using *Nocardia corallina* B-276. *Molecules* 17, 3148–3154. doi: 10.3390/molecules17033148
- Lin, B., and Tao, Y. (2017). Whole-cell biocatalysts by design. *Microb Cell Fact.* 16, 106–106. doi: 10.1186/s12934-017-0724-7
- Lin, B.-X., Zhang, Z.-J., Liu, W.-F., Dong, Z.-Y., and Tao, Y. (2013). Enhanced production of N-acetyl-D-neuraminic acid by multi-approach whole-cell biocatalyst. *Appl. Microbiol. Biotechnol.* 97, 4775–4784. doi: 10.1007/s00253-013-4754-8
- Litsanov, B., Brocker, M., and Bott, M. (2012). Toward homosuccinate fermentation: metabolic engineering of *Corynebacterium glutamicum* for anaerobic production of succinate from glucose and formate. *Appl. Environ. Microbiol.* 78, 3325–3337. doi: 10.1128/AEM.07790-11
- Liu, X., and Parales, R. E. (2009). Bacterial chemotaxis to atrazine and related s-triazines. *Appl. Environ. Microbiol.* 75, 5481–5488. doi: 10.1128/aem.01030-09
- Liu, Y., Wang, F., and Tan, T. (2009). Cyclic resolution of racemic ibuprofen via coupled efficient lipase and acid-base catalysis. *Chirality* 21, 349–353. doi: 10.1002/chir.20578
- Lombard, V., Golaconda Ramulu, H., Drula, E., Coutinho, P. M., and Henrissat, B. (2013). The carbohydrate-active enzymes database (CAZy) in 2013. *Nucleic Acids Res.* 42, D490–D495. doi: 10.1093/nar/gkt1178
- Lombardi, P. (2002). Exemestane, a new steroidal aromatase inhibitor of clinical relevance. *Biochim. Biophys. Acta* 1587, 326–337. doi: 10.1016/S0925-4439(02)00096-0
- Lottrup, G., Andersson, A. M., Leffers, H., Mortensen, G. K., Toppari, J., Skakkebaek, N., et al. (2006). Possible impact of phthalates on infant reproductive health. *Int. J. Androl.* 29, 172–180. doi: 10.1111/j.1365-2605.2005.00642.x
- Lu, Y., Tang, F., Wang, Y., Zhao, J., Zeng, X., Luo, Q., et al. (2009). Biodegradation of dimethyl phthalate, diethyl phthalate and di-n-butyl phthalate by *Rhodococcus* sp. L4 isolated from activated sludge. *J. Hazard. Mater.* 168, 938–943. doi: 10.1016/j.jhazmat.2009.02.126
- Lu, Y., Wang, J., Deng, Z., Wu, H., Deng, Q., Tan, H., et al. (2013). Isolation and characterization of fatty acid methyl ester (FAME)-producing *Streptomyces* sp. S 161 from sheep (*Ovis aries*) faeces. *Lett. Appl. Microbiol.* 57, 200–205. doi: 10.1111/lam.12096
- Ma, T., Li, G., Li, J., Liang, F., and Liu, R. (2006). Desulfurization of dibenzothiophene by *Bacillus subtilis* recombinants carrying dszABC and dszD genes. *Biotechnol. Lett.* 28, 1095–1100. doi: 10.1007/s10529-006-9056-0
- Maass, D., Todescato, D., Moritz, D. E., Oliveira, J. V., Oliveira, D., Ulson de Souza, A. A., et al. (2015). Desulfurization and denitrogenation of heavy gas oil by

- Rhodococcus erythropolis* ATCC 4277. *Bioprocess Biosyst. Eng.* 38, 1447–1453. doi: 10.1007/s00449-015-1386-7
- Maghsoudi, S., Vossoughi, M., Kheirloom, A., Tanaka, E., and Katoh, S. (2001). Biotransformation of hydrocarbons and diesel fuels by *Rhodococcus* sp. strain P32C1. *Biochem. Eng. J.* 8, 151–156. doi: 10.1016/S1369-703X(01)00097-3
- Mandelbaum, R. T., Allan, D. L., and Wackett, L. P. (1995). Isolation and characterization of a *Pseudomonas* sp. that mineralizes the s-triazine herbicide atrazine. *Appl. Environ. Microbiol.* 61, 1451–1457.
- Matsui, R., Takagi, K., Sakakibara, F., Abe, T., and Shiiba, K. (2016). Identification and characterization of 1,4-dioxane-degrading microbe separated from surface seawater by the seawater-charcoal perfusion apparatus. *Biodegradation* 27, 155–163. doi: 10.1007/s10532-016-9763-8
- Matsumura, E., Sakai, M., Hayashi, K., Murakami, S., Takenaka, S., and Aoki, K. (2006). Constitutive expression of catABC genes in the aniline-assimilating bacterium *Rhodococcus* species AN-22: production, purification, characterization and gene analysis of CatA, CatB and CatC. *Biochem. J.* 393(Pt 1), 219–226. doi: 10.1042/bj20050740
- Mattam, A. J., Clomburg, J. M., Gonzalez, R., and Yazdani, S. S. (2013). Fermentation of glycerol and production of valuable chemical and biofuel molecules. *Biotechnol. Lett.* 35, 831–842. doi: 10.1007/s10529-013-1240-4
- Meyer, H., and Ruesing, M. (2008). “Lonza-Examples of bioprocesses for the production of nutraceuticals,” in *Paper Presented at the World Congress on Industrial Biotechnology & Bioprocessing*, Chicago, IL.
- Mitsukura, K., Kondo, Y., Yoshida, T., and Nagasawa, T. (2006). Regioselective hydroxylation of adamantane by *Streptomyces griseoplanus* cells. *Appl. Microbiol. Biotechnol.* 71, 502–504. doi: 10.1007/s00253-005-0167-7
- Mitsukura, K., Suzuki, M., Tada, K., Yoshida, T., and Nagasawa, T. (2010). Asymmetric synthesis of chiral cyclic amine from cyclic imine by bacterial whole-cell catalyst of enantioselective imine reductase. *Org. Biomol. Chem.* 8, 4533–4535. doi: 10.1039/c0ob00353k
- Mitsukura, K., Yoshida, T., and Nagasawa, T. (2002). Synthesis of (R)-2-phenylpropanoic acid from its racemate through an isomerase-involving reaction by *Nocardia diaphanozonaria*. *Biotechnol. Lett.* 24, 1615–1621. doi: 10.1023/A:1020353631566
- Mohamed Mel, S., Al-Yacoub, Z. H., and Vedakumar, J. V. (2015). Biocatalytic desulfurization of thiophenic compounds and crude oil by newly isolated bacteria. *Front. Microbiol.* 6:112. doi: 10.3389/fmicb.2015.00112
- Mohebbi, G., Ball, A. S., Rasekh, B., and Kaytash, A. (2007). Biotransformation potential of a newly isolated bacterium, RIPI90A. *Enzyme Microb. Technol.* 40, 578–584. doi: 10.1016/j.enzmictec.2006.05.012
- Mukhtar, S., Zaheer, A., Aiysha, D., Malik, K., and Mehnaz, S. (2017). Actinomycetes: a source of industrially important enzymes. *J. Proteomics Bioinform.* 10, 316–319. doi: 10.4172/jpb.1000456
- Müller, A. L. H., Picoloto, R. S., de Azevedo Mello, P., Ferrão, M. F., dos Santos, M. D. F. P., Guimarães, R. C. L., et al. (2012). Total sulfur determination in residues of crude oil distillation using FT-IR/ATR and variable selection methods. *Spectrochim. Acta A Mol. Biomol. Spectrosc.* 89, 82–87. doi: 10.1016/j.saa.2011.12.001
- Murohisa, T., and Iida, M. (1993). Some new intermediates in microbial side chain degradation of β -sitosterol. *J. Ferment. Bioeng.* 76, 174–177. doi: 10.1016/0922-338X(93)90003-Q
- Mycroft, Z., Gomis, M., Mines, P., Law, P., and Bugg, T. D. (2015). Biocatalytic conversion of lignin to aromatic dicarboxylic acids in *Rhodococcus jostii* RHA1 by re-routing aromatic degradation pathways. *Green Chem.* 17, 4974–4979. doi: 10.1039/C5GC01347J
- Neumann, G., Teras, R., Monson, L., Kivisaar, M., Schauer, F., and Heipieper, H. J. (2004). Simultaneous degradation of atrazine and phenol by *Pseudomonas* sp. strain ADP: effects of toxicity and adaptation. *Appl. Environ. Microbiol.* 70, 1907–1912. doi: 10.1128/AEM.70.4.1907-1912.2004
- Nigam, V. K., Khandelwal, A. K., Gothwal, R. K., Mohan, M. K., Choudhury, B., Vidyarthi, A. S., et al. (2009). Nitrilase-catalysed conversion of acrylonitrile by free and immobilized cells of *Streptomyces* sp. *J. Biosci.* 34, 21–26. doi: 10.1007/s12038-009-0005-7
- Nordin, K., Unell, M., and Jansson, J. K. (2005). Novel 4-chlorophenol degradation gene cluster and degradation route via hydroxyquinol in *Arthrobacter chlorophenolicus* A6. *Appl. Environ. Microbiol.* 71, 6538–6544. doi: 10.1128/AEM.71.11.6538-6544.2005
- Olaniran, A. O., and Igbinsola, E. O. (2011). Chlorophenols and other related derivatives of environmental concern: properties, distribution and microbial degradation processes. *Chemosphere* 83, 1297–1306. doi: 10.1016/j.chemosphere.2011.04.009
- Oyama, M., Kakinoki, T., Inoue, D., and Michihiko, I. (2013). Isolation and characterization of tetrahydrofuran-degrading bacteria for 1, 4-dioxane-containing wastewater treatment by co-metabolic degradation. *J. Water Environ. Technol.* 11, 11–19. doi: 10.2965/jwet.2013.11
- Pandey, J., Heipieper, H. J., Chauhan, A., Arora, P. K., Prakash, D., Takeo, M., et al. (2011). Reductive dehalogenation mediated initiation of aerobic degradation of 2-chloro-4-nitrophenol (2C4NP) by *Burkholderia* sp. strain SJ98. *Appl. Microbiol. Biotechnol.* 92, 597–607. doi: 10.1007/s00253-011-3254-y
- Parales, R. E., Adamus, J. E., White, N., and May, H. D. (1994). Degradation of 1,4-dioxane by an actinomycete in pure culture. *Appl. Environ. Microbiol.* 60, 4527–4530.
- Peralta-Yahya, P. P., Zhang, F., Del Cardayre, S. B., and Keasling, J. D. (2012). Microbial engineering for the production of advanced biofuels. *Nature* 488, 320–328. doi: 10.1038/nature11478
- Peters-Wendisch, P., Stolz, M., Etterich, H., Kennerknecht, N., Sahm, H., and Eggeling, L. (2005). Metabolic engineering of *Corynebacterium glutamicum* for L-serine production. *Appl. Environ. Microbiol.* 71, 7139–7144. doi: 10.1128/AEM.71.11.7139-7144
- Phelan, R. M., Sekurova, O. N., Keasling, J. D., and Zotchev, S. B. (2014). Engineering terpene biosynthesis in *Streptomyces* for production of the advanced biofuel precursor bisabolene. *ACS Synth. Biol.* 4, 393–399. doi: 10.1021/sb5002517
- Pignatello, R., Panto, V., Salmaso, S., Bersani, S., Pistara, V., Kepe, V., et al. (2008). Flurbiprofen derivatives in Alzheimer's disease: synthesis, pharmacokinetic and biological assessment of lipoamino acid prodrugs. *Bioconjug. Chem.* 19, 349–357. doi: 10.1021/bc700312y
- Pimentel-Elardo, S. M., Kozytska, S., Bugni, T. S., Ireland, C. M., Moll, H., and Hentschel, U. (2010). Anti-parasitic compounds from *Streptomyces* sp. strains isolated from Mediterranean sponges. *Mar. Drugs* 8, 373–380. doi: 10.3390/md8020373
- Prakash, D., Nawani, N., Prakash, M., Bodas, M., Mandal, A., Khetmalas, M., et al. (2013). Actinomycetes: a repository of green catalysts with a potential revenue resource. *Biomed Res. Int.* 2013:264020. doi: 10.1155/2013/264020
- Priyadarsini, P., and Dhanasekaran, D. (2015). Diversity of soil allelopathic Actinobacteria in Tiruchirappalli district, Tamilnadu, India. *J. Saudi Soc. Agric. Sci.* 14, 54–60. doi: 10.1016/j.jssas.2013.07.001
- Raj, J., Seth, A., Prasad, S., and Bhalla, T. C. (2007). Bioconversion of butyronitrile to butyramide using whole cells of *Rhodococcus rhodochrous* PA-34. *Appl. Microbiol. Biotechnol.* 74, 535–539. doi: 10.1007/s00253-006-0693-y
- Ralebits, T. K., Senior, E., and van Verseveld, H. W. (2002). Microbial aspects of atrazine degradation in natural environments. *Biodegradation* 13, 11–19. doi: 10.1023/A:1016329628618
- Ramteke, P. W., Maurice, N. G., Joseph, B., and Wadher, B. J. (2013). Nitrile-converting enzymes: an eco-friendly tool for industrial biocatalysis. *Biotechnol. Appl. Biochem.* 60, 459–481. doi: 10.1002/bab.1139
- Roh, C., Seo, S. H., Choi, K. Y., Cha, M., Pandey, B. P., Kim, J. H., et al. (2009). Regioselective hydroxylation of isoflavones by *Streptomyces avermitilis* MA-4680. *J. Biosci. Bioeng.* 108, 41–46. doi: 10.1016/j.jbiosc.2009.02.021
- Rohr, J. R., and McCoy, K. A. (2010). A qualitative meta-analysis reveals consistent effects of atrazine on freshwater fish and amphibians. *Environmen. Health Perspect.* 118, 20–32. doi: 10.1289/ehp.0901164
- Rousseaux, S., Hartmann, A., and Soulas, G. (2001). Isolation and characterisation of new Gram-negative and Gram-positive atrazine degrading bacteria from different French soils. *FEMS Microbiol. Ecol.* 36, 211–222. doi: 10.1111/j.1574-6941.2001.tb00842.x
- Saa, L., Jaureguibeitia, A., Largo, E., Llama, M. J., and Serra, J. L. (2010). Cloning, purification and characterization of two components of phenol hydroxylase from *Rhodococcus erythropolis* UPV-1. *Appl. Microbiol. Biotechnol.* 86, 201–211. doi: 10.1007/s00253-009-2251-x
- Santhi, V. A., and Mustafa, A. M. (2013). Assessment of organochlorine pesticides and plasticisers in the Selangor River basin and possible pollution sources. *Environ. Monit. Assess.* 185, 1541–1554. doi: 10.1007/s10661-012-2649-2

- Santoshkumar, M., Veeranagouda, Y., Lee, K., and Karegoudar, T. B. (2011). Utilization of aliphatic nitrile by *Paracoccus* sp SKG isolated from chemical waste samples. *Int. Biodeterior. Biodegradation* 65, 153–159. doi: 10.1016/j.ibiod.2010.10.008
- Sen, S. E., and Anliker, K. S. (1996). ¹H NMR analysis of R/S ibuprofen by the formation of diastereomeric pairs: microscale stereochemistry experiment for the undergraduate organic laboratory. *J. Chem. Educ.* 73:569. doi: 10.1021/ed073p569
- Sgobba, E., Blöbaum, L., and Wendisch, V. F. (2018). Production of food and feed additives from non-food-competing feedstocks: valorizing N-acetylmuramic acid for amino acid and carotenoid fermentation with *Corynebacterium glutamicum*. *Front. Microbiol.* 9:2046. doi: 10.3389/fmicb.2018.02046
- Shafi, R., and Hutchings, G. J. (2000). Hydrosulfurization of hindered dibenzothiophenes: an overview. *Catal. Today* 59, 423–442. doi: 10.1016/S0920-5861(00)00308-4
- Smith, K. M., Cho, K.-M., and Liao, J. C. (2010). Engineering *Corynebacterium glutamicum* for isobutanol production. *Appl. Microbiol. Biotechnol.* 87, 1045–1055. doi: 10.1007/s00253-010-2522-6
- Snell, D., and Colby, J. (1999). Enantioselective hydrolysis of racemic ibuprofen amide to s-(+)-ibuprofen by *Rhodococcus* AJ270. *Enzyme Microb. Technol.* 24, 160–163. doi: 10.1016/S0141-0229(98)00097-0
- Solecka, J., Zajko, J., Postek, M., and Rajnisz, A. (2012). Biologically active secondary metabolites from Actinomycetes. *Open Life Sci.* 7, 373–390. doi: 10.2478/s11535-012-0036-1
- Solomon, K. R., Carr, J. A., Du Preez, L. H., Giesy, J. P., Kendall, R. J., Smith, E. E., et al. (2008). Effects of atrazine on fish, amphibians, and aquatic reptiles: a critical review. *Crit. Rev. Toxicol.* 38, 721–772. doi: 10.1080/10408440802116496
- Solyanikova, I., and Golovleva, L. (2011). Biochemical features of the degradation of pollutants by *Rhodococcus* as a basis for contaminated wastewater and soil cleanup. *Microbiology* 80, 579–594. doi: 10.1134/S0026261711050158
- Sousa, S. F., Sousa, J. F., Barbosa, A. C., Ferreira, C. E., Neves, R. P., Ribeiro, A. J., et al. (2016). Improving the biodesulfurization of crude oil and derivatives: a qm/mm investigation of the catalytic mechanism of NADH-FMN oxidoreductase (DszD). *J. Phys. Chem. A* 120, 5300–5306. doi: 10.1021/acs.jpca.6b01536
- Sripalakit, P., Wichai, U., and Saraphanchotiwitthaya, A. (2006). Biotransformation of various natural sterols to androsthenones by *Mycobacterium* sp. and some steroid-converting microbial strains. *J. Mol. Catal. B Enzym.* 41, 49–54. doi: 10.1016/j.molcatb.2006.04.007
- Steinmann, J. G., Phillips, J. H., Sanders, W. J., and Kiessling, L. L. (2001). Synthesis of cyclic sulfates by halocyclization. *Org. Lett.* 3, 3557–3559. doi: 10.1021/ol016674b
- Stepien, D. K., Diehl, P., Helm, J., Thoms, A., and Puttmann, W. (2014). Fate of 1,4-dioxane in the aquatic environment: from sewage to drinking water. *Water Res.* 48, 406–419. doi: 10.1016/j.watres.2013.09.057
- Szentirmai, A. (1990). Microbial physiology of sidechain degradation of sterols. *J. Ind. Microbiol.* 6, 101–115. doi: 10.1007/BF01576429
- Tappe, W., Groeneweg, J., and Jantsch, B. (2002). Diffuse atrazine pollution in German aquifers. *Biodegradation* 13, 3–10. doi: 10.1023/A:1016325527709
- Topp, E., Mulbry, W. M., Zhu, H., Nour, S. M., and Cuppels, D. (2000). Characterization of s-triazine herbicide metabolism by a *Nocardioideis* sp. isolated from agricultural soils. *Appl. Environ. Microbiol.* 66, 3134–3141. doi: 10.1128/AEM.66.8.3134-3141.2000
- Trung, T. Q., Kim, J. M., and Kim, K. H. (2006). Preparative method of R-(+)-ibuprofen by diastereomer crystallization. *Arch. Pharm. Res.* 29, 108–111. doi: 10.1007/BF02977477
- Udaka, S. (1960). Screening method for microorganisms accumulating metabolites and its use in the isolation of *Micrococcus glutamicus*. *J. Bacteriol.* 79, 754–755.
- Ulrich, E. M., Morrison, C. N., Goldsmith, M. R., and Foreman, W. T. (2012). Chiral pesticides: identification, description, and environmental implications. *Rev. Environ. Contam. Toxicol.* 217, 1–74. doi: 10.1007/978-1-4614-2329-4_1
- van Afferden, M., Schacht, S., Klein, J., and Trüper, H. G. (1990). Degradation of dibenzothiophene by *Brevibacterium* sp. DO. *Arch. Microbiol.* 153, 324–328. doi: 10.1007/BF00249000
- Van Hamme, J. D., Singh, A., and Ward, O. P. (2003). Recent advances in petroleum microbiology. *Microbiol. Mol. Biol. Rev.* 67, 503–549. doi: 10.1128/MMBR.67.4.503-549.2003
- Van Keulen, F., Correia, C., and Da Fonseca, M. (1998). Solvent selection for the biotransformation of terpenes by *Pseudomonas putida*. *J. Mol. Catal. B Enzym.* 5, 295–299. doi: 10.1016/S1381-1177(98)00054-X
- Vesela, A. B., Pelantova, H., Sulc, M., Mackova, M., Lovecka, P., Thimova, M., et al. (2012). Biotransformation of benzonitrile herbicides via the nitrile hydratase-amidase pathway in rhodococci. *J. Ind. Microbiol. Biotechnol.* 39, 1811–1819. doi: 10.1007/s10295-012-1184-z
- Wadhwa, L., and Smith, K. E. (2000). Progesterone side-chain cleavage by *Bacillus sphaericus*. *FEMS Microbiol. Lett.* 192, 179–183. doi: 10.1111/j.1574-6968.2000.tb09379.x
- Wang, W., Ma, T., Lian, K., Zhang, Y., Tian, H., Ji, K., et al. (2013). Genetic analysis of benzoethiophene biodesulfurization pathway of *Gordonia terrae* strain C-6. *PLoS One* 8:e84386. doi: 10.1371/journal.pone.0084386
- Ward, T. R., and Köhler, V. (2015). Editorial overview: biocatalysis and biotransformation: bio-inspired, bio-based and bio-linked catalysis. *Curr. Opin. Chem. Biol.* 25, v–vi. doi: 10.1016/j.cbpa.2015.02.022
- Webster, N. A., Ramsden, D. K., and Hughes, J. (2001). Comparative characterisation of two *Rhodococcus* species as potential biocatalysts for ammonium acrylate production. *Biotechnol. Lett.* 23, 95–101. doi: 10.1023/A:1010389115549
- Whited, G. M., Feher, F. J., Benko, D. A., Cervin, M. A., Chotani, G. K., McAuliffe, J. C., et al. (2010). Technology update: development of a gas-phase bioprocess for isoprene-monomer production using metabolic pathway engineering. *Ind. Biotechnol.* 6, 152–163. doi: 10.1089/ind.2010.6.152
- Wu, X., Wang, Y., Liang, R., Dai, Q., Jin, D., and Chao, W. (2011). Biodegradation of an endocrine-disrupting chemical di-n-butyl phthalate by newly isolated *Agrobacterium* sp. and the biochemical pathway. *Process Biochem.* 46, 1090–1094. doi: 10.1016/j.procbio.2011.01.031
- Xu, P., Yu, B., Li, F. L., Cai, X. F., and Ma, C. Q. (2006). Microbial degradation of sulfur, nitrogen and oxygen heterocycles. *Trends Microbiol.* 14, 398–405. doi: 10.1016/j.tim.2006.07.002
- Xun, L., Topp, E., and Orser, C. (1992). Purification and characterization of a tetrachloro-p-hydroquinone reductive dehalogenase from a *Flavobacterium* sp. *J. Bacteriol.* 174, 8003–8007. doi: 10.1128/jb.174.24.8003-8007.1992
- Yamamoto, S., Suda, M., Niimi, S., Inui, M., and Yukawa, H. (2013). Strain optimization for efficient isobutanol production using *Corynebacterium glutamicum* under oxygen deprivation. *Biotechnol. Bioeng.* 110, 2938–2948. doi: 10.1002/bit.24961
- Yu, L. L., Li, Z. Y., Peng, C. S., Li, Z. Y., and Guo, Y. W. (2009). Neobacillamide A, a novel thiazole-containing alkaloid from the marine bacterium *Bacillus vallismortis* C89, associated with South China Sea sponge *Dysidea avara*. *Helv. Chim. Acta* 92, 607–612. doi: 10.1002/hlca.200800349
- Zahoor, A., Lindner, S. N., and Wendisch, V. F. (2012). Metabolic engineering of *Corynebacterium glutamicum* aimed at alternative carbon sources and new products. *Comput. Struct. Biotechnol. J.* 3:e201210004. doi: 10.5936/csbi.201210004
- Zhang, M., and Yu, Y. (2013). Dehydration of ethanol to ethylene. *Ind. Eng. Chem. Res.* 52, 9505–9514. doi: 10.1021/ie401157c
- Zheng, Y. G., Chen, J., Liu, Z. Q., Wu, M. H., Xing, L. Y., and Shen, Y. C. (2008). Isolation, identification and characterization of *Bacillus subtilis* ZJB-063, a versatile nitrile-converting bacterium. *Appl. Microbiol. Biotechnol.* 77, 985–993. doi: 10.1007/s00253-007-1236-x

Conflict of Interest Statement: The authors declare that the research was conducted in the absence of any commercial or financial relationships that could be construed as a potential conflict of interest.

Copyright © 2019 Anteneh and Franco. This is an open-access article distributed under the terms of the Creative Commons Attribution License (CC BY). The use, distribution or reproduction in other forums is permitted, provided the original author(s) and the copyright owner(s) are credited and that the original publication in this journal is cited, in accordance with accepted academic practice. No use, distribution or reproduction is permitted which does not comply with these terms.



A Waking Review: Old and Novel Insights into the Spore Germination in *Streptomyces*

Jan Bobek^{1,2,3*}, Klára Šmídová^{1,3} and Matouš Čihák¹

¹ Institute of Immunology and Microbiology, First Faculty of Medicine, Charles University, Prague, Czechia, ² Chemistry Department, Faculty of Science, Jan Evangelista Purkyně University in Ústí nad Labem, Ústí nad Labem, Czechia, ³ Institute of Microbiology of the Czech Academy of Sciences, Prague, Czechia

OPEN ACCESS

Edited by:

Dirk Tischler,
Freiburg University of Mining
and Technology, Germany

Reviewed by:

Susan Schlimpert,
John Innes Centre (BBSRC),
United Kingdom
Philippe Constant,
Institut National de la Recherche
Scientifique (INRS), Canada

*Correspondence:

Jan Bobek
jan.bobek@lf1.cuni.cz

Specialty section:

This article was submitted to
Microbial Physiology and Metabolism,
a section of the journal
Frontiers in Microbiology

Received: 28 August 2017

Accepted: 26 October 2017

Published: 13 November 2017

Citation:

Bobek J, Šmídová K and Čihák M
(2017) A Waking Review: Old
and Novel Insights into the Spore
Germination in *Streptomyces*.
Front. Microbiol. 8:2205.
doi: 10.3389/fmicb.2017.02205

The complex development undergone by *Streptomyces* encompasses transitions from vegetative mycelial forms to reproductive aerial hyphae that differentiate into chains of single-celled spores. Whereas their mycelial life – connected with spore formation and antibiotic production – is deeply investigated, spore germination as the counterpoint in their life cycle has received much less attention. Still, germination represents a system of transformation from metabolic zero point to a new living lap. There are several aspects of germination that may attract our attention: (1) Dormant spores are strikingly well-prepared for the future metabolic restart; they possess stable transcriptome, hydrolytic enzymes, chaperones, and other required macromolecules stabilized in a trehalose milieu; (2) Germination itself is a specific sequence of events leading to a complete morphological remodeling that include spore swelling, cell wall reconstruction, and eventually germ tube emergences; (3) Still not fully unveiled are the strategies that enable the process, including a single cell's signal transduction and gene expression control, as well as intercellular communication and the probability of germination across the whole population. This review summarizes our current knowledge about the germination process in *Streptomyces*, while focusing on the aforementioned points.

Keywords: dormancy, germination, *Streptomyces*, spore, cell wall, gene expression, metabolism, signaling

INTRODUCTION

Soil microorganisms are exposed to periodic nutrient exhaustions and various abiotic and biotic stresses that inhibit growth. An important survival strategy for many bacteria and fungi in the face of such physiological stresses is the cells' transition into a dormant state. In the dormant state, cells arrest their growth, discontinue replication and transform themselves into metabolically inactive (or with limited activity), widely resistant forms. Several bacterial clades living in soil, such as *Actinomyces*, *Streptomyces*, and *Micromonospora*, differentiate into dormant fungi-like uninucleoid spores (arthrospores or exospores). Arthrospores significantly differ from the endospores of *Bacilli* and *Clostridia* in morphology and function. The endospores exhibit striking resistance to a wide range of environmental stresses, such as heat, desiccation, and ultraviolet radiation (Setlow, 2007; Galperin et al., 2012). Their abilities to survive harsh conditions result from multi-layered surface structures and extremely low water content (Setlow et al., 2006; Henriques and Moran, 2007). The well-studied endospores of *Bacillus subtilis* contain high levels of dipicolinic acid in chelation with divalent cations (Ca²⁺) and extremely stable small spore proteins

(Setlow et al., 2006). All these features contribute to the overall robust endospore resistance. The streptomycete arthrospores, on the other hand, are more reminiscent of the spores of eukaryotic fungi, possibly due to their convergent evolution in the soil environment. *Penicillium* species, for example, produce conidiophores (analogous to streptomycete aerial hyphae, see below) that bear individually constricted conidiospores (Foster et al., 1945). Both, streptomycetes and molds produce large numbers of small hydrophobic spores with similar properties; both contain, for example, a relatively thick coat (Briza et al., 1990; Pammer et al., 1992; Neiman, 2005), protective small molecules including sugars (such as trehalose, see below), and heat shock proteins (Wyatt et al., 2013). Spores of these organisms not only guard genetic information during unfavorable conditions, but are also adapted to wind dispersal and may remain airborne for long periods.

Their complex life cycle and the described similarities with eukaryotic fungi make streptomycetes unique organisms within the bacterial kingdom. However, comprehensive information about the diverse features of spore germination in this antibiotic-producing clade is still missing. This review attempts to fill this gap.

The process of germination, when either considering the germination rate of a single spore or the probability of germination within a spore population, varies between different *Streptomyces*. Some species (mainly *S. viridochromogenes* and *S. granaticolor*) exhibit fast and robust germination with nearly all spores germinating. That is also why this organism was subjected to many initial germination experiments (Hirsch and Ensign, 1976a,b; Mikulik et al., 1977; Bobek et al., 2004; Xu and Vetsigian, 2017). In contrast, other species (e.g., *S. coelicolor* and *S. venezuelae*) germinate more slowly with a fraction of spores that does not germinate at all. These exhibit more complex germination behavior and possess a fraction of germlings that stop growing soon after germination, probably due to produced inhibitory compounds, such as germicidins and hypnosins, that affect their development (Petersen et al., 1993; Aoki et al., 2007, 2011; Ma et al., 2017; Xu and Vetsigian, 2017). Over time, *S. coelicolor* became a widely used model streptomycetes whose genome was the first to be resolved and best annotated within the genus (Bentley et al., 2002). Therefore, the later genome-wide expression analyses of germinating spores have also been conducted on this strain (Strakova et al., 2013a,b, 2014; Bobek et al., 2014). Hence, most of the findings mentioned here come from the experimental results obtained with *S. coelicolor*.

THE *Streptomyces* CELL CYCLE AND SPOROGENESIS

Our knowledge of the complex life of *Streptomyces* with a certain emphasis on the process of sporulation and spore maturation (together here called as sporogenesis) offers many clues for understanding the readiness of spores for successful germination. The life cycle of *Streptomyces*, similarly as in the other arthrospore-forming bacteria, encompasses a development of a network of branched hyphae that grow into the substrate thus

creating a vegetative mycelium. The subsequent development of aerial hyphae and spores is considered to be the cell's response to nutrient depletion. The sporulation-specific regulon is activated after repression of sporulation-specific genes by the BldD-c-di-GMP complex is released (Tschowri et al., 2014; Bush et al., 2015). A part of the vegetative mycelium lyses to be used as a surrogate of nutrients. During this developmental phase the activity of secondary metabolism reaches its maximum to synthesize various bioactive compounds, including antibiotics, in its effort to avoid competitive organisms.

The aerial mycelium of *Streptomyces* is covered with a rodlet layer, a network of pairwise amyloid fibrils (Wildermuth et al., 1971) that consist of chaplin and rodlin proteins (Claessen et al., 2004). This hydrophobic structure lowers the water surface tension thereby enabling the hyphae to grow apically into the air (Elliot and Talbot, 2004; Claessen et al., 2006). The erected sporogenic hyphae are dissected by sporulation septa. The sporulation septation is synchronized with a segregation of chromosomes thus forming unigenomic pre-spore compartments (Ausmees et al., 2007; Wang et al., 2007; Jakimowicz and van Wezel, 2012; Ditekowski et al., 2013). This process is controlled by a family of SsgA-like proteins (SALP) found exclusively in differentiating actinomycetes (Sigle et al., 2015). Their member SsgA is a protein essential for sporulation in *S. coelicolor*; in concert with SsgB it dynamically controls the assembly of FtsZ rings at septation sites (van Wezel et al., 2000; Keijser et al., 2003; Sevcikova and Kormanec, 2003; Willemse et al., 2011). The role of SsgA is related to the *de novo* peptidoglycan synthesis; SsgA has been suggested to mark future germination sites and when the protein is overproduced, individual spores generate many germ tubes. SsgC, whose deletion leads to hypersporulation, has been suggested to function as an antagonist of SsgA. The SALP proteins also include SsgD that ensures the development of the thick spore wall and SsgG that controls regular localization of division sites (Noens et al., 2005, 2007; Traag and van Wezel, 2008).

The following process of spore maturation is the transition of the dissected aerial hyphae into the mature ovoid spores. Not much is known about this phase. When spores are only partially mature (harvested at an earlier stage of sporulation), they germinate remarkably faster and more synchronously. On the other hand, the fully matured spores exhibit less viability and longer lag-phase in conditions suitable for germination (Hirsch and Ensign, 1976a). These differences hint at further but not yet fully understood processes associated with spore maturation, presumably involving the stabilization of nucleic acids and proteins, deactivation of the metabolic apparatus, desiccation, and changes in the cell wall structure. The spore's wall thickening is dependent on the so called *Streptomyces*-spore-wall-synthesizing complex (SSSC), a system somewhat similar to the elongasome of rod-shaped bacteria (Kleinschmitz et al., 2011). Members involved in this complex are the cytoskeletal actin-like proteins, MreB and Mbl that cooperate in spore wall synthesis (Mazza et al., 2006; Heichlinger et al., 2011). Maturation is further accompanied by DNA condensation and spore pigmentation, such as the production of gray spore pigment in *S. coelicolor* (Kelemen et al., 1998). After maturation, the

rodlet layer forms a thin, basket-like fibrous sheath around the thickened spore wall (Claessen et al., 2002, 2003; Elliot et al., 2003) and cell wall hydrolases under control of other SALP members, SsgE and SsgF, separate individual spores allowing for their dispersal into the environment (Traag and van Wezel, 2008; Flardh and Buttner, 2009; Haiser et al., 2009).

DORMANT SPORE EQUIPMENT

Dormant spores of streptomycetes are the only haploid state in the development of this multicellular mycelial bacterium. Their main function is to safeguard genetic information throughout unfavorable conditions and consequently spread it into new niches. All the macromolecules that are needed for the future launch of germination have to be pre-synthesized before dormancy. Yet, it remains unclear whether dormant spores possess none or limited metabolism. Despite the commonly held belief that dormant spores are metabolically inactive, Liot and Constant suggested some metabolic activity of dormant spores as their experiments showed that mature spores of *S. avermitilis* (suspended in Tris-HCl) are able to oxidize atmospheric H₂ to supply maintenance energy (Constant et al., 2008; Liot and Constant, 2016). A fascinating example of metabolically active spores comes from another soil-inhabiting actinomycete genus, *Actinoplanes*, which produces flagellated spores (zoospores) that guided by chemotaxis (sugars, amino acids, aromatic compounds, and mineral ions) are temporarily able to rapidly swim (Palleroni, 1976; Jang et al., 2016).

Generally, other than the thick cell wall, the lack of water in spores ensures their resistance to thermal extremities and to other physical and chemical effects (Kalakoutskii and Agre, 1976). On the other hand, the dehydrated state results in immobility and changed conformation of macromolecules; the condensation of nucleic acids and an inactive form of proteins. The endospores of *Bacilli* contain a significant amount (20%) of dipicolinic acid (Setlow et al., 2006) that stabilizes their macromolecule structures under dehydrated conditions. In the spores of streptomycetes that lack the Ca-dipicolinate, the stabilization and protection of macromolecules is provided by trehalose, instead. During spore resuscitation, the protective role is transferred to present protein chaperones that help other proteins reobtain their functional conformation (Bobek et al., 2004).

Spores subjected to germination in the presence of the antibiotic rifampicin that inhibits the initiation of transcription were still able to synthesize proteins (termed early proteins) over the experimental period. This result suggested that there is also a pool of stable mRNAs, functional ribosomes, and translational apparatus that have been preserved during spore maturation (Mikulik et al., 2002).

In addition, preserved hydrolytic enzymes are accessible for the initial reconstruction of the cell wall (Haiser et al., 2009). In *S. coelicolor*, several hydrolases that might take their part in the cell envelope reconstruction (SCO1061, SCO1725, SCO3487, and SCO5466) were shown to be stored throughout spore dormancy and not synthesized *de novo* during germination (Strakova et al.,

2013a). This suggests that cells possess the required enzymatic equipment from the sporulation and/or spore maturation period.

While common opinion has, until recent times, stipulated that spores require external nutrients to launch germination (Flardh and Buttner, 2009), *B. subtilis* spores were recently shown to germinate even in an environment lacking all germination factors (Sturm and Dworkin, 2015; van Vliet, 2015). The launch of germination was stochastic (discussed below) and depended on the level of a transcription factor involved in spore assembly. In the case of *Streptomyces*, the probability of germination was suggested to be dependent on an insoluble protein NepA (de Jong et al., 2009). NepA is a structural part of the streptomycete spore wall which was shown to maintain the spore's dormancy. In the absence of this protein spores germinate faster and more synchronously. Even spores lacking NepA protein were able to produce hyphae (after 3 days) and form mycelial clumps (after 7 days of cultivation) when cultivated in water (de Jong et al., 2009). This would not be possible if the spores did not possess intracellular nutrient sources, such as trehalose (Ranade and Vining, 1993) and polyphosphates (volutin) (Ghorbel et al., 2006; Strakova et al., 2013b) that promote the metabolic restart before the external sugar can be sensed and assimilated. Various strains of *Streptomyces* have been reported to contain high trehalose levels in their spores. For example in the glucose excess, spores of *S. griseus* accumulate trehalose that comprises up to 25% of their dry weight (McBride and Ensign, 1987a). Trehalose is also abundant in *S. venezuelae* spores, whereas glycogen and polyhydroxybutyrate are absent, which stands in contrast to vegetative hyphae (Ranade and Vining, 1993). It has been shown that sporogenic hyphae convert present glycogen to trehalose during the final period of spore maturation in *S. brasiliensis* (Rueda et al., 2001).

Trehalose is a disaccharide consisting of two glucose molecules that are bound together in α , α -1,1-glycosidic linkage. Trehalose associates in clusters resulting in a large, continuous aggregates formation (Sapir and Harries, 2011). According to the water displacement theory, trehalose present in a system replaces water under desiccation conditions (Sola-Penna and Meyer-Fernandes, 1998). Trehalose is present in various organisms; from Archaea to animals where it may serve as a source of carbon and energy or act as a signaling molecule (Elbein et al., 2003). The unique α , α -1,1-glycosidic linkage makes trehalose non-reducing and therefore unreactive, making it the best intracellular macromolecules stabilizer. Thanks to its ability to make hydrogen bonds with membranes and nucleic acids, as well as its ability to modify the solvation layer of proteins (Sola-Penna and Meyer-Fernandes, 1998), trehalose is capable of protecting cellular membranes, DNA, enzymes (though in their inactive forms), and even whole microorganisms (Yoshinaga et al., 1997; Kandrór et al., 2002; Jain and Roy, 2010). The sugar may thus help the cells cope with heat, freezing, desiccation, radiation, and oxidative stresses (Hottiger et al., 1989; Wiemken, 1990; De Virgilio et al., 1994; Yoshinaga et al., 1997; An et al., 2000; Benaroudj et al., 2001; Fillinger et al., 2001). Its multi-protective role is of special need in dormant stages; the sugar is thought to form a gel phase in anhydrous conditions, which prevents aggregation

of macromolecules. Subsequent rehydration allows normal restoration of cell metabolism. Consequently, trehalose, as a protective sugar, is quite abundant in bacterial cells, such as those of *Mycobacterium*, including *M. smegmatis* and *M. tuberculosis* (Elbein and Mitchell, 1973), in spores of *Myxococcus* (McBride and Zusman, 1989) and *Streptomyces* (Martin et al., 1986), or in spores of eukaryotic yeast and fungi (Trevelyan and Harrison, 1956; Nwaka and Holzer, 1998). Trehalose is also located inside mycobacterial and corynebacterial cell wall structures (Lederer, 1976).

THE SPORES' AWAKENING

Minimal or no metabolic activity enables the spores to survive harsh conditions such as high temperatures or the presence of antibiotics and thus stay persevered for years. To awake, spores require at least aqueous conditions (Hirsch and Ensign, 1976b). Germination is faster and more convenient, however, in the presence of required nutrients and other germination stimuli (Paredes-Sabja et al., 2011). Despite this, the scattering remains high in the germination rate within a single population. This being the case, Jyothikumar et al. (2008) showed by means of time-lapse microscopy that germination tubes occurred between 3.75 and 7.5 h in their experimental conditions. The known stimuli that consequently lead to a more synchronous development are heat shock (Hirsch and Ensign, 1976a), mechanical disruption of the spore envelopes (Mikulik et al., 1977; Stastna, 1977; Miguelez et al., 1993), or the presence of peptidoglycan residues (Shah et al., 2008). But how may metabolically inert spores detect optimal environmental conditions? As was shown in the case of the *B. subtilis* spores, germination is launched stochastically, though at much lower frequency in poor environments (Paidhungat and Setlow, 2000; Epstein, 2009; Sturm and Dworkin, 2015). If the environmental conditions remain adverse, for example because of the lack of nutrients, the germinating spore will eventually die (van Vliet, 2015). Thus spores of *Saccharomyces cerevisiae*, an eukaryotic yeast, that launch germination in a poor glucose solution, without any additional nutrients, are not able to further develop bud emergences in these conditions (Chen et al., 2000). In the optimal environment, however, spores may even stimulate each other's development. In addition to the spore-forming *Streptomyces* (Xu and Vetsigian, 2017) and *Bacilli* (Chen et al., 2006; Sturm and Dworkin, 2015; van Vliet, 2015), the stochastic development from a dormant state was observed in non-sporulating *Escherichia coli* and *M. smegmatis* as well (Balaban et al., 2004; Buerger et al., 2012). Such a strategy where successful pioneers wake other fellows up in a favorable environment is probably advantageous and cost-effective from the perspective of the whole population.

GERMINATION STAGES

Germination is associated with a complete reconstruction of the cell that involves highly accelerating metabolic activity,

morphological changes that start with uncoating, and reconstitution of the cellular content. Spore germination is a sequential process and thus can be divided into three distinctive steps (defined by Hardisson et al., 1978): darkening, swelling, and germ tube emergence (**Figure 1**).

(a) Darkening is associated with cell wall reconstruction

The first step could be described as a transition from pure physical processes, such as osmosis, that progressively activate initial biochemical activities requiring energy sources. During this step spores lose their hydrophobicity resulting in water influx, swelling, and the subsequent loss of heat resistance. These processes change the optical features of spores and allow the cells to re-activate metabolism within the only several minutes after germination initiation. The darkening is caused by the loss of light refraction which requires bivalent cations Ca^{2+} , Mg^{2+} , Mn^{2+} , Zn^{2+} , and Fe^{2+} (Hardisson et al., 1978; Eaton and Ensign, 1980; Salas et al., 1983). The binding sites for calcium and magnesium are provided by both, the carboxyl units of peptidoglycan and the polyphosphate groups of teichoic acid in the spore wall (Thomas and Rice, 2014). Relatively early the spores undergo an uncoating, during which calcium accumulated in the spore envelope is gradually released (Eaton and Ensign, 1980; Salas et al., 1983). This process is mediated by a calcium-binding protein CabC whose disruption leads to prematurely germinating spores on the spore chain, while an overexpression of the gene delays their development (Wang et al., 2008). During uncoating, spore lysozyme-like hydrolases are reactivated and facilitate changes in spore morphology and optical features. These enzymes provide lysis and facilitate the reconstruction of cell wall peptidoglycan to allow the entrance of external nutrients. Mutants of two cell wall hydrolases, RpfA and SwlA, exhibited slower germination (Haiser et al., 2009). The hydrolases cleave covalent bonds inside the peptidoglycan layer; an act that must be well-coordinated with the new cell wall synthesis. RpfA belongs to a class of so called resuscitation-promoting factors, Rpf, a subgroup of lysozyme-like transglycosylases, which hydrolyze the beta-(1,4)-glycosidic bond between *N*-acetylglucosamine and *N*-acetylmuramic acid (Mukamolova et al., 1998b, 2002, 2006; Cohen-Gonsaud et al., 2004; Keep et al., 2006; Telkov et al., 2006; Hett et al., 2008; Haiser et al., 2009; Ruggiero et al., 2009). These muralytic enzymes are known to participate in the restoration of active growth from dormancy not only in *Streptomyces* but also in other actinobacteria, like *Mycobacterium* and *Micrococcus* (Mukamolova et al., 1998a, 2006; Keep et al., 2006). *S. coelicolor* possesses five Rpf proteins (RpfA to RpfE) (Haiser et al., 2009) whose individual mutants delay germination to varying extents; with RpfA and RpfE having a stronger effect than RpfC and RpfD. This differs to what can be observed in the wild type (Sexton et al., 2015). Although a multiple *rpf* mutant (with deletion of all five *rpf* genes) revealed a highly impaired germination,

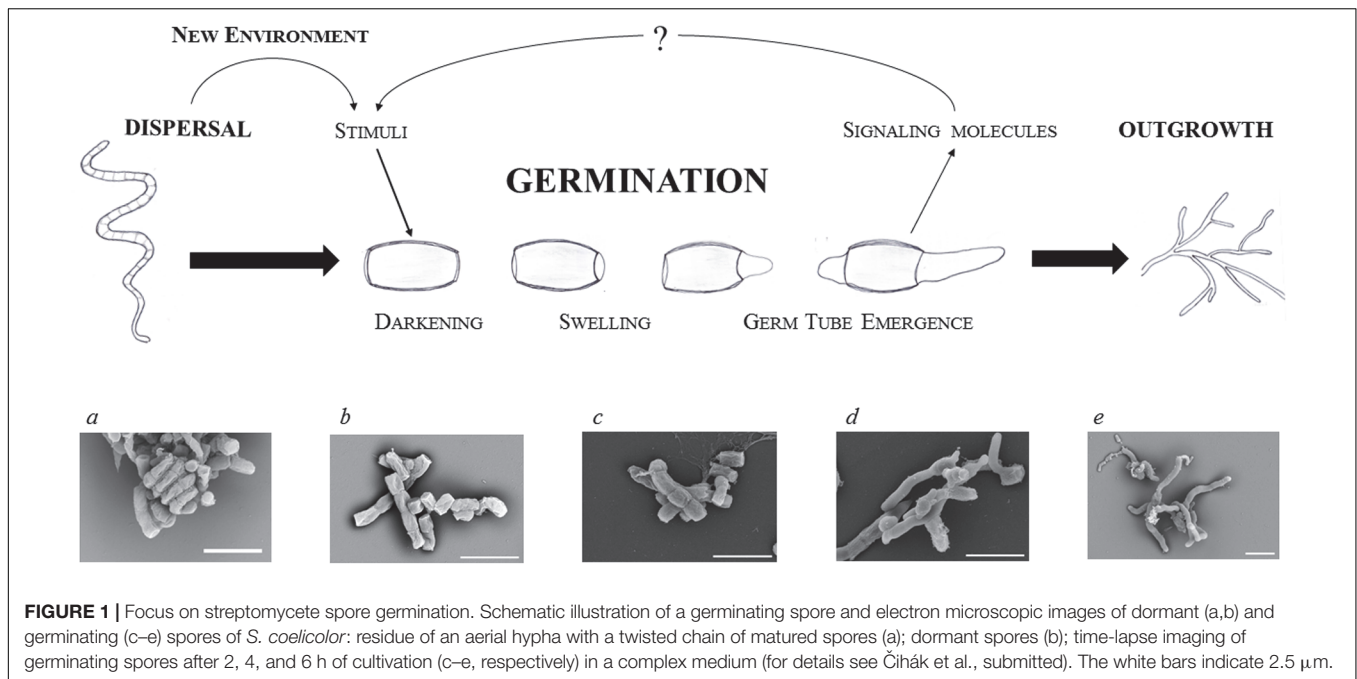


FIGURE 1 | Focus on streptomycete spore germination. Schematic illustration of a germinating spore and electron microscopic images of dormant (a,b) and germinating (c–e) spores of *S. coelicolor*: residue of an aerial hypha with a twisted chain of matured spores (a); dormant spores (b); time-lapse imaging of germinating spores after 2, 4, and 6 h of cultivation (c–e, respectively) in a complex medium (for details see Čihák et al., submitted). The white bars indicate 2.5 μm.

the strain was able to germinate within 12 h. This suggests that the Rpf hydrolase family is highly important but not essential for a smooth germination. The Rpf family could probably be substituted by other cell wall hydrolases. Three *Streptomyces* cell wall lytic enzymes (SwlA to SwlC) are examples of such possible candidates that may be responsible for the proper thickness of the dormant spore wall ensuring its heat resistance (Haiser et al., 2009). In this reference one may find an overview of predicted streptomycete cell wall hydrolase genes as well.

- (b) Enzymatic activities are recovered during swelling. Continual influx of water causes spores to swell. A dramatic intracellular decline of the trehalose level has been observed in *S. griseus* during spore swelling (McBride and Ensign, 1987b, 1990). A similar effect was also observed in *M. smegmatis* (Shleeva et al., 2017), *Neurospora* (Sussman and Lingappa, 1959; Sussman, 1961), and *Dictyostelium discoideum* (Roth and Sussman, 1966; Ceccarini, 1967). Consequently, the glucose level increases in swelled spores, suggesting a restored activity of the trehalase enzyme due to an increased concentration of intracellular ATP (McBride and Ensign, 1987b). The hydrolysis of trehalose appears to be an essential step in spore germination (Nwaka and Holzer, 1998). Based on observations of the yeast *S. cerevisiae*, trehalase possesses an inactive form which is activated by phosphorylation in a cAMP-dependent manner (Thevelein, 1984). The restored glucose subsequently provides an internal energy source for the revived enzymes and initial development. Only after the intracellular concentration of trehalose declines do the protected proteins refold into their active forms with the help of their respective chaperones (Singer and Lindquist, 1998).

The hydration of the cytoplasm supports the re-activation of assorted proteins and ribosomes that are preserved from dormancy (Cowan et al., 2003). Bound chaperones GroEL, Trigger factor and DnaK assist in the reactivation of the proteosynthetic apparatus and nascent proteins (Bobek et al., 2004). These chaperones as well as others (GrpE and peptidyl-prolyl *cis-trans* isomerases) are constitutively expressed throughout the germination course suggesting that their presence is constantly necessary (Strakova et al., 2013a). Within several minutes of the germination starting, the ribosomes present are fully functional and new proteins are translated from the stable mRNA stock (Strakova et al., 2013b). The proteosynthesis accelerates between 30 and 60 min (Strakova et al., 2013a). At this stage spores are metabolically active and able to utilize primarily internal energy sources, such as trehalose (see below; Elbein, 1974; Crowe et al., 1984), to obtain carbon, nitrogen and energy (Hey-Ferguson et al., 1973; McBride and Ensign, 1987a). The obtained energy is exploited not only for the intensive proteosynthesis (Mikulik et al., 1984, 2008, 2011; Paleckova et al., 2006) but also for the first DNA replication, which occurs just before or simultaneously with the germ tube emergence within about 60 min of germination in *S. granaticolor* (Mikulik et al., 1977) or 30–60 min later in *S. coelicolor* (Ruban-Osmialowska et al., 2006; Wolanski et al., 2011). Later the spores are able to detect external nutrient sources and as a response they adjust metabolic pathways. They are capable of this due to the activity of present pleiotropic gene expression regulators acting on both transcriptional (BldD, cyclic AMP-receptor protein Crp, and sigma and anti-sigma factors) and translational (ribonuclease RNase III) levels, as was shown in *S. coelicolor* (Strakova et al., 2013a).

- (c) The vegetative growth starts with germ tube emergence. The eventual germ tube emergence is a microscopically observable event that provides the basis for the apically growing hyphae. The not yet septated tubes rise from the inner wall of spore (Glauert and Hopwood, 1961) and progress through the outer rodlet layer. An important role is carried out by the chaperonin-like protein SsgA that localizes sites of germ tube emergences. This protein is located at the sites of the germ tip appearance (Noens et al., 2007). In *S. coelicolor* one or two germination tubes appear after 180 min of germination and elongate by apical tip extension. At this developmental point two or three DNA replisomes were demonstrated (Ruban-Osmialowska et al., 2006; Wolanski et al., 2011). The critical determinant of the vegetative growth is the DivIVA protein that localizes at hyphal tips ensuring a new cell wall outgrowth (Flardh, 2003a; Flardh et al., 2012; Hempel et al., 2012; Richards et al., 2012). Interestingly, DivIVA is expressed from early on after spore hydration and its synthesis increases during the whole process of germination (Strakova et al., 2013a). As was also shown, cell division-associated protein FtsZ (SCO2082, Grantcharova et al., 2005), which is the BldD target, and cell growth-associated protein FilP (SCO5396, Flardh, 2003b; Bagchi et al., 2008) are expressed at 300 min of *S. coelicolor*'s germination. FilP protein, which is associated with DivIVA, accumulates in the tips of young hyphae and is also expressed soon after germination starts (Strakova et al., 2013a). FilP resemble eukaryotic intermediate filaments forming a tangled cytoskeletal network that confers to rigidity and elasticity of hyphae (Kelemen, 2017). The onset of these proteins was previously proposed as the point when the germination phase finalizes (Strakova et al., 2013a).

PROTEOME RECONSTITUTION AND TRANSCRIPTION CONTROL DURING GERMINATION

Several genome-wide studies on gene expression during the streptomycete spore germination have recently been conducted (Bobek et al., 2004, 2014; Piette et al., 2005; Strakova et al., 2013a,b). Furthermore, a biocomputational modeling (Strakova et al., 2013a,b, 2014) was employed to obtain a global view on protein synthesis and to characterize the regulatory networks. The expression profiles of individual proteins from 13 time points throughout the course of germination have been sorted and divided among differential functional groups. A study analyzing the protein synthesis changes between consecutive time intervals revealed that the transcriptional apparatus is indeed highly active from the first 30 min of germination but surprisingly, most of the mRNAs preserved from dormancy are consequently degraded during the rehydration (Strakova et al., 2013a; Bobek et al., 2014). The degradation affects mRNAs from the majority of functional protein groups, i.e., amino acid, carbohydrate, lipid and energy metabolism, proteasomes, and DNA repair pathways. This does not mean, however, that the activity of these functional groups

is disabled. For example, besides those mentioned, the degraded mRNAs also encode proteins involved in translation. This occurs despite the intensive protein synthesis, suggesting that the fully active translational apparatus is available from dormancy and is re-activated very rapidly when the germination starts. Subsequently, but still during the first 30 min of germination, the level of most mRNA groups increases again, but now more likely as a relevant response to the available sources and cell requirements under new conditions.

The activity of the transcriptional apparatus is strictly dependent on the set of sigma factors present in distinctive time points. They direct specific developmental tasks, such as the cell wall reconstitution, protein refolding, or the osmotic stress response, and therefore they must be fully accessible at specific points during germination (Bobek et al., 2014). Thus, SigW sigma factor (SCO0632), whose homolog in *B. subtilis* directs the synthesis of cell wall hydrolases (Helmman, 2006), is already expressed in *S. coelicolor* during the initial rehydration event, suggesting a similar role in the cell wall reconstruction. At 30 min of germination, a set of other sigma factors is activated, including HrdD and the stress responding ECF family sigma factors SigR, SigE, SigD, and SigH. SigR as well as SigH direct cellular responses to osmotic stress (Kormanec et al., 2000; Kelemen et al., 2001; Viollier et al., 2003; Zdanowski et al., 2006; Shu et al., 2009; Kallifidas et al., 2010; Sevcikova et al., 2010). Moreover, the SigR sigma factor, whose regulon comprise DnaK and ClpB chaperones, ensures control over the process of protein re-folding (Kallifidas et al., 2010). SigE possibly takes part in cell envelope reconstruction control, similarly to SigW in the early phase (Paget et al., 1999; Hong et al., 2002). However, the highest increase in its cellular level during germination is exhibited by *S. coelicolor*'s SigQ sigma factor (SCO4908; Bobek et al., 2014), whose regulon is now being studied. Most of the sigma factors mentioned are known to respond to stress conditions. Several members of the stress response apparatus that are involved in the antioxidant defense – superoxide dismutase SodF2 (SCO0999), catalase (SCO0379), and thioredoxins TrxA (SCO3889) and TrxA4 (SCO5419) – were also shown to be expressed soon after spore hydration in *S. coelicolor* (Strakova et al., 2013a). The detoxification system thus reflects the increased metabolic activity. Based on the fact that the stress responding proteins and their regulators (sigma factors) are highly active during germination, it could be proposed that germination itself evokes stress-like conditions, due to the entry of water, oxygen radicals, and salts into the reviving spores.

The ATP level increases approximately 11-fold during germination (Hirsch and Ensign, 1978). Its production is ensured by ATP synthase, whose expression is abolished in the *crp*[−] mutant strain (see below). ATP is essential not only as an energy source for the basal metabolism (Eaton and Ensign, 1980) but also for cyclic AMP (cAMP) synthesis (Piette et al., 2005). The cAMP is a signal molecule which accumulates during germination and is bound by the cAMP-receptor protein Crp, an important transcription regulator (Susstrunk et al., 1998; Derouaux et al., 2004). Both *Streptomyces* mutant strains in which either *cya* (a gene encoding adenylate cyclase that catalyzes conversion of ATP to cAMP) or the *crp* gene were deleted exhibited a similar,

dramatic defect in germination. The germination defect caused by the missing or inactive Crp system can be explained by the subsequent absence of several members of the affected Crp regulon that play a crucial role in germination. Other than ATP synthase, the Crp regulon encompasses the cell wall hydrolases and chaperones (Piette et al., 2005). Piette et al. (2005) described morphological differences between spores of *S. coelicolor* wild type and its *crp*[−] mutant strains. The spore wall of the *crp*[−] strain was twice as thick as that of the wild type strain. This can be related to the suppressed expression of another cell wall hydrolase, SCO5466, in the *crp*[−] strain during germination. Besides SCO5466, the expression of the above mentioned RpfA hydrolase is also under regulation of Crp (St-Onge et al., 2015). One may assume that the Cya-cAMP-Crp system might control the muralytic activity of hydrated spores, among other processes, allowing for cell wall reconstruction; an indispensable procedure for successful germination. A differential protein expression analysis between the wild type and *crp*[−] strains, provided by the same authors, revealed decreased expression of protein chaperones GroEL1, GroEL2, DnaK that could have a negative effect on protein folding and thus negatively affect the germination in the *crp*[−] strain. The crucial role played by the Cya-cAMP-Crp system in germination may however rely on the aforementioned trehalose hydrolysis control.

SECONDARY METABOLISM OF GERMINATING SPORES

In natural soil environments, germination of spores and seeds from different organisms is affected by a plethora of external factors. These include population density of organisms of the same species, the presence of rival organisms, and respective intra- or inter-species communication. In laboratory conditions, physiological differences, including inhibition of development or degradation of signaling compounds, were observed when *Streptomyces* had been cultivated together with *B. subtilis* or with bacteria containing mycolic acids in their cell walls (Onaka et al., 2011; Traxler et al., 2013).

Germinating spores produce signals that play a role in their own communication framework. The production of an unknown activator that would induce germination under optimal conditions can be expected based on an experiment in which monocultural spores of *S. venezuelae* germinated significantly faster in higher spore densities or in a medium supplemented by its own, earlier germlings (Xu and Vetsigian, 2017). On the other hand, a similar experiment provided by the same authors revealed a reduction of the germinating spores at higher spore densities in *S. coelicolor*. The existence of germination inhibitors produced by the germlings was firstly shown in *S. viridochromogenes* (Grund and Ensign, 1985) and later also in *S. coelicolor* (Song et al., 2006). These germination inhibitors include germicidins, gramicidine S, and hypnosin (Ensign, 1978; Grund and Ensign, 1985; Setlow, 2003; Aoki et al., 2007, 2011). At least four germicidin homologs are produced by Gcs, a type III polyketide synthase in *S. coelicolor* (Song et al., 2006). The expression of its gene (SCO7221) highly increases at 30 min of germination, as can be found in the whole

genome expression data in Strakova et al. (2013a). The hypnosin, whose genetic substantiality is not clear, is bound to the spore surface and released in wet conditions thus probably preventing premature germination of spore chains on aerial mycelia (Xu and Vetsigian, 2017).

Recent analytical technologies allow more detailed investigations into the production of small molecular compounds. Using high-performance liquid chromatography-mass spectrometry, three different compounds – a sesquiterpenoid antibiotic albaflavone, the polyketide germicidin A, and the chalcone – were detected to be synthesized upon germination in *S. coelicolor*. The two latter compounds revealed an inhibitory effect on the germination process (Čihák et al., submitted). Germicidin A is known as an autoregulatory germination inhibitor of *Streptomyces* and other bacteria (Petersen et al., 1993). The compound is expected to be a widespread interspecies regulator affecting germination of various sporogenic organisms. Chalcones, as well as other flavonoids and phenolic compounds, are important signaling molecules in plant-microbe symbioses, being essential for the plant survival (Maxwell et al., 1989; Diaz-Tielas et al., 2012). Although *Streptomyces* produce flavonoids [e.g., THN and flaviolin by *S. coelicolor* (Zhao et al., 2005)], the only streptomycete chalcone derivative is known in naringerin biosynthesis, a typical plant secondary metabolite produced by *Streptomyces clavuligerus* (Alvarez-Alvarez et al., 2015). The presence of different germination inhibitors in *S. coelicolor* is in accordance with the fact that the germination rate of this strain is much slower and even decreased with a higher spore densities, as mentioned above.

Several streptomycete antibiotics produced during sporulation, such as neomycin in *S. fradiae*, streptomycin in *S. griseus* (Barabas and Szabo, 1968), or actinorhodin in *S. coelicolor* (Čihák et al., submitted) are known to be bound on the spore envelopes and released into the environment during germination. These antibiotics protect the germinating spores against environmental challenges before the internal biosynthetic pathways are re-activated. Some antibiotics, such as cephamycin C and clavulanic acid both synthesized by *S. clavuligerus* are known to be produced soon after germination (Sanchez and Brana, 1996).

PERSPECTIVES

Spore germination in *Streptomyces* represents an exceptional study model of bacterial cell differentiation that presents a complete transformation of cellular morphology and the restoration of all physiological processes. More detailed knowledge about the structure of dormant spores may provide clues for understanding their readiness to trigger metabolic activity and cell reconstitution.

An interesting area that deserves our attention is the probability of germination and germination control. As discussed in this review, the cell awakening is launched in an aquatic milieu; the probability of awakening differs, possibly depending on the accessibility to nutrients and on other biotic and abiotic factors.

Stochastic germination seems to be a widespread strategy of spore-forming organisms that has evolved to ensure the survival of whole populations. From the one-cell perspective, spores represent a safe but non-reproductive state, whereas germination is a risky and irreversible process. From the point of view of the whole population, early germinating pioneers take advantage by occupying vacant niches whereas a hesitant strategy is preferable when conditions become harsh. Therefore, one may assume that the onset of germination is subject to various controlling mechanisms that respond to external signals and activate or suppress the process as is needed. The characterization of these signals and their sensors has not been established to date. The transferred signals are eventually reflected in complete cell reconstruction. This requires the activity of specific genes whose expression is directed by a unique set of transcriptional factors. Characterizing these factors and clarifying their regulons would shed more light on the process by which dormant spores are awakened.

REFERENCES

- Alvarez-Alvarez, R., Botas, A., Albillos, S. M., Rumero, A., Martin, J. F., and Liras, P. (2015). Molecular genetics of naringenin biosynthesis, a typical plant secondary metabolite produced by *Streptomyces clavuligerus*. *Microb. Cell Fact.* 14, 178. doi: 10.1186/s12934-015-0373-7
- An, T. Z., Iwakiri, M., Edashige, K., Sakurai, T., and Kasai, M. (2000). Factors affecting the survival of frozen-thawed mouse spermatozoa. *Cryobiology* 40, 237–249. doi: 10.1006/cryo.2000.2245
- Aoki, Y., Matsumoto, D., Kawaide, H., and Natsume, M. (2011). Physiological role of germicidins in spore germination and hyphal elongation in *Streptomyces coelicolor* A3(2). *J. Antibiot.* 64, 607–611. doi: 10.1038/ja.2011.59
- Aoki, Y., Yoshida, M., Kawaide, H., Abe, H., and Natsume, M. (2007). Isolation and characterization of a spore germination inhibitor from *Streptomyces* sp. CB-1-1, a phytopathogen causing root tumor of melon. *Biosci. Biotechnol. Biochem.* 71, 986–992. doi: 10.1271/bbb.60649
- Ausmees, N., Wahlstedt, H., Bagchi, S., Elliot, M. A., Buttner, M. J., and Flardh, K. (2007). SmeA, a small membrane protein with multiple functions in *Streptomyces* sporulation including targeting of a SpoIIIE/FtsK-like protein to cell division septa. *Mol. Microbiol.* 65, 1458–1473. doi: 10.1111/j.1365-2958.2007.05877.x
- Bagchi, S., Tomenius, H., Belova, L. M., and Ausmees, N. (2008). Intermediate filament-like proteins in bacteria and a cytoskeletal function in *Streptomyces*. *Mol. Microbiol.* 70, 1037–1050. doi: 10.1111/j.1365-2958.2008.06473.x
- Balaban, N. Q., Merrin, J., Chait, R., Kowalik, L., and Leibler, S. (2004). Bacterial persistence as a phenotypic switch. *Science* 305, 1622–1625. doi: 10.1126/science.1099390
- Barabas, G., and Szabo, G. (1968). Role of streptomycin in the life of *Streptomyces griseus*: streptidine-containing fractions in the cell walls of *Streptomyces griseus* strains. *Can. J. Microbiol.* 14, 1325–1331. doi: 10.1139/m68-222
- Benaroudj, N., Lee, D. H., and Goldberg, A. L. (2001). Trehalose accumulation during cellular stress protects cells and cellular proteins from damage by oxygen radicals. *J. Biol. Chem.* 276, 24261–24267. doi: 10.1074/jbc.M101487200
- Bentley, S. D., Chater, K. F., Cerdeno-Tarraga, A. M., Challis, G. L., Thomson, N. R., James, K. D., et al. (2002). Complete genome sequence of the model actinomycete *Streptomyces coelicolor* A3(2). *Nature* 417, 141–147. doi: 10.1038/417141a
- Bobek, J., Halada, P., Angelis, J., Vohradsky, J., and Mikulik, K. (2004). Activation and expression of proteins during synchronous germination of aerial spores of *Streptomyces granaticolor*. *Proteomics* 4, 3864–3880. doi: 10.1002/pmic.200400818
- Bobek, J., Strakova, E., Zikova, A., and Vohradsky, J. (2014). Changes in activity of metabolic and regulatory pathways during germination of *S. coelicolor*. *BMC Genomics* 15:1173. doi: 10.1186/1471-2164-15-1173

AUTHOR CONTRIBUTIONS

JB wrote the whole manuscript, MČ analyzed the knowledge about metabolic activities of germinating spores, KŠ analyzed the knowledge about transcriptional activities of germinating spores.

ACKNOWLEDGMENTS

The authors are very grateful to Dr. Oldrich Benada and to Dr. Olga Kofronova for electron microscopic pictures of germinating spores. This work was supported by a project of Charles University in Prague: Progress Q26/LF1 to JB, SVV260369 to KŠ, a grant of the Grant Agency of the Charles University (www.cuni.cz/UK-33.html) under contract no. 160214 to KŠ, a project of J. E. Purkinje University: UJEP-SGS-173-07-01 to JB, and by the Czech research infrastructure for systems biology C4SYS (project no. LM2015055) to JB.

- Briza, P., Breitenbach, M., Ellinger, A., and Segall, J. (1990). Isolation of two developmentally regulated genes involved in spore wall maturation in *Saccharomyces cerevisiae*. *Genes Dev.* 4, 1775–1789. doi: 10.1101/gad.4.10.1775
- Buerger, S., Spoering, A., Gavrish, E., Leslin, C., Ling, L., and Epstein, S. S. (2012). Microbial scout hypothesis, stochastic exit from dormancy, and the nature of slow growers. *Appl. Environ. Microbiol.* 78, 3221–3228. doi: 10.1128/AEM.07307-11
- Bush, M. J., Tschowri, N., Schlimpert, S., Flardh, K., and Buttner, M. J. (2015). c-di-GMP signalling and the regulation of developmental transitions in streptomycetes. *Nat. Rev. Microbiol.* 13, 749–760. doi: 10.1038/nrmicro3546
- Ceccarini, C. (1967). The biochemical relationship between trehalase and trehalose during growth and differentiation in the cellular slime mold, *Dictyostelium discoideum*. *Biochim. Biophys. Acta* 148, 114–124. doi: 10.1016/0304-4165(67)90285-1
- Chen, D., Huang, S. S., and Li, Y. Q. (2006). Real-time detection of kinetic germination and heterogeneity of single *Bacillus* spores by laser tweezers Raman spectroscopy. *Anal. Chem.* 78, 6936–6941. doi: 10.1021/ac061090e
- Chen, K. C., Csikasz-Nagy, A., Györfy, B., Val, J., Novak, B., and Tyson, J. J. (2000). Kinetic analysis of a molecular model of the budding yeast cell cycle. *Mol. Biol. Cell* 11, 369–391. doi: 10.1091/mbc.11.1.369
- Claessen, D., de Jong, W., Dijkhuizen, L., and Wosten, H. A. (2006). Regulation of *Streptomyces* development: reach for the sky! *Trends Microbiol.* 14, 313–319. doi: 10.1016/j.tim.2006.05.008
- Claessen, D., Rink, R., de Jong, W., Siebring, J., de Vreugd, P., Boersma, F. G., et al. (2003). A novel class of secreted hydrophobic proteins is involved in aerial hyphae formation in *Streptomyces coelicolor* by forming amyloid-like fibrils. *Genes Dev.* 17, 1714–1726. doi: 10.1101/gad.264303
- Claessen, D., Stokroos, I., Deelstra, H. J., Penninga, N. A., Bormann, C., Salas, J. A., et al. (2004). The formation of the rodlet layer of streptomycetes is the result of the interplay between rodlines and chaplins. *Mol. Microbiol.* 53, 433–443. doi: 10.1111/j.1365-2958.2004.04143.x
- Claessen, D., Wosten, H. A., van Keulen, G., Faber, O. G., Alves, A. M., Meijer, W. G., et al. (2002). Two novel homologous proteins of *Streptomyces coelicolor* and *Streptomyces lividans* are involved in the formation of the rodlet layer and mediate attachment to a hydrophobic surface. *Mol. Microbiol.* 44, 1483–1492. doi: 10.1046/j.1365-2958.2002.02980.x
- Cohen-Gonsaud, M., Keep, N. H., Davies, A. P., Ward, J., Henderson, B., and Labesse, G. (2004). Resuscitation-promoting factors possess a lysozyme-like domain. *Trends Biochem. Sci.* 29, 7–10. doi: 10.1016/j.tibs.2003.10.009
- Constant, P., Poissant, L., and Villemur, R. (2008). Isolation of *Streptomyces* sp. PCB7, the first microorganism demonstrating high-affinity uptake of tropospheric H₂. *ISME J.* 2, 1066–1076. doi: 10.1038/ismej.2008.59
- Cowan, A. E., Koppel, D. E., Setlow, B., and Setlow, P. (2003). A soluble protein is immobile in dormant spores of *Bacillus subtilis* but is mobile in germinated

- spores: implications for spore dormancy. *Proc. Natl. Acad. Sci. U.S.A.* 100, 4209–4214. doi: 10.1073/pnas.0636762100
- Crowe, J. H., Crowe, L. M., and Chapman, D. (1984). Preservation of membranes in anhydrobiotic organisms: the role of trehalose. *Science* 223, 701–703. doi: 10.1126/science.223.4637.701
- de Jong, W., Manteca, A., Sanchez, J., Bucca, G., Smith, C. P., Dijkhuizen, L., et al. (2009). NepA is a structural cell wall protein involved in maintenance of spore dormancy in *Streptomyces coelicolor*. *Mol. Microbiol.* 71, 1591–1603. doi: 10.1111/j.1365-2958.2009.06633.x
- De Virgilio, C., Hottiger, T., Dominguez, J., Boller, T., and Wiemken, A. (1994). The role of trehalose synthesis for the acquisition of thermotolerance in yeast. I. Genetic evidence that trehalose is a thermoprotectant. *Eur. J. Biochem.* 219, 179–186. doi: 10.1111/j.1432-1033.1994.tb19928.x
- Derouaux, A., Halici, S., Nofthart, H., Neutelings, T., Moutzourelis, G., Dusart, J., et al. (2004). Deletion of a cyclic AMP receptor protein homologue diminishes germination and affects morphological development of *Streptomyces coelicolor*. *J. Bacteriol.* 186, 1893–1897. doi: 10.1128/JB.186.6.1893-1897.2004
- Diaz-Tielas, C., Grana, E., Reigosa, M. J., and Sanchez-Moreiras, A. M. (2012). The role of peroxidases on the mode of action of chalcone in *Arabidopsis* roots. *Plant Signal. Behav.* 7, 1274–1276. doi: 10.4161/psb.21594
- Ditkowski, B., Holmes, N., Rydzak, J., Donczew, M., Bezulska, M., Ginda, K., et al. (2013). Dynamic interplay of ParA with the polarity protein, Scy, coordinates the growth with chromosome segregation in *Streptomyces coelicolor*. *Open Biol.* 3:130006. doi: 10.1098/rsob.130006
- Eaton, D., and Ensign, J. C. (1980). *Streptomyces viridochromogenes* spore germination initiated by calcium ions. *J. Bacteriol.* 143, 377–382.
- Elbein, A. D. (1974). The metabolism of alpha, alpha-trehalose. *Adv. Carbohydr. Chem. Biochem.* 30, 227–256. doi: 10.1016/S0065-2318(08)60266-8
- Elbein, A. D., and Mitchell, M. (1973). Levels of glycogen and trehalose in *Mycobacterium smegmatis* and the purification and properties of the glycogen synthetase. *J. Bacteriol.* 113, 863–873.
- Elbein, A. D., Pan, Y. T., Pastuszak, I., and Carroll, D. (2003). New insights on trehalose: a multifunctional molecule. *Glycobiology* 13, 17R–27R. doi: 10.1093/glycob/cwg047
- Elliot, M. A., Karoonuthaisiri, N., Huang, J., Bibb, M. J., Cohen, S. N., Kao, C. M., et al. (2003). The chaplins: a family of hydrophobic cell-surface proteins involved in aerial mycelium formation in *Streptomyces coelicolor*. *Genes Dev.* 17, 1727–1740. doi: 10.1101/gad.264403
- Elliot, M. A., and Talbot, N. J. (2004). Building filaments in the air: aerial morphogenesis in bacteria and fungi. *Curr. Opin. Microbiol.* 7, 594–601. doi: 10.1016/j.mib.2004.10.013
- Ensign, J. C. (1978). Formation, properties, and germination of actinomycete spores. *Annu. Rev. Microbiol.* 32, 185–219. doi: 10.1146/annurev.mi.32.100178.001153
- Epstein, S. S. (2009). Microbial awakenings. *Nature* 457:1083. doi: 10.1038/4571083a
- Fillinger, S., Chaveroche, M. K., van Dijk, P., de Vries, R., Ruijter, G., Thevelein, J., et al. (2001). Trehalose is required for the acquisition of tolerance to a variety of stresses in the filamentous fungus *Aspergillus nidulans*. *Microbiology* 147(Pt 7), 1851–1862. doi: 10.1099/00221287-147-7-1851
- Flardh, K. (2003a). Essential role of DivIVA in polar growth and morphogenesis in *Streptomyces coelicolor* A3(2). *Mol. Microbiol.* 49, 1523–1536. doi: 10.1046/j.1365-2958.2003.03660.x
- Flardh, K. (2003b). Growth polarity and cell division in *Streptomyces*. *Curr. Opin. Microbiol.* 6, 564–571. doi: 10.1016/j.mib.2003.10.011
- Flardh, K., and Buttner, M. J. (2009). *Streptomyces* morphogenetics: dissecting differentiation in a filamentous bacterium. *Nat. Rev. Microbiol.* 7, 36–49. doi: 10.1038/nrmicro1968
- Flardh, K., Richards, D. M., Hempel, A. M., Howard, M., and Buttner, M. J. (2012). Regulation of apical growth and hyphal branching in *Streptomyces*. *Curr. Opin. Microbiol.* 15, 737–743. doi: 10.1016/j.mib.2012.10.012
- Foster, J. W., Mc, D. L., Woodruff H.B., Stokes, J. L. (1945). Microbiological aspects of penicillin; conidiospore formation in submerged cultures of *Penicillium notatum*. *J. Bacteriol.* 50, 365–368.
- Galperin, M. Y., Mekhedov, S. L., Puigbo, P., Smirnov, S., Wolf, Y. I., and Rigden, D. J. (2012). Genomic determinants of sporulation in *Bacilli* and *Clostridia*: towards the minimal set of sporulation-specific genes. *Environ. Microbiol.* 14, 2870–2890. doi: 10.1111/j.1462-2920.2012.02841.x
- Ghorbel, S., Smirnov, A., Chouayekh, H., Sperandio, B., Esnault, C., Kormanec, J., et al. (2006). Regulation of ppk expression and in vivo function of Ppk in *Streptomyces lividans* TK24. *J. Bacteriol.* 188, 6269–6276. doi: 10.1128/JB.00202-06
- Glauert, A. M., and Hopwood, D. A. (1961). The fine structure of *Streptomyces violaceoruber* (S. *coelicolor*). III. The walls of the mycelium and spores. *J. Biophys. Biochem. Cytol.* 10, 505–516. doi: 10.1083/jcb.10.4.505
- Grantcharova, N., Lustig, U., and Flardh, K. (2005). Dynamics of FtsZ assembly during sporulation in *Streptomyces coelicolor* A3(2). *J. Bacteriol.* 187, 3227–3237. doi: 10.1128/JB.187.9.3227-3237.2005
- Grund, A. D., and Ensign, J. C. (1985). Properties of the germination inhibitor of *Streptomyces viridochromogenes* spores. *J. Gen. Microbiol.* 131, 833–847. doi: 10.1099/00221287-131-4-833
- Haider, H. J., Yousef, M. R., and Elliot, M. A. (2009). Cell wall hydrolases affect germination, vegetative growth, and sporulation in *Streptomyces coelicolor*. *J. Bacteriol.* 191, 6501–6512. doi: 10.1128/JB.00767-09
- Hardisson, C., Manzanal, M. B., Salas, J. A., and Suarez, J. E. (1978). Fine structure, physiology and biochemistry of arthrospore germination in *Streptomyces antibioticus*. *J. Gen. Microbiol.* 105, 203–214. doi: 10.1099/00221287-105-2-203
- Heichlinger, A., Ammelburg, M., Kleinschnitz, E. M., Latus, A., Maldener, I., Flardh, K., et al. (2011). The MreB-like protein Mbl of *Streptomyces coelicolor* A3(2) depends on MreB for proper localization and contributes to spore wall synthesis. *J. Bacteriol.* 193, 1533–1542. doi: 10.1128/JB.01100-10
- Helmann, J. D. (2006). Deciphering a complex genetic regulatory network: the *Bacillus subtilis* sigmaW protein and intrinsic resistance to antimicrobial compounds. *Sci. Prog.* 89(Pt 3–4), 243–266. doi: 10.3184/003685006783238290
- Hempel, A. M., Cantlay, S., Molle, V., Wang, S. B., Naldrett, M. J., Parker, J. L., et al. (2012). The Ser/Thr protein kinase AfsK regulates polar growth and hyphal branching in the filamentous bacteria *Streptomyces*. *Proc. Natl. Acad. Sci. U.S.A.* 109, E2371–E2379. doi: 10.1073/pnas.1207409109
- Henriques, A. O., and Moran, C. P. Jr. (2007). Structure, assembly, and function of the spore surface layers. *Annu. Rev. Microbiol.* 61, 555–588. doi: 10.1146/annurev.micro.61.080706.093224
- Hett, E. C., Chao, M. C., Deng, L. L., and Rubin, E. J. (2008). A mycobacterial enzyme essential for cell division synergizes with resuscitation-promoting factor. *PLOS Pathog.* 4:e1000001. doi: 10.1371/journal.ppat.1000001
- Hey-Ferguson, A., Mitchell, M., and Elbein, A. D. (1973). Trehalose metabolism in germinating spores of *Streptomyces hygroscopicus*. *J. Bacteriol.* 116, 1084–1085.
- Hirsch, C. F., and Ensign, J. C. (1976a). Heat activation of *Streptomyces viridochromogenes* spores. *J. Bacteriol.* 126, 24–30.
- Hirsch, C. F., and Ensign, J. C. (1976b). Nutritionally defined conditions for germination of *Streptomyces viridochromogenes* spores. *J. Bacteriol.* 126, 13–23.
- Hirsch, C. F., and Ensign, J. C. (1978). Some properties of *Streptomyces viridochromogenes* spores. *J. Bacteriol.* 134, 1056–1063.
- Hong, H. J., Paget, M. S., and Buttner, M. J. (2002). A signal transduction system in *Streptomyces coelicolor* that activates the expression of a putative cell wall glycan operon in response to vancomycin and other cell wall-specific antibiotics. *Mol. Microbiol.* 44, 1199–1211. doi: 10.1046/j.1365-2958.2002.02960.x
- Hottiger, T., Boller, T., and Wiemken, A. (1989). Correlation of trehalose content and heat resistance in yeast mutants altered in the RAS/adenylate cyclase pathway: is trehalose a thermoprotectant? *FEBS Lett.* 255, 431–434. doi: 10.1016/0014-5793(89)81139-1
- Jain, N. K., and Roy, I. (2010). Trehalose and protein stability. *Curr. Protoc. Protein Sci.* 59, 4.9.1–4.9.12. doi: 10.1002/0471140864.ps0409s59
- Jakimowicz, D., and van Wezel, G. P. (2012). Cell division and DNA segregation in *Streptomyces*: how to build a septum in the middle of nowhere? *Mol. Microbiol.* 85, 393–404. doi: 10.1111/j.1365-2958.2012.08107.x
- Jang, M. S., Mouri, Y., Uchida, K., Aizawa, S., Hayakawa, M., Fujita, N., et al. (2016). Genetic and transcriptional analyses of the flagellar gene cluster in *Actinoplanes missouriensis*. *J. Bacteriol.* 198, 2219–2227. doi: 10.1128/JB.00306-16
- Jyothikumar, V., Tilley, E. J., Wali, R., and Herron, P. R. (2008). Time-lapse microscopy of *Streptomyces coelicolor* growth and sporulation. *Appl. Environ. Microbiol.* 74, 6774–6781. doi: 10.1128/AEM.01233-08
- Kalakoutsii, L. V., and Agre, N. S. (1976). Comparative aspects of development and differentiation in actinomycetes. *Bacteriol. Rev.* 40, 469–524.
- Kallifidas, D., Thomas, D., Doughty, P., and Paget, M. S. (2010). The sigmaR regulon of *Streptomyces coelicolor* A32 reveals a key role in protein

- quality control during disulphide stress. *Microbiology* 156(Pt 6), 1661–1672. doi: 10.1099/mic.0.037804-0
- Kandror, O., DeLeon, A., and Goldberg, A. L. (2002). Trehalose synthesis is induced upon exposure of *Escherichia coli* to cold and is essential for viability at low temperatures. *Proc. Natl. Acad. Sci. U.S.A.* 99, 9727–9732. doi: 10.1073/pnas.142314099
- Keep, N. H., Ward, J. M., Robertson, G., Cohen-Gonsaud, M., and Henderson, B. (2006). Bacterial resuscitation factors: revival of viable but non-culturable bacteria. *Cell Mol. Life Sci.* 63, 2555–2559. doi: 10.1007/s00018-006-6188-2
- Keijser, B. J., Noens, E. E., Kraal, B., Koerten, H. K., and van Wezel, G. P. (2003). The *Streptomyces coelicolor* ssgB gene is required for early stages of sporulation. *FEMS Microbiol. Lett.* 225, 59–67. doi: 10.1016/S0378-1097(03)00481-6
- Kelemen, G. H. (2017). Intermediate filaments supporting cell shape and growth in bacteria. *Subcell. Biochem.* 84, 161–211. doi: 10.1007/978-3-319-53047-5_6
- Kelemen, G. H., Brian, P., Flardh, K., Chamberlin, L., Chater, K. F., and Buttner, M. J. (1998). Developmental regulation of transcription of whiE, a locus specifying the polyketide spore pigment in *Streptomyces coelicolor* A3 (2). *J. Bacteriol.* 180, 2515–2521.
- Kelemen, G. H., Viollier, P. H., Tenor, J., Marri, L., Buttner, M. J., and Thompson, C. J. (2001). A connection between stress and development in the multicellular prokaryote *Streptomyces coelicolor* A3(2). *Mol. Microbiol.* 40, 804–814. doi: 10.1046/j.1365-2958.2001.02417.x
- Kleinschmitt, E. M., Heichlinger, A., Schirner, K., Winkler, J., Latus, A., Maldener, I., et al. (2011). Proteins encoded by the mre gene cluster in *Streptomyces coelicolor* A3(2) cooperate in spore wall synthesis. *Mol. Microbiol.* 79, 1367–1379. doi: 10.1111/j.1365-2958.2010.07529.x
- Kormanec, J., Sevcikova, B., Halgasova, N., Knirschova, R., and Rezuchova, B. (2000). Identification and transcriptional characterization of the gene encoding the stress-response sigma factor sigma(H) in *Streptomyces coelicolor* A3(2). *FEMS Microbiol. Lett.* 189, 31–38.
- Lederer, E. (1976). Cord factor and related trehalose esters. *Chem. Phys. Lipids* 16, 91–106. doi: 10.1016/0009-3084(76)90001-3
- Liot, Q., and Constant, P. (2016). Breathing air to save energy—new insights into the ecophysiological role of high-affinity [NiFe]-hydrogenase in *Streptomyces avermitilis*. *Microbiol. Open* 5, 47–59. doi: 10.1002/mbo3.310
- Ma, M., Rateb, M. E., Yang, D., Rudolf, J. D., Zhu, X., Huang, Y., et al. (2017). Germicidins H-J from *Streptomyces* sp. CB00361. *J. Antibiot. (Tokyo)* 70, 200–203. doi: 10.1038/ja.2016.100
- Martin, M. C., Diaz, L. A., Manzanal, M. B., and Hardisson, C. (1986). Role of trehalose in the spores of *Streptomyces*. *FEMS Microbiol. Lett.* 35, 49–54. doi: 10.1016/0378-1097(86)90160-6
- Maxwell, C. A., Hartwig, U. A., Joseph, C. M., and Phillips, D. A. (1989). A chalcone and two related flavonoids released from alfalfa roots induce nod genes of *Rhizobium meliloti*. *Plant Physiol.* 91, 842–847. doi: 10.1104/pp.91.3.842
- Mazza, P., Noens, E. E., Schirner, K., Grantcharova, N., Mommaas, A. M., Koerten, H. K., et al. (2006). MreB of *Streptomyces coelicolor* is not essential for vegetative growth but is required for the integrity of aerial hyphae and spores. *Mol. Microbiol.* 60, 838–852. doi: 10.1111/j.1365-2958.2006.05134.x
- McBride, M. J., and Ensign, J. C. (1987a). Effects of intracellular trehalose content on *Streptomyces griseus* spores. *J. Bacteriol.* 169, 4995–5001. doi: 10.1128/jb.169.11.4995-5001.1987
- McBride, M. J., and Ensign, J. C. (1987b). Metabolism of endogenous trehalose by *Streptomyces griseus* spores and by spores or cells of other actinomycetes. *J. Bacteriol.* 169, 5002–5007. doi: 10.1128/jb.169.11.5002-5007.1987
- McBride, M. J., and Ensign, J. C. (1990). Regulation of trehalose metabolism by *Streptomyces griseus* spores. *J. Bacteriol.* 172, 3637–3643. doi: 10.1128/jb.172.7.3637-3643.1990
- McBride, M. J., and Zusman, D. R. (1989). Trehalose accumulation in vegetative cells and spores of *Myxococcus xanthus*. *J. Bacteriol.* 171, 6383–6386. doi: 10.1128/jb.171.11.6383-6386.1989
- Miguel, E. M., Martin, C., Hardisson, C., and Manzanal, M. B. (1993). Synchronous germination of *Streptomyces antibioticus* spores: tool for the analysis of hyphal growth in liquid cultures. *FEMS Microbiol. Lett.* 109, 123–129. doi: 10.1111/j.1574-6968.1993.tb06156.x
- Mikulik, K., Bobek, J., Bezouskova, S., Benada, O., and Kofronova, O. (2002). Expression of proteins and protein kinase activity during germination of aerial spores of *Streptomyces granaticolor*. *Biochem. Biophys. Res. Commun.* 299, 335–342. doi: 10.1016/S0006-291X(02)02606-2
- Mikulik, K., Bobek, J., Zikova, A., Smetakova, M., and Bezouskova, S. (2011). Phosphorylation of ribosomal proteins influences subunit association and translation of poly (U) in *Streptomyces coelicolor*. *Mol. Biosyst.* 7, 817–823. doi: 10.1039/c0mb00174k
- Mikulik, K., Janda, I., Maskova, H., Stastna, J., and Jiranova, A. (1977). Macromolecular synthesis accompanying the transition from spores to vegetative forms of *Streptomyces granaticolor*. *Folia Microbiol.* 22, 252–261. doi: 10.1007/BF02877654
- Mikulik, K., Janda, I., Weiser, J., Stastna, J., and Jiranova, A. (1984). RNA and ribosomal protein patterns during aerial spore germination in *Streptomyces granaticolor*. *Eur. J. Biochem.* 145, 381–388. doi: 10.1111/j.1432-1033.1984.tb08565.x
- Mikulik, K., Paleckova, P., Felsberg, J., Bobek, J., Zidkova, J., and Halada, P. (2008). SsrA genes of streptomycetes and association of proteins to the tmRNA during development and cellular differentiation. *Proteomics* 8, 1429–1441. doi: 10.1002/pmic.200700560
- Mukamolova, G. V., Kaprelyants, A. S., Young, D. I., Young, M., and Kell, D. B. (1998a). A bacterial cytokine. *Proc. Natl. Acad. Sci. U.S.A.* 95, 8916–8921. doi: 10.1073/pnas.95.15.8916
- Mukamolova, G. V., Yanopolskaya, N. D., Kell, D. B., and Kaprelyants, A. S. (1998b). On resuscitation from the dormant state of *Micrococcus luteus*. *Antonie Van Leeuwenhoek* 73, 237–243. doi: 10.1023/A:1000881918216
- Mukamolova, G. V., Murzin, A. G., Salina, E. G., Demina, G. R., Kell, D. B., Kaprelyants, A. S., et al. (2006). Muralytic activity of *Micrococcus luteus* Rpf and its relationship to physiological activity in promoting bacterial growth and resuscitation. *Mol. Microbiol.* 59, 84–98. doi: 10.1111/j.1365-2958.2005.04930.x
- Mukamolova, G. V., Turapov, O. A., Kazarian, K., Telkov, M., Kaprelyants, A. S., Kell, D. B., et al. (2002). The rpf gene of *Micrococcus luteus* encodes an essential secreted growth factor. *Mol. Microbiol.* 46, 611–621. doi: 10.1046/j.1365-2958.2002.03183.x
- Neiman, A. M. (2005). Ascospore formation in the yeast *Saccharomyces cerevisiae*. *Microbiol. Mol. Biol. Rev.* 69, 565–584. doi: 10.1128/MMBR.69.4.565-584.2005
- Noens, E. E., Mersinias, V., Traag, B. A., Smith, C. P., Koerten, H. K., and van Wezel, G. P. (2005). SsgA-like proteins determine the fate of peptidoglycan during sporulation of *Streptomyces coelicolor*. *Mol. Microbiol.* 58, 929–944. doi: 10.1111/j.1365-2958.2005.04883.x
- Noens, E. E., Mersinias, V., Willemsse, J., Traag, B. A., Laing, E., Chater, K. F., et al. (2007). Loss of the controlled localization of growth stage-specific cell-wall synthesis pleiotropically affects developmental gene expression in an ssgA mutant of *Streptomyces coelicolor*. *Mol. Microbiol.* 64, 1244–1259. doi: 10.1111/j.1365-2958.2007.05732.x
- Nwaka, S., and Holzer, H. (1998). Molecular biology of trehalose and the trehalases in the yeast *Saccharomyces cerevisiae*. *Prog. Nucleic Acid Res. Mol. Biol.* 58, 197–237. doi: 10.1016/S0079-6603(08)60037-9
- Onaka, H., Mori, Y., Igarashi, Y., and Furumai, T. (2011). Mycolic acid-containing bacteria induce natural-product biosynthesis in *Streptomyces* species. *Appl. Environ. Microbiol.* 77, 400–406. doi: 10.1128/AEM.01337-10
- Paget, M. S., Chamberlin, L., Atrih, A., Foster, S. J., and Buttner, M. J. (1999). Evidence that the extracytoplasmic function sigma factor sigmaE is required for normal cell wall structure in *Streptomyces coelicolor* A3(2). *J. Bacteriol.* 181, 204–211.
- Paidhungat, M., and Setlow, P. (2000). Role of ger proteins in nutrient and nonnutrient triggering of spore germination in *Bacillus subtilis*. *J. Bacteriol.* 182, 2513–2519. doi: 10.1128/JB.182.9.2513-2519.2000
- Paleckova, P., Bobek, J., Felsberg, J., and Mikulik, K. (2006). Activity of translation system and abundance of tmRNA during development of *Streptomyces aureofaciens* producing tetracycline. *Folia Microbiol.* 51, 517–524. doi: 10.1007/BF02931615
- Palleroni, N. J. (1976). Chemotaxis in *Actinoplanes*. *Arch. Microbiol.* 110, 13–18. doi: 10.1007/BF00416963
- Pammer, M., Briza, P., Ellinger, A., Schuster, T., Stucka, R., Feldmann, H., et al. (1992). *DIT101 (CSD2, CAL1)*, a cell cycle-regulated yeast gene required for synthesis of chitin in cell walls and chitosan in spore walls. *Yeast* 8, 1089–1099. doi: 10.1002/yea.320081211

- Paredes-Sabja, D., Setlow, P., and Sarker, M. R. (2011). Germination of spores of *Bacillales* and *Clostridiales* species: mechanisms and proteins involved. *Trends Microbiol.* 19, 85–94. doi: 10.1016/j.tim.2010.10.004
- Petersen, F., Zahner, H., Metzger, J. W., Freund, S., and Hummel, R. P. (1993). Germicidin, an autoregulative germination inhibitor of *Streptomyces viridochromogenes* NRRL B-1551. *J. Antibiot.* 46, 1126–1138. doi: 10.7164/antibiotics.46.1126
- Piette, A., Derouaux, A., Gerkens, P., Noens, E. E., Mazzucchielli, G., Vion, S., et al. (2005). From dormant to germinating spores of *Streptomyces coelicolor* A3(2): new perspectives from the crp null mutant. *J. Proteome Res.* 4, 1699–1708. doi: 10.1021/pr050155b
- Ranade, N., and Vining, L. C. (1993). Accumulation of intracellular carbon reserves in relation to chloramphenicol biosynthesis by *Streptomyces venezuelae*. *Can. J. Microbiol.* 39, 377–383. doi: 10.1139/m93-055
- Richards, D. M., Hempel, A. M., Flardh, K., Buttner, M. J., and Howard, M. (2012). Mechanistic basis of branch-site selection in filamentous bacteria. *PLOS Comput. Biol.* 8:e1002423. doi: 10.1371/journal.pcbi.1002423
- Roth, R., and Sussman, M. (1966). Trehalose synthesis in the cellular slime mold *Dictyostelium discoideum*. *Biochim. Biophys. Acta* 122, 225–231. doi: 10.1016/0926-6593(66)90064-6
- Ruban-Osmialowska, B., Jakimowicz, D., Smulczyk-Krawczynszyn, A., Chater, K. F., and Zakrzewska-Czerwinski, J. (2006). Replisome localization in vegetative and aerial hyphae of *Streptomyces coelicolor*. *J. Bacteriol.* 188, 7311–7316. doi: 10.1128/JB.00940-06
- Rueda, B., Miguelez, E. M., Hardisson, C., and Manzanal, M. B. (2001). Changes in glycogen and trehalose content of *Streptomyces brasiliensis* hyphae during growth in liquid cultures under sporulating and non-sporulating conditions. *FEMS Microbiol. Lett.* 194, 181–185. doi: 10.1111/j.1574-6968.2001.tb09466.x
- Ruggiero, A., Tizzano, B., Pedone, E., Pedone, C., Wilmanns, M., and Berisio, R. (2009). Crystal structure of the resuscitation-promoting factor (DeltaDUF)RpfB from *M. tuberculosis*. *J. Mol. Biol.* 385, 153–162. doi: 10.1016/j.jmb.2008.10.042
- Salas, J. A., Guijarro, J. A., and Hardisson, C. (1983). High calcium content in *Streptomyces* spores and its release as an early event during spore germination. *J. Bacteriol.* 155, 1316–1323.
- Sanchez, L., and Brana, A. F. (1996). Cell density influences antibiotic biosynthesis in *Streptomyces clavuligerus*. *Microbiology* 142(Pt 5), 1209–1220. doi: 10.1099/13500872-142-5-1209
- Sapir, L., and Harries, D. (2011). Linking trehalose self-association with binary aqueous solution equation of state. *J. Phys. Chem. B* 115, 624–634. doi: 10.1021/jp109780n
- Setlow, B., Atluri, S., Kitchel, R., Koziol-Dube, K., and Setlow, P. (2006). Role of dipicolinic acid in resistance and stability of spores of *Bacillus subtilis* with or without DNA-protective alpha/beta-type small acid-soluble proteins. *J. Bacteriol.* 188, 3740–3747. doi: 10.1128/JB.00212-06
- Setlow, P. (2003). Spore germination. *Curr. Opin. Microbiol.* 6, 550–556. doi: 10.1016/j.mib.2003.10.001
- Setlow, P. (2007). I will survive: DNA protection in bacterial spores. *Trends Microbiol.* 15, 172–180. doi: 10.1016/j.tim.2007.02.004
- Sevcikova, B., and Kormanec, J. (2003). The ssgB gene, encoding a member of the regulon of stress-response sigma factor sigmaH, is essential for aerial mycelium septation in *Streptomyces coelicolor* A3(2). *Arch. Microbiol.* 180, 380–384. doi: 10.1007/s00203-003-0603-y
- Sevcikova, B., Rezuchova, B., Homerova, D., and Kormanec, J. (2010). The anti-sigma factor BldG is involved in activation of the stress response sigma factor sigma(H) in *Streptomyces coelicolor* A3(2). *J. Bacteriol.* 192, 5674–5681. doi: 10.1128/JB.00828-10
- Sexton, D. L., St-Onge, R. J., Haier, H. J., Yousef, M. R., Brady, L., Gao, C., et al. (2015). Resuscitation-promoting factors are cell wall-lytic enzymes with important roles in the germination and growth of *Streptomyces coelicolor*. *J. Bacteriol.* 197, 848–860. doi: 10.1128/JB.02464-14
- Shah, I. M., Laaberki, M. H., Popham, D. L., and Dworkin, J. (2008). A eukaryotic-like Ser/Thr kinase signals bacteria to exit dormancy in response to peptidoglycan fragments. *Cell* 135, 486–496. doi: 10.1016/j.cell.2008.08.039
- Shleeva, M. O., Trutneva, K. A., Demina, G. R., Zinin, A. I., Sorokoumova, G. M., Laptinskaya, P. K., et al. (2017). Free trehalose accumulation in dormant *Mycobacterium smegmatis* cells and its breakdown in early resuscitation phase. *Front. Microbiol.* 8:524. doi: 10.3389/fmicb.2017.00524
- Shu, D., Chen, L., Wang, W., Yu, Z., Ren, C., Zhang, W., et al. (2009). afsQ1-Q2-sigQ is a pleiotropic but conditionally required signal transduction system for both secondary metabolism and morphological development in *Streptomyces coelicolor*. *Appl. Microbiol. Biotechnol.* 81, 1149–1160. doi: 10.1007/s00253-008-1738-1
- Sigle, S., Ladwig, N., Wohlleben, W., and Muth, G. (2015). Synthesis of the spore envelope in the developmental life cycle of *Streptomyces coelicolor*. *Int. J. Med. Microbiol.* 305, 183–189. doi: 10.1016/j.ijmm.2014.12.014
- Singer, M. A., and Lindquist, S. (1998). Multiple effects of trehalose on protein folding in vitro and in vivo. *Mol. Cell* 1, 639–648. doi: 10.1016/S1097-2765(00)80064-7
- Sola-Penna, M., and Meyer-Fernandes, J. R. (1998). Stabilization against thermal inactivation promoted by sugars on enzyme structure and function: why is trehalose more effective than other sugars? *Arch. Biochem. Biophys.* 360, 10–14. doi: 10.1006/abbi.1998.0906
- Song, L., Barona-Gomez, F., Corre, C., Xiang, L., Udawary, D. W., Austin, M. B., et al. (2006). Type III polyketide synthase beta-ketoacyl-ACP starter unit and ethylmalonyl-CoA extender unit selectivity discovered by *Streptomyces coelicolor* genome mining. *J. Am. Chem. Soc.* 128, 14754–14755. doi: 10.1021/ja065247w
- Stastna, J. (1977). A method of rapid wetting and synchronous germination of streptomycete spores. *Folia Microbiol.* 22, 137–138. doi: 10.1007/BF02881639
- St-Onge, R. J., Haier, H. J., Yousef, M. R., Sherwood, E., Tschowri, N., Al-Bassam, M., et al. (2015). Nucleotide second messenger-mediated regulation of a muralytic enzyme in *Streptomyces*. *Mol. Microbiol.* 96, 779–795. doi: 10.1111/mmi.12971
- Strakova, E., Bobek, J., Zikova, A., Rehulka, P., Benada, O., Rehulkova, H., et al. (2013a). Systems insight into the spore germination of *Streptomyces coelicolor*. *J. Proteome Res.* 12, 525–536. doi: 10.1021/pr300980v
- Strakova, E., Bobek, J., Zikova, A., and Vohradsky, J. (2013b). Global features of gene expression on the proteome and transcriptome levels in *S. coelicolor* during germination. *PLOS ONE* 8:e72842. doi: 10.1371/journal.pone.0072842
- Strakova, E., Zikova, A., and Vohradsky, J. (2014). Inference of sigma factor controlled networks by using numerical modeling applied to microarray time series data of the germinating prokaryote. *Nucleic Acids Res.* 42, 748–763. doi: 10.1093/nar/gkt917
- Sturm, A., and Dworkin, J. (2015). Phenotypic diversity as a mechanism to exit cellular dormancy. *Curr. Biol.* 25, 2272–2277. doi: 10.1016/j.cub.2015.07.018
- Sussman, A. S. (1961). The role of trehalose in the activation of dormant ascospores of neurospora. *Q. Rev. Biol.* 36, 109–116. doi: 10.1086/403332
- Sussman, A. S., and Lingappa, B. T. (1959). Role of trehalose in ascospores of neurospora tetrasperma. *Science* 130:1343. doi: 10.1126/science.130.3385.1343
- Susstrunk, U., Pidoux, J., Taubert, S., Ullmann, A., and Thompson, C. J. (1998). Pleiotropic effects of cAMP on germination, antibiotic biosynthesis and morphological development in *Streptomyces coelicolor*. *Mol. Microbiol.* 30, 33–46. doi: 10.1046/j.1365-2958.1998.01033.x
- Telkov, M. V., Demina, G. R., Voloshin, S. A., Salina, E. G., Dudik, T. V., Stekhanova, T. N., et al. (2006). Proteins of the Rpf (resuscitation promoting factor) family are peptidoglycan hydrolases. *Biochemistry* 71, 414–422. doi: 10.1134/S0006297906040092
- Thevelein, J. M. (1984). Regulation of trehalose mobilization in fungi. *Microbiol. Rev.* 48, 42–59.
- Thomas, K. J. III, and Rice, C. V. (2014). Revised model of calcium and magnesium binding to the bacterial cell wall. *Biometals* 27, 1361–1370. doi: 10.1007/s10534-014-9797-5
- Traag, B. A., and van Wezel, G. P. (2008). The SsgA-like proteins in actinomycetes: small proteins up to a big task. *Antonie Van Leeuwenhoek* 94, 85–97. doi: 10.1007/s10482-008-9225-3
- Traxler, M. F., Watrous, J. D., Alexandrov, T., Dorrestein, P. C., and Kolter, R. (2013). Interspecies interactions stimulate diversification of the *Streptomyces coelicolor* secreted metabolome. *mBio* 4:e00459-13. doi: 10.1128/mBio.00459-13
- Trevelyan, W. E., and Harrison, J. S. (1956). Studies on yeast metabolism. 5. The trehalose content of baker's yeast during anaerobic fermentation. *Biochem. J.* 62, 177–183. doi: 10.1042/bj0620177b

- Tschowri, N., Schumacher, M. A., Schlimpert, S., Chinnam, N. B., Findlay, K. C., Brennan, R. G., et al. (2014). Tetrameric c-di-GMP mediates effective transcription factor dimerization to control *Streptomyces* development. *Cell* 158, 1136–1147. doi: 10.1016/j.cell.2014.07.022
- van Vliet, S. (2015). Bacterial dormancy: how to decide when to wake up. *Curr. Biol.* 25, R753–R755. doi: 10.1016/j.cub.2015.07.039
- van Wezel, G. P., van der Meulen, J., Kawamoto, S., Luiten, R. G., Koerten, H. K., and Kraal, B. (2000). *ssgA* is essential for sporulation of *Streptomyces coelicolor* A3(2) and affects hyphal development by stimulating septum formation. *J. Bacteriol.* 182, 5653–5662. doi: 10.1128/JB.182.20.5653-5662.2000
- Viollier, P. H., Weihofen, A., Folcher, M., and Thompson, C. J. (2003). Post-transcriptional regulation of the *Streptomyces coelicolor* stress responsive sigma factor, SigH, involves translational control, proteolytic processing, and an anti-sigma factor homolog. *J. Mol. Biol.* 325, 637–649. doi: 10.1016/S0022-2836(02)01280-9
- Wang, L., Yu, Y., He, X., Zhou, X., Deng, Z., Chater, K. F., et al. (2007). Role of an FtsK-like protein in genetic stability in *Streptomyces coelicolor* A3(2). *J. Bacteriol.* 189, 2310–2318. doi: 10.1128/JB.01660-06
- Wang, S. L., Fan, K. Q., Yang, X., Lin, Z. X., Xu, X. P., and Yang, K. Q. (2008). CabC, an EF-hand calcium-binding protein, is involved in Ca²⁺-mediated regulation of spore germination and aerial hypha formation in *Streptomyces coelicolor*. *J. Bacteriol.* 190, 4061–4068. doi: 10.1128/JB.01954-07
- Wiemken, A. (1990). Trehalose in yeast, stress protectant rather than reserve carbohydrate. *Antonie Van Leeuwenhoek* 58, 209–217. doi: 10.1007/BF00548935
- Wildermuth, H., Wehrli, E., and Horne, R. W. (1971). The surface structure of spores and aerial mycelium in *Streptomyces coelicolor*. *J. Ultrastruct. Res.* 35, 168–180. doi: 10.1016/S0022-5320(71)80149-1
- Willemse, J., Borst, J. W., de Waal, E., Bisseling, T., and van Wezel, G. P. (2011). Positive control of cell division: FtsZ is recruited by SsgB during sporulation of *Streptomyces*. *Genes Dev.* 25, 89–99. doi: 10.1101/gad.600211
- Wolanski, M., Wali, R., Tilley, E., Jakimowicz, D., Zakrzewska-Czerwinska, J., and Herron, P. (2011). Replisome trafficking in growing vegetative hyphae of *Streptomyces coelicolor* A3(2). *J. Bacteriol.* 193, 1273–1275. doi: 10.1128/JB.01326-10
- Wyatt, T. T., Wosten, H. A., and Dijksterhuis, J. (2013). Fungal spores for dispersion in space and time. *Adv. Appl. Microbiol.* 85, 43–91. doi: 10.1016/B978-0-12-407672-3.00002-2
- Xu, Y., and Vetsigian, K. (2017). Phenotypic variability and community interactions of germinating *Streptomyces* spores. *Sci. Rep.* 7, 699. doi: 10.1038/s41598-017-00792-7
- Yoshinaga, K., Yoshioka, H., Kurosaki, H., Hirasawa, M., Uritani, M., and Hasegawa, K. (1997). Protection by trehalose of DNA from radiation damage. *Biosci. Biotechnol. Biochem.* 61, 160–161. doi: 10.1271/bbb.61.160
- Zdanowski, K., Doughty, P., Jakimowicz, P., O'Hara, L., Buttner, M. J., Paget, M. S., et al. (2006). Assignment of the zinc ligands in RsrA, a redox-sensing ZAS protein from *Streptomyces coelicolor*. *Biochemistry* 45, 8294–8300. doi: 10.1021/bi060711v
- Zhao, B., Guengerich, F. P., Bellamine, A., Lamb, D. C., Izumikawa, M., Lei, L., et al. (2005). Binding of two flavin substrate molecules, oxidative coupling, and crystal structure of *Streptomyces coelicolor* A3(2) cytochrome P450 158A2. *J. Biol. Chem.* 280, 11599–11607. doi: 10.1074/jbc.M410933200

Conflict of Interest Statement: The authors declare that the research was conducted in the absence of any commercial or financial relationships that could be construed as a potential conflict of interest.

Copyright © 2017 Bobek, Šmídová and Čihák. This is an open-access article distributed under the terms of the Creative Commons Attribution License (CC BY). The use, distribution or reproduction in other forums is permitted, provided the original author(s) or licensor are credited and that the original publication in this journal is cited, in accordance with accepted academic practice. No use, distribution or reproduction is permitted which does not comply with these terms.



Germination and Growth Analysis of *Streptomyces lividans* at the Single-Cell Level Under Varying Medium Compositions

Joachim Koepff^{††}, Christian Carsten Sachs^{††}, Wolfgang Wiechert^{1,2},
Dietrich Kohlheyer^{1,3}, Katharina Nöh¹, Marco Oldiges^{1,4} and Alexander Grünberger^{1,5*}

¹ Institute of Bio- and Geosciences, IBG-1: Biotechnology, Forschungszentrum Jülich GmbH, Jülich, Germany,

² Computational Systems Biotechnology, RWTH Aachen University – Aachener Verfahrenstechnik, Aachen, Germany,

³ Microscale Bioengineering, RWTH Aachen University – Aachener Verfahrenstechnik, Aachen, Germany, ⁴ Institute of Biotechnology, RWTH Aachen University, Aachen, Germany, ⁵ Multiscale Bioengineering, Bielefeld University, Bielefeld, Germany

OPEN ACCESS

Edited by:

Dirk Tischler,
Ruhr-Universität Bochum, Germany

Reviewed by:

Susan Schlimpert,
John Innes Centre, United Kingdom
Josef Trögl,
Jan Evangelista Purkyně University
in Ústí nad Labem, Czechia

*Correspondence:

Alexander Grünberger
alexander.gruenberger@uni-
bielefeld.de

^{††} These authors have contributed
equally to this work

Specialty section:

This article was submitted to
Microbial Physiology and Metabolism,
a section of the journal
Frontiers in Microbiology

Received: 09 August 2018

Accepted: 19 October 2018

Published: 22 November 2018

Citation:

Koepff J, Sachs CC, Wiechert W,
Kohlheyer D, Nöh K, Oldiges M and
Grünberger A (2018) Germination
and Growth Analysis of *Streptomyces*
lividans at the Single-Cell Level Under
Varying Medium Compositions.
Front. Microbiol. 9:2680.
doi: 10.3389/fmicb.2018.02680

Quantitative single-cell cultivation has provided fundamental contributions to our understanding of heterogeneity among industrially used microorganisms. Filamentous growing *Streptomyces* species are emerging platform organisms for industrial production processes, but their exploitation is still limited due to often reported high batch-to-batch variations and unexpected growth and production differences. Population heterogeneity is suspected to be one responsible factor, which is so far not systematically investigated at the single-cell level. Novel microfluidic single-cell cultivation devices offer promising solutions to investigate these phenomena. In this study, we investigated the germination and growth behavior of *Streptomyces lividans* TK24 under varying medium compositions on different complexity levels (i.e., mycelial growth, hyphal growth and tip elongation) on single-cell level. Our analysis reveals a remarkable stability within growth and germination of spores and early mycelium development when exposed to constant and defined environments. We show that spores undergo long metabolic adaptation processes of up to > 30 h to adjust to new medium conditions, rather than using a “persister” strategy as a possibility to cope with rapidly changing environments. Due to this uniform behavior, we conclude that *S. lividans* can be cultivated quite robustly under constant environmental conditions as provided by microfluidic cultivation approaches. Failure and non-reproducible cultivations are thus most likely to be found in less controllable larger-scale cultivation workflows and as a result of environmental gradients within large-scale cultivations.

Keywords: *Streptomyces lividans*, filamentous growth, microfluidics, single-cell cultivation, germination, tip elongation rate, heterogeneity

Abbreviations: AA00, Pure minimal salt cultivation medium; AA04, Minimal salt medium, supplemented 4 selected amino acids; AA08, Minimal salt medium, supplemented 8 selected amino acids; AA20, Minimal salt medium, supplemented with all 20 proteinogenic amino acids; CAS, Minimal salt medium, supplemented with Bacto™ Casamino Acids; CM, Complex cultivation medium; HGU, Hyphal growth unit; MSCC, Microfluidic single cell cultivation; MTPC, Microtiter-plate cultivation; *S. lividans*, *Streptomyces lividans* TK24.

INTRODUCTION

Streptomyces is one of the most promising genera in industrial research for novel target molecules and structures (Bérdy, 2005; Olano et al., 2009), as their secondary metabolism facilitates the formation of more than 7,500 biologically active compounds (Bérdy, 2005). Among those are, for example the majority of antibiotics in clinical and agricultural use today (Chater, 2016). On top of that, several members of this genus, such as *Streptomyces lividans*, have been promoted as promising production hosts for heterologous proteins, due to their high secretory capacity (Sevillano et al., 2016; Anné et al., 2017). Together with the sequenced genome (Rückert et al., 2015) and established state-of-the-art genome editing techniques available (Cobb et al., 2015; Rebets et al., 2016; Wang et al., 2016), Streptomyces are nowadays well accessible for targeted metabolic engineering approaches.

However, their fungus-like filamentous growth behavior often impedes the implementation of novel production processes (Claessen et al., 2014; van Dissel et al., 2015; Chater, 2016). High batch-to-batch variations and unexpected growth and production differences are reported frequently, caused by the complex mechanism of growth (van Wezel et al., 2006; van Dissel et al., 2014) and the linked implications on production yield and titers (D'Huys et al., 2011). So far it is known that, besides the genetic background, the apparent growth morphology (van Dissel et al., 2015) is highly sensitive at least toward media composition (Reichl et al., 1992), dissolved oxygen concentration (van Dissel et al., 2014), surface tension (Walisko et al., 2015), and energy input (Belmar-Beiny and Thomas, 1991; Koepff et al., 2017). Even the role of germling agglomeration originating from different spores, aggregating in early growth states and thereby contributing significantly to pellet size variations and culture inhomogeneity has been discussed (Zacchetti et al., 2016).

With all these variability factors in mind, the question remains how the organisms' intrinsic heterogeneity contributes to the high batch-to-batch variations. Pinpointing cellular heterogeneity at population, spore and mycelium level may help to assess reproducibility issues and reduce the burden of unpredictability in bioprocess development. Therefore, the impact of intrinsic cellular heterogeneity as well as the contribution of different substrate complexity (here: availability of different amino-acids and complex compounds) during germination and early mycelium formation needs to be investigated.

Microscopic time-lapse imaging technologies have developed over the last three decades as preferred technique for in-depth mycelial growth investigations. The first video based analysis on the germination and mycelium formation of *Streptomyces* was already published in 1990 (Reichl et al., 1990a,b). Reichl et al., analyzed various growth parameters, such as individual hyphal length, number of branches as well as HGU. Later, the same analytical approach was applied to investigate filamentous fungi (Spohr et al., 1998; Pollack et al., 2008). Thereby, a temperature controlled growth chamber placed under a camera-equipped light microscope was used for cultivation. In further time-lapse studies *Streptomyces* was grown on solid

media, either using small agar patches (Hempel et al., 2008) or plugs (Jyothikumar et al., 2008; Willemse et al., 2012), flattening the three-dimensional mycelial structures. Recently, a microfluidic cultivation device was applied to investigate the whole *Streptomyces* life-cycle, including germination, mycelium formation and sporulation (Schlimpert et al., 2016). Nowadays, such miniaturized cultivation systems can be operated at highly constant environmental conditions regarding the cultivation medium, temperature and oxygen concentration. At the same time single microfluidic devices enable high throughput analysis and the application of statistical methods due to a high degree of parallelization (Dusny and Schmid, 2015). These unique features allow investigating large cell numbers to unravel cell-to-cell heterogeneity induced by biological and intrinsic factors, independently from environmental fluctuations. Xu and Vetsigian (2017) investigated spores of *Streptomyces* disclosing phenotypic variability and interactions between communities. Performing cultivations on agarose-pads, they systematically investigated the sporulation and growth of four different *Streptomyces* strains and identified differences in the germination fraction, depending on the strain and differences in the level of medium dilution.

In this study, we investigated the growth characteristics as well as the variability in germination and early stage mycelium development of *S. lividans* TK24 via MSCC inside hundreds of picoliter sized growth chambers. Live-cell imaging and subsequent data analysis was performed by a tailor-made image based data processing workflow. In a first step, our new MSCC approach was validated by accompanying MTPC applied as our reference system. In a second step, six different media compositions with decreasing complexity in terms of available substrate spectrum were applied to investigate phenotypic growth variations of *S. lividans* on the level of entire populations, single spores, and individual mycelia.

MATERIALS AND METHODS

Strains and Media

All experiments were conducted using *S. lividans* TK24, a plasmid-free derivative of *S. lividans* 66 (Cruz-Morales et al., 2013), which is a close relative of *S. coelicolor* A3(2), generally regarded as the best genetically characterized *Streptomyces* strain (Hopwood, 1999).

To prepare *S. lividans* spore solutions the protocol published by Kieser et al. (2000) was applied: Solid corn steep agar (Hobbs et al., 1989) cultures were grown for 10 days at 28°C to obtain well-sporulated mycelium. By pipetting 10 mL sterile PBS with 20% (vol/vol) glycerol onto an agar surface and gentle scratching with a sterilized spreader rod, the spores were dispersed and subsequently separated from remaining hyphae fragments by a custom-made cotton wool filter, before being stored at -20°C as permanent culture.

For main-culture in chip or MTP cultivations, all together six different media compositions were applied (Table 1). Full complex phage medium (CM) (Korn et al., 1978), consists of 5 g·L⁻¹ peptone, 5 g·L⁻¹ yeast extract, 5 g·L⁻¹ meat

extract, $0.5 \text{ g}\cdot\text{L}^{-1} \text{ MgSO}_4\cdot 7 \text{ H}_2\text{O}$ and $0.74 \text{ g}\cdot\text{L}^{-1} \text{ CaCl}_2\cdot 2\text{H}_2\text{O}$. The basic minimal medium was composed of $2.07 \text{ g}\cdot\text{L}^{-1} \text{ NaH}_2\text{PO}_4\cdot 1 \text{ H}_2\text{O}$, $2.6 \text{ g}\cdot\text{L}^{-1} \text{ K}_2\text{HPO}_4$, $0.6 \text{ g}\cdot\text{L}^{-1} \text{ MgSO}_4\cdot 7 \text{ H}_2\text{O}$, $3.0 \text{ g}\cdot\text{L}^{-1} (\text{NH}_4)_2\text{SO}_4$ and $10 \text{ g}\cdot\text{L}^{-1} \text{ D-glucose}$, 100 mM 2-(N-morpholino)ethanesulfonic acid (MES) as well as several trace elements ($1 \text{ mg}\cdot\text{L}^{-1} \text{ ZnSO}_4\cdot 7 \text{ H}_2\text{O}$, $1 \text{ mg}\cdot\text{L}^{-1} \text{ FeSO}_4\cdot 7 \text{ H}_2\text{O}$, $1 \text{ mg}\cdot\text{L}^{-1} \text{ MnCl}_2\cdot 4 \text{ H}_2\text{O}$, $1 \text{ mg}\cdot\text{L}^{-1} \text{ CaCl}_2$), having the pH adjusted to 6.8 using $1 \text{ M H}_2\text{SO}_4$. To supplement the minimal media, either $2 \text{ g}\cdot\text{L}^{-1}$ hydrolyzed milk protein (Bacto™ Casamino Acids, MM_CAS) or $2 \text{ g}\cdot\text{L}^{-1}$ of 3 different amino acids mixtures were added (Table 1), with ratios following the natural abundances in *Streptomyces* protein (Kieser et al., 2000). Additionally, minimal media without any supplementation was used as reference medium. The detailed compositions are provided in Supplementary Material S1.

Microfluidic Cultivation Conditions

Microfluidic single-cell cultivations (MSCCs) were performed using a modified version of the polydimethylsiloxane (PDMS) cultivation device described by Grünberger et al. (2015) (Figure 1A). The chip system consists of 8 arrays of monolayer cultivation chambers ($1 \times w \times h = 90 \times 40 \times 1 \text{ }\mu\text{m}$), with 40 chambers each (Figures 1B,C). For fabrication details the reader is referred to Grünberger et al. (2013). The microfluidic chip was mounted onto a motorized inverted microscope (Nikon Eclipse Ti, Nikon, Japan) equipped with an incubator (PeCon Series 2000, PeCon GmbH, Germany) for temperature control. A *S. lividans* spore suspension with a concentration of $\sim 10^6$ spores $\cdot\text{mL}^{-1}$ was inoculated into the chip, according to the loading procedure as described earlier for *Escherichia coli* (Probst et al., 2015). Fluidic connections were established by silicone tubing (Tygon S-54-HL, ID = 0.25 mm, OD = 0.76 mm, Saint-Gobain, United States) and dispensing needles (ID = 0.2 mm, OD = 0.42 mm, Nordson EFD, United States). Media were infused at approx. $200 \text{ nL}\cdot\text{min}^{-1}$ after cell inoculation by a syringe pump (neMESYS, cetoni GmbH, Germany). The media described above were systematically tested as growth media. Specific growth chambers which were most suitable for imaging

were selected manually. Each experiment was stopped, as soon as the mycelia started to overgrow the chamber volume.

Image Processing and Data Analysis

Image analyses were performed using the analysis software *myceliso* (Sachs et al., 2018). For each image frame, the growth chamber was automatically detected and used as a region of interest (ROI), removing the need for separate image registration. Time lapse image stacks (Figure 1D) were segmented (Figure 1E), skeletonized (Figure 1F) and automatically tracked (Figure 1G) using the *myceliso* software. Automated filtering (standard *myceliso* settings) during the tracking process was applied in order to remove artifacts due to tracking errors: (a) tracked hyphae must be tracked for at least 5 consecutive time points, (b) they must reach a length longer $10 \text{ }\mu\text{m}$ at the end of the track, (c) be grown for at least $5 \text{ }\mu\text{m}$, (d) hyphae must not have an elongation rate greater than $100 \text{ }\mu\text{m}\cdot\text{h}^{-1}$. To exclude erroneous segmentations due to densely packed mycelia, tracking was only performed until 20% coverage of the growth chamber was reached. Analysis results were visually checked using *myceliso* Inspector, and a subset of positions was chosen, which (i) contained a properly grown mycelium (centered, viable) and (ii) were analyzed without obvious errors. Data was collected by *myceliso* in hierarchical data format 5 (HDF5) files and further subjected to statistical evaluation using Python with commonly available modules (i.e., numpy, scipy, pandas, and matplotlib): data of individual positions was collected for interpretation and visualization, means and standard deviations calculated. Germination delay was determined for each position by the time where the first trackable hypha occurred. Growth rate of the total mycelium length was determined per chamber by assuming exponential growth and employing a log-linear regression model with $R^2 > 0.9$. HGU was determined by finding the maximum of the quotient the smoothed time-resolved data “total mycelium length” divided by “count of tips” during the exponential growth phase. Means of different media compositions were statistically assessed using both equal and unequal variance (Student's/Welch's) *t*-test. Data analysis and figure generation is available as a Jupyter notebook in the Supplementary Analysis Data (Supplementary Data Sheet 2).

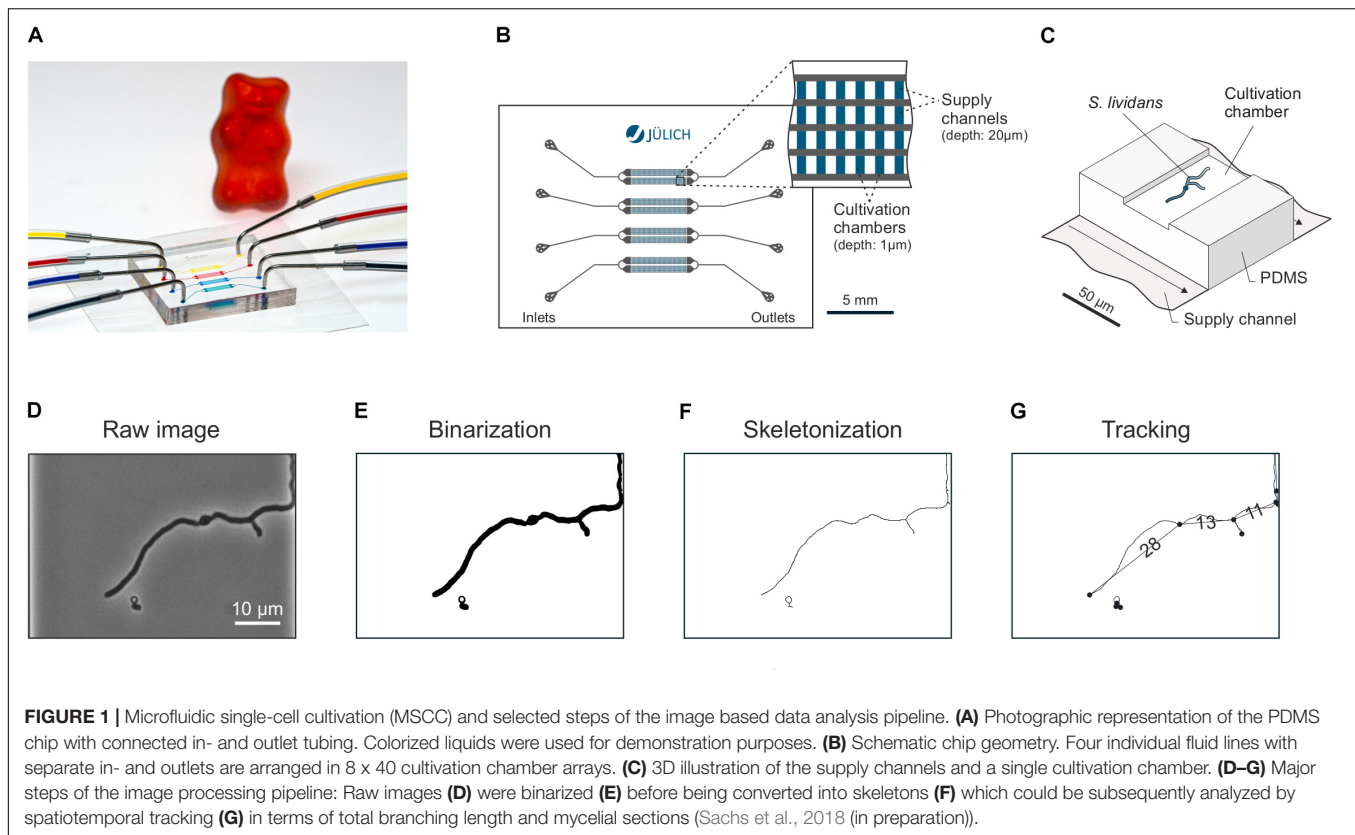
TABLE 1 | Media compositions and supplementation for both: chip- and MTP-based cultivation.

Medium ID	Medium basis	Supplementation	Final concentration
CM	Complex phage medium	–	–
CAS	Minimal medium	Bacto™ Casamino acids	$2 \text{ g}\cdot\text{L}^{-1}$
AA20	Minimal medium	All 20 proteinogenic amino acids	$2 \text{ g}\cdot\text{L}^{-1}$
AA08	Minimal medium	Arg, Asn, Asp, Glu, Leu, Met, Phe, Thr	$2 \text{ g}\cdot\text{L}^{-1}$
AA04	Minimal medium	Asn, Leu, Met, Phe	$2 \text{ g}\cdot\text{L}^{-1}$
AA00	Minimal medium	–	–

Selection for 8 (MM_08) and 4 (MM_04) amino acids was done according to the proposal in Nowruzi et al. (2008). The individual amino acid concentrations are provided in Supplementary Material S1.

Microtiter-Plate Cultivation (MTPC) of *S. lividans*

Microtiter-plate cultivation was performed in 48-well FlowerPlates® (MTP-48-BOH) covered by gas permeable sealing foils (F-GP-10) in an automated cultivation device (BioLector, m2p-labs GmbH, Germany) as previously described (Koepff et al., 2017) with the following modifications: Wells, prefilled with $1000 \text{ }\mu\text{L}$ cultivation medium were inoculated using $50 \text{ }\mu\text{L}$ spore suspension with an concentration of $\sim 10^6$ spores $\cdot\text{mL}^{-1}$. Cultivation parameters were set to 800 rpm shaking frequency, cultivation temperature of 30°C , 85% relative humidity and a 10 min recording interval for scattered light measurements. In all experiments MTP-cultivation was performed parallel to chip experiments, using the identical spore vial for inoculation, ensuring identical start conditions for all cultures.



Data Analysis of MTPC Online Signals

Scattered light signal was blanked in each well separately, by the average of the first 10 values. Lag-phase was calculated as the time difference between cultivation start and the beginning of exponential-like growth behavior in the scattered-light signal. Specific growth rate was determined on spline interpolation (10 knot points) of scattered light data as described elsewhere (Radek et al., 2017).

RESULTS AND DISCUSSION

Validating Microfluidic Single-Cell Against Submerge Microtiter-Plate Cultivation

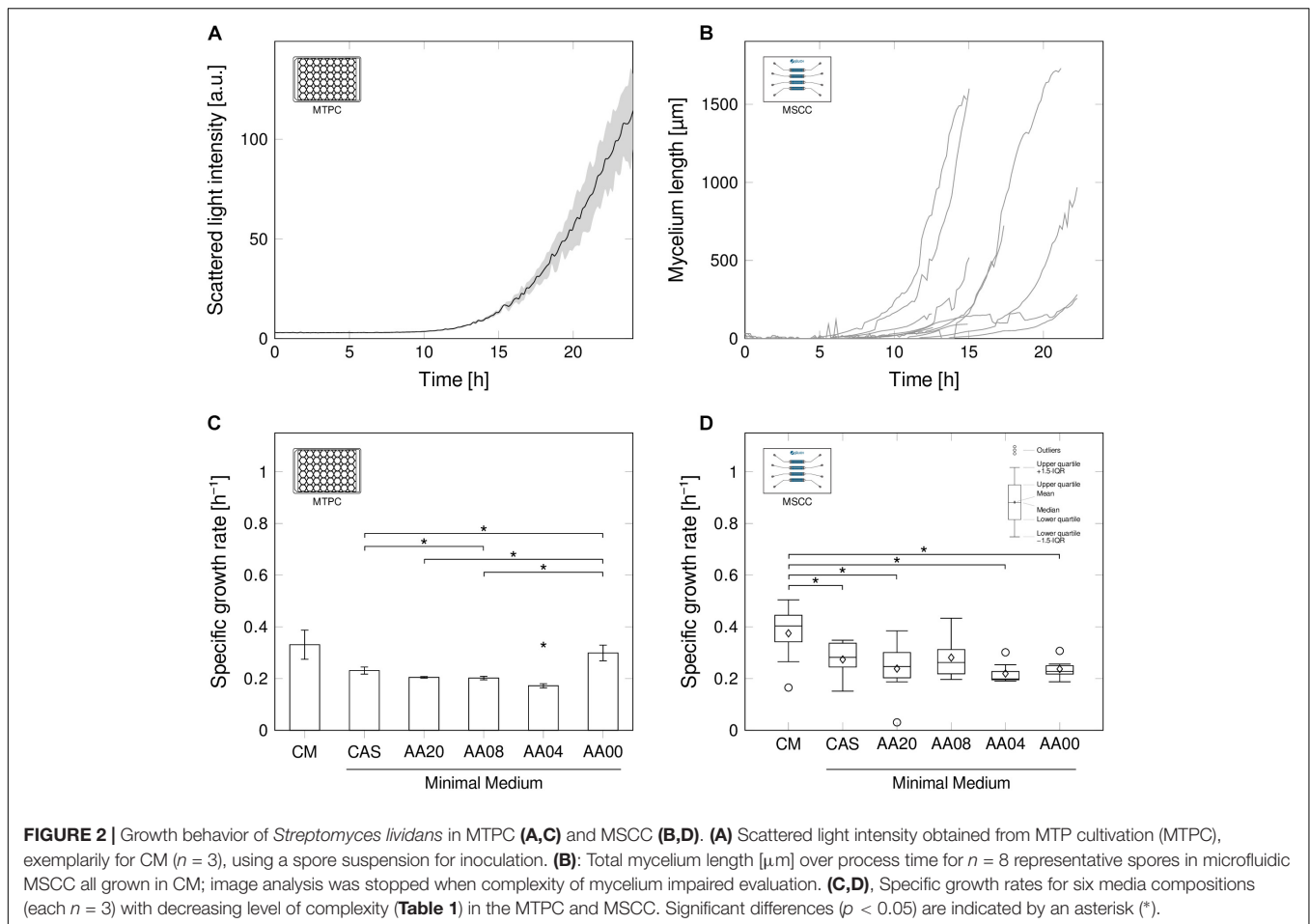
For research and production purposes, *S. lividans* is typically grown in agitated bioreactor environments in submerge cultures (Kieser et al., 2000; van Dissel et al., 2014). Under such conditions, the organism shows normal growth kinetics in biomass related signals, such as scattered light intensity (Figure 2A). After a lag-phase, in which no growth is detectable, an exponential increase of scattered light is recorded, then limitations occur, which cause stagnation and at a later stage even decrease of the signal pattern.

However, the optically derived scattered light signal, alike all other macroscopic biomass signals, describes an average status of the culture as it is affected by all scattering particles within the

liquid volume. Its aggregate character therefore is not suitable to unravel mycelial growth in detail: It remains unclear whether the flat-line signal pattern within the first hours of cultivation reflects a biological adaption process (lag-phase) before germination of the spores, or if the growth activities are simply occurring below the signal detection limit. Therefore, such averaged signals cannot be used to resolve heterogeneities and variability occurring within the mycelium of individual spores and in-between mycelia emerging from different spores.

To disclose the activity of single spores and single mycelia, we cultivated *S. lividans* inside MSCC devices under continuous time-lapse imaging (Figure 2B). PDMS based chip manufacturing enabled us to tailor an application-specific microfluidic device (Figure 1), suitable for *S. lividans* cultivation in its early stage of germination. The height of the growth chambers ($\sim 1 \mu\text{m}$) in the used device approximately match the diameter of single spores thereby aligning the cellular growth in 2D monolayers. Constant environmental conditions were ensured by the continuous and balanced medium supply adjacent to both openings of each cultivation chamber.

Evaluating the total development of mycelial length for individual spores grown in CM (Figure 2B) basically revealed a comparable exponential growth pattern in comparison to the MTPC reference system. Nevertheless, the microfluidic analysis unraveled the presence of spore-to-spore variation, as the culture-wide scattered light signal indicated. Growth initiation occurred in a wide temporal distribution, but also the exponential growth behavior varied between individually



evolving mycelia. Still, growth rates obtained from the MTP reference system (Figure 2C) and from single spores in the microfluidic chip (Figure 2D) approach are generally comparable under all six investigated media compositions, ranging from full complex (CM), to pure minimal medium (AA00) with supplemented minimal medium steps in-between (for detailed media compositions see Table 1). Once more, this notable result underlines, that MSCC can mirror submerge conditions (Grünberger et al., 2013).

As expected, the highest specific growth rates ($0.38 \text{ h}^{-1} \pm 0.11 \text{ h}^{-1}$ in MSCC, $0.33 \text{ h}^{-1} \pm 0.06 \text{ h}^{-1}$ in MTPC) were obtained in CM, as a broad spectrum of available substrates facilitates the faster formation of new mycelial structures. In the remaining media compositions, the estimated growth rates ranged in MSCC between $0.27 \text{ h}^{-1} \pm 0.07 \text{ h}^{-1}$ for CAS and $0.22 \text{ h}^{-1} \pm 0.04 \text{ h}^{-1}$ for AA04. In MTPC, the growth rates were $0.23 \text{ h}^{-1} \pm 0.01 \text{ h}^{-1}$ for CAS and $0.17 \text{ h}^{-1} \pm 0.01 \text{ h}^{-1}$ for AA04. Thus the growth rate on CM was significantly higher, compared to the growth rate of the media compositions CAS, AA20, AA04, AA00 (all $p < 0.05$). No significant growth rate difference was found between CM and AA8 ($p = 0.11$).

The slightly higher growth rates, obtained in MSCC (see Supplementary Material S2) fits well to previously reported results for different biological systems and cultivation conditions

(Unthan et al., 2014; Dusny and Schmid, 2015). This trend may be caused by the differences of the cultivation modes (batch vs. continuous) or, in case of MTPC, potentially the presence of nutrient gradients in the cultivation wells leading to temporally changing conditions. This renders a direct and absolute rate comparison between the two systems difficult.

Interestingly, not only the growth rate, but also growth rate distributions were found to be a function of the media complexity: Highest growth rate fluctuations between individual spores as well as between parallel wells in the MTP setup were observed in CM. These fluctuating rates may contribute to pellet size distributions, as recently reported for CM cultivations (Zacchetti et al., 2016). Also, significantly reduced size distributions were reported herein for minimal media setups, which is again an agreement to the rate fluctuations in the corresponding media setups (Figure 2D).

Spore Germination Time Point Considering Inner-Culture Variations

Whereas in MTPC and other established cultivation systems only average lag-phases are determinable, MSCC allows investigating the initial delay until germination of individual spores (Figure 3).

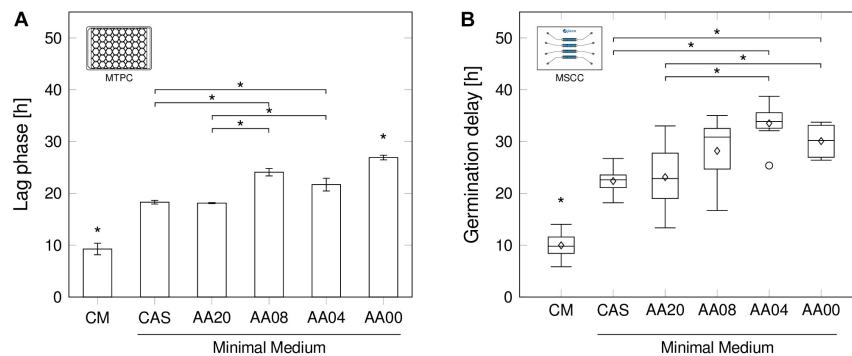


FIGURE 3 | Lag-phase and germination delay by decreasing medium complexity. **(A)** Lag-phase durations in shaken MTPC for all six medium conditions. Error bars calculated from $n = 3$ biologically independent replicates. **(B)** Germination delays determined by MSCC in $n \geq 6$ cultivation chambers. Box plot annotation identical to **Figure 2D**. Determination methods for lag-phases and germination delays are provided in the methods section. Significant differences ($p < 0.05$) are indicated by an asterisk (*).

A clear dependency of the medium complexity on the germination delay, namely the time difference between inoculation and spore germination, was observed in both cultivation systems (**Figure 3**). During MSCC (**Figure 3B**) the spores began to form primary hyphae after already $10.0 \text{ h} \pm 2.4 \text{ h}$, when being cultivated in CM, while significant longer delays were found in all other media applied in this work (up to $33.5 \text{ h} \pm 3.9 \text{ h}$ in AA04) (all p -values < 0.05). Interestingly, very comparable mean values were obtained for the complex amino acid combination CAS and the artificial AA20 mixture. In both media spores show a significant faster spore germination compared to medium AA04 and AA00 (all p -values < 0.05). In contrast, the media with 4 (AA04) and 8 (AA08) supplemented amino acids do not have a positive influence on the germination delay, since the non-supplemented negative-control (AA00) showed comparable delays.

Remarkably, the mentioned effects above, obtained by chip-based cultivation (**Figure 3B**), showed equivalent tendencies for the observed lag-phase durations, derived from MTPCs (**Figure 3A**). The absolute values ranged between $9.3 \text{ h} \pm 1.1 \text{ h}$ for CM and $27.0 \text{ h} \pm 0.5 \text{ h}$ in AA00 medium. Although the cultivation systems highly differ by design and mode of operation, average spore germination seems not to be affected significantly.

The lag-phase is generally understood to be an adaptation process upon a change of the environmental condition, possibly resulting in a homogenous switching into a new phenotype or a phenotypic (stochastic vs. responsive) diversification into two phenotypes (Kotte et al., 2014). In the present study, these altered conditions may include the availability of substrates. Here, the remaining question depicts the occurrence of intrinsic cellular heterogeneity toward germination time points, as it may illuminate underlying regulation mechanisms and adaptation strategies. By studying the distribution of the single-spore germination time points, we found that interestingly all germinating spores in the observed growth chambers showed quite robust and consistent behavior with standard deviations between 2.4 h (CM, $10.0 \text{ h} \pm 2.4 \text{ h}$) and 3.9 h (AA04, $33.5 \text{ h} \pm 3.9 \text{ h}$).

In opposition to that, when some spores show a rapid germination, while others remain dormant as persistent cells, backing up the population in case of emerging more disadvantageous conditions a bimodal behaviour would have been suspected. Such a bimodal behavior has been observed for microbial adaption processes upon the availability of different carbon sources (Solopova et al., 2014). Differences in the germination delay in CM and between the minimal media might be due to the modifications in amino-acid availability (Ensign, 1978) or a combination with other unknown complex medium compounds, rather than the cultivation method. This lays the foundation, to use MSCC as a future screening tool for further germination studies with different medium compositions. Please note, that the overall spore germination behavior is quite low (36.12%, **Supplementary Material S3**), but comparable for all media (CAS = 31%; AA20–AA00 = 33%), while only with CM higher outgrowth values (CM = 61%) were reached. The latter number is well comparable to published results, where in similar CM a germination fraction of $\sim 45\%$ was observed after 24 h for *S. coelicolor* (Xu and Vetsigian, 2017). Interestingly, during the inoculation procedure of spores into separate cultivation chambers and subsequent continuous perfusion with fresh cultivation medium, the accumulation of germicidins (germination inhibiting agents) was presumably avoided. These substances were reported to be secreted by germinating spores to prevent the germination of neighboring spores (Aoki et al., 2011; Xu and Vetsigian, 2017), but should not have an influence during MSCC.

Intra-Mycelial Variations: Hyphal Elongation Rates of Individual Apical Growth Tips – Within a Single Spore and In-Between Spores

Beside the previously discussed spore-level parameters, image analysis allows to take a deeper look at underlying inner-spore growth performances and fluctuations. This was realized by dissecting the developing mycelium into individual hyphae segments, separated at the branching points (**Figures 1G**,

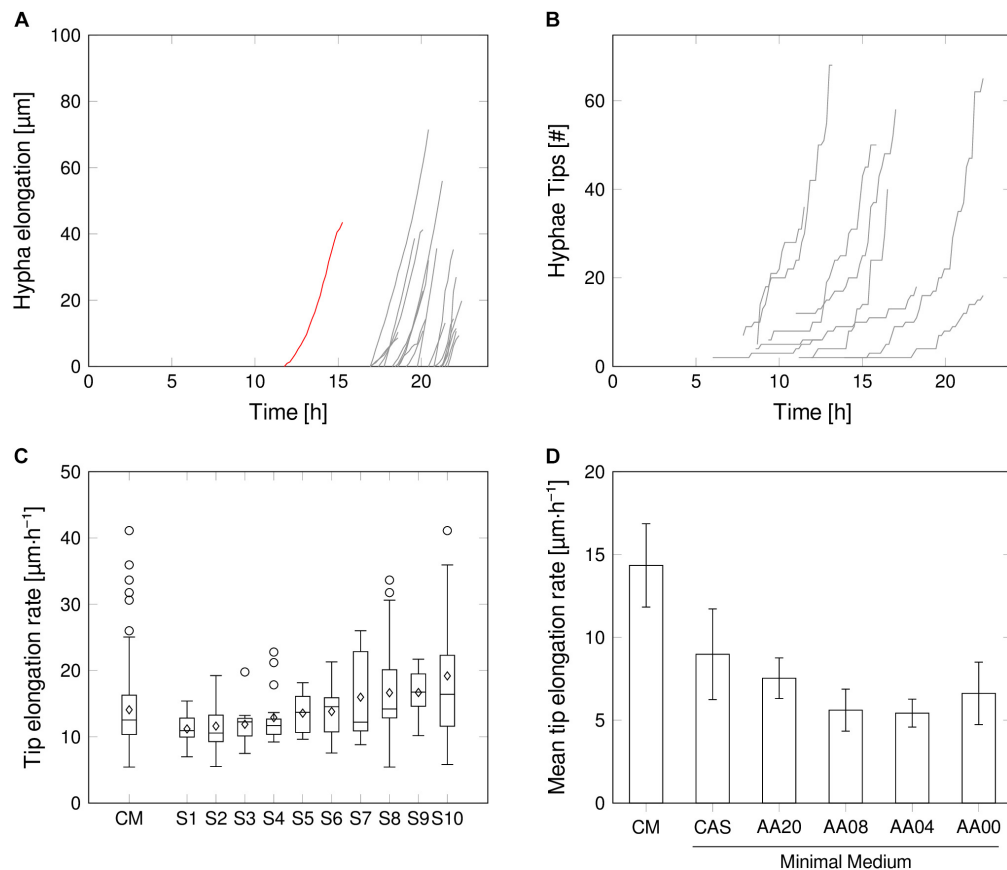


FIGURE 4 | Intrinsic growth heterogeneity on mycelium level. **(A)** Additional length of the developing mycelium in one representative chamber. Primary hyphae (red) and subsequent hyphae after branching (gray). **(B)** Number of hyphal tips, exemplarily for several spores in complex medium. **(C)** Tip elongation rate distribution for all and 10 representative spores supplied with CM. Outliers may be provoked by missing or falsely annotated links between image frames. **(D)** Average tip elongation rate (average of mean tip elongation rate of all evaluated spores of each medium condition). Detailed tip elongation rates for each medium condition are provided in **Supplementary Material S4**.

4A). Notably, the primary hypha, arising from the spore, showed an approximate exponentially increasing tip elongation rate within the first hours after germination. In contrast, all subsequent branches grew at linear rates right after branching. A similar growth pattern discrimination between the first and subsequent mycelial segments was already previously reported (Allan and Prosser, 1983; Kretschmer, 1988; Reichl et al., 1990a; Yang et al., 1992). This underlines the suitability of the developed microfluidic cultivation system for comparative growth studies. The exponential development of the total mycelial length therefore is a result of the exponential increase of branching points rather than of the growth of the individual tips (Figure 4B).

Within the mycelial network of a single spore, the elongation rates fluctuated strongly (Figure 4C), resulting in a mean elongation rate of $14.1 \mu\text{m}\cdot\text{h}^{-1} \pm 6.1 \mu\text{m}\cdot\text{h}^{-1}$ in CM, over all observed spores (Figure 4C). However, this points to a robust phenomenon, as no pronounced variations in the rate distribution were found when comparing different spores, supplied by the same medium (Figure 4D and **Supplementary Material S2**). Thus, inner-spore tip elongation

rate variations probably will not have a strong effect on macroscopic heterogeneities. Here, the limited chamber height due to fabrication design could influence data interpretation, as it may lead to friction of hyphae and result in unsteady growth behavior over time. The same holds true for inaccuracies within cell detection over time, due to limitations of the automated image-analysis workflow.

The HGU, which describes the average length of a hyphal segment, follows a similar trend as the mean tip elongation rate (**Supplementary Material S5**). Highest HGU was found in CM with an average of $28.7 \mu\text{m}$, which is in well accordance with previous results for *S. tendae* (Reichl et al., 1992) and *S. coelicolor* (Allan and Prosser, 1983) on a comparable medium. Interestingly, various amino acid supplementations did not have a strong influence on the HGU as all remaining media setups resulted in average HGUs between $14.3 \mu\text{m}$ (AA04) and $17.4 \mu\text{m}$ (CAS). Even though there is not much known about the effect of minimal media supplementation on HGUs in filamentous bacteria, in tendency reduced HGUs have been reported for MM setups in comparison to CM, but with a high dependency on carbon (glucose) availability (Reichl et al., 1992). In the present

study, however, all minimal media setups contained an identical concentration of glucose ($10 \text{ g} \cdot \text{L}^{-1}$) and, except for AA00, a stoichiometrically adjusted amount of amino acids. From our results such a general relation between richness of medium and branching frequency cannot be deduced. By far the strongest fluctuations in HGUs between spores were recorded for CM as expressed by a standard deviation of $21.7 \mu\text{m}$. The larger pellet size variations reported for complex compared to minimal media (Zacchetti et al., 2016) may therefore be explained by this issue. In minimal media setups reduced HGU fluctuations were obtained where the variations decrease with the medium complexity.

DISCUSSION

Inner-culture variability resulting in unfavorable fluctuation in growth and production are repeatedly reported for members of the *Streptomyces* genus, and are known to constitute a risk when employing members of this genus in industrial production processes (van Dissel et al., 2014). Several genetic and especially environmental effectors have been identified over the years, known to contribute to the observed cultivation difficulties. As bulk measurements can occlude the observation of heterogeneously reacting subpopulations, we choose to investigate inner-*Streptomyces* heterogeneity using MSCC in combination with an automated image analysis, allowing for individual, unbiased investigation of growth parameters per spore and mycelium.

We validated the MSCC for filamentous *Streptomyces* against an established MTP cultivation method (Koepff et al., 2017). Here a high comparability was obtained between the two systems in germination and early-stage mycelium formation. Differing not only in working volume by a factor of 10^6 , but also by their cultivation mode (perfusion vs. batch), this was a notable finding, confirming the applicability of MSCC in further screening and in-depth growth investigations for filamentous bacteria. The MSCC has therefore proven – again – to be a useful and efficient tool to deeply investigate inner-culture heterogeneity also in filamentous organisms. To operate this technology to its potential, time-lapse microscopy accompanied by a powerful image processing and data analysis software pipeline is a necessary prerequisite. By analyzing $\approx 680 \text{ GB}$ of image stacks in a reproducible and unbiased manner, it is possible to draw comprehensive statements across different hierarchical morphological levels that would otherwise be impossible to derive.

Even though there are variation in mycelium growth, germination and tip elongation, these variations are a reproducible phenomenon in each set of spores and therefore probably not the driving force behind discussed reproducibility issues and inner-culture heterogeneities. While CM provides a faster growth performance in all recorded parameters, it goes along with the burden of higher fluctuations on spore level (average mycelium growth rate, germination time delay) and mycelium level (tip elongation rate, HGU). When inner-culture homogeneity is the main objective, minimal medium setups are to be preferred. Even though there are inner-culture fluctuations, especially due to individual spore germination delays, still a

robust inner growth performance of the organism prevails. In conclusion, this single-cell characterization shifts the focus back to the already known, especially environmental factors such as gradients within large-scale processes (Lara et al., 2006) and variabilities/variances within cultivation workflows (Koepff et al., 2017), known to trigger batch-to-batch and inner-culture fluctuations. Filamentous organisms, even more as their bisecting microbial competitors, demand for highly standardized and constant cultivation conditions. If such conditions are provided, it should be possible to obtain reproducible cultivation results. This strongly underlines the need to investigate the impact of gradients in large-scale production when using filamentous organisms, as done manifold for bisecting production hosts such as *E. coli* (Löffler et al., 2016) and *C. glutamicum* (Limberg et al., 2017).

Further progress within microfluidic fabrication techniques, will allow the investigation of more complex biological questions in MSCC, for example the emulation of large-scale bioprocesses by exposing cells to altering medium conditions over time (Binder et al., 2017). An improved understanding of the origin, reason and impact of heterogeneities in *Streptomyces* large-scale cultivation will lay the foundation for improved bioprocesses and cultivation pipelines.

AUTHOR CONTRIBUTIONS

JK and AG conceived the study. JK and AG performed the experiments. CS analyzed the data. JK, AG, and CS interpreted the results. JK and CS wrote the first draft. JK, CS, DK, KN, MO, and AG discussed the findings. WW, DK, KN, MO, and AG copyedited the manuscript. WW provided the funding.

FUNDING

The research leading to these results has received funding from the European Commission's Seventh Framework Program (FP7/2007-2013, KBBE.2013.3.6-02: Synthetic Biology toward applications) under the grant agreement STREPSYNTH (Project No. 613877). Further funding was received from the Enabling Spaces Program "Helmholtz Innovation Labs" of German Helmholtz Association to support the "Microbial Bioprocess Lab – A Helmholtz Innovation Lab." CS was supported by the Deutsche Forschungsgemeinschaft (WI 1705/16-2). AG was supported by a postdoctoral grant provided by the Helmholtz Association (PD-311). DK was supported by the Helmholtz Association (VH-NG-1029). We acknowledge support for the Article Processing Charge by the Deutsche Forschungsgemeinschaft and the Open Access Publication Fund of Bielefeld University.

SUPPLEMENTARY MATERIAL

The Supplementary Material for this article can be found online at: <https://www.frontiersin.org/articles/10.3389/fmicb.2018.02680/full#supplementary-material>

REFERENCES

- Allan, E. J., and Prosser, J. I. (1983). Mycelial growth and branching of *Streptomyces coelicolor* A3(2) on solid medium. *Microbiology* 129, 2029–2036. doi: 10.1099/00221287-129-7-2029
- Anné, J., Economou, A., and Bernaerts, K. (2017). Protein secretion in gram-positive bacteria: from multiple pathways to biotechnology. *Curr. Top. Microbiol. Immunol.* 404, 267–308. doi: 10.1007/82_2016_49
- Aoki, Y., Matsumoto, D., Kawaide, H., and Natsume, M. (2011). Physiological role of germicidins in spore germination and hyphal elongation in *Streptomyces coelicolor* A3(2). *J. Antibiot.* 64, 607–611. doi: 10.1038/ja.2011.59
- Belmar-Beiny, M. T., and Thomas, C. R. (1991). Morphology and clavulanic acid production of *Streptomyces clavuligerus*. Effect of stirrer speed in batch fermentations. *Biotechnol. Bioeng.* 37, 456–462. doi: 10.1002/bit.260370507
- Bérdy, J. (2005). Bioactive microbial metabolites. *J. Antibiot.* 58, 1–26. doi: 10.1038/ja.2005.1
- Binder, D., Drepper, T., Jaeger, K.-E., Delvigne, F., Wiechert, W., Kohlheyer, D., et al. (2017). Homogenizing bacterial cell factories. Analysis and engineering of phenotypic heterogeneity. *Metab. Eng.* 42, 145–156. doi: 10.1016/j.ymben.2017.06.009
- Chater, K. F. (2016). Recent advances in understanding *Streptomyces*. *F1000Res.* 5:2795. doi: 10.12688/f1000research.9534.1
- Claessen, D., Rozen, D. E., Kuipers, O. P., Sogaard-Andersen, L., and van Wezel, G. P. (2014). Bacterial solutions to multicellularity. A tale of biofilms, filaments and fruiting bodies. *Nat. Rev. Microbiol.* 12, 115–124. doi: 10.1038/nrmicro3178
- Cobb, R. E., Wang, Y., and Zhao, H. (2015). High-efficiency multiplex genome editing of *Streptomyces* species using an engineered CRISPR/Cas system. *ACS Synth. Biol.* 4, 723–728. doi: 10.1021/sb500351f
- Cruz-Morales, P., Vijgenboom, E., Iruegas-Bocardo, F., Girard, G., Yáñez-Guerra, L. A., Ramos-Aboites, H. E., et al. (2013). The genome sequence of *Streptomyces lividans* 66 reveals a novel tRNA-dependent peptide biosynthetic system within a metal-related genomic island. *Gen. Biol. Evol.* 5, 1165–1175. doi: 10.1093/gbe/evt082
- D’Huys, P.-J., Lule, I., van Hove, S., Vercammen, D., Wouters, C., Bernaerts, K., et al. (2011). Amino acid uptake profiling of wild type and recombinant *Streptomyces lividans* TK24 batch fermentations. *J. Biotechnol.* 152, 132–143. doi: 10.1016/j.jbiotec.2010.08.011
- Dusny, C., and Schmid, A. (2015). Microfluidic single-cell analysis links boundary environments and individual microbial phenotypes. *Environ. Microbiol.* 17, 1839–1856. doi: 10.1111/1462-2920.12667
- Ensign, J. C. (1978). Formation, properties, and germination of actinomycete spores. *Annu. Rev. Microbiol.* 32, 185–219. doi: 10.1146/annurev.mi.32.100178.001153
- Grünberger, A., Probst, C., Helfrich, S., Nanda, A., Stute, B., Wiechert, W., et al. (2015). Spatiotemporal microbial single-cell analysis using a high-throughput microfluidics cultivation platform. *Cytometry A* 87, 1101–1115. doi: 10.1002/cyto.a.22779
- Grünberger, A., Probst, C., Heyer, A., Wiechert, W., Frunzke, J., and Kohlheyer, D. (2013). Microfluidic picoliter bioreactor for microbial single-cell analysis: fabrication, system setup, and operation. *J. Vis. Exp.* 82:50560. doi: 10.3791/50560
- Hempel, A. M., Wang, S.-B., Letek, M., Gil, J. A., and Flärdh, K. (2008). Assemblies of DivIVA mark sites for hyphal branching and can establish new zones of cell wall growth in *Streptomyces coelicolor*. *J. Bacteriol.* 190, 7579–7583. doi: 10.1128/JB.00839-08
- Hobbs, G., Frazer, C. M., Gardner, D. C. J., Cullum, J. A., and Oliver, S. G. (1989). Dispersed growth of *Streptomyces* in liquid culture. *Appl. Microbiol. Biotechnol.* 31, 272–277. doi: 10.1007/BF00258408
- Hopwood, D. A. (1999). Forty years of genetics with *Streptomyces*: from in vivo through in vitro to in silico. *Microbiology* 145(Pt 9), 2183–2202. doi: 10.1099/00221287-145-9-2183
- Jyothikumar, V., Tilley, E. J., Wali, R., and Herron, P. R. (2008). Time-lapse microscopy of *Streptomyces coelicolor* growth and sporulation. *Appl. Environ. Microbiol.* 74, 6774–6781. doi: 10.1128/AEM.01233-08
- Kieser, T., Bibb, M. J., Buttner, M. J., Chater, K. F., and Hopwood, D. A. (2000). *Practical Streptomyces Genetics*. Norwich: John Innes Foundation.
- Koepff, J., Keller, M., Tsolis, C. K., Busche, T., Rückert, C., Hamed, M. B., et al. (2017). Fast and reliable strain characterization of *Streptomyces lividans* through micro-scale cultivation. *Biotechnol. Bioeng.* 114, 2011–2022. doi: 10.1002/bit.26321
- Korn, F., Weingärtner, B., and Kutzner, H. J. (1978). “A study of twenty actinophages: morphology, serological relationship and host range,” in *Genetics of the Actinomycetales*, ed. J. H. Thumim (Stuttgart: Fischer), 251–270.
- Kotte, O., Volkmer, B., Radzikowski, J. L., and Heinemann, M. (2014). Phenotypic bistability in *Escherichia coli*’s central carbon metabolism. *Mol. Syst. Biol.* 10:736. doi: 10.15252/msb.20135022
- Kretschmer, S. (1988). Stepwise increase of elongation rate in individual hyphae of *Streptomyces granaticolor* during outgrowth. *J. Basic Microbiol.* 28, 35–43. doi: 10.1002/jobm.3620280106
- Lara, A. R., Galindo, E., Ramírez, O. T., and Palomares, L. A. (2006). Living with heterogeneities in bioreactors: understanding the effects of environmental gradients on cells. *Mol. Biotechnol.* 34, 355–382.
- Limberg, M. H., Schulte, J., Aryani, T., Mahr, R., Baumgart, M., Bott, M., et al. (2017). Metabolic profile of 1,5-diaminopentane producing *Corynebacterium glutamicum* under scale-down conditions. Blueprint for robustness to bioreactor inhomogeneities. *Biotechnol. Bioeng.* 114, 560–575. doi: 10.1002/bit.26184
- Löffler, M., Simen, J. D., Jäger, G., Schäferhoff, K., Freund, A., and Takors, R. (2016). Engineering *E. coli* for large-scale production – Strategies considering ATP expenses and transcriptional responses. *Metab. Eng.* 38, 73–85. doi: 10.1016/j.ymben.2016.06.008
- Nowruz, K., Elkamel, A., Scharer, J. M., Cossar, D., and Moo-Young, M. (2008). Development of a minimal defined medium for recombinant human interleukin-3 production by *Streptomyces lividans* 66. *Biotechnol. Bioeng.* 99, 214–222. doi: 10.1002/bit.21566
- Olano, C., Méndez, C., and Salas, J. A. (2009). Antitumor compounds from marine actinomycetes. *Mar. Drugs* 7, 210–248. doi: 10.3390/md7020210
- Pollack, J. K., Li, Z. J., and Marten, M. R. (2008). Fungal mycelia show lag time before re-growth on endogenous carbon. *Biotechnol. Bioeng.* 100, 458–465. doi: 10.1002/bit.21779
- Probst, C., Grünberger, A., Braun, N., Helfrich, S., Nöh, K., Wiechert, W., et al. (2015). Rapid inoculation of single bacteria into parallel picoliter fermentation chambers. *Anal. Methods* 7, 91–98. doi: 10.1039/C4AY02257B
- Radek, A., Tenhaef, N., Müller, M.-F., Brüsseler, C., Polen, T., Wiechert, W., et al. (2017). Miniaturized and automated adaptive laboratory evolution: evolving *Corynebacterium glutamicum* towards an improved D-Xylose utilization. *Bioresour. Technol.* 245(Pt B), 1377–1385.
- Rebets, Y., Kormanec, J., Lutzhetzky, A., Bernaerts, K., and Anné, J. (2016). “Cloning and expression of metagenomic DNA in *Streptomyces lividans* and subsequent fermentation for optimized production,” in *Metagenomics Methods and Protocols*, ed. R. Daniel (Berlin: Springer), 850–858.
- Reichl, U., Buschulte, T. K., and Gilles, E. D. (1990a). Study of the early growth and branching of *Streptomyces tendae* by means of an image processing system. *J. Microsc.* 158(Pt 1), 55–62.
- Reichl, U., Yang, H., Gilles, E.-D., and Wolf, H. (1990b). An improved method for measuring the interseptal spacing in hyphae of *Streptomyces tendae* by fluorescence microscopy coupled with image processing. *FEMS Microbiol. Lett.* 67, 207–210. doi: 10.1111/j.1574-6968.1990.tb13864.x
- Reichl, U., King, R., and Gilles, E. D. (1992). Effect of temperature and medium composition on mycelial growth of *Streptomyces tendae* in submerged culture. *J. Basic Microbiol.* 32, 193–200. doi: 10.1002/jobm.3620320308
- Rückert, C., Albersmeier, A., Busche, T., Jaenicke, S., Winkler, A., and Friðjónsson, ÖH. (2015). Complete genome sequence of *Streptomyces lividans* TK24. *J. Biotechnol.* 199, 21–22. doi: 10.1016/j.jbiotec.2015.02.004
- Sachs, C. C., Koepff, J., Wiechert, W., Grünberger, A., and Nöh, K. (2018). *Mycelyso: Analysis of Streptomyces Mycelium Live Cell Imaging*. Available at: <https://github.com/modsim/mycelysy>
- Schlumpert, S., Flärdh, K., and Buttner, M. (2016). Fluorescence time-lapse imaging of the complete *S. venezuelae* life cycle using a microfluidic device. *J. Vis. Exp.* 108:53863. doi: 10.3791/53863
- Sevillano, L., Vijgenboom, E., van Wezel, G. P., Díaz, M., and Santamaría, R. I. (2016). New approaches to achieve high level enzyme production in

- Streptomyces lividans*. *Microb. Cell Fact.* 15, 15–28. doi: 10.1186/s12934-016-0425-7
- Solopova, A., van Gestel, J., Weissing, F. J., Bachmann, H., Teusink, B., Kok, J., et al. (2014). Bet-hedging during bacterial diauxic shift. *Proc. Natl. Acad. Sci. U.S.A.* 111, 7427–7432. doi: 10.1073/pnas.1320063111
- Spohr, A., Dam-Mikkelsen, C., Carlsen, M., Nielsen, J., and Villadsen, J. (1998). On-line study of fungal morphology during submerged growth in a small flow-through cell. *Biotechnol. Bioeng.* 58, 541–553. doi: 10.1002/(SICI)1097-0290(19980605)58:5
- Unthan, S., Grünberger, A., van Ooyen, J., Gatgens, J., Heinrich, J., Paczia, N., et al. (2014). Beyond growth rate 0.6: what drives *Corynebacterium glutamicum* to higher growth rates in defined medium. *Biotechnol. Bioeng.* 111, 359–371. doi: 10.1002/bit.25103
- van Dissel, D., Claessen, D., Roth, M., and van Wezel, G. P. (2015). A novel locus for mycelial aggregation forms a gateway to improved *Streptomyces* cell factories. *Microb. Cell Fact.* 14:44. doi: 10.1186/s12934-015-0224-6
- van Dissel, D., Claessen, D., and van Wezel, G. P. (2014). Morphogenesis of *Streptomyces* in submerged cultures. *Adv. Appl. Microbiol.* 89, 1–45. doi: 10.1016/B978-0-12-800259-9.00001-9
- van Wezel, G. P., Krabben, P., Traag, B. A., Keijser, B. J. F., Kerste, R., Vijgenboom, E., et al. (2006). Unlocking *Streptomyces* spp. for use as sustainable industrial production platforms by morphological engineering. *Appl. Environ. Microbiol.* 72, 5283–5288. doi: 10.1128/AEM.00808-06
- Walisko, R., Moench-Tegeder, J., Blotenberg, J., Wucherpfennig, T., and Krull, R. (2015). The taming of the shrew—controlling the morphology of filamentous eukaryotic and prokaryotic microorganisms. *Adv. Biochem. Eng. Biotechnol.* 149, 1–27. doi: 10.1007/10_2015_322
- Wang, Y., Cobb, R. E., and Zhao, H. (2016). High-efficiency genome editing of *Streptomyces* species by an engineered CRISPR/Cas system. *Methods Enzymol.* 575, 271–284. doi: 10.1016/bs.mie.2016.03.014
- Willemse, J., Ruban-Ośmiałowska, B., Widdick, D., Celler, K., Hutchings, M. I., van Wezel, G. P., et al. (2012). Dynamic localization of Tat protein transport machinery components in *Streptomyces coelicolor*. *J. Bacteriol.* 194, 6272–6281. doi: 10.1128/JB.01425-12
- Xu, Y., and Vetsigian, K. (2017). Phenotypic variability and community interactions of germinating *Streptomyces* spores. *Sci. Rep.* 7:699. doi: 10.1038/s41598-017-00792-7
- Yang, H., King, R., Reichl, U., and Gilles, E. D. (1992). Mathematical model for apical growth, septation, and branching of mycelial microorganisms. *Biotechnol. Bioeng.* 39, 49–58. doi: 10.1002/bit.260390109
- Zacchetti, B., Willemse, J., Recter, B., van Dissel, D., van Wezel, G. P., Wosten, H. A. B., et al. (2016). Aggregation of germlings is a major contributing factor towards mycelial heterogeneity of *Streptomyces*. *Sci. Rep.* 6:27045. doi: 10.1038/srep27045

Conflict of Interest Statement: The authors declare that the research was conducted in the absence of any commercial or financial relationships that could be construed as a potential conflict of interest.

Copyright © 2018 Koepff, Sachs, Wiechert, Kohlheyer, Nöh, Oldiges and Grünberger. This is an open-access article distributed under the terms of the Creative Commons Attribution License (CC BY). The use, distribution or reproduction in other forums is permitted, provided the original author(s) and the copyright owner(s) are credited and that the original publication in this journal is cited, in accordance with accepted academic practice. No use, distribution or reproduction is permitted which does not comply with these terms.



Secondary Metabolites Produced during the Germination of *Streptomyces coelicolor*

Matouš Čihák¹, Zdeněk Kameník², Klára Šmídová^{1,2}, Natalie Bergman³, Oldřich Benada^{2,3}, Olga Kofroňová², Kateřina Petříčková¹ and Jan Bobek^{1,2,3*}

¹ First Faculty of Medicine, Institute of Immunology and Microbiology, Charles University, Prague, Czechia, ² Institute of Microbiology, The Czech Academy of Sciences, Prague, Czechia, ³ Chemistry Department, Faculty of Science, J. E. Purkinje University, Ústí nad Labem, Czechia

OPEN ACCESS

Edited by:

Dirk Tischler,
Freiburg University of Mining and
Technology, Germany

Reviewed by:

Dennis Claessen,
Leiden University, Netherlands
Yinhua Lu,
Shanghai Institutes for Biological
Sciences (CAS), China

*Correspondence:

Jan Bobek
jan.bobek@lf1.cuni.cz

Specialty section:

This article was submitted to
Microbial Physiology and Metabolism,
a section of the journal
Frontiers in Microbiology

Received: 29 August 2017

Accepted: 30 November 2017

Published: 13 December 2017

Citation:

Čihák M, Kameník Z, Šmídová K,
Bergman N, Benada O, Kofroňová O,
Petříčková K and Bobek J (2017)
Secondary Metabolites Produced
during the Germination of
Streptomyces coelicolor.
Front. Microbiol. 8:2495.
doi: 10.3389/fmicb.2017.02495

Spore awakening is a series of actions that starts with purely physical processes and continues via the launching of gene expression and metabolic activities, eventually achieving a vegetative phase of growth. In spore-forming microorganisms, the germination process is controlled by intra- and inter-species communication. However, in the *Streptomyces* clade, which is capable of developing a plethora of valuable compounds, the chemical signals produced during germination have not been systematically studied before. Our previously published data revealed that several secondary metabolite biosynthetic genes are expressed during germination. Therefore, we focus here on the secondary metabolite production during this developmental stage. Using high-performance liquid chromatography-mass spectrometry, we found that the sesquiterpenoid antibiotic albaflavenone, the polyketide germicidin A, and chalcone are produced during germination of the model streptomycete, *S. coelicolor*. Interestingly, the last two compounds revealed an inhibitory effect on the germination process. The secondary metabolites originating from the early stage of microbial growth may coordinate the development of the producer (*quorum sensing*) and/or play a role in competitive microflora repression (*quorum quenching*) in their nature environments.

Keywords: spore germination, *Streptomyces*, cell signaling, secondary metabolism, albaflavenone, germicidin, chalcone

INTRODUCTION

A large variety of compounds is produced by various microorganisms by means of specialized biosynthetic pathways. Although the special (or secondary) metabolites (Hopwood, 2007; Baltz, 2008; van Keulen and Dyson, 2014) are not essential for growth and reproduction, they often provide the producing organism with a bioactive role (Keller et al., 2005). Reaching further than a cell itself physically can, the small diffusible molecules may give an advantage to its producer by effectively adapting to extracellular conditions to some degree. They may provide defense (or attack), competition, signaling, or interspecies interactions, depending on the environmental cues, thus increasing the likelihood of survival in an inhospitable environment (Brachmann et al., 2013; Martinez et al., 2017). The bioactivity of the small molecules is mostly achieved by affecting transcription in receiving cells (Camilli and Bassler, 2006).

Secondary metabolism is of special interest in *Streptomyces*, a clade of multicellular bacteria that occupies a high position in the developmental hierarchy of bacteria due to their advanced morphology and physiology. Streptomycetes have evolved a plethora of biosynthetic pathways to produce various secondary metabolites, especially signal molecules (see below), or antibiotics (van Keulen and Dyson, 2014). These compounds provide the organism with a competitive advantage, protection from unfavorable living conditions and/or facilitate interspecies interactions (Maxwell et al., 1989).

The genes for the biosynthesis of streptomycete secondary metabolites are mostly clustered and their expression is highly regulated (Bentley et al., 2002; Tanaka et al., 2013). The model *S. coelicolor* possesses the best annotated genome that encodes biosynthetic pathways for more than 20 secondary metabolites (Bentley et al., 2002). The chemical structure has so far been elucidated in less than 30 percent of the compounds, belonging to the following groups of natural substances: polyketides, pyrones, peptides, siderophores, γ -butyrolactones, butenolides, furans, terpenoids, fatty acids, oligopyrroles, and deoxysugars (van Keulen and Dyson, 2014). The remaining 70 percent are called “cryptic compounds” as they are not produced at standard laboratory conditions (Bentley et al., 2002; Ikeda et al., 2003; Ohnishi et al., 2008; Tanaka et al., 2013; van Keulen and Dyson, 2014). To activate these cryptic pathways, streptomycetes are cultivated under non-standard physical and nutritional conditions or co-cultured with other microorganisms (Wakefield et al., 2017). Genetic manipulations within the genes (Luo et al., 2013) or the transfer of the whole biosynthetic gene cluster into a heterologous producer (Kalan et al., 2013; Tanaka et al., 2013) are also commonly used strategies. The successful activation of the biosynthetic pathways often leads to biosynthesis of previously unknown compounds (Ikeda et al., 2003; Ohnishi et al., 2008; Gomez-Escribano et al., 2012; Tanaka et al., 2013). For example, a polyketide alkaloid, coelimycin P1 (so-called yellow pigment), is produced from the *cpk* cryptic gene cluster in *S. coelicolor* (Gomez-Escribano et al., 2012).

The complicated development of streptomycetes requires highly sophisticated control mechanisms mediated by multiple molecules linked to signaling cascades (Kelemen and Buttner, 1998; Claessen et al., 2006; Gao et al., 2012). A widely studied signaling system is *quorum sensing*, in which stimuli are spread within a population and induce appropriate responses (Phelan et al., 2011). Based on the signal assessment, the organism can adapt to its environment and coordinate further development in response to local population densities (Waters and Bassler, 2005). One of the assumptions made in this work is that cellular signaling is also employed in spore germination (see below). However, the nature of the signaling in this developmental phase remains unclear, as do the chemical characteristics and the possible regulatory effect of the produced substances.

Streptomyces undergo a cellular differentiation that resembles the fungal life cycle (Seipke et al., 2012). Their growth starts with germinating spores that develop into a vegetative mycelium of branching hyphae. Subsequent development of aerial hyphae is considered to be a cell response to nutrient depletion; most of the secondary metabolites are formed at this developmental

stage (Sello and Buttner, 2008; Seipke et al., 2012). The aerial hyphae are dissected into chains of uninucleoid spores. Spores are subjected to maturation which ensures their survival in unfavorable conditions and allows them to spread into new niches.

The dormant state of spores is characterized by limited metabolic activity or its complete stagnation (McCormick and Flardh, 2012). Subsequent germination is the spore's transition into a metabolically active vegetative phase. Reactivation of the dormant exospore takes place in an aqueous environment. In addition to energy sources (e.g., trehalose) and various nutrients (Ranade and Vining, 1993), the dormant spores of streptomycetes also contain transcriptome which is a remnant of sporulation and spore maturation (Mikulik et al., 2002). The residual pool of mRNA appears to be necessary for the initial germination phase, serving as a template for the early synthesis of proteins, such as chaperones and hydrolases. Whereas chaperones are indispensable in the re-activation of present proteins upon their release from the trehalose milieu (Bobek et al., 2017), hydrolases reconstitute the thick hydrophobic spore cell wall (Bobek et al., 2004; Haiser et al., 2009).

Further development requires the re-activation of the transcriptional apparatus (Paleckova et al., 2006; Mikulik et al., 2008, 2011) controlled by the activity of a set of sigma factors, whose expression takes place from the very beginning of the process (Bobek et al., 2014; Strakova et al., 2014). Genome-wide expression data revealed that the activity of most metabolic pathways is stabilized after the first DNA replication that occurs between 120 and 150 min of germination of *S. coelicolor* (Bobek et al., 2014). After this period, morphologically observable changes, like the first germ tube emerging from the spore, occur (Kelemen and Buttner, 1998; Claessen et al., 2006; Ohnishi et al., 2008).

In the case of non-activated spores, it was found that about 10–20% of spores do not germinate even under optimal incubation conditions (Yoshida and Kobayashi, 1994). Sole spores of *S. viridochromogenes* have been shown to germinate more slowly than in the dense population (Xu and Vetsigian, 2017). This indicates an existence of germination activator produced into the medium. On the other hand, the extract from the *S. viridochromogenes* supernatant has been shown to inhibit the germination of unactivated spores when added prior to incubation (Hirsch and Ensign, 1976a). The inhibitor present was later isolated (along with other congeners) and described as germicidin A (Petersen et al., 1993; Aoki et al., 2011; Ma et al., 2017). The launch of germination within a spore population is stochastic, as was shown not only in streptomycetes (Xu and Vetsigian, 2017) but also in other spore-forming bacteria (van Vliet, 2015). The probability of germination within a population differs between different streptomycete strains; *S. viridochromogenes* and *S. granaticolor* exhibit fast and robust germination whereas *S. coelicolor* and *S. venezuelae* show more complex behavior with a fraction of germings that stop growing soon after germination (Mikulik et al., 1977; Bobek et al., 2004; Xu and Vetsigian, 2017). Activity of early released compounds, germination activators and inhibitors, may affect the stochasticity of germination in order to adapt the germination strategy to

environmental conditions (Petersen et al., 1993; Aoki et al., 2007, 2011; Ma et al., 2017). Since it is considered to be non-productive (Seipke et al., 2012), the initial developmental phase has hitherto not been given sufficient attention. It is nevertheless apparent from the genome-wide expression analysis of *S. coelicolor*'s germinating spores (germlings) performed by Strakova (Strakova et al., 2013), that 163 genes involved in the biosynthesis of secondary metabolites are transcribed during germination (including those cryptic). It is for this reason that we chose to focus on the biosynthetic activities of the germinating spores of *S. coelicolor* in this article. Secondary metabolites produced in this phase would possibly function as germinative signals in the frame of intercellular communication (Rutherford and Bassler, 2012; Brachmann et al., 2013) or may suppress competing microflora.

MATERIALS AND METHODS

Preparation of *Streptomyces* Spores

Streptomyces coelicolor M145 was cultivated on cellophane discs on solid agar plates (0.4% yeast extract, 1% malt extract, 0.4% glucose, 2.5% bacterial agar, pH 7.2) at 28°C for 14 days. Harvested dormant spores were filtered through cotton wool and used to screen for associated secondary metabolites. Spores mixed with 20% glycerol were stored frozen at −20°C.

Germination and Microbial Growth

Spores were washed twice in 10 mL sterile distilled water and resuspended in 50 mL NMMP (Kieser et al., 2000), R3 (Shima et al., 1996), or AM (Bobek et al., 2004) liquid medium to a final spore concentration 10^8 mL^{−1}. Glucose, glycerol, or mannitol was used as a carbon source. For boosting synchronicity of the population, spores were incubated for 10 min at 50°C, followed by 6-h germination at 37°C (Hirsch and Ensign, 1976a; Kieser et al., 2000) before screening for produced secondary metabolites.

To prepare samples from the stationary phase of growth, *S. coelicolor* was further cultivated 48 h at 29°C in the same medium. The grown mycelium or supernatant was then used in the screening for produced secondary metabolites.

Solid Phase Extraction of Secondary Metabolites

Secondary metabolites were taken from the culture supernatants extracted using ethyl acetate (Rajan and Kannabiran, 2014), QuEChERS (Schenck and Hobbs, 2004), or solid phase extraction (Kamenik et al., 2010), which was found to be the most suitable and was carried out as follows. An Oasis HLB 3cc 60 mg cartridge (hydrophilic-lipophilic balanced sorbent, Waters, USA) was conditioned with 3 mL methanol (LC-MS grade, Biosolve, Netherlands), equilibrated with 3 mL water (prepared using Milli-Q water purifier, Millipore, USA) and then 3 mL culture supernatant (pH adjusted to 3 with formic acid, 98–100%, Merck, Germany) was loaded. Subsequently, the cartridge was washed with 3 mL water and absorbed substances were eluted with 1.5 mL methanol. The eluent was evaporated to dryness (Concentrator Plus, 2013 model, Eppendorf), reconstituted in 200 µL 50% methanol and centrifuged at $12,000 \times g$ for 5 min.

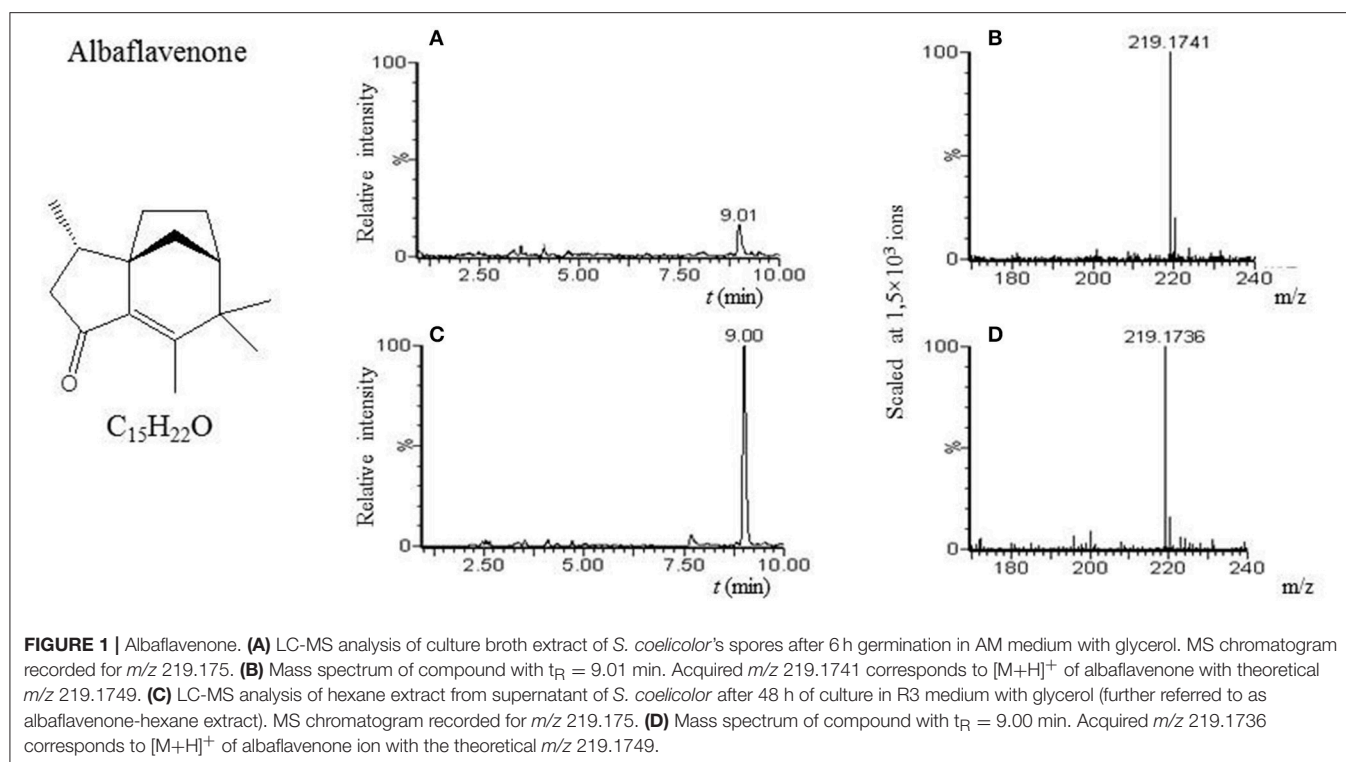
LC-MS Analyses

LC-MS analyses were performed on the Acquity UPLC system with 2996 PDA detection system (194–600 nm) connected to LCT premier XE time-of-flight mass spectrometer (Waters, USA). Five µL of sample was loaded onto the Acquity UPLC BEH C18 LC column (50 mm × 2.1 mm I.D., particle size 1.7 µm, Waters) kept at 40°C and eluted with a two-component mobile phase, A and B, consisting of 0.1% formic acid and acetonitrile, respectively, at the flow rate of 0.4 mL min^{−1}. The analyses were performed under a linear gradient program (min/%B) 0/5; 1.5/5; 15/70; 18/99 followed by a 1.0-min column clean-up (99% B) and 1.5-min equilibration (5% B). The mass spectrometer operated in the positive “W” mode with capillary voltage set at +2,800 V, cone voltage +40 V, desolvation gas temperature, 350°C; ion source block temperature, 120°C; cone gas flow, 50 L h^{−1}; desolvation gas flow, 800 L h^{−1}; scan time of 0.15 s; inter-scan delay of 0.01 s. The mass accuracy was kept below 6 ppm using lock spray technology with leucine enkephalin as the reference compound (2 ng µL^{−1}, 5 µL min^{−1}). MS chromatograms were extracted for [M+H]⁺ ions with the tolerance window of 0.03 Da, smoothed with mean smoothing method (window size; 4 scans, number of smooths, 2). The data were processed by MassLynx V4.1 (Waters).

Bioactivity Assays

Although albaflavenone is not commercially available, we have verified its presence using LC-MS in the hexane extract from the supernatant after 48 h of *S. coelicolor*'s growth in R3 medium with glycerol as the carbon source. Cells were centrifuged for 5 min ($7,000 \times g$). The supernatant was extracted three times with 300 mL of *n*-hexane (Lach-Ner, Prague, Czech Republic). The cells were washed in distilled water and mycelial products were extracted with 200 mL of *n*-hexane. Cells were removed by filtration. After separation of the phases, the *n*-hexane layers were pooled (below called as albaflavenone-hexane extract, Figure 1B).

Germicidin A standard was purchased from Cayman Pharma (the Czech Republic), chalcone's standard was obtained from Sigma-Aldrich (Merck, Germany). Dimethylsulfoxid (DMSO) was purchased from Lach-Ner (Czech Republic). On a six-sector culture microtiter plate, ONA medium (1.4% Oxoid nutrient agar, pH 7.2; Kieser et al., 2000) with a linear concentration gradient of germicidin A 0–8 µg mL^{−1} (standard dissolved in sterile distilled water) or chalcone 0–8 µg mL^{−1} (standard dissolved in DMSO), or the albaflavenone-hexane extract (concentration unknown) was poured into three sectors as follows. Pure ONA medium was poured into an inclined plate and allowed to solidify to form a wedge; the plate was then placed horizontally and ONA medium containing selected compound in concentration 8 µg mL^{−1} was poured to form a complementary wedge. The remaining three sectors were filled with either pure ONA medium for control cultivation respective to germicidin A, or ONA medium with DMSO for control cultivation respective to chalcone, or ONA medium with hexane for control cultivation respective to albaflavenone. 10^5 spores were spread on each sector and incubated 48 h at 29°C. Number of colony-forming units (CFU) was assessed and compared.



A Dehydrogenase Activity Test

Two milliliter of the alabaflavenone-hexane extract was mixed with 5 mL R3 medium with glycerol and used for 6 h germination of 5×10^6 spores. A negative control culture was performed in 5 mL R3 medium with glycerol with 2 mL pure hexane. The dehydrogenase activity test (as described in Burdock et al., 2011) was used to measure metabolic activity of germinating spores by means of triphenyl tetrazolium chloride (TTC). After the germination course, cells were incubated in the presence of TTC and an electron-donating substrate for 1 h. Rising triphenyl formazan (TF) was extracted using ethanol and its concentration was determined colorimetrically by measuring the optical density at wavelength of 484 nm. The absorbances were compared between the tested and negative control samples.

Scanning Electron Microscopy

Streptomyces spores were fixed with 3% glutaraldehyde overnight at 4°C. The fixed spores were extensively washed and then allowed to sediment at 4°C overnight onto circular coverslips treated with poly-L-lysine. The coverslips with attached spores were dehydrated through an alcohol series followed by absolute acetone and critical point dried from liquid CO₂ in a K850 Critical Point Dryer (Quorum Technologies Ltd, Ringmer, UK). The dried samples were sputter-coated with 3 nm of platinum in a Q150T Turbo-Pumped Sputter Coater (Quorum Technologies Ltd, Ringmer, UK). The final samples were examined in a FEI Nova NanoSEM scanning electron microscope (FEI, Brno, Czech Republic) at 5 kV using CBS and TLD detectors. Beam deceleration mode of scanning electron microscope was used in some cases for minimization of charging artifacts.

RESULTS

In Silico Analysis of the Expressed Secondary Metabolite Biosynthetic Genes during Germination of *S. coelicolor*

Genes that are expressed in the consecutive time points of germination have been reported by Strakova (Strakova et al., 2013). From their dataset we selected genes whose products are involved in the biosynthesis of secondary metabolites by *S. coelicolor*, according to the StrepDB database (<http://strepdb.streptomyces.org.uk>), where the annotated *S. coelicolor* genes are categorized into metabolic groups. We updated the list of secondary metabolites with regard to newly published findings (Zhao et al., 2009; van Keulen and Dyson, 2014). The resulting list of genes is summarized in Table 1. Predicted secondary metabolites, whose respective genes are expressed during germination, include polyketides, pyrones, peptides, siderophores, terpenoids, oligopyrroles, and fatty acids.

Secondary Metabolites Produced by *S. coelicolor* during Germination and/or in the Stationary Phase

The fact that genes whose products are involved in the secondary metabolite biosynthesis were transcribed during germination encouraged us to investigate whether germinating spores produce respective compounds up to the 6th hour of their development. For this purpose, we performed an LC-MS analysis of the culture supernatants. In order to ensure that any detected compound is synthesized *de novo* during

TABLE 1 | An overview of biosynthetic genes expressed during germination, according to Strakova et al. (2013).

Secondary metabolites	Biosynthetic (SCO) genes expressed during germination
Actinorhodin and related congeners	0331; 3978; 4280; 5072-5079; 5081-5086; 5088-5090
Albaflavenone	5223
Calcium-dependent antibiotic (CDA)	3210; 3212; 3214; 3220-3221; 3223; 3225; 3227; 3228; 3230-3232; 3234-3237; 3239; 3241-3242; 3246; 3249
Coellobactin	7682-7684; 7686-7687; 7689-7691
Coellichelin	0490-0498
Coelmycin P1	6273-6275; 6277-6287
Desferrioxamines B, E, G ₁ a D ₁	2783-2784
Eicosapentaenoic acid (EPA)	0124-0125
Flaviolin, THN	1206
Geosmin	6073
Hopanoids, ATBH	6759-6763; 6765; 6767; 6769; 6771
Isorenieratene, β -carotene	0187-0191
Streptorubin B, undecylprodigiosin	0126-0127; 5877-5878; 5881; 5891-5894; 5898
Triketid pyrones	7670-7671
Tw95a	5314; 5318; 5320

TABLE 2 | Secondary metabolites detected in the stationary phase of growth.

Secondary metabolite	Medium (carbon source)	Molecular formula	Theoretical mass (m/z)	Acquired mass (m/z)	Mass error (ppm)
γ - actinorhodin	R3, AM, NMMP (glycerol, mannitol, glucose)	C ₃₂ H ₂₂ O ₁₄	631.1090	631.1081	1.40
Actinorhodinic acid	R3, AM, NMMP (glycerol, mannitol, glucose)	C ₃₂ H ₂₆ O ₁₆	667.1300	667.1289	1.60
Albaflavenone	R3 (glycerol)	C ₁₅ H ₂₂ O	219.1736	219.1749	5.90
CDA	R3 (glycerol)	C ₆₇ H ₇₈ N ₁₄ O ₂₆	1495.5290	1495.5292	0.10
Coelmycin P1	R3 (glycerol)	C ₁₇ H ₂₀ N ₂ O ₄ S	349.1222	349.1229	2.00
Chalcone	R3 (glycerol/mannitol)	C ₁₅ H ₁₂ O	209.0960	209.0966	2.90
Desferrioxamine B	R3 (glycerol/mannitol) AM (glycerol/mannitol)	C ₂₅ H ₄₈ N ₆ O ₈	561.3625	561.3612	2.30
Desferrioxamine D ₁	AM (glucose/mannitol)	C ₂₇ H ₅₀ N ₆ O ₉	603.3711	603.3718	1.20
Desferrioxamine E	R3 (glycerol/mannitol) AM (glucose/glycerol) NMMP (glucose/mannitol)	C ₂₇ H ₄₈ N ₆ O ₉	601.3561	601.3561	0.00
Desferrioxamine G ₁	AM (glucose/glycerol)	C ₂₇ H ₅₀ N ₆ O ₁₀	619.3677	619.3667	1.60
Germicidin A	R3 (glycerol/mannitol) AM (glucose/mannitol)	C ₁₁ H ₁₆ O ₃	197.1170	197.1178	4.10
Germicidin B	R3 (glycerol/mannitol) NMMP (glucose/mannitol)	C ₁₀ H ₁₄ O ₃	183.1016	183.1021	2.73
Kalafungin	R3 (mannitol)	C ₁₆ H ₁₂ O ₆	301.0709	301.0714	1.00
Streptorubin B	R3 (glycerol/mannitol) AM (glucose/glycerol)	C ₂₅ H ₃₃ N ₃ O	392.2696	392.2702	1.50
Undecylprodigiosin	R3 (glycerol/mannitol) AM (glucose/glycerol)	C ₂₅ H ₃₅ N ₃ O	394.2866	394.2858	2.00

germination, we included dormant spores (non-activated) as negative control samples in the analysis. As a positive control that tests effectiveness of our detection method, samples from the sporulation phase were included too. The compounds detected only in the sporulation phase (after 48 h of cultivation) but absent from the germination are listed in **Table 2**.

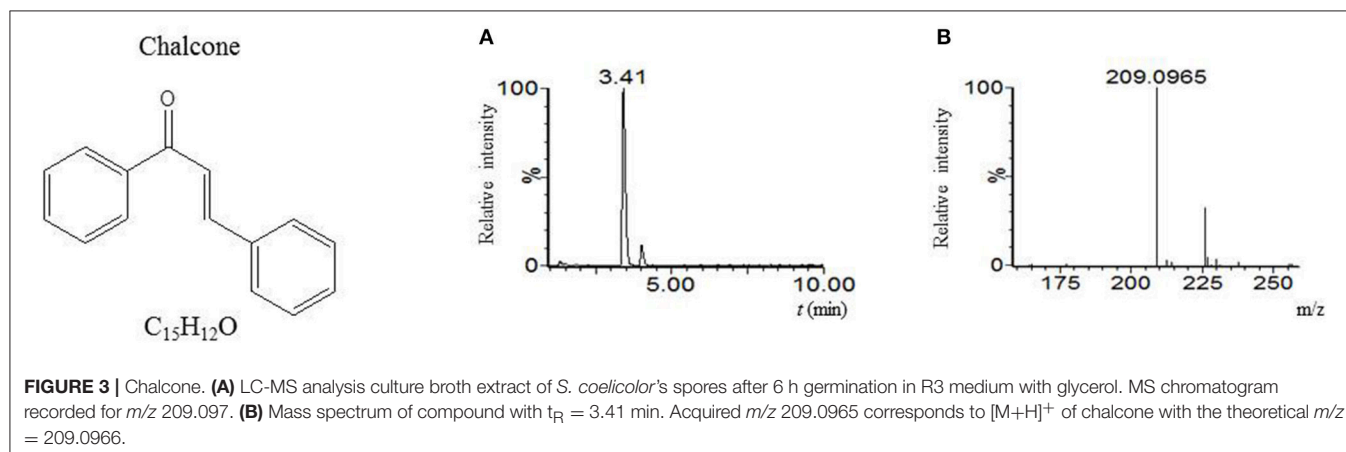
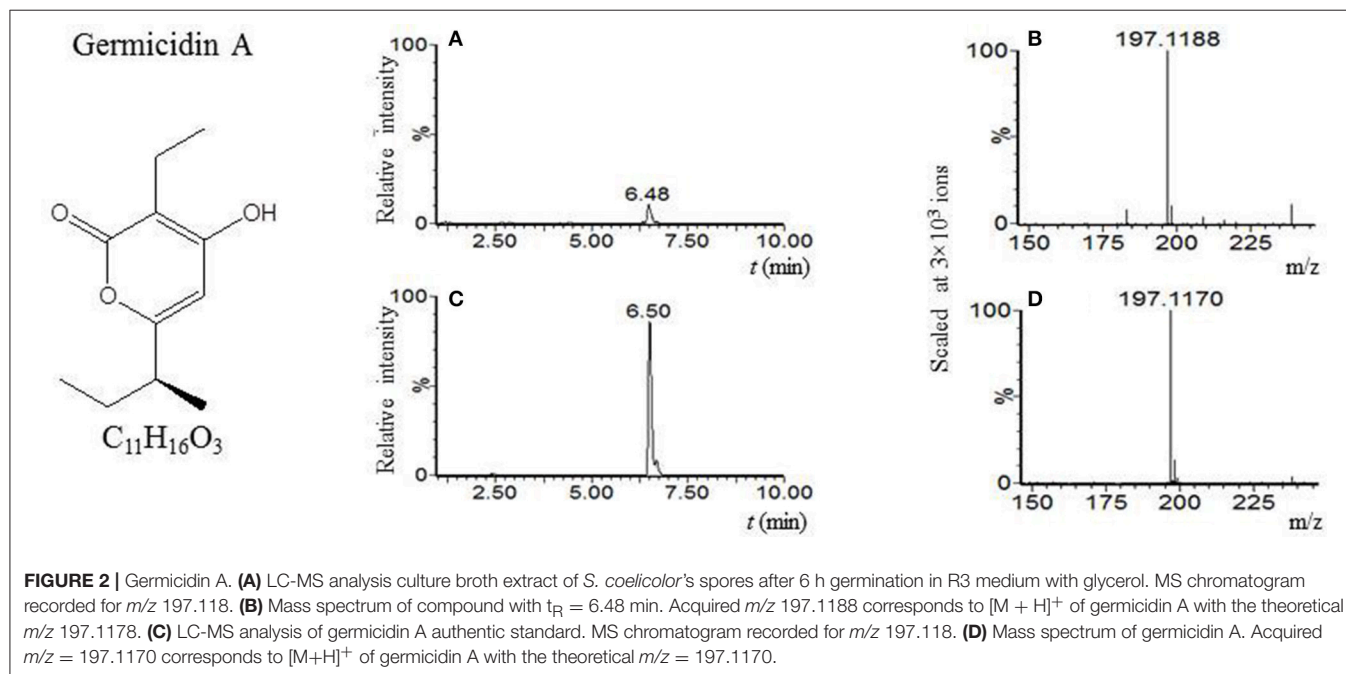
Our LC-MS measurements revealed, however, that the *S. coelicolor*'s germlings produce three different compounds with masses corresponding to the sesquiterpenoid antibiotic albaflavenone, the polyketide germicidin A, and chalcone (**Table 3**; **Figures 1–3**, respectively). Furthermore, the identity of germicidin A was confirmed by comparing the actual retention time with the original standard obtained from Cayman Pharma (**Figure 2**).

Actinorhodin Production

Actinorhodin compounds (actinorhodinic acid and γ -actinorhodin) were detected in both dormant and germinating spores, as well as in samples from the stationary phase of growth (**Table 2**). Streptomycetes produced these compounds after 48 h of cultivation in R3, AM, and NMMP medium, regardless of carbon source (glucose, glycerol, or mannitol). Although the suspensions of dormant spores were washed in distilled water, we found that dormant spores also contained these blue pigments. We also found actinorhodinic acid and γ -actinorhodin in the cell-free supernatant after spore germination in AM medium. All supernatants containing the blue pigments also exhibited a pH-dependent color change.

TABLE 3 | Secondary metabolites produced during germination.

Secondary metabolite	Medium (carbon source)	Molecular formula	Theoretical mass (m/z)	Acquired mass (m/z)	Mass error (ppm)
Albaflavone	AM (glycerol)	$C_{15}H_{22}O$	219.1741	219.1749	3.70
Germicidin A	R3 (glycerol/mannitol) AM (glucose/mannitol)	$C_{11}H_{16}O_3$	197.1188	197.1178	5.10
Chalcone	R3 (glycerol/mannitol)	$C_{15}H_{12}O$	209.0965	209.0966	0.50



pH-Dependent Biosynthetic Activity of Germlings

Biosynthesis of albaflavone involves the activity of cytochrome P450 (CYP170A1) which, depending on pH, can either act as a monooxygenase (pH 7.0–8.2) or as a farnesene synthase (5.5–6.5) (Zhao et al., 2009). Whereas β -farnesene was not synthesized in cultures in R3, NMMP, and AM medium at pH 7.0–7.2, we showed that the germlings produce a substance corresponding to

albaflavone. To see whether β -farnesene is produced in more acidic conditions, we performed a germination experiment in R3 medium with glycerol at pH 6.0. Secondary metabolites were extracted by the solid phase extraction, followed by the LC-MS analysis. To compare, we used an extract after 6 h of cultivation at pH 7.2 without changing the other conditions. Although the direct production of β -farnesene was not found, it is clear from the total ionic and base peak chromatograms that under different

pH conditions *S. coelicolor* produces a different spectrum of substances (Figure 4). Further analysis was beyond the scope of this manuscript.

Biological Effects of Albaflavenone, Germicidin A, and Chalcone

Since albaflavenone was not commercially available, its possible effect on germination was tested using the albaflavenone-hexane extract (see Methods). A negative control, which contained pure hexane, was included in the experiment. No quantitative or phenotypic changes were observed in the tested conditions (Figure 5C). To verify this result, a dehydrogenase activity test was performed (Figure 5D). Metabolic activity of living cells that are present in the medium during germination was determined as a function of their dehydrogenase activity, proportional to the concentration of rising TF measured by the optical density at 484 nm (see Methods for details). The optical density increased in time during germination at the same rate in both tested and control samples; the albaflavenone-hexane extract created no observable effect.

The biological effect of the other two secondary metabolites on germination was examined using standards of germicidin A (Cayman Pharma) and chalcone (Sigma-Aldrich). Experiments were performed on six-section cultivation titration plates (Gama Group). Three fields in one column contained ONA medium with a gradient of tested compound (0–8 $\mu\text{g mL}^{-1}$) and pure medium without the tested substance was poured into the fields in the other column as negative controls. Results were evaluated in terms of the number of colony forming units (CFU) and phenotypic changes.

Germicidin A

Germicidin A clearly inhibited the germination of *S. coelicolor* from the concentration of 4 $\mu\text{g mL}^{-1}$ (Figure 5A). The average number of colony-forming units (germinating spores) was 20 on an ONA medium with the linear gradient of germicidin A at 4 $\mu\text{g mL}^{-1}$ and lower; 60 colonies were grown without germicidin A as a negative control. The tested colonies were of the same shape and size as their controls. Actinorhodin production was quantitatively the same.

Chalcone

Our initial experiments showed that chalcone suppressed germination of *S. coelicolor* in concentrations down to 8 $\mu\text{g mL}^{-1}$ on the solid medium (Figure 5B). The average number of CFU was 20 on a medium with a chalcone gradient (0–8 $\mu\text{g mL}^{-1}$), contrary to 70 colonies on the chalcone-free medium. The size of the colonies was inversely proportional to the chalcone concentrations; the colonies were significantly smaller compared to the negative control, suggesting a slower germination rate and/or vegetative growth. Moreover, in the presence of chalcone, actinorhodin was not produced throughout the whole cell cycle. The effect of chalcone was additionally examined in R3 liquid medium. Whereas the concentration 8 $\mu\text{g mL}^{-1}$ revealed to be subinhibitory, the chalcone concentration of 80 $\mu\text{g mL}^{-1}$ completely suppressed the development as could be seen in electronmicroscopic images taken from the germination course in the 4th and 6th hour of cultivation Figure 6. As could be seen in the image, the developing germ tubes disrupt in the presence of chalcone, leaving empty cell envelopes.

DISCUSSION

Although many secondary metabolites of streptomycetes have been discovered, they were most often isolated from the stationary phase of growth, i.e., in the context of the formation of aerial mycelium (Janecek et al., 1997; Kieser et al., 2000; van Keulen and Dyson, 2014). However, our *in silico* search within the gene expression data (Strakova et al., 2013; Bobek et al., 2014) revealed a number of genes (including those cryptic) responsible for the biosynthesis of secondary metabolites to be expressed during the course of *S. coelicolor*'s germination (see Table 1); especially genes responsible for the synthesis of desferrioxamines (sco2783–2784), gray spore pigment (sco5314, sco5318, sco5320), or yellow coelimycin P1 (sco6273–6276, sco6277–6287, so called *cpk* cryptic gene cluster) (Lahey et al., 1983; Gomez-Escribano et al., 2012). We therefore focused our work on whether germinating spores are capable of activating the respective biosynthetic pathways and producing any compound within the 6 h of germination.

Metabolites that could be bound to the spore surface or present in germination medium were identified by means of the LC-MS analysis. Simultaneously, the secondary metabolites produced during the sporulation phase and those associated with the dormant spores were also included in the analysis in order to state whether the compounds found in the samples from germlings were synthesized *de novo*. The cultivations were carried out in three different liquid media (R3, NMMP, and AM,

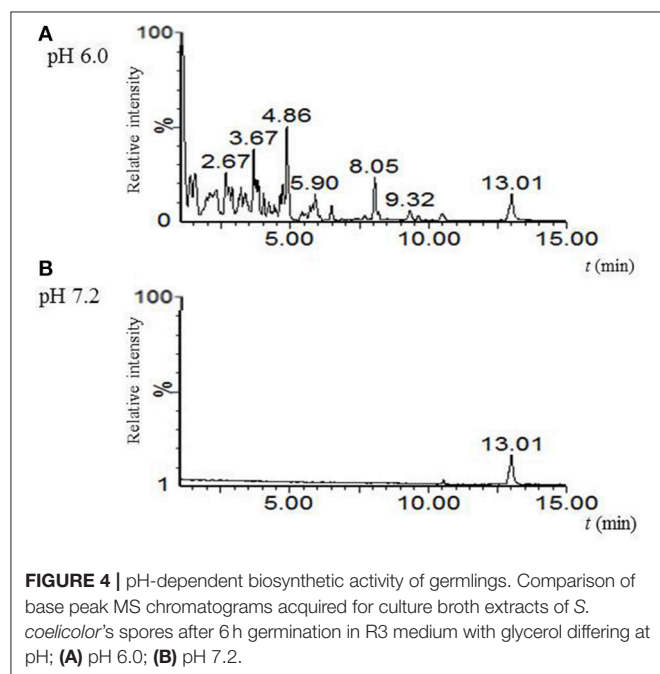
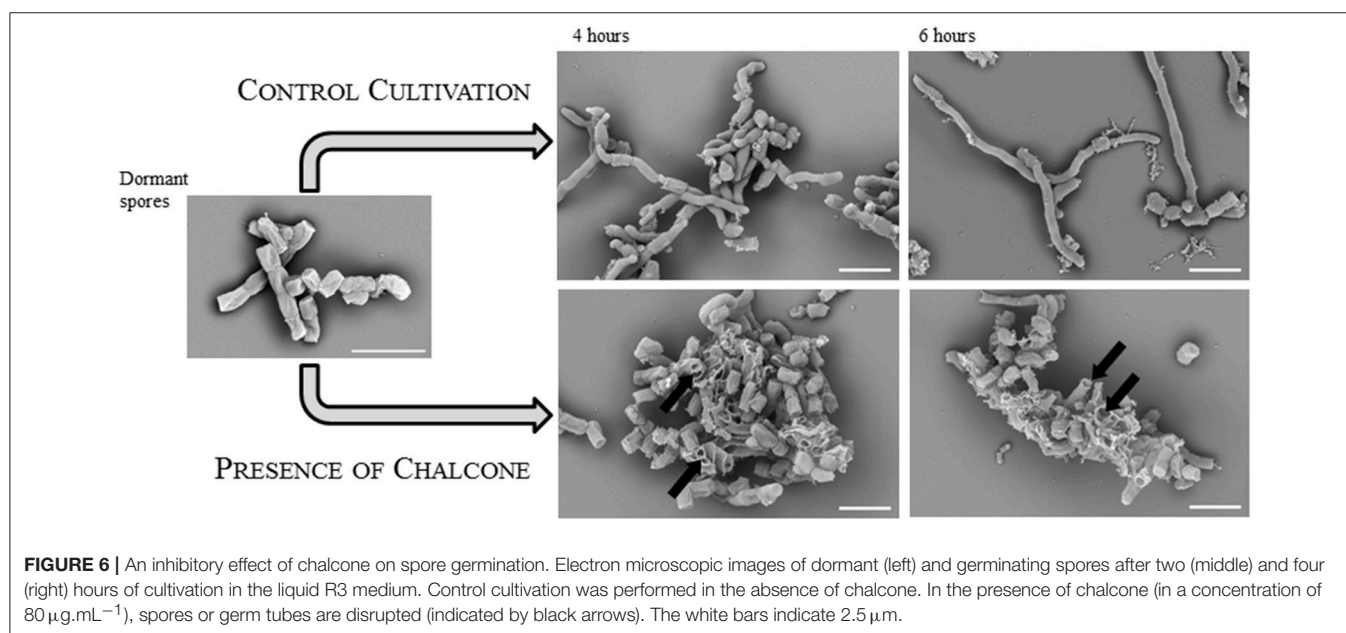
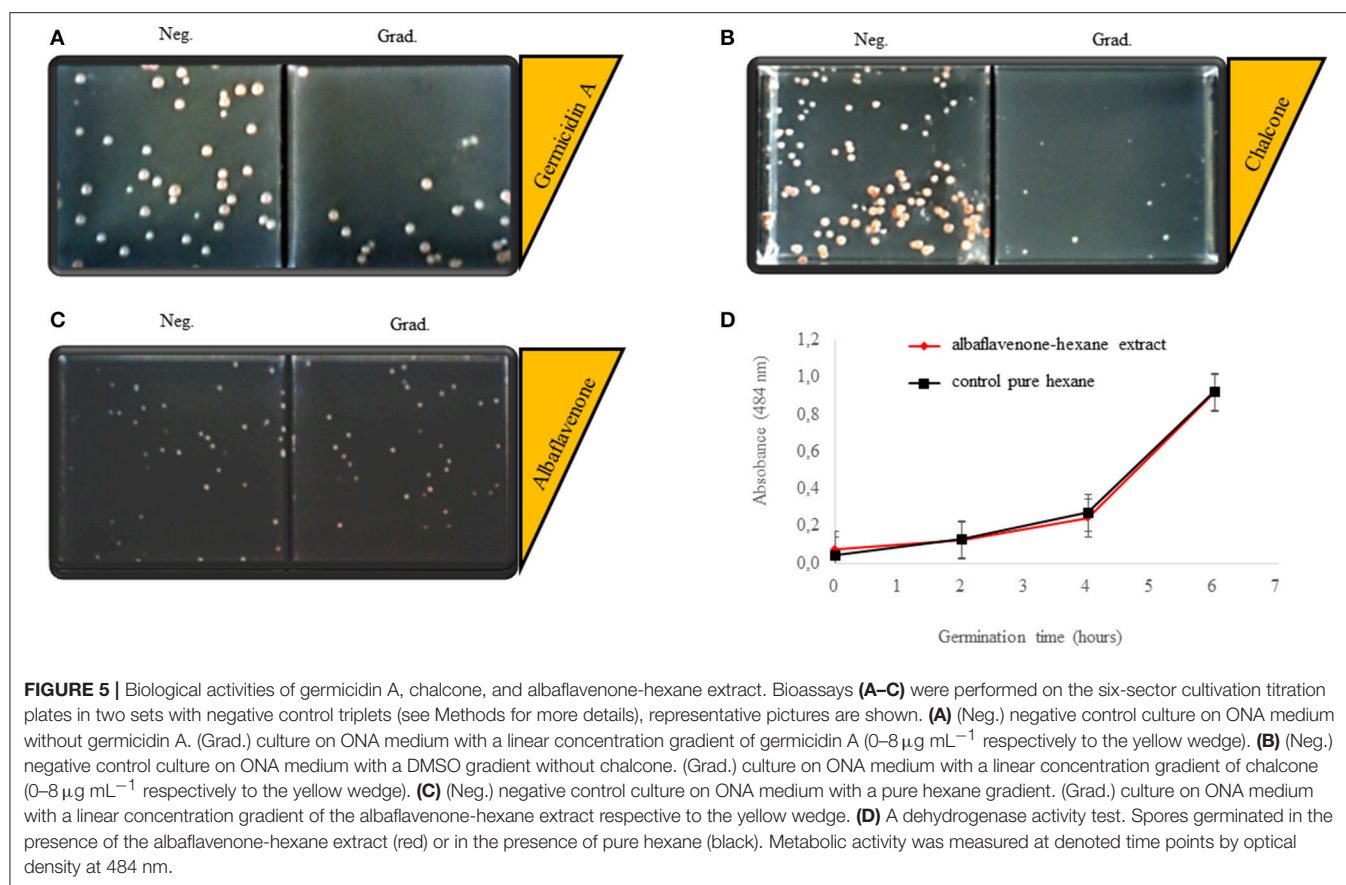


FIGURE 4 | pH-dependent biosynthetic activity of germlings. Comparison of base peak MS chromatograms acquired for culture broth extracts of *S. coelicolor*'s spores after 6 h germination in R3 medium with glycerol differing at pH: (A) pH 6.0; (B) pH 7.2.



see Methods). The nutritionally rich medium R3 was chosen for the capacity of *S. coelicolor* to produce a number of structurally distinct secondary metabolites in it, such as actinorhodin (Shima et al., 1996) or coelimycin P1 (Gomez-Escribano et al., 2012).

In contrast to the R3 medium, the minimal liquid medium NMMP, a poorer medium in which streptomycetes produce fewer secondary metabolites (Hodgson, 1982), was also used. The reason is that NMMP enables the testing of the effects

of various ions and nutrients on the production of secondary metabolites. The AM medium containing 20 amino acids was also implemented into our experiments as it had been specifically designed for germination experiments and was used throughout the whole genome expression analyses (Bobek et al., 2004; Strakova et al., 2013). It is known that the presence of different carbon and energy sources in the medium qualitatively affects secondary metabolism (Janecek et al., 1997). That is why the presence of various sugars—glucose, glycerol, and mannitol—in all three media types was tested. In accordance with previously published data (Kieser et al., 2000), both glycerol and mannitol were revealed to be a more suitable source of carbon for secondary metabolites production in the R3 medium in our experiments. Mannitol and glucose exhibited a higher capacity for secondary metabolism when NMMP medium was used and glycerol was shown to have a higher capacity in cases where AM medium was used. Our results also showed that both nutritionally richer media R3 and AM are more suited to germination and the production of secondary metabolites than the minimal NMMP medium, probably due to the presence of Ca^{2+} ions (Eaton and Ensign, 1980; Lakey et al., 1983), L-amino acids (Hirsch and Ensign, 1976b), or various carbon sources (Romero-Rodriguez et al., 2016) in the richer media.

The elution methods with ethylacetate (Rajan and Kannabiran, 2014) or the QuEChERS (Schenck and Hobbs, 2004) were not the most appropriate for isolation of secondary metabolites. Therefore, solid phase extraction (Kamenik et al., 2010) was applied with optimization for streptomyces secondary metabolites. These extracts from supernatants of *S. coelicolor*'s cultures were used for LC-MS analyses.

Secondary Metabolites of *S. coelicolor* Not Produced during Germination

Most of the secondary metabolites, whose biosynthetic genes had previously been shown to be expressed during germination (Strakova et al., 2013), were not detected in samples from germination. These include 21 genes (including sco3230-3232 that encode CDA peptide-synthetase I-III) from the *cda* gene cluster [encoding synthesis of the calcium-dependent-antibiotic (CDA)], the cryptic gene cluster *cpk* (genes sco6273-6288, encoding synthesis of a polyketide antibiotic coelimycin P1), genes sco5314, sco5318, and sco5320 (encoding synthesis of the gray spore pigment), and genes sco5877-5878, sco5881, sco5891-5894, and sco5898 from the so-called *red* gene cluster (encoding synthesis of undecylprodigiosin), and genes sco2783-2784 from the *desABCD* cluster (sco2782-2785, controlling the synthesis of desferrioxamines). Despite the respective gene expression, biosynthesis of more complex secondary metabolites may not occur, since gene expression is only a requirement for biosynthesis and not evidence of it actually taking place.

On the other hand, we found two actinorhodin congeners - actinorhodinic acid and γ -actinorhodin (Bystrykh et al., 1996; Okamoto et al., 2009) in all tested developmental phases, i.e., stationary phase, dormant and germinating spores. In germinating spores, expression of several involved genes: sco5072-5086, sco5088, and sco5090 had been found (Strakova

et al., 2013). Despite the detected expression, we cannot exclude the possibility that the presence of actinorhodin originates from the stationary phase rather than from *de novo* synthesis in germination (therefore the compounds are not listed in Table 3). The reason is that actinorhodin (as well as other aromatic pigments derived from the type II and type III polyketide synthases) is known to be bound on the spore envelopes throughout dormancy (Davis and Chater, 1990; Bystrykh et al., 1996; Funa et al., 1999; Tahlan et al., 2007). This was also confirmed by the actinorhodin detection in our samples of dormant spores even after several washings.

Secondary Metabolites of *S. coelicolor* Produced during Germination

The latest study on the topic (Xu and Vetsigian, 2017) concludes that the germination of *S. coelicolor* M145 may be positively or negatively affected by unknown substances produced by the germlings themselves or by other streptomyces species (e.g., *S. venezuelae*). The results presented here unveiled that *S. coelicolor* produces three secondary metabolites during germination, belonging to the terpenoids (albaflavenone) and polyketides (germicidin A, chalcone). As these compounds have not been detected in dormant spore extracts, we assume that they are produced *de novo* during germination. They show a variety of biological effects and thus perhaps help *S. coelicolor* suppress competitive microflora or coordinate its own development at the early stage of development. The biosynthetic pathways of the detected substances encompass only a few simple reaction steps that do not require complicated precursors and whose biosynthetic genes are expressed during germination, as can be found in gene expression data (Strakova et al., 2013). In contrast, structurally complex metabolites (like the CDA) were not detected in germination (see above).

Albaflavenone

Tricyclic sesquiterpenoid albaflavenone has an aroma similar to geosmin (Gerber and Lechevalier, 1965; Gurtler et al., 1994). Its biosynthesis requires only two genes: sco5222-5223 (Moody et al., 2012). The expression of these genes can be suppressed by cAMP-receptor protein, Crp, which also occurs in other bacteria (e.g., in *Escherichia coli*). The cAMP-Crp control system is a key regulator of germination, secondary metabolism, and further development of *S. coelicolor* (Derouaux et al., 2004; Gao et al., 2012; Bobek et al., 2017). The system also influences the expression of biosynthetic gene clusters in *S. coelicolor* that extend beyond albaflavenone actinorhodin, prodigiosin, CDA, and coelimycin (Gao et al., 2012).

So far, the production of albaflavone in streptomyces has been described only in the stationary growth in *S. albidoflavus* (Gurtler et al., 1994), *S. coelicolor*, *S. viridochromogenes*, *S. avermitilis*, *S. griseoflavus*, *S. Ghanaensis*, and *S. albus* (Moody et al., 2012). However, the expression data analysis shows that the gene sco5223 is activated in germination (Strakova et al., 2013), indicating the possible formation of this metabolite during the initial 6 h of cultivation. We actually found a substance corresponding to albaflavenone in the germination sample in the AM medium with glycerol. The compound was also detected

in samples from the stationary phase (positive control in R3 medium with glycerol), but not samples from dormant spores, indicating its germination-associated *de novo* synthesis.

Albaflavenone is not commercially available, which is why we used hexane extracts, where the compound was detected by LC-MS, for testing its biological activities. We did not see any effect, however. On the other hand, it can be assumed that the albaflavenone produced during the germination provides an advantage in a highly competitive soil environment because it has a demonstrable antibacterial effect on *Bacillus subtilis* at the concentration of $8 \mu\text{g mL}^{-1}$ (Gurtler et al., 1994). Moreover, if albaflavenone was incorporated into the hydrophobic envelope of spores, as other terpenoids do incorporate into the lipophilic membrane layers, it would affect the permeability of the envelopes leading to an intense water influx into spores, thereby accelerating their germination. If we reason that the thickness of the hydrophobic spore envelope is not unified (Lee and Rho, 1993), then the water influx comes into different spores in a different intensity, and therefore, naturally, germination is a non-synchronous process (Hirsch and Ensign, 1976a; Xu and Vetsigian, 2017). The spores already germinated would produce albaflavenone as a signal that environmental conditions are appropriate for the growth of the whole population.

β -farnesene is a sesquiterpene relative to albaflavenone with a wide range of bioactivities (Gibson and Pickett, 1983; Avé et al., 1987) that serves as a precursor of a number of biosynthetic pathways, including the geosmin synthesis. The synthesis of both albaflavenone and β -farnesene is dependent on the type of activity carried out by cytochrome P450 (CYP170A1). It may function either as P450 monooxygenase or as P420 farnesene-synthase. It has been shown that the farnesene-synthase activity predominates at pH 5.5–6.5 and in the presence of bivalent cations (Mg^{2+} , Mn^{2+} , Ca^{2+}), while at pH 7.0–8.2, it functions as the monooxygenase, oxidizing epi-isozizaen first to albaflavenol, and then to albaflavenone (Moody et al., 2012). Conformation and final enzymatic activity of CYP170A1 is thus affected by the pH of the environment. We presume that *S. coelicolor* may exploit the dual pH-dependent activity of the enzyme in order to detect optimal external conditions. Therefore, we tested whether the biosynthetic activity is dependent on the pH of the medium during germination. For the experiment we performed the same R3 medium with a pH of either 7.2 or 6.0. Although we were not able to directly demonstrate the production of β -farnesene, we proved that the spectrum of detected substances significantly differed. Further experiments are required to confirm the expected pH-dependent signaling activity of the albaflavenon/ β -farnesene systems.

Germicidin A

Gcs protein (a polyketide synthase type III, PKS III) is involved in the germicidin biosynthesis in *S. coelicolor* (Chemler et al., 2012). However, expression of its gene *sco7221* during germination was below the detection limit (Strakova et al., 2013). The germicidin biosynthesis could also be related to the activity of other genes *sco7670–7671*, whose expression is active in germination (Strakova et al., 2013).

Germicidin A production has previously been described in germination spores and in the stationary growth stage of *S. viridochromogenes* (Hirsch and Ensign, 1978; Petersen et al., 1993). It was also isolated after more than 24 h of submerged cultivation of *S. coelicolor* and other streptomyces (Petersen et al., 1993; Aoki et al., 2011; Ma et al., 2017). The results of our work, however, show for the first time that germicidin A is produced by germlings of *S. coelicolor* (in R3 medium with glycerol or mannitol, and in AM medium with glucose or glycerol). In contrast, germicidin B in germinating *S. coelicolor* was not produced, which is consistent with the results reported in *S. viridochromogenes* (Petersen et al., 1993). On the other hand, both polyketides, germicidin A and germicidin B, were detected here in samples from the stationary phase (in both, R3 medium with glycerol, or mannitol and NMMP medium with glucose or mannitol).

Germicidins belong to a richly represented group of α -pyrone natural substances found in bacteria, fungi, plants, and animals (Schaberle, 2016). Pyrones have many biological effects and signal molecules for *quorum sensing* can be found among them (Brachmann et al., 2013). Germicidin A is a known reversible inhibitor of spore germination; it prevents the germination at very low concentrations of 40 pg mL^{-1} ; i.e., only 2,400 molecules per spore (Petersen et al., 1993). We verified this biological effect in *S. coelicolor*, where germicidin A had a marked adverse effect on germination already at as low a concentration in medium as $4 \mu\text{g mL}^{-1}$. It is known that germicidin A affects the respiration of spores and mycelia by interacting with the membrane Ca^{2+} -ATPase, inactivating the enzyme. By this mechanism, germicidin not only prevents spores from generating sufficient energy for germination but also inhibits hyphal growth (Eaton and Ensign, 1980; Grund and Ensign, 1985; Aoki et al., 2011). Germicidin A also exhibits antibacterial activity against gram-positive bacteria such as *Bacillus subtilis*, *Arthrobacter crystallopoietes*, or *Mycobacterium smegmatis* (Grund and Ensign, 1985; Aoki et al., 2011).

Because of its inhibitory effect, the production of germicidin during germination in optimal conditions might, at first glance, seem surprising. Its production by germinating spores might help to co-ordinate germination within the population. Its self-regulating function could maintain a portion of spores in their dormant state for a prolonged period as a reserve if the environment proves to be unfavorable or when germination occurs in higher spore densities. Conversely, the ungerminated spores can be further propagated in the environment and, after overcoming the reversible inhibition, can spread in new niches.

Chalcone

The detection of chalcone in *Streptomyces* has not yet been proven to our knowledge. Its tentative identification presented here is based on the accurate mass of analyzed supernatants from the stationary phase and germination in R3 medium with glycerol or mannitol. Chalcones are intermediates of flavonoid biosynthesis where the key role in their synthesis plays 1,3,6,8-tetrahydroxynaphthalene-synthase. One of its precursors is the naringenin-chalcone, whose involvement in the flavonoid

naringenin biosynthesis was described in *S. clavuligerus* (Alvarez-Alvarez et al., 2015). The enzyme, which belongs to PKS III, is closely related to the plant chalcone synthase (Izumikawa et al., 2003). Its sco1206 gene in *S. coelicolor* is expressed during germination (Strakova et al., 2013).

Chalcone is apparently an instrument of interspecies interaction, as there are referred its antifungal, phytotoxic and insecticidal effects are outlined (Diaz-Tielas et al., 2012). Chalcone could also function as a signaling molecule in a symbiotic relationship, such as 4,4'-dihydroxy-2'-methoxychalcone produced by legumes that induce transcription of *nod* genes in symbiotic rhizobacteria. The products of these genes, Nod factors, are involved in the symbiosis where rhizobacteria produce nitrogen for plants (Maxwell et al., 1989).

Interestingly, other flavonoids - quercetin, kaempferol, and myricetin—are known to stimulate pollen germination in *Nicotiana tabacum* L. (Ylstra et al., 1992). Therefore, we expected that chalcones produced by germinating spores would stimulate germination under favorable environmental conditions. Experimentally, however, we verified the opposite as the chalcone of *S. coelicolor* remarkably inhibited germination. At a concentration of 300 $\mu\text{g mL}^{-1}$, it completely suppressed growth and at 8 $\mu\text{g mL}^{-1}$ and lower the compound visibly inhibited spore germination, colony differentiation, and actinorhodin production on solid medium. Electron microscopic images taken from liquid cultivation revealed disrupted germ tubes. This finding correlates with a described activity of chalcone which was shown to interfere with cell membrane of *Staphylococcus aureus* (Sivakumar et al., 2009).

CONCLUSION

In this work the production of secondary metabolites in germinating streptomycetes is systematically analyzed for the first time. Our investigation was based on the hypothesis that germinating spores exploit intercellular communications (*quorum sensing*) to support a coordinated development in its early stage as well as interspecies communication (*quorum quenching*) to suppress metabolic activities of competing microflora (Chen et al., 2000). This work succeeds the previous transcriptomic analysis of germination in streptomycetes (Strakova et al., 2013), which has shown the expression of genes from different antibiotic clusters. Here using LC-MS, we detected three potentially important secondary metabolites—sesquiterpenoid albaflavene, and polyketides germicidin A, and chalcone—that are synthesized during spore germination of *S. coelicolor*. All three detected compound possess capacities to suppress

competitive microflora at the early stage of development. Their biosynthetic pathways are simple, having only a few reaction steps that do not require complex precursors.

Albaflavene had been previously detected only in the stationary phase of growth of certain streptomycetes (Gurtler et al., 1994; Moody et al., 2012). It exhibits an antibacterial effect and could serve as a germination signal for coordinated development or as a factor of interspecific communication (these suggestions are not proven here). In contrary, the two other compounds revealed inhibitory effects on germination that may explain slower germination rate and less synchronicity in the model *S. coelicolor*, in comparison with other *Streptomyces* species, such as *S. viridochromogenes*. Our data are consistent with the known inhibitory effect of the supernatant of *S. coelicolor* on its own germination (Xu and Vetsigian, 2017).

The widespread autoregulator of germination, germicidin A, is known to be produced by germinating spores of *S. viridochromogenes*. Here it was shown that the germings of *S. coelicolor* are also capable of its production. Chalcone is probably one of the precursors of biosynthesis of a not yet described flavonoid in *S. coelicolor*. During germination it functions as a germination inhibitor that may serve as a means of interspecies communication.

AUTHOR CONTRIBUTIONS

MČ managed all experiments and evaluated data; MČ and KP performed analytical samples; MČ and ZK performed LC-MS measurements; KŠ and NB performed cultures and experimental design for germination; OB and OK performed the electron microscopy; JB conceived the project and wrote the manuscript.

ACKNOWLEDGMENTS

Access to the electron microscopy facility, supported by the project LO1509 of the Ministry of Education, Youth and Sports of the Czech Republic and by the Operational Program Prague–Competitiveness project (CZ.2.16/3.1.00/24023) supported by the European Union, is gratefully acknowledged. This work was supported by a project by Charles University in Prague: Progres Q26/LF1 to JB, SVV260369 to KŠ, a grant of the Grant Agency of the Charles University (www.cuni.cz/UK-33.html) under contract no. 160214 to KŠ, a project of J. E. Purkinje University: UJEP-SGS-173-07-01 to JB, and by the Czech research infrastructure for systems biology C4SYS (project no. LM2015055) to JB.

REFERENCES

- Alvarez-Alvarez, R., Botas, A., Albillos, S. M., Rumero, A., Martin, J. F., and Liras, P. (2015). Molecular genetics of naringenin biosynthesis, a typical plant secondary metabolite produced by *Streptomyces clavuligerus*. *Microb. Cell Fact.* 14:178. doi: 10.1186/s12934-015-0373-7
- Aoki, Y., Matsumoto, D., Kawaide, H., and Natsume, M. (2011). Physiological role of germicidins in spore germination and hyphal elongation in *Streptomyces coelicolor* A3(2). *J. Antibiot.* 64, 607–611. doi: 10.1038/ja.2011.59
- Aoki, Y., Yoshida, M., Kawaide, H., Abe, H., and Natsume, M. (2007). Isolation and characterization of a spore germination inhibitor from *Streptomyces* sp. CB-1-1, a phytopathogen causing root tumor of melon. *Biosci. Biotechnol. Biochem.* 71, 986–992. doi: 10.1271/bbb.60649
- Avé, D. A., Gregory, P., and Tingey, W. M. (1987). Aphid repellent sesquiterpenes in glandular trichomes of *Solanum berthaultii* and *S. tuberosum*.

- Entomol. Experim. Appl. 44, 131–138. doi: 10.1111/j.1570-7458.1987.tb01057.x
- Baltz, R. H. (2008). Renaissance in antibacterial discovery from actinomycetes. *Curr. Opin. Pharmacol.* 8, 557–563. doi: 10.1016/j.coph.2008.04.008
- Bentley, S. D., Chater, K. F., Cerdeno-Tarraga, A. M., Challis, G. L., Thomson, N. R., James, K. D., et al. (2002). Complete genome sequence of the model actinomycete *Streptomyces coelicolor* A3(2). *Nature* 417, 141–147. doi: 10.1038/417141a
- Bobek, J., Halada, P., Angelis, J., Vohradsky, J., and Mikulík, K. (2004). Activation and expression of proteins during synchronous germination of aerial spores of *Streptomyces granaticolor*. *Proteomics* 4, 3864–3880. doi: 10.1002/pmic.200400818
- Bobek, J., Šmídová, K., and Čihák, M. (2017). A waking review: old and novel insights into the spore germination in *Streptomyces*. *Front. Microbiol.* 8:2205. doi: 10.3389/fmicb.2017.02205
- Bobek, J., Strakova, E., Zikova, A., and Vohradsky, J. (2014). Changes in activity of metabolic and regulatory pathways during germination of *S. coelicolor*. *BMC Genomics* 15:1173. doi: 10.1186/1471-2164-15-1173
- Brachmann, A. O., Brameyer, S., Kresovic, D., Hitkova, I., Kopp, Y., Manske, C., et al. (2013). Pyrones as bacterial signaling molecules. *Nat. Chem. Biol.* 9, 573–578. doi: 10.1038/nchembio.1295
- Burdock, T. J., Brooks, M. S., and Ghaly, A. E. (2011). A dehydrogenase activity test for monitoring the growth of *Streptomyces venezuelae* in a nutrient rich medium. *J. Bioprocess Biotechnol.* 1:101. doi: 10.4172/2155-9821.1000101
- Bystrykh, L. V., Fernandez-Moreno, M. A., Herrema, J. K., Malfartida, F., Hopwood, D. A., and Dijkhuizen, L. (1996). Production of actinorhodin-related "blue pigments" by *Streptomyces coelicolor* A3(2). *J. Bacteriol.* 178, 2238–2244. doi: 10.1128/jb.178.8.2238-2244.1996
- Camilli, A., and Bassler, B. L. (2006). Bacterial small-molecule signaling pathways. *Science* 311, 1113–1116. doi: 10.1126/science.1121357
- Chemler, J. A., Buchholz, T. J., Geders, T. W., Akey, D. L., Rath, C. M., Chlipala, G. E., et al. (2012). Biochemical and structural characterization of germicidin synthase: analysis of a type III polyketide synthase that employs acyl-ACP as a starter unit donor. *J. Am. Chem. Soc.* 134, 7359–7366. doi: 10.1021/ja2112228
- Chen, K. C., Csikasz-Nagy, A., Györfy, B., Val, J., Novak, B., and Tyson, J. J. (2000). Kinetic analysis of a molecular model of the budding yeast cell cycle. *Mol. Biol. Cell* 11, 369–391. doi: 10.1091/mbc.11.1.369
- Claessen, D., de Jong, W., Dijkhuizen, L., and Wosten, H. A. (2006). Regulation of *Streptomyces* development: reach for the sky! *Trends Microbiol.* 14, 313–319. doi: 10.1016/j.tim.2006.05.008
- Davis, N. K., and Chater, K. F. (1990). Spore colour in *Streptomyces coelicolor* A3(2) involves the developmentally regulated synthesis of a compound biosynthetically related to polyketide antibiotics. *Mol. Microbiol.* 4, 1679–1691. doi: 10.1111/j.1365-2958.1990.tb00545.x
- Derouaux, A., Halici, S., Nothaft, H., Neutelings, T., Moutzourelis, G., Dusart, J., et al. (2004). Deletion of a cyclic AMP receptor protein homologue diminishes germination and affects morphological development of *Streptomyces coelicolor*. *J. Bacteriol.* 186, 1893–1897. doi: 10.1128/JB.186.6.1893-1897.2004
- Diaz-Tielas, C., Grana, E., Reigosa, M. J., and Sanchez-Moreiras, A. M. (2012). The role of peroxidases on the mode of action of chalcone in *Arabidopsis* roots. *Plant Signal. Behav.* 7, 1274–1276. doi: 10.4161/psb.21594
- Eaton, D., and Ensign, J. C. (1980). *Streptomyces viridochromogenes* spore germination initiated by calcium ions. *J. Bacteriol.* 143, 377–382.
- Funa, N., Ohnishi, Y., Fujii, I., Shibuya, M., Ebizuka, Y., and Horinouchi, S. (1999). A new pathway for polyketide synthesis in microorganisms. *Nature* 400, 897–899. doi: 10.1038/23748
- Gao, C., Hindra, Mulder, D., Yin, C., and Elliot, M. A. (2012). Crp is a global regulator of antibiotic production in streptomycetes. *MBio* 3:e00407-12. doi: 10.1128/mBio.00407-12
- Gerber, N. N., and Lechevalier, H. A. (1965). Geosmin, an earthy-smelling substance isolated from actinomycetes. *Appl. Microbiol.* 13, 935–938.
- Gibson, R. W., and Pickett, J. A. (1983). Wild potato repels aphids by release of aphid alarm pheromone. *Nature* 302, 608–609. doi: 10.1038/302608a0
- Gomez-Escribano, J. P., Song, L., Fox, D. J., Yeo, V., Bibb, M. J., and Challis, G. (2012). Structure and biosynthesis of the unusual polyketide alkaloid coelimycin P1, a metabolic product of the cpk gene cluster of *Streptomyces coelicolor* M145. *Chem. Sci.* 3, 2716–2720. doi: 10.1039/c2sc20410j
- Grund, A. D., and Ensign, J. C. (1985). Properties of the germination inhibitor of *Streptomyces viridochromogenes* spores. *J. Gen. Microbiol.* 131, 833–847. doi: 10.1099/00221287-131-4-833
- Gurtler, H., Pedersen, R., Anthoni, U., Christophersen, C., Nielsen, P. H., Wellington, E. M., et al. (1994). Albalavene, a sesquiterpene ketone with a zizaene skeleton produced by a streptomycete with a new rope morphology. *J. Antibiot.* 47, 434–439. doi: 10.7164/antibiotics.47.434
- Haiser, H. J., Yousef, M. R., and Elliot, M. A. (2009). Cell wall hydrolases affect germination, vegetative growth, and sporulation in *Streptomyces coelicolor*. *J. Bacteriol.* 191, 6501–6512. doi: 10.1128/JB.00767-09
- Hirsch, C. F., and Ensign, J. C. (1976a). Heat activation of *Streptomyces viridochromogenes* spores. *J. Bacteriol.* 126, 24–30.
- Hirsch, C. F., and Ensign, J. C. (1976b). Nutritionally defined conditions for germination of *Streptomyces viridochromogenes* spores. *J. Bacteriol.* 126, 13–23.
- Hirsch, C. F., and Ensign, J. C. (1978). Some properties of *Streptomyces viridochromogenes* spores. *J. Bacteriol.* 134, 1056–1063.
- Hodgson, D. (1982). Glucose repression of carbon source uptake and metabolism in *Streptomyces coelicolor* A3(2) and its perturbation in mutants resistant to 2-deoxyglucose. *Micro Soc.* 128, 2417–2430. doi: 10.1099/00221287-128-10-2417
- Hopwood, D. A. (2007). How do antibiotic-producing bacteria ensure their self-resistance before antibiotic biosynthesis incapacitates them? *Mol. Microbiol.* 63, 937–940. doi: 10.1111/j.1365-2958.2006.05584.x
- Ikedo, H., Ishikawa, J., Hanamoto, A., Shinose, M., Kikuchi, H., Shiba, T., et al. (2003). Complete genome sequence and comparative analysis of the industrial microorganism *Streptomyces avermitilis*. *Nat. Biotechnol.* 21, 526–531. doi: 10.1038/nbt820
- Izumikawa, M., Shipley, P. R., Hopke, J. N., O'Hare, T., Xiang, L., Noel, J. P., et al. (2003). Expression and characterization of the type III polyketide synthase 1,3,6,8-tetrahydroxynaphthalene synthase from *Streptomyces coelicolor* A3(2). *J. Ind. Microbiol. Biotechnol.* 30, 510–515. doi: 10.1007/s10295-003-0075-8
- Janecek, J., Tichý, P., Spizek, J., and Vanek, Z. (1997). Constitution of the metabolic type of streptomycetes during the first hours of cultivation. *Folia Microbiol.* 42, 75–96. doi: 10.1007/BF02898713
- Kalan, L., Gessner, A., Thaker, M. N., Wagglechner, N., Zhu, X., Szawiola, A., et al. (2013). A cryptic polyene biosynthetic gene cluster in *Streptomyces calvus* is expressed upon complementation with a functional bldA gene. *Chem. Biol.* 20, 1214–1224. doi: 10.1016/j.chembiol.2013.09.006
- Kamenik, Z., Hadacek, F., Mareckova, M., Ulanova, D., Kopecky, J., Chobot, V., et al. (2010). Ultra-high-performance liquid chromatography fingerprinting method for chemical screening of metabolites in cultivation broth. *J. Chromatogr. A* 1217, 8016–8025. doi: 10.1016/j.chroma.2010.08.031
- Kelemen, G. H., and Buttner, M. J. (1998). Initiation of aerial mycelium formation in *Streptomyces*. *Curr. Opin. Microbiol.* 1, 656–662. doi: 10.1016/S1369-5274(98)80111-2
- Keller, N. P., Turner, G., and Bennett, J. W. (2005). Fungal secondary metabolism - from biochemistry to genomics. *Nat. Rev. Microbiol.* 3, 937–947. doi: 10.1038/nrmicro1286
- Kieser, T., Bibb, M. J., Buttner, M. J., Chater, K. F., and Hopwood, D. A. (2000). *Practical Streptomyces Genetics*, 2nd Edn. Norwich: John Innes Foundation.
- Lakey, J. H., Lea, E. J., Rudd, B. A., Wright, H. M., and Hopwood, D. A. (1983). A new channel-forming antibiotic from *Streptomyces coelicolor* A3(2) which requires calcium for its activity. *J. Gen. Microbiol.* 129, 3565–3573. doi: 10.1099/00221287-129-12-3565
- Lee, K. J., and Rho, Y. T. (1993). Characteristics of spores formed by surface and submerged cultures of *Streptomyces albidoflavus* SMF301. *J. Gen. Microbiol.* 139, 3131–3137. doi: 10.1099/00221287-139-12-3131
- Luo, Y., Huang, H., Liang, J., Wang, M., Lu, L., Shao, Z., et al. (2013). Activation and characterization of a cryptic polycyclic tetramate macrolactam biosynthetic gene cluster. *Nat. Commun.* 4:894. doi: 10.1038/ncomms3894
- Ma, M., Rateb, M. E., Yang, D., Rudolf, J. D., Zhu, X., Huang, Y., et al. (2017). Germicidins H-J from *Streptomyces* sp. CB00361. *J. Antibiot.* 70, 200–203. doi: 10.1038/ja.2016.100
- Martinez, G., Regente, M., Jacobi, S., Del Rio, M., Pinedo, M., and de la Canal, L. (2017). Chlorogenic acid is a fungicide active against phytopathogenic fungi. *Pestic. Biochem. Physiol.* 140, 30–35. doi: 10.1016/j.pestbp.2017.05.012

- Maxwell, C. A., Hartwig, U. A., Joseph, C. M., and Phillips, D. A. (1989). A chalcone and two related flavonoids released from alfalfa roots induce nod genes of rhizobium meliloti. *Plant Physiol.* 91, 842–847. doi: 10.1104/pp.91.3.842
- McCormick, J. R., and Flardh, K. (2012). Signals and regulators that govern *Streptomyces* development. *FEMS Microbiol. Rev.* 36, 206–231. doi: 10.1111/j.1574-6976.2011.00317.x
- Mikulík, K., Bobek, J., Bezouskova, S., Benada, O., and Kofronova, O. (2002). Expression of proteins and protein kinase activity during germination of aerial spores of *Streptomyces granaticolor*. *Biochem. Biophys. Res. Commun.* 299, 335–342. doi: 10.1016/S0006-291X(02)02606-2
- Mikulík, K., Bobek, J., Zikova, A., Smetakova, M., and Bezouskova, S. (2011). Phosphorylation of ribosomal proteins influences subunit association and translation of poly (U) in *Streptomyces coelicolor*. *Mol. Biosyst.* 7, 817–823. doi: 10.1039/C0MB00174K
- Mikulík, K., Janda, I., Maskova, H., Stastna, J., and Jiranova, A. (1977). Macromolecular synthesis accompanying the transition from spores to vegetative forms of *Streptomyces granaticolor*. *Folia Microbiol.* 22, 252–261. doi: 10.1007/BF02877654
- Mikulík, K., Paleckova, P., Felsberg, J., Bobek, J., Zidkova, J., and Halada, P. (2008). SsrA genes of streptomycetes and association of proteins to the tmRNA during development and cellular differentiation. *Proteomics* 8, 1429–1441. doi: 10.1002/pmic.200700560
- Moody, S. C., Zhao, B., Lei, L., Nelson, D. R., Mullins, J. G., Waterman, M. R., et al. (2012). Investigating conservation of the albaflavone biosynthetic pathway and CYP170 bifunctionality in streptomycetes. *FEBS J.* 279, 1640–1649. doi: 10.1111/j.1742-4658.2011.08447.x
- Ohnishi, Y., Ishikawa, J., Hara, H., Suzuki, H., Ikenoya, M., Ikeda, H., et al. (2008). Genome sequence of the streptomycin-producing microorganism *Streptomyces griseus* IFO 13350. *J. Bacteriol.* 190, 4050–4060. doi: 10.1128/JB.00204-08
- Okamoto, S., Taguchi, T., Ochi, K., and Ichinose, K. (2009). Biosynthesis of actinorhodin and related antibiotics: discovery of alternative routes for quinone formation encoded in the act gene cluster. *Chem. Biol.* 16, 226–236. doi: 10.1016/j.chembiol.2009.01.015
- Paleckova, P., Bobek, J., Felsberg, J., and Mikulík, K. (2006). Activity of translation system and abundance of tmRNA during development of *Streptomyces aureofaciens* producing tetracycline. *Folia Microbiol.* 51, 517–524. doi: 10.1007/BF02931615
- Petersen, F., Zahner, H., Metzger, J. W., Freund, S., and Hummel, R. P. (1993). Germicidin, an autoregulative germination inhibitor of *Streptomyces viridochromogenes* NRRL B-1551. *J. Antibiot.* 46, 1126–1138. doi: 10.7164/antibiotics.46.1126
- Phelan, V. V., Liu, W. T., Pogliano, K., and Dorrestein, P. C. (2011). Microbial metabolic exchange—the chemotype-to-phenotype link. *Nat. Chem. Biol.* 8, 26–35. doi: 10.1038/nchembio.739
- Rajan, B. M., and Kannabiran, K. (2014). Extraction and identification of antibacterial secondary metabolites from marine *Streptomyces* sp. VITBRK2. *Int. J. Mol. Cell. Med.* 3, 130–137.
- Ranade, N., and Vining, L. C. (1993). Accumulation of intracellular carbon reserves in relation to chloramphenicol biosynthesis by *Streptomyces venezuelae*. *Can. J. Microbiol.* 39, 377–383. doi: 10.1139/m93-055
- Romero-Rodriguez, A., Ruiz-Villafan, B., Tierrafria, V. H., Rodriguez-Sanoja, R., and Sanchez, S. (2016). Carbon catabolite regulation of secondary metabolite formation and morphological differentiation in *Streptomyces coelicolor*. *Appl. Biochem. Biotechnol.* 180, 1152–1166. doi: 10.1007/s12010-016-2158-9
- Rutherford, S. T., and Bassler, B. L. (2012). Bacterial quorum sensing: its role in virulence and possibilities for its control. *Cold Spring Harb. Perspect. Med.* 2:a012427. doi: 10.1101/cshperspect.a012427
- Schaberle, T. F. (2016). Biosynthesis of alpha-pyrone. *Beilstein J. Org. Chem.* 12, 571–588. doi: 10.3762/bjoc.12.56
- Schenck, F. J., and Hobbs, J. E. (2004). Evaluation of the quick, easy, cheap, effective, rugged, and safe (QuEChERS) approach to pesticide residue analysis. *Bull. Environ. Contam. Toxicol.* 73, 24–30. doi: 10.1007/s00128-004-0388-y
- Seipke, R. F., Kaltenpoth, M., and Hutchings, M. I. (2012). *Streptomyces* as symbionts: an emerging and widespread theme? *FEMS Microbiol. Rev.* 36, 862–876. doi: 10.1111/j.1574-6976.2011.00313.x
- Sello, J. K., and Buttner, M. J. (2008). The gene encoding RNase III in *Streptomyces coelicolor* is transcribed during exponential phase and is required for antibiotic production and for proper sporulation. *J. Bacteriol.* 190, 4079–4083. doi: 10.1128/JB.01889-07
- Shima, J., Hesketh, A., Okamoto, S., Kawamoto, S., and Ochi, K. (1996). Induction of actinorhodin production by rpsL (encoding ribosomal protein S12) mutations that confer streptomycin resistance in *Streptomyces lividans* and *Streptomyces coelicolor* A3(2). *J. Bacteriol.* 178, 7276–7284. doi: 10.1128/jb.178.24.7276-7284.1996
- Sivakumar, P. M., Priya, S., and Doble, M. (2009). Synthesis, biological evaluation, mechanism of action and quantitative structure-activity relationship studies of chalcones as antibacterial agents. *Chem. Biol. Drug Des.* 73, 403–415. doi: 10.1111/j.1747-0285.2009.00793.x
- Strakova, E., Bobek, J., Zikova, A., Rehulka, P., Benada, O., Rehulkova, H., et al. (2013). Systems insight into the spore germination of *Streptomyces coelicolor*. *J. Proteome Res.* 12, 525–536. doi: 10.1021/pr300980v
- Strakova, E., Zikova, A., and Vohradsky, J. (2014). Inference of sigma factor controlled networks by using numerical modeling applied to microarray time series data of the germinating prokaryote. *Nucleic Acids Res.* 42, 748–763. doi: 10.1093/nar/gkt917
- Tahlan, K., Ahn, S. K., Sing, A., Bodnaruk, T. D., Willems, A. R., Davidson, A. R., et al. (2007). Initiation of actinorhodin export in *Streptomyces coelicolor*. *Mol. Microbiol.* 63, 951–961. doi: 10.1111/j.1365-2958.2006.05559.x
- Tanaka, Y., Kasahara, K., Hirose, Y., Murakami, K., Kugimiya, R., and Ochi, K. (2013). Activation and products of the cryptic secondary metabolite biosynthetic gene clusters by rifampin resistance (rpoB) mutations in actinomycetes. *J. Bacteriol.* 195, 2959–2970. doi: 10.1128/JB.00147-13
- van Keulen, G., and Dyson, P. J. (2014). Production of specialized metabolites by *Streptomyces coelicolor* A3(2). *Adv. Appl. Microbiol.* 89, 217–266. doi: 10.1016/B978-0-12-800259-9.00006-8
- van Vliet, S. (2015). Bacterial dormancy: how to decide when to wake up. *Curr. Biol.* 25, R753–R755. doi: 10.1016/j.cub.2015.07.039
- Wakefield, J., Hassan, H. M., Jaspars, M., Ebel, R., and Rateb, M. E. (2017). Dual induction of new microbial secondary metabolites by fungal bacterial co-cultivation. *Front. Microbiol.* 8:1284. doi: 10.3389/fmicb.2017.01284
- Waters, C. M., and Bassler, B. L. (2005). Quorum sensing: cell-to-cell communication in bacteria. *Annu. Rev. Cell Dev. Biol.* 21, 319–346. doi: 10.1146/annurev.cellbio.21.012704.131001
- Xu, Y., and Vetsigian, K. (2017). Phenotypic variability and community interactions of germinating *Streptomyces* spores. *Sci. Rep.* 7:699. doi: 10.1038/s41598-017-00792-7
- Ylstra, B., Touraev, A., Moreno, R. M., Stoger, E., van Tunen, A. J., Vicente, O., et al. (1992). Flavonols stimulate development, germination, and tube growth of tobacco pollen. *Plant Physiol.* 100, 902–907. doi: 10.1104/pp.100.2.902
- Yoshida, M., and Kobayashi, K. (1994). Morphogenesis of the pathogenic *Streptomyces* sp. causing root tumor of melon on the culture medium. *Ann. Phytopathol. Soc. Jpn.* 60, 514–522. doi: 10.3186/jjphytopath.60.514
- Zhao, B., Lei, L., Vassilyev, D. G., Lin, X., Cane, D. E., Kelly, S. L., et al. (2009). Crystal structure of albaflavone monooxygenase containing a moonlighting terpene synthase active site. *J. Biol. Chem.* 284, 36711–36719. doi: 10.1074/jbc.M109.064683

Conflict of Interest Statement: The authors declare that the research was conducted in the absence of any commercial or financial relationships that could be construed as a potential conflict of interest.

Copyright © 2017 Čihák, Kameník, Šmídová, Bergman, Benada, Kofronová, Petříčková and Bobek. This is an open-access article distributed under the terms of the Creative Commons Attribution License (CC BY). The use, distribution or reproduction in other forums is permitted, provided the original author(s) or licensor are credited and that the original publication in this journal is cited, in accordance with accepted academic practice. No use, distribution or reproduction is permitted which does not comply with these terms.



RNase III-Binding-mRNAs Revealed Novel Complementary Transcripts in *Streptomyces*

Dita Šetinová¹, Klára Šmídová¹, Pavel Pohl², Inesa Musić² and Jan Bobek^{1, 2, 3*}

¹ First Faculty of Medicine, Institute of Immunology and Microbiology, Charles University, Prague, Czechia, ² Chemistry Department, Faculty of Science, J. E. Purkinje University, Ústí nad Labem, Czechia, ³ Institute of Microbiology, Academy of Sciences of the Czech Republic, Prague, Czechia

OPEN ACCESS

Edited by:

Dirk Tischler,
Freiburg University of Mining and
Technology, Germany

Reviewed by:

Francis Repolla,
Institut National de la Recherche
Agronomique (INRA), France
Gerd M. Seibold,
University of Ulm, Germany
Edgardo Sepulveda,
Center for Scientific Research and
Higher Education at Ensenada,
Mexico

*Correspondence:

Jan Bobek
jan.bobek@lf1.cuni.cz

Specialty section:

This article was submitted to
Microbial Physiology and Metabolism,
a section of the journal
Frontiers in Microbiology

Received: 30 August 2017

Accepted: 26 December 2017

Published: 15 January 2018

Citation:

Šetinová D, Šmídová K, Pohl P,
Musić I and Bobek J (2018) RNase
III-Binding-mRNAs Revealed Novel
Complementary Transcripts in
Streptomyces.
Front. Microbiol. 8:2693.
doi: 10.3389/fmicb.2017.02693

cis-Antisense RNAs (asRNAs) provide very simple and effective gene expression control due to the perfect complementarity between regulated and regulatory transcripts. In *Streptomyces*, the antibiotic-producing clade, the antisense control system is not yet understood, although it might direct the organism's complex development. Initial studies in *Streptomyces* have found a number of asRNAs. Apart from this, hundreds of mRNAs have been shown to bind RNase III, the double strand-specific endoribonuclease. In this study, we tested 17 mRNAs that have been previously co-precipitated with RNase III for antisense expression. Our RACE mapping showed that all of these mRNAs possess cognate asRNA. Additional tests for antisense expression uncovered *as-adiA*, *as-rnc*, *as3983*, *as-sigB*, *as-sigH*, and *as-sigR* RNAs. Northern blots detected the expression profiles of 18 novel transcripts. Noteworthy, we also found that only a minority of asRNAs respond to the absence of RNase III enzyme by increasing their cellular levels. Our findings suggest that antisense expression is widespread in *Streptomyces*, including genes of such important developmental regulators, as AdpA, RNase III, and sigma factors.

Keywords: *cis*-antisense RNA, RNase III, *Streptomyces*, antibiotics, gene expression control

INTRODUCTION

Bacterial small RNAs are important post-transcriptional regulators that control a variety of cell processes. A large majority of these RNAs acts on target mRNAs via base pairing, an antisense mechanism that leads to positive or negative regulation of the target gene, as reviewed in Thomason (Thomason and Storz, 2010). Such antisense RNAs fall into two groups: *cis*- (asRNAs) and *trans*-encoded (sRNAs) (Romby and Charpentier, 2010).

The *trans*-acting sRNAs are encoded distinctly from their target mRNA(s), which is also the reason why the sRNA-mRNA pair mostly shares reduced complementarity. On the other hand, the sRNAs are usually able to act on multiple targets. The *trans*-encoded sRNAs have been extensively characterized and discussed in many reviews (Papenfert and Vogel, 2009; Waters and Storz, 2009). The limited base pairing requires the RNA chaperone protein Hfq in a number of bacteria. However, Hfq is either missing or its homolog has not yet been found in several bacterial clades, including Actinomycetes (Sun et al., 2002).

Reported proportions of *cis*-antisense expression in various bacteria vary from 13% in *Bacillus subtilis* (Nicolas et al., 2012), 27% in *Synechocystis* PCC6803 (Mitschke et al., 2011a), 30% in

Anabaena (Mitschke et al., 2011b), 46% in *Helicobacter pylori* (Sharma et al., 2010), and up to 49% in *Staphylococcus aureus* (Lasa et al., 2011). These transcripts are encoded on the DNA strand opposite to their specific targets. Both asRNA and mRNA are produced by overlapping transcription, thus sharing perfect complementarity (summarized in Lasa et al., 2012). The ability of asRNAs to modulate mRNA levels is not only mediated by post-transcriptional mechanisms but they may also directly impact transcription due to collisions between RNA polymerases traveling in opposite directions [transcription interference, for review see Thomason (Thomason and Storz, 2010)]. The mechanisms of post-transcriptional action of asRNAs may be divided into two groups: (i) asRNA influences the stability of the target mRNA by either tagging for degradation or stabilizing its structure and/or (ii) asRNA affects translation either by blocking or promoting ribosome access to the ribosome binding site (Geissmann et al., 2009; Lasa et al., 2011).

In many cases of negative antisense control, the sense-antisense RNA complex formation results in its rapid cleavage. In many bacteria, two dominant endoribonucleases, RNase E and RNase III, are involved in the degradation process. The RNase E enzyme, as a member of the degradosome complex with Hfq in *E. coli*, cleaves single-stranded RNA (reviewed in Carpousis et al., 2009). The RNase III enzyme cleaves double-stranded RNA (MacRae and Doudna, 2007). Although RNase III was initially shown to be associated with the processing of ribosomal RNAs (Carpousis et al., 2009; Taverniti et al., 2011), its involvement in the degradation of sense/antisense pairs is being reported in an increasing number of publications (Blomberg et al., 1990; Gerdes et al., 1992; Lasa et al., 2011, 2012; Durand et al., 2012; Lioliou et al., 2012; Lybecker et al., 2014a,b; Le Rhun et al., 2016).

In *Staphylococcus aureus*, deep sequencing of the short RNA fraction revealed a massive accumulation of 22-nucleotide RNA fragments generated by the RNase III cleavage of paired transcripts (Lasa et al., 2011). More than 75% of the fragments corresponded to the overlapping transcription from most regions of the chromosome. The number of short RNA fragments was significantly decreased in an RNase III-deletion strain. In contrast, such a collection of short RNA fragments was not found when using a similar transcriptome analysis for the Gram-negative bacterium *Salmonella enterica* (Viegas et al., 2007).

Bacteria of the genus *Streptomyces* undergo a complex mycelial life cycle. Their growth starts with the germination of spores that develop into a vegetative mycelium of branching hyphae. Subsequent development of aerial hyphae is considered to be a cell response to nutrient depletion (Chater and Losick, 1997). At this stage part of the vegetative mycelium is lysed and can be used as a nutrient source, while the synthesis of antibiotics reaches its maximum presumably to avoid competitive organisms. Eventually, the aerial hyphae are dissected into spores by sporulation septa, producing chains of uninucleoid spores.

The complexity of the morphological and physiological differentiation in *Streptomyces* can be documented by the existence of more than 900 transcriptional protein regulators that control the metabolic and developmental transitions. Among them, over 60 sigma factors have been identified thus far

(Gruber and Gross, 2003). Besides sigma factors, one of the most pleiotropic transcription regulators is AdpA. AdpA is expressed in an A-factor-dependent manner in *Streptomyces griseus* and acts as a transcriptional repressor as well as an activator thus controlling expression of several hundred genes during *Streptomyces* development (Higo et al., 2012). In *Streptomyces coelicolor*, not only could AdpA-mRNA bind purified RNase III *in vitro*, but, as also shown, AdpA and RNase III coordinated the expression of each other in a posttranscriptional feedback loop (Xu et al., 2010). This finding may rationally explain the *rnc* (RNase III-deficient) mutant phenotype that affects expression of genes involved in sporulation and antibiotic production.

Although RNase III from the *Streptomyces* genus was recently shown to assist processing of ribosomal RNAs (Jones et al., 2014), it came to light as a global regulator of antibiotic biosynthesis (Adamidis and Champness, 1992; Aceti and Champness, 1998; Huang et al., 2005; Gatewood et al., 2012; Lee et al., 2013; Jones et al., 2014). In *Streptomyces coelicolor*, the deletion of the gene encoding RNase III [*rnc* gene, also termed as *absB* (Adamidis and Champness, 1992)] leads to a severely reduced production of at least four antibiotics (actinorhodin, undecylprodigiosin, CDA, and methylenomycin) (Price et al., 1999; Chang et al., 2005; Sello and Buttner, 2008). Microarray analysis was used to compare the levels of gene expression in the *S. coelicolor* parental strain and the RNase III mutant strain (Huang et al., 2005). A wide effect of the ribonuclease was found, mainly on genes connected with sporulation and antibiotic production. In the *rnc* mutant strain, sporulation genes were up-regulated, whereas activators of the antibiotic biosynthetic pathways (e.g., *actII-ORF4*, *redD*, *redZ*, and *cdaR*) were down-regulated, which is consistent with defects in antibiotic production. However, Strakova (Strakova et al., 2013) revealed that *rnc* expression is activated from the first hour of germination, suggesting a more general role for RNase III, either in ribosomal RNA or in asRNA processing. Subsequent microarray and co-immunoprecipitation analyses, performed by Gatewood (Gatewood et al., 2012), revealed at least 777 mRNAs bound by the RNase III enzyme. The authors also showed that the absence of the enzyme directly or indirectly affected the levels of hundreds of mRNAs and at least two small RNAs. These very valuable results greatly inspired the work described in this paper.

Confirmation of the expected employment of small RNAs in the regulation of cell processes, including primary metabolism, developmental transitions, antibiotic production, and various stress responses is being increasingly reported (Palečková et al., 2007; Pánek et al., 2008; Swiercz et al., 2008; D'Alia et al., 2010; Mikulík et al., 2014). Hundreds of *cis*-acting asRNAs were identified using RNA sequencing in two recent studies (Vockenhuber et al., 2011; Moody et al., 2013). Here, we further exploited Gatewood's results to see if there are connections between asRNAs and RNase III, which have not yet been reported in *Streptomyces*. We selected 17 mRNAs that are bound by the RNase III enzyme *in vivo* as stated in Gatewood et al. (2012) to check if they possessed an antisense transcript. Surprisingly, the search for asRNAs within the selected group of mRNAs was 100% successful. Moreover, additional analyses revealed antisense transcripts to selected mRNAs that encode RNase III

and several transcription regulators (AdpA, SigB, SigH, and SigR).

Although our data did not elucidate the exact role of newly found asRNAs in the RNase III-degradation pathway, the current findings further demonstrate that the antisense mechanism is widely present in *Streptomyces* and antisense RNAs are possibly involved in developmental and antibiotic synthesis control.

MATERIALS AND METHODS

Bacterial Strain, Cultivation

In this study, the *Streptomyces coelicolor* wild-type (wt) strain M145 (Kieser et al., 2000) and its RNase III-deletion strain derivative [*rnc*, M145 *rnc::aac(3)IV* (Sello and Buttner, 2008)] were used. 10^8 spores were inoculated on solid R2YE medium (Kieser et al., 2000) covered by cellophane at 29°C. Bacterial samples were collected after 24, 48, and 72 h of cultivation, where each time point represented a different developmental stage, i.e., vegetative mycelium, aerial mycelium, and spores.

RNA Isolation

Total RNA was isolated using a TRIzol method (Van Dessel et al., 2004). Harvested cells were immediately submerged in TRIzol reagent (Ambion) on ice (1 ml of TRIzol per 50 cm² of culture dish surface area). Five glass beads (3 mm in diameter) were added to the cell suspension. The cells were disrupted using a Minilys homogenizer (Precellys) twice for 2 min at 3,000 rpm and twice for 2 min at 4,000 rpm, cooled on ice between the cycles. The samples were subsequently centrifuged for 2 min at 10,000 g and purified in TRIzol/chloroform (5:1) and chloroform. For RNA precipitation, the samples were incubated in isopropanol at −20°C overnight and centrifuged for 30 min at 10,000 g. RNA samples were washed in ethanol and resuspended in 30 µl of RNase-free water. Residual DNA in the RNA samples was removed by DNase I treatment (Ambion). Typically, a concentration between 1 and 3.5 µg/µl was obtained. RNA quality was checked on a 1% agarose gel.

5' and 3' Race

RNA samples were isolated after 48 h of cultivation of both wt and *rnc* strains. Antisense RNA expressions were tested by means of the FirstChoice RLM-RACE Kit (Ambion) following the manufacturer's protocol with the several exceptions:

1. Because the uncapped 5' ends of bacterial RNAs are sensitive to the CIP (calf intestinal phosphatase) enzyme dephosphorylation, the treatment was omitted from the 5' RACE procedure.
2. A gene-specific primer (see **Figure 1**) was used instead of random decamers in the 5' RACE. The 5' RACE primers as well as the probes used for Northern blot hybridizations were designed to cover the ribosome binding site and start codon of a cognate mRNA. All of the primers were designed using the Primer3 software (<http://sourceforge.net/projects/primer3/>) (Untergasser et al., 2012).
3. The PrimeScript (Takara, 100 units per 10 µl of reaction mixture) reverse transcriptase was always included in the

experiment. Negative control lacking the enzyme was always attached to the experiment.

4. The reverse transcription proceeded at 42°C for 45 min and 48°C for 10 min.
5. Preceding the 3' RACE, total RNA samples were polyadenylated by 5 units of Poly(A) Polymerase I (New England Biolabs), according the manufacturer's protocol.

Final PCR products were separated on a 1.2% agarose gel. Products that were found in samples but absent in negative controls were excised and purified using the Qiagen MinElute PCR purification kit. The purified products were cloned into the TOPO vector using the TOPO TA Cloning (Invitrogen) and transformed into *E. coli* One Shot TOP10F' competent cells (Invitrogen). Plasmids containing the cDNA inserts were extracted using the QIAprep Miniprep kit, and sequenced to map 5' and 3' ends of RNAs reverse-transcribed.

Reverse Transcription and PCR

Experiments were performed according to the reverse transcription and PCR protocols described in the FirstChoice RLM-RACE Kit using gene specific DNA probes (details in Results and discussion). The PrimeScript (Takara, 100 units per 10 µl of reaction mixture) was used as a reverse transcriptase. A negative control PCR reaction used the original RNA sample as a template.

Northern Blot Analysis

RNA samples (30 µg) were denatured for 10 min at 70°C in RNA loading buffer (95% formamide, 0.1% bromophenol blue, 0.1% xylene cyanol, 10 mM EDTA) and separated in a 1% agarose gel containing formaldehyde, provided by the NorthernMax Kit (Ambion). Separated samples were transferred onto positively charged nylon membranes (ZetaProbe, Bio-Rad) by electroblotting at 240 mA for 45 min. The nylon membrane was UV-crosslinked.

Oligonucleotides were radioactively labeled on their 5' ends by γ -³²P-ATP using T4 polynucleotide kinase (Thermo Scientific) and purified (QIAquick Nucleotide Removal Kit, Qiagen). Hybridization was performed in ULTRAhyb hybridization buffer (Ambion) overnight at 37–42°C. The membranes were then washed twice with 2xSSC, 0.1% SDS (NorthernMax kit) at room temperature and once with 0.1xSSC, 0.1% SDS (NorthernMax kit) at 42°C. The membranes were dried and exposed in a BAS cassette on the imaging plate (Fuji-Film) for 4 days. The signals were visualized using a Phosphorimager FX (Bio-Rad) and quantified using QuantityOne analysis software (Bio-Rad), where the signals were standardized proportionally to the 5S RNA levels. Each northern blot was performed at least twice with samples from separate cultivations in the same conditions.

RESULTS

Using the RNA-seq approach, Gatewood (Gatewood et al., 2012) compared gene expression between the *S. coelicolor* M145 wild type strain and the JSE1880 *rnc*-mutant strain. The authors found that approximately 10% of all mRNAs from the vegetative

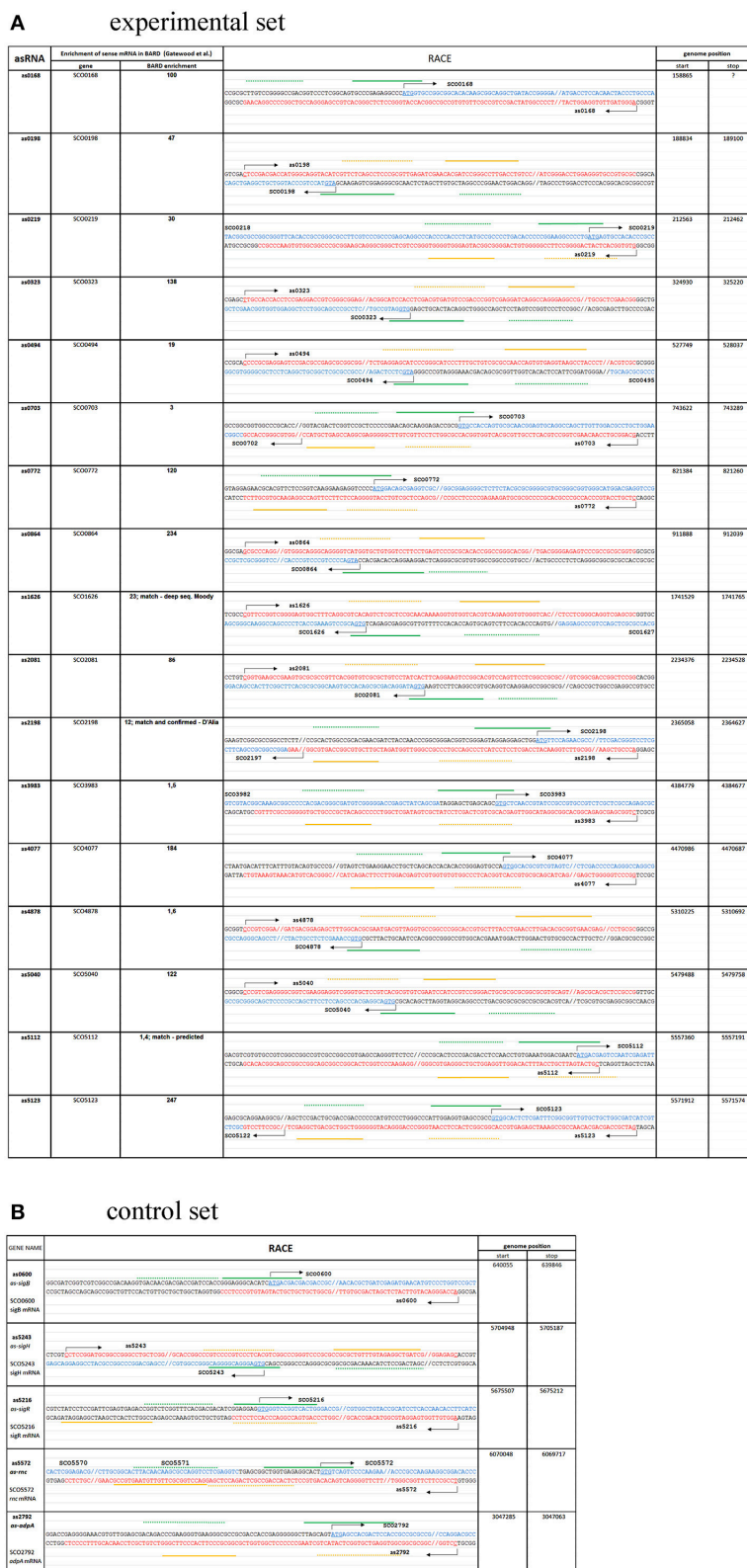


FIGURE 1 | Novel asRNAs revealed by 5' and 3' RACE method, and their genome locations (sequence of asRNA in red, sequence of mRNA in blue). Transcriptional start sites are indicated by arrows. Full green line represents 5' RACE inner primers, dotted green line represents 5' RACE outer primers, full orange line represents 3' RACE inner primers, dotted orange line represents 3' RACE outer primers. **(A)** Experimental set; **(B)** Control set; (see text for details).

state of growth were directly or indirectly affected by RNase III. In addition, they applied RNA immunoprecipitation to detect mRNAs targeted by the enzyme (referred to in their paper as BARD, bead-antibody-RNA-D70A strain). However, the necessity of involvement of other transcripts for the binding of the double-strand-specific enzyme to the mRNAs is still unknown in the case of *Streptomyces*. *In vitro* assays showed that the RNase III digests mRNA transcripts SCO3982 to SCO3988 and SCO5737 unattended (i.e., without asRNA) (Gatewood et al., 2012), whereas another unattended transcript, SCO0762, was not cleaved (Xu et al., 2008). Although *Streptomyces* as GC rich bacteria form highly structured RNAs, naturally occurring stem-loop structures of most mRNAs are too short to be bound by the RNase III enzyme that requires a minimum of approximately 20 bp of double stranded RNA for binding *in vivo* (Robertson, 1982).

RNase III-Binding mRNAs and Small RNAs Genome Vicinities

Here, to probe if the antisense RNA expression occurs in the vicinity of the RNase III-binding mRNAs (or alternatively, the binding is not complexed with asRNA), we firstly analyzed the genes whose transcripts are affected by RNase III (i.e., those mRNAs that are increased by more than two-fold in the JSE1880 *rnc*-mutant or detected in BARD as listed in the **Table S2** in Gatewood; Gatewood et al., 2012). We asked whether in the proximity of these genes lies a gene encoding for any of 1713 small RNAs found or predicted in *S. coelicolor* up-to-date (Pánek et al., 2008; Swiercz et al., 2008; D'Alia et al., 2010; Vockenhuber et al., 2011; Moody et al., 2013) that could act on the messenger by the antisense mechanism. We found out that from the 153 mRNAs increased in JSE1880 (at a single experimental time point), 45 neighbor with one of the 1713 small RNAs that could thus theoretically act as an asRNA. From these 45 mRNAs, 21 mRNAs were listed in the BARD, i.e., they bind RNase III. These data, summarized in **Table 1**, encouraged us to search for novel asRNAs expressed in the opposite direction to other RNase III-binding mRNAs.

Experimental Search for Novel cis-Antisense Transcripts

Genes for the experimental analyses had been selected independently of the *in silico* search above. We altogether tested 30 genes for the possible novel antisense expression. The initial experimental set consisted of 17 exemplar genes which we selected out of a total of 37 genes whose mRNAs were enriched in the BARD, i.e., they co-precipitated with RNase III (listed in **Table 2**, see also Gatewood's Table 2 and Table S3 in Gatewood et al., 2012). Within this set, only *as1625*, *as2198*, and *as5112* genes have been predicted before (see **Table 1**). The control set consisted of three other genes—SCO5737, *adpA*, and *rnc* (the gene of RNase III) that had been previously shown to be directly targeted by RNase III *in vitro* (Xu et al., 2008, 2010; Gatewood et al., 2012). Additionally, to determine whether the existence of antisense transcripts involves only those messengers bound by RNase III or is even more widespread, we decided to add into the control set the genes whose transcripts have not been shown

to bind RNase III. For these tests, we selected 10 genes encoding sigma factors (HrdA, HrdB, HrdC, HrdD, SigB, SigD, SigE, SigH, SigR, and WhiG) as important transcriptional regulators that govern gene expression, controlling cell development and/or responses to various stresses (Bobek et al., 2014).

We reasoned that many asRNAs overlap the ribosome binding site and the start codon of their target, possibly leading to negative translational control. Following this, all of the DNA primers used here to find antisense transcripts have been designed accordingly (**Figure 1**). To demonstrate expression of antisense transcripts, 5' RACE analyses were performed using the primers. Sequence(s) extended from the primer was/were PCR amplified and sequenced. To avoid false positive results, each reverse transcription was accompanied with a negative control sample lacking the reverse transcriptase in the reaction. The resulting electrophoretograms of both the experimental and the negative control samples were compared to exclude non-unspecific fragments in the experimental sample from sequencing.

From the total of 30 samples tested (involving both the experimental and the control set), 22 revealed a novel antisense transcript in *cis* (5' end(s) detected; see **Table 2**).

From the 17 samples of the experimental set (i.e., our selection from those mRNAs enriched in the BARD), 17 cognate asRNAs were detected (three of them have been predicted previously as could be seen in **Table 1**), signifying a 100% outcome within this group (**Figure 1A**). The 3' RACE revealed 16 3' ends within the experimental set (*scr0168* unsuccessful, northern blot was not performed).

In the control set (**Figure 1B**), our RACE data detected transcripts antisense to *adpA* (*as-adpA*), *rnc* (*as-rnc*), and three sigma factor genes (*as-sigB*, *as-sigH*, *as-sigR*). Seven sigma factor genes and the transcript SCO5737, which is bound by RNase III *in vitro*, did not reveal antisense expression.

Due to our primer design, we did not detect such antisense transcripts acting on messenger's 3' end [in Moody (Moody et al., 2013) termed as cutoRNAs]. Also the experimental approach did not allow identification of *trans*-encoded sRNAs, although similar complementary sequence on the genome could be found (as examples, novel RNAs as0772, as0600, as3983, and as5216 could theoretically act on other targets throughout the genome).

Sometimes the RACE analysis may produce false positive results due to the RNA self-priming during the reverse transcription which could be theoretically caused by stem-loop structures formation. In order to confirm the existence of the newly found *cis*-antisense transcripts and to compare their expression during *Streptomyces* cell development (24, 48, and 72 h at standard growth conditions, see methods), we performed northern blot analyses. From the total of 22 analyzed, 18 asRNAs revealed an apparent signal (**Figure 2**; for the raw northern blot images see **Presentation 1** in Supplementary Material). The signals of the remaining four were too weak or undetectable.

Details describing expression profiles of asRNAs are summarized in **Table S1** and signal quantification is presented in **Table S2** online, where the listed relative values proportional to the 5S RNA controls correspond with intracellular levels of the analyzed transcripts.

TABLE 1 | *In silico* search for sRNA genes adjacent to mRNAs that are up-regulated in *rnc* mutant.

Selected genes whose expression increased in JSE1880 (blue indicate transcripts present in the BARD; Gatewood et al., 2012)		Antisense/adjacent small RNAs (scr = small coelicolor RNA)	References	Relative orientation of asRNA gene to its possible mRNA target (red arrow) and the second adjacent gene (black arrow), * unknown (ambiguous) strand of asRNA gene, => orientation of asRNA gene, cutoRNA—antisense transcripts acting on messenger's 3' end			Comment
SCO	0499	scr	0500	Moody et al., 2013	Ambiguous	-> * <-	mRNA up-regulated in JSE1880 (Gatewood et al., 2012)
SCO	0500	scr	0500	Moody et al., 2013	Ambiguous	-> * <-	mRNA up-regulated in JSE1880 (Gatewood et al., 2012)
SCO	1150	scr	1150	Moody et al., 2013	cutoRNA	-> <=<-	mRNA up-regulated in JSE1880 (Gatewood et al., 2012)
SCO	1565	scr	1566	Swiercz et al., 2008	Ambiguous	<- * ->	Predicted
SCO	1626	scr	1625	Moody et al., 2013	cutoRNA	-> <=<-	as1625 analyzed here
SCO	1630	scr	1631	Swiercz et al., 2008	Ambiguous	<- * <-	Predicted
SCO	1659	scr	1659	Swiercz et al., 2008	Ambiguous	-> * ->	Predicted
SCO	1700	scr	1700	D'Alia et al., 2010	cis asRNA	<- => <-	Predicted by RNAz (D'Alia et al., 2010)
SCO	1906	scr	1907	Swiercz et al., 2008	Ambiguous	<- * <-	Predicted
SCO	2197	scr	2198	Swiercz et al., 2008	Ambiguous	<- * ->	Predicted
SCO	2198	scr	2198	D'Alia et al., 2010	cis asRNA	<- <=>	Confirmed, as2198 analyzed here
SCO	3003	scr	3004	Swiercz et al., 2008	Ambiguous	<- * ->	Predicted
SCO	3113	scr	3114	Swiercz et al., 2008	Ambiguous	-> * <-	Predicted
SCO	3132	scr	3133	D'Alia et al., 2010	cis asRNA	-> <=<-	Predicted by RNAz (D'Alia et al., 2010)
SCO	3216	scr	3216	Swiercz et al., 2008	Ambiguous	<- * ->	Predicted
SCO	3217	scr	3217	Swiercz et al., 2008	Ambiguous	-> * ->	Predicted
SCO	4095	scr	4096	Swiercz et al., 2008	Ambiguous	-> * ->	Predicted
SCO	4142	scr	4143	Swiercz et al., 2008	Ambiguous	<- * <-	Predicted
SCO	4144	scr	4145	Swiercz et al., 2008	Ambiguous	<- * <-	Predicted
SCO	4145	scr	4145	Swiercz et al., 2008	Ambiguous	<- * <-	Predicted
SCO	4145	scr	4146	Swiercz et al., 2008	Ambiguous	<- * ->	Predicted
SCO	4229	scr	4229	Swiercz et al., 2008	ambiguous	<- * ->	Predicted
SCO	4249	scr	4249	Swiercz et al., 2008	Ambiguous	<- * ->	Predicted
SCO	4283	scr	4283	Moody et al., 2013	cutoRNA	-> <=<-	mRNA up-regulated in JSE1880 (Gatewood et al., 2012)
SCO	4698	scr	4699	Moody et al., 2013	Ambiguous	-> <=>	Predicted
SCO	4748	scr	4749	Moody et al., 2013	cutoRNA	-> => <-	mRNA up-regulated in JSE1880 (Gatewood et al., 2012)
SCO	4882	scr	4883	Swiercz et al., 2008	Ambiguous	-> * ->	Predicted
SCO	4947	scr	4947	Swiercz et al., 2008	Ambiguous	-> * ->	Predicted
SCO	5106	scr	5106	Moody et al., 2013	cutoRNA	-> => <-	mRNA up-regulated in JSE1880 (Gatewood et al., 2012)
SCO	5112	scr	5112	Swiercz et al., 2008	cis asRNA	-> * ->	Predicted, as5112 analyzed here
SCO	5142	scr	5143	Moody et al., 2013	Ambiguous	-> <=>	Predicted
SCO	5145	scr	5145	Swiercz et al., 2008	Ambiguous	<- * ->	Predicted
SCO	5145	scr	5146	Moody et al., 2013	cutoRNA	-> => <-	mRNA up-regulated in JSE1880 (Gatewood et al., 2012)
SCO	5163	scr	5164	Swiercz et al., 2008	Ambiguous	<- * ->	Predicted
SCO	5476	scr	5476	Swiercz et al., 2008	Ambiguous	-> * ->	Predicted
SCO	5519	scr	5518	Moody et al., 2013	Ambiguous	<- * ->	Predicted
SCO	5520	scr	5521	Swiercz et al., 2008	Ambiguous	-> * ->	Predicted
SCO	5521	scr	5521	Swiercz et al., 2008	Ambiguous	-> * ->	Predicted

(Continued)

TABLE 1 | Continued

Selected genes whose expression increased in JSE1880 (blue indicate transcripts present in the BARD; Gatewood et al., 2012)	Antisense/adjacent small RNAs (scr = small coelicolor RNA)	References	Relative orientation of asRNA gene to its possible mRNA target (red arrow) and the second adjacent gene (black arrow), * unknown (ambiguous) strand of asRNA gene, => orientation of asRNA gene, cutoRNA—antisense transcripts acting on messenger's 3' end	Comment
SCO	5536 scr	5536 Pánek et al., 2008	Ambiguous <- * ->	Termed #234
SCO	5537 scr	5537 Swiercz et al., 2008	Ambiguous -> * <-	Predicted
SCO	5757 scr	5756 Swiercz et al., 2008	Ambiguous -> * ->	Predicted
SCO	6277 scr	6277 Moody et al., 2013	cis asRNA -> <=>	mRNA up-regulated in JSE1880 (Gatewood et al., 2012)
SCO	6283 scr	6284 Moody et al., 2013	Ambiguous -> * ->	Predicted
SCO	6284 scr	6284 Moody et al., 2013	Ambiguous -> * ->	Predicted
SCO	6284 scr	6285 Moody et al., 2013	Ambiguous -> <=>	Predicted
SCO	6396 scr	6396 Moody et al., 2013	Ambiguous -> * ->	Predicted
SCO	6716 scr	6716 Moody et al., 2013	cutoRNA -> <=>	mRNA up-regulated in JSE1880 (Gatewood et al., 2012)
SCO	6716 scr	6717 Moody et al., 2013	cutoRNA -> => <-	-
SCO	6728 scr	6729 Moody et al., 2013	cutoRNA -> => <-	mRNA up-regulated in JSE1880 (Gatewood et al., 2012)

Vice Versa: *scr2101* Small RNAs Found in BARD (Gatewood et al., 2012) Is Antisense to the SCO2100-SCO2101 Transcript

In Gatewood's work, expression of two small RNAs, *scr6925* and *scr2101*, was enriched in the *rnc* strain (scr = small *S. coelicolor* RNA). These data imply their antisense role and subsequent processing by the RNase III enzyme. The expression of *scr2101* was previously revealed by Swiercz (Swiercz et al., 2008). Gatewood et al. (2012) showed that the molecule is up-regulated in the JSE1880 strain (lacking the RNase III), where its level was 7-fold higher compared to that in the wild type strain. *scr2101* was also shown to be bound by the enzyme (presented in the BARD, although its enrichment was only 0.57). As the RNA's gene lies on the opposite strand between SCO2100 and SCO2101, we raised the question whether these two protein-coding genes form an operon, producing one common transcript targeted by the *scr2101* antisense RNA. The potential SCO2100-SCO2101 common transcript was used here as a template for reverse transcription using a DNA probe complementary to the 5' end of the SCO2101 mRNA (TGTCCCGGCTGCTCCAGGGA). The second DNA primer, used for the following PCR amplification, was identical to the 3' end of the SCO2100 mRNA sequence (CGTAGGTCCCCGCCCGCT), thus forming a 635-nt product, which was indeed produced. Use of a negative control PCR reaction, where the original RNA was used instead of a template, eliminated the risk of false positive results (Figure S1). This finding suggests that the antisense function of *scr2101* (which thus should be termed as *as2101*) targets the region between two open reading frames. Although the binding experiments are outside the scope of this paper, our findings raise demand to expand the RNase III-binding analyses to the unannotated sRNA transcriptome.

DISCUSSION

Novel asRNAs to mRNAs That Bind RNase III *in Vitro*

The double stranded stems of stem-loop mRNA structures are thought to be too short to be digested by the RNase III enzyme (Robertson, 1982). On the other hand, one may argue that the stem-loop structures on several mRNAs are the only possible targets for RNase III activity. Indeed, the enzyme is involved in pre-rRNA, tRNA, and polycistronic RNA processing (Conrad and Rauhut, 2002; Drider and Condon, 2004), where such stem-loop structures are present and possibly long enough to be cleaved by the enzyme. Gatewood clearly showed that some lone mRNAs are targeted and cleaved by RNase III *in vitro* (SCO5737, or the SCO3982 to SCO3988 mRNA region). In accordance to the first example, our experiments did not reveal any antisense transcript to the SCO5737 (which encodes a polynucleotide phosphorylase). Its mRNA transcript is 2,220 nt in length, and thus might be capable of forming several longer double-stranded regions observed by RNAfold (<http://rna.tbi.univie.ac.at/cgi-bin/RNAWebSuite/RFold.cgi>; fig. not shown), which are most likely targeted by the RNase III enzyme *in vitro*.

On the other hand, we show that at least one member of the SCO3982-SCO3988 operon – SCO3983 possesses an antisense gene. Its transcript, *as3983*, is 103 nt long and exhibited a strongest expression signal in vegetative cells (24 h) of the *rnc* strain. The mRNA also had a strong signal at 24 h and 48 h, even elevated in the *rnc* strain. Moreover, we observed that the *as3983* sequence is nearly identical to the region adjacent to SCO3268 and theoretically may thus also act on this transcript *in trans*.

TABLE 2 | The list of analyzed genes.

Genes selected for the analyses			Encoded protein	Relation of mRNA to RNase III		RACE			
				Ratio enrichment in BARD	Fold increase in JSE1880	5'/3' end detection result	Original strain from which the final RACE data were determined	Northern blot detection result	5'end-antisense expression independently confirmed by RNA-seq data*
				Data taken from Gatewood et al. (2012)					
Experimental set (mRNA co-precipitated with RNase III <i>in vivo</i>)	SCO	0168	Possible regulatory protein	100	2.41	+/-	WT	-	+/+
	SCO	0198	Hypothetical protein	47.6	2.70	+/+	WT	+	-/-
	SCO	0219	Putative nitrate reductase delta chain	30	2.18	+/+	WT, RNC	+	-/-
	SCO	0323	Hypothetical protein	138	1.62	+/+	WT, RNC	+	+/+
	SCO	0494	Probable iron-siderophore binding lipoprotein	19	-2.14	+/+	RNC	+	-/-
	SCO	0703	Putative regulatory protein	119	1.36	+/+	RNC	+	-/-
	SCO	0772	Putative regulatory protein	3	2.46	+/+	WT, RNC	+	+/+
	SCO	0864	Probable ECF-family sigma factor	234	1.70	+/+	WT	+	-/-
	SCO	1626	Cytochrome P450	22.8	-2.6	+/+	WT, RNC	+	+/+
	SCO	2081	Hypothetical protein	86	1.23	+/+	WT, RNC	-	-/-
	SCO	2198	Glutamine synthetase I	12.4	2.9	+/+	RNC	+	+/+
	SCO	3983	Hypothetical protein	1.5	2.14	+/+	WT, RNC	+	+/+
	SCO	4077	Hypothetical protein	184	-1.01	+/+	WT, RNC	+	+/+
	SCO	4878	Glycosyltransferase	1.6	2.00	+/+	RNC	-	+/+
	SCO	5040	Hypothetical protein	122	1.22	+/+	RNC	-	-/-
	SCO	5112	Putative ABC transport system integral membrane protein, BldKA	1.4	2.56	+/+	WT, RNC	+	+/+
	SCO	5123	Small membrane protein	247	1.24	+/+	WT, RNC	+	+/+
	Control set	SCO	2792	AdpA		<i>In vitro</i> binding	+/+	RNC	+
SCO		5572	RNase III		<i>In vitro</i> binding	+/+	WT	+	+/+
SCO		5737	Guanosine pentaphosphate synthetase/polyribonucleotide nucleotidyltransferase		<i>In vitro</i> binding	-/-	-	-	+/+
SCO		0600	RNA polymerase sigma factor SigB		Unknown	+/+	WT	+	+/+
SCO		0895	RNA polymerase sigma factor HrdC		Unknown	-/-	-	-	+/+
SCO		2465	RNA polymerase sigma factor HrdA		Unknown	-/-	-	-	+/+
SCO		3202	RNA polymerase sigma factor HrdD		Unknown	-/-	-	-	+/+
SCO		3356	RNA polymerase sigma factor SigE		Unknown	-/-	-	-	+/+
SCO		4769	RNA polymerase sigma factor SigD		Unknown	-/-	-	-	+/+
SCO		5216	RNA polymerase sigma factor SigR		Unknown	+/+	WT	+	+/+
SCO		5243	RNA polymerase sigma factor SigH		Unknown	+/+	WT	+	+/+
SCO		5621	RNA polymerase sigma factor WhiG		Unknown	-/-	-	-	-/-
SCO	5820	RNA polymerase sigma factor HrdB		Unknown	-/-	-	-	+/+	

*The expression was confirmed from the RNA-Seq data (Vockenhuber et al., 2011)/(Moody et al., 2013).

In addition to the identified as3983 RNA, we have found antisense transcripts to two other mRNAs targeted by RNase III *in vitro*. These two mRNAs code important developmental regulators that influence antibiotic production—AdpA and the RNase III itself.

According to Gatewood's results, the *adpA* mRNA was enriched 22-fold in the BARD. Therefore, we asked whether AdpA expression is controlled by an antisense mechanism. Indeed, our RACE analysis revealed a 223-nt long antisense transcript termed *as-adpA* (Figure 1B) and although subsequent

northern blot weakly detected the transcript in the wt strain (faint signal at 72 h stage of growth, **Figure 2B**), it was clearly found in the *rnc* strain at later stages, peaking at the 48 h old mycelium.

The *rnc* gene (SCO5572) that encodes the RNase III enzyme is the last member of a three gene operon, about 2,000 nt in length, that also encodes a hypothetical protein SCO5570 and a ribosomal protein L32 (SCO5571). A point mutation at amino acid position 120 of the RNase III protein causes deficiency in the ribonucleolytic activity of the enzyme, whereas its ability to bind double stranded RNAs remains intact (Huang et al., 2005). Observations that the *rnc* mRNA abundance is increased in these mutants led to discovery that RNase III cleaves among others its own transcript (Xu et al., 2008). Consistently, our northern blot analyses did not detect the *rnc* transcript in the wt strain, though we clearly confirmed the *as-rnc* RNA, which was detectable during the time course. Hence the antisense mechanism is probably involved in gene expression control of regulatory proteins such as the RNase III enzyme or the AdpA transcription regulator. Our future effort will be focused on more detailed characterization of the involvement of these two novel asRNAs in *Streptomyces* development.

as2198 RNA as an Example from the Experimental Set

as2198 is an asRNA to the *glnA* gene (SCO2198, encoding a glutamine synthase) and was previously independently shown to be expressed, termed *cnc2198.1* (D'Alia et al., 2010). The authors performed a detailed functional analysis and revealed that overexpression of *cnc2198.1* affects growth rate and antibiotic production. In the overexpression strain, the intracellular level of the targeted GlnA protein was decreased by 40%. The authors speculated that the *glnA-cnc2198.1* RNA complex blocks *glnA* translation, which may lead to its subsequent degradation. We further hypothesize that the complex is degraded by the RNase III enzyme, as our northern blot revealed that the asRNA level is increased in the *rnc* mutant. Our RACE mapping estimated the size of the antisense transcript to be 432 nt, nearly four times longer than the 121 nt transcript described by D'Alia et al. (2010). Moreover, the detected 3' end overlapped the adjacent SCO2197, revealing that *as2198* is in fact the 5'UTR of the SCO2197 mRNA. The fact that our northern blot showed a second, weaker fragment of 425 nt in size, could mean that the SCO2197 gene possesses another promoter or its transcript is further processed. Both of the detected fragments, as well as the cognate SCO2198 mRNA, had the strongest expression signals in samples from vegetative 24-h old cells, even strengthened in the *rnc* strain.

Are the Sense-Antisense Transcripts Cleaved by RNase III?

Because the sense mRNAs of the antisense transcripts found here are targeted by RNase III (or at least, their expression was negatively affected in the presence of the enzyme), we speculated that the RNase III enzyme is the most likely candidate for the paired transcript degradations. The 18 northern blot positive

results proved the existence of novel asRNAs. However, only five of those asRNAs were increased in the *rnc* strain when compared to the expression in the wild type strain. These included *as0494*, *as0864*, *as2198*, *as3983*, and the *as-adpA*. On the other hand, in two other cases, our northern blots suggest even a positive effect of the presence of RNase III enzyme on the cellular level of asRNAs (*as0323* and *as5112*, see below). Consistently, Gatewood (Gatewood et al., 2012) showed that the majority of known sRNAs, detected in their RNA-seq analysis, do not exhibit significant expression differences between the wild-type and the *rnc*-deletion mutant. As another example of sense-antisense RNA pair with an undistinguishable or even a positive effect of the enzyme on its stability in *Streptomyces* is the *scr4677*-SCO4676 complex (Hindra et al., 2014). The possibility that the RNase III enzyme does not always post-transcriptionally degrade sense-antisense complexes is also inferred from a study on sRNA degradation by three different RNases (RNase Y, J1, and III) in another Gram-positive bacterial model, *Bacillus subtilis* (Durand et al., 2012). In *Bacillus*, RNase III depletion has little effect on antisense RNAs observed by high-resolution tiling arrays. Although several RNAs showed increased abundance in the RNase III mutant, their half-lives were not affected by the enzyme, as observed by northern blot analysis. The authors concluded that the role of RNase III in *Bacillus subtilis* lies more likely in indirect transcriptional control rather than post-transcriptional RNA turnover. One may argue that the function of the enzyme might be substituted by other ribonucleases in *rnc* mutants. As the RNase III-binding mRNAs may serve as a fruitful source for novel antisense transcript discoveries, we can assume that the mRNA-asRNA pairs are targeted by the enzyme but not always degraded. An involvement of some other RNA-binding proteins, such as RNA helicase or Hfq-like protein which has not been found in *Streptomyces* yet, could be expected (Gerhart Wagner, Uppsala University, Sweden, personal communication). On the other hand, the possibility that in other cases the antisense transcripts might protect their mRNA targets against the RNase III cleavage should be taken in mind. Clarification of the exact role of RNase III enzyme in *Streptomyces* remains to be established.

asRNAs as a Potential Part of the Gene Expression Control System in *Streptomyces*

The genus *Streptomyces* can be presented as a model bacterial group lying on the top of prokaryotic cellular complexity. Their 8–10 Mbp long genome encodes all the developmental stages, including morphological changes (spore formation and germination, vegetative branching hyphae, aerial twisting mycelium), secondary metabolite production (antibiotics and a variety of other bioactive compounds, siderophores, pigments, etc.) and a capacity to respond to all possible environmental changes (diverse stresses) that are encountered. Developmental transitions and environmental intricacy require advanced regulatory networks that involve a concerted action of more than 900 transcription regulatory proteins known thus far. Here we unveiled 22 novel antisense transcripts, out of which 18 were

confirmed by northern blot analyses. These results suggest an equivalent role and possibly even bigger number of non-protein-coding RNA regulators. The *cis*-antisense transcripts are efficient gene expression modulators with minimal space requirements on their genome (Georg and Hess, 2011), with a theoretical capability to act on nearly all genes. Moreover, the mode of their action (whether based on co-transcriptional collision or post-transcriptional 100% complementarity) is simple and effective. Our work suggests that antisense transcription is widespread in *Streptomyces* and somehow connected with the function of RNase III, although the absence of the *rnc* gene did not greatly influence the majority of the transcripts. It is noteworthy that the majority of antisense transcripts found here escaped previous sRNA predictions and/or whole genome searches, suggesting that their expression level is often low and may be lost during statistical background subtraction. Nevertheless, the results in this work confirm the extensiveness of the antisense transcripts and raise the demand for elucidation of their role in gene expression control in *Streptomyces*.

AUTHOR CONTRIBUTIONS

DŠ, PP, IM, and KŠ conceived the RACE and northern blot experiments, JB performed the *in silico* analysis and provided the project design, analyzed the results and wrote the manuscript. All authors reviewed the manuscript.

REFERENCES

- Aceti, D. J., and Champness, W. C. (1998). Transcriptional regulation of *Streptomyces coelicolor* pathway-specific antibiotic regulators by the *absA* and *absB* loci. *J. Bacteriol.* 180, 3100–3106.
- Adamidis, T., and Champness, W. (1992). Genetic analysis of *absB*, a *Streptomyces coelicolor* locus involved in global antibiotic regulation. *J. Bacteriol.* 174, 4622–4628. doi: 10.1128/jb.174.14.4622-4628.1992
- Blomberg, P., Wagner, E. G., and Nordström, K. (1990). Control of replication of plasmid R1: the duplex between the antisense RNA, CopA, and its target, CopT, is processed specifically *in vivo* and *in vitro* by RNase III. *EMBO J.* 9, 2331–2340.
- Bobek, J., Strakova, E., Zikova, A., and Vohradsky, J. (2014). Changes in activity of metabolic and regulatory pathways during germination of *S. coelicolor*. *BMC Genomics* 15:1173. doi: 10.1186/1471-2164-15-1173
- Carpousis, A. J., Luisi, B. F., and McDowall, K. J. (2009). Endonucleolytic initiation of mRNA decay in *Escherichia coli*. *Prog. Mol. Biol. Transl. Sci.* 85, 91–135. doi: 10.1016/S0079-6603(08)00803-9
- Chang, S. A., Bralley, P., and Jones, G. H. (2005). The *absB* gene encodes a double strand-specific endoribonuclease that cleaves the read-through transcript of the *rpsO*-*pnp* operon in *Streptomyces coelicolor*. *J. Biol. Chem.* 280, 33213–33219. doi: 10.1074/jbc.M503440200
- Chater, K., and Losick, R. (1997). “Mycelial life style of *Streptomyces coelicolor* A3 (2) and its relatives,” in *Bacteria as Multicellular Organisms*, eds K. F. Chater, R. Losick, and American Society for Microbiology (New York, NY: Oxford University Press), 149–182.
- Conrad, C., and Rahut, R. (2002). Ribonuclease III: new sense from nuisance. *Int. J. Biochem. Cell Biol.* 34, 116–129. doi: 10.1016/S1357-2725(01)00112-1
- D’Alia, D., Nieselt, K., Steigle, S., Müller, J., Verbarg, I., and Takano, E. (2010). Noncoding RNA of glutamine synthetase I modulates antibiotic production in *Streptomyces coelicolor* A3(2). *J. Bacteriol.* 192, 1160–1164. doi: 10.1128/JB.01374-09

ACKNOWLEDGMENTS

Authors are very grateful to Prof. Beatrix Suess, Dr. Michael Vockenhuber, and Dr. Marie Elliot for checking their RNA-Seq expression data to verify the results presented here. This work was supported by a project of J. E. Purkinje University: UJEP-SGS-173-07-01 to JB, PP, IM, a project of Charles University in Prague: Progres Q26/LF1 to JB, SVV260369 to DŠ and KŠ, by the Czech research infrastructure for systems biology C4SYS (project no. LM2015055) to JB, and a grant of the Grant Agency of the Charles University (www.cuni.cz/UK-33.html) under contract no. 160214 to KŠ and 290215 to DŠ.

SUPPLEMENTARY MATERIAL

The Supplementary Material for this article can be found online at: <https://www.frontiersin.org/articles/10.3389/fmicb.2017.02693/full#supplementary-material>

Figure S1 | SCO2100-SCO2101 RT-PCR. RNA samples were isolated from both wt (lane 1) and *rnc* (lane 2) 48 h old cultures from the R2YE medium. The first probe TGTCCCGGCTGCTCCAGGGA primed the reverse transcription reaction and together with the second probe CGTAGGTCCCGCCCGCT was used in the subsequent PCR. Additional samples originated from both strains but lacking reverse transcriptase in the reaction were used as negative controls (lanes 3 and 4).

Table S1 | Description of the expression profiles of detected asRNAs.

Table S2 | Quantification of the northern blot signals presented in Figure 2.

Presentation 1 | Raw northern blot images.

- Drider, D., and Condon, C. (2004). The continuing story of endoribonuclease III. *J. Mol. Microbiol. Biotechnol.* 8, 195–200. doi: 10.1159/000086700
- Durand, S., Gilet, L., Bessières, P., Nicolas, P., and Condon, C. (2012). Three essential ribonucleases-RNase Y, J1, and III-control the abundance of a majority of *Bacillus subtilis* mRNAs. *PLoS Genet.* 8:e1002520. doi: 10.1371/journal.pgen.1002520
- Gatewood, M. L., Bralley, P., Weil, M. R., and Jones, G. H. (2012). RNA-Seq and RNA immunoprecipitation analyses of the transcriptome of *Streptomyces coelicolor* identify substrates for RNase III. *J. Bacteriol.* 194, 2228–2237. doi: 10.1128/JB.06541-11
- Geissmann, T., Marzi, S., and Romby, P. (2009). The role of mRNA structure in translational control in bacteria. *RNA Biol.* 6, 153–160. doi: 10.4161/rna.6.2.8047
- Georg, J., and Hess, W. R. (2011). *cis*-antisense RNA, another level of gene regulation in bacteria. *Microbiol. Mol. Biol. Rev.* 75, 286–300. doi: 10.1128/MMBR.00032-10
- Gerdes, K., Nielsen, A., Thorsted, P., and Wagner, E. G. (1992). Mechanism of killer gene activation. Antisense RNA-dependent RNase III cleavage ensures rapid turn-over of the stable *hok*, *srnB* and *pndA* effector messenger RNAs. *J. Mol. Biol.* 226, 637–649. doi: 10.1016/0022-2836(92)90621-P
- Gruber, T. M., and Gross, C. A. (2003). Multiple sigma subunits and the partitioning of bacterial transcription space. *Annu. Rev. Microbiol.* 57, 441–466. doi: 10.1146/annurev.micro.57.030502.090913
- Higo, A., Hara, H., Horinouchi, S., and Ohnishi, Y. (2012). Genome-wide distribution of AdpA, a global regulator for secondary metabolism and morphological differentiation in *Streptomyces*, revealed the extent and complexity of the AdpA regulatory network. *DNA Res.* 19, 259–273. doi: 10.1093/dnares/dss010
- Hindra, Moody, M. J., Jones, S. E., and Elliot, M. A. (2014). Complex intra-operonic dynamics mediated by a small RNA in *Streptomyces coelicolor*. *PLoS ONE* 9:e85856. doi: 10.1371/journal.pone.0085856

- Huang, J., Shi, J., Molle, V., Sohlberg, B., Weaver, D., Bibb, M. J., et al. (2005). Cross-regulation among disparate antibiotic biosynthetic pathways of *Streptomyces coelicolor*. *Mol. Microbiol.* 58, 1276–1287. doi: 10.1111/j.1365-2958.2005.04879.x
- Jones, S. E., Leong, V., Ortega, J., and Elliot, M. A. (2014). Development, antibiotic production, and ribosome assembly in *Streptomyces venezuelae* are impacted by RNase J and RNase III deletion. *J. Bacteriol.* 196, 4253–4267. doi: 10.1128/JB.02205-14
- Kieser, T., B. M., Buttner, M. J., Chater, K. F., and Hopwood, D. A. (2000). *Practical Streptomyces Genetics*, 2nd Edn. Norwich: John Innes Foundation.
- Lasa, I., Toledo-Arana, A., Dobin, A., Villanueva, M., de los Mozos, I. R., Vergara-Irigaray, M., et al. (2011). Genome-wide antisense transcription drives mRNA processing in bacteria. *Proc. Natl. Acad. Sci. U.S.A.* 108, 20172–20177. doi: 10.1073/pnas.1113521108
- Lasa, I., Toledo-Arana, A., and Gingeras, T. R. (2012). An effort to make sense of antisense transcription in bacteria. *RNA Biol.* 9, 1039–1044. doi: 10.4161/rna.21167
- Lee, J. H., Gatewood, M. L., and Jones, G. H. (2013). RNase III is required for actinomycin production in *Streptomyces antibioticus*. *Appl. Environ. Microbiol.* 79, 6447–6451. doi: 10.1128/AEM.02272-13
- Le Rhun, A., Beer, Y. Y., Reimegård, J., Chylinski, K., and Charpentier, E. (2016). RNA sequencing uncovers antisense RNAs and novel small RNAs in *Streptococcus pyogenes*. *RNA Biol.* 13, 177–195. doi: 10.1080/15476286.2015.1110674
- Lioliou, E., Sharma, C. M., Caldelari, I., Helfer, A. C., Fechter, P., Vandenesch, F., et al. (2012). Global regulatory functions of the *Staphylococcus aureus* endoribonuclease III in gene expression. *PLoS Genet.* 8:e1002782. doi: 10.1371/journal.pgen.1002782
- Lybecker, M., Bilusic, I., and Raghavan, R. (2014a). Pervasive transcription: detecting functional RNAs in bacteria. *Transcription* 5:e944039. doi: 10.4161/21541272.2014.944039
- Lybecker, M., Zimmermann, B., Bilusic, I., Tukhtubaeva, N., and Schroeder, R. (2014b). The double-stranded transcriptome of *Escherichia coli*. *Proc. Natl. Acad. Sci. U.S.A.* 111, 3134–3139. doi: 10.1073/pnas.1315974111
- MacRae, I. J., and Doudna, J. A. (2007). Ribonuclease revisited: structural insights into ribonuclease III family enzymes. *Curr. Opin. Struct. Biol.* 17, 138–145. doi: 10.1016/j.sbi.2006.12.002
- Mikulík, K., Bobek, J., Zidková, J., and Felsberg, J. (2014). 6S RNA modulates growth and antibiotic production in *Streptomyces coelicolor*. *Appl. Microbiol. Biotechnol.* 98, 7185–7197. doi: 10.1007/s00253-014-5806-4
- Mitschke, J., Georg, J., Scholz, I., Sharma, C. M., Dienst, D., Bantscheff, J., et al. (2011a). An experimentally anchored map of transcriptional start sites in the model cyanobacterium *Synechocystis* sp. PCC6803. *Proc. Natl. Acad. Sci. U.S.A.* 108, 2124–2129. doi: 10.1073/pnas.1015154108
- Mitschke, J., Vioque, A., Haas, F., Hess, W. R., and Muro-Pastor, A. M. (2011b). Dynamics of transcriptional start site selection during nitrogen stress-induced cell differentiation in *Anabaena* sp. PCC7120. *Proc. Natl. Acad. Sci. U.S.A.* 108, 20130–20135. doi: 10.1073/pnas.1112724108
- Moody, M. J., Young, R. A., Jones, S. E., and Elliot, M. A. (2013). Comparative analysis of non-coding RNAs in the antibiotic-producing *Streptomyces* bacteria. *BMC Genomics* 14:558. doi: 10.1186/1471-2164-14-558
- Nicolas, P., Mäder, U., Dervyn, E., Rochat, T., Leduc, A., Pigeonneau, N., et al. (2012). Condition-dependent transcriptome reveals high-level regulatory architecture in *Bacillus subtilis*. *Science* 335, 1103–1106. doi: 10.1126/science.1206848
- Palečková, P., Felsberg, J., Bobek, J., and Mikulík, K. (2007). tmRNA abundance in *Streptomyces aureofaciens*, *S. griseus* and *S. collinus* under stress-inducing conditions. *Folia Microbiol. (Praha)* 52, 463–470. doi: 10.1007/BF02932105
- Pánek, J., Bobek, J., Mikulík, K., Basler, M., and Vohradský, J. (2008). Biocomputational prediction of small non-coding RNAs in *Streptomyces*. *BMC Genomics* 9:217. doi: 10.1186/1471-2164-9-217
- Papenfort, K., and Vogel, J. (2009). Multiple target regulation by small noncoding RNAs rewires gene expression at the post-transcriptional level. *Res. Microbiol.* 160, 278–287. doi: 10.1016/j.resmic.2009.03.004
- Price, B., Adamidis, T., Kong, R., and Champness, W. (1999). A *Streptomyces coelicolor* antibiotic regulatory gene, absB, encodes an RNase III homolog. *J. Bacteriol.* 181, 6142–6151.
- Robertson, H. D. (1982). *Escherichia coli* ribonuclease III cleavage sites. *Cell* 30, 669–672. doi: 10.1016/0092-8674(82)90270-7
- Romby, P., and Charpentier, E. (2010). An overview of RNAs with regulatory functions in gram-positive bacteria. *Cell. Mol. Life Sci.* 67, 217–237. doi: 10.1007/s00018-009-0162-8
- Sello, J. K., and Buttner, M. J. (2008). The gene encoding RNase III in *Streptomyces coelicolor* is transcribed during exponential phase and is required for antibiotic production and for proper sporulation. *J. Bacteriol.* 190, 4079–4083. doi: 10.1128/JB.01889-07
- Sharma, C. M., Hoffmann, S., Darfeuille, F., Reignier, J., Findeiss, S., Sittka, A., et al. (2010). The primary transcriptome of the major human pathogen *Helicobacter pylori*. *Nature* 464, 250–255. doi: 10.1038/nature08756
- Strakova, E., Bobek, J., Zikova, A., Rehulka, P., Benada, O., Rehulkova, H., et al. (2013). Systems insight into the spore germination of *Streptomyces coelicolor*. *J. Proteome Res.* 12, 525–536. doi: 10.1021/pr300980v
- Sun, X., Zhulin, I., and Wartell, R. M. (2002). Predicted structure and phyletic distribution of the RNA-binding protein Hfq. *Nucleic Acids Res.* 30, 3662–3671. doi: 10.1093/nar/gkf508
- Swiercz, J. P., Hindra, Bobek, J., Bobek, J., Haiser, H. J., Di Berardo, C., et al. (2008). Small non-coding RNAs in *Streptomyces coelicolor*. *Nucleic Acids Res.* 36, 7240–7251. doi: 10.1093/nar/gkn898
- Taverniti, V., Forti, F., Ghisotti, D., and Putzer, H. (2011). Mycobacterium smegmatis RNase J is a 5'-3' exo-/endoribonuclease and both RNase J and RNase E are involved in ribosomal RNA maturation. *Mol. Microbiol.* 82, 1260–1276. doi: 10.1111/j.1365-2958.2011.07888.x
- Thomason, M. K., and Storz, G. (2010). Bacterial antisense RNAs: how many are there, and what are they doing? *Annu. Rev. Genet.* 44, 167–188. doi: 10.1146/annurev-genet-102209-163523
- Untergasser, A., Cutcutache, I., Koressaar, T., Ye, J., Faircloth, B. C., Remm, M., et al. (2012). Primer3—new capabilities and interfaces. *Nucleic Acids Res.* 40:e115. doi: 10.1093/nar/gks596
- Van Dessel, W., Van Mellaert, L., Geukens, N., Lammertyn, E., and Anné, J. (2004). Isolation of high quality RNA from *Streptomyces*. *J. Microbiol. Methods* 58, 135–137. doi: 10.1016/j.mimet.2004.03.015
- Viegas, S. C., Pfeiffer, V., Sittka, A., Silva, I. J., Vogel, J., and Arraiano, C. M. (2007). Characterization of the role of ribonucleases in *Salmonella* small RNA decay. *Nucleic Acids Res.* 35, 7651–7664. doi: 10.1093/nar/gkm916
- Vockenhuber, M. P., Sharma, C. M., Statt, M. G., Schmidt, D., Xu, Z., Dietrich, S., et al. (2011). Deep sequencing-based identification of small non-coding RNAs in *Streptomyces coelicolor*. *RNA Biol.* 8, 468–477. doi: 10.4161/rna.83.14421
- Waters, L. S., and Storz, G. (2009). Regulatory RNAs in bacteria. *Cell* 136, 615–628. doi: 10.1016/j.cell.2009.01.043
- Xu, W., Huang, J., and Cohen, S. N. (2008). Autoregulation of AbsB (RNase III) expression in *Streptomyces coelicolor* by endoribonucleolytic cleavage of absB operon transcripts. *J. Bacteriol.* 190, 5526–5530. doi: 10.1128/JB.00558-08
- Xu, W., Huang, J., Lin, R., Shi, J., and Cohen, S. N. (2010). Regulation of morphological differentiation in *S. coelicolor* by RNase III (AbsB) cleavage of mRNA encoding the AdpA transcription factor. *Mol. Microbiol.* 75, 781–791. doi: 10.1111/j.1365-2958.2009.07023.x

Conflict of Interest Statement: The authors declare that the research was conducted in the absence of any commercial or financial relationships that could be construed as a potential conflict of interest.

Copyright © 2018 Šetinová, Šmídová, Pohl, Musić and Bobek. This is an open-access article distributed under the terms of the Creative Commons Attribution License (CC BY). The use, distribution or reproduction in other forums is permitted, provided the original author(s) or licensor are credited and that the original publication in this journal is cited, in accordance with accepted academic practice. No use, distribution or reproduction is permitted which does not comply with these terms.



The SCO4117 ECF Sigma Factor Pleiotropically Controls Secondary Metabolism and Morphogenesis in *Streptomyces coelicolor*

María T. López-García, Paula Yagüe, Nathaly González-Quiñónez, Beatriz Rioseras and Angel Manteca*

Área de Microbiología, Departamento de Biología Funcional e IUOPA, Facultad de Medicina, Universidad de Oviedo, Oviedo, Spain

OPEN ACCESS

Edited by:

Dirk Tischler,
Freiburg University of Mining and
Technology, Germany

Reviewed by:

Thorsten Mascher,
Technische Universität Dresden,
Germany

Dennis Claessen,
Leiden University, Netherlands

*Correspondence:

Angel Manteca
mantecaangel@uniovi.es

Specialty section:

This article was submitted to
Microbial Physiology and Metabolism,
a section of the journal
Frontiers in Microbiology

Received: 14 August 2017

Accepted: 09 February 2018

Published: 21 February 2018

Citation:

López-García MT, Yagüe P,
González-Quiñónez N, Rioseras B and
Manteca A (2018) The SCO4117 ECF
Sigma Factor Pleiotropically Controls
Secondary Metabolism and
Morphogenesis in *Streptomyces*
coelicolor. *Front. Microbiol.* 9:312.
doi: 10.3389/fmicb.2018.00312

Extracytoplasmic function (ECF) sigma factors are a major type of bacterial signal-transducers whose biological functions remain poorly characterized in streptomycetes. In this work we studied SCO4117, a conserved ECF sigma factor from the ECF52 family overexpressed during substrate and aerial mycelium stages. The ECF52 sigma factors harbor, in addition to the ECF sigma factor domain, a zinc finger domain, a transmembrane region, a proline-rich C-terminal extension, and a carbohydrate-binding domain. This class of ECF sigma factors is exclusive to Actinobacteria. We demonstrate that SCO4117 is an activator of secondary metabolism, aerial mycelium differentiation, and sporulation, in all the culture media (sucrose-free R5A, GYM, MM, and SFM) analyzed. Aerial mycelium formation and sporulation are delayed in a SCO4117 knockout strain. Actinorhodin production is delayed and calcium-dependent antibiotic production is diminished, in the Δ SCO4117 mutant. By contrast, undecylprodigiosin production do not show significant variations. The expression of genes encoding secondary metabolism pathways (deoxysugar synthases, actinorhodin biosynthetic genes) and genes involved in differentiation (*rdl*, *chp*, *nepA*, *ssgB*) was dramatically reduced (up to 300-fold) in the SCO4117 knockout. A putative motif bound, with the consensus “CSGYN-17bps-SRHA” sequence, was identified in the promoter region of 29 genes showing affected transcription in the SCO4117 mutant, including one of the SCO4117 promoters. SCO4117 is a conserved gene with complex regulation at the transcriptional and post-translational levels and the first member of the ECF52 family characterized.

Keywords: *Streptomyces*, ECF, sigma factor, differentiation, secondary metabolism, antibiotic

INTRODUCTION

Extracytoplasmic function (ECF) sigma factors, together with one- and two-component systems, are a major type of bacterial signal-transducing proteins (Huang et al., 2015). The ECF sigma factors belong to the σ^{70} family, but harbor only two of the four conserved regions of this group (σ^2 and σ^4 regions), which is sufficient for promoter recognition and RNA

polymerase recruitment (reviewed in Mascher, 2013). The ECF sigma factors activate genes that confer resistance to agents that threaten the integrity of the envelope or cellular homeostasis (Kormanec et al., 2016) and are tightly regulated by diverse and complex mechanisms (Mascher, 2013). Most ECF sigma factors are negatively regulated by anti- σ factors (ASF), usually co-expressed with its target ECF sigma factor. The correct stimulus leads to the inactivation of the ASF and allows the ECF sigma factors to bind to their target promoters and RNA polymerase (Mascher, 2013). However, several ECF sigma factors lack a known ASF and are therefore differently regulated (Staron et al., 2009; Huang et al., 2015). Members of the ECF41 and ECF42 families possess C-terminal extensions that regulate their activities, thereby acting like ASFs (Gómez-Santos et al., 2011; Wecke et al., 2012), while the activity of other ECF sigma factors was proposed to be regulated by ASF-independent transcriptional regulators and post-translational modifications (Ser/Thr/Tyr phosphorylation) (Mascher, 2013).

Streptomyces is a genus of Gram-positive soil bacteria of great importance for biotechnology given their ability to produce a large array of bioactive compounds, including antibiotics, anticancer agents, immunosuppressants, and industrial enzymes (Hopwood, 2007). *Streptomyces* has a complex morphogenesis that includes hyphal differentiation and sporulation. In high density laboratory cultures, after spore germination, a fully compartmentalized mycelium (MI) initiates the development until it undergoes an ordered process of programmed cell death (PCD) and develops into a second multinucleated mycelium (substrate mycelium, early MII). This mycelium further develops into aerial hyphae and makes the hydrophobic proteins necessary for growth into the air (reviewed in Yagüe et al., 2013a). Secondary metabolism and differentiation are largely controlled by specific sigma factors that enable the recognition of specific promoters, directing the expression of specific genes (reviewed in Kormanec et al., 2016). *Streptomyces coelicolor*, the best-characterized *Streptomyces* strain, harbors 65 σ factors, including principal σ factors (*hrdA-D*), general stress response σ factors, and ECF sigma factors (Kormanec et al., 2016). The *S. coelicolor* genome encodes for 51 ECF sigma factors, of which only four have been characterized so far: SigE, required for a normal cell wall structure (Hutchings et al., 2006); SigR, a global regulator of redox homeostasis (Feeney et al., 2017); SigT, regulating actinorhodin production in response to nitrogen stress (Feng et al., 2011); and σ BldN, an ECF sigma factor required for aerial mycelium formation (Bibb et al., 2012).

The ECF52 family of sigma factors is characterized by long C-terminal extensions that contain a zinc finger domain, a variable number of transmembrane helices and a long proline-rich C-terminal extension, which includes a carbohydrate-binding domain (Huang et al., 2015; **Figure 1**). Members of this family are only present in Actinobacteria (Huang et al., 2015). In this work, we studied *SCO4117*, a conserved ECF52 sigma factor that was detected as overexpressed during the substrate and aerial

mycelia stages of *Streptomyces* development (Yagüe et al., 2013b), suggesting a role in the regulation of secondary metabolism and differentiation. To our knowledge, *SCO4117* is the first member of the ECF52 sigma factors that has been characterized.

MATERIALS AND METHODS

Bacterial Strains and Culture Conditions

All *Streptomyces* and *Escherichia coli* strains used in this work are listed in **Table 1**. Spores were harvested from SFM solid plates (Kieser, 2000) after growth at 30°C for 7 days. The differentiation analyses were carried out on GYM plates covered with cellophane and on minimal medium (MM) plates supplemented with glucose (10 g/l), both inoculated with 10⁷ spores from a fresh water suspension and cultured at 30°C. The samples for quantification of actinorhodin and undecylprodigiosin production were obtained from 100-ml sucrose-free R5A (Fernández et al., 1998) cultures grown at 30°C and 200 rpm in 500-ml flasks. Calcium-dependent antibiotic (CDA) production was measured on nutritive agar from Oxoid. *E. coli* strains were cultured in LB and 2xTY media at 37°C. The following antibiotics were added to select plasmid-bearing and mutant strains: ampicillin (100 µg/ml), apramycin (100 µg/ml for *E. coli*, 25 µg/ml for *S. coelicolor*), chloramphenicol (25 µg/ml), hygromycin (100 µg/ml for *E. coli*, 200 µg/ml for *S. coelicolor*), kanamycin (50 µg/ml), and nalidixic acid (25 µg/ml).

Nucleic Acid Manipulations

Genomic DNA isolation and conjugation were performed following standard methods (Kieser, 2000; Sambrook and Russell, 2001).

Total RNA samples were isolated as previously described (Rioseras et al., 2016) using RNeasy Mini spin columns and treated with DNase I (Qiagen). The quantity and integrity of the RNA samples were measured with Nanodrop 2000 (Thermo Scientific) and 2100 Bioanalyzer (Agilent).

SCO4117 Mutagenesis

The *SCO4117* ORF was replaced with the apramycin resistance cassette. The fragments upstream (UP-1944pb) and downstream (DW-2234pb) of *SCO4117* were amplified by PCR from *S. coelicolor* DNA using the primers SCO159-SCO160 and SCO163-SCO164, respectively. The PCR products were cloned and sequenced in pCRTM-Blunt II-TOPO[®] obtaining pTOPO-UP and pTOPO-DW. The DW fragment was liberated from pTOPO-DW by *EcoRV*/*PstI* digestion and subcloned in pTOPO-UP digested with the same restriction enzymes. The resulting plasmid, pTOPO-UPDW, was linearized with *PstI* and ligated with a *PstI*-fragment from pIJ773 containing an apramycin resistance cassette with an *oriT*, obtaining p Δ SCO4117. This vector was introduced in the wild-type strain by conjugation and double recombinants were selected as kanamycin-sensitive and apramycin-resistant. Southern hybridization and PCR amplification with SCO134 and 4117R (**Table 1**) primers were performed to check the Δ SCO4117 mutant.

Abbreviations: ECF, extracytoplasmic function; ASF, anti-sigma factor; CDA, calcium dependent antibiotic; PCD, programmed cell death; ORF, open reading frame; NGS, next generation sequencing; RT-PCR, reverse transcription PCR.

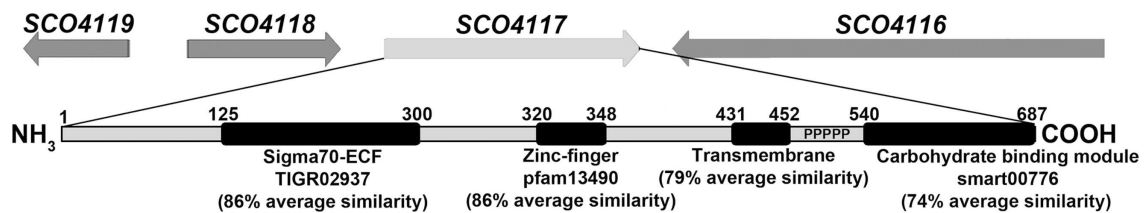


FIGURE 1 | SCO4117 structure. Outline of the SCO4116-SCO4119 region, showing the SCO4117 conserved domains and average similarities between SCO4117 and their orthologs in *S. griseus*, *S. avermitilis*, *S. lividans*, *S. clavuligerus*, and *S. venezuelae*. Ps indicate the proline-rich C-terminal extension.

To discard polar effects in the expression of the *SCO4117* neighbor genes due to the apramycin gene insertion, we recreated the *SCO4117* knockout by CRISPR-Cas9. We used the system designed by Tong et al. (2015). The 20-nt target sequence was selected inside the *SCO4117* and amplified by PCR with the primers SCO215 and sgRNA-R. The product of 110 bps was digested with *NcoI/SnaBI* and cloned in *NcoI/SnaBI*-digested pCRISPR-Cas9, obtaining pCRISPR-SgSCO4117. The *SCO4117*-surrounding regions were amplified by PCR with SCO216/SCO217 and SCO218/SCO219 primers. The couple of DNA fragments were combined by overlap extension PCR (Lee et al., 2010) with the primers SCO216/SCO219. The PCR product was cloned and sequenced in pCRTM-Blunt II-TOPO[®]. The insert was released with *EcoRV* and cloned into pCRISPR-SgSCO4117 digested with *StuI*. The final vector pCRISPR-SCO4117A was introduced into the *S. coelicolor* wild-type strain by conjugation. The conjugants harboring the plasmid were selected using apramycin resistance, plated in SFM and grown at 37°C for 3 days for plasmid clearance. Mutations were confirmed by PCR using the primers Mut4117F and Mut4117R (Table 1).

The SCO4117 mutant harboring the nucleotides encoding for the first 305 amino acids of *SCO4117*, those including the sigma factor domain (Figure 1), was created by CRISPR-Cas9. The 20-nt target sequence was selected inside the *SCO4117*, but outside the first 305 amino acids (Figure 1) and amplified by PCR with the primers SCO215/sgRNA-R. The SCO220/SCO221 and SCO222/SCO219 primers were used (primer SCO222 contain the SCO4117 stop codon in frame with the first 305 amino acids) to amplify the *SCO4117* sigma factor-surrounding regions. DNA fragments were combined by overlap extension PCR with the primers SCO220/SCO219. The amplicon was cloned and sequenced in pCRTM-Blunt II-TOPO[®]. The insert was released with *EcoRV* and cloned into pCRISPR-SgSCO4117 digested with *StuI*, obtaining vector pCRISPR-SCO4117B. Conjugation, mutagenesis, and mutant confirmation was performed as described above (Table 1).

S. coelicolor Δ*SCO4117* Complementation

The complementation of *S. coelicolor* Δ*SCO4117* was performed via the integration of plasmid pMS82 (Gregory et al., 2003), harboring the *SCO4117* ORF and an upstream region large enough to include the two promoter regions identified by Jeong et al. (2016). The *SCO4117* was amplified from the *S. coelicolor* chromosome using the primers SCO134 and 4117R. The 2171 bp-fragment was cloned in pCRTM-Blunt II-TOPO[®] and sequenced

to check the absence of mutations. A *SpeI* fragment obtained from TOPO-4117 was ligated into pMS82 digested with *SpeI* resulting in pMS82-*SCO4117*. This plasmid was transferred by conjugation to the *S. coelicolor* Δ*SCO4117* mutant. The conjugants harboring the plasmid were selected by hygromycin resistance and the correct plasmid insertion at the *SCO4848 attB* site was verified by PCR using the primers SCO4848F and pMS82R (Table 1).

Restoration of the wild-type genotype of the Δ*SCO4117* mutant was achieved using the CRISPR-Cas9 system for *Streptomyces* designed by Tong et al. (2015). The 20-nt target sequence was selected inside the apramycin resistance cassette, replacing *SCO4117* and amplified by PCR with the primers SCO197 and sgRNA-R. The 120-bps product was digested with *NcoI/SnaBI* and cloned in *NcoI/SnaBI*-digested pCRISPR-Cas9 obtaining pCRISPR-120. A single fragment of 3.7 kb, containing the complete *SCO4117* sequence and the surrounding regions, was amplified by PCR from *S. coelicolor* chromosome using SCO4117-FA and SCO4117-R primers. The product was then cloned and sequenced in pCRTM-Blunt II-TOPO[®]. The resulting plasmid was digested with *EcoRV/SpeI* to liberate a 3.7 kb fragment. The *SpeI*-end was filled with the Klenow enzyme and the product was cloned into pCRISPR-120 linearized with *StuI*. The final vector pCRISPR-4117, was introduced in *S. coelicolor* Δ*SCO4117* by conjugation. Conjugant selection and plasmid clearance were performed as described above. Restoration of the wild-type genotype was checked by the loss of apramycin resistance (Table 1).

Viability Staining

Samples were obtained from GYM plates covered with cellophane at different developmental stages. The bacteria were stained with SYTO 9 and propidium iodide (LIVE/DEAD BacLight Bacterial Viability Kit, Invitrogen, L-13152) and observed under a Leica TCS-SP8 confocal laser-scanning microscope at wavelengths of 488 and 568 nm excitation and at 530 (green) or 640 nm (red) emissions.

Antibiotic Production and Protein Quantification

Undecylprodigiosin and actinorhodin were quantified spectrophotometrically according to Tsao et al. (1985) and Bystrykh et al. (1996). For actinorhodin quantification, KOH was added to the culture samples at a final concentration of 1N. Cellular pellets were discarded by centrifugation

TABLE 1 | Bacterial strains, plasmids, cosmids, and primers used in this study.

Strain, plasmid, cosmid	Description	Reference
<i>S.coelicolor</i> M145	SCP1 ⁺ SCP2 ⁺ , reference strain	Kieser, 2000
<i>S.coelicolor</i> ΔSCO4117	SCO4117 replaced with <i>acc(3)/IV</i> , Apr ^R	This study
<i>E. coli</i> TOP10	F [−] <i>mcrA</i> Δ(<i>mrr-hsdRMS-mcrBC</i>) φ80 <i>lacZ</i> ΔM15 Δ <i>lacX74</i> <i>recA1</i> <i>araD139</i> Δ(<i>ara-leu</i>)7697 <i>galU</i> <i>galK</i> <i>rpsL</i> <i>endA1</i> <i>nupG</i>	Invitrogen
<i>E. coli</i> ET12567	<i>dam-13::Tn9</i> , <i>dcm-6</i> , <i>hsdM</i> , <i>hsdR</i>	MacNeil et al., 1992
<i>E. coli</i> ET12567/pUZ8002	<i>E. coli</i> ET12567 harboring pUZ8002, a not self-transmissible plasmid which can mobilize <i>oriT</i> -containing plasmids by conjugation	Flett et al., 1997
<i>Bacillus subtilis</i>	Indicator microorganism for CDA bioassay	
PLASMIDS AND COSMIDS		
pMS82	Integrative and conjugative vector, Hyg ^R	Gregory et al., 2003
PCR TM -Blunt II-TOPO [®]	Zero Blunt [®] TOPO [®] PCR Cloning Kit, Kan ^R	Invitrogen
pIJ773	Apr cassette in pIJ699	Gust et al., 2003
pΔSCO4117	SCO4117 deletion construction, a <i>Streptomyces</i> non-replicative plasmid transmissible by conjugation, Apr ^R Kan ^R	This study
pMS82-SCO4117	Integrative and conjugative plasmid derived from pMS82 with the completed SCO4117 gen under its own promoter control. Hyg ^R	This study
pCRISPR-Cas9	Conjugative and thermosensitive plasmid harboring Cas9	Tong et al., 2015
pCRISPR-120	pCRISPR-Cas9 harboring the apramycin resistance target sequence	This study
pCRISPR-SCO4117	pCRISPR-120 harboring a 3.7 kb DNA fragment including SCO4117	This study
pCRISPR-SgSCO4117	pCRISPR-Cas9 harboring the target SCO4117 sequence	This study
pCRISPR-SCO4117A	pCRISPR-SgSCO4117 harboring a 2.5 kb fragment used to create the SCO4117 knockout	This study
pCRISPR-SCO4117B	pCRISPR-SgSCO4117 harboring a 2.2 kb fragment used to create the truncated SCO4117 gene harboring the sigma factor domain	This study
PRIMERS		
SCO134	GACGTGCTGCTGGTCATAGC	This study
SCO4117R	GGGACTAGTGACGCCGCCGAAGTGG	This study
SCO159	GGAGGCGATGTCCATCTGTT	This study
SCO160	TCAACGCTCATCGCGAAAG	This study
SCO163	CTGCAGGCCAGTCCCGCTTCAC	This study
SCO164	GATATCACTCCTGGTCTCGACAACT	This study
SCO4848F	CGTCGTATCCCCCTCGGTTG	Gonzalez-Quinonez et al., 2016
pMS82R	GAGCCGGGAAAGCTCATTCA	Gonzalez-Quinonez et al., 2016
SCO197	CATGCCATGGTTCCGCGATGAGCGTTGAAAGTTTTAGAGCTAGAAATAGC	This study
sgRNA-R	ACGCCTACGTAAAAAAGCACCGACTCGGTGCC	Tong et al., 2015
SCO4117-FA	GGGGGATATCACGACCGTGATCTCGGCC	This study
RT-SCO4117-F	CGACGACACGGCCTACGA	This study
RT-SCO4117-R	CGCACCGCCTGAAGCAT	This study
hrdB-F	CGCGGCATGCTCTTCCT	Kurt et al., 2013
hrdB-R	AGGTGGCGTACGTGGAGAAC	Kurt et al., 2013
bldN-F	CTCACCAGCGAGACCTTTCTGC	This study
bldN-R	TCGTTGGCGTCGAGCATCT	This study
SCO1178-F	TCAAGGTCCGGCAGGTCTA	This study
SCO1178-R	CCGTCTCCTGCTTGGT	This study
chpA-F	CTCGTCTCGTCTCGACTT	Straight et al., 2006
chpA-R	GTCGTTCTCGCACTTGTTGC	Straight et al., 2006
chpH-F	CACCGGTGGTCTGGTTCTC	Straight et al., 2006
chpH-R	ATCACGGAGATCGTGTTGC	Straight et al., 2006
SCO2748-F	GAGATCACCCCGAAACTGG	This study
SCO2748-R	AAGTGCCAGTCGATGACGTT	This study
actVA2-F	ACTACGCCTCCAGAACCTC	This study
actVA2-R	TTGTGCCCGCGATGTC	This study

(Continued)

TABLE 1 | Continued

Strain, plasmid, cosmid	Description	Reference
redF-F	CGGAGAACAAGGGCAAGC	This study
redF-R	CAGGGGGATGGCGAAG	This study
actII4-F	GCGGCTTTTGAATGC	This study
actII4-R	GCAGGGTCTCGTTCAGC	This study
SCO215	CATGCCATGGCAGCTCGCTCCACTGGTAGAGTTTATAGCTAGAAATAGC	This study
SCO216	GATATCCGGGAACCAACGTCGCACGG	This study
SCO217	CGGTTCCGCAGGCTCCTACGCGGAAAGCCCCGCCAAC	This study
SCO218	GTTGGCGGGGCTTTCCGCGTAGGAGCCTGCGGAACCG	This study
SCO219	GATATCTGCAGGTGCGGATGATGCAC	This study
SCO220	GATATCCGTATCTCCTTCCCCGAACG	This study
SCO221	CGGTTCCGCAGGCTCCTACTGGAGGTAGGCCTGCTTG	This study
SCO222	CAAGCAGGCCTACCTCCAGTAGGAGCCTGCGGAACCG	This study
Mut4117F	CCCTGTCGCAACCTCTGC	This study
Mut4117R	GACGGGCACCCTGCG	This study

and actinorhodin concentration was spectrophotometrically determined at 640 nm applying the linear Beer–Lambert relationship ($\epsilon_{640} = 25,320$). The culture samples for undecylprodigiosin quantification were vacuum-dried, resuspended in methanol, acidified with 0.5N HCl and spectrophotometrically assayed at 530 nm, using the Beer–Lambert relationship to estimate concentration ($\epsilon_{530} = 100,500$).

CDA production was determined via a bioassay against *Bacillus subtilis*. Oxoid nutritive agar (ONA) plates (90 mm in diameter) were inoculated with 5 μ l of a *Streptomyces* spore suspension at 1×10^5 spores/ml and incubated at 30°C. After 2 days, the plates were overlayed with 5 ml of soft ONA (0.75% agar), inoculated with *B. subtilis* (OD = 0.25) and supplemented with $\text{Ca}(\text{NO}_3)_2$ (60 mM). Negative controls were performed in parallel without adding calcium. Inhibitory halos were measured after 15 h at 30°C.

Growth was determined by measuring the protein concentration with the Bradford assay (Biorad) and a bovine serum albumin standard (Sigma). Total protein extracts were obtained mixing a volume of culture with a volume of 1 M NaOH, boiling for 5 min, and removing cell debris by centrifugation at 7740 g.

RNA-Seq and Bioinformatic Analysis

Next-generation sequencing (NGS) was performed by Stab Vida (Caparica, Portugal) from two biological replicates using the Δ SCO4117 mutant and the *S. coelicolor* wild-type strain. Ribosomal RNA was depleted with the Ribo-Zero Bacteria Kit (Illumina), and the cDNA library construction was carried out using the TruSeq Stranded mRNA Library Preparation Kit (Illumina). The DNA was sequenced in the Illumina HiSeq 2500 platform using 100-bp paired-end sequencing reads (at least 20 M reads per sample). Raw data are available via the Gene Expression Omnibus database (accession GSE107661).

Bioinformatic analysis of the sequenced data was performed under the Linux operative system using the following software:

FastQC to check the quality of the sequences, Cutadapt for trimming sequences, Bowtie2 for mapping with the *Streptomyces coelicolor* genome and Cuffdiff for differential expression test analysis (Trapnell et al., 2012). Variations in transcript abundances were considered significant if they had a p -value < 0.03 (Supplementary Table 1). Transcript abundances without significant variations (p -values higher than 0.03) are shown in Supplementary Table 2.

The transmembrane topology of the SCO4117 gene was analyzed using the Phobius software (<http://phobius.sbc.su.se/>). The SCO4117 orthologs were obtained from the Strepdb database (<http://strepdb.streptomyces.org.uk/>): SLI_4349 (*S. lividans*), SAV_3491 (*S. avermitilis*), SVEN15_3779 (*S. venezuelae*), SGR_3904 (*S. griseus*), and SCLAV_3143/ SCLAV_3144 (*S. clavuligerus*). Amino acid similarities were estimated using the software package Lalign (http://www.ch.embnet.org/software/LALIGN_form.html).

SCO4117 Motif Bound Search

The 46 genes significantly down-regulated in the Δ SCO4117 mutant were grouped into 33 putative operons (Supplementary Table 1). A library of putative regulatory sequences has compiled from the 250 nucleotide-long sequences located upstream of the putative operons. BioProspector (Liu et al., 2001) was used to search for bipartite overrepresented motifs in these sequences. Searches were performed only in the forward strand, and the following parameters were varied iteratively: the lengths of the -35 and -10 motifs were varied between 5 and 7 nucleotides; the spacer length was varied between 15 and 20 nucleotides in 1-nucleotide intervals. From all generated motifs, the highest scoring bipartite motif was selected. The motif logo was created using Weblogo (Crooks et al., 2004).

Quantitative RT-PCR (qRT-PCR)

A High-Capacity cDNA Reverse Transcription Kit (Applied Biosystems) was used to synthesize cDNA from 0.5 μ g of RNA from two biological replicates. Real-Time PCRs of the SCO4117

gene were carried out on an ABI PRISM 7900 HT thermocycler (Applied Biosystems). The reactions were performed in triplicate, containing 2 μ l of 2-fold diluted cDNA, 10 μ l of SYBR Green PCR Master Mix (Applied Biosystems), and 300 nM of specific primers (RT-SCO4117-F/R) (listed in **Table 1**) in a final volume of 20 μ l. The *hrdB* (SCO5820, amplified using primers hrdB-F/R) was used as reference since its expression showed no variation between strains in our RNA-seq results (Supplementary Table 2). The DNA contamination and primer dimer amplification were tested in negative controls replacing cDNA by RNA or water. Amplification conditions were as follows: 2 min at 50°C, 10 min at 90°C, 40 repetitions of 15 s at 95°C, and 1 min at 60°C. Primer efficiencies were measured using serial dilutions of genomic DNA as template and the relative quantification of gene expression was performed by the $\Delta\Delta$ Ct method (Livak and Schmittgen, 2001).

The expression of the most differentially expressed genes between the *SCO4117* mutant and the wild strain was validated by qRT-PCR: *SCO5077*, *actVA2*; *SCO2478*, reductase activated by actinorhodin; and *SCO1178* epimerase. We also analyzed key genes from the actinorhodin (*actII-4*, *SCO5085*) and undecylprodigiosin (*redF*, *SCO5898*) clusters; one of the bald genes (*bldN*, *SCO3323*); two of the genes participating in the aerial hyphae formation (*chpA*, *SCO2716* / *chpH*, *SCO1675*); and *SCO0761*, a hypothetical protein (primers are listed in **Table 1**). The correlation between transcript abundances quantified by RNA-seq and qRT-PCR was adequate (regression coefficient of 0.71) (Supplementary Figure 1).

RESULTS

SCO4117 Gene Structure and Conservation in the *Streptomyces* Genus

Gene *SCO4117*, the only member of the ECF52 family present in *S. coelicolor*, encodes a conserved multidomain protein (average protein similarity of 68.4% among *S. griseus*, *S. avermitilis*, *S. lividans*, *S. clavuligerus*, and *S. venezuelae*). The *SCO4117* harbors a putative ECF sigma factor domain (conserved domain database accession TRIGR02937, 86% average similarity), a putative zinc finger domain (pfam13490, 86% average similarity), a putative transmembrane domain (79% average similarity), a putative carbohydrate-binding module (smart00776, 74% average similarity), and a proline-rich region separating the transmembrane and the carbohydrate module (**Figure 1**). Surprisingly, in the case of the *S. clavuligerus* ortholog, there is a stop codon separating the carbohydrate-binding domain module ORF (*SCLAV_3143*) from the other domain ORFs (*SCLAV_3144*) (<http://streptdb.streptomyces.org.uk/>), perhaps due to an error in the sequence at the proline-rich region. Gene *SCO4117* is localized downstream the actinorhodin positive regulator *atrA* (*SCO4118*), but both genes were described as being expressed independently (Uguru et al., 2005). This synteny is maintained in all *Streptomyces* species analyzed, with the exception of *Streptomyces avermitilis*, in which the *SCO4117* and *atrA* orthologs (*SAV_3491* and *SAV_4110* respectively) are separated.

Mutation of *SCO4117* Affects Antibiotic Production and Morphogenesis in Different Culture Conditions (Liquid and Solid) and Media (Sucrose-Free R5A, GYM, MM, SFM)

The *S. coelicolor* *SCO4117* knockout mutant (Δ *SCO4117*) do not show a significant variation in growth (**Figure 2A**), or in the maximum amount of actinorhodin and undecylprodigiosin production (**Figures 2B,C**), in sucrose-free R5A liquid cultures. However, the mutant shows a delay in actinorhodin production compared to the wild-type strain (**Figure 2B**). The *SCO4117* knockout mutant showed lower CDA production (**Figure 2D**) and a delay in MII differentiation (notice the discontinuities characterizing the MI hyphae in the mutant at 24 h) (**Figure 2F**) (Manteca et al., 2006) and sporulation (**Figures 2E,F**) in solid GYM solid cultures. The delay in development was not complemented when *SCO4117* and an upstream region large enough to include the two promoter regions identified by Jeong et al. (2016) were introduced into the mutant using the integrative plasmid pMS82-*SCO4117* (**Figure 2G**). As discussed below, the *SCO4117* gene expression was not restored in the complemented mutant (the *SCO4117* transcript abundance was 4-fold less than in the wild-type strain) (**Figure 2H**). Interestingly, the Δ *SCO4117* phenotype was only restored when a copy of the *SCO4117* ORF was introduced at the native position in the Δ *SCO4117* mutant, using the CRISPR-Cas9 methodology (**Figure 2I**). This result discards the possibility of artifactual mutations at chromosomal positions different to *SCO4117*, generating the phenotypes observed.

As discussed below, the above data suggest a complex regulation of the expression of the *SCO4117* gene. Polar effects in the expression of *SCO4117* neighbor genes due to the apramycin-resistance gene transcription, are unlikely, because, as detailed below, we did not detect significant variations in the expression of the *SCO4116* and *SCO4118* genes in the Δ *SCO4117* mutant compared to the wild-type strain (Supplementary Table 2). In order to further discard a possible effect of the apramycin-resistance gene in the phenotypes observed, we recreated the knockout mutant by CRISPR/Cas9. We eliminated the *SCO4117* ORF, obtaining the CRISPR/Cas9- Δ *SCO4117* mutant (strain “1” in **Figures 3A,B**). This mutant, shows a phenotype similar to the Δ *SCO4117* mutant (strain “2” in **Figures 3A,B**).

SCO4117 Gene Expression during *S. coelicolor* Development

The expression of *SCO4117* was analyzed at three key developmental stages (MI, 17 h; aerial mycelia, 48 h; sporulating mycelia, 72 h) by qRT-PCR, in solid GYM cultures of the wild-type strain. As reported previously in our transcriptomic work (Yagüe et al., 2013b), *SCO4117* is overexpressed during the sporulating stage in the *S. coelicolor* wild-type strain (**Figure 3C**).

The *SCO4117* Sigma Factor Regulates the Expression of Its Own Gene

A mutant expressing the sigma factor domain from the *SCO4117* ORF was created by CRISPR/Cas9 (CRISPR/Cas9- σ mutant) (**Figure 1**). The CRISPR/Cas9- σ mutant shows a

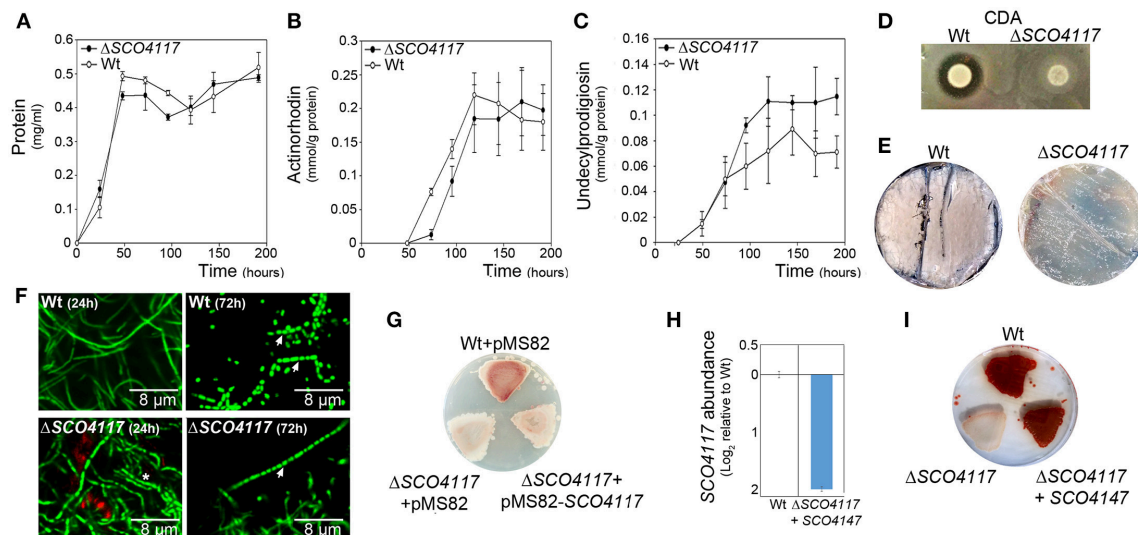


FIGURE 2 | Phenotypic analyses of the Δ SCO4117 mutant. **(A)** Growth curve. **(B)** Actinorhodin production. **(C)** Undecylprodigiosin production. **(D)** CDA production. **(E)** Macroscopic view of sporulation (gray color) in the Δ SCO4117 mutant compared to the wild strain in GYM plates at 85 h. **(F)** Confocal laser fluorescence microscopy pictures (SYTO9-PI staining) of the Δ SCO4117 mutant illustrating delay in MII differentiation (24 h) and sporulation (72 h) compared to the *S. coelicolor* M145 wild-type strain (GYM plates). Arrows indicate spore chains; the asterisk indicates the discontinuities characterizing the MI compartmentalized hyphae. **(G)** Macroscopic view of antibiotic production (red color) in the wild-type strain, the Δ SCO4117 mutant harboring plasmid pMS82 and the Δ SCO4117 mutant harboring plasmid pMS82-SCO4117, all of them grown in MM plates at 5 days. **(H)** SCO4117 transcript abundance in the Δ SCO4117 mutant harboring pMS82-SCO4117 (complemented mutant) compared to the wild-type strain in GYM plates at 17 h. **(I)** Macroscopic view of antibiotic production (red color) in the Δ SCO4117 restored mutant in MM plates at 5 days.

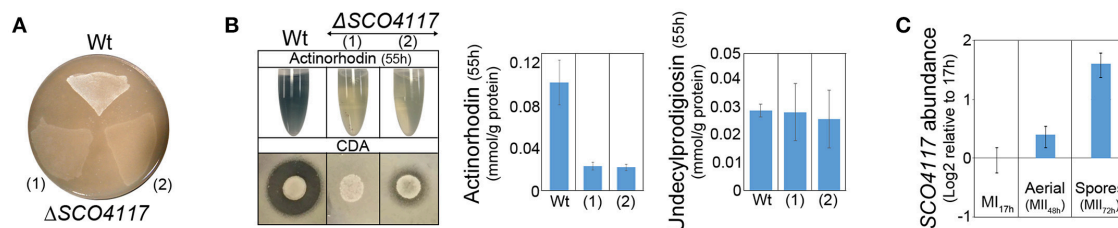


FIGURE 3 | Phenotypic analyses of the CRISPR/Cas9- Δ SCO4117 mutant and SCO4117 gene expression. **(A)** Macroscopic view of aerial mycelium development (white color) in the Δ SCO4117 mutant (1) and in the CRISPR/Cas9- Δ SCO4117 mutant (2), both grown in SFM plates at 2 days. **(B)** Actinorhodin (sucrose-free R5A extracellular medium, purple color), CDA and undecylprodigiosin production in the Δ SCO4117 and CRISPR/Cas9- Δ SCO4117 mutants compared to the wild-type strain. **(C)** SCO4117 transcript abundance at 17, 48, and 72 h in the *S. coelicolor* wild-type strain.

delayed actinorhodin production and lower CDA production than the wild-type strain (Supplementary Figure 2). Sporulation is also delayed, but it is faster than in the CRISPR/Cas9- Δ SCO4117 knockout mutant (Figure 4A). Interestingly, the expression of SCO4117 is slightly up-regulated (1.3-fold) in the CRISPR/Cas9- σ mutant compared to the wild strain (Figure 4B), suggesting that the sigma factor domain regulates the expression of its own gene.

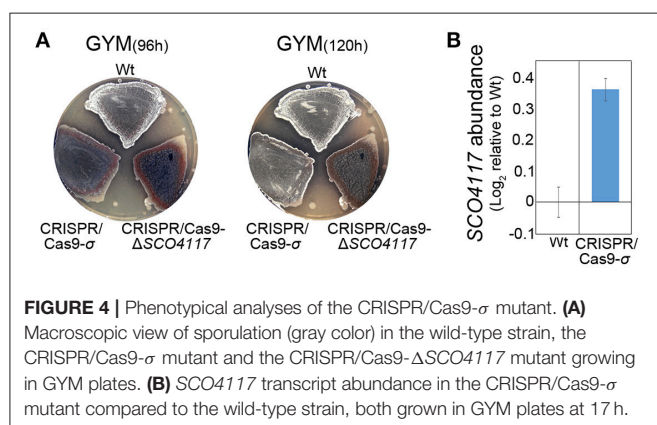
Comparison of Δ SCO4117 and *S. coelicolor* Wild-Type Transcriptomes

The differences between the Δ SCO4117 mutant and the wild-type transcriptomes were analyzed at 44 h on solid GYM cultures, the developmental conditions preceding the differences observed in sporulation (Figures 2E,F). Fifty-six genes showed altered expression in the Δ SCO4117 mutant compared to the

wild-type strain (Supplementary Table 1). As expected, the SCO4117 transcript was absent in the Δ SCO4117 knockout (Supplementary Table 1). The expression of the SCO4117 neighbor genes (SCO4116 and SCO4118) was not significantly affected (Supplementary Table 2). Particularly interesting is that 46 of 56 transcripts, 82% of the total, are down-regulated in the Δ SCO4117 mutant compared to the wild strain (green bars in Figure 5, Supplementary Table 1), suggesting a pleiotropic activator effect of the SCO4117 ECF which is absent in the knockout mutant. 7,679 transcripts did not show significant variations (*p*-values higher than 0.03) (Figure 5).

Several key developmental and physiological genes were differentially expressed in the Δ SCO4117 mutant compared to the wild-type strain (Figure 5; Table 2). The expression of genes involved in secondary metabolism (deoxysugar synthases and

actinorhodin biosynthetic genes) was highly down-regulated (up to 0.003, i.e., up-regulated 333-fold in the wild-type strain). The expression of genes involved in aerial mycelium formation and sporulation (*chaplins*, *rodmins*, *nepA*, *ssgB*, *SCO7449*) was also highly down-regulated in the mutant (up to 0.005, i.e., up-regulated up to 200-fold in the wild-type strain) (Figure 5; Table 2). *SCO4684* (encoding the ScoF3 cold shock protein) was down-regulated in the mutant. The other 22 transcripts down-regulated in the Δ *SCO4117* mutant, included, in addition to *SCO4117*, transcripts of genes encoding enzymes, stress and secreted proteins, as well as uncharacterized proteins (Supplementary Table 1). The 10 transcripts up-regulated in the Δ *SCO4117* mutant included: *SCO0194*, encoding a putative sigma factor; *SCO2162*, encoding a quinolinate synthetase; *SCO6102*, encoding a nitrite/sulphite reductase; and 6 transcripts from uncharacterized genes (Figure 5; Table 2).



SCO4117 DNA Motif Bound

The 46 genes encoding transcripts down-regulated in the Δ *SCO4117* mutant (Figure 5) (Supplementary Table 1) might harbor *SCO4117* motif bounds in their promoters. These genes were grouped into 33 putative operons (Supplementary Table 1) whose promoter regions were analyzed (see Materials and Methods). Twenty-nine promoters harbored the putative “*CSGYN*-17bps-SRHA” *SCO4117* motif bound at their promoter regions (Figure 6) (Supplementary Table 1).

DISCUSSION

The study of the *Streptomyces coelicolor* *SCO4117* knockout mutant revealed that the *SCO4117* ECF sigma factor is a pleiotropic activator of antibiotic production (actinorhodin and CDA) in solid and liquid cultures (Figures 2B–D). Aerial mycelium differentiation and sporulation are also enhanced by *SCO4117* in solid sporulating cultures (Figures 2E,F). The effect of *SCO4117* activating the expression of secondary metabolism and differentiation was corroborated by transcriptomics. The expression of secondary metabolism (deoxysugar synthases, actinorhodin) and differentiation genes (*bld*, *rhl*, *chp*, *nepA*, *ssgB*) was dramatically reduced (up to 300-fold) in the knockout strain compared to the *S. coelicolor* wild strain. The effect of *SCO4117* in secondary metabolism was not universal, since the expression of some secondary metabolite genes (for instance the undecylprodigiosin genes) did not appear to be affected (Supplementary Table 2).

Gene *SCO4117* encodes a multidomain ECF sigma factor belonging to the ECF52 family (Figure 1). A putative *SCO4117* motif bound (“*CSGYN*-17bps-SRHA”) was identified

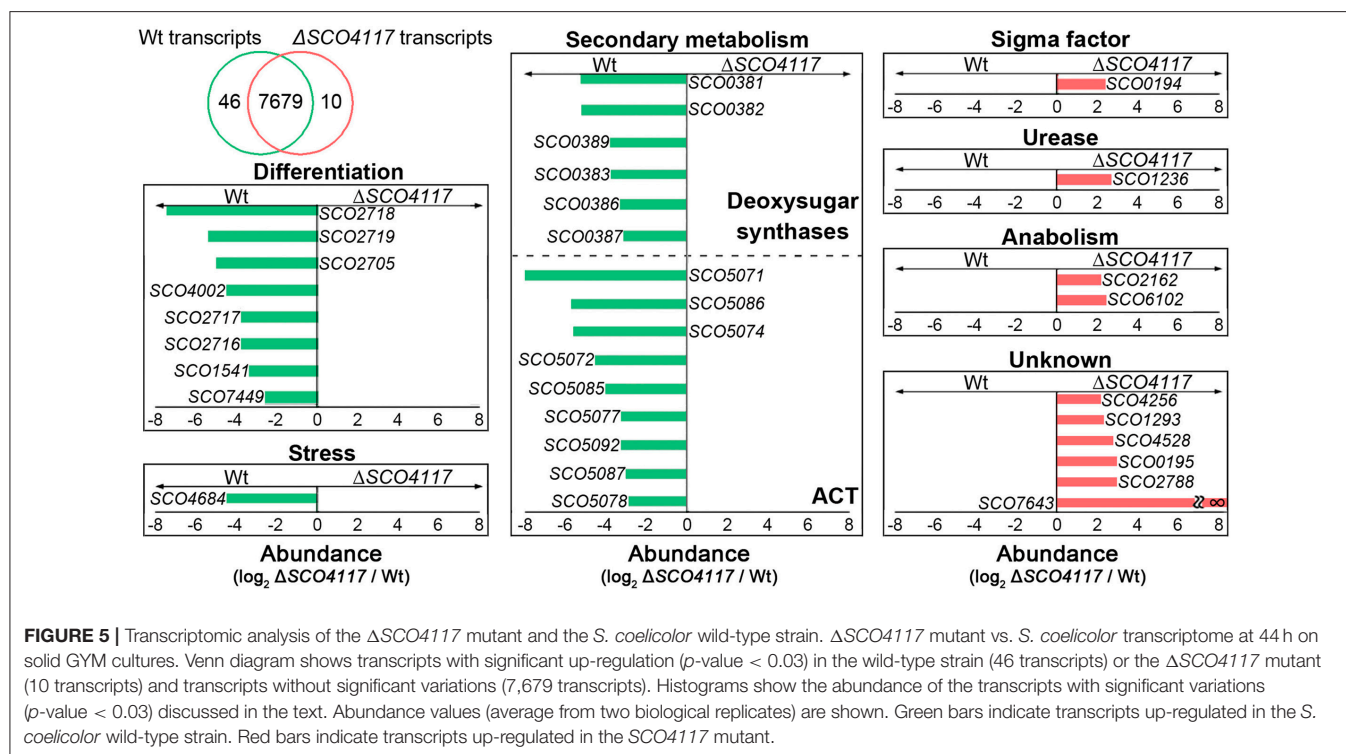


TABLE 2 | Abundance values of transcripts showing significant variations (p -value < 0.03) between the Δ SCO4117 mutant and the *S. coelicolor* M145 wild-type strain quantified in MM solid cultures (44 h), and grouped into functional categories.

Function		SCO no ^o	Gene	Log ₂ fold-change (Δ SCO4117/Wt)	Fold-change (Δ SCO4117/Wt)
Secondary metabolism	Deoxysugar synthases	SCO0381	Glycosyl transferase	-5.2	0.03
		SCO0382	Dehydrogenase	-5.2	0.03
		SCO0383	Glycosyl transferase	-3.8	0.07
		SCO0386	Asparagine synthetase	-3.3	0.1
		SCO0387	Oxidoreductase	-3.1	0.1
		SCO0389	Lipoprotein	-3.8	0.07
	ACT	SCO5071	Dehydrogenase	-8	0.003
		SCO5072	Dehydrogenase	-4.5	0.04
		SCO5074	Dehydratase	-5.6	0.02
		SCO5077	<i>actVA2</i>	-3.3	0.1
		SCO5078	<i>actVA3</i>	-2.8	0.1
		SCO5085	<i>actII-4</i>	-4	0.06
		SCO5086	<i>actIII</i>	-5.7	0.02
		SCO5087	<i>actIORF1</i>	-3	0.1
		SCO5092	<i>actVB</i>	-3	0.1
Differentiation		SCO1541	<i>sbgB</i>	-3.4	0.09
		SCO2705	<i>chpF</i>	-5.1	0.03
		SCO2716	<i>chpA</i>	-3.8	0.07
		SCO2717	<i>chpD</i>	-3.8	0.07
		SCO2718	<i>rdlA</i>	-7.5	0.005
		SCO2719	<i>rdlB</i>	-5.5	0.02
		SCO4002	<i>nepA</i>	-4.5	0.04
		SCO7449	Spore pigmentation ^a	-2.6	0.2
Stress		SCO4684	<i>scoF3</i>	-4.5	0.05
Regulators		SCO0194	Sigma factor	2.4	5.2
Catabolic enzymes		SCO1236	Urease	2.7	6.5
Anabolic enzymes		SCO2162	Quinolinate synthetase	2.2	4.6
		SCO6102	Nitrite/sulphite reductase	2.5	5.7
Unknown		SCO4256	Hypothetical protein	2.2	4.6
		SCO1293	Putative acetyltransferase	2.3	4.9
		SCO4258	Putative hydrolytic protein	2.8	6.9
		SCO0195	Putative lipoprotein	2.9	7.5
		SCO2788	Hypothetical protein	2.9	7.5
		SCO7643	Hypothetical protein	∞^b	∞^b

The genes discussed in the text are indicated.

^a Secreted protein related to spore pigmentation (Salerno et al., 2013).

^b Transcripts not detected in the wild-type strain.

(Figure 6). This motif differs from the theoretical ECF52 sigma factor promoter signature predicted by Pinto and Mascher (2016). Both motif bounds are theoretical, but the promoter signature identified in this work was present in the promoter regions of 29 putative operons down-regulated in the SCO4117 knockout mutant. Further experimentation will be necessary to unequivocally identify the ECF52 sigma factor promoter signature. Unfortunately, our attempts to overproduce the SCO4117 protein to study its interaction

with the identified motif, were unsuccessful (data not shown).

SCO4117 gene expression has a complex regulation. Two promoters were identified controlling the expression of this gene (Jeong et al., 2016), one of them harboring the putative SCO4117 motif bound identified in this work. However, further uncharacterized regulation should exist, as the two promoters together with the SCO4117 ORF, did not complement the wild-type phenotype (Figure 2G), or the SCO4117 gene expression



FIGURE 6 | SCO4117 putative DNA motif bound. Putative SCO4117 motif bound logo ("CSGYN-17bps-SRHA") identified in the promoter region of 29 genes showing affected transcription in the SCO4117 mutant (Supplementary Table 1). The logo was created using Weblogo (Crooks et al., 2004).

(Figure 2H), in the *SCO4117* knockout. Polar effects in the expression of the *SCO4117* neighbor genes due to the apramycin gene insertion, were discarded, because the expression of the *SCO4116* and *SCO4118* genes does not show significant variations in the Δ *SCO4117* compared to the wild strain (Supplementary Table 2) and because the same phenotypes were observed in the CRISPR/Cas9- Δ *SCO4117* mutant and in the insertional Δ *SCO4117* knockout (Figure 3). Our results, might indicate the existence of unknown promoters controlling the expression of *SCO4117*, perhaps a cotranscription of the *atrA* and *SCO4117* genes from the *atrA* promoter. However, Uguru et al. (2005) described a putative transcription terminator between *SCO4118* and *SCO4117*. They also demonstrated that the *atrA* knockout phenotype (severe reduction in the amount of actinorhodin production) is complemented by a DNA fragment containing *atrA*, but lacking *SCO4117* (Uguru et al., 2005). The putative SCO4117 motif bound found in one of the *SCO4117* promoters (Figure 6) (Supplementary Table 1), suggests a positive autoregulation of *SCO4117* gene expression. This autoregulation was observed in a strain expressing a truncated version of SCO4117 lacking the zinc-finger domain, the transmembrane region and the carbohydrate binding module, in which the expression of *SCO4117* is activated (Figure 4B). Positive gene expression autoregulation is common in ECF sigma factors, allowing the amplification of the activation signal (Helmann, 2002; Pinto and Mascher, 2016). Further work will be necessary to fully understand the regulation of the *SCO4117* gene transcription.

The developmental effect of the expression of a truncated version of the *SCO4117* gene encoding the σ factor domain in the CRISPR/Cas9- σ mutant (delay in differentiation/sporulation) was lesser than in the absence of the whole gene in the Δ *SCO4117* mutant (Figure 4), indicating that the σ factor domain itself can modulate development. These results suggest a complex post-translational regulation of the SCO4117 activity which might involve the excision of the ECF sigma factor domain from the membrane by an uncharacterized protease. In fact, Pinto and Mascher (2016) proposed this kind of regulation for ECF52 sigma factors: the sigma factor domain might be activated by the carbohydrate-binding module, leading to a proteolytic cascade or conformational changes that inactivate the zinc-finger domain to ultimately release an active form of the ECF sigma factor. Interestingly, in a previous study, we discovered that

SCO4117 is phosphorylated at Ser 15 and Thr 231, suggesting a putative regulation of the SCO4117 activity by phosphorylation (Manteca et al., 2011). Further work will be necessary to fully understand the post-translational regulation of the SCO4117 activity.

Overall, in this work, we demonstrated pleiotropic effects on the regulation of secondary metabolism and differentiation of *SCO4117*, the first member of the ECF52 family characterized. Gene *SCO4117* is a conserved gene overexpressed during substrate and aerial mycelium stages, with complex regulation at the transcriptional and post-translational levels.

AUTHOR CONTRIBUTIONS

ML-G, PY, NG-Q, and BR performed the experiments. ML-G and AM planned the experiments and wrote the manuscript.

FUNDING

We thank the European Research Council (ERC Starting Grant; Strp-differentiation 280304) and the Spanish "Ministerio de Economía y Competitividad" (MINECO; BIO2015-65709-R) for financial support. NG-Q was funded by a Severo Ochoa fellowship (FICYT, "Consejería de Educación y Cien2cia, Spain").

ACKNOWLEDGMENTS

We thank Dr. Daniela Pinto ("Universität Dresden") for her unselfish search of the SCO4117 motif bound; Prof. Maggie Smith (University of York) for providing the pMS82 plasmid; Angel Martinez Nistal, and Marta Alonso Guervos ("Servicios Científico-Técnicos de la Universidad de Oviedo") for their support with confocal microscopy; Beatriz Gutierrez Magan (Universidad de Oviedo, Dpto. Biología Funcional, Área de Microbiología) for laboratory assistance and Proof-Reading-Service.com for proofreading the final manuscript.

SUPPLEMENTARY MATERIAL

The Supplementary Material for this article can be found online at: <https://www.frontiersin.org/articles/10.3389/fmicb.2018.00312/full#supplementary-material>

REFERENCES

- Bibb, M. J., Domonkos, A., Chandra, G., and Buttner, M. J. (2012). Expression of the chaplin and rodlin hydrophobic sheath proteins in *Streptomyces venezuelae* is controlled by sigma(BldN) and a cognate anti-sigma factor, RsbN. *Mol. Microbiol.* 84, 1033–1049. doi: 10.1111/j.1365-2958.2012.08070.x
- Bystrykh, L. V., Fernández-Moreno, M. A., Herrema, J. K., Malpartida, F., Hopwood, D. A., and Dijkhuizen, L. (1996). Production of actinorhodin-related “blue pigments” by *Streptomyces coelicolor* A3(2). *J. Bacteriol.* 178, 2238–2244. doi: 10.1128/jb.178.8.2238-2244.1996
- Crooks, G. E., Hon, G., Chandonia, J. M., and Brenner, S. E. (2004). WebLogo: a sequence logo generator. *Genome Res.* 14, 1188–1190. doi: 10.1101/gr.849004
- Feeney, M. A., Chandra, G., Findlay, K. C., Paget, M. S. B., and Buttner, M. J. (2017). Translational control of the SigR-directed oxidative stress response in *Streptomyces* via IF3-mediated repression of a noncanonical GTC start codon. *MBio.* 8:e00815-17. doi: 10.1128/mBio.00815-17
- Feng, W. H., Mao, X. M., Liu, Z. H., and Li, Y. Q. (2011). The ECF sigma factor SigT regulates actinorhodin production in response to nitrogen stress in *Streptomyces coelicolor*. *Appl. Microbiol. Biotechnol.* 92, 1009–1021. doi: 10.1007/s00253-011-3619-2
- Fernández, E., Weissbach, U., Sánchez Reillo, C., Braña, A. F., Méndez, C., Rohr, J., et al. (1998). Identification of two genes from *Streptomyces argillaceus* encoding glycosyltransferases involved in transfer of a disaccharide during biosynthesis of the antitumor drug mithramycin. *J. Bacteriol.* 180, 4929–4937.
- Flett, F., Mersinias, V., and Smith, C. P. (1997). High efficiency intergeneric conjugal transfer of plasmid DNA from *Escherichia coli* to methyl DNA-restricting streptomycetes. *FEMS Microbiol. Lett.* 155, 223–229. doi: 10.1111/j.1574-6968.1997.tb13882.x
- Gómez-Santos, N., Perez, J., Sánchez-Sutil, M. C., Moraleda-Muñoz, A., and Muñoz-Dorado, J. (2011). CorE from *Myxococcus xanthus* is a copper-dependent RNA polymerase sigma factor. *PLoS Genet.* 7:e1002106. doi: 10.1371/journal.pgen.1002106
- Gonzalez-Quinonez, N., López-García, M. T., Yagüe, P., Rioseras, B., Pisciotta, A., Alduina, R., et al. (2016). New PhiBT1 site-specific integrative vectors with neutral phenotype in Streptomyces. *Appl. Microbiol. Biotechnol.* 100, 2797–2808. doi: 10.1007/s00253-015-7271-0
- Gregory, M. A., Till, R., and Smith, M. C. (2003). Integration site for Streptomyces phage phiBT1 and development of site-specific integrating vectors. *J. Bacteriol.* 185, 5320–5323. doi: 10.1128/JB.185.17.5320-5323.2003
- Gust, B., Challis, G. L., Fowler, K., Kieser, T., and Chater, K. F. (2003). PCR-targeted Streptomyces gene replacement identifies a protein domain needed for biosynthesis of the sesquiterpene soil odor geosmin. *Proc. Natl. Acad. Sci. U.S.A.* 100, 1541–1546. doi: 10.1073/pnas.0337542100
- Helmann, J. D. (2002). The extracytoplasmic function (ECF) sigma factors. *Adv. Microb. Physiol.* 46, 47–110. doi: 10.1016/S0065-2911(02)46002-X
- Hopwood, D. A., (2007). *Streptomyces in Nature and Medicine: The Antibiotic Makers*. New York, NY; Oxford: Oxford University Press.
- Huang, X., Pinto, D., Fritz, G., and Mascher, T. (2015). Environmental sensing in actinobacteria: a comprehensive survey on the signaling capacity of this phylum. *J. Bacteriol.* 197, 2517–2535. doi: 10.1128/JB.00176-15
- Hutchings, M. I., Hong, H. J., Leibovitz, E., Sutcliffe, I. C., and Buttner, M. J. (2006). The sigma(E) cell envelope stress response of *Streptomyces coelicolor* is influenced by a novel lipoprotein, CseA. *J. Bacteriol.* 188, 7222–7229. doi: 10.1128/JB.00818-06
- Jeong, Y., Kim, J. N., Kim, M. W., Bucca, G., Cho, S., Yoon, Y. J., et al. (2016). The dynamic transcriptional and translational landscape of the model antibiotic producer *Streptomyces coelicolor* A3(2). *Nat. Commun.* 7:11605. doi: 10.1038/ncomms11605
- Kieser, T. (2000). *Practical Streptomyces Genetics*. Norwich: John Innes Foundation.
- Kormanec, J., Sevcikova, B., Novakova, R., Homerova, D., Rezuchova, B., and Mingyar, E. (2016). “The complex roles and regulation of stress response σ factors in *Streptomyces coelicolor*,” in *Stress and Environmental Regulation of Gene Expression and Adaptation in Bacteria*, ed F. J. de Bruijn (Hoboken, NJ: Wiley-Blackwell), 328–343.
- Kurt, A., Álvarez-Álvarez, R., Liras, P., and Özcengiz, G. (2013). Role of the cmcH-ccaR intergenic region and ccaR overexpression in cephamycin C biosynthesis in *Streptomyces clavuligerus*. *Appl. Microbiol. Biotechnol.* 97, 5869–5880. doi: 10.1007/s00253-013-4721-4
- Lee, J., Shin, M. K., Ryu, D. K., Kim, S., and Ryu, W. S. (2010). Insertion and deletion mutagenesis by overlap extension PCR. *Methods Mol. Biol.* 634, 137–146. doi: 10.1007/978-1-60761-652-8_10
- Liu, X., Brutlag, D. L., and Liu, J. S. (2001). Bioprospector: discovering conserved DNA motifs in upstream regulatory regions of co-expressed genes. *Pac. Symp. Biocomput.* 6, 127–138. doi: 10.1142/9789814447362_0014
- Livak, K. J., and Schmittgen, T. D. (2001). Analysis of relative gene expression data using real-time quantitative PCR and the 2(-Delta Delta C(T)) Method. *Methods* 25, 402–408. doi: 10.1006/meth.2001.1262
- MacNeil, D. J., Gewain, K. M., Ruby, C. L., Dezeny, G., Gibbons, P. H., and MacNeil, T. (1992). Analysis of *Streptomyces avermitilis* genes required for avermectin biosynthesis utilizing a novel integration vector. *Gene* 111, 61–68. doi: 10.1016/0378-1119(92)90603-M
- Manteca, A., Fernandez, M., and Sanchez, J. (2006). Cytological and biochemical evidence for an early cell dismantling event in surface cultures of *Streptomyces antibioticus*. *Res. Microbiol.* 157, 143–152. doi: 10.1016/j.resmic.2005.07.003
- Manteca, A., Ye, J., Sánchez, J., and Jensen, O. N. (2011). Phosphoproteome analysis of Streptomyces development reveals extensive protein phosphorylation accompanying bacterial differentiation. *J. Proteome Res.* 10, 5481–5492. doi: 10.1021/pr200762y
- Mascher, T. (2013). Signaling diversity and evolution of extracytoplasmic function (ECF) sigma factors. *Curr. Opin. Microbiol.* 16, 148–155. doi: 10.1016/j.mib.2013.02.001
- Pinto, D., and Mascher, T. (2016). “The ECF classification: a phylogenetic reflection of the regulatory diversity in the extracytoplasmic function sigma factor protein family,” in *Stress and Environmental Control of Gene Expression in Bacteria*, ed F. J. de Bruijn (Hoboken, NJ: Wiley-Blackwell), 64–96.
- Rioseras, B., Yagüe, P., López-García, M. T., Gonzalez-Quinonez, N., Binda, E., Marinelli, F., et al. (2016). Characterization of SCO4439, a D-alanyl-D-alanine carboxypeptidase involved in spore cell wall maturation, resistance, and germination in *Streptomyces coelicolor*. *Sci. Rep.* 6:21659. doi: 10.1038/srep21659
- Salerno, P., Persson, J., Bucca, G., Laing, E., Ausmees, N., Smith, C. P., et al. (2013). Identification of new developmentally regulated genes involved in *Streptomyces coelicolor* sporulation. *BMC Microbiol.* 13:281. doi: 10.1186/1471-2180-13-281
- Sambrook, J., and Russell, D. W. (2001). *Molecular Cloning: A Laboratory Manual*. Cold Spring Harbor, NY: Cold Spring Harbor Laboratory Press.
- Staron, A., Sofia, H. J., Dietrich, S., Ulrich, L. E., Liesegang, H., and Mascher, T. (2009). The third pillar of bacterial signal transduction: classification of the extracytoplasmic function (ECF) sigma factor protein family. *Mol. Microbiol.* 74, 557–581. doi: 10.1111/j.1365-2958.2009.06870.x
- Straight, P. D., Willey, J. M., and Kolter, R. (2006). Interactions between *Streptomyces coelicolor* and *Bacillus subtilis*: role of surfactants in raising aerial structures. *J. Bacteriol.* 188, 4918–4925. doi: 10.1128/JB.00162-06
- Tong, Y., Charusanti, P., Zhang, L., Weber, T., and Lee, S. Y. (2015). CRISPR-Cas9 based engineering of actinomycetal genomes. *ACS Synth. Biol.* 4, 1020–1029. doi: 10.1021/acssynbio.5b00038
- Trapnell, C., Roberts, A., Goff, L., Pertea, G., Kim, D., Kelley, D. R., et al. (2012). Differential gene and transcript expression analysis of RNA-seq experiments with TopHat and Cufflinks. *Nat. Protoc.* 7, 562–578. doi: 10.1038/nprot.2012.016
- Tsao, S. W., Rudd, B. A., He, X. G., Chang, C. J., and Floss, H. G. (1985). Identification of a red pigment from *Streptomyces coelicolor* A3(2) as a mixture of prodigiosin derivatives. *J. Antibiot.* 38, 128–131. doi: 10.7164/antibiotics.38.128
- Uguru, G. C., Stephens, K. E., Stead, J. A., Towle, J. E., Baumberg, S., and McDowall, K. J. (2005). Transcriptional activation of the pathway-specific regulator of the actinorhodin biosynthetic genes in *Streptomyces coelicolor*. *Mol. Microbiol.* 58, 131–150. doi: 10.1111/j.1365-2958.2005.04817.x
- Wecke, T., Halang, P., Staron, A., Dufour, Y. S., Donohue, T. J., and Mascher, T. (2012). Extracytoplasmic function sigma factors of the widely distributed

- group ECF41 contain a fused regulatory domain. *Microbiologyopen* 1, 194–213. doi: 10.1002/mbo3.22
- Yagüe, P., López-García, M. T., Rioseras, B., Sánchez, J., and Manteca, A. (2013a). Pre-sporulation stages of *Streptomyces* differentiation: state-of-the-art and future perspectives. *FEMS Microbiol. Lett.* 342, 79–88. doi: 10.1111/1574-6968.12128
- Yagüe, P., Rodríguez-García, A., López-García, M. T., Martín, J. F., Rioseras, B., Sánchez, J., et al. (2013b). Transcriptomic analysis of *Streptomyces coelicolor* differentiation in solid sporulating cultures: first compartmentalized and second multinucleated mycelia have different and distinctive transcriptomes. *PLoS ONE* 8:e60665. doi: 10.1371/journal.pone.0060665

Conflict of Interest Statement: The authors declare that the research was conducted in the absence of any commercial or financial relationships that could be construed as a potential conflict of interest.

Copyright © 2018 López-García, Yagüe, González-Quirón, Rioseras and Manteca. This is an open-access article distributed under the terms of the Creative Commons Attribution License (CC BY). The use, distribution or reproduction in other forums is permitted, provided the original author(s) and the copyright owner are credited and that the original publication in this journal is cited, in accordance with accepted academic practice. No use, distribution or reproduction is permitted which does not comply with these terms.



ArgR of *Streptomyces coelicolor* Is a Pleiotropic Transcriptional Regulator: Effect on the Transcriptome, Antibiotic Production, and Differentiation in Liquid Cultures

Alma Botas^{1,2}, Rosario Pérez-Redondo², Antonio Rodríguez-García^{1,2}, Rubén Álvarez-Álvarez¹, Paula Yagüe³, Angel Manteca³ and Paloma Liras^{1*}

¹ Área de Microbiología, Departamento de Biología Molecular, Universidad de León, León, Spain, ² Instituto de Biotecnología de León, León, Spain, ³ Área de Microbiología, Departamento de Biología Funcional e IUOPA, Universidad de Oviedo, Oviedo, Spain

OPEN ACCESS

Edited by:

Dirk Tischler,
Freiburg University of Mining and
Technology, Germany

Reviewed by:

Andreas Burkovski,
University of Erlangen-Nuremberg,
Germany
Erhard Bremer,
University of Marburg, Germany

*Correspondence:

Paloma Liras
paloma.liras@unileon.es

Specialty section:

This article was submitted to
Microbial Physiology and Metabolism,
a section of the journal
Frontiers in Microbiology

Received: 07 September 2017

Accepted: 15 February 2018

Published: 01 March 2018

Citation:

Botas A, Pérez-Redondo R, Rodríguez-García A, Álvarez-Álvarez R, Yagüe P, Manteca A and Liras P (2018) ArgR of *Streptomyces coelicolor* Is a Pleiotropic Transcriptional Regulator: Effect on the Transcriptome, Antibiotic Production, and Differentiation in Liquid Cultures. *Front. Microbiol.* 9:361. doi: 10.3389/fmicb.2018.00361

ArgR is a well-characterized transcriptional repressor controlling the expression of arginine and pyrimidine biosynthetic genes in bacteria. In this work, the biological role of *Streptomyces coelicolor* ArgR was analyzed by comparing the transcriptomes of *S. coelicolor* Δ argR and its parental strain, *S. coelicolor* M145, at five different times over a 66-h period. The effect of *S. coelicolor* ArgR was more widespread than that of the orthologous protein of *Escherichia coli*, affecting the expression of 1544 genes along the microarray time series. This *S. coelicolor* regulator repressed the expression of arginine and pyrimidine biosynthetic genes, but it also modulated the expression of genes not previously described to be regulated by ArgR: genes involved in nitrogen metabolism and nitrate utilization; the *act*, *red*, and *cpk* genes for antibiotic production; genes for the synthesis of the osmotic stress protector ectoine; genes related to hydrophobic cover formation and sporulation (*chaplins*, *rodmins*, *ramR*, and *whi* genes); all the *cwg* genes encoding proteins for glycan cell wall biosynthesis; and genes involved in gas vesicle formation. Many of these genes contain ARG boxes for ArgR binding. ArgR binding to seven new ARG boxes, located upstream or near the *ectA-ectB*, *afsS*, *afsR*, *glnR*, and *redH* genes, was tested by DNA band-shift assays. These data and those of previously assayed fragments permitted the construction of an improved model of the ArgR binding site. Interestingly, the overexpression of sporulation genes observed in the Δ argR mutant in our culture conditions correlated with a sporulation-like process, an uncommon phenotype.

Keywords: ArgR, arginine, ARG box, *S. coelicolor*, transcriptomics, sporulation, antibiotics

INTRODUCTION

Biosynthesis of amino acids is regulated in microorganisms when these nutrients are abundant in the culture medium. ArgR first described in *Escherichia coli* is the model for the ArgR repressor superfamily; this transcriptional regulator, in response to the presence of arginine, represses the expression of arginine biosynthesis genes using arginine as a co-repressor and decreases the

activity of arginine biosynthesis enzymes (Maas, 1994). A similar effect was found for pyrimidine biosynthesis. The ArgR protein is widely distributed in bacteria, acting mostly as a repressor of genes for arginine uptake and biosynthesis (Cunin et al., 1983) but may also act as an activator, as in the *aot* operon for arginine and ornithine uptake in *Pseudomonas* (Nishijyo et al., 1998; Lu et al., 2004). It is an essential accessory protein in the site-specific resolution of ColE1 oligomers in *E. coli* (Stirling et al., 1988).

In gram-positive bacteria, the control of arginine and pyrimidine biosynthesis in *Lactococcus lactis* (Larsen et al., 2008) and the repression of the corynebacteria *argCJBDFR* operon by ArgR are well documented (Yim et al., 2011). L-arginine has been overproduced in a corynebacteria industrial strain by increasing the copy number of the arginine operon genes in an ArgR-defective mutant (Xu et al., 2012). The *Bacillus* *AhrC* repressor, homologous to ArgR, represses the *argCAEBD-cpa-argF* gene cluster in the presence of arginine (Smith et al., 1989) and activates arginine catabolism genes in cooperation with the RocR activator (Gardan et al., 1997).

In *Streptomyces coelicolor* and *Streptomyces clavuligerus*, a repression system of the arginine biosynthesis genes homologous to those of other bacteria has been described (Soutar and Baumberg, 1996; Rodríguez-García et al., 1997). The effect of arginine as the ArgR co-repressor is weak in *Streptomyces*, and high levels of this amino acid are required to observe repression of arginine biosynthesis genes or a decrease in arginine biosynthesis enzyme activities (Rodríguez-García et al., 1997). Arginine, when added to *S. coelicolor* cultures at 25 mM, only affected the expression of 27 arginine-related genes (0.35% of the genome; Pérez-Redondo et al., 2012).

The crystallized hexameric ArgR repressor of *E. coli* is formed by two trimers (van Duyne et al., 1996). It has been demonstrated to interact with the operator region of *argF* (Grandori et al., 1995) by binding specific DNA sequences known as ARG boxes. A standard ARG box in *E. coli* is formed by two 18-bp sequences separated by 3 bp and is located close to the promoters of ArgR-controlled genes (Tian et al., 1992). In *E. coli*, ArgR binding to the ARG boxes strictly depends on L-arginine as the co-repressor (van Duyne et al., 1996). In corynebacteria, the ArgR C-terminal end contains a conserved GTIAGDDTL/I oligomerization domain (amino acids 146–154 in *S. coelicolor* ArgR), which has been demonstrated to be essential for arginine binding (Yim et al., 2011). ArgR proteins in *Bacillus* (Dion et al., 1997) show lower specificity and dependency on L-arginine as co-repressor, exhibit an equilibrium trimer-hexamer and bind to ARG boxes normally separated by 2 bp (Song et al., 2002).

DNase I footprinting and electrophoresis mobility shift assay experiments analyzing the binding of *B. subtilis* *AhrC* to the *argCJBDR* operon of *S. clavuligerus* and the binding of ArgR to the *S. coelicolor* arginine biosynthesis genes (*argC*, *argG*, *arcB*, and *argH*) revealed the presence of ARG boxes arranged as two 20-bp contiguous sequences in these actinomycetes (Rodríguez-García et al., 1997; Pérez-Redondo et al., 2012; Botas, 2013), as in the *Bacillus* system (Dion et al., 1997; Song et al., 2002).

Pérez-Redondo et al. (2012) studied the *S. coelicolor* transcriptome at a single developmental time-point (32 h), identifying 459 genes regulated by ArgR. These genes were

involved in purine and pyrimidine biosynthesis, cell morphology, and antibiotic production. In this work, we analyzed the differences between the transcriptomes of the parental strain and a $\Delta argR$ mutant at five different time-points in the culture development, which allowed us to confirm the previous results and significantly increase the number of ArgR-controlled genes at other time points and ratify the significance of data obtained in the single developmental point from previous experiments (Pérez-Redondo et al., 2012). Novel DNA binding experiments enabled the location and characterization of new functional ARG boxes and redefinition of the ARG box model in *S. coelicolor*. A bioinformatic search was performed to locate additional putative ARG boxes that could explain the regulatory role of the ArgR protein. In addition, a sporulation-like phenomenon in liquid culture was observed in the $\Delta argR$ mutant strain. Sporulation is unusual in *S. coelicolor* and has never been reported for *Streptomyces argR* mutants.

MATERIALS AND METHODS

Strains and Culture Conditions

S. coelicolor M145 was used as a control strain (Bentley et al., 2002). *S. coelicolor* $\Delta argR$ derives from the former strain and is a mutant with a deletion in the *argR* gene (Pérez-Redondo et al., 2012). For transcriptomic studies, *S. coelicolor* strains were inoculated in a defined MG medium containing 50 g/l starch, 12 mM glutamic acid as the only nitrogen source, 2.5 mM phosphate and salts (Doull and Vining, 1989; Pérez-Redondo et al., 2012), using 10^8 spores stored in glycerol at -80°C . The cultures were grown at 30°C and 300 rpm in triplicate in 500-ml baffled flasks containing 100 ml of medium. Actinorhodin and undecylprodigiosin were spectrophotometrically determined at 640 and 530 nm, respectively, as previously described (Kieser et al., 2000). Dry weight was determined in culture samples (2 ml) washed twice with deionized-ultrapure water and dried for 80 h at 60°C . Growth was similar for both strains (not shown).

RNA Isolation, Microarray Hybridization, and Transcriptomic Data Analysis

Samples from three independent *S. coelicolor* M145 and *S. coelicolor* $\Delta argR$ cultures were taken at five time points: 32, 42 (exponential phase start and end) 49, 56, and 66 h (stationary phase). RNA samples with RIN values above 8.5 (2100 Bioanalyzer, Agilent) were employed. Cy5-gDNA and Cy3-cDNA labeling, hybridization in the Sco-Chip²-v2 microarrays (Oxford Gene Technology), washing, scanning, and signal quantification were performed as indicated in Yagüe et al. (2014). Fluorescence intensities were processed and normalized using the limma package (Smyth, 2004) in the R environment as indicated previously (Yagüe et al., 2014), except that quality weights were estimated for the non-control spots (43,798) of each array (Table S1). These weights were used for normalization and linear model statistics. For each gene, the normalized Mg values were calculated as the average among three replicates of the binary logarithms of the Cy3-cDNA signal divided by the Cy5-gDNA signal (log Cy3/Cy5). Probe values were previously averaged if more than one probe for a gene were present (mean of

4.6 probes per gene in the arrays). For each culture time, comparisons between the M_g values of the mutant and parental strains were the basis of the statistical results and corresponded to the M_c value (fold change). A threshold of 0.01 for the Benjamini-Hochberg adjusted p -values was used to identify significantly differentially expressed genes. This resulted in 1544 genes (out of a total of 7,721 present in the microarray), which passed the threshold in at least one comparison. Significantly differential expression profiles were identified in the time-course microarray experiment by means of maSigPro (Conesa et al., 2006) and grouped in 10 profiles. The GEO accession number for microarray data is GSE58666.

qRT-PCR

The qRT-PCR was performed in triplicate RNA samples with the oligonucleotides shown in Table S2, as previously described (López-García et al., 2010). RNA was retrotranscribed to cDNA using random primers and the Invitrogen SuperScript III commercial kit. Amplification and quantification of DNA by qRT-PCR was performed using a StepOnePlus thermocycler using SYBR Green PCR Master Mix (both from Applied Biosystems). The baseline and threshold cycle determination was performed using Sequence Detection Software (Applied Biosystems).

The reactions were prepared in a final volume of 20 μ l. A template of 2 μ l of undiluted (or 2- to 10-fold diluted) cDNA was used to give C_t detection between cycles 15 and 25. The final concentration of 300 μ M oligonucleotides increased the highest amplification of the specific product at a lower C_t without primer dimer formation. The RNA was confirmed to be free of DNA contamination using negative controls where template cDNA was replaced with RNA.

The relative quantification of the expression differences of a target gene between mutant and control strains was performed using the $\Delta\Delta C_t$ method (Livak and Schmittgen, 2001). As a reference, the *hrdB* gene, encoding a constitutive *Streptomyces* sigma factor (Buttner et al., 1990), was used.

The efficiency of each oligonucleotide pair was determined by amplifying serial dilutions of genomic DNA (six different dilutions, each amplified in triplicate) and measuring the slope of the resulting line of C_t plotted against the logarithm of DNA concentration. Slope values between -3.6 and -3.1 were regarded as valid, indicating efficiencies of 90–100%, which were required to apply the $\Delta\Delta C_t$ method.

The relative expression of a gene in the mutant strain is given by $2^{-\Delta\Delta C_t}$, where $\Delta\Delta C_t$ indicates the difference between the ΔC_t of both strains analyzed, obtained from the difference in the C_t of the target gene and the reference gene in each strain. Relative expression above 1 indicated that the analyzed gene is overexpressed in the mutant strain, while values below 1 indicate its repression.

DNA Band-Shift Studies and Structure of the ArgR Binding Site

To improve the previous model of the ArgR binding site (Pérez-Redondo et al., 2012), we used the DNA band-shift assays (EMSA, electrophoretic mobility shift assay) results for 50 DNA

fragments. The conditions used were as indicated in a previous work (Pérez-Redondo et al., 2012).

In brief, ArgR protein was purified from *E. coli* as a Strep-tag fused protein. DNA fragments to be tested by EMSA were amplified using specific oligonucleotides (Table S2), cloned in pBluescript SK+ (Stratagene), and labeled by PCR with Universal 6-FAM oligonucleotides to obtain fluorescent probes. The DNA-protein binding reaction contained: 5 μ L buffer (10 mM Tris-HCl, pH 7.4, 5 mM MgCl₂, 2.5 mM CaCl₂, 250 mM KCl, 0.5 mM DTT, 10 mM L-arginine, pH 7.4), poly-(dIdC) 1.3 μ g/mL, glycerol 10%, 6-FAM-labeled probe 2 nM, and Strep-ArgR protein 0.8 μ M in 15 μ L. This mixture was incubated for 30 min at 30°C and immediately resolved in a 5% acrylamide gel using 0.5x TBE as running buffer at 50 V. Competition experiments were done with increasing amounts of unlabeled specific probe. The chromosomal sequences of the probes used for DNA binding shift are included in Table S3.

To improve the previous model of the ArgR binding site (Pérez-Redondo et al., 2012), we used the EMSA which resulted in 50 DNA fragments shifted. The chromosomal sequences of the probes used for DNA band-shift assays, obtained by PCR amplification, are included in Table S3. These sequences were chosen among those containing putative ArgR binding sites, according to the previous model. A three-step process was conducted to identify ARG boxes in the sequences of the positive probes and to build a new binding-site model. First, the MEME algorithm, available through the MEME server (Bailey et al., 2009), was used for motif discovery using two search strategies: (i) the discriminative mode, fed with both sets of positive and negative sequences and searching for palindromes 14–20 nt in length (ZOOPS option), detected a total of 25 ARG boxes in the input positive sequences and built an ARG box model 14 nt in length (named ARGNE04); (ii) the normal mode, searching for palindromes 18–20 nt in length with the ANR option, detected 14 sites among the set of positive probes and produced a model 20 nt in length (ARGNE05). Second, the sequences giving positive DNA band-shift were scanned with both the ARGNE04 and ARGNE05 models using the FIMO algorithm (Grant et al., 2011). The results were manually inspected to determine the most likely binding site(s) in each positive sequence, in terms of sequence conservation, location relative to the translation start site of the regulated gene, and the presence of a unique ARG box or two tandemly arranged ARG boxes (Table 1). Third, 37 ARG boxes were well-conserved sequences that were selected among the 44 boxes identified in the previous analysis and used to build the final model using information theory algorithms (Schneider, 1997).

Viability Stain

Culture samples were obtained and processed for microscopy at different incubation time-points, as previously described (Manteca et al., 2007, 2008). To detect the dead cell population, the cells were stained with the cell-impermeant nucleic acid stain propidium iodide (PI), which only penetrates bacteria with damaged membranes. In addition, SYTO 9 green fluorescent nucleic acid stain, which labels all cells (LIVE/DEAD BacLight Bacterial Viability Kit, Invitrogen) was used to detect viable

TABLE 1 | ARG boxes detected in DNA fragments bound by ArgR in DNA band-shift assays.

Regulated gene(s)	Gene name	Product	ARG box identifier	Sequence	Chromosomal coordinates			Distance to start codon	R _i (bit)
					Left	Right			
SCO256 ^{a,f}		Short chain oxidoreductase-like	AB.SCO0256_1	GCCCGCACGCTGTTGGCAG	245912	245931		55	5.8
SCO256 ^{a,f}		Short chain oxidoreductase-like	AB.SCO0256_2	CACCGCAGAGAGCGGGAG	245932	245951		35	7.7
SCO1086 ^a		Hypothetical protein	AB.SCO1086_1	CAGTCAATGACTTTTCAGGT	1146431	1146450		5	5.0
SCO1086		Hypothetical protein	AB.SCO1086_2	GAACGCATACCTATGCAGTG	1146451	1146470		25	15.7
SCO1236	<i>ureA</i>	Urease gamma subunit	AB.SCO1236_0	GATTGATTACCGATGCAGTC	1310778	1310797		183	7.4
SCO1483 ^c	<i>pyrA</i>	Carbamoylphosphate synthetase L chain	AB.SCO1483_0	GGTGGAAACAGGTAGCGGCG	1587621	1587640		209	5.6
SCO1487	<i>pyrB</i>	Aspartate carbamoyltransferase	AB.SCO1487_0	CTCCGTAAGGCGATTTCATGC	1591396	1591415		9	9.3
SCO1488	<i>pyrR</i>	Pyrimidine operon regulatory protein	AB.SCO1488_0	TGTTGCTTTGCCATACGAAA	1592070	1592089		−13	7.4
SCO1489	<i>bidD</i>	BidD, transcriptional regulator	AB.SCO1489_0	CGCTGCGTAACCTACAGTG	1592299	1592318		63	9.6
SCO1570 ^a	<i>argH</i>	Argininosuccinate lyase	AB.SCO1570_1	TCATGCATGAGTATGCAGAA	1681889	1681908		30	16.3
SCO1570	<i>argH</i>	Argininosuccinate lyase	AB.SCO1570_2	CTCTGCATGTTTCGTCAATC	1681909	1681928		50	4.4
SCO1580 ^c	<i>argC</i>	N-acetyl-γ-glutamyl-l-phosphate reductase	AB.SCO1580_A0	GCCCGCATACCCACTCGCTC	1691417	1691436		−44	9.5
SCO1580 ^{a,d}	<i>argC</i>	N-acetyl-γ-glutamyl-l-phosphate reductase	AB.SCO1580_B1	GAGAGCATGACTATACGTGC	1691479	1691498		18 −3	9.1
SCO1580 ^d	<i>argC</i>	N-acetyl-γ-glutamyl-l-phosphate reductase	AB.SCO1580_B2	CGATGCACGTTTATGCAATG	1691499	1691518		38 −23	13.3
SCO1864 ^{c,e}		Putative acetyltransferase	AB.SCO1864_0	ATTCTGAACCCCATCCGGCG	1998411	1998430		38	3.8
SCO2015		2',3'-cyclic-nt 2'-phosphodiesterase-like	AB.SCO2015_0	CCACGCATGACCACTCAACA	2157812	2157831		159	11.4
SCO2055 ^b		Hypothetical protein	AB.SCO2055_1	GTTCCGACGGTACGCAGTG	2202678	2202697		63	11.8
SCO2055		Hypothetical protein	AB.SCO2055_2	GCATGAACGGTTGTACGAAG	2202699	2202718		42	9.0
SCO2231-2 ^b	<i>malE-R</i>	Maltose-binding, transcriptional repressor	AB.SCO2231-2_A1	TGCTGCAAAAATGTGCAAGA	2400395	2400414		136 237	10.7
SCO2231-2	<i>malE-R</i>	Maltose-binding, transcriptional repressor	AB.SCO2231-2_A2	ATCTCCGAAAGTTATCCGGGC	2400416	2400435		157 216	5.1
SCO2231-2	<i>malE-R</i>	Maltose-binding, transcriptional repressor	AB.SCO2231-2_B0	CTCTGCAAGCTCTTGCCGCC	2400507	2400526		248 125	11.9
SCO2529	<i>snpA</i>	Metalloprotease	AB.SCO2529_0	GTCCGTATCAGTATGCGGGA	2727401	2727420		144	10.7
SCO2686 ^{b,c,f}		Putative luxR-family transcriptional regulator	AB.SCO2686_A1	TAITGAGCGTCTCTTCAAAA	2930741	2930760		−98	5.5
SCO2686 ^{c,f}		Putative luxR-family transcriptional regulator	AB.SCO2686_A2	TGCGGCATAGAAGTGOAGTC	2930762	2930781		−77	7.3
SCO2686 ^f		Putative luxR-family transcriptional regulator	AB.SCO2686_B0	CAATGCATGATCATGCCACA	2930862	2930881		23	12.6
SCO3034 ^f	<i>whiB</i>	Sporulation regulatory protein	AB.SCO3034_0	GGAACCAAGCCCATGCAATA	3321156	3321175		140	9.4
SCO3067 ^f	<i>arsI/sigI</i>	Anti anti sigma factor/sigma factor SigI	AB.SCO3067_0	CACAGAACACACTTGGGGTC	3360549	3360568		108 126	7.6
SCO3943 ^{b,f}	<i>rstP</i>	Putative transcriptional regulator	AB.SCO3943_A0	GGACGCATATGCACGGGTTG	4339185	4339204		39	10.2
SCO3943 ^{b,f}	<i>rstP</i>	Putative transcriptional regulator	AB.SCO3943_B0	TTCTGCAAGATCATTAATGC	4339215	4339234		69	9.4
SCO3978-9 ^f		Oxidoreductase TeIR-like regulator	AB.SCO3978-9_0	TAACGGATAGCTTTTCATAA	4381976	4381995		27 35	9.2
SCO4158 ^f		LacI-family regulatory protein-like	AB.SCO4158_0	CCTTGGATGACCTTGGGCC	4576182	4576201		48	11.3
SCO4293 ^f		Putative threonine synthase	AB.SCO4293_0	GCCTCCATGGCTGTGCAGAC	4708595	4708614		−7	14.5
SCO4425	<i>afsS</i>	Sigma-like protein	AB.SCO4425_0	TGCCGGACGGCGCGCGGAG	4842637	4842656		64	8.8
SCO4426 ^{c,f}	<i>afsR</i>	Regulatory protein	AB.SCO4426_0	TTTGCTTTGTTATGCCGAC	4845804	4845823		36	1.2
SCO5226 ^f	<i>nrpA</i>	Ribonucleotide-diphosphate reductase	AB.SCO5226_0	GACTGGACAGGCGTGCGCGC	5688301	5688320		158	9.2

(Continued)

TABLE 1 | Continued

Regulated gene(s)	Gene name	Product	ARG box identifier	Sequence	Chromosomal coordinates			Ri (bit)
					Left	Right	Distance to start codon	
SCO5326-7 ^f		Hypothetical protein	AB.SCO5326-7_0	GCCTCGTTGGTCATGCATCC	5796724	5796743	146 -7	8.9
SCO5583	<i>amtB</i>	Ammonium transporter	AB.SCO5583_0	CCATGCCAGGTCATTCGGAG	6085777	6085796	235	10.2
SCO5864 ^f		Conserved hypothetical protein	AB.SCO5864_0	CTCTCCGTGATCATGCACCC	6421332	6421351	267	11.8
SCO5896 ^c	<i>redH</i>	Phosphoenolpyruvate-utilizing enzyme	AB.SCO5896_0	GACGGCGTGGGCCCTGCAGAA	6461067	6461086	-1669	6.3
SCO5976 ^a	<i>arcB</i>	Ornithine carbamoyltransferase	AB.SCO5976_1	CGCTGTATAGAAATTCAGAA	6550325	6550344	55	8.2
SCO5976	<i>arcB</i>	Ornithine carbamoyltransferase	AB.SCO5976_2	GTTTGGTATAGACTTCCAGAA	6550345	6550364	35	9.6
SCO7036 ^a	<i>argG</i>	Argininosuccinate synthase	AB.SCO7036_1	CTTTGCATGGTCATGCGTAA	7824734	7824753	18	17.2
SCO7036	<i>argG</i>	Argininosuccinate synthase	AB.SCO7036_2	TGATGCATACCTCTTCTATG	7824754	7824773	-2	8.1
SCO7314	<i>sigM</i>	Probable RNA polymerase sigma factor	AB.SCO7314_0	ATCCGGCATGCTCATAGAAAC	8120535	8120554	-13	9.5

a, No separation between the ARG boxes; b, One nucleotide separation between ARG boxes; c, Not included in the model; d, Binding site "A" might to control both SCO1580 and SCO1581 genes; e, Alternative box located 27 nt before; f, Differential transcription not observed.

cells. In the presence of both stains, bacteria with intact cell membranes appeared to fluoresce green, whereas bacteria with damaged membranes appear red. After being left to sit at least 10 min in the dark, the samples were examined under a Leica TCS-SP2-AOBS confocal laser-scanning microscope at a wavelength of either 488 or 568 nm excitation and 530 nm (green) or 630 nm (red) emission, respectively (optical sections ~0.2 μm). Images were mixed using Leica Confocal Software. In some cases, samples were also examined in differential interference contrast mode using the same equipment.

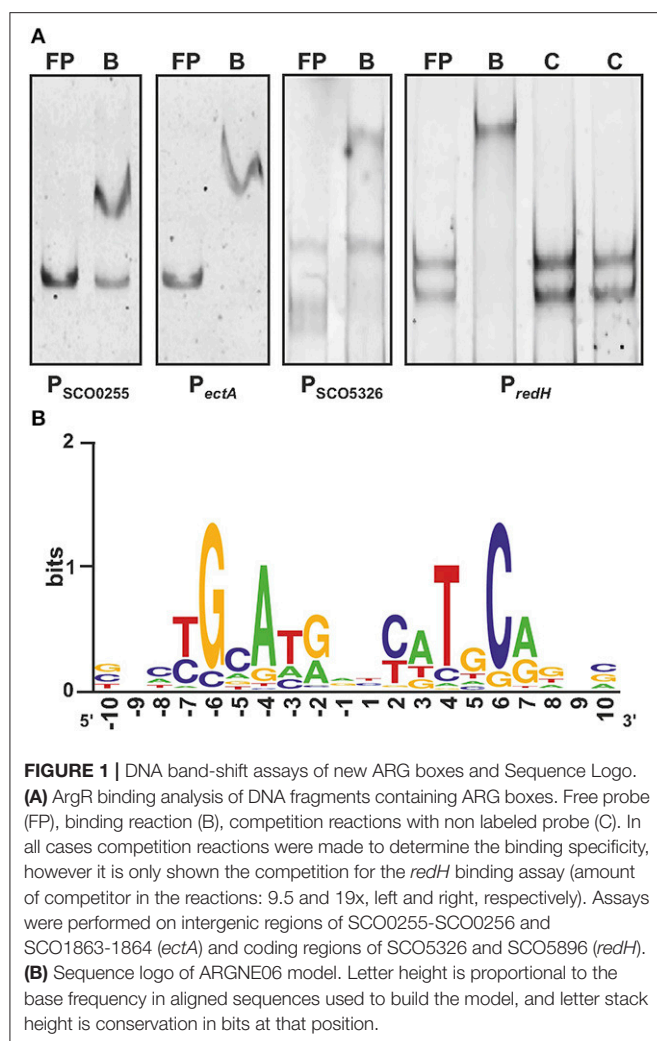
Images were processed with ImageJ. Compartmentalized hyphae were counted using the cell counter plugin (<https://imagej.nih.gov/ij/plugins/cell-counter.html>). The percentage of hyphae suffering segmentation (sporulation-like) was estimated by counting 727 hyphae among numerous pictures, and two different biological replicates, visualized independently in the same focal plane. The average segment length was estimated from 226 measurements (Figure S1).

RESULTS

Construction of a New Model to Analyse ArgR Binding in *S. coelicolor*

Previous footprinting, EMSA and *in vivo* luciferase-fused sequence data demonstrated ArgR binding to several gene promoters (Rodríguez-García et al., 1997; Pérez-Redondo et al., 2012). ArgR binding sites (ARG boxes) are imperfect palindromes up to 20 nt in length (two turns of the DNA helix). Most evident ArgR binding sites were identified in the arginine biosynthesis promoters of *S. clavuligerus* (Rodríguez-García et al., 1997) and *S. coelicolor* (Pérez-Redondo et al., 2012). All binding sites are composed of two contiguous ARG boxes, although DNA band-shift studies showed ArgR binding sites, formed by a unique ARG box (Pérez-Redondo et al., 2012). A bioinformatics model of the *S. coelicolor* ARG box was built according to these sequences (Pérez-Redondo et al., 2012). In this work, the results of EMSA with 50 DNA fragments (27 previously published) were used to build an improved model of the ArgR binding site. Of these 50 fragments assayed, 30 yielded mobility shifts, and 20 fragments failed to show ArgR binding (Table S3). Seven novel positive fragments correspond to the intergenic regions of SCO0255-SCO0256 and SCO1863-SCO1864 (*ectA-ectB*) genes, to the upstream regions of SCO4425 (*afsS*) and SCO4426 (*afsR*) genes, and to the coding regions of SCO4159 (*glnR*), SCO5326 and SCO5896 (*redH*). All the experimental data described in Materials and Methods allowed that a new model of the ARG box was built (Figure 1). The total conservation of this model is $R_{sequence} = 9.9$ bits, and the R_i value of the consensus sequence is 20.9 bits.

The new model was used to analyse the ArgR binding sites present in the DNA fragments giving positive EMSA. A total of 44 ARG functional boxes were identified, showing various conservation values (Table 1). These ARG boxes were arranged into three types of binding sites: (1) typical binding sites formed by two contiguous ARG boxes, such as those of *arg* genes; (2) binding sites formed by two tandem ARG boxes but separated



by one nucleotide; and (3) binding sites formed by a single ARG box. In the promoter of the *rstP* gene, there are two possible ARG boxes separated by 10 nucleotides. It is possible that both boxes form a single binding site or constitute two independent sites.

To identify ARG boxes in the genes transcriptionally affected by the lack of ArgR (see below), a bioinformatic search was conducted in the *S. coelicolor* chromosome. The list of predicted ArgR binding sites was filtered by probability (p -value $< 10^{-5}$) and information content ($R_i > 10.0$ bit) (Table S4A). The 315 ArgR putative sites shown control 221 differentially expressed genes, at either the gene located downstream of the ARG site or the next. In addition, many ArgR binding sites with lower probability were identified, some of which were related to differentially transcribed genes; some are shown in Table S4B. The functionality of most of these ARG boxes remains to be validated.

Transcriptomic Studies of *S. coelicolor* M145 and *S. coelicolor* Δ argR

Gene expression was analyzed in MG liquid cultures of *S. coelicolor* M145 and *S. coelicolor* Δ argR, employing three

biological replicates at five time points. A total of 1544 genes (~20% of the *S. coelicolor* genome) showed differences in expression (signification level $p < 0.01$) in at least one of the 5 time points analyzed. These transcripts corresponded to the genes involved in amino acid metabolism (75 genes), purine and pyrimidine metabolism (31 genes), nitrogen and phosphate control (20 genes), DNA repair and recombination (25 genes), structure and morphology (78 genes), secondary metabolism (74 genes), coenzyme biosynthesis (13 genes), two-component systems (57 genes), regulators and sigma factors (106 genes), or membrane protein-encoding genes (160 genes). Many genes were related to protein secretion or had unknown functions (767 genes), and others were unclassified genes (138) (Table S5). The differentially expressed genes in the control strain and Δ argR mutant were fitted into ten prototypical expression patterns (Figure 2). ArgR behaves mainly as a repressor (profiles 1, 2, 3, and 4) but can also be a weak activator (profiles 5, 6, 7, and 8), and few genes showed either repression or activation at various growth times (profiles 9 and 10). It has to be noted that 50% of the genes did not fit any of the 10 maSigPro profiles. Only 45 of the 7,721 genes scanned were deregulated at all times.

Genes Related to Amino Acids and Pyrimidine Biosynthesis

The genes most affected by the absence of ArgR were those involved in arginine biosynthesis (Figure 3A). They were overexpressed in the Δ argR mutant, in agreement with previous observations for type II ArgR repressors (Tian et al., 1992). Fold changes (or Mc values) for these transcripts oscillated between 7- and 38-fold upregulation in the mutant, and *argC* was the most upregulated gene (Table S5). Conserved ARG boxes were located upstream of *argC*, *argH*, *argR*, *arcB*, and in the intergenic *argG-gabD* bidirectional promoter region (Pérez-Redondo et al., 2012; Table 1). Amino acid biosynthesis genes, such as *hpdD* (SCO2927) and *glyA3* (SCO5364) involved in glycine-serine-threonine metabolism or *gabD* (SCO7035) encoding a succinate semialdehyde dehydrogenase, were upregulated in the Δ argR mutant (Table S5). Especially remarkable was the effect on gene SCO1086, encoding a protein with a transglutaminase domain (125-fold upregulation) (Table S5).

Genes for pyrimidine biosynthesis were highly upregulated in the Δ argR strain, with fold changes close to 4.0; *pyrB* and *pyrR* were the most upregulated genes (Figure 3B; Table S5). Conserved ARG boxes are present upstream of *pyrB*, *pyrA*, *pyrD*, and *pyrR* (Table 1), and some were already confirmed to be bound by ArgR *in vitro* (Pérez-Redondo et al., 2012). The ribonucleotide reductases, forming deoxyribonucleotides in an oxygen-dependent (*nrdABS*) or oxygen-independent (*nrdRJ*) manner, were upregulated by the absence of ArgR but only at the early exponential growth phase (32 h) (Pérez-Redondo et al., 2012). The same was true for the *cobB* and *cobQ* genes required for cobalamin B12 formation, a cofactor controlling *nrdABS* transcription (Table S5).

Genes Related to Nitrogen Metabolism

The expression of nitrogen metabolism genes (*glnII*, *glnA*, *amtB*, *glnK*, and *glnD*) in *S. coelicolor* M145 is shown in Figure 3C.

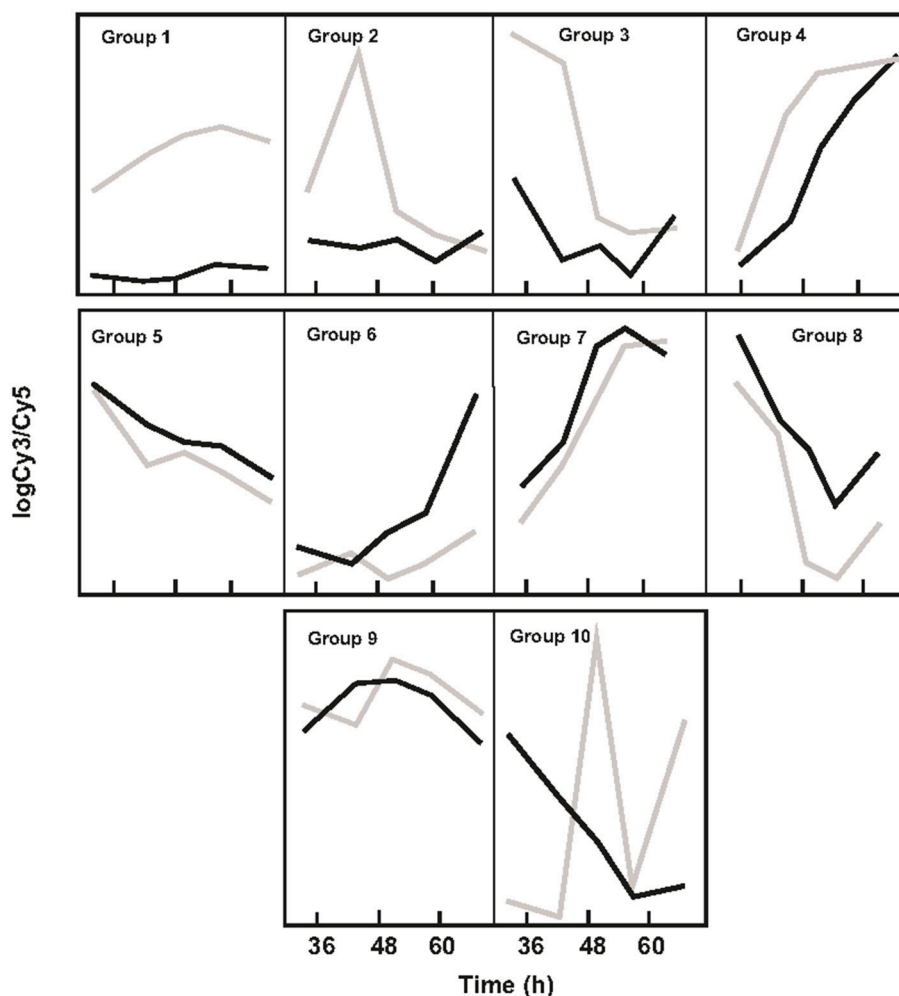


FIGURE 2 | Clustering of gene expression profiles in *S. coelicolor* M145 and *S. coelicolor* $\Delta argR$. *S. coelicolor* M145 gene expression is indicated by black lines; expression of *S. coelicolor* $\Delta argR$ gene is indicated by gray lines. Clustering was obtained using maSigPro Program.

These genes showed high expression at early times, moderate expression between 42 and 56 h, and another increase at the end of the culture. This pattern does not clearly fit any of the profiles shown in **Figure 2**. The $\Delta argR$ mutant displayed expression similar to the control strain between 42 and 56 h of growth, but the strong upregulation at early and late times observed in the control strain did not occur in the mutant (**Figure 3C**).

S. coelicolor grows on nitrate as sole nitrogen source, and it possesses three gene clusters for nitrate reduction: SCO0216 to SCO0219 and SCO4947 to SCO4750, complexes 2 and 3, respectively, and SCO6532 to SCO6535 (Fischer et al., 2010). All genes encoding for the nitrate reductase complex 3 are underexpressed in the $\Delta argR$ mutant (**Figure 3D**), with an expression profile that fitted in group 6, as shown in **Figure 2**. Functional ARG boxes are present upstream of *amtB* (Pérez-Redondo et al., 2012) and in the 3' region of SCO4159, *glnR* (**Table 1**).

Membrane and Secretion Proteins

Approximately 150 genes encoding proteins related to secretion and 160 genes for membrane proteins were up- or down-regulated in expression compared to the parental and the $\Delta argR$ strains (**Table S5**). Some of these genes were strongly underexpressed (SCO4251 and SCO6934) in the mutant at early or late culture times. Other genes, especially SCO0615, SCO0665, SCO6375, and SCO2704, are overexpressed in the $\Delta argR$ mutant (**Table S5**).

Secondary Metabolism Gene Clusters

Lack of ArgR affects the production of the pigmented antibiotics actinorhodin and undecylprodigiosin (Pérez-Redondo et al., 2012). Red and Act production in the control strain reached 6 and 50 nmol/mg dry weight and were detected at 56 and 66 h, respectively. The mutant antibiotic production was reduced to 12% (for Act) and 8% (for Red) of the levels detected in the parental strain (not shown).

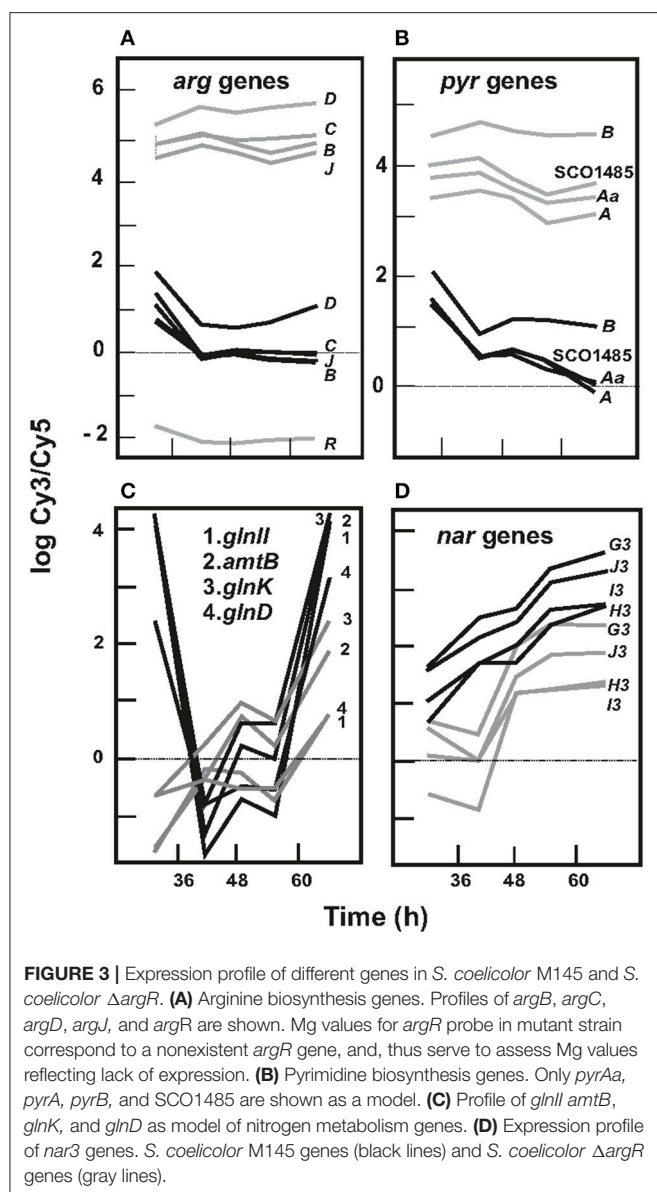


FIGURE 3 | Expression profile of different genes in *S. coelicolor* M145 and *S. coelicolor* Δ argR. (A) Arginine biosynthesis genes. Profiles of *argB*, *argC*, *argD*, *argJ*, and *argR* are shown. Mg values for *argR* probe in mutant strain correspond to a nonexistent *argR* gene, and, thus serve to assess Mg values reflecting lack of expression. (B) Pyrimidine biosynthesis genes. Only *pyrAa*, *pyrB*, and SCO1485 are shown as a model. (C) Profile of *glnI*, *amtB*, *glnK*, and *glnD* as model of nitrogen metabolism genes. (D) Expression profile of *nar3* genes. *S. coelicolor* M145 genes (black lines) and *S. coelicolor* Δ argR genes (gray lines).

All genes for actinorhodin biosynthesis (SCO5071 to SCO5092) shared the same expression profile with growth (group 6 in Figure 2). Expression of the *act* genes in the parental strain decreased from 32 to 42 h and increased steadily thereafter to reach a 6-fold level, whereas the genes expression in the mutant was always lower (18–55% of the level of the parental strain) and increased after 49 h to reach a final level 23% lower than that of the parental strain (Figure 4A).

The 23 genes involved in undecylprodigiosin biosynthesis (SCO5877 to SCO5899) were repressed in the Δ argR mutant with respect to the control strain (Figure 4B), following a group 7 profile. As shown below, the coding sequence of *redH*, SCO5896, contains a functional ARG box (6.3 bits, Table 1).

Expression of the *cpk* gene cluster (SCO6268 to SCO6288) for the biosynthesis of the polyketide coelimycin P1 (Gomez-Escribano et al., 2012) was also altered in the

Δ argR mutant. The *cpk* genes' expression decreased steadily in the control strain with time, while in the Δ argR mutant, the transcription increased to a maximum at the 49 h sampling time and then decreased. However, the complex transcription profile of these genes (group 10, Figure 2) suggests control mechanisms in addition to those due to ArgR. Transcription of genes located close to the *cpk* cluster, as for the γ -butyrolactone-receptor (*scbR*) and the genes involved in γ -butyrolactone synthesis (*scbA*, *scbB*), was also affected by the Δ argR deletion and showed the same expression profile 10 (Figure 2; Table S5). Genes of the *act*, *red*, and *cpk* clusters are putatively under the control of ARG boxes (Table S4).

Secondary metabolism genes with expression altered in the Δ argR mutant include SCO7700 and SCO7701, which are involved in methylisoborneol biosynthesis, and *eshA* (SCO7699), a regulator of secondary metabolism (Saito et al., 2003, 2006); all of these show the expression profile of group 2. The *whiE* genes (SCO5314–5320), related to the synthesis of the TW95a pigment (Kelemen et al., 1998), are strongly upregulated in the Δ argR mutant (Table S5). A less pronounced effect (group 2, Figure 2) was observed in SCO1206 to SCO1208 genes for the synthesis of the tetrahydroxynaphthalene pigment (Table S5). The geosmine biosynthesis gene SCO6073 was underexpressed in the mutant at late times (49 to 66 h, Table S5). A secondary metabolite, ectoine, confers protection against osmotic stress and stabilizes proteins at high temperature and extreme pH to the cells (Bursy et al., 2008; Kol et al., 2010). The ectoine biosynthesis gene cluster (SCO1864 to SCO1867) was weakly overexpressed (1.5 to 3-fold) in the Δ argR mutant, showing the profile of group 3 (Table S5). A DNA fragment from the SCO1863–SCO1864 intergenic region was retarded *in vitro* by the ArgR protein (Table 1).

Transcriptional Analysis of Genes Involved in Differentiation, Sporulation, and Gas Vesicle Formation

Clear expression differences were found in genes involved in hydrophobic cover formation (rodmins and chaplins), sporulation (*ram*, *whi*), cell wall glycan biosynthesis (*cwg*) and gas vesicle formation (*gvp*) (Table 2).

Genes for Rodlins and Chaplins

The rodlet layer formed by chaplins and rodmins (Claessen et al., 2004) is partially responsible for the hydrophobicity in aerial hyphae and spores. The genes encoding chaplins (*chpA*, *chpB*, *chpC*, *chpD*, and *chpG*) and rodmins (*rdlA* and *rdlB*) were upregulated in the Δ argR mutant. This overexpression was particularly high in the exponential growth phase (Table 2). The *chpA*, *rdlB*, and *rdlA* gene expression increased 30-, 52-, and 114-fold, respectively, at 42 h (Figure 5, upper panels), while *chpC* and *chpB* were less affected (4.5-fold increase, Table 2).

Cwg Genes

The *cwg* cluster (SCO6179 to SCO6190) is tentatively involved in glycan cell wall synthesis (Hong et al., 2002). All *cwg* genes were overexpressed (1.3 to 4.3-fold) in the Δ argR mutant (Figure 5, middle panels).

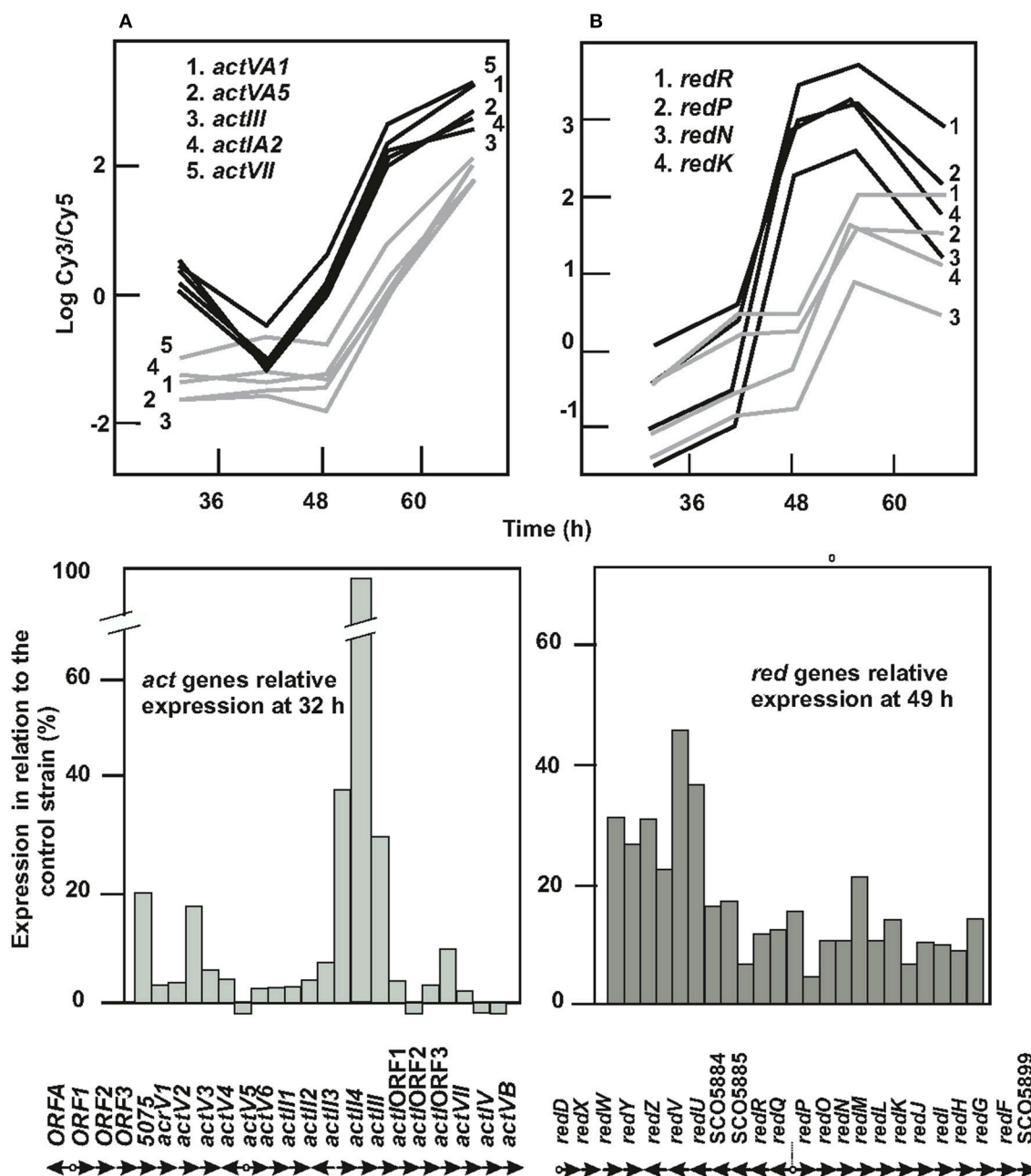


FIGURE 4 | Expression of *act* and *red* genes in *S. coelicolor* M145 and *S. coelicolor* $\Delta argR$. **(A)** Actinorhodin biosynthesis genes. Expression profile of *actVA1*, *actVA5*, *actIII*, *actIA2*, and *actVII* are shown as model (upper left panel). In lower left panel, columns show the relative expression of each *act* gene in *S. coelicolor* $\Delta argR$ at 32 h compared to *S. coelicolor* M145 expression, taken as 100. The corresponding genes are indicated below. **(B)** Undecylprodigiosin biosynthesis genes. Expression profile of *redR*, *redP*, *redN*, and *redK* are shown as a model (upper right panel). In lower right panel columns show relative expression of each *red* gene in *S. coelicolor* $\Delta argR$ at 49 h compared to *S. coelicolor* M145 expression, taken as 100. The corresponding *red* genes are indicated below. *S. coelicolor* M145 genes (black lines), *S. coelicolor* $\Delta argR$ genes (gray lines). The time point at which the expression difference between strains of both sets of genes is maximal (32 or 49 h) have been chosen for representation in lower panels.

Genes for Gas Vesicles

Two independent gene clusters involved in gas vesicle formation (*gvp* genes) were present in the *S. coelicolor* M145 genome. Both clusters showed low and relatively constant expression along the developmental time course in the control strain. However, in

cultures of *S. coelicolor* $\Delta argR$, all *gvp* genes were overexpressed. Cluster I gene expression (SCO0649-SCO0657) slowly increased and peaked at 42 h, as shown for the model gene *gvpA* (Figure 5, lower left panel). Transcription for genes in cluster II (SCO6499-SCO6508) increased along with time in the mutant, showing

TABLE 2 | Genes related to morphology differentially expressed in *S. coelicolor* M145 and *S. coelicolor* Δ argR (1).

Code	Product	Gene	Mc Δ argR-M145					p BH Δ argR-M145				
			32 h	42h	49h	56h	66h	32 h	42 h	49 h	56 h	66 h
SCO0649	Putative gas vesicle synthesis protein	<i>gvpO2</i>	0.328	3.008	1.143	0.467	−0.183	0.856	0.000	0.021	0.557	0.870
SCO0650	Putative gas vesicle synthesis protein	<i>gvpA2</i>	0.274	3.122	1.713	0.522	1.138	0.868	0.000	0.000	0.414	0.011
SCO0651	Putative gas vesicle synthesis protein	<i>gvpF2</i>	0.230	1.843	0.510	0.216	0.035	0.799	0.000	0.092	0.681	0.967
SCO0652	Putative gas vesicle synthesis protein	<i>gvpG2</i>	0.632	2.872	1.248	0.227	0.106	0.381	0.000	0.009	0.803	0.929
SCO0653	Conserved hypothetical protein	<i>gvpY2</i>	0.023	1.157	−0.160	0.047	−0.012	0.999	0.004	0.715	0.964	0.992
SCO0654	Conserved hypothetical protein	<i>gvpZ2</i>	0.224	2.443	0.979	0.211	0.204	0.909	0.000	0.015	0.781	0.790
SCO0655	Putative gas vesicle synthesis protein.	<i>gvpJ2</i>	0.185	1.283	0.827	0.230	−0.231	0.945	0.001	0.030	0.754	0.736
SCO1415	Putative membrane protein	<i>smeA</i>	1.002	3.040	1.923	0.302	0.088	0.302	0.000	0.006	0.823	0.960
SCO1416	Putative membrane protein	<i>sffA</i>	0.738	1.982	1.474	0.449	0.310	0.066	0.000	0.000	0.353	0.517
SCO1489	BldD, transcriptional regulator of developmental genes	<i>bldD</i>	0.329	0.778	0.621	0.414	0.183	0.230	0.000	0.004	0.086	0.525
SCO1541	SsgA-like protein	<i>ssgB</i>	1.211	4.936	1.902	−0.010	−1.258	0.056	0.000	0.001	0.995	0.023
SCO1674	Putative secreted protein	<i>chpC</i>	0.522	1.634	0.363	0.484	−0.984	0.488	0.000	0.426	0.473	0.031
SCO1800	Putative small secreted protein	<i>chpE</i>	−0.016	0.082	−0.883	0.319	−0.490	0.999	0.848	0.009	0.520	0.182
SCO2082	Cell division protein	<i>ftsZ</i>	0.307	0.678	0.093	0.048	−0.159	0.244	0.001	0.658	0.915	0.578
SCO2716	Putative secreted protein	<i>chpA</i>	3.918	4.953	2.124	1.431	0.310	0.000	0.000	0.000	0.015	0.734
SCO2717	Putative small membrane protein	<i>chpD</i>	0.689	2.057	0.388	0.304	−1.100	0.609	0.003	0.592	0.822	0.141
SCO2718	Putative secreted protein	<i>rdlA</i>	5.182	6.836	3.209	2.305	0.705	0.000	0.000	0.000	0.005	0.486
SCO2719	Putative secreted protein	<i>rdlB</i>	4.621	5.711	2.595	1.667	0.496	0.000	0.000	0.000	0.018	0.596
SCO2786	beta-N-acetylhexosaminidase	<i>hexA</i>	0.345	0.305	−0.240	−0.283	−1.345	0.091	0.077	0.154	0.197	0.000
SCO3356	ECF sigma factor	<i>sigE</i>	0.042	−0.592	0.158	0.275	0.640	0.999	0.001	0.387	0.232	0.001
SCO3404	Cell division protein ftsH homolog	<i>ftsH2</i>	−0.007	0.548	0.059	0.067	0.249	0.999	0.009	0.807	0.883	0.330
SCO3925	IcIR-type transcriptional regulator of ssgA	<i>ssgR</i>	0.594	1.519	0.329	−0.152	−0.429	0.159	0.000	0.322	0.815	0.271
SCO3926	Sporulation factor	<i>ssgA</i>	0.785	2.219	1.472	0.728	−0.671	0.127	0.000	0.001	0.164	0.139
SCO4035	RNA polymerase sigma factor	<i>sigF</i>	0.373	0.740	−0.049	−0.181	−0.407	0.394	0.009	0.888	0.717	0.206
SCO4767	Putative regulatory protein	<i>whiD</i>	−0.014	1.989	0.352	0.822	1.462	1.000	0.001	0.586	0.339	0.019
SCO4923	Conserved hypothetical protein		−0.203	−0.397	0.073	−0.171	0.038	0.232	0.002	0.584	0.330	0.896
SCO5046	Hypothetical protein	<i>wblI</i>	0.068	0.391	−0.258	−0.741	−1.258	0.999	0.126	0.302	0.008	0.000
SCO5240	Sporulation transcription factor-like	<i>wblE</i>	0.200	0.750	−0.189	−0.368	−0.704	0.706	0.001	0.422	0.222	0.003
SCO5314	whiE protein VII	<i>whiE</i> -ORFVII	0.333	5.188	2.766	0.383	0.223	0.942	0.000	0.000	0.768	0.890
SCO5315	polyketide cyclase	<i>whiE</i> -ORFVI	0.469	2.869	1.951	0.814	0.034	0.741	0.000	0.001	0.306	0.983
SCO5316	acyl carrier protein	<i>whiE</i> -ORFV	1.023	5.555	2.857	0.694	0.454	0.270	0.000	0.000	0.500	0.679
SCO5317	polyketide beta-ketoacyl synthase beta	<i>whiE</i> -ORFIV	0.023	1.395	0.409	−0.087	−0.314	0.999	0.003	0.388	0.941	0.683
SCO5318	polyketide beta-ketoacyl synthase alpha	<i>whiE</i> -ORFIII	0.143	3.152	1.263	−0.178	0.024	0.995	0.000	0.008	0.851	0.985
SCO5319	whiE protein II	<i>whiE</i> -ORFII	0.245	2.398	1.389	0.101	0.216	0.960	0.000	0.014	0.944	0.860
SCO5320	whiE protein I	<i>whiE</i> -ORFI	0.083	2.182	0.777	0.100	0.030	0.999	0.000	0.073	0.928	0.981
SCO5321	polyketide hydroxylase	<i>whiE</i> -ORFVIII	0.023	1.479	0.325	−0.024	−0.125	0.999	0.000	0.374	0.980	0.877
SCO5580	Putative prokaryotic docking protein	<i>ftsY</i>	0.058	0.027	0.290	0.242	0.746	0.999	0.938	0.233	0.526	0.003
SCO5819	Sporulation transcription factor, WhiH	<i>whiH</i>	1.978	3.388	1.448	1.197	−0.647	0.000	0.000	0.004	0.026	0.241
SCO6029	Two-component regulator	<i>whiI</i>	2.696	3.526	1.840	1.287	0.261	0.000	0.000	0.002	0.039	0.807
SCO6131	Putative carboxypeptidase		0.039	−0.815	−0.648	0.002	0.563	0.999	0.001	0.010	0.998	0.027
SCO6180	Putative transferase	<i>cwgB</i>	0.225	1.275	1.786	1.779	1.527	0.572	0.000	0.000	0.000	0.000
SCO6181	Putative transferase	<i>cwgC</i>	0.047	0.777	1.267	1.303	1.058	0.999	0.001	0.000	0.000	0.000
SCO6182	Putative dehydratase	<i>cwgD</i>	0.148	0.396	0.682	1.108	0.695	0.822	0.061	0.002	0.000	0.002
SCO6183	Putative transferase	<i>cwgE</i>	0.325	0.084	1.086	1.551	1.017	0.492	0.817	0.000	0.000	0.001
SCO6185	Putative transferase	<i>cwgG</i>	0.361	1.704	2.092	1.867	1.200	0.341	0.000	0.000	0.000	0.000
SCO6186	Putative phosphoheptose isomerase	<i>cwgH</i>	0.592	0.846	1.200	0.942	0.746	0.148	0.009	0.001	0.010	0.025
SCO6187	Putative bifunctional synthase/transferase	<i>cwgI</i>	0.313	0.338	0.943	0.896	0.213	0.573	0.286	0.003	0.007	0.652
SCO6188	Putative transferase	<i>cwgJ</i>	0.087	0.440	0.826	0.766	0.627	0.990	0.111	0.004	0.011	0.024

(Continued)

TABLE 2 | Continued

Code	Product	Gene	Mc $\Delta argR$ -M145					p BH $\Delta argR$ -M145				
			32 h	42h	49h	56h	66h	32 h	42 h	49 h	56 h	66 h
SCO6499	Putative gas vesicle synthesis protein	<i>gvpO</i>	0.185	0.799	1.259	1.507	2.420	0.990	0.170	0.023	0.018	0.000
SCO6500	Putative gas vesicle synthesis protein	<i>gvpA</i>	0.163	0.669	1.206	1.464	2.244	0.973	0.108	0.004	0.001	0.000
SCO6501	Putative gas vesicle synthesis protein	<i>gvpF</i>	0.196	0.720	0.843	1.014	1.662	0.836	0.011	0.005	0.001	0.000
SCO6502	Putative gas vesicle synthesis protein	<i>gvpG</i>	0.263	0.787	0.602	0.923	1.691	0.879	0.068	0.152	0.065	0.000
SCO6503	Hypothetical protein SC1E6.12	<i>gvpY</i>	0.126	0.396	0.521	0.767	0.966	0.978	0.271	0.114	0.049	0.006
SCO6504	Conserved hypothetical protein SC1E6.13	<i>gvpZ</i>	0.323	0.781	0.777	1.201	1.910	0.722	0.039	0.035	0.005	0.000
SCO6505	Putative gas vesicle synthesis protein	<i>gvpJ</i>	−0.077	0.408	0.768	1.036	1.300	0.999	0.183	0.011	0.002	0.000
SCO6506	Putative gas vesicle protein	<i>gvpL</i>	0.172	−0.088	0.420	0.645	1.143	0.860	0.796	0.104	0.033	0.000
SCO6507	Putative gas vesicle synthesis protein	<i>gvpS</i>	−0.375	−0.076	−0.440	0.416	0.955	0.391	0.840	0.109	0.284	0.001
SCO6682	Hypothetical protein SC5A7.32	<i>ramS</i>	−2.158	−0.491	−0.152	−1.645	−1.481	0.004	0.532	0.854	0.034	0.036
SCO6685	Two-component system response regulator	<i>ramR</i>	−0.570	−0.394	−1.116	−0.741	−0.697	0.091	0.177	0.000	0.019	0.016
SCO6715	Putative transcriptional regulator	<i>wblH</i>	−0.505	0.203	−0.231	0.671	2.427	0.817	0.828	0.775	0.549	0.001
SCO7050	Putative D-alanyl-D-alanine carboxypeptidase		0.437	0.851	0.460	0.249	0.169	0.306	0.004	0.111	0.605	0.750
SCO7257	Putative secreted protein	<i>chpB</i>	1.118	2.174	0.504	0.415	−0.223	0.017	0.000	0.221	0.520	0.772
SCO7699	EshA protein	<i>eshA</i>	1.043	2.524	0.185	−0.018	−2.170	0.030	0.000	0.688	0.988	0.000

(1) For each gene, the Mc value is the binary log of the differential transcription between the mutant and the wild strain. A positive Mc value indicates upregulation, and a negative one, downregulation. Data are the average of three biological replicates and Benjamini-Hochberg adjusted p-values are indicated. Bold numbers indicate p-values below the threshold (0.01) set to identify significantly differentially expressed genes.

2- to 4-fold higher expression than in the control strain in the stationary phase; as a prototype gene of cluster II, *gvpA*₂ expression is shown in **Figure 5** (right lower panel).

Genes Related to Spore Formation and Differentiation

All *whi* genes were involved in sporulation and aerial hyphae formation (Davis and Chater, 1992), with the exception of *whiJ* and *whiA*, which were significantly upregulated by the absence of ArgR (**Table 2**). The *whiD*, *whiI*, and *whiH* genes (**Figure 6**, upper panels) and the eight *whiE* genes (*orfI* to *orfVIII*), which are involved in the formation of the spore pigment (Kelemen et al., 1998) (**Figure 6**, lower panels), were most overexpressed in the mutant. The ARG box located in the *whiB* promoter region (Ri 9.4 bits, **Table 1**) was demonstrated to bind ArgR in previous DNA band-shift studies (Pérez-Redondo et al., 2012), and several *whi* genes are under the predicted control of ARG boxes (**Table S4**).

The *ramR* gene, which encodes an orphan response regulator related to the SapB peptide and aerial mycelium formation (San Paolo et al., 2006), was weakly down-regulated in the $\Delta argR$ mutant (**Table S5**). The transcription of genes for key sporulation regulatory proteins, such as *ssgR*, *ssgA*, *ssgB*, and *smeA-sffA* (van Wezel et al., 2000a; Traag et al., 2004; Ausmees et al., 2007; Willemse et al., 2011), were all upregulated in the mutant (**Table 2**).

Other genes related to morphological differentiation had smaller, but significant, differences in expression between the parental and $\Delta argR$ mutant strains. These were the developmental transcriptional regulator *blbD* (Elliot et al., 2001), which presents functional ARG boxes upstream of its coding sequence (Pérez-Redondo et al., 2012); *wblH*, a target of WhiA

(Bush et al., 2013); and *ftsZ*, a key protein of cell division (van Wezel et al., 2000b; Bush et al., 2013). All weakly increased w their expression at the first three sampling times (**Table S5**). Also upregulated in the $\Delta argR$ mutant were *hexA*, encoding for an N-acetylhexosaminidase involved in glycan degradation (Mark et al., 1998); SCO4923, putatively involved in septum formation; SCO7050, for a D,D-carboxypeptidase-like protein; and SCO7699, reported to be involved in sporulation (**Table 2**).

Analysis of S. coelicolor M145 and $\Delta argR$ Mutant Differentiation

The mycelium from liquid cultures of the $\Delta argR$ mutant showed a dark, brownish pigment, which was not observed in the *S. coelicolor* M145 mycelium (compare **Figure 7A** with **Figure 7E**). Morphological differentiation was analyzed in liquid cultures using confocal microscopy. The most important difference between *S. coelicolor* M145 and the $\Delta argR$ mutant was the presence of nucleoid segregation (**Figure 7G**), and the formation of round segments (**Figure 7H**) with an average length of $0.9 \mu\text{m} \pm 0.1$ in the $\Delta argR$ mutant, resembling the segmentation observed during sporulation in solid cultures. Hypha segmentation began at 27 h of culture and affected $4.3\% \pm 0.1$ of the hyphae (**Figure S1**).

Validation of Transcriptomic Data by qRT-PCR

Transcriptomic data were validated using qRT-PCR at two developmental time points for thirteen of the genes related to differentiation and secondary metabolism: *whiH*, *rdlB*, SCO1588, *cwgB*, *chpA*, *whiE-orfV*, *gvpO*, *pyrB*, *ramR*, *glnII*, *scbR*, *redW*, and *actV1* (**Figure 8**). The expression levels of 14 additional

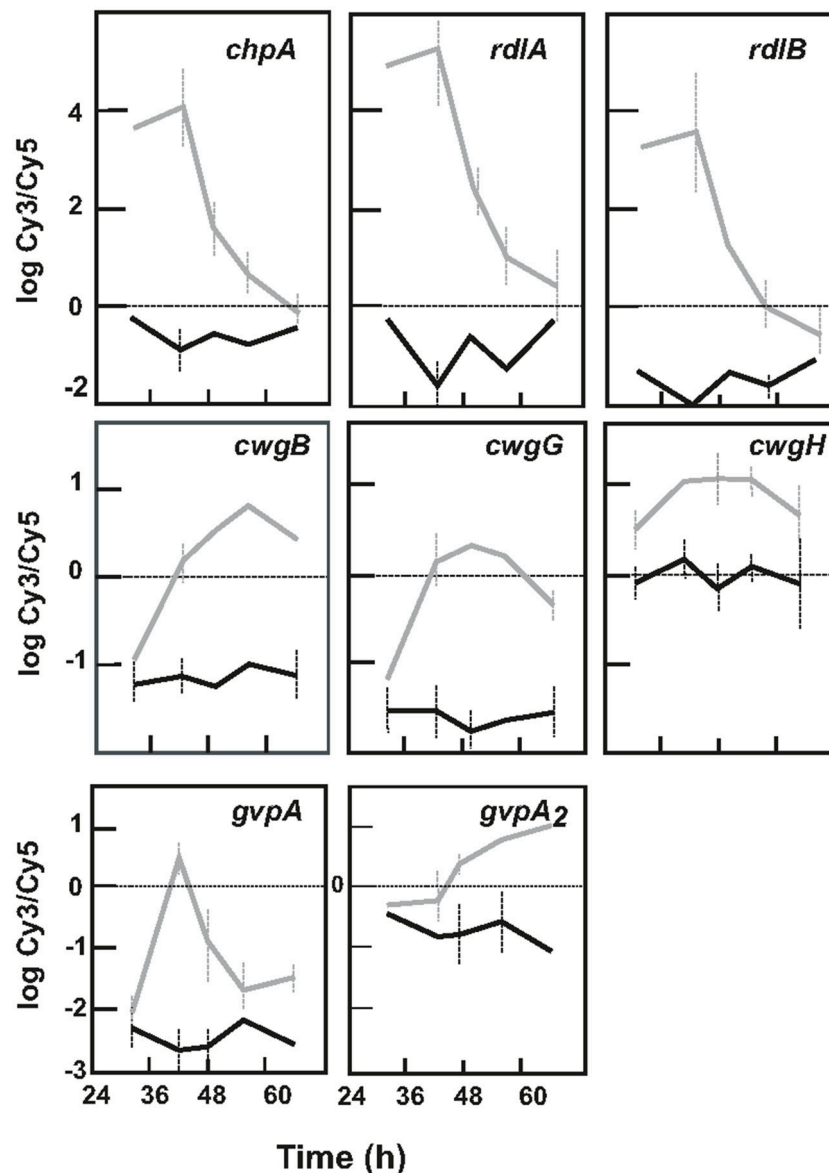


FIGURE 5 | Expression of genes related to differentiation in *S. coelicolor* M145 and *S. coelicolor* $\Delta argR$. **(Upper panels)** Expression profile of genes encoding chaplins (*chpA* as model) and rodlin (*rdlA*, *rdlB*). **(Middle panels)** Expression profile of *cwg* genes. Expression of *cwgB*, *cwgG*, and *cwgH* are shown as model. **(Lower panels)** Expression of genes for gas vesicles: *gvpA* and *gvpA₂* are shown as model of genes for gas vesicle clusters I and II. *S. coelicolor* M145 genes (black lines), *S. coelicolor* $\Delta argR$ genes (gray lines). Standard deviation is represented by discontinuous bars.

genes from all the expression profiles shown in **Figure 1** were also validated (Figure S2). The correlation between the qRT-PCR and microarray results for the 27 genes was very good, with an R^2 value of 0.926 (**Figure 8**), confirming the reliability of the transcriptomic data.

DISCUSSION

The differences in the transcriptomes of *S. coelicolor* M145 and the $\Delta argR$ mutant strain were previously studied at a single developmental time point (Pérez-Redondo et al., 2012).

The current studies were extended by analyzing five different developmental stages in the culture.

The existence of ARG boxes in ArgR controlled genes suggests a modulator role of ArgR in the transcription. The information content (R_i) of the operators formed by a single ARG box, listed in **Table 1**, ranged from 1.2 bit (*afsR*) to 14.5 bit (SCO4293). The presence of one or two ARG boxes, the distance between them, the R_i value, and their location in relation to other regulatory signals, may account for different ArgR binding affinities and allow fine-tuned regulation of the expression of the controlled genes. ARG boxes were predicted in the genome using the new

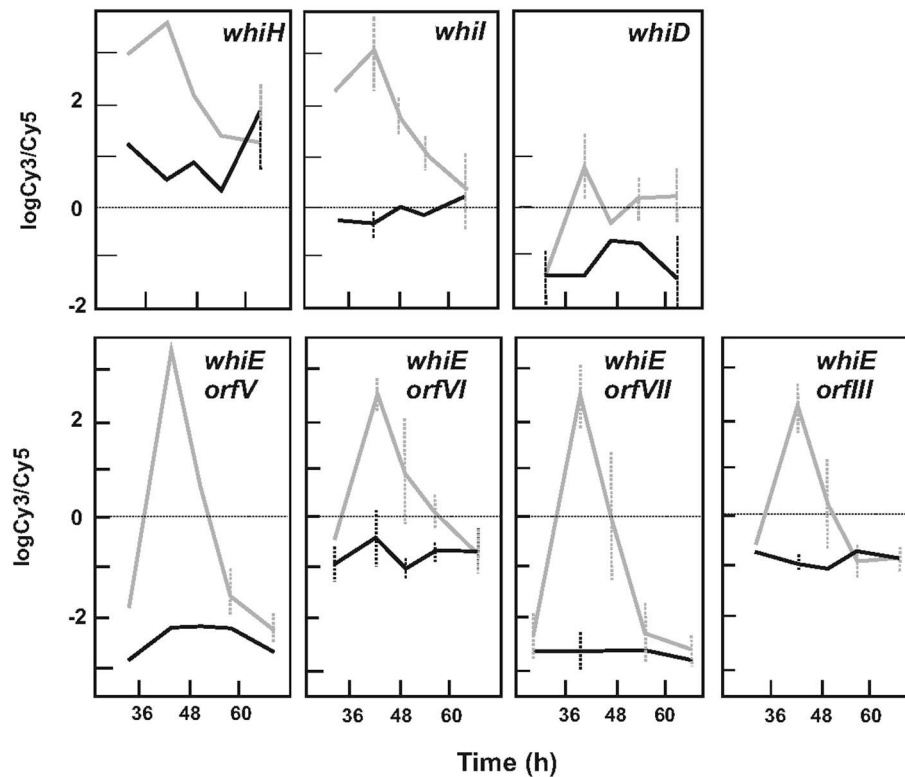


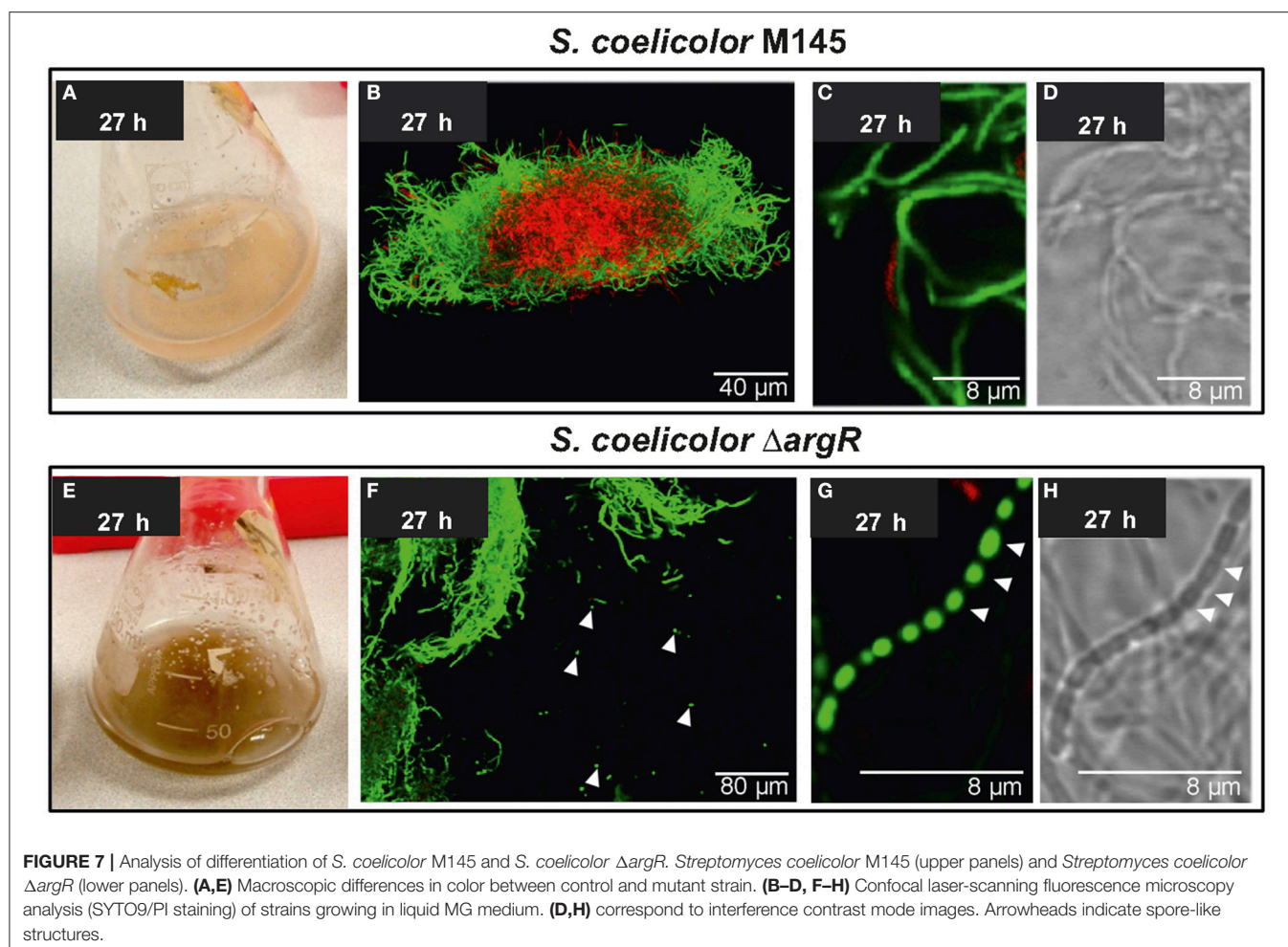
FIGURE 6 | Expression profile of *whi* genes in *S. coelicolor* M145 and *S. coelicolor* Δ argR. **(Upper panels)** Expression of *whiH*, *whiI*, and *whiD* genes. **(Lower panels)** Expression of *whiE* cluster genes. The *whiE*-orfV, orfVI, orfVII, and orfIII are shown as models. *S. coelicolor* M145 genes (black lines), *S. coelicolor* Δ argR genes (gray lines). Standard deviation is represented by discontinuous bars.

model (Table S4). Those sites, if functional, might account for the altered transcription in the Δ argR mutant. Alternatively, in the absence of an ArgR binding site, the regulatory role of ArgR in the expression would be indirect.

This study demonstrates that ArgR is a pleiotropic regulator, which in *S. coelicolor* represses more than the genes for arginine and pyrimidine biosynthesis (Cunin et al., 1983; Larsen et al., 2008). A total of 1,544 genes out of the 7,721 analyzed were significantly deregulated at least once according to the microarray experiment (Table S5). Forty-five genes were always overexpressed (e.g., at 5 time points) in the ArgR mutant (Table S5), which suggests that the ArgR protein exerts a tight control over their transcription. Most of them, 29 out of these 45 genes (64%) had the profile of group 1 (Figure 2), including the 15 genes related to arginine and pyrimidine biosynthesis. The other 16 genes did not fit any of the 10 groups determined by maSigPro. The function of many of these 29 genes is unknown, although SCO6824-SCO6827 resembles a polyketide synthesis gene cluster and *sigM* (SCO7314) has been reported to be involved in osmotic stress control (Lee et al., 2005). ArgR direct control over some of these 45 deregulated genes was demonstrated by binding to functional ARG boxes located upstream of SCO1086, *pyrA*, *pyrB*, *pyrR*, *bldD*, *argH*, *argC*, *arcB*, *argG*, and *sigM* (Table 1), and non-tested, but predicted ARG boxes could account for the control of SCO2864-SCO2869, SCO6205-SCO6206, SCO6824-SCO6827

genes (Table S4). However, most of the deregulated genes (1499) were over- or under-expressed at one, two, three or four time points, indicating a ArgR relaxed control and/or interaction with other regulators. The nitrogen metabolism genes are controlled in *S. coelicolor* by GlnR, the global regulator of nitrogen assimilation, by NnaR (Amin et al., 2012) and also by PhoP, the global regulator of phosphate metabolism (Rodríguez-García et al., 2009; Sola-Landa et al., 2013). We found that, in addition, some nitrogen metabolism genes (*glnII*, *amtB*, *glnK*, *glnD*) are regulated by ArgR. This was a direct effect, since expression of *glnR* and *phoP* was not affected in the Δ argR mutant. Arginine is a nitrogen-rich storage compound in many organisms (Llácer et al., 2008), and the discovery of ArgR binding-ARG boxes (Pérez-Redondo et al., 2012) in the *glnR* and *amtB* genes, supports a direct regulatory role for ArgR in nitrogen metabolism.

A similar situation occurs in cell wall biosynthesis genes (*cwg*), which were upregulated in the Δ argR mutant. The *cwg* genes were predicted to be transcribed from the *cwgA* upstream promoter, which is controlled by SigE (Hong et al., 2002) in response to the signal transmitted by the two component system CseC-CseB (Paget et al., 1999). Our results suggest an additional ArgR regulation of *cwg* genes. Expression of genes for secondary metabolite biosynthesis was also altered in the Δ argR mutant. The *act* and *red* genes were repressed, and genes for the TW95a



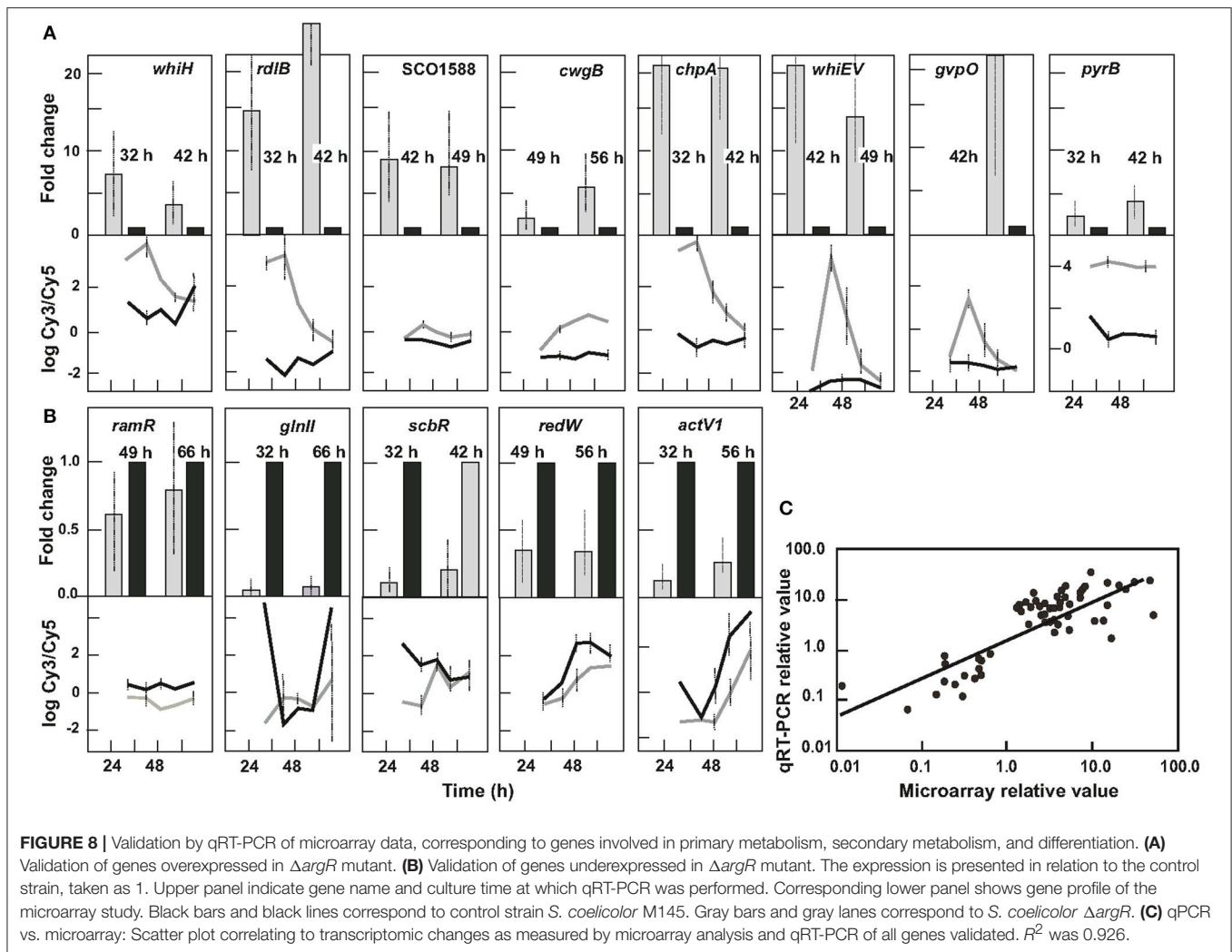
pigment, and coelomicin were overexpressed. The genes for ectoine biosynthesis, controlled by GlnR (Shao et al., 2015), were overexpressed at all time points.

In *S. coelicolor* the *gvp* genes for a putative regulator and gas vesicle structural proteins are located in two duplicated clusters. These gas-filled vesicles are required in aquatic organisms for flotation, but have never been found in soil-dwelling bacteria and the presence of these gene clusters (Offner et al., 1998) is surprising. In fact, disruption of the *gvp* gene clusters does not affect the buoyancy of *Streptomyces* cells in liquid cultures (van Keulen et al., 2005). An induction of *gvp* genes was found following exposure to high concentrations of salt, and it has been proposed that gas vesicles may counteract hyperosmotic stress. The expression of both *S. coelicolor* *gvp* clusters was upregulated in the $\Delta argR$ strain. The Gvp proteins have a very high content of arginine, glutamate, and proline, up to 42% of the protein total amino acids in GvpA₂, and might have evolved in soil *Actinobacteria* as nitrogen storage material, which might explain the ArgR control on their biosynthesis.

Some putative ArgR binding sequences were found in these differentially expressed genes, including ARG boxes located in coding regions. The presence of binding sequences for regulatory

proteins in coding sequences is not unusual; in a study of the PHO regulon in *S. coelicolor*, almost 70% of the PhoP-chromatin-immunoprecipitated enriched fragments, and ~50% of the bioinformatically located PHO boxes, were located in coding sequences (Allenby et al., 2012).

DNA band-shift studies using ArgR protein identified 24 regions containing ARG boxes (Pérez-Redondo et al., 2012). Here, we show additional DNA fragments bound by ArgR *in vitro* (Figure 1A). However, other DNA fragments tested with putative ARG boxes showed no band retardation on EMSA (Table S3). The lack of binding in sequences putatively involved in regulation is not rare. The presence of ARG boxes might not be sufficient indicator of affinity binding *in vitro*. In fact, Sola-Landa et al. (2008) selected, with very stringent criteria, 20 promoters containing PHO boxes but were able to confirm the functionality of only 40% of them using an *in vitro* gel-shift assay. A lack of binding may derive from low Ri boxes but also depends on the correct spatial configuration of the DNA in the fragment used, the *in vivo* requirement of additional accessory proteins or cofactors that increase the affinity binding of the regulatory protein, and/or the requirement of *in vivo* modifications of the binding regulator (Wade et al., 2007). This is



the case for RocR and AhrC cooperation in *Bacillus* to activate expression of arginine catabolism genes (Gardan et al., 1997) or the cooperation of the regulatory proteins FarR and ArgR in corynebacteria, to control *argB* expression and intracellular ornithine levels (Lee et al., 2011).

The relationship between ArgR and hyphae differentiation remained unexplored. As detailed above, *S. coelicolor* $\Delta argR$ mutants showed a spectacular phenotype in liquid cultures, resulting in the formation of spore-like chains. Microscopy analysis displayed the division and separation of nucleoids and the physical strangulation of hypha, forming chains of individual round segments in mutant liquid cultures, two principal events associated with sporulation (Figure 7). While sporulation in liquid cultures has occasionally been described in other *Streptomyces* strains (Lee and Rho, 1993; Rho and Lee, 1994; Rueda et al., 2001), in *S. coelicolor* it is very unusual and has only been reported in flask cultures submitted to either nutritional downshift or Ca^{2+} supplementation (Daza et al., 1989), in *S. coelicolor* strains overexpressing *ssgA* (van Wezel et al., 2000a), and recently, in 2-L bioreactors (Rioseras et al.,

2014). The signals triggering sporulation in *Streptomyces* hyphae (the upper parts of the aerial mycelia in solid cultures; the border of the mycelial pellets in liquid cultures) remain poorly characterized. Our results suggest that the arginine metabolism can contribute to modulate sporulation.

The differentiation signals activating sporulation and secondary metabolism are not completely known, especially in liquid cultures (Salerno et al., 2013). This work suggests that ArgR contributes to the regulation of these processes blocking sporulation in liquid cultures of the parental strain. In addition, this phenotype correlates with the overexpression in the $\Delta argR$ mutant of genes involved in hydrophobic cover formation, differentiation, and sporulation (e.g., chaplins, rodlin, most *whi* genes, *ramR*, *ssgR*, *ssgA*, *smeA-sffA*). Several possible ARG boxes were associated with the *whi* genes, suggesting a direct interaction with ArgR. In the case of rodlin and chaplin genes, no putative regulatory sequences were bioinformatically detected, indicating possible indirect regulation through other genes. Small but significant differences were found for some genes related to sporulation, such as *sigF* (Kelemen et al., 1996), or

to hyphae septation, such as *ftsZ* and *ftsH2*, but not for other genes involved in the formation of the cytokinetic Z ring (*ftsW*, *ftsI*, *ftsQ*), (Grantcharova et al., 2003). No significant differences were found for other genes, such as rodlin and chaplin genes, genes related to aerial mycelium formation (*ramCSAB*) (Keijser et al., 2002; O'Connor and Nodwell, 2005), hyphae elongation or cellular division (*whiA*, *crgA*) (Flårdh et al., 1999). The regulatory genes differentially expressed in the Δ *argR* mutant with respect to the *S. coelicolor* parental strain are potential regulators of sporulation-like processes detected in liquid cultures. Further work is necessary to achieve a deeper characterization of the biochemical mechanism behind activation of sporulation in liquid cultures.

In summary, this work demonstrates that the ArgR protein is more pleiotropic than other bacterial ArgRs, affecting the expression of 1544 genes and triggering a sporulation-like process under the growth conditions used in this work. A new weight matrix was developed for the identification of novel ARG boxes, and a database containing the expression data of genes differentially expressed in the Δ *argR* mutant was generated.

AUTHOR CONTRIBUTIONS

PL, AR-G, and AM: conceived and designed research. AB, RP-R, RÁ-Á, and PY: performed research. AR-G: did the bioinformatics

studies. PY and AM: did the differentiation studies. PL: wrote the manuscript.

FUNDING

Grant BIO2013-34723 from the Spanish Ministry of Science and Innovation to PL. Work in the AM's laboratory was funded by the European Research Council (ERC Starting Grant; Strp-differentiation 280304) and by the Spanish Ministry of Economy and Competitiveness (Grant BIO2015-65709-R).

ACKNOWLEDGMENTS

We greatly appreciate Juan F. Martín for the valuable discussions on the experimental work and suggestions for the manuscript. We appreciate the help of Springer Nature Authors Service to improve the language of the article, of María Teresa López-García in solving practical issues in the laboratory, and also the collaboration with DISMED SA.

SUPPLEMENTARY MATERIAL

The Supplementary Material for this article can be found online at: <https://www.frontiersin.org/articles/10.3389/fmicb.2018.00361/full#supplementary-material>

REFERENCES

- Allenby, N. E. E., Laing, E., Bucca, G., Kierzek, A. M., and Collin, C. P. (2012). Diverse control of metabolism and other cellular processes in *Streptomyces coelicolor* by the PhoP transcription factor: genome-wide identification of *in vivo* targets. *Nucleic Acid Res.* 40, 9543–9556. doi: 10.1093/nar/gks766
- Amin, R., Reuther, J., Bera, A., Wohlleben, W., and Mast, Y. (2012). A novel GlnR target gene, is involved in nitrite assimilation in *Streptomyces coelicolor*. *Microbiology* 158, 1172–1182. doi: 10.1099/mic.0.054817-0.
- Ausmees, N., Wahlstedt, H., Bagchi, S., Elliot, M. A., Buttner, M. J., and Flårdh, K. (2007). A small membrane protein with multiple functions in *Streptomyces* sporulation including targeting of a SpoIIIE/FtsK-like protein to cell division septa. *Mol. Microbiol.* 65, 1458–1473. doi: 10.1111/j.1365-2958.2007.05877.x
- Bailey, T. L., Bodén, M., Buske, F. A., Frith, M., Grant, C. E., Clementi, L., et al. (2009). MEME SUITE: tools for motif discovery and searching. *Nucleic Acids Res.* 37, W202–W208. doi: 10.1093/nar/gkp335
- Bentley, S. D., Chater, K. F., Cerde-o-Tárraga, A. M., Challis, G. L., Thomson, N. R., James, K. D., et al. (2002). Complete genome sequence of the model actinomycete *Streptomyces coelicolor* A3(2). *Nature* 417, 141–147. doi: 10.1038/417141a
- Botas, A. (2013). *Regulación del Metabolismo en Streptomyces: Control por ArgR*, Ph.D. thesis, University of León.
- Bursy, J., Kuhlmann, A. U., Pittelkow, M. H., Jebbar, M., Pierik, A. J., and Bremer, E. (2008). Synthesis and uptake of the compatible solutes ectoine and 5-hydroxyectoine by *Streptomyces coelicolor* A3(2) in response to salt and heat stresses. *Appl. Environ. Microbiol.* 74, 7286–7296. doi: 10.1128/AEM.00768-08
- Bush, M. J., Bibb, M. J., Chandra, G., Findlay, K. C., and Buttner, M. J. (2013). Genes required for aerial growth, cell division, and chromosome segregation are targets of WhiA before sporulation in *Streptomyces venezuelae*. *mBio* 24, e00684–e00613. doi: 10.1128/mBio.00684-13
- Buttner, M. J., Chater, K. F., and Bibb, M. J. (1990). Cloning, disruption, and transcriptional analysis of three RNA polymerase sigma factor genes of *Streptomyces coelicolor* A3(2). *J. Bacteriol.* 172, 3367–3378. doi: 10.1128/jb.172.6.3367-3378.1990
- Claessen, D., Stokroos, I., Deelstra, H. J., Penninga, N. A., Bormann, C., Salas, J. A., et al. (2004). The formation of the rodlet layer of streptomycetes is the result of the interplay between rodlin and chaplins. *Mol. Microbiol.* 53, 433–443. doi: 10.1111/j.1365-2958.2004.04143.x
- Conesa, A., Nueda, M. J., Ferrer, A., and Talon, M. (2006). maSigPro: a method to identify significantly differential expression profiles in time-course microarray experiments. *Bioinformatics* 22, 1096–1102. doi: 10.1093/bioinformatics/btl056
- Cunin, R., Eckhardt, T., Piette, J., Boyen, A., Piérard, A., and Glandsdorff, N. (1983). Molecular basis for modulated regulation of gene expression in the arginine regulon of *Escherichia coli* K-12. *Nucleic Acid Res.* 11, 5007–5018. doi: 10.1093/nar/11.15.5007
- Davis, N. K., and Chater, K. F. (1992). The *Streptomyces coelicolor* whiB gene encodes a small transcription factor-like protein dispensable for growth but essential for sporulation. *Mol. Gen. Genet.* 232, 351–358. doi: 10.1007/BF00266237
- Daza, A., Martín, J. F., Domínguez, A., and Gil, J. A. (1989). Sporulation of several species of *Streptomyces* in submerged cultures after nutritional downshift. *J. Gen. Microbiol.* 135, 2483–2491. doi: 10.1099/00221287-135-9-2483
- Dion, M., Charlier, D., Wang, H., Gigot, D., Savchenko, A., Hallet, J. N., et al. (1997). The highly thermostable arginine repressor of *Bacillus stearothermophilus*: gene cloning and repressor-operator interactions. *Mol. Microbiol.* 25, 385–398. doi: 10.1046/j.1365-2958.1997.4781845.x
- Doull, J. L., and Vining, L. C. (1989). Nutritional control of actinorhodin production by *Streptomyces coelicolor* A3(2): suppressive effects of nitrogen and phosphate. *Appl. Microbiol. Biotechnol.* 32, 449–454. doi: 10.1007/BF00903781
- Elliot, M. A., Bibb, M. J., Buttner, M. J., and Leskiw, B. K. (2001). BldD is a direct regulator of key developmental genes in *Streptomyces coelicolor* A3(2). *Mol. Microbiol.* 40, 257–269. doi: 10.1046/j.1365-2958.2001.02387.x
- Fischer, M., Alderson, J., van Keulen, G., White, J., and Sawers, R. G. (2010). The obligate aerobic *Streptomyces coelicolor* A3(2) synthesizes three active respiratory nitrate reductases. *Microbiology* 156, 3166–3179. doi: 10.1099/mic.0.042572-0
- Flårdh, K., Findlay, K. C., and Chater, K. F. (1999). Association of early sporulation genes with suggested developmental decision points in *Streptomyces coelicolor* A3(2). *Microbiology* 145, 2229–2243. doi: 10.1099/00221287-145-9-2229

- Gardan, R., Rapoport, G., and Débarbouillé, M. (1997). Role of the transcriptional activator RocR in the arginine-degradation pathway of *Bacillus subtilis*. *Mol. Microbiol.* 24, 825–837. doi: 10.1046/j.1365-2958.1997.3881754.x
- Gomez-Escribano, J. P., Song, L., Fox, D. J., Yeo, V., Bibb, M. J., and Challis, G. L. (2012). Structure and biosynthesis of the unusual polyketide alkaloid coelimycin P1, a metabolic product of the cpk gene cluster of *Streptomyces coelicolor* M145. *Chem. Sci.* 3, 2716–2720. doi: 10.1039/c2sc20410j
- Grandori, R., Lavie, T. A., Pflumm, M., Tian, G., Nierbach, H., Maas, W. K., et al. (1995). The DNA binding domain of the hexameric arginine repressor. *J. Mol. Biol.* 254, 150–162. doi: 10.1006/jmbi.1995.0607
- Grant, C. E., Bailey, T. L., and Noble, W. S. (2011). FIMO: scanning for occurrences of a given motif. *Bioinformatics* 27, 1017–1018. doi: 10.1093/bioinformatics/btr064
- Grantcharova, N., Ubhayasekera, W., Mowbray, S. L., McCormick, J. R., and Flärdh, K. (2003). A missense mutation in *ftsZ* differentially affects vegetative and developmentally controlled cell division in *Streptomyces coelicolor* A3(2). *Mol. Microbiol.* 47, 645–656. doi: 10.1046/j.1365-2958.2003.03334.x
- Hong, H. J., Paget, M. S., and Buttner, M. J. (2002). A signal transduction system in *Streptomyces coelicolor* that activates the expression of a putative cell wall glycan operon in response to vancomycin and other cell wall-specific antibiotics. *Mol. Microbiol.* 44, 1199–1211. doi: 10.1046/j.1365-2958.2002.02960.x
- Keijser, B. J., van Wezel, G. P., Canters, G. W., and Vijgenboom, E. (2002). Developmental regulation of the *Streptomyces lividans* *ram* genes: involvement of RamR in regulation of the *ramCSAB* operon. *J. Bacteriol.* 184, 4420–4429. doi: 10.1128/JB.184.16.4420-4429.2002
- Kelemen, G. H., Brian, P., Flärdh, K., Chamberlin, L., Chater, J. F., and Buttner, M. J. (1998). Developmental regulation of transcription of *whiE*, a locus specifying the polyketide spore pigment in *Streptomyces coelicolor* A3(2). *J. Bacteriol.* 180, 2515–2521.
- Kelemen, G. H., Brown, G. L., Kormanec, J., Potůčková, L., Chater, K. F., and Buttner, M. J. (1996). The positions of the sigma-factor genes, *whiG* and *sigF*, in the hierarchy controlling the development of spore chains in the aerial hyphae of *Streptomyces coelicolor* A3(2). *Mol. Microbiol.* 21, 593–603. doi: 10.1111/j.1365-2958.1996.tb02567.x
- Kieser, T., Bibb, M. J., Buttner, M. J., Chater, K. F., and Hopwood, D. A. (2000). *Practical Streptomyces Genetics*. Norwich: John Innes Foundation.
- Kol, S., Merlo, M. E., Scheltema, R. A., de Vries, M., Vonk, R. J., Kikkert, N. A., et al. (2010). Metabolomic characterization of the salt stress response in *Streptomyces coelicolor*. *Appl. Environ. Microbiol.* 76, 2574–2581. doi: 10.1128/AEM.01992-09
- Larsen, R., van Hijum, S. A., Martinussen, J., Kuipers, O. P., and Kok, J. (2008). Transcriptome analysis of the *Lactococcus lactis* ArgR and AhrC regulons. *Appl. Environ. Microbiol.* 74, 4768–4771. doi: 10.1128/AEM.00117-08
- Lee, E. J., Karoonuthaisiri, N., Kim, H. S., Park, J. H., Cha, C. J., Kao, C. M., et al. (2005). A master regulator σ B governs osmotic and oxidative response as well as differentiation via a network of sigma factors in *Streptomyces coelicolor*. *Mol. Microbiol.* 57, 1252–1264. doi: 10.1111/j.1365-2958.2005.04761.x
- Lee, K. J., and Rho, Y. T. (1993). Characteristics of spores formed by surface and submerged cultures of *Streptomyces albidoflavus* SMF301. *J. Gen. Microbiol.* 139, 3131–3137. doi: 10.1099/00221287-139-12-3131
- Lee, S. Y., Park, J.-M., Lee, J. H., Chang, S.-T., Park, J.-S., Kim, Y.-H., et al. (2011). Interaction of transcriptional repressor ArgR with the transcriptional regulator FarR at the *argB* promoter region in *Corynebacterium glutamicum*. *Appl. Environ. Microbiol.* 77, 711–718. doi: 10.1128/AEM.01610-10
- Livak, K. J., and Schmittgen, T. D. (2001). Analysis of relative gene expression data using real time quantitative PCR and the $2^{-\Delta\Delta Ct}$. *Methods* 25, 402–408. doi: 10.1006/meth.2001.1262
- Llácer, J. L., Fita, I., and Rubio, V. (2008). Arginine and nitrogen storage. *Curr. Opin. Struct. Biol.* 18, 673–681. doi: 10.1016/j.sbi.2008.11.002
- López-García, T., Santamarta, I., and Liras, P. (2010). Morphological differentiation and clavulanic acid formation are affected in a *Streptomyces clavuligerus* *adpA*-deleted mutant. *Microbiology* 156, 2354–2365. doi: 10.1099/mic.0.035956-0
- Lu, C.-D., Yang, Z., and Li, W. (2004). Transcriptome analysis of the ArgR regulon in *Pseudomonas aeruginosa*. *J. Bacteriol.* 186, 3855–3861. doi: 10.1128/JB.186.12.3855-3861.2004
- Maas, W. K. (1994). The arginine repressor of *Escherichia coli*. *Microbiol. Rev.* 58, 631–640.
- Manteca, A., Alvarez, R., Salazar, N., Yagüe, P., and Sánchez, J. (2008). Mycelium differentiation and antibiotic production in submerged cultures of *Streptomyces coelicolor*. *Appl. Environ. Microbiol.* 74, 3877–3886. doi: 10.1128/AEM.02715-07
- Manteca, A., Claessen, D., López-Iglesias, C., and Sánchez, J. (2007). Aerial hyphae in surface cultures of *Streptomyces lividans* and *Streptomyces coelicolor* originate from viable segments surviving an early programmed cell death event. *FEMS Microbiol. Lett.* 274, 118–125. doi: 10.1111/j.1574-6968.2007.00825.x
- Mark, B. L., Wasney, G. A., Salo, T. J., Khan, A. R., Cao, Z., Robbins, P. W., et al. (1998). Structural and functional characterization of *Streptomyces pilatus* β -N-acetylhexosaminidase by comparative molecular modeling and site-directed mutagenesis. *J. Biol. Chem.* 273, 19618–19624. doi: 10.1074/jbc.273.31.19618
- Nishijyo, T., Park, S. M., Lu, C. D., Itoh, Y., and Abdelal, A. T. (1998). Molecular characterization and regulation of an operon encoding system for transport of arginine and ornithine and the ArgR regulatory protein in *Pseudomonas aeruginosa*. *J. Bacteriol.* 180, 5559–5566.
- O'Connor, T. J., and Nodwell, J. R. (2005). Pivotal roles for the receiver domain in the mechanism of action of the response regulator RamR of *Streptomyces coelicolor*. *J. Mol. Biol.* 351, 1030–1047. doi: 10.1016/j.jmb.2005.06.053
- Offner, S., Ziese, U., Wanner, G., Typke, D., and Pfeifer, F. (1998). Structural studies of halobacterial gas vesicles. *Microbiology* 144, 1331–1334. doi: 10.1099/00221287-144-5-1331
- Paget, M. S., Leibovitz, E., and Buttner, M. J. (1999). A putative two-component signal transduction system regulates sigmaE, a sigma factor required for normal cell wall integrity in *Streptomyces coelicolor* A3(2). *Mol. Microbiol.* 33, 97–107. doi: 10.1046/j.1365-2958.1999.01452.x
- Pérez-Redondo, R., Rodríguez-García, A., Botas, A., Santamarta, I., Martín, J. F., and Liras, P. (2012). ArgR of *Streptomyces coelicolor* is a versatile regulator. *PLoS ONE* 7:e32697. doi: 10.1371/journal.pone.0032697
- Rho, Y. T., and Lee, K. J. (1994). Kinetic characterization of sporulation in *Streptomyces albidoflavus* SMF301 during submerged culture. *Microbiology* 140, 2061–2065. doi: 10.1099/13500872-140-8-2061
- Riosera, B., López-García, M. T., Yagüe, P., Sánchez, J., and Manteca, A. (2014). Mycelium differentiation and development of *Streptomyces coelicolor* in lab-scale bioreactors: programmed cell death, differentiation, and lysis are closely linked to undecylprodigiosin and actinorhodin production. *Bioresour. Technol.* 151, 191–198. doi: 10.1016/j.biortech.2013.10.068
- Rodríguez-García, A., Ludovice, M., Martín, J. F., and Liras, P. (1997). Arginine boxes and the *argR* gene in *Streptomyces clavuligerus*: evidence for a clear regulation of the arginine pathway. *Mol. Microbiol.* 25, 219–228. doi: 10.1046/j.1365-2958.1997.4511815.x
- Rodríguez-García, A., Sola-Landa, A., Apel, K., Santos-Beneit, F., and Martín, J. F. (2009). Phosphate control over nitrogen metabolism in *Streptomyces coelicolor*: direct and indirect negative control of *glnR*, *glnA*, *glnI* and *amtB* expression by the response regulator PhoP. *Nucleic Acids Res.* 37, 3230–3242. doi: 10.1093/nar/gkp162
- Rueda, B., Miguélez, E. M., Hardisson, C., and Manzanal, M. B. (2001). Mycelial differentiation and spore formation by *Streptomyces brasiliensis* in submerged culture. *Can. J. Microbiol.* 47, 1042–1047. doi: 10.1139/w01-109
- Saito, N., Matsubara, K., Watanabe, M., Kato, F., and Ochi, K. (2003). Genetic and biochemical characterization of EshA, a protein that forms large multimers and affects developmental processes in *Streptomyces griseus*. *J. Biol. Chem.* 278, 5902–5911. doi: 10.1074/jbc.M208564200
- Saito, N., Xu, J., Hosaka, T., Okamoto, S., Aoki, H., Bibb, M. J., et al. (2006). EshA accentuates ppGpp accumulation and is conditionally required for antibiotic production in *Streptomyces coelicolor* A3(2). *J. Bacteriol.* 188, 4952–4961. doi: 10.1128/JB.00343-06
- Salerno, P., Persson, J., Bucca, G., Laing, E., Ausmees, N., Smith, C. P., et al. (2013). Identification of new developmentally regulated genes involved in *Streptomyces coelicolor* sporulation. *BMC Microbiol.* 13:28. doi: 10.1186/1471-2180-13-281
- San Paolo, S., Huang, J., Cohen, S. N., and Thompson, C. J. (2006). *rag* genes: novel components of the Ram regulon that trigger morphological differentiation in *Streptomyces coelicolor*. *Mol. Microbiol.* 61, 1167–1186. doi: 10.1111/j.1365-2958.2006.05304.x
- Schneider, T. D. (1997). Information content of individual genetic sequences. *J. Theor. Biol.* 189, 427–441. doi: 10.1006/jtbi.1997.0540
- Shao, Z., Deng, W., Li, S., He, J., Ren, S., Huang, W., et al. (2015). GlnR-mediated regulation of *ectABCD* transcription expands the role of the

- GlnR regulon to osmotic stress management. *J. Bacteriol.* 197, 3041–3047. doi: 10.1128/JB.00185-15
- Smith, M. C. M., Czaplowski, L., North, A. K., Baumberg, S., and Stockley, P. G. (1989). Sequences required for regulation of arginine biosynthesis promoters are conserved between *Bacillus subtilis* and *Escherichia coli*. *Mol. Microbiol.* 3, 23–28. doi: 10.1111/j.1365-2958.1989.tb00099.x
- Smyth, G. K. (2004). Linear models and empirical Bayes methods for assessing differential expression in microarray experiments. *Stat. Appl. Genet. Mol. Biol.* 3, 1–25. doi: 10.2202/1544-6115.1027
- Sola-Landa, A., Rodríguez-García, A., Amin, R., Wohlleben, W., and Martín, J. F. (2013). Competition between the GlnR and PhoP regulators for the glnA and amtB promoters in *Streptomyces coelicolor*. *Nucleic Acids Res.* 41, 1767–1782. doi: 10.1093/nar/gks1203
- Sola-Landa, A., Rodríguez-García, A., Apel, A. K., and Martín, J. F. (2008). Target genes and structure of the direct repeats in the DNA-binding sequences of the response regulator PhoP in *Streptomyces coelicolor*. *Nucleic Acids Res.* 36, 1358–1368. doi: 10.1093/nar/gkm1150
- Song, H., Wang, H., Gigot, D., Dimova, D., Sakanyan, V., Glansdorff, N., et al. (2002). Transcription regulation in thermophilic bacteria: high resolution contact probing of *Bacillus stearothermophilus* and *Thermotoga neapolitana* arginine repressor-operator interactions. *J. Mol. Biol.* 315, 255–274. doi: 10.1006/jmbi.2001.5236
- Soutar, A., and Baumberg, S. (1996). Implication of a repression system, homologous to those of other bacteria, in the control of arginine biosynthesis genes in *Streptomyces coelicolor*. *Mol. Gen. Genet.* 251, 245–251.
- Stirling, C. J., Szatmari, G., Stewart, G., Smith, M. C., and Sherratt, D. J. (1988). The arginine repressor is essential for plasmid-stabilizing site-specific recombination at the ColE1 *cer* locus. *EMBO J.* 7, 4389–4395.
- Tian, G., Lim, D., Carey, J., and Maas, W. K. (1992). Binding of the arginine repressor of *Escherichia coli* K12 to its operator sites. *J. Mol. Biol.* 226, 387–397. doi: 10.1016/0022-2836(92)90954-I
- Traag, B. A., Kelemen, G. H., and van Wezel, G. P. (2004). Transcription of the sporulation gene *ssgA* is activated by the IclR-type regulator SsgR in a *whi*-independent manner in *Streptomyces coelicolor* A3(2). *Mol. Microbiol.* 53, 985–1000. doi: 10.1111/j.1365-2958.2004.04186.x
- van Duyn, G. D., Ghosh, G., Maas, W. K., and Sigler, P. B. (1996). Structure of the oligomerization and L-arginine binding domain of the arginine repressor of *Escherichia coli*. *J. Mol. Biol.* 256, 377–391. doi: 10.1006/jmbi.1996.0093
- van Keulen, G., Hopwood, D. A., Dijkhuizen, L., and Sawers, R. G. (2005). Gas vesicles in actinomycetes: old buoys in novel habitats? *Trends Microbiol.* 13, 350–354. doi: 10.1016/j.tim.2005.06.006
- van Wezel, G. P., van der Meulen, J., Kawamoto, S., Luiten, R. G., Koerten, H. K., and Kraal, B. (2000a). *ssgA* is essential for sporulation of A3(2) and affects hyphal development by stimulating septum formation. *J. Bacteriol.* 182, 5653–5662. doi: 10.1128/JB.182.20.5653-5662.2000
- van Wezel, G. P., van der Meulen, J., Taal, E., Koerten, H., and Kraal, B. (2000b). Effects of increased and deregulated expression of cell division genes on the morphology and on antibiotic production of streptomycetes. *Antonie van Leeuwenhoek* 78, 269–276. doi: 10.1023/A:1010267708249
- Wade, J. T., Struhl, K., Busby, S. J., and Grainger, D. C. (2007). Genomic analysis of protein-DNA interactions in bacteria: insights into transcription and chromosome organization. *Mol. Microbiol.* 65, 21–26. doi: 10.1111/j.1365-2958.2007.05781.x
- Willemse, J., Borst, J. W., de Waal, E., Bisseling, T., and van Wezel, G. P. (2011). Positive control of cell division: FtsZ is recruited by SsgB during sporulation of *Streptomyces*. *Gen. Develop.* 25, 89–99. doi: 10.1101/gad.600211
- Xu, M., Rao, Z., Yang, J., Xia, H., Dou, W., Jin, J., et al. (2012). Heterologous and homologous expression of the arginine biosynthetic argC~H cluster from *Corynebacterium crenatum* for improvement of (L)-arginine production. *J. Ind. Microbiol. Biotechnol.* 39, 495–502. doi: 10.1007/s10295-011-1042-4
- Yagüe, P., Rodríguez-García, A., López-García, M. T., Rioseras, B., Martín, J. F., Sánchez, J., et al. (2014). Transcriptomic analysis of liquid non-sporulating *streptomyces coelicolor* cultures demonstrates the existence of a complex differentiation comparable to that occurring in solid sporulating cultures. *PLoS ONE* 9:e86296. doi: 10.1371/journal.pone.0086296
- Yim, S.-H., Jung, S., Lee, S., Cheon, C., Song, E., Lee, S.-S., et al. (2011). Purification and characterization of an arginine regulatory protein, ArgR in *Corynebacterium glutamicum*. *J. Ind. Microb. Biotechnol.* 38, 2011–2020. doi: 10.1007/s10295-011-0977-9

Conflict of Interest Statement: The authors declare that the research was conducted in the absence of any commercial or financial relationships that could be construed as a potential conflict of interest.

Copyright © 2018 Botas, Pérez-Redondo, Rodríguez-García, Álvarez-Álvarez, Yagüe, Manteca and Liras. This is an open-access article distributed under the terms of the Creative Commons Attribution License (CC BY). The use, distribution or reproduction in other forums is permitted, provided the original author(s) and the copyright owner are credited and that the original publication in this journal is cited, in accordance with accepted academic practice. No use, distribution or reproduction is permitted which does not comply with these terms.



Plant-Growth Promotion and Biocontrol Properties of Three *Streptomyces* spp. Isolates to Control Bacterial Rice Pathogens

Zulma Rocío Suárez-Moreno^{1*}, Diana Marcela Vinchira-Villarraga²,
Diana Isabel Vergara-Morales¹, Leonardo Castellanos³, Freddy A. Ramos³,
Corrado Guarnaccia⁴, Giuliano Degrassi⁵, Vittorio Venturi⁵ and
Nubia Moreno-Sarmiento^{2*}

OPEN ACCESS

Edited by:

Dirk Tischler,
Ruhr-Universität Bochum, Germany

Reviewed by:

Collin M. Timm,
Johns Hopkins University,
United States
Jan Bobek,
Charles University, Czechia
Matouš Čihák,
Contipro Inc., Czechia,
in collaboration with reviewer JB

*Correspondence:

Zulma Rocío Suárez-Moreno
zrsuarezm@gmail.com;
zulma.suarez@vecol.com.co
Nubia Moreno-Sarmiento
ncmorenos@unal.edu.co

Specialty section:

This article was submitted to
Microbial Physiology and Metabolism,
a section of the journal
Frontiers in Microbiology

Received: 31 August 2018

Accepted: 04 February 2019

Published: 25 February 2019

Citation:

Suárez-Moreno ZR,
Vinchira-Villarraga DM,
Vergara-Morales DI, Castellanos L,
Ramos FA, Guarnaccia C, Degrassi G,
Venturi V and Moreno-Sarmiento N
(2019) Plant-Growth Promotion
and Biocontrol Properties of Three
Streptomyces spp. Isolates to Control
Bacterial Rice Pathogens.
Front. Microbiol. 10:290.
doi: 10.3389/fmicb.2019.00290

¹ Investigación y el Desarrollo, Biocultivos S.A., Bogotá, Colombia, ² Instituto de Biotecnología, Universidad Nacional de Colombia, Bogotá, Colombia, ³ Departamento de Química, Universidad Nacional de Colombia, Bogotá, Colombia, ⁴ Biotechnology Development Unit, International Centre for Genetic Engineering and Biotechnology, Trieste, Italy, ⁵ Bacteriology and Plant Bacteriology Group, International Centre for Genetic Engineering and Biotechnology, Trieste, Italy

Bacterial Panicle Blight caused by *Burkholderia glumae* is a major disease of rice, which has dramatically affected rice production around the world in the last years. In this study we describe the assessment of three *Streptomyces* isolates as biocontrol agents for *B. glumae*. Additionally, the presence of other plant-growth promoting abilities and their possible beneficial effects upon their inoculation on rice plants was evaluated as an ecological analysis for their future inoculation in rice crops. Two isolates (A20 and 5.1) inhibited growth of virulent *B. glumae* strains, as well as a wide range of bacterial and fungal species, while a third strain (7.1) showed only antifungal activity. *In vitro* tests demonstrated the ability of these strains to produce siderophores, Indoleacetic acid (IAA), extracellular enzymes and solubilizing phosphate. Greenhouse experiments with two rice cultivars indicated that *Streptomyces* A20 is able to colonize rice plants and promote plant growth in both cultivars. Furthermore, an *egfp* tagged mutant was generated and colonization experiments were performed, indicating that *Streptomyces* A20 –GFP was strongly associated with root hairs, which may be related to the plant growth promotion observed in the gnotobiotic experiments. In order to characterize the antimicrobial compounds produced by strain A20 bacteria, mass spectrometry analyses were performed. This technique indicated that A20 produced several antimicrobial compounds with sizes below 3 kDa and three of these molecules were identified as Streptotricins D, E and F. These findings indicate the potential of *Streptomyces* A20 as a biocontrol inoculant to protect rice plants against bacterial diseases.

Keywords: *Streptomyces*, biological control, plant growth promotion, *Burkholderia glumae*, streptothricins

Abbreviations: ACC, 1-aminocyclopropane-1-carboxylate; BPB, Bacterial panicle Blight; CMC, carboxymethylcellulose; IAA, Indoleacetic Acid; LC-MS, liquid chromatography–mass spectrometry; MLST, Multilocus Sequence Typing; PGPB, Plant-Growth Promoting Bacteria; SBR, Sheath Brown Rot.

INTRODUCTION

Bacterial Panicle Blight (BPB) caused by *Burkholderia glumae* is a bacterial disease of rice with an increasing occurrence in South America since its first detection in 2007 (Correa et al., 2007; Castillo et al., 2011; Ham et al., 2011). This bacterial pathogen was first detected in Japan (Goto and Ohata, 1956; Tanii et al., 1976) and is currently widespread around the world. In the last 20 years, *B. glumae* has shown a significant occurrence in rice-growing countries in Latin America and United States causing grain rot and seedling rot of rice (Zeigler and Alvarez, 1987; Correa et al., 2007; Nandakumar et al., 2007; Diago et al., 2009; Nandakumar et al., 2009). *B. glumae* causes bacterial wilt in a wide variety of plant hosts, but disease in rice is the most studied due to the dramatic economic effects of BPB in rice yields (Jeong et al., 2003). Major symptoms of this BPB include panicle blight, seedling blight, and sheath rot, with a linear lesion extending downward from the leaf blade collar forms on the flag leaf. Affected panicles may have one or all of their florets blighted with grains not filling or aborting, which causes typical upright brown panicles due to the failure of grain filling (Goto and Ohata, 1956; Kurita and Tabei, 1967; Goto et al., 1987; Zeigler and Alvarez, 1987).

In Latin America and the United States, rice yield reductions due to BPB have reached 75% in severely infested fields as a result of a reduction in grain weight, sterility of florets and inhibition of seed germination (Correa et al., 2007; Nandakumar et al., 2007, 2009; Diago et al., 2009). In addition to the problems due to BPB, losses due to SBR caused by the phytopathogen *Pseudomonas fuscovaginae* have increased dramatically in rice-producing countries like Indonesia, Malaysia, and Colombia, with losses up to 76% (Razak et al., 2009). The occurrence of both pathogens has been favored by changes in climatic conditions and it is believed that these diseases may occur more frequently in tropical and semi-tropical countries.

The main current approaches to control *B. glumae* include rice breeding to obtain tolerant rice varieties (Mizobuchi et al., 2013) and isolation and identification of virulent strains, which have been analyzed at genomic level to identify putative virulence genes differing among them (Francis et al., 2013; Fory et al., 2014). Also, improvement of diagnostic tools for achieving detection at early stages of rice development, and intense diffusion and training of farmers in symptoms-detection in the fields have been used as an approach to diminish the incidence of *B. glumae* (Sayler et al., 2006; Kawanishi et al., 2011). Furthermore, recently transcriptome studies for the pathosystem rice-*B. glumae* have contributed to an understanding of the gene expression of this pathogen along rice development (Kim et al., 2014; Magbanua et al., 2014). Nonetheless, these approaches are not always efficient, considering that virulent strains are polymorphic and have developed resistance to chemical treatments (Hikichi et al., 2001; Karki et al., 2012).

In spite of the dramatic losses due to *P. fuscovaginae* and *B. glumae*, no biological or chemical approach has proven to be successful for controlling them in Latin America, and consequently, sustainable alternatives for reducing these two bacterial diseases of rice in the region are urgently needed.

A possible alternative is a biocontrol approach, which involves the use of disease-suppressive microorganisms to control pathogens and improve plant health (Handelsman and Stabb, 1996). Major aspects of biocontrol are bioprospecting for new active isolates as well as understanding the mechanisms of pathogen antagonism for their future improvement and broader use.

Many *Streptomyces* strains are considered biocontrol agents, since they produce a wide range of antimicrobials, can persist in harsh environments, and efficiently colonize the rhizosphere of different plant species including rice (Qin et al., 2011; Kinkel et al., 2012). Furthermore, *Streptomyces* are able to elicit induced resistance, as it has been described before (Conn et al., 2008; Kurth et al., 2014). Because of these features, it is not surprising that diverse *Streptomyces* strains had been studied to control fungal and bacterial diseases of rice like Bacterial Leaf Blight caused by *Xanthomonas oryzae*, however very few *Streptomyces* are currently being developed as biocontrol products.

Research and development of biocontrol products commonly focuses on four major points: (1) studying the biocontrol traits for microbial agents, (2) assessment of the plant-microorganism interaction, (3) monitoring the beneficial and ecological effects of inoculation of each agent in the rhizosphere, and finally (4) verifying proper release of the microbial agents upon inoculation of crops with formulated products (Herrmann and Lesueur, 2013; Miransari, 2013). In this study, we describe the isolation and characterization of three *Streptomyces* isolates and assess their potential as biocontrol agents in order to explore their interaction and possible beneficial effects upon inoculation of rice plants. Colonization and plant growth promotion experiments were performed in sterile and non-sterile conditions as an approach to evaluate the ecological effects of their use in rice fields, and the colonization patterns were visualized microscopically for one isolate.

MATERIALS AND METHODS

Isolation and Identification of *Streptomyces*-Like Isolates

Forty-five samples of rhizospheric soils were collected from rice-cultivated fields in Tolima (Colombia). In order to conduct this research, the ANLA (Autoridad Nacional de Licencias Ambientales) and the Ministry of Environment (Ministerio de Ambiente y Desarrollo Sostenible) were requested for permission to collect samples and study the recovered bacteria.

Briefly, plants roots were removed from the soil and subsequently handshaked for 10 min to remove bulk soil. The remaining adhering soil was considered as rhizospheric soil, and was collected by handshaking roots for 10 min in a sterile plastic bag. Rhizospheric soil samples (4–5 g for each) were then mixed with 1 g of CaCO₃. Samples were further dried at 45°C for 1 h, as described previously (Gurung et al., 2009). Actinobacteria were subsequently isolated by spread plate technique following the serial dilution of soil samples on starch casein agar (Starch 10 g/L, Casein 1 g/L, K₂HPO₄ 0.5 g/L, Agar 13 g/L) and incubated at 30°C for a week. In order to select *Streptomyces*-like bacteria, microscopic and macroscopic characteristics of the

obtained colonies were assessed resulting in a total of 60 isolates, which were further purified and sub-cultured. Single colonies were characterized by their colony morphology in International *Streptomyces* Project media (ISP2, ISP3, ISP4), Nutrient agar and Mueller Hinton Agar (**Supplementary Figure S1**). Catalase, oxidase and their carbon source utilization were tested, as suggested for *Streptomyces*-like bacteria (Shirling and Gottlieb, 1968; Goodfellow, 2012).

Antimicrobial Activity Assays

Actinobacteria strains were grown for 5 days in M3.7 liquid media (glucose 5 g/L, Yeast Extract 5 g/L, $(\text{NH}_4)_2\text{SO}_4$ 5 g/L, Corn gluten 5 g/L, CaCO_3 2 g/L, NaCl 2 g/L, FeSO_4 1 mg/L, starch 10 g/L pH 7.2). Five-day cultures were used for antimicrobial tests. Antibacterial activities against 21 strains from 15 species (**Supplementary Table S1**) were determined by using the Kirby-Bauer agar well-diffusion method, modified from the CLSI 2011 guidelines (Clinical Laboratory Standards Institute, 2011). Briefly, each strain to be tested was grown overnight in LB media, and its OD_{600} was determined. Bacterial absorbance was then adjusted to 0.25, and a cotton swab was fully immersed in each bacterial dilution. The inoculated swab was used to spread the entire surface of a Mueller Hinton Agar plate, containing 25 mL of agar five times. Seven mm (diameter) wells were perforated in the agar, and 50 μL of each actinobacterial culture were poured into the well. Plates were subsequently incubated at 30 or 37°C (according to the best temperature for each bacteria to be tested). Inhibition zones were measured after 24 h of incubation. Antibacterial assays were also performed against a collection of 48 *B. glumae* isolates recovered from rice plants exhibiting symptoms of BPB (kindly provided by FEDEARROZ-Colombia).

Antifungal activities against 9 fungal plant pathogens (**Supplementary Table S1**) were measured as described previously (Kanini et al., 2013). For this assay, fungal strains were grown in Potato Dextrose Agar (PDA) plates for 3 days at 25°C, and two 6 mm disks of mycelium from each phytopathogenic fungi were then placed in opposites edges of a new PDA plate. Following fungal inoculation, two 6 mm wells were open in opposite sides of the PDA plate, containing 50 μL of a 5-day culture for each Actinobacteria strain tested. The plates were incubated at 28°C for 5 days and antagonistic activity was estimated by measuring the growth inhibition zone.

Taxonomical Identification and Multilocus Sequence Analysis (MLST)

Three strains were selected based on their wide range of antimicrobial activity. Genomic DNA was isolated by using the Salting-out procedure described previously (Pospiech and Neumann, 1995), with few modifications. Briefly, single colonies of each isolate were grown in 30 mL Tryptic Soy Broth, with shaking at 30°C for 48 h. Cells were harvested by centrifugation and washed with 10% sucrose, and suspended in 5 mL of STE Buffer (75 mM NaCl, 25 mM EDTA pH 8.0, 20 mM Tris-HCl pH 7.5), containing heat-treated pancreatic RNase A at 10 mg/mL. Hundred microliters of lysozyme (50 mg/mL) were added to the mixture and incubated for 1 h at 37°C, with

gentle tapping at intervals. This was followed by the addition of 140 μL of proteinase K (20 mg/mL) and 600 μL of 10% SDS, with further incubation at 55°C for 2 h. Two mL of 5M NaCl were added and mixed by inversion until the temperature of the suspension reached the 37°C. The samples were cooled to room temperature and extracted twice with 5 mL of chloroform. Aqueous fractions were separated by centrifuging at 10000 g for 10 min at 4°C, and genomic DNA was precipitated by adding one volume of isopropanol, mixed by inversion and centrifuged 15 min at 15000 rpm. The obtained DNA pellet was rinsed with 70% ethanol, air-dried and suspended in 100 μL of DNase-free sterile water.

Taxonomical identification was first approached by PCR amplification, sequencing, and analysis of the entire 16S rRNA locus by using primers 16S_A and 16S_B described by Cui et al. (2001), and the cleaned PCR products were directly sequenced using universal primers 27F, 500F, 818R and 1492R (**Supplementary Table S1**). Closely related sequences were obtained from RDP (Ribosomal Database Project) (Cole et al., 2014) and EZTaxon (Kim et al., 2012). Obtained sequences were imported into MEGA6 software and aligned with ClustalW for phylogenetic analysis (Thompson et al., 1994).

Multilocus Sequence Typing was used to elucidate a further taxonomical affiliation (Guo et al., 2008; Rong et al., 2009). Briefly, five loci (*gyrB*, *atpD*, *recA*, *trpB*, and *rpoB*) were PCR amplified and purified by using the EuroGOLD Gel extraction Kit (EuroCLONE, Italy). Each fragment was then sequenced by using primers described previously (Guo et al., 2008), and listed in **Supplementary Table S1**. The sequences for all loci for each strain were concatenated head to tail in frame and exported in FASTA format. Sequences were aligned using CLCbio Mainworkbench 6.9.1 (CLC-Bio Qiagen) and MEGA 6.0 (Tamura et al., 2011). A phylogenetic tree was constructed from the concatenated sequences of all six loci, and representative *Streptomyces* strains available in the *Streptomyces* MLST database (Jolley and Maiden, 2010)¹ Maximum likelihood algorithm trees were generated with MEGA based on the Tamura-Nei model (Tamura and Nei, 1993), and a tree with the highest log likelihood was generated calculating the percentage of trees in which the associated taxa clustered together. Initial trees for the heuristic search were obtained automatically by applying Neighbor-Join and BioNJ algorithms (Gascuel, 1997) to a matrix of pairwise distances estimated using the Maximum Composite Likelihood (MCL) approach, and then selecting the topology with superior log-likelihood value.

In vitro Assessment of Plant Growth Promotion (PGP) Traits

Biological nitrogen fixation, phosphate solubilization, indoleacetic acid production (IAA), ACC deaminase and extracellular enzyme production were evaluated. For this purpose, each isolate was grown in 100 mL M3.7 medium for 5 days, and each assay was performed with three independent cultures for each strain.

¹<http://pubmlst.org/Streptomyces/>

Biological Nitrogen Fixation

To test biological nitrogen fixation, Acetylene Reduction Assay (ARA) was performed as described elsewhere (Hardy et al., 1968). To this purpose, 100 μ L of washed cells were inoculated into 17 mL of semisolid NFB medium in 25 mL serum bottles with a cotton cap, and cultures were maintained at 30°C, without agitation (Dobereiner, 1995). After 5 days, 2 mL of acetylene were injected into the flask and a rubber stopper was used to replace the cotton cap. The acetylene and ethylene concentrations of each sample were determined by gas chromatography, using a chromatograph Varian 3400-G-crom, equipped with a flame ionization detector and a capillary column (Hayesep Porapak N 80/100 column; 6' X 1/8"). Ethylene and acetylene estimation was done by integrating the area under the curve for each compound, at retention times of 1.417 and 2.40 min, respectively.

Phosphate Solubilization

Phosphate solubilizing abilities were qualitatively determined by inoculating single colonies of each strain in National Botanical Research Institute's Phosphate growth medium (NBRIP) (Nautiyal, 1999) and SRS media (Sundara-Rao and Sinha, 1963). Plates were incubated at 30°C for 5 days, and colonies with a clear orange halo in NBRIP media and/or a purple color in SRS media were marked positive for phosphate solubilization. A quantitative determination was performed by growing each strain in 100 mL of NBRIP liquid media supplemented with 5 g/L CaCO_3 , for 5 days. Subsequently, the solubilized phosphate present in the supernatant was measured with the Spectroquant Phosphor Kit (Merck).

Siderophore Production

Siderophore production was determined in Chrome Azurol Blue agar (Schwyn and Neilands, 1987), modified to use KOH to adjust the pH, as suggested previously (Mahmoud and Abdallah, 2001).

ACC Deaminase Production

1-aminocyclopropane-1-carboxylate (ACC) deaminase production was determined by checking the ability of each strain to use ACC as sole nitrogen source. For this purpose, single colonies were inoculated in Dorwin-Foster media (DF) supplemented with 3 mM ACC as sole nitrogen source, or with 2 g/L $(\text{NH}_4)_2\text{SO}_4$ as growth control (Belimov et al., 2001; El-tarabily, 2008). In each case, 2 μ L of a 10^6 CFU/mL culture, were spotted on the surface of a DF plate with or without N source, and growth was evaluated after 5 days at 30°C, and *Burkholderia unamae* MT1 641T was included as a positive control. An absence of phenotypic changes in growth or sporulation of the isolates in the medium supplemented with ACC in comparison with an $(\text{NH}_4)_2\text{SO}_4$ supplemented medium were considered as indicators of the capacity of the microorganisms to use ACC as a source of nitrogen mediated by the production of ACC-deaminase.

Indoleacetic Acid

For the quantitative determination of Indoleacetic acid (IAA) and IAA-like molecules, the colorimetric Salkowski's assay was performed (Tang and Bonner, 1948). For this purpose, each

Streptomyces strain was grown in 20 mL Tryptic Soy Broth (TBS) supplemented with 60 mM tryptophan. After 4 days, 1 mL of Salkowski reagent (Glickmann and Dessaux, 1995) was pipetted into test tubes containing 1 mL of culture spent supernatant. The tubes containing the mixture were gently vortexed and left for 30 min for development of color at room temperature ($26 \pm 1^\circ\text{C}$). The intensity of the color was spectrophotometrically determined at 535 nm.

Extracellular Enzyme Production

Extracellular enzyme production was evaluated *in vitro*. Cellulolytic activity was evaluated by spotting 2 μ L of 5-day old cultures on the surface of CMC-media plates, in which CMC was the sole carbon source. Spots were incubated at 30°C for 4 days, and then strains were assayed for their ability to degrade CMC by flooding each plate with a 0.2% Congo red solution for 15 min, followed by washing with 1 M NaCl. Activity halos dimensions were then measured from the border of the colony to the outer edge of the halo. Similarly, ligninolytic activities were determined in guaiacol containing media and positive activity was scored when a red halo was formed around colonies, due to the oxidation of the substrate to tetraguaiacol, as described previously (Nagadesi and Arya, 2012).

Plant-Growth Promotion Experiments

Gnotobiotic Experiments

Gnotobiotic inoculation experiments were performed in rice cultivars FEDEARROZ 733 (F733) and FEDEARROZ 60 (F60). For this purpose, rice seeds were surface sterilized and pre-germinated in 1% agar, for 5 days in complete darkness (Mattos et al., 2008). Each seed was then transferred into glass flasks (15 cm \times 4 cm) with 40 mL of semisolid Hoagland media previously inoculated with 10^3 CFU/mL of each strain. To this end, each strain was grown in M3.7 media, and cells were suspended in sterile saline solution and added to the semi-solid medium to reach a final concentration of 10^3 CFU/mL, before solidification of the medium.

Plantlets were then transferred to a greenhouse (Relative humidity $43\% \pm 8.6$, Average Temperature $24^\circ\text{C} \pm 5.2$, natural light). *Azotobacter chroococcum* (APFN010) and *Azospirillum brasilense* (AZPP010) strains (10^5 CFU/mL) were used as positive controls, and sterile water was used as negative control. Each treatment included two biological replicates (two independent colonies for each bacterial strain), and 10 plants were inoculated with each inoculum. The entire experiment was performed twice, and biometric properties (root and shoot fresh weight, plant dry weight, and length) were measured 15 days post-inoculation.

Soil Inoculation Experiments

Inoculation experiments were also performed in sterile and non-sterile soil using cultivars F733 and F60 with pregerminated seeds, as described above. For these assays, 10 mL from a 10^8 CFU/mL inoculum were mixed with 250 g of sterile soil, to reach a concentration of 10^5 CFU/g. Subsequently, pre-germinated seeds were planted inside the pot and plants were kept in the greenhouse at 25°C for 31 days post-inoculation. *A. chroococcum* (APFN010) and *A. brasilense* (AZPP010) strains were used

as positive controls, and sterile water was used as negative control. Each treatment included two biological replicates (two independent colonies for each bacterial strain), and 10 plants were inoculated with each inoculum. Biometric properties (root and shoot fresh weight, plant dry weight and length) were measured 31 days post-inoculation. Dry weight for each plant was determined after drying the plant material at 50°C, until obtaining a constant weight.

Plant Colonization Experiments

To assess the ability of the three *Streptomyces* for rice plant colonization, two independent assays were performed under gnotobiotic and soil conditions as described before, using in each case three biological replicates for each strain, with five plants per replicate. Bacterial strains were re-isolated from the rhizoplane by cutting and washing 2 cm segments of each plant root and placing the excised root segments on the surface of ISP3 plates. Roots of the soil experiment were placed on ISP3 medium supplemented with nalidixic acid (20 µg/ml) and nitrofurantoin (10 µg/ml) to inhibit the growth of other soil microorganisms. The identity of colonies recovered from the roots was verified from their phenotype and their antimicrobial profile.

To verify endophytic colonization, inoculated plants were surface sterilized with 1% sodium hypochlorite and 70% ethanol for 4 min each, followed by several washes with sterile water. Each plant was then excised in the root, plant shoot and leaves, and each part was macerated with a sterile pestle. Each suspension was then serially diluted and plated in ISP3 plates. Surface sterilization was regarded as optimum when no growth was observed: (1) after placing the processed plants on ISP3 plates, and (2) after plating 100 µL from the last wash in ISP3 (see more details from the experimental set-up in **Supplementary Figure S2**).

Finally, to test the persistence and viability of isolates in the soil, rhizospheric soil portions were sampled from each treatment. 1 g of each sample was diluted in Tween 80 (0.1% v/v) and plated in ISP3 medium supplemented with nalidixic acid and nitrofurantoin. Results were evaluated after 4 days incubation at 30°C and reported as CFU/g soil rhizosphere.

Fluorescence Microscopy

An *egfp* tagged mutant from *Streptomyces* sp. A20 was generated by intergeneric conjugation with *Escherichia coli* S17-1 λ pir harboring pIJ8641 plasmid, (kindly provided by M. Bibb from the John Innes Centre-Norwich, United Kingdom) (Sun et al., 1999; Kieser et al., 2000; Willey et al., 2007), and transconjugants were selected into Apramycin ISP3 plates (100 µg/ml). Fluorescent transconjugants were further selected for gnotobiotic inoculation experiments as described before, using either semisolid Hoagland or sterile vermiculite supplemented with Apramycin (100 µg/ml). For these experiments, 15 plants were inoculated with A20pIJ8641, non-tagged *Streptomyces* A20, and a non-inoculated set of plants was included as a control. To assess the colonization process three roots were evaluated for each treatment at days 1, 2, 3, 10, and 15 days post inoculation. In each evaluation day, the roots were excised from the matrix, washed three times with sterile water and cut in

3 mm × 3 mm fragments. Observations were performed in an Olympus BX41 Microscope with a CCD Infinity 3 Camera (dichroic mirror DM500; excitation filter BP460-490 and barrier filter BA520IF).

Purification and Characterization of Antimicrobial Compounds

Streptomyces A20 was grown in 80 L M3.7 media in a 100 L stirrer tank bioreactor with constant shaking (40 rpm) at 25°C. After 4 days, 1 L of culture was centrifuged and spent supernatants were filter-sterilized using a 0.22 µm membrane. Bioassay-guided fractionation of A20 fermentation sterile supernatants was then performed by a sequential partition with ethyl acetate (2 × 500 mL), followed by butanol (4 × 500 mL) extraction (**Supplementary Figure S3**), to yield organic (EtOAc), butanolic and residual aqueous fraction (ABP fractions). Each fraction was evaporated to dryness and suspended into sterile water to be subjected to antibacterial assays. Active fractions were first purified by ultra-filtration by using 1, 3, and 10 kDa Amicon filters (Millipore).

Several chromatographic techniques were used to purify antimicrobial compounds produced by strain *Streptomyces* A20. Briefly, residual aqueous fractions from butanol extraction were dried and suspended into buffer A (sodium acetate 0.05 M pH 5.5) to be loaded into a strong anion exchanger column, Q Sepharose Fast Flow, previously equilibrated and washed with buffer A, using a BioRad Biologic Duoflow chromatography system. Compounds bound to the column were eluted with a linear gradient of increasing NaCl concentration (0–1M). Antimicrobial compounds present in the flowthrough, were purified by loading it into an S Sepharose™ Fast Flow column (cation exchange chromatography), and antimicrobial compounds were eluted again with a gradient of increasing NaCl concentration. Antimicrobial fractions were then suspended into 20 mM ammonium acetate, containing 0.1% heptafluorobutyric acid (HFBA), and injected onto a semipreparative C18 reversed phase column (1x 25 cm). Three fractions were recovered due to their antibacterial activity and were further analyzed by LC-MS.

Samples for LC-MS were dissolved in 90% methanol and 10 µl injected onto a Gemini C18 column (2 × 150 mm, 5 µm; Phenomenex, Torrance, CA, United States) and separated using a gradient from water to 90% acetonitrile mobile phases containing 0.1% formic acid at 0.2 ml min⁻¹. The column effluent was delivered to an ESI ion trap mass spectrometer (Amazon SL, Bruker Daltonics, Bremen, Germany) and mass spectra collected in positive ion mode in the range 200–2000 m/z.

Statistical Analysis

Most experiments were performed at least three times and means are given. Statistical analyses included unpaired *t*-tests and ANOVA with Dunnett's post-test and were performed with PRISM 4.0 software (GraphPad Software, San Diego CA, United States). A *P*-value of < 0.05 was considered significant.

DNA Sequencing and Nucleotide Sequence Accession Numbers

16S rRNA nucleotide sequences for strains *Streptomyces* A20, 5.1, 7.1 and *Streptomyces racemochromogenes* DSM 40194 were deposited in GenBank/EMBL/DDBJ, under the accession numbers KP082880, KP082881, KP082882, and KP082883.

RESULTS

Isolation and Identification of *Streptomyces* Strains With Anti-bacterial Activity From Rice Cultivated Soils

Sixty actinobacterial-like isolates were obtained from Colombian soils upon enrichment with CaCO₃ however, only three isolates denoted as A20, 5.1 and 7.1 showed antimicrobial activity against either two plant pathogenic bacterial strains of *B. glumae* and *P. fuscovaginae*, or fungal phytopathogens. Strains A.20 and 5.1 showed both antibacterial and antifungal activity, whereas strain 7.1 showed only antifungal activity (Table 1).

Biochemical tests indicated that these three strains were catalase positive; oxidase negative, and their carbon source analysis indicated that all strains were able to metabolize glucose, but were unable to use rhamnose, arabinose, xylose or mannitol as carbon source (Table 2). Taxonomical analyses derived from 16S rRNA sequencing confirmed that all three strains belong to the genus *Streptomyces* and similarity calculations of the 16S rRNA locus, based on Maximum Likelihood and Neighbor Joining analyses indicated that the closest relatives for strain A20 were *S. racemochromogenes*/*S. polychromogenes* and *S. flavotricini* with similarity values of 99.93 and 99.8 % respectively, placing this strain within the previously described clade 38 (Labeda et al., 2012). A similar analysis located strain 7.1 within clades 2 and 71 with similarity values of 99.89 and 99.79% to *S. chrestomyceticus*, *S. corchorusii*/*S. canarius*. Strain 5.1 was related to the *S. roseovorticillatus* clade 65, having 98.9% similarity to *Streptomyces kashimirensis* and *S. salmonis* (Figure 1A).

In order to improve the taxonomical identification, MLST was performed for all three strains, and type strain *S. racemochromogenes* DSM 40194. MLST analyses for 12 strains, including the closest neighbors for each isolate revealed that all six loci have unique sequences compared to all available allele types in the MLST *Streptomyces* database. MLST profiles for strains 5.1 and 7.1 defined these two isolates as independent entities, and MLST profiles for close neighbors these two should be obtained to improve their taxonomical identification.

All loci obtained for strain A20 were highly similar to those obtained for strain *S. racemochromogenes* DSM 40194, and concatenated loci for both strains shared 97.2% identity at sequence level, however evolutionary distance calculated with Kimura 2 parameters, was above the species-definitive MLSA distance of 0.007 (0.028) (Figure 1B) (Rong and Huang, 2012; Labeda et al., 2014). Further studies may be required to generate MLST profiles for other type strains from this cluster in order to verify these results and define if strain A20 corresponds to a known species or may be described as a new species.

Streptomyces A20, 5.1, and 7.1 Exhibit a Wide Range of Antimicrobial Activity

In order to study the strength and range of antimicrobial activity, all three selected strains were tested by Kirby-Bauer well-diffusion assays, which indicated that *Streptomyces* strains A20 and 5.1 could inhibit the growth of a wide range of bacterial and fungal phytopathogens to varying degrees, whereas strain 7.1 was able to inhibit mainly fungal phytopathogens (Table 1). Strain A20 showed the wider range of activity, with antimicrobial effects against 20 out of 21 bacterial species tested, and against all fungal pathogens evaluated (Figure 2). All three *Streptomyces* strains were also tested against a collection of 48 pathogenic *B. glumae* isolates isolated from Colombian rice-growing areas. In these assays, *Streptomyces* strains A20 and 5.1 exhibited antimicrobial activities against 91.48 and 78.72% of pathogens tested, respectively. Remarkably most of the pathogenic *B. glumae* isolates were inhibited by *Streptomyces* A20.

Streptomyces Strains Isolated From Colombian Soils Are Able to Promote Rice Growth in Several Rice Cultivars

In vitro tests suggested that all three strains were able to produce siderophores, as well as proteolytic enzymes. All three strains also showed an ability to produce IAA and ACC deaminase, but none of the *Streptomyces* isolates could fix nitrogen. *Streptomyces* strain 7.1 was able to solubilize inorganic phosphate and showed a remarkable cellulolytic ability (Table 3 and Figure 3).

Gnotobiotic inoculation experiments suggested that strain A20 was able to promote rice growth in comparison to non-inoculated plants, since it generated increases in shoot length and fresh weight in roots and plants of two different cultivars being however statistically significant only for cultivar F60 (Figure 4A). *Streptomyces* 7.1 was able to increase root and shoot fresh weight in the cultivar F733 and did not have any effect on rice cultivar F60. *Streptomyces* 5.1 did not show any increase in any of the evaluated parameters, in any of the cultivars tested. In soil experiments, *Streptomyces* 5.1 was able to improve the fresh weight of roots and shoots in cultivar F733, and strains A20 and 7.1 displayed the ability to significantly increase all the biometric parameters evaluated in cultivar F733 in comparison to the non-inoculated control (Figure 4B and Supplementary Figure S4).

Plant growth promotion experiments were performed both with sterile and non-sterile conditions in order to compare the performance of the three strains in such environments and foresee their behavior under natural conditions. In non-sterile soil, plants inoculated with *Streptomyces* A20 and *Streptomyces* 7.1 showed increases in their biometric parameters, with the same trend they showed in the gnotobiotic experiments. In contrast, strain *Streptomyces* 5.1 was able to increase plant length and fresh weight in plantlets from cultivar 733 (Figure 4C). Importantly, plantlets from non-sterile soils were smaller due to the presence of fungal strains, observed along the process (data not shown), which were

TABLE 1 | Antibacterial and antifungal activity of *Streptomyces* A20, 5.1, and 7.1.

Strain	A20	5.1	7.1
Antibacterial activity			
<i>Acidovorax avenae</i> CIAT 4008-2	++	++	–
<i>Acinetobacter baumannii</i> ATCC 19606	+	–	–
<i>Bacillus</i> sp. C636	+	+	–
<i>Bacillus subtilis</i> ATCC 21556	+	+++	–
<i>Burkholderia glumae</i> 320012	+++	++++	–
<i>Burkholderia glumae</i> AU6208	+++	+++	–
<i>Burkholderia glumae</i> CIAT 4026	++	+++	–
<i>Burkholderia gladioli</i> CIAT 3704-1	+	+++	–
<i>Burkholderia gladioli</i> CIAT 3962	+	++	–
<i>Chromobacterium violaceum</i> ATCC 31532	++	++++	–
<i>Enterobacter aerogenes</i> 7ARG	+	–	–
<i>Escherichia coli</i> DH5 α	+++	++	–
<i>Escherichia coli</i> ATCC 23724	+++	–	–
<i>Escherichia coli</i> ATCC 25922	++	+	–
<i>Klebsiella pneumoniae</i> ATCC 700603	+	++	–
<i>Pseudomonas putida</i> F117 pKRC12	+++	–	–
<i>Pseudomonas aeruginosa</i> ATCC 27853	–	++	–
<i>Pseudomonas fuscovaginae</i> CIAT 3638-19	+	++++	–
<i>Pseudomonas fuscovaginae</i> CIAT 3668 π 3	+	++	–
<i>Staphylococcus aureus</i> ATCC 25923	+	+++	–
Antifungal activity			
<i>Fusarium</i> sp. DC9	+	+	–
<i>Fusarium</i> sp. DC 13B	+	+	–
<i>Fusarium oxysporum</i>	+	+	+
<i>Gaeumannomyces</i> sp.	+	+	+
<i>Phomopsis</i> sp.	+	+	–
<i>Ulocladium</i> sp.	+	+	+
<i>Rhizoctonia solani</i>	+	+	–
<i>Colletotrichum</i> sp. 24C	+	+	+
<i>Colletotrichum</i> sp. 26B	+	+	+

Results are means of three inhibition halo-diameter (mm) measurements in three independent replicates for each strain tested. Antibacterial activity: (–) No inhibition detected, (+) 5–10 mm, (++) 11–15 mm, (+++) 16–20 mm, (+++++) > 20 mm. Antifungal activity: (–) No inhibition detected, (+) Inhibition zone detectable.

TABLE 2 | Biochemical characterization of *Streptomyces* A20, 5.1 and 7.1.

Strain	Cat	Oxi	Glu	Suc	Fru	Rha	Ara	Ino	Xyl	Man
A20	+	–	+	–	–	–	–	–	–	–
7.1	+	–	+	+	+	–	–	–	–	–
5.1	+	–	+	–	–	–	–	+	–	–

(–) No sugar fermentation detected or negative reaction. (+) sugar fermentation detected or positive reaction. Cat, Catalase. Oxi, Oxidase. Glu, Glucose. Suc, Sucrose. Fru, Fructose. Rha, Rhamnose. Ara, Arabinose. Ino, Inositol. Xyl, Xylose. Man, Mannitol.

most likely controlled by antifungal metabolites produced by isolates A20 and 5.1.

***Streptomyces* A20, 5.1, and 7.1 Are Able to Colonize Two Different Rice Cultivars Under Gnotobiotic and Soil Conditions**

Colonization experiments indicated that all *Streptomyces* strains tested were able to colonize the roots, since they were recovered from the rhizoplane in gnotobiotic experiments with roots from cultivars F733 and F60, even after 31 days post-inoculation

(dpi) (Table 4 and Supplementary Material S2). *Streptomyces* A20 and *Streptomyces* 7.1 were also able to colonize the root endosphere, as they were recovered from a percentage of surface sterilized plants (80 and 20 %, respectively) grown in a gnotobiotic system.

An *egfp* tagged mutant was generated for strain A20 and colonization experiments were performed. Our results indicated that *egfp* expressing strain strongly associated with root hairs (Figure 5). Also, our experiments suggested that *Streptomyces* A20 first established itself in the main root and on the surface of the rice seeds (1 dpi, Figure 5), followed by the formation

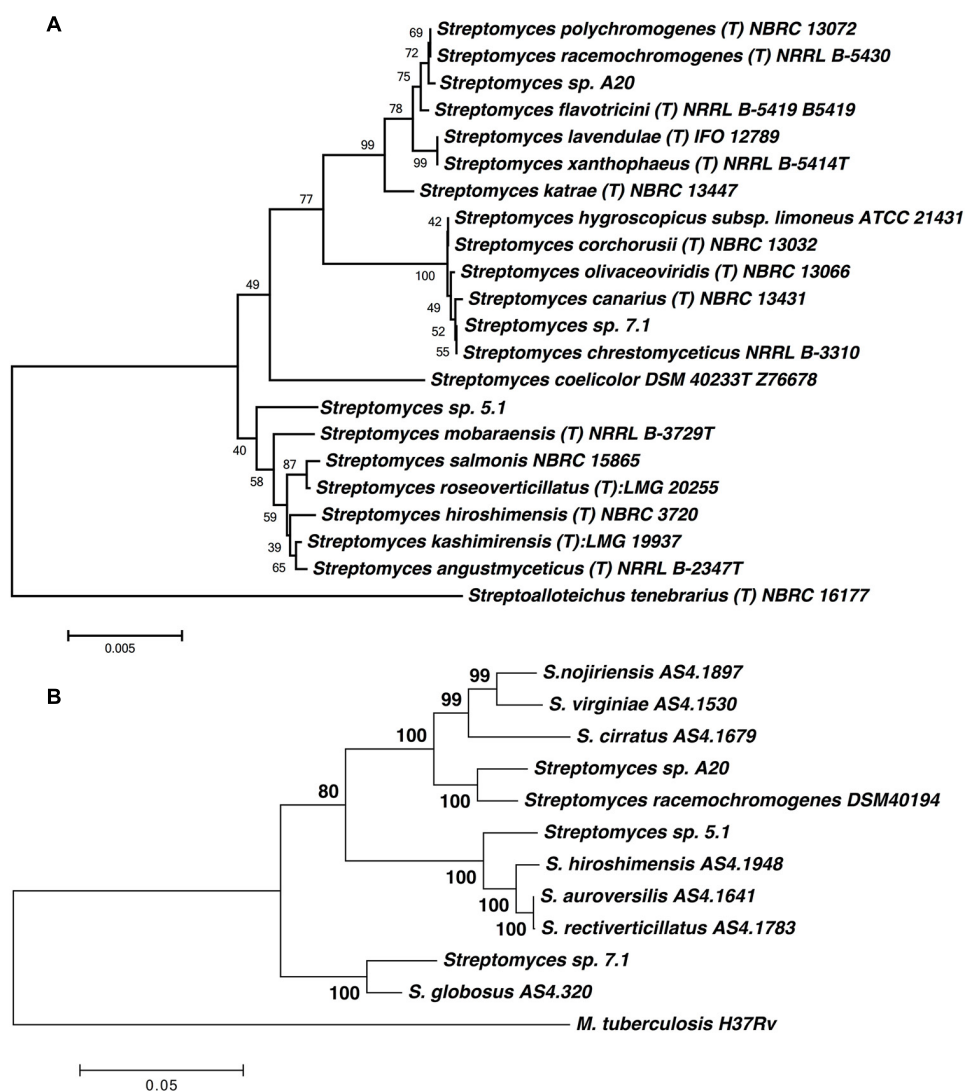


FIGURE 1 | (A) Phylogenetic tree based on 16S rRNA sequences of the *Streptomyces* strains. The evolutionary history was inferred using the Neighbor-Joining method (Saitou and Nei, 1987). The tree is drawn to scale, with branch lengths in the same units as those of the evolutionary distances used to infer the phylogenetic tree. Numbers at branch nodes are bootstrap values. Sequence from *Streptoalloteichus tenebrarius* NBRC 16177 was included as outgroup.

(B) Phylogenetic tree based on MLST analyses from five loci (*gyrB*, *atpD*, *recA*, *trpB*, and *rpoB*). The tree was drawn to scale using Maximum Likelihood method and Tamura-Nei model, with branch lengths measured in the number of substitutions per site. The analysis involved 12 nucleotide sequences. All positions containing gaps and missing data were eliminated. There were a total of 2896 positions in the final dataset.

of micro-colonies between 2 and 3 dpi, and the colonization of secondary roots (**Figure 5**). After 10 days of growth, *Streptomyces* A20 had colonized the points of emergence for secondary roots and the surface of the main and secondary roots. After 15 days an overall colonization from the surface of the root is observed both in vermiculite and semisolid Hoagland media.

***Streptomyces* A20 Produces Several Hydrophilic Charged Compounds**

Strain A20 was chosen for further characterization of antimicrobial metabolites. Bioassay-guided extraction of A20 spent supernatants with solvents of increasing-polarity

suggested that the antimicrobial compounds produced by this strain are hydrophilic ionic compounds since they remain in the aqueous fraction after the butanol extraction (**Supplementary Figure S3**). Ultrafiltration assays followed by antimicrobial activity assays indicated that the antimicrobial compounds present in residual aqueous fractions have sizes below 3 kDa (**Table 5**). Cation-exchange chromatography generated three more fractions with antimicrobial activity (namely fractions 21, 32, and 33), which were further submitted to ion-pairing chromatography in order to obtain defined peaks with antimicrobial activity. This technique allowed the resolution of 2 identical peaks in fractions 32 and 33, and one single peak in fraction 21, which possessed antibacterial

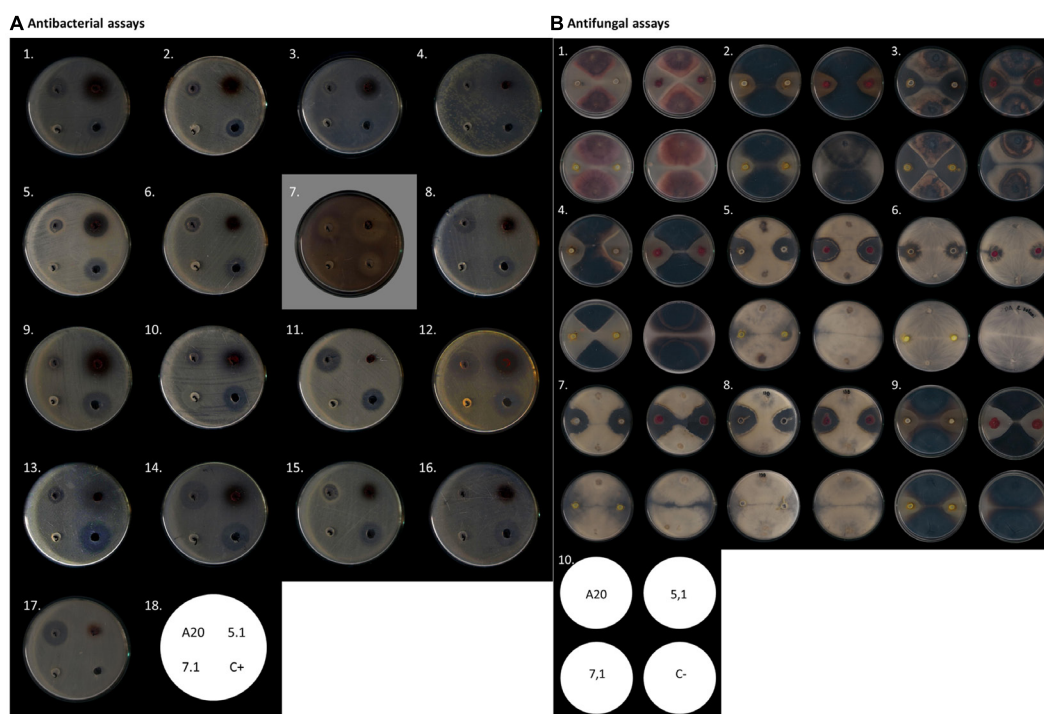


FIGURE 2 | Antimicrobial activity of *Streptomyces* A20, 5.1, and 7.1. **(A)** Antibacterial assays by Kirby-Bauer well diffusion test. In the figure from left to right: (1) *A. avenae* CIAT 4008-2, (2) *A. baumannii* ATCC19606, (3) *S. aureus* ATCC 25923, (4) *B. glumae* CIAT 4026, (5) *B. subtilis* ATCC 21556, (6) *Bacillus* C636, (7) *C. violaceum* ATCC 31532, (8) *E. coli* ATCC12167, (9) *B. gladioli* CIAT 3962, (10) *B. gladioli* CIAT 3704-1, (11) *E. coli* ATCC23724, (12) *B. glumae* 320012, (13) *P. fuscovaginae* CIAT 3638-19, (14) *E. coli* DH5 α , (15) *K. pneumoniae* ATCC 700603, (16) *P. aeruginosa* ATCC 27853, (17) *P. putida* F117. (18) Assay scheme. **(B).** Antifungal assay as described by Kanini et al. (2013). In the figure from left to right: (1) *Fusarium oxysporum*, (2) *Gaeumannomyces* sp., (3) *Colletotrichum* sp. 24C, (4) *Colletotrichum* sp. 26B, (5) *Phomopsis* sp. DC1B, (6) *Rhizoctonia solani*, (7) *Fusarium* sp. DC9, (8) *Fusarium* sp. DC13B, (9) *Ulocladium* sp., (10) Assay scheme.

activity. All the fractions were subsequently subjected to mass spectrometry analysis. Results have indicated that strain A20 produces three compounds with same spectra patterns and m/z values (503.3, 631.4, and 759.4), to those reported for Streptothricin F, D and E, as suggested by comparison of their mass spectra (Figure 6) (Ji et al., 2007; Maruyama and Hamano, 2009). Characterization of the streptothricin D was confirmed as follows: the MS/MS spectra for the parent ion at m/z 759.4 $[M+H]^+$, proposed as the pseudomolecular ion for Streptothricine D, presented daughter ions at m/z 589 $[M-L_3]^+$, 571 $[M-L_3-H_2O]^+$, 554 $[M-L_3-H_2O-NH_3]^+$, 553 $[M-L_3-H_2O-H_2O]^+$, and 510 $[M-L_3-H_2O-H_2O-CONH_2]^+$ where the L_3 represents the chain of three lysine residues of Streptothricin D, as suggested previously (Ji et al., 2007, 2008, 2009). These analyses were also applied for Streptothricin E and F, indicating the presence of an ion m/z 171, a signature peak characteristic of streptolidine lactam for all Streptothricins (Figure 6) (Ji et al., 2009).

DISCUSSION

High densities of antagonistic *Streptomyces* sp. have been associated with plant disease suppression in many soils, and thus biocontrol via bioinoculants is today regarded as a promising

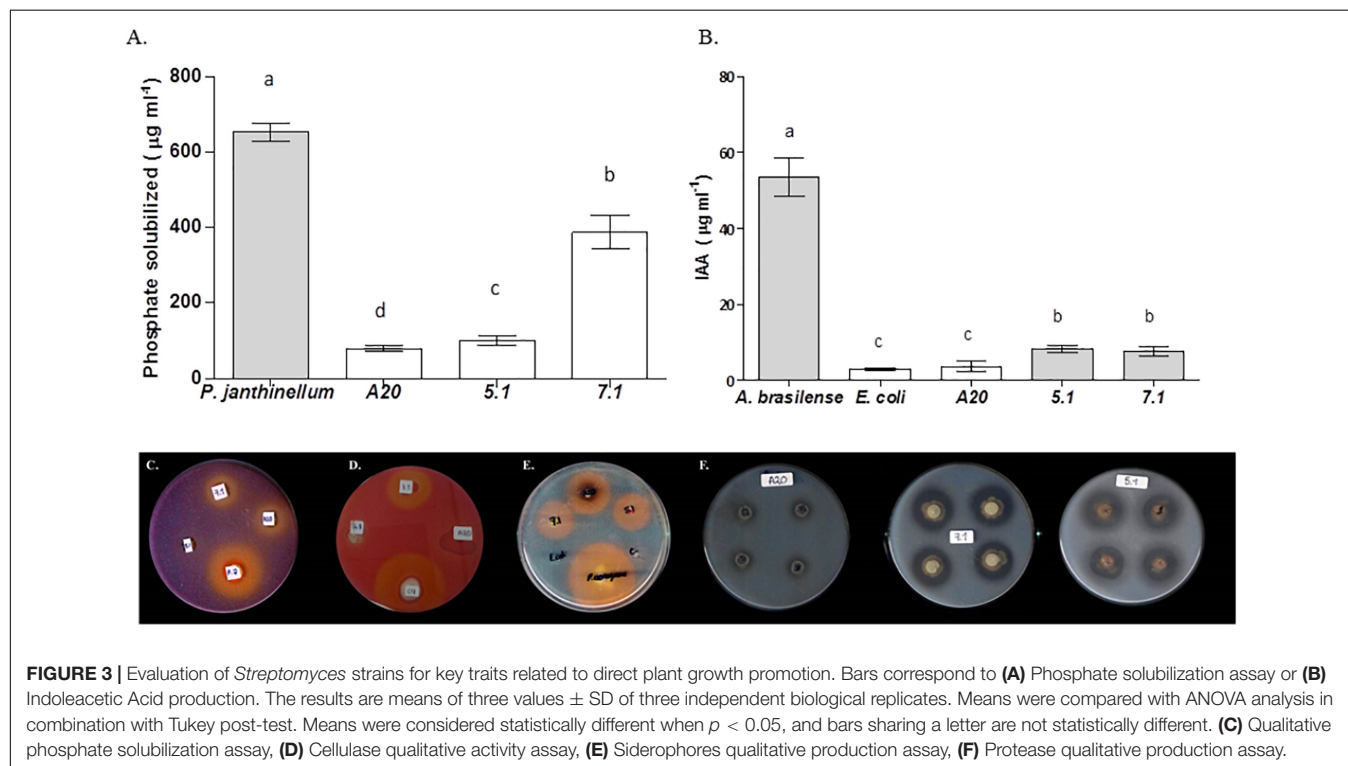
alternative for the management of bacterial diseases. These potential biocontrol bacteria can combine several mechanisms to inhibit pathogens in soil; which include nutrient competition, production of degradative enzymes, nitrous oxide production and quorum quenching (Kinkel et al., 2012). *Streptomyces* spp. have been widely recognized for their potential for controlling fungal pathogens, including *Fusarium moniliforme*, *Fusarium oxysporum* f. sp. *ciceri*, *Rhizoctonia solani*, *R. bataticola*, *Magnaporthe grisea*, and *Magnaporthe oryzae* (Emmert and Handelsman, 1999; Samac and Kinkel, 2001; Taechowisan et al., 2003; Tian et al., 2007; Zarandi et al., 2009; Gopalakrishnan et al., 2011; Kanini et al., 2013), as well as rice bacterial pathogen *Xanthomonas oryzae* pv. *oryzae* (Hastuti et al., 2012). Furthermore, diversity of secondary metabolite production among *Streptomyces* has supported the formulation of inoculants for biocontrol like Mycostop® (Verdera, Finland) and Actinovate (Natural Industries, Incorporated, United States), based on *S. griseoviridis* K61 and *S. lidicus* WYEC 108, respectively.

Biocontrol agent selection is not a simple task due to the diversity of agents and interactions with the host plant (Mota et al., 2017). Efficient selection strategies have been proposed in order to increase the possibility of identifying organisms that can be produced in a large scale and maintain their viability and efficiency for extended periods of time (Schisler et al., 1997; Köhl et al., 2011). This study presents a

TABLE 3 | Traits related with direct plant growth promotion.

Strain	Quantitative assay			Qualitative assay				
	BNF	Phosphate solubilization ($\mu\text{g mL}^{-1}$)	IAA ($\mu\text{g mL}^{-1}$)	Siderophore Production	ACC deaminase	Proteases (mm)	Cellulase activity (mm)	Ligninolytic activity
A20	UD	79.53 \pm 7.43 ^a	4.07 \pm 1.83 ^a	+	UD	12 \pm 1.64	UD	UD
5.1	UD	101.54 \pm 12.57 ^b	7.98 \pm 0.87 ^b	+	UD	9.64 \pm 1.24	UD	UD
7.1	UD	388.53 \pm 43.66 ^c	7.7 \pm 1.3 ^b	+	UD	17.43 \pm 1.5	21.43 \pm 2.06	UD

Each assay was done three times with three biological replicates, and values represent their means \pm standard deviation. One way-ANOVA ($p < 0.05$) was used to compare means. Values sharing a letter, within a column are not statistically different. UD, Undetectable activity. BNF, Biological Nitrogen Fixation. IAA, Indoleacetic Acid Production.

**TABLE 4** | Bacterial counts in colonization experiments.

Strain/cultivar	Rhizoplane	Rhizosphere	Endosphere CFU (g dry weight) ⁻¹ *		
			Root*	2 cm*	Leaves*
A20 (733)	+	1.66 $\times 10^6 \pm 0.21$ a	1.65 $\times 10^2 \pm 0.18$ a	1 $\times 10^4$	–
A20 (60)	+	1.3 $\times 10^6 \pm 0.43$ a	3.43 $\times 10^2 \pm 0.40$ a	1 $\times 10^2$	–
7.1 (733)	+	4.23 $\times 10^6 \pm 0.68$ c	4.93 $\times 10^2 \pm 0.3$ a	–	–
7.1 (60)	+	7.8 $\times 10^5 \pm 1.17$ a,b	1.7 $\times 10^3 \pm 0.172$ b	–	–
5.1 (733)	+	2.13 $\times 10^6 \pm 0.32$ a	–	–	–
5.1 (60)	–	4.9 $\times 10^4 \pm 2.8$ b	–	–	–

Numbers represent means \pm Standard Deviation for three biological replicates for each strain, with five plants per replicate. Different letters within a column indicate that values are statistically different, according to one way-ANOVA test ($p < 0.05$). *Endophytic colonization assay was performed under gnotobiotic condition.

systematic assessment of *Streptomyces* strains for development of bioinoculants able to promote plant growth and control rice phytopathogens like *B. glumae* and *P. fuscovaginae*. Our approach included: (1) Screening for actinobacterial isolates

from the rice rhizosphere, favoring selection of bacteria from the same ecological niche; (2) Screening for PGPR and biocontrol properties *in vitro*, (3) Taxonomical identification for isolates with broader antimicrobial activity, (4) Assessment

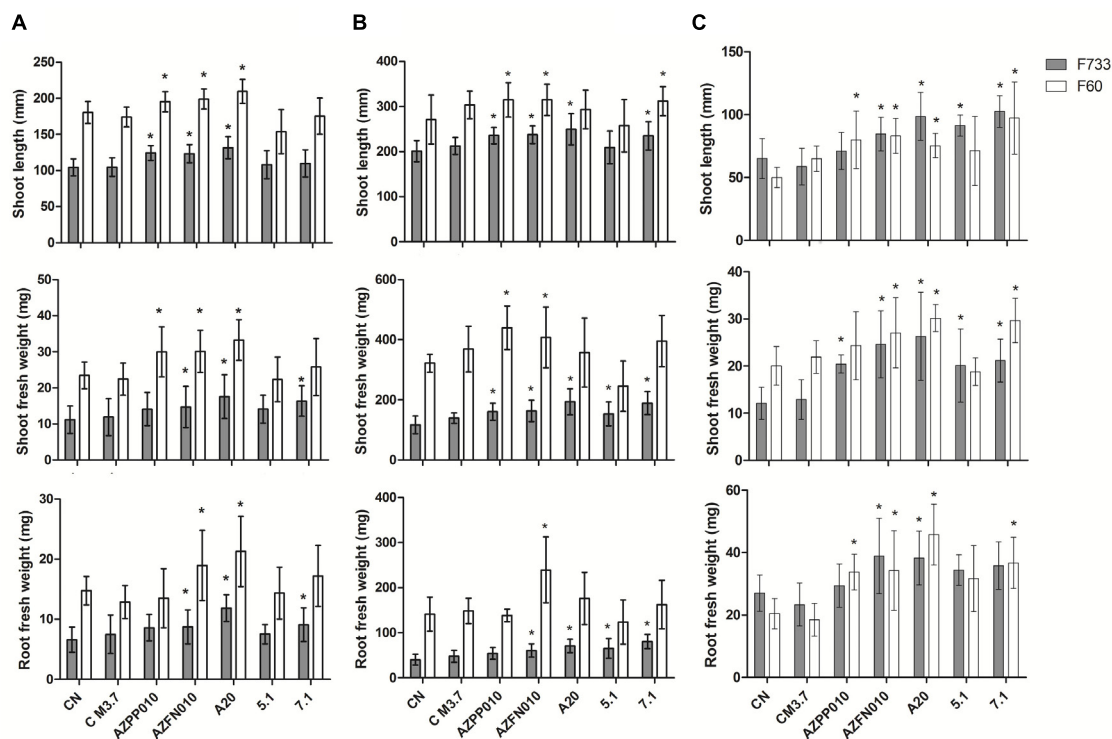


FIGURE 4 | Plant-growth promotion experiments. Bars correspond to (A) Gnotobiotic assay, (B) Sterile Soil assay, and (C) Non-sterile soil assay. The results are means of twenty values \pm SD, from two independent biological replicates. Means were compared with ANOVA analysis in combination with Tukey post-test, means were considered statistically different when $p < 0.05$. Bars with (*) above are statistically different from the negative control. CN, Negative control. C M3.7, Medium control. AZPP010, *A. brasilense*. AZFN010, *A. chroococcum*.

of plant growth promotion and colonization, *in vivo*, and (4) Antimicrobial compounds identification.

Sixty actinobacterial-like isolates were obtained from Colombian soils upon enrichment with CaCO_3 , but only three of them (A20, 5.1 and 7.1) showed antibacterial activity against pathogenic bacterial strains of both *B. glumae* and *P. fuscovaginae*. Taxonomical analyses based on 16S rRNA confirmed that all three strains belong to the genus *Streptomyces*, and MLST results suggested that these isolates might represent new species within the genus. Evolutionary distance analyses between concatenated loci from isolate A20 and type strain *S. racemochromogenes* DSM 40194 suggested that *Streptomyces* A20 is likely to be a new member of this species clade.

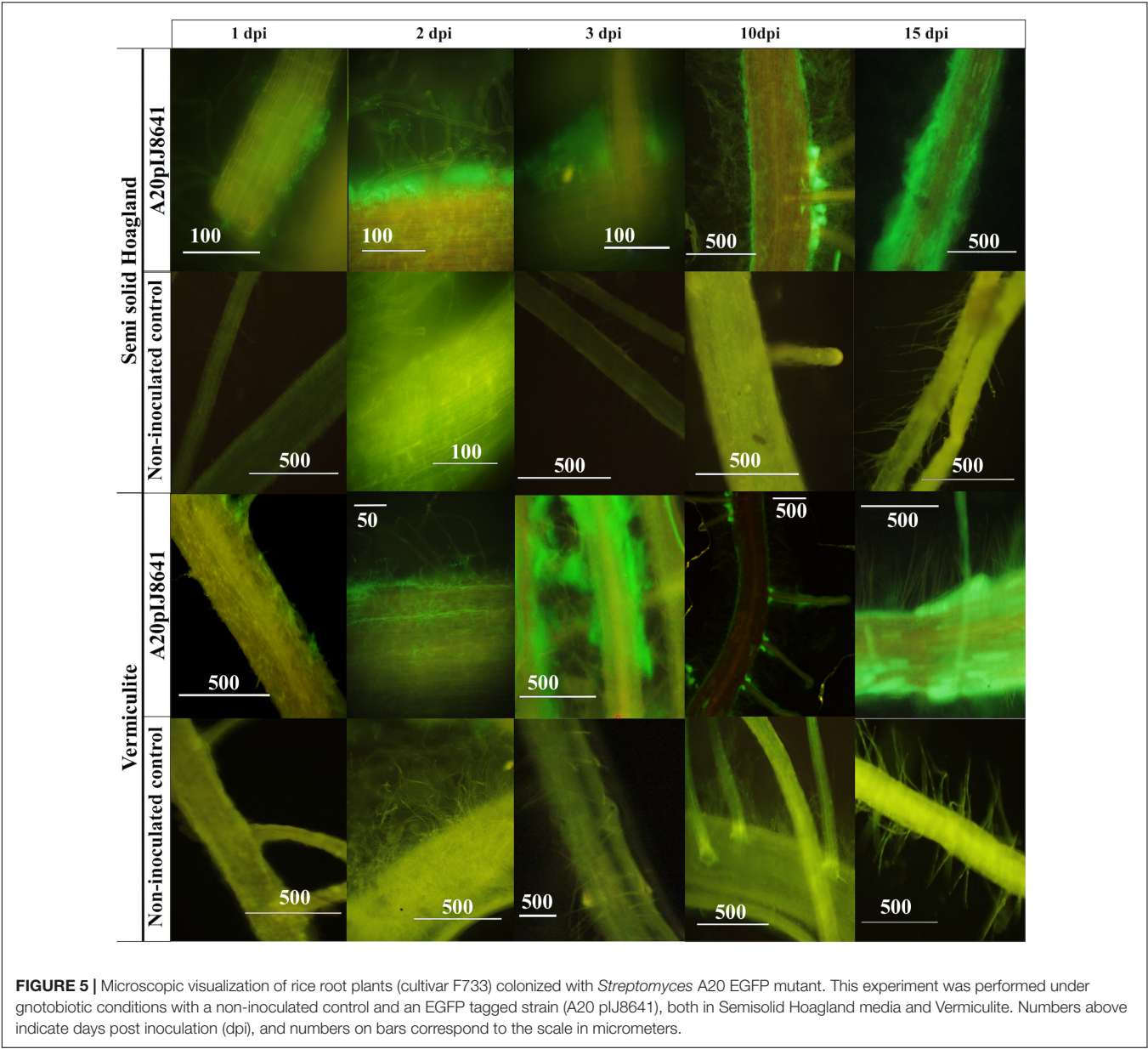
Those selected isolates were further studied, regarding their antimicrobial potential, plant growth promotion and plant colonization. Despite their common origin (rice rhizosphere), all strains showed a different spectrum of action, being *Streptomyces* A20 able to inhibit growth for a broader range of bacterial and fungal phytopathogens. When tested against 48 *B. glumae* pathogenic isolates, most of them were also inhibited by *Streptomyces* A20, which indicated that this isolate could be potentially used, alone or in combination with other strains to control BPB.

Production of broad-spectrum antimicrobials has been reported for plant-associated *Streptomyces* species, supporting

their use to control fungal and nematode phytopathogens (Emmert and Handelsman, 1999; Samac and Kinkel, 2001; Taechowisan et al., 2003; Tian et al., 2004; Zarandi et al., 2009). Furthermore, biogeographic studies about the ecology of *Streptomyces* have hypothesized that *Streptomyces* with broad and highly potent inhibitory phenotypes might be competitive 'hot spots,' which have selected for populations that are useful inhibitors of resource competitors, which may be the case for rice rhizosphere (Schlatter and Kinkel, 2014; Behie et al., 2016).

The three selected strains were tested *in vitro* for properties that are known to be important for plant growth promoting activities of bacteria, such as the production of siderophores, solubilization of inorganic phosphate, phytohormone levels etc. Overall, these suggested that all three strains can solubilize phosphate and produce siderophores, proteases, and IAA, which are also typical of plant-associated Actinobacteria, and have been related to plant-growth promotion (Nimnoi et al., 2010; Bouizgarne and Aouamar, 2014; Carvalho et al., 2017).

Many biocontrol bacteria are only capable of preventing or limiting the establishment of soilborne pathogens after colonizing plant roots, as root colonization is necessary for the suppression of root pathogens (Mota et al., 2017). As a result, several studies have been directed at identifying the different bacterial traits that may contribute to their *rhizospheric competence* (De Weert and Bloemberg, 2006). Since *in vitro* experiments revealed that



Streptomyces A20, 5.1 and 7.1 strains carry several features important for biocontrol and plant growth promotion, we were interested in assessing plant growth promotion and colonization *in vivo*, using two cultivars of rice. Plant growth promotion experiments were performed both with sterile and non-sterile conditions in order to compare the performance of these strains in such environments and foresee their behavior under natural conditions. Our results indicated that in non-sterile soil, plants inoculated with *Streptomyces* A20 and *Streptomyces* 7.1 showed significant increases in their biometric parameters, with the same trend they showed in the gnotobiotic experiments. Furthermore, colonization experiments indicated that all *Streptomyces* strains tested were able to colonize the roots, since they were able to prevail in close association with roots, in two different cultivars, even after 31 days post-inoculation (dpi).

TABLE 5 | Ultrafiltration analyses for antimicrobial compounds produced by A20.

Fraction	<i>P. fuscovaginae</i> UPB0736	<i>B. glumae</i> AU6208
Aqueous phase (FAB)	+	+
<3 kDa	+	+
3–10 kDa	–	–
>10 kDa	–	–

Ultrafiltration was performed with Amicon filters, by centrifuging at 1300 rpm × 30–40 min. Each fraction was ultrafiltrated, and the retentate was washed and centrifuged twice to avoid aggregate formation. (+) Positive antagonist activity (–) antagonist activity no detectable.

Interestingly, *Streptomyces* A20 and *Streptomyces* 7.1 were also able to colonize the root endosphere, as they were recovered from a percentage of surface sterilized plants (80 and 20%,

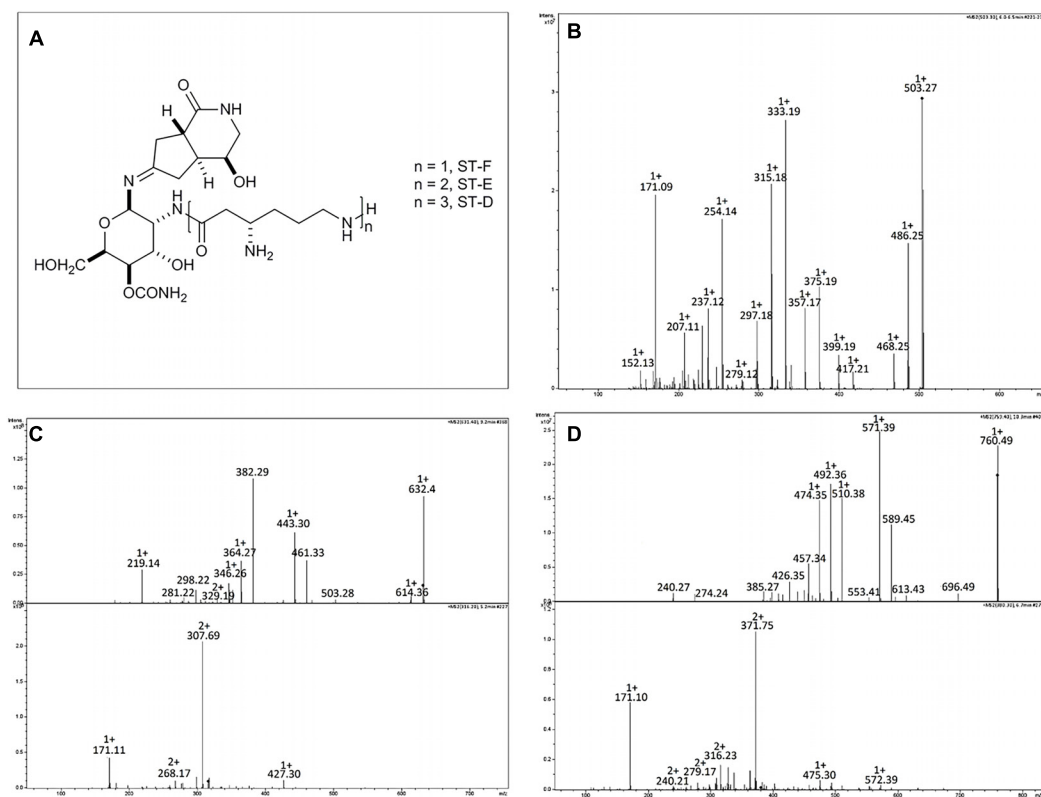


FIGURE 6 | Structure and HPLC/ESI-MS analysis of the metabolites produced by strain *Streptomyces* A20. **(A)** Structures of the streptothricin-class antibiotics. MS/MS Spectra for **(B)** Streptothricin F (m/z 503.3), **(C)** Streptothricin D (m/z 631.4), and **(D)** Streptothricin E (m/z 759.5). For Streptothricins D and E lower panel corresponds to the MS/MS analysis of the doubly charged ion species for each compound. Analyzed compounds were obtained from fraction 16 collected in the RP-HPLC from the original fraction 32.

respectively), grown in a gnotobiotic system. This last trend was not observed for plants grown in soil indicating that it might be due to the growth conditions, as well as possible competition against the other microbiota present in the soil and associated to the plant. These results are consistent with similar findings reported for other Actinobacteria, including *Streptomyces* strains (*S. cyaneus*, *S. lanatus*, and *S. galilaues*), which were also recovered from the endosphere of the roots (Tian et al., 2004, 2007; Knief et al., 2012). Field experiments with more extended growth periods may be required to determine if these strains can colonize the endosphere under natural conditions.

In order to monitor the rice colonization process by strain *Streptomyces* A20, colonization experiments were performed with an *egfp* tagged mutant. Our results indicated that *egfp* expressing strain strongly associated with root hairs and experiments in inoculated and non-inoculated plants showed an increase in root-hair formation, which may be related to the plant growth promotion observed in the gnotobiotic experiments.

Antimicrobial compound identification is convenient when developing biocontrol products. In this study, several chromatographic techniques were used to purify antimicrobial compounds produced by strain A20, that exhibited antibacterial activity against *B. glumae* AU6208 and *P. fuscovaginae* UPB0736. Results indicated that strain A20 produces three

close related compounds, according to their similar spectra patterns (m/z values at 503.3, 631.4, and 759.4). The mass spectra and their MS/MS study allowed identifying those compounds as Streptothricin F, D and E. A typical streptothricin structure consists of a streptolidine, a carbamoyl-D-gulosamine and a β-lysine chain, which varies from one to six units in streptothricins F to A, respectively (Khokhlov and Shutova, 1972; Telesnina et al., 1973; Khokhlov, 1983). Streptothricins (STs) were the earliest reported antibiotics with a broad antimicrobial spectrum from actinomycetes and are found in approximately 10% of randomly collected soil actinomycetes. These compounds are also known as nourseothricins, racemomycins, and yazumycins, and the first member of this group, designated ST-F, was isolated from *Streptomyces lavendulae* in 1943 (Waksman, 1943; Maruyama and Hamano, 2009).

STs are known to inhibit protein biosynthesis in prokaryotic cells and strongly inhibit the growth of eukaryotes like fungi and have been suggested as a selection marker for a wide range of organisms including bacteria, yeast, filamentous fungi, and plant cells. A known example is Nourseothricin (CloNat), an effective selective agent for molecular cloning technologies in fungi and plants (Goldstein and McCusker, 1999; Kochupurakkal and Iglehart, 2013). Despite their wide range of antimicrobial activity, STs are not currently indicated for clinical or veterinary

uses because of their inherent toxicity, including nephrotoxicity (Hartl et al., 1986). On the other hand, streptothricins are currently being tested as fungistatic agents in agriculture for the treatment of blast and other plant diseases (Goo et al., 1996). Lastly, STs have been registered as agrochemical fungicides in China (Kusumoto et al., 1982).

As indicated in the *Streptomyces* chemical database StreptomeDB (Lucas et al., 2013), streptothricins production has been reported for *Streptomyces ginsengensis*, *S. rochei*, *S. flavus*, *S. lavendulae*, *S. griseus*, *S. roseochromogenes*, and *S. noursei*. Maruyama and Hamano reported an extended study describing the genetic cluster responsible of the streptothricin synthesis in *S. rochei* NBRC12908. Interestingly, this cluster includes a self-resistance gene encoding a ST acetyltransferase (SAT). In addition degenerate primers were proposed as a tool to identify SAT-related immunity genes using highly conserved amino acid sequences of SATs identified in ST-resistant microorganisms (Maruyama et al., 2012). We did not obtain amplification for a potential SAT locus using genomic DNA from *Streptomyces* A20 (data not shown); this may indicate that this locus in strain A20 differs at sequence level from those reported so far, although it is also possible that strain A20 possesses a different mechanism for ST tolerance.

Plant growth promotion, colonization abilities and antimicrobial activities shown by strain *Streptomyces* A20 suggest that this strain could be used for plant growth promotion and biocontrol in rice. One significant advantage for this isolate is that it was initially recovered from rice sown soils, and thus it fulfills the premise that microorganisms chosen for inoculation should ideally be selected from local ecological niches and re-inoculated into the same environments, to ensure the desired benefits. Field experiments are necessary to further verify the effects on rice plants under natural growth conditions. Further studies will allow establishing the relationship between application of strain *Streptomyces* A20 and plant disease suppression, as well as the spatial-temporal dynamics of the pathogens and antagonists in soil (Johnson and Dileone, 1999).

AUTHOR CONTRIBUTIONS

ZS-M, DV-V, and DV-M performed the experiments for bacterial isolation, identification and antimicrobial screening and plant experiments. LC and FR designed chemical fractionation schemes for the elucidation of bioactive compounds and data analyses for all chromatographic techniques. CG and GD developed ultrafiltration studies, chromatography and mass spectrometry experiments for compound elucidation and provided advice about data analyses. ZS-M, NM-S, LC, FR, GD, and VV contributed to the conception and design of the study. NM-S was the leader of the project. All authors contributed to the manuscript revision, read and approved the submitted version.

FUNDING

ZS-M was supported by a fellowship from the program “Inserción Laboral de Doctores en Empresas Colombianas-535” from

COLCIENCIAS (Contract No. 0185-2012). ZS-M and DV-M were funded by an ICGEB Short-term fellowship to perform collaborative research at ICGEB-Trieste.

ACKNOWLEDGMENTS

ZS-M thanks the Program “Inserción Laboral de Doctores en Empresas Colombianas” (535) for the granted scholarship. ZS-M and DV-M thank ICGEB-Trieste for the granted fellowships to perform research in Italy. Strains of *Burkholderia* spp and fungal strains were kindly provided by the Biotechnology Institute of the Universidad Nacional de Colombia. *E. coli* S17-1 λ pir harboring pIJ8641 plasmid was kindly provided by M. Bibb from the John Innes Centre, Norwich, United Kingdom. *Chromobacterium violaceum* ATCC31532 was kindly provided by Prof. Catalina Arévalo Ferro, Departamento de Biología, Universidad Nacional de Colombia.

SUPPLEMENTARY MATERIAL

The Supplementary Material for this article can be found online at: <https://www.frontiersin.org/articles/10.3389/fmicb.2019.00290/full#supplementary-material>

FIGURE S1 | The figure shows the plate count technique used for the determination of Colony-Forming Units of *Streptomyces* isolates (A) and the macroscopic and microscopic characterization of the selected *Streptomyces* strains (B).

FIGURE S2 | Rice colonization assays. Two independent assays were performed under gnotobiotic and soil conditions, using three biological replicates for each strain, with five plants per replicate in two rice cultivars (F60 and F733). Bacterial strains were re-isolated from the rhizoplane by cutting and washing 2 cm segments of each plant root and placing the excised root segments on the surface of ISP3 plates. To assess the ability of each strain to colonize the rhizoplane, samples were macerated and serially diluted and plated on ISP3 plates. Note that strain *Streptomyces* A20 was able to colonize both cultivars. To verify endophytic colonization, inoculated plants were surface sterilized and each plant was then excised in the root, plant shoot and leaves, and each part was macerated with a sterile pestle. Each suspension was then serially diluted and plated in ISP3 plates, and surface sterilization was regarded as optimum when no growth was observed after placing the processed plants on nutrient agar plates. This experiment suggests that strains A20 and 7.1 are able to colonize the endosphere of both cultivars. Furthermore, microscopy of the treated roots, stained with Lactophenol blue suggests the presence of *Streptomyces* A20 mycelium on and around the surface of and adventitious root (see arrows).

FIGURE S3 | Bioassay-guided fractionation of A20 antibacterial compounds. (A) Fractionation Scheme. (B) Antimicrobial assays in *B. glumae* AU6208 and *P. fuscovaginae* UPB0736. The red numbers in the fractionating scheme (A) correspond to the fractions tested in the Kirby-Bauer test shown in (B). Control plates include Gentamycin (Gm) as positive control for antimicrobial activity, and Water (W) as negative control. To exclude any effect from the media, media, M3.7 was processed in the same way, and fractions 3, 4, 5, and 6 were tested in control plates.

FIGURE S4 | Picture of inoculated rice plants (Cultivar 733) with *Streptomyces* spp. strains vs. controls. *Streptomyces* 5.1 was able to improve the fresh weight of roots and shoots in cultivar 733, and strains A20 and 7.1 displayed the ability to significantly increase all the biometric parameters evaluated in cultivar F733 in comparison to the non-inoculated control. *Azotobacter chroococcum* was used as positive control for plant growth promotion (AC).

TABLE S1 | Microbial strains and primers used in this study.

REFERENCES

- Behie, S. W., Bonet, B., Zacharia, V. M., McClung, D. J., and Traxler, M. F. (2016). Molecules to ecosystems: actinomycete natural products in situ. *Front. Microbiol.* 7:2149. doi: 10.3389/fmicb.2016.02149
- Belimov, A., Safronova, V. I., and Sergeyeva, T. A. (2001). Characterization of plant growth promoting rhizobacteria isolated from polluted soils and containing 11-aminocyclopropane-1-carboxylate deaminase. *Can. J. Microbiol.* 47, 642–652. doi: 10.1139/w01-062
- Bouizgarne, B., and Aouamar, A. A. B. (2014). "Diversity of Plant Associated Actinobacteria," in *Bacterial Diversity in Sustainable Agriculture*, ed. D. K. Maheshwari (Cham: Springer International Publishing), 41–99.
- Carvalho, M. F., Ma, Y., Oliveira, R. S., and Freitas, H. (2017). "Endophytic Actinobacteria for Sustainable Agricultural Applications," in *Endophytes: Crop Productivity and Protection*, Vol. 2, eds D. K. Maheshwari and K. Annapurna (Cham: Springer International Publishing), 163–189. doi: 10.1007/978-3-319-66544-3_8
- Castillo, L. A., Pineda, D., Ospina, J., Echeverry, J., Perafan, R., and Garcés, G. (2011). Cambio climático y producción de Arroz. *Revista Arroz* 58, 5–12.
- Clinical Laboratory Standards Institute (2011). *Performance Standards for Antimicrobial Susceptibility Testing: Twenty-first Informational Supplement CLSI document M100-S21*. Wayne, PA: CLSI.
- Cole, J. R., Wang, Q., Fish, J. A., Chai, B., McGarrell, D. M., Sun, Y., et al. (2014). Ribosomal database project: data and tools for high throughput rRNA analysis. *Nucleic Acids Res.* 42, D633–D642. doi: 10.1093/nar/gkt1244
- Conn, V. M., Walker, A. R., and Franco, C. M. (2008). Endophytic actinobacteria induce defense pathways in *Arabidopsis thaliana*. *Mol. Plant Microbe Interact.* 21, 208–218. doi: 10.1094/MPMI-21-2-0208
- Correa, F., Perez, C. R., and Saavedra, E. (2007). Añublo bacterial de la panícula del arroz. *Revista Arroz* 468, 26–31.
- Cui, X., Mao, P. H., Zeng, M., Li, W. J., Zhang, L. P., Xu, L. H., et al. (2001). Streptimonospora salina gen. nov., sp. nov., a new member of the family Nocardioaceae. *Int. J. Syst. Evol. Microbiol.* 51, 357–363. doi: 10.1099/00207713-51-2-357
- De Weert, S., and Bloemberg, G. V. (2006). "Rhizosphere competence and the role of root colonization in biocontrol," in *Plant-Associated Bacteria*, ed. S. S. Gnanamanickam (Dordrecht: Springer Netherlands), 317–333.
- Diago, M., Ospina, J., Peirez, C. R., Saavedra, J., Echeverri, J., Cuevas, J., et al. (2009). Un buen manejo del cultivo, verdadera barrera contra el añublo bacterial. *Revista Arroz* 57, 30–38.
- Dobereiner, J. (1995). "Isolation and identification of aerobic nitrogen fixing bacteria from soil and plants," in *Methods in Applied Soil Microbiology and Biochemistry*, eds K. Alef and P. Nampieri (London: Academic Press), 161–174.
- El-tarabily, K. A. (2008). Promotion of tomato (*Lycopersicon esculentum* Mill.) plant growth by rhizosphere competent 1-aminocyclopropane-1-carboxylic acid deaminase - producing streptomycete actinomycetes. *Plant Soil* 308, 161–174. doi: 10.1007/s11104-008-9616-2
- Emmert, E. A., and Handelsman, J. (1999). Biocontrol of plant disease: a gram positive perspective. *FEMS Microbiol. Lett.* 171, 1–9. doi: 10.1111/j.1574-6968.1999.tb13405.x
- Fory, P. A., Triplett, L. R., Ballen, C., Abello, J. F., Duitama, J., Aricapa, G., et al. (2014). Comparative analysis of two emerging rice seed bacterial pathogens. *Phytopathology* 104, 436–444. doi: 10.1094/PHYTO-07-13-0186-R
- Francis, F., Kim, J., Ramajaj, T., Farmer, A., Rush, M. C., and Ham, J. H. (2013). Comparative genomic analysis of two *Burkholderia glumae* strains from different geographic origins reveals a high degree of plasticity in genome structure associated with genomic islands. *Mol. Genet. Genomics* 288, 195–203. doi: 10.1007/s00438-013-0744-x
- Gascuel, O. (1997). BIONJ: an improved version of the NJ algorithm based on a simple model of sequence data. *Mol. Biol. Evol.* 14, 685–695. doi: 10.1093/oxfordjournals.molbev.a025808
- Glickmann, E., and Dessaux, Y. (1995). A critical examination of the specificity of the salkowski reagent for indolic compounds produced by phytopathogenic bacteria. *Appl. Environ. Microbiol.* 61, 793–796.
- Goldstein, A. L., and McCusker, J. H. (1999). Three new dominant drug resistance cassettes for gene disruption in *Saccharomyces cerevisiae*. *Yeast* 15, 1541–1553. doi: 10.1002/(SICI)1097-0061(199910)
- Goo, Y. M., Kim, O. Y., Joe, Y. A., Lee, Y. B., Ju, J., Kim, B. T., et al. (1996). A new streptothricin family antibiotic producing *Streptomyces* spp. SNUS 8810-111; characterization of the producing organisms, fermentation, isolation, and structure elucidation of antibiotic. *Arch. Pharm. Res.* 19, 153–159. doi: 10.1007/BF02976852
- Goodfellow, M. (2012). "Phylum XXVI. Actinobacteria phyl. nov," in *Bergey's Manual of Systematic Bacteriology*, eds W. B. Whitman, M. Goodfellow, P. Kämpfer, H. J. Busse, M. E. Trujillo, W. Ludwig, et al. (New York, NY: Springer Science Business Media), 34–2028. doi: 10.1007/978-0-387-68233-4
- Gopalakrishnan, S., Pande, S., Sharma, M., Humayun, P., Kiran, B. K., Sandeep, D., et al. (2011). Evaluation of actinomycete isolates obtained from herbal vermicompost for the biological control of *Fusarium* wilt of chickpea. *Crop Prot.* 30, 1070–1078. doi: 10.1016/j.cropro.2011.03.006
- Goto, K., Nishiyama, K., and Ohata, K. (1987). Bacteria causing grain rot of rice. *Ann. Phytopathol. Soc. Jpn.* 53, 141–149. doi: 10.3186/jjphytopath.53.141
- Goto, K., and Ohata, K. (1956). New bacterial diseases on rice (brown stripe and grain rot). *Ann. Phytopathol. Soc. Jpn.* 21, 46–47.
- Guo, Y., Zheng, W., Rong, X., and Huang, H. Y. (2008). A multilocus phylogeny of the *Streptomyces* griseus 16S rRNA gene clade: use of multilocus sequence analysis for streptomycete systematics. *Int. J. Syst. Evol. Microbiol.* 2008, 149–159. doi: 10.1099/ijs.0.65224-0
- Gurung, T. D., Sherpa, C., Agrawal, V. P., and Lekhak, B. (2009). Isolation and characterization of antibacterial actinomycetes from soil samples of kalapathar, mount everest region. *Nepal J. Sci. Technol.* 10, 173–182. doi: 10.3126/njst.v10i0.2957
- Ham, J. H., Melanson, R. A., and Rush, M. C. (2011). *Burkholderia glumae*: next major pathogen of rice? *Mol. Plant Pathol.* 12, 329–339. doi: 10.1111/j.1364-3703.2010.00676.x
- Handelsman, J., and Stabb, E. V. (1996). Biocontrol of soilborne plant pathogens. *Plant Cell* 8, 1855–1869. doi: 10.1105/tpc.8.10.1855
- Hardy, R. W., Holsten, R. D., Jackson, E. K., and Burns, R. C. (1968). The acetylene-ethylene assay for N(2) fixation: laboratory and field evaluation. *Plant Physiol.* 43, 1185–1207. doi: 10.1104/pp.43.8.1185
- Hartl, A., Guttner, J., Stockel, U., and Hoffmann, H. (1986). Acute and subchronic toxicity of nourseothricin in laboratory animals. *Arch. Exp. Veterinarmed.* 40, 727–735.
- Hastuti, R. D., Lestari, Y., Saraswati, R., and Suwanto, A. (2012). Capability of *Streptomyces* spp. in controlling bacterial leaf blight disease in rice plants. *Am. J. Agric. Biol. Sci.* 7, 217–223. doi: 10.3844/ajabssp.2012.217.223
- Herrmann, L., and Lesueur, D. (2013). Challenges of formulation and quality of biofertilizers for successful inoculation. *Appl. Microbiol. Biotechnol.* 97, 8859–8873. doi: 10.1007/s00253-013-5228-8
- Hikichi, Y., Tsujiguchi, K., Maeda, Y., and Okuno, T. (2001). Development of increased oxolinic acid-resistance in *Burkholderia glumae*. *J. Gen. Plant Pathol.* 67, 57–62. doi: 10.1007/PL00012988
- Jeong, Y., Kim, J., Kim, S., Kang, Y., Nagamatsu, T., and Hwang, I. (2003). Toxoflavin produced by *Burkholderia glumae* causing rice grain rot is responsible for inducing bacterial wilt in many field crops. *Plant Dis.* 87, 890–895. doi: 10.1094/PDIS.2003.87.8.890
- Ji, Z., Wang, M., Wei, S., Zhang, J., and Wu, W. (2009). Isolation, structure elucidation and antibacterial activities of streptothricin acids. *J. Antibiot.* 62, 233–237. doi: 10.1038/ja.2009.16
- Ji, Z., Wang, M., Zhang, J., Wei, S., and Wu, W. (2007). Two new members of streptothricin class antibiotics from *Streptomyces qinlingensis* sp. nov. *J. Antibiot.* 60, 739–744. doi: 10.1038/ja.2007.96
- Ji, Z., Wei, S., Zhang, J., Wu, W., and Wang, M. (2008). Identification of streptothricin class antibiotics in the early-stage of antibiotics screening by electrospray ionization mass spectrometry. *J. Antibiot.* 61, 660–667. doi: 10.1038/ja.2008.93
- Johnson, K. B., and Dileone, J. A. (1999). Effect of antibiosis on antagonist dose-plant disease response relationships for the biological control of crown gall of tomato and cherry. *Phytopathology* 89, 974–980. doi: 10.1094/PHYTO.1999.89.10.974
- Jolley, K. A., and Maiden, M. C. (2010). BIGSdb: scalable analysis of bacterial genome variation at the population level. *BMC Bioinformatics* 11:595. doi: 10.1186/1471-2105-11-595
- Kanini, G. S., Katsifas, E. A., Savvides, A. L., Hatzinikolaou, D. G., and Karagouni, A. D. (2013). Greek indigenous streptomycetes as biocontrol agents against the

- soil-borne fungal plant pathogen *Rhizoctonia solani*. *J. Appl. Microbiol.* 114, 1468–1479. doi: 10.1111/jam.12138
- Karki, H. S., Shrestha, B. K., Han, J. W., Groth, D. E., Barphagha, I. K., Rush, M. C., et al. (2012). Diversities in virulence, antifungal activity, pigmentation and DNA fingerprint among strains of *Burkholderia glumae*. *PLoS One* 7:e45376. doi: 10.1371/journal.pone.0045376
- Kawanishi, T., Shiraishi, T., Okano, Y., Sugawara, K., Hashimoto, M., Maejima, K., et al. (2011). New detection systems of bacteria using highly selective media designed by SMART: selective medium-design algorithm restricted by two constraints. *PLoS One* 6:e16512. doi: 10.1371/journal.pone.0016512
- Khokhlov, A. S. (1983). Achievements in the study of streptothricin antibiotics. *Antibiotiki* 28, 613–622.
- Khokhlov, A. S., and Shutova, K. I. (1972). Chemical structure of streptothricins. *J. Antibiot.* 25, 501–508. doi: 10.7164/antibiotics.25.501
- Kieser, T., Bibb, M. J., Buttner, K. F., Chater, K. F., and Hopwood, D. A. (2000). *Practical Streptomyces Genetics*. Norwich: The John Innes Foundation.
- Kim, O. S., Cho, Y. J., Lee, K., Yoon, S. H., Kim, M., Na, H., et al. (2012). Introducing EzTaxon-e: a prokaryotic 16S rRNA gene sequence database with phylotypes that represent uncultured species. *Int. J. Syst. Evol. Microbiol.* 62(Pt 3), 716–721. doi: 10.1099/ijs.0.038075-0
- Kim, S., Park, J., Lee, J., Shin, D., Park, D. S., Lim, J. S., et al. (2014). Understanding pathogenic *Burkholderia glumae* metabolic and signaling pathways within rice tissues through in vivo transcriptome analyses. *Gene* 547, 77–85. doi: 10.1016/j.gene.2014.06.029
- Kinkel, L. L., Schlatter, D. C., Bakker, M. G., and Arenz, B. E. (2012). *Streptomyces* competition and co-evolution in relation to plant disease suppression. *Res. Microbiol.* 163, 490–499. doi: 10.1016/j.resmic.2012.07.005
- Knief, C., Delmotte, N., Chaffron, S., Stark, M., Innerebner, G., Wassmann, R., et al. (2012). Metaproteogenomic analysis of microbial communities in the phyllosphere and rhizosphere of rice. *ISME J.* 6, 1378–1390. doi: 10.1038/ismej.2011.192
- Kochupurakkal, B. S., and Iglehart, J. D. (2013). Nourseothricin N-acetyl transferase: a positive selection marker for mammalian cells. *PLoS One* 8:e68509. doi: 10.1371/journal.pone.0068509
- Köhl, J., Postma, J., Nicot, P., Ruocco, M., and Blum, B. (2011). Stepwise screening of microorganisms for commercial use in biological control of plant-pathogenic fungi and bacteria. *Biol. Control* 57, 1–12. doi: 10.1016/j.biocontrol.2010.12.004
- Kurita, T., and Tabei, H. (1967). On the pathogenic bacterium of bacterial grain rot of rice. *Ann. Phytopathol. Soc. Jpn.* 33:111.
- Kurth, F., Mailander, S., Bonn, M., Feldhahn, L., Herrmann, S., Grosse, I., et al. (2014). *Streptomyces*-induced resistance against oak powdery mildew involves host plant responses in defense, photosynthesis, and secondary metabolism pathways. *Mol. Plant Microbe Interact.* 27, 891–900. doi: 10.1094/MPMI-10-13-0296-R
- Kusumoto, S., Kambayashi, Y., Imaoka, S., Shima, K., and Shiba, T. (1982). Total chemical structure of streptothricin. *J. Antibiot.* 35, 925–927. doi: 10.7164/antibiotics.35.925
- Labeda, D. P., Doroghazi, J. R., Ju, K. S., and Metcalf, W. W. (2014). Taxonomic evaluation of *Streptomyces albus* and related species using multilocus sequence analysis and proposals to amend the description of *Streptomyces albus* and describe *Streptomyces pathocidini* sp. nov. *Int. J. Syst. Evol. Microbiol.* 64(Pt 3), 894–900. doi: 10.1099/ijs.0.058107-0
- Labeda, D. P., Goodfellow, M., Brown, R., Ward, A. C., Lanoot, B., Vannanneyt, M., et al. (2012). Phylogenetic study of the species within the family Streptomycetaceae. *Antonie Van Leeuwenhoek* 101, 73–104. doi: 10.1007/s10482-011-9656-0
- Lucas, X., Senger, C., Erxleben, A., Gruning, B. A., Doring, K., Mosch, J., et al. (2013). StreptomeDB: a resource for natural compounds isolated from *Streptomyces* species. *Nucleic Acids Res.* 41, D1130–D1136. doi: 10.1093/nar/gks1253
- Magbanua, Z. V., Arick, M. II, Buza, T., Hsu, C. Y., Showmaker, K. C., Chouvarine, P., et al. (2014). Transcriptomic dissection of the rice-*Burkholderia glumae* interaction. *BMC Genomics* 15:755. doi: 10.1186/1471-2164-15-755
- Mahmoud, A. L. E., and Abdallah, M. A. (2001). Siderophores production by some microorganisms and their effect on *Bradyrhizobium*-mungbean symbiosis. *Int. J. Agric. Biol.* 3, 157–162.
- Maruyama, C., and Hamano, Y. (2009). The biological function of the bacterial isochorismatase-like hydrolase SttH. *Biosci. Biotechnol. Biochem.* 73, 2494–2500. doi: 10.1271/bbb.90499
- Maruyama, C., Toyoda, J., Kato, Y., Izumikawa, M., Takagi, M., Shin-ya, K., et al. (2012). A stand-alone adenylation domain forms amide bonds in streptothricin biosynthesis. *Nat. Chem. Biol.* 8, 791–797. doi: 10.1038/nchembio.1040
- Mattiuzzo, M., Bertani, I., Ferluga, S., Cabrio, L., Bigirimana, J., Guarnaccia, C., et al. (2010). The plant pathogen *Pseudomonas fuscovaginae* contains two conserved quorum sensing systems involved in virulence and negatively regulated by RsaL and the novel regulator RsaM. *Environ. Microbiol.* 13, 145–162. doi: 10.1111/j.1462-2920.2010.02316.x
- Mattos, K. A., Padua, V. L., Romeiro, A., Hallack, L. F., Neves, B. C., Ulisses, T. M., et al. (2008). Endophytic colonization of rice (*Oryza sativa* L.) by the diazotrophic bacterium *Burkholderia kururiensis* and its ability to enhance plant growth. *An. Acad. Bras. Cienc.* 80, 477–493. doi: 10.1590/S0001-37652008000300009
- Miransari, M. (2013). Soil microbes and the availability of soil nutrients. *Acta Physiol. Plant* 35, 3075–3084. doi: 10.1007/s11738-013-1338-2
- Mizobuchi, R., Sato, H., Fukuoka, S., Tanabata, T., Tsushima, S., Imbe, T., et al. (2013). Mapping a quantitative trait locus for resistance to bacterial grain rot in rice. *Rice* 6:13. doi: 10.1186/1939-8433-6-13
- Moreno, N. (2011). Optimising carbon and nitrogen sources for *Azotobacter chroococcum* growth. *Afr. J. Biotechnol.* 10, 2951–2958. doi: 10.5897/AJB10.1484
- Moreno, N., and Rojas, J. (2008). Producción y formulación de prototipos de un biofertilizante a partir de bacterias nativas asociadas al cultivo de arroz (*Oryza sativa*). *Rev. Colomb. Biotechnol.* 10, 50–62.
- Mota, M. S., Gomes, C. B., Souza Junior, I. T., and Moura, A. B. (2017). Bacterial selection for biological control of plant disease: criterion determination and validation. *Braz. J. Microbiol.* 48, 62–70. doi: 10.1016/j.bjm.2016.09.003
- Nagadesi, P. K., and Arya, A. (2012). Lignocellulolytic activity of wood-inhabiting fungi from ratanmahal wildlife sanctuary gujarat, india. *Biotechnol. Adv.* 12, 30–36.
- Nandakumar, R., Rush, M. C., and Correa, F. (2007). Association of *Burkholderia glumae* and *Burkholderia gladioli* with panicle blight symptoms on rice in panama. *Plant Dis.* 91:767. doi: 10.1094/PDIS-91-6-0767C
- Nandakumar, R., Shahjahan, A. K. M., Yuan, X. L., Dickstein, E. R., Groth, D. E., Clarck, C. A., et al. (2009). *Burkholderia glumae* and *B. gladioli* cause bacterial panicle blight in rice in the Southern United States. *Plant Dis.* 93, 896–905. doi: 10.1094/PDIS-93-9-0896
- Nautiyal, C. S. (1999). An efficient microbiological growth medium for screening phosphate solubilizing microorganisms. *FEMS Microbiol. Lett.* 170, 265–270. doi: 10.1111/j.1574-6968.1999.tb13383.x
- Nimnoi, P., Pongsilp, N., and Lumyong, S. (2010). Endophytic actinomycetes isolated from *Aquilaria crassna* pierre ex Lec and screening of plant growth promoters production. *World J. Microbiol. Biotechnol.* 26, 193–203. doi: 10.1007/s11274-009-0159-3
- Pospiech, A., and Neumann, B. (1995). A versatile quick-prep of genomic DNA from Gram-positive bacteria. *Trends Genet.* 11, 217–218. doi: 10.1016/S0168-9525(00)89052-6
- Qin, S., Xing, K., Jiang, J. H., Xu, L. H., and Li, W. J. (2011). Biodiversity, bioactive natural products and biotechnological potential of plant-associated endophytic actinobacteria. *Appl. Microbiol. Biotechnol.* 89, 457–473. doi: 10.1007/s00253-010-2923-2926
- Razak, A. A., Zainudin, N. A., Sidiq, S., Ismail, N. A., Mohamad, N. I., and Baharuddin, S. (2009). Sheat brown rot disease of rice caused by *Pseudomonas fuscovaginae* in the peninsular Malaysia. *J. Plant Prot. Res.* 49, 244–249. doi: 10.2478/v10045-009-0037-x
- Riedel, K., Hentzer, M., Geisenberger, O., Huber, B., Steidle, A., Wu, H., et al. (2001). N-acylhomoserine-lactone-mediated communication between *Pseudomonas aeruginosa* and *Burkholderia cepacia* in mixed biofilms. *Microbiology* 147(Pt 12), 3249–3262. doi: 10.1099/00221287-147-12-3249
- Rong, X., Guo, Y., and Huang, H. Y. (2009). Proposal to reclassify the *Streptomyces albidoflavus* clade on the basis of multilocus sequence analysis and DNA–DNA hybridization, and taxonomic elucidation of *Streptomyces griseus* subsp. *solvifaciens*. *Syst. Appl. Microbiol.* 32, 314–322. doi: 10.1016/j.syapm.2009.05.003
- Rong, X., and Huang, Y. (2012). Taxonomic evaluation of the *Streptomyces hygroscopicus* clade using multilocus sequence analysis and DNA–DNA

- hybridization, validating the MLSA scheme for systematics of the whole genus. *Syst. Appl. Microbiol.* 35, 7–18. doi: 10.1016/j.syapm.2011.10.004
- Saitou, N., and Nei, M. (1987). The neighbor-joining method: a new method for reconstructing phylogenetic trees. *Mol. Biol. Evol.* 4, 406–425. doi: 10.1093/oxfordjournals.molbev.a040454
- Samac, D. A., and Kinkel, L. L. (2001). Suppression of the root-lesion nematode (*Pratylenchus penetrans*) in alfalfa (*Medicago sativa*) by *Streptomyces* spp. *Plant Soil* 235, 35–44. doi: 10.1023/a:1011820002779
- Sayler, R. J., Cartwright, R. D., and Yang, K. Y. (2006). Genetic characterization and real-time PCR detection of *Burkholderia glumae*, a newly emerging bacterial pathogen of rice in the United States. *Plant Dis.* 90, 603–610. doi: 10.1094/PD-90-0603
- Scervino, J. M., Prieto, M., Della Mónica, I., Recchi, M., Moreno, N., and Godeas, A. (2010). Soil fungal isolates produce different organic acid patterns involved in phosphate salts solubilization. *Biol. Fertil. Soils* 46, 755–763. doi: 10.1007/s00374-010-0482-8
- Schisler, D. A., Slininger, P. J., and Bothast, R. J. (1997). Effects of antagonist cell concentration and two-strain mixtures on biological control of fusarium dry rot of potatoes. *Phytopathology* 87, 177–183. doi: 10.1094/PHYTO.1997.87.2.177
- Schlatter, D. C., and Kinkel, L. L. (2014). Global biogeography of *Streptomyces* antibiotic inhibition, resistance, and resource use. *FEMS Microbiol. Ecol.* 88, 386–397. doi: 10.1111/1574-6941.12307
- Schwyn, B., and Neilands, J. B. (1987). Universal chemical assay for the detection and determination of siderophores. *Anal. Biochem.* 160, 47–56. doi: 10.1016/0003-2697(87)90612-9
- Shirling, E., and Gottlieb, D. (1968). Cooperative descriptions of type cultures of *Streptomyces* III. Additional species descriptions from first and second studies. *Int. J. Syst. Bacteriol.* 18, 279–392. doi: 10.1099/00207713-18-4-27
- Sun, J., Kelemen, G. H., Fernandez-Abalos, J. M., and Bibb, M. J. (1999). Green fluorescent protein as a reporter for spatial and temporal gene expression in *Streptomyces coelicolor* A3(2). *Microbiology* 145(Pt 9), 2221–2227. doi: 10.1099/00221287-145-9-2221
- Sundara-Rao, W. V. B., and Sinha, M. K. (1963). Phosphate dissolving microorganisms in the soil and rhizosphere. *Indian J. Agric. Sci.* 33, 272–278.
- Taechowisan, T., Peberdy, J. F., and Lumyong, S. (2003). Chitinase production by endophytic *Streptomyces aureofaciens* CMUAc130 and its antagonism against phytopathogenic fungi. *Ann. Microbiol.* 53, 447–461.
- Tamura, K., and Nei, M. (1993). Estimation of the number of nucleotide substitutions in the control region of mitochondrial DNA in humans and chimpanzees. *Mol. Biol. Evol.* 10, 512–526. doi: 10.1093/oxfordjournals.molbev.a040023
- Tamura, K., Peterson, D., Peterson, N., Stecher, G., Nei, M., and Kumar, S. (2011). MEGA5: molecular evolutionary genetics analysis using maximum likelihood, evolutionary distance, and maximum parsimony methods. *Mol. Biol. Evol.* 28, 2731–2739. doi: 10.1093/molbev/msr121
- Tang, Y. W., and Bonner, J. (1948). The enzymatic inactivation of indole acetic acid; the physiology of the enzyme. *Am. J. Bot.* 35, 570–578. doi: 10.1002/j.1537-2197.1948.tb08123.x
- Tanii, A., Miyajima, K., and Akita, T. (1976). The sheath brown rot disease of rice plant and its causal bacterium. *Ann. Phytopathol. Soc. Jpn.* 42, 540–548. doi: 10.3186/jjphytopath.42.540
- Telesnina, G. N., Riabova, I. D., Shutova, K. I., and Khokhlov, A. S. (1973). Mechanism of action of streptothricins. *Dokl. Akad. Nauk SSSR* 213, 743–745.
- Thompson, J. D., Higgins, D. G., and Gibson, T. J. (1994). CLUSTAL W: improving the sensitivity of progressive multiple sequence alignment through sequence weighting, position-specific gap penalties and weight matrix choice. *Nucleic Acids Res.* 22, 4673–4680. doi: 10.1093/nar/22.22.4673
- Tian, X., Cao, L., Tan, H., Han, W., Chen, M., Liu, Y., et al. (2007). Diversity of cultivated and uncultivated actinobacterial endophytes in the stems and roots of rice. *Microb. Ecol.* 53, 700–707. doi: 10.1007/s00248-006-9163-9164
- Tian, X. L., Cao, L. X., Tan, H. M., Zeng, Q. G., Jia, Y. Y., Han, W. Q., et al. (2004). Study on the communities of endophytic fungi and endophytic actinomycetes from rice and their antipathogenic activities in vitro. *World J. Microbiol. Biotechnol.* 20, 303–309. doi: 10.1023/B:WIBI.0000023843.83692.3f
- Waksman, S. A. (1943). Production and activity of streptothricin. *J. Bacteriol.* 46, 299–310.
- Weinberg, J. B., Alexander, B. D., Majure, J. M., Williams, L. W., Kim, J. Y., Vandamme, P., et al. (2007). *Burkholderia glumae* infection in an infant with chronic granulomatous disease. *J. Clin. Microbiol.* 45, 662–665. doi: 10.1128/JCM.02058-06
- Wiley, J. M., Sherwood, L. M., and Woolverton, C. J. (2007). *Prescott, Harley, and Klein's Microbiology*. New York, NY: McGraw Hill.
- Zarandi, M. E., Bonjar, G. H. S., Dehkaei, F. P., Moosavi, S. A. A., Farokhi, P. R., and Aghighi, S. A. (2009). Biological control of rice blast (*Magnaporthe oryzae*) by use of *Streptomyces sindeneusis* isolate 263 in greenhouse. *Am. J. Appl. Sci.* 6, 194–199. doi: 10.3844/ajassp.2009.194.199
- Zeigler, R. S., and Alvarez, E. (1987). Grain discoloration of rice caused by *Pseudomonas glumae* in Latin America. *Plant Dis.* 73:368. doi: 10.1094/PD-73-0368B

Conflict of Interest Statement: The authors declare that the research was conducted in the absence of any commercial or financial relationships that could be construed as a potential conflict of interest.

Copyright © 2019 Suárez-Moreno, Vinchira-Villarraga, Vergara-Morales, Castellanos, Ramos, Guarnaccia, Degrassi, Venturi and Moreno-Sarmiento. This is an open-access article distributed under the terms of the Creative Commons Attribution License (CC BY). The use, distribution or reproduction in other forums is permitted, provided the original author(s) and the copyright owner(s) are credited and that the original publication in this journal is cited, in accordance with accepted academic practice. No use, distribution or reproduction is permitted which does not comply with these terms.

Advantages of publishing in Frontiers



OPEN ACCESS

Articles are free to read
for greatest visibility
and readership



FAST PUBLICATION

Around 90 days
from submission
to decision



HIGH QUALITY PEER-REVIEW

Rigorous, collaborative,
and constructive
peer-review



TRANSPARENT PEER-REVIEW

Editors and reviewers
acknowledged by name
on published articles

Frontiers

Avenue du Tribunal-Fédéral 34
1005 Lausanne | Switzerland

Visit us: www.frontiersin.org

Contact us: info@frontiersin.org | +41 21 510 17 00



REPRODUCIBILITY OF RESEARCH

Support open data
and methods to enhance
research reproducibility



DIGITAL PUBLISHING

Articles designed
for optimal readership
across devices



FOLLOW US

@frontiersin



IMPACT METRICS

Advanced article metrics
track visibility across
digital media



EXTENSIVE PROMOTION

Marketing
and promotion
of impactful research



LOOP RESEARCH NETWORK

Our network
increases your
article's readership